



INVESTIGATION INTO THE CLEANING BEHAVIOUR OF NANOFUIDS ON  
CRUDE OIL CONTAMINATED SOILS AT OPTIMUM CONDITIONS

By

RITA NGOZI EDOGA

ID NO: 200509238

A DISSERTATION

Submitted to the Graduate School in accordance with  
the Requirements for the Award of Doctor of Philosophy  
degree in  
School of Chemical and Process Engineering, University of  
Leeds  
Leeds, United Kingdom

Doctoral Committee,

Professor Graham Huggan (School of English)

Professor Michelle Peckham (School of Molecular & Cellular Biology)

November-2015

## **Declaration**

I hereby declare that the Thesis titled “Investigation into the Cleaning Behavior of Nanofluids on Crude Oil Contaminated Soils at Optimum Conditions” which is a dissertation submitted by me in partial fulfillment of the requirements for the award of Doctor of Philosophy degree is my work and has never been submitted any where for the award of any degree prior to this date. I duly acknowledged all the equations in the thesis used by me.

Clearance was obtained from the Institutional Ethics Committee for carrying out the study.

Signature: .....

Date: .....

## **Certification**

I, Rita Edoga hereby certify that I had personally carried out the work depicted in the thesis entitled ‘‘INVESTGATON INTO THE CLEANING BEHAVIOUR OF NANOFLUIDS ON CRUDE OIL CONTAMINATED SOILS AT OPTIMUM CONDITIONS’’ and to the best of my knowledge that this dissertation I have submitted meets all the required institutional formatting guidelines as specified in the most recent edition of the Thesis/Dissertation writer’s Guide.No part of the thesis has been submitted for the award of any other degree prior to this date.

Name: Mrs Rita Edoga.....Date:

## **Dedication**

This Dissertation is dedicated to God Almighty that has been making everything possible for me and my family members - Prof M.O.Edoga, Joseph Edoga and Joel Edoga, at all times.

## **Acknowledgements**

First of all, I would like to express my deep gratitude to my able supervisor, co-supervisors and internal assessor, Dr Ali Hassanpour Rudbari, Dr Darron Dixon – Hardy, Prof Yulong Ding and Dr Olivier Cayre for their advice and encouragement throughout the period of my 4 years study. More so, I would like to thank University of Leeds – SCAPE for the opportunity given to me to work on this project and for providing me with an office space, laboratories as well as equipment.

I am very grateful to the Technicians who assisted me in the various laboratories that I used in the course of this work especially David Lawlor, Sussane Patel, Peter Dawson, Adrian Cunliffe and Sarah Dona.

My special thanks also go to all the staff and students of University of Leeds who contributed towards the successful completion of this study, especially Prof. William Gale, Natalie Wells, ERI secretaries - S.Heathen, David Haynes as well as IPSE secretaries.

Lastly, I would like to sincerely thank all my families and friends in Nigeria and Leeds for all their love, moral support and prayers towards the success of the programme.

This project would not have been possible at all without the financial support of Petroleum Technology Development Fund (PTDF), Abuja – Nigeria. I sincerely express my gratitude to PTDF, the sponsor of my programme in University of Leeds, United Kingdom.

Above all, I thank God Almighty for His love, blessings and protection throughout the period of the study.

## Table of contents

Declaration.....	ii
Certification .....	iii
Dedication .....	iv
Acknowledgements.....	v
Table of contents.....	vi
Table of Figures .....	x
List of Abbreviations .....	xxvii
SYNOPSIS (ABSTRACT) .....	xxviii
1 Chapter 1.0 Introduction .....	1
1.1 Background .....	1
1.2 Causes of soil contamination .....	5
1.2.1.1 Limitations.....	7
1.3 Report Outline .....	9
2 Chapter 2.0 Literature Review .....	11
2.1 Soil properties .....	11
2.2 Porosity.....	11
2.2.1 Permeability (Hydraulic conductivity) .....	12
2.2.2 Saturation .....	12
2.3 Fluid Properties .....	13
2.3.1 Density .....	13
2.3.2 Surface and interfacial tension (IFT) .....	14
2.3.3 Viscosity .....	15
2.4 Properties of Fluid-Soil Interaction.....	15
2.4.1 Wettability.....	15
2.4.2 Classification of wettability .....	16
2.4.3 Methods of wettability measurement.....	17
2.4.4 Amott method for the calculation of Wettability Index (WI).....	17
2.4.4.1 USBM Test .....	19
2.4.4.2 Contact angle .....	19
2.4.4.3 The static and dynamic sessile drop method .....	20

2.4.4.4	Applications of contact angle .....	21
2.4.5	Contact angle and wettability.....	21
2.4.5.1	Spreading, wetting, and contactangle .....	23
2.5	Saturation .....	24
2.5.1	Capillary Pressure .....	25
2.5.2	The Effects of Wettability on Capillary Pressure .....	26
2.5.3	Effective and Relative Permeability .....	27
2.5.4	Effects of Wettability on Relative Permeability .....	27
2.5.5	Crude oil.....	28
2.5.6	Classification of Hydrocarbon Reservoir Fluids.....	29
2.5.7	Chemical components .....	32
2.5.8	Petroleum and petroleum products .....	33
2.5.8.1	Petroleum definition .....	33
2.5.8.2	Chemistry of Petroleum.....	35
2.5.8.3	Chemical Compounds and Wettability.....	36
2.5.9	Recovery of crude Oil.....	37
2.5.10	Use of Nanotechnology as Enhanced Oil Recovery .....	37
<b>2.5.11</b>	<b>Nanoparticles and Nano fluids.....</b>	<b>37</b>
2.5.11.1	Backgrounds .....	37
	Properties of Nanofluids.....	41
	Viscosity .....	41
	Density.....	41
	Specific heat capacity .....	41
2.6	PREPARATION OF NANOFUIDS.....	43
<b>2.6.1</b>	<b>Production of Nano fluids.....</b>	<b>43</b>
2.6.1.1	One-Step Methods .....	43
2.6.1.2	Two-Step Methods .....	44
2.6.2	STABILITY OF NANOFUIDS .....	44
2.6.3	Methods of Improving the Stability of a Nanofluid.....	45
2.6.4	Stability Evaluation.....	46
2.6.5	Surfactants.....	47

2.7	THERMOPHYSICAL PROPERTIES OF NANOFUIDS .....	48
2.7.1	Thermal Conductivity: .....	48
2.7.2	Heat Transfer .....	49
2.7.3	Contact Angle .....	51
2.7.4	Porosity and contact angle .....	52
<b>2.8</b>	<b>Application of Nano fluids.....</b>	<b>52</b>
2.8.1	Nano fluid Detergent.....	54
2.8.2	Application of Nanotechnology in Oil and Gas Industries.....	54
2.8.3	Remediation methods.....	56
<b>2.8.4</b>	<b>Natural processes .....</b>	<b>57</b>
<b>3</b>	<b>Chapter 3.0   MATERIALS AND METHODS  .....</b>	<b>74</b>
3.1	Materials and Equipment .....	74
3.1.1	Surface tension.....	90
3.1.2	Contact angle measurements.....	92
4	4.0: Soil preparation and characterization.....	95
4.1	Study site .....	95
5	Chapter 5.0.....	108
5.1.1	Characterization of the mineral oil used in the experiment. ....	108
6	6.1 General soil physical and chemical properties.....	156
	CURRICULUM VITAE .....	195
	NAME: Rita Ngozi, EDOGA (Mrs) .....	195
	Appendices.....	197
	A Properties of experimental materials.....	197
	A.1 Nanoparticles .....	197
	A.2 Organic and Inorganic Compounds .....	198
	A.3 Characterization of experimental nanofluids [57] .....	199
	A.3.1 Particle size distribution .....	199
	B.Results from the measurements of soil sample and Fluid properties.....	217
	B.1 Permeability measurements .....	217
	B.1 is the measurement of porosity results.....	217
	B.3 Results from the mean permeability. ....	217



C. Results from the total surface area of the different nanofluids is calculated using three equations:.....	221
D. Results from the surface tension of both pure and surfacted nanofluids.....	224
E Thermal Conductivity enhancement (%) .....	225
G.Thermal optical/Absorbancy Results for the different nanofluids .....	228
H.Summary of the wettability of the different nanofluids.....	230
H.2Surfacted nanofluids .....	232
Table I- 1Measured contact angles of the different nanofluids .....	234
Table J- 2 Wettability parameters for surfacted nanofluids. ....	236
Table K- 1Effect of pH on the zetapotential and absorbency of the different surfacted nanofluids.....	236
L.Soil contamination with mineral oil and cleanup process with the different nanofluids .....	237
M. Thermal Analysis of soil after cleanup process .....	242
M.1 Soil Analysis .....	242
This graph is reported by replotting the generated tga data into weight loss and heatflow considering the temperature and time as shown on FigureA-36 .....	244

## Table of Figures

Figure 1-1 Soil contaminated sites [100] .....	1
Figure 2-1 Interfacial tension acts perpendicular to the interface between the two immiscible fluids [126] .....	14
Figure 2-2 Contact angle measurements through the water phase [107] .....	20
Figure 2-3 Schematic of advancing and receding contact angles .....	20
Figure 2-4 Illustration of the nomenclature used for defining the contact angle [126] .....	22
Figure 2-5 Illustration of interfacial tension for a two-phase system with water and oil on a soil surface [10b] .....	23
Figure 2-6 Illustration of a porous system of mixed wettability .....	23
Figure 2-7 Illustration of the capillary pressure as a function of saturation showing the drainage and imbibition curve .....	26
Figure 2-8 Visualization of the effect of wettability on the relative permeability curves .....	28
Figure 2-9 Examples of typical hydrocarbon components. Normal hexane and iso-hexane are paraffins. Cyclohexane belongs to the naphthenes, and aromatic benzene [51]. .....	33
Figure 2-10 Helical Coiled Tubing (Heat Exchanger) Layout [69c] .....	51
Figure 2-11 A water droplet in equilibrium over a horizontal solid surface .....	51
Figure 3-1. Al <sub>2</sub> O <sub>3</sub> nanoparticles .....	78
Figure 3-2 TiO <sub>2</sub> nanoparticles .....	78
Figure 3-3. Deionised water .....	78
Figure 3-4 ZnO powder .....	78
Figure 3-5 Al <sub>2</sub> O <sub>3</sub> nanoparticles Figure 3-6 Deionised water Figure 3-7 Al <sub>2</sub> O <sub>3</sub> nanofluid .....	79
Figure 3-8 Photographic view of a Malvern 4800 zetasizer .....	85
Figure 3-9 A sketch block diagram of Dynamic Light Scattering instrument .....	85
Figure 3-10 Photographic view of pH meter .....	86
Figure 3-11 Photographic View of UV-Vis Spectrophotometer .....	87
Figure 3-12 Absorption Cell/Cuvettes .....	87
Figure 3-13 More reviewed on water droplet in equilibrium over a horizontal solid surface. .....	88
Figure 3-14 Photographic view of a Picnometer for measuring the density of mineral oil and nanofluids .....	89
Figure 3-15. Photographic view of Bohlin Rheometer .....	89
Figure 3-16 Photographic view of Attension Theta (Potential meter) .....	92
Figure 3-17 The picture view of Contact Angle Instrument .....	93

Figure4-1.Illustration of the Constant Head permeability test apparatus experimental setup .	96
Figure 4-2 Burette/Imbibition Flask with Core soil sample .....	97
Figure 4-3 Laboratory clean-up experimental Set-up of oil contaminated soil using nano fluid .....	97
Figure 4-4 White mineral oil.....	98
Figure 4-5 HV160.....	98
Figure 4-6 Refined golden Oil recovered from the contaminated soil using nanofluids.....	100
Figure 4-7 Set-up of the Cam 100 (KSV instrument) camera .....	103
Figure5-1 Viscosity of the experimental mineral oil [57] .....	110
Figure 5-2 Particle size distribution of pure 0.3 vol% $Al_2O_3$ water nanofluid .....	111
Figure 5-3 Particle Size Distribution of 0.3wt% $Al_2O_3$ + 0.03wt% SDBS- deionised water nanofluid .....	112
Figure 5-4 Particle size distribution of pure 0.7 vol% $Al_2O_3$ water nanofluid .....	113
Figure5-5 Particle Size Distribution of 0.7wt% $Al_2O_3$ + 0.07wt%SDBS –deionised water nanofluid .....	114
Figure 5-6 Particle size distribution of 1vol% pure $Al_2O_3$ water nanofluid .....	115
Figure 5-7 Particle Size Distribution of 1wt% $Al_2O_3$ + 0.1wt%SDBS –deionised water nanofluid .....	116
Figure 5-8 Total surface area of the different monotype nanofluids. ....	119
Figure 5-9 Total surface area of the different monotype nanofluids [137].....	120
Figure 5-10 Total surface area of the different hybrid nanofluids [137]. ....	121
Figure 5-11 Comparison of cleaning efficiency with total surface area of Monotype nanofluids .....	122
Figure 5-12 Comparison of cleaning efficiency with total surface area of hybrid nanofluids .....	122
Figure 5-13 Measured density of experimental mineral oil Hv1 60 .....	123
Figure 5-14 Experimental results of monotype nanofluids density measurements .....	124
Figure 5-15 Comparison of the density of the various hybrid nanofluids .....	125
Figure 5-16 Measured surface tension of the various weight fractions of the pure monotype nanofluids.....	126
Figure 5-17 Measured surface tension of the various weight fractions of the surf acted monotype nanofluids.....	127
Figure 5-18 Surface tension of hybrid nanofluids .....	128

Figure 5-19 Surface tension of different hybrid nanofluids.....	128
Figure 5-20 .Vertically flipped frames recorded during the measurements .....	129
Figure 5-21 Viscosities of the experimental oils .....	130
Figure 5-22 Viscosity of Poly Cambol oil .....	131
Figure 5-23 Viscosity of High Viscosity Index Oil .....	131
Figure 5-24 Viscosity of Mineral oil .....	132
Figure 5-25 Viscosity of 0.3wt% concentration of the various nanofluids against temperature .....	132
Figure 5-26 Viscosity of 0.7wt% concentration of the various nanofluids against temperature .....	133
Figure 5-27 Viscosity of 1.0wt% concentration of different nanofluids against temperature [57] .....	134
Figure 5-28 Viscosity of the various pure hybrid nanofluids .....	134
Figure 5-29 Viscosity of surfacted hybrid nanofluids .....	135
Figure 5-30 Viscosities of the different 0.3 vol% nanofluids against temperature .....	135
Figure 5-31 Zetapotential of the different monotype nanofluids vs pH for optimum stabilization .....	136
Figure 5-32 Zeta potential of the different hybrid nanofluids vs.pH for optimum stabilization .....	136
Figure 5-33 Experimental results of the cleaning efficiency of the different pure monotype nanofluids.....	137
Figure 5-34 Comparison of the cleaning efficiency of different surfacted monotype nanofluids .....	138
Figure 5-35 Comparison of the cleaning efficiency different pure (series 4) and surfacted (series 5) hybrid nanofluids.....	139
Figure 5-36 Comparison of cleaning efficiency with surface tension of pure monotype nanofluids.....	139
Figure 5-37 Comparison of cleaning efficiency and surface tension of surfacted monotype nanofluids.....	140
Figure 5-38 Comparison of cleaning efficiency and surface area of pure hybrid nanofluids	141
Figure 5-39 Comparison of cleaning efficiency and surface tension of surfacted hybrid nanofluids.....	141
Figure 5-40 Cleaning efficiency (%) of different concentrations of Al <sub>2</sub> O <sub>3</sub> monotype deionised water nanofluid (%), Table 5-4.....	142

Figure 5-41 Cleaning efficiency of different concentrations of TiO <sub>2</sub> water nanofluid (%)..	142
Figure 5-42 Cleaning efficiency of different concentrations of ZnO water nanofluid (%), Table 5-4 .....	143
Figure 5-43 Comparison of cleaning efficiency values for different monotype -water nanofluids .....	143
Figure 5-44 Wavelength of the different pure monotype nanofluids .....	146
Figure 5-45 Wavelength of different surfacted monotype nanofluids .....	147
Figure 5-46 Wavelength of the various surfacted monotype nanofluids Series6 - 1.0%ZnO = 860nm .....	147
Figure 5-47 Comparison of wave length of pure (series 3) and surfacted (series 6) hybrid nanofluids.....	148
Figure 5-48 Effect of pH on the absorbency of different surfacted monotype nanofluids. ...	148
Figure 5-49 Effect of pH on the zetapotential and absorbency for surfacted monotype nanofluids.....	149
Figure 5-50 Effect of pH on the zetapotential and absorbency of the surfacted hybrid nanofluids.....	150
Figure 5-51 Effect of pH on absorbency of surfacted hybrid nanofluids.Series3 - pH and ..	150
Figure 5-52 Effect of mass fraction of SDBS surfactant on absorbency of the surfacted monotype nanofluids.....	151
Figure 5-53 Absorbancy of surfacted ZnO with different mass fraction of Na <sub>2</sub> HPO <sub>4</sub> .....	152
Figure 5-54 Absorbancy of the different surfacted monotype nanofluids.....	153
Figure 5-55 Absorbancy of the surfacted hybrid nanofluids .....	153
Figure 5-56 Comparison of the total surface area of the different monotype nanofluids .....	154
Figure 5-57 Comparison of the total surface area of the different hybrid nanofluids .....	155
Figure 5-58 Total surface area of the hybrid nanofluids. (Series3 – surfacted hybrids & series5 – Pure hybrids .....	156
Figure 6-1 Measured oil-wet of the various pure monotype nanofluids during the cleanup process.....	158
Figure 6-2 Measured water-wet of the various pure hybrid nanofluids during the cleanup process.....	159
Figure 6-3 Measured oil-wet of the various surfacted monotype nanofluids during the cleanup process.....	160
Figure 6-4 Measured oil-wet of the various surfacted hybrid nanofluids during the cleanup process.....	160

Figure 6-5 Comparison of lwo from pure and surfacted monotype nanofluids.....	161
Figure 6-6 Comparison of lwo from pure and surfacted hybrid nanofluids .....	162
Figure 6-7 Measured contact angles of the different monotype nanofluids .....	162
Figure 6-8 Measured contact angles $\theta$ of the different hybrid nanofluids.....	163
Figure 6-9 Measured wettability with contact angles of the best surfacted hybrid nanofluid .....	164
Figure 6-10 Effect of wettability on relative permeability of surfacted nanofluids based on Brook – Corey.....	168
Figure 6-11 Effect of wettability on relative permeability curves for surfacted nanofluids (oil – wet formation) based on modified Brook-Corey method [170]. .....	169
Figure 6-12 Effect of wettability on relative permeability of pure nanofluids based on Brook – Corey equation .....	170
Figure 6-13Effect of wettability on relative permeability of pure nanofluids (Strongly w ater – wet soil) based on modified Brook – Corey (Caig’s rules of thumb, Table 6.2b, [170]. .....	170

Figure A- 1 Particle size distribution of pure (without surfactant) 0.3 vol% $\text{Al}_2\text{O}_3$ water nanofluid .....	199
Figure A- 2 Particle Size Distribution of 0.3wt% $\text{Al}_2\text{O}_3$ + 0.03wt% SDBS- deionised water nanofluid .....	200
Figure A- 3 Particle size distribution of pure 0.7 vol% $\text{Al}_2\text{O}_3$ water nanofluid .....	201
Figure A- 4 Particle Size Distribution of 0.7wt% $\text{Al}_2\text{O}_3$ + 0.07wt%SDBS –deionised water nanofluid .....	201
Figure A- 5 Particle size distribution of 1vol% $\text{Al}_2\text{O}_3$ water nanofluid without surfactant ..	202
Figure A- 6 Particle Size Distribution of 1wt% $\text{Al}_2\text{O}_3$ + 0.1wt%SDBS –deionised water nanofluid. ....	202
Figure A- 7 Particle size distribution of 0.3vol% $\text{TiO}_2$ water nanofluid without surfactant.	203
Figure A- 8 Particle Size Distribution of 0.3wt% $\text{TiO}_2$ + 0.03wt%SDBS – deionised water nanofluid. ....	203
Figure A- 9 Particle size distribution of pure 0.7vol% $\text{TiO}_2$ water nanofluid .....	204
Figure A- 10 Particle Size Distribution of 0.7wt% $\text{TiO}_2$ + 0.07wt%SDBS – deionised water nanofluid. ....	204
Figure A- 11 Particle size distribution of pure 1.0 vol% $\text{TiO}_2$ water nanofluid .....	205
Figure A- 12 Particle Size Distribution of 1wt% $\text{TiO}_2$ + 0.1wt%SDBS – deionised water nanofluid. ....	205
Figure A- 13 Particle Size Distribution of pure 0.3wt% $\text{ZnO}$ -water nanofluid.....	206
Figure A- 14 Particle Size Distribution of 0.3wt% $\text{ZnO}$ + 0.15wt% $\text{Na}_2\text{HPO}_4$ – deionised water nanofluid. ....	207
Figure A- 15 Particle Size Distribution of 0.7wt% pure $\text{ZnO}$ water nanofluid. ....	207
Figure A- 16 Particle Size Distribution of 0.7wt% surfacted $\text{ZnO}$ + 0.35wt% $\text{Na}_2\text{HPO}_4$ – deionised water nanofluid. ....	208
Figure A- 17 Particle Size Distribution of 1wt% pure $\text{ZnO}$ -water nanofluid.....	208
Figure A- 18 Particle Size Distribution of 1wt% $\text{ZnO}$ + 0.5wt% $\text{Na}_2\text{HPO}_4$ –deionised water nanofluid. ....	209
Figure A- 19 Particle size distribution of pure 0.3wt% $\text{Al}_2\text{O}_3$ + 0.7wt% $\text{TiO}_2$ - deionised water nanofluid .....	209
Figure A- 20 Particle size distribution of 0.3wt% $\text{Al}_2\text{O}_3$ + 0.7wt% $\text{TiO}_2$ + 0.1wt% SDBS - deionised water nanofluid .....	210
Figure A- 21 Particle size distribution of 0.7 pure $\text{Al}_2\text{O}_3$ + 0.3 $\text{TiO}_2$ deionised water nanofluid .....	210

Figure A- 22 Particle size distribution of 0.3wt%TiO <sub>2</sub> + 0.7wt%Al <sub>2</sub> O <sub>3</sub> + 0.03wt%SDBS + 0.07wt%SDBS – deionised water nanofluid.....	211
Figure A- 23 Particle size distribution of pure 0.3Al <sub>2</sub> O <sub>3</sub> + 0.7ZnO vol% deionised water nanofluid .....	212
Figure A- 24 Particle size distribution of 0.7wt%ZnO + 0.3wt% Al <sub>2</sub> O <sub>3</sub> + 0.35wt%Na <sub>2</sub> HPO <sub>4</sub> + 0.03wt%SDBS .....	212
Figure A- 25 Particle size distribution of pure 0.3ZnO + 0.7Al <sub>2</sub> O <sub>3</sub> vol% deionised water nanofluid .....	213
Figure A- 26 Particle size distribution of 0.3wt% ZnO + 0.7wt% Al <sub>2</sub> O <sub>3</sub> + 0.15wt% Na <sub>2</sub> HPO <sub>4</sub> + 0.07wt% SDBS – deionised water. ....	213
Figure A- 27 Particle size distribution of pure 0.3TiO <sub>2</sub> + 0.7 ZnO vol% deionised water nanofluid. ....	214
Figure A- 28 Particle size distribution of 0.7ZnO + 0.3TiO <sub>2</sub> + 0.35wt%Na <sub>2</sub> HPO <sub>4</sub> + 0.03wt%SDBS – deionised water .....	214
Figure A- 29 Particle size distribution of 0.3ZnO + 0.7TiO <sub>2</sub> vol% –water nanofluid .....	215
Figure A- 30 Particle size distribution of 0.3wt%ZnO + 0.7wt%TiO <sub>2</sub> + 0.15wt%Na <sub>2</sub> HPO <sub>4</sub> + 0.07wt%SDBS -deionised water nanofluid .....	215
Figure A- 31 Particle size distribution of pure 0.3Al <sub>2</sub> O <sub>3</sub> + 0.3TiO <sub>2</sub> + 0.3ZnO vol% deionised water nanofluid. ....	216
Figure A- 32 Particle size distribution of surfacted 0.3Al <sub>2</sub> O <sub>3</sub> + 0.3TiO <sub>2</sub> + 0.3ZnO vol% deionised water nanofluid.....	216
Figure A- 33 10g Soil contaminated with 5g Oil HV1 and cleaned in Tga without nanofluid [57].....	243
Figure A- 34 Tga heat flow of 21.33mgoil contaminated soil sample analysis cleaned without nanofluid. ....	243
Figure A- 35 Weight loss and heatflow of 0.3 Al <sub>2</sub> O <sub>3</sub> /water –nanofluid.....	244
Figure A- 36 10g Soil contaminated with 5g Oil HV1 and cleaned with pure 0.3vol%Al <sub>2</sub> O <sub>3</sub> . ....	244
Figure A- 37 Mass loss per min and heatflow per min of surfacted 0.3wt%Al <sub>2</sub> O <sub>3</sub> /water.....	244
Figure A- 38 Heatflow for surfacted 0.3Al <sub>2</sub> O <sub>3</sub> /water .....	245
Figure A- 39 Heatflow for surfacted 0.3Al <sub>2</sub> O <sub>3</sub> /water .....	245
Figure A- 40 Weight loss per second of the contaminated soil cleaned with pure0.7Al <sub>2</sub> O <sub>3</sub> /water .....	246



Figure A- 41 Heatflow for pure 0.7Al <sub>2</sub> O <sub>3</sub> /water.....	247
Figure A- 42 Heatflow for 0.7Al <sub>2</sub> O <sub>3</sub> /water.....	247
Figure A- 43 Mass loss per min and heatflow per min of surfacted 0.7Al <sub>2</sub> O <sub>3</sub> /Water .....	248
Figure A- 44 Heatflow for surfacted 0.7Al <sub>2</sub> O <sub>3</sub> /water .....	248
Figure A- 45 Heatflow for surfacted 0.7Al <sub>2</sub> O <sub>3</sub> /water .....	248
Figure A- 46 Heatflow for surfacted 0.7Al <sub>2</sub> O <sub>3</sub> /water .....	249
Figure A- 47 Mass loss per min and heatflow per min of pure 1.0wt% Al <sub>2</sub> O <sub>3</sub> /water .....	250
Figure A- 48 Heatflow for pure 1.0Al <sub>2</sub> O <sub>3</sub> /water.....	250
Figure A- 49 Heatflow for pure 1.0Al <sub>2</sub> O <sub>3</sub> /water.....	251
Figure A- 50 Mass loss per min and heatflow per min of surfacted 1.0Al <sub>2</sub> O <sub>3</sub> /water .....	251
Figure A- 51 Heatflow for surfacted1.0Al <sub>2</sub> O <sub>3</sub> /water. ....	252
Figure A- 52 Heatflow for surfacted 1.0Al <sub>2</sub> O <sub>3</sub> /water. ....	252
Figure A- 53 Weight loss and heatflow of pure 1.0 TiO <sub>2</sub> -Water.....	253
Figure A- 54 0.3vol% TiO <sub>2</sub> at controlled temperature in Thermal Analyzer. ....	254
Figure A- 55 Mass loss per min and heatflow per min of Surfacted 0.3TiO <sub>2</sub> /water .....	254
Figure A- 56 Heatflow for surfacted 0.3TiO <sub>2</sub> /water.....	254
Figure A- 57 Heatflow for surfacted 0.3TiO <sub>2</sub> /water.....	255
Figure A- 58 Mass loss per min and heatflow per min of pure 0.7TiO <sub>2</sub> /water.....	256
Figure A- 59 Weight loss per second of the contaminated soil cleaned with pure 0.7TiO <sub>2</sub> /water .....	256
Figure A- 60 Comparison of weight loss with temperature for heatflow of 0.7TiO <sub>2</sub> /water..	257
Figure A- 61 Mass loss per min and heatflow per min of surfacted 0.7TiO <sub>2</sub> .....	257
Figure A- 62 Heatflow for surfacted 0.7TiO <sub>2</sub> /water.....	258
Figure A- 63 Heatflow for surfacted 0.7TiO <sub>2</sub> /water.....	258
Figure A- 64 Mass loss per min and heatflow per min of pure 1.0TiO <sub>2</sub> /water.....	259
Figure A- 65 Weight loss per second of the contaminated soil cleaned with pure 1.0TiO <sub>2</sub> /water. ....	259
Figure A- 66 Heatflow for pure 1.0TiO <sub>2</sub> .nanofluid .....	260
Figure A- 67 Heatflow for pure 1.0TiO <sub>2</sub> /water. ....	260
Figure A- 68 Heatflow for surfacted1.0 TiO <sub>2</sub> /water.....	261
Figure A- 69 Heatflow for surfacted 1.0 TiO <sub>2</sub> /water.....	261
Figure A- 70 Weight loss per second of contaminated soil cleaned with pure0.3wt% ZnO/water .....	262

Figure A- 71 Weight loss per second of the contaminated soil cleaned with surfacted 0.3ZnO/water. ....	262
Figure A- 72 10g Soil contaminated with 5g oil HV1 and cleaned with 15g pure 0.7ZnO deionised water nanofluid .....	263
Figure A- 73 Heatflow for pure 0.7ZnO/water. ....	263
Figure A- 74 Heatflow for contaminated soil cleaned with pure 0.7ZnO/water nanofluid. ...	264
Figure A- 75 Heatflow for contaminated soil cleaned with pure 1.0ZnO/water. ....	264
Figure A- 76 Heatflow for contaminated soil cleaned with surfacted 1g ZnO nanofluid .....	265
Figure A- 77 Further result on heatflow for soil cleaned with surfacted 1.0%ZnO/water. ...	265
Figure A- 78 Heatflow for contained soil cleaned with surfacted 1.0ZnO/water per second. ....	266
Figure A- 79 Mass loss per min and heat flow of pure 0.3Al <sub>2</sub> O <sub>3</sub> + 0.7TiO <sub>2</sub> /water .....	267
Figure A- 80 Weight loss per second of surfacted 0.3Al <sub>2</sub> O <sub>3</sub> + 0.7TiO <sub>2</sub> /water .....	267
Figure A- 81 Comparison of temperature with weight loss of soil sample cleaned .....	267
Figure A- 82 Heatflow for sample cleaned with surfacted 0.3Al <sub>2</sub> O <sub>3</sub> + 0.7TiO <sub>2</sub> /water. ....	268
Figure A- 83 Heatflow for 0.3Al <sub>2</sub> O <sub>3</sub> + 0.7TiO <sub>2</sub> /water per second.....	269
Figure A- 84 Further result on Heatflow for sample cleaned with pure 0.3Al <sub>2</sub> O <sub>3</sub> + 0.7TiO <sub>2</sub> /water.....	269
Figure A- 85 Weight loss of soil cleaned with pure 0.7Al <sub>2</sub> O <sub>3</sub> + 0.3TiO <sub>2</sub> /water .....	270
Figure A- 86 Weight loss per second of heatflow for pure 0.7Al <sub>2</sub> O <sub>3</sub> + 0.3TiO <sub>2</sub> .....	270
Figure A- 87 Weight loss per second for soil sample cleaned with 0.7Al <sub>2</sub> O <sub>3</sub> + 0.3TiO <sub>2</sub> /water .....	271
Figure A- 88 Comparison of weight loss with temperature for heatflow of 0.7Al <sub>2</sub> O <sub>3</sub> + 0.3TiO <sub>2</sub> /water.....	271
Figure A- 89 Comparison of weight loss with temperature for sample cleaned surfacted 0.7Al <sub>2</sub> O <sub>3</sub> + 0.3TiO <sub>2</sub> /water.....	272
Figure A- 90 Mass loss per second of contaminated soil cleaned with pure 0.3ZnO + 0.7Al <sub>2</sub> O <sub>3</sub> /water.....	272
Figure A- 91 Weight loss per second of soil cleaned with pure 0.3ZnO + 0.7Al <sub>2</sub> O <sub>3</sub> /water..	273
Figure A- 92 Comparison of weight loss with temperature rise for soil sample cleaned surfacted 0.3ZnO + 0.7Al <sub>2</sub> O <sub>3</sub> /water. ....	273
Figure A- 93 Mass loss per min and heat flow of soil cleaned with pure 0.7ZnO + 0.3Al <sub>2</sub> O <sub>3</sub> /water .....	274

Figure A- 94 Weight loss per second for pure 0.7ZnO + 0.3Al <sub>2</sub> O <sub>3</sub> /water.....	274
Figure A- 95 Heatflow for pure 0.7ZnO + 0.3Al <sub>2</sub> O <sub>3</sub> /water. ....	275
Figure A- 96 Weight loss per second of surfacted 0.3Al <sub>2</sub> O <sub>3</sub> + 0.7ZnO/water.....	275
Figure A- 97 Comparison of weight loss with temperature for soil cleaned with surfacted 0.3Al <sub>2</sub> O <sub>3</sub> + 0.7ZnO/water. ....	276
Figure A- 98 Mass loss per min and heat flow of soil cleaned with pure 0.3TiO <sub>2</sub> + 7ZnO/water .....	276
Figure A- 99 Weight loss per second for soil cleaned with pure 0.3ZnO+0.7TiO <sub>2</sub> /water ....	277
Figure A- 100 Comparison of weight loss with temperature for heatflow of 0.3ZnO + 0.7TiO <sub>2</sub> /water.....	277
Figure A- 101 Weight loss of soil sample cleaned with pure 0.3ZnO+0.7TiO <sub>2</sub> /water.....	278
Figure A- 102 Comparison of weight loss with temperature for heatflow of pure 0.3ZnO + 0.7TiO <sub>2</sub> /water.....	278
Figure A- 103 Weight loss per second for soil cleaned with pure 0.3TiO <sub>2</sub> + 0.7ZnO/water	279
Figure A- 104 Comparison of weight loss with temperature for soil sample cleaned with surfacted 0.3TiO <sub>2</sub> + 0.7ZnO/water.....	279
Figure A- 105 Comparison of weight loss of contaminated soil cleaned with surfacted 0.3TiO <sub>2</sub> + 0.7ZnO/water .....	280
Figure A- 106 Comparison of weight loss of contaminated soil cleaned with surfacted 0.3ZnO + 0.7TiO <sub>2</sub> /water. ....	280
Figure A- 107 Comparison of weight loss with time for soil sample cleaned with surfacted 0.3ZnO + 0.7TiO <sub>2</sub> /water .....	281
Figure A- 108 Mass loss per min of soil cleaned with pure0.3Al <sub>2</sub> O <sub>3</sub> + 0.3ZnO + 0.3TiO <sub>2</sub> /water .....	281
Figure A- 109 Heatflow for soil cleaned with pure 0.3Al <sub>2</sub> O <sub>3</sub> + 0.3TiO <sub>2</sub> + 0.3ZnO .....	282
Figure A- 110 Weight loss per second of surfacted 0.3Al <sub>2</sub> O <sub>3</sub> + 0.3TiO <sub>2</sub> + 0.3ZnO/water ...	282
Figure A- 111 Comparison of temperature with weight loss of surfacted 0.3Al <sub>2</sub> O <sub>3</sub> + 0.3TiO <sub>2</sub> + 0.3ZnO/water. ....	283
Figure A- 112 Comparison of weight loss with temperature for soil sample cleaned with surfacted 0.3Al <sub>2</sub> O <sub>3</sub> +0.3TiO <sub>2</sub> + 0.3ZnO/water.....	283
Figure A- 113 10g Soil contaminated with 4.4g Oil HV1 and cleaned with 10g 0.3vol% Al <sub>2</sub> O <sub>3</sub> .....	284
Figure A- 114 Tga heatflow curve of 27.89mg oil-0.3vol% Al <sub>2</sub> O <sub>3</sub> nanofluid soil after cleanup .....	285

Figure A- 115 Tga heatflow curve of 27.78mg oil-0.3vol% TiO <sub>2</sub> nanofluid soil after cleanup	285
Figure A- 116 Heat flow curve of 26.01mg oil-0.7vol% ZnO nanofluid soil after cleanup [41a].	285
Figure A- 117 Heat flow curve of 28.24mg oil-0.3vol% ZnO nanofluid soil after cleanup.	286
Figure A- 118 Tga heat flow of 21.33 mg oil contaminated soil sample analysis	286
Figure A- 119 Heat flow of 37.13mg oil contaminated soil sample after cleanup	286
Figure A- 120 Experimental results of Thermal Capacity of the different monotype nanofluids	287
Figure A- 121 The DSC machine and Crucible sealing press (Mettler Toledo)	287
Figure A- 122 Mettler Toledo Tga helical test Coil Heat Exchanger	288
Figure A- 123 Specific heat capacity of the various monotype nanofluids	291
Figure A- 124 Specific heat capacity of the different hybrid nanofluids[57].	292
Figure A- 125 Thermal capacity of the different monotype nanofluids[57].	293
Figure A- 126 Comparison of thermal capacity of different hybrid nanofluids[57]	293
Figure A- 127 Heat transfer rate of monotype nanofluids.	293
Figure A- 128 Heat transfer rate of the various hybrid nanofluids.	294
Figure A- 129 Photographic view of KD2 Pro thermal property analyzer	294
Figure A- 130 Thermal Conductivity of different pure monotype nanofluids.	295
Figure A- 131 Comparison of thermal conductivity of surfacted monotype nanofluids	296
Figure A- 132 Comparison of the thermal conductivity of the different hybrid nanofluids	297
Figure A- 133 Effect of volume fraction on thermal conductivity of surfacted monotype nanofluids.	297
Figure A- 134 Effect of volume fraction on thermal conductivity of surfacted hybrid nanofluids	298

Table 2-1 Wettability index (WI) and contact angle for different wetting conditions .....	22
Table 2-2 Relationship between wettability, contact angle USBM and Amott – Harvey wettability indices [10b] .....	22
Table 2-3 2005Composition and Percentage of the Trecate crude oil (AGIP, 1995) Enrollment in local colleges,.....	29
Table 2-4.Composition of hydrocarbon elements by weight.....	34
Table 2-5 Porosity and contact angle values.....	52
Table 2-6Summary of the major remediation methods .....	71
Table 3-1 List of Materials .....	74
Table 3-2List of Equipment .....	74
Table 3-3 Samples ZnO/TiO <sub>2</sub> /Al <sub>2</sub> O <sub>3</sub> formulation & preparation using fractorial designs 23 .	79
Table3-4 Formulation 2. Using 3, 3 Simplex Lattice Design .....	81
Table 3-5 (2,2) Simplex Lattice Design for formulation of mixture of two surfactants.....	82
Table 3-6 Process Variables design using 3, 3 Simplex Lattice Design for optimum cleanin	82
Table 3-7 (3,3) Simplex Lattice Design for formulation of time,( max 60 mins) for optimum .....	83
Table 3-8 (3,2) Simplex Lattice Design for formulation of mixture of soil with two oil grades. ....	83
Table 3-9 Measured surface tension data for the different nanofluids .....	90
Table 4-1 <b>Summary of Experimental set-up</b> using 2 x 3 factorial designs (2 <sup>3</sup> ) for simulation and cleaning of crude oil contaminated soils. ....	100
Table 4-2 Critical phase saturation & relative permeability data based on [26, 27] .....	105
Table 4-3 Summary of the different parameters used for the calculations. ....	106
Table 5-1Physical and chemical properties of the experimental mineral oil.....	108
Table 5-2 Physical and Chemical properties of the experimental mineral oil (IARC 1984).108	
Table 5-3 Property table for organic compounds used in the experiments [22].....	109
Table 5-4 Property table for water (which is an inorganic compound) [22] .....	109
Table 5-5 Characterization of different pure nanofluids and their combinations/hybrids at 25°C [57].....	117
Table 5-6 Characterization of different surfacted nanofluids and their combinations/hybrids at 25°C [41a, 123] .....	118
Table 5-7 Viscosities of Poly Cambol oil, HV1 60 oil & white liquid mineral oil .....	130
Table 5-8 Comparison of the cleaning efficiency of the different pure and surfacted nanofluids .....	144

Table 5-9 Total surface area (nm <sup>2</sup> ) of the different nanofluids calculated with equation (C1.1) in Appendix C.....	144
Table 5-10 Total surface area (nm <sup>2</sup> ) with the cleaning efficiency (%)......	145
Table 5-11 Comparison of the cleaning efficiency of the different nanofluids.....	153
Table 6-1 Mean physical properties of the soils .....	156
Table 6-2 Distribution of pore sizes, porosity (%) for the treatments as a function of soil depth.Means ± standard error of the mean).Pore size (µm) (>50 µm) .....	157
Table 6-3 Hydraulic conductivity (permeability) results.....	157
Table 6-4 Calculation of wettability index & contact angleθ for pure nanofluids .....	164
Table 6-5 Calculation of wettability index & contact angleθ for surfacted nanofluids.....	166
Table 6-6 Relative permeability of the best surfacted nanofluid (Recalculated values from the former graph (Fig6-11) for surfacted nanofluids).....	169
Table 6-7 Helical Test Coil Heat Exchanger Specifications .....	288
Table 0-1 Statistical analysis of the experimental results.....	298
Table 0-2 Comparison of pure TiO <sub>2</sub> /water with surfacted TiO <sub>2</sub> /water.....	299
Table 0-3 Comparison of pure TiO <sub>2</sub> /water with process variables .....	300
Table 0-4 Comparison of effects of temperature and time on weight loss .....	300
Table 0-5 Comparison of weight loss with temp and time for the contaminated soil cleaned with pure TiO <sub>2</sub> /water.....	301
Table 0-6 Statistical Analysis of time and temp on weight loss using T-Test (Paired Samples Test) .....	301
Table 0-7 Model Summary .....	302
Table 0-8 ANOVA for Surfacted TiO <sub>2</sub> nanofluids .....	303
Table 0-9 Oneway ANOVA for Time by temp(effect of temperature and time on weight loss) .....	303
Table 0-10Oneway ANOVA for weight loss by Temperature for surfacted TiO <sub>2</sub> .....	304
Table 0-11 Satistical analysis for surfacted TiO <sub>2</sub> .....	<b>Error! Bookmark not defined.</b>
Table 0-12 Model Summary .....	305
Table 0-13 ANOVA for Surfacted TiO <sub>2</sub> nanofluids .....	306
Table 0-15Oneway ANOVA for weight loss by Temperature for surfacted TiO <sub>2</sub> .....	308
Table 0-16 Satistical analysis for surfacted TiO <sub>2</sub> .....	308
Table 0-17 Pure 0.3Al <sub>2</sub> O <sub>3</sub> +0.3TiO <sub>2</sub> +0.3ZnO/water.....	310

Table 0-23 Comparison of surfacted best nanofluids - TiO <sub>2</sub> and 0.3Al <sub>2</sub> O <sub>3</sub> +0.3TiO <sub>2</sub> +0.3ZnO .....	313
Table 0-24 Descriptive Statistics .....	313
Table 0-25 Comparing the two means using <b>Paired Samples Correlations</b> .....	314
Table 0-26 Model Coefficients <sup>a</sup> for the best nanofluid.....	<b>Error! Bookmark not defined.</b>
Table 0-27 Paired Samples Statistics .....	316
Table 0-28 Final Comparison of the best nanofluids with process variables .....	317
Table 0-29 Summary of statistical parameters of wettability and cleaning efficiency .....	318
Table 0-30 Descriptive Statistics .....	318
Table 0-31 Summary of the Table 6.11 for better understanding of the effects of wettability on the cleaning efficiency with process variables of the different nanofluids.....	320
Table 0-32 The values of % oil removed in the contaminated soils.....	322

Table A- 1 Properties of Alumina Nanopowder. ....	197
Table A- 2 Properties of Titanium Oxide Nanopowder.....	197
Table A- 3 Properties of Zinc Oxide Nanopowder, ZnO.....	197
Table A- 4 Properties of Disodium Phosphate Na <sub>2</sub> HPO <sub>4</sub> (inorganic compound).....	197
Table A- 5 Properties of Sodium dodecyl Sulphate (Organic compound) .....	198
Table A- 6 Property table for water (which is an inorganic compound) [19].....	198
Table A- 7 Property table for organic compounds used in the experiments [19] .....	198
Table A- 8 Porosity (%) measurement.....	217
Table A- 9 Result of bulk density (g/m <sup>3</sup> ) measurements .....	217
Table A- 10 Hydraulic conductivity (permeability) results .....	217
Table A- 11 The density of mineral oil, nanofluids and distilled water was measured with a picnometer of 25ml at room temperature of 25°C. ....	218
Table A- 12 Viscosity of different nanofluids without surfactants.....	218
Table A- 13 Viscosity of different hybrid - water nanofluids without surfactants .....	218
Table A- 14 Viscosity of different monotype nanofluids with surfactants.....	219
Table A- 15 Viscosity of different hybrid nanofluids with surfactants .....	219
Table A- 16 Viscosity of pure hybrid nanofluids .....	220
Table A- 17 Measured density of experimental mineral oil Hv160 .....	220
Table A- 18 Measured density of different monotype nanofluids.....	220
Table A- 19 Measured density of different hybrid nanofluids .....	221
Table A- 20 Total surface area of the different nanofluids calculated using equation (C1.1) .....	221
Table A- 21 Total surface area of the different nanofluids calculated using equation (C1.2) .....	222
Table A- 22 Total surface area of the different nanofluids calculated using equation (C.1.3)[106].....	223
Table A- 23 Surface tension results .....	224
Table A- 24 Surface tension of the different nanofluids.....	224
Table A- 25 Thermal Conductivity enhancement (%).....	225
Table A- 26 Thermal conductivity (W/m-k) of the various hybrid nanofluids.....	226
Table A- 27 Thermal conductivity of the various Monotype nanofluids .....	226
Table A- 28 Specific heat capacity and thermal capacity of the various nanofluids .....	227
Table A- 29 Specific heat capacity of the different nanofluids concentration (%) .....	227



Table A- 30 Summary of thermal capacity of the different pure hybrid nanofluids .....	227
Table A- 31 Thermal capacity of pure monotype nanofluids .....	228
Table A- 32 Thermal capacity of pure monotype nanofluids .....	228
Table A- 33 Pure nanofluids thermal optical results .....	228
Table A- 34 Results of thermaloptical measurement for surfacted monotype nanofluids. ...	228
Table A- 35 Thermal optical of the different nanofluids .....	229
Table A- 36 Wettability index of pure nanofluids.....	230
Table A- 37 Wettability index of Surfacted nanofluids.....	232
Table A- 38 Comparison of lwo from pure and surfacted nanofluids .....	233
Table A- 39 Comparison of pure and surfacted nanofluids .....	234
Table A- 40 Measured contact angles of the different nanofluids.....	234
Table A- 41 Comparison of wettability with contact angle. ....	235
Table A- 42 Wettability parameters for pure nanofluids .....	235
Table A- 43 Wettability parameters for surfacted nanofluids .....	236
Table A- 44 Effect of pH on the zetapotential and absorbency of the different surfacted nanofluids.....	236
Table A- 45 Soil contamination & cleanup process with pure and surfacted nanofluids.....	237
Table A- 46 Statistical analysis of the experimental results .....	298
Table A- 47 Comparison of pure TiO <sub>2</sub> /water with surfacted TiO <sub>2</sub> /water .....	299
Table A- 48 Comparison of pure TiO <sub>2</sub> /water with process variables .....	300
Table A- 49 Comparison of effects of temperature and time on weight loss .....	300
Table A- 50 Comparison of weight loss with temp and time for the contaminated soil cleaned with pure TiO <sub>2</sub> /water.....	301
Table A- 51 Statistical Analysis of time and temp on weight loss using T-Test (Paired Samples Test) .....	301
Table A- 52 Model Summary .....	302
Table A- 53 ANOVA for Surfacted TiO <sub>2</sub> nanofluids .....	303
Table A- 54 Oneway ANOVA for Time by temp(effect of temperature and time on weight loss) .....	303
Table A- 55 Oneway ANOVA for weight loss by Temperature for surfacted TiO <sub>2</sub> .....	304
Table A- 56 Paired Samples Test.....	305
Table A- 57 Model Summary .....	305
Table A- 58 ANOVA for Surfacted TiO <sub>2</sub> nanofluids .....	306

Table A- 59 Oneway ANOVA for Time by temp(effect of temperature and time on weight loss)	307
Table A- 60 Oneway ANOVA for weight loss by Temperature for surfacted TiO <sub>2</sub>	308
Table A- 61 Statistical analysis for surfacted TiO <sub>2</sub>	308
Table A- 62 Pure 0.3Al <sub>2</sub> O <sub>3</sub> +0.3TiO <sub>2</sub> +0.3ZnO/water	310
Table A- 63 Paired Samples Test	311
Table A- 64 Correlations process variables and weight loss.	311
Table A- 65 Model Summary And Regression of time on weight loss (ANOVAa)	312
Table A- 66 Effect of process variables on Surfacted 0.3Al <sub>2</sub> O <sub>3</sub> +0.3TiO <sub>2</sub> +0.3ZnO/water	312
Table A- 67 Comparison of surfacted best nanofluids - TiO <sub>2</sub> and 0.3Al <sub>2</sub> O <sub>3</sub> +0.3TiO <sub>2</sub> +0.3ZnO	313
Table A- 68 Descriptive Statistics for surfacted best nanofluids - TiO <sub>2</sub> and 0.3Al <sub>2</sub> O <sub>3</sub> +0.3TiO <sub>2</sub> +0.3ZnO	313
Table A- 69 T-Test for surfacted best nanofluids - TiO <sub>2</sub> and 0.3Al <sub>2</sub> O <sub>3</sub> +0.3TiO <sub>2</sub> +0.3ZnO	313
Table A- 70 Comparing the two means using <b>Paired Samples Correlations</b> .	314
Table A- 71 Correlation of surfacted TiO <sub>2</sub> and surfacted 0.3Al <sub>2</sub> O <sub>3</sub> + 0.3TiO <sub>2</sub> +0.3ZnO/water.	314
Table A- 72 Model Coefficients <sup>a</sup> for the best nanofluid	316
Table A- 73 Paired Samples Statistics for surfacted TiO <sub>2</sub> and surfacted 0.3Al <sub>2</sub> O <sub>3</sub> +0.3TiO <sub>2</sub> +0.3ZnO with process variables	316
Table A- 74 Final Comparison of the best nanofluids with process variables	317
Table A- 75 Summary of statistical parameters of wettability and cleaning efficiency	318
Table A- 76 Comparison of wettability, cleaning efficiency with process variables	319
Table A- 77 Summary of the Table A-76 for better understanding of the effects of wettability on the cleaning efficiency with process variables of the different nanofluids	320
Table A- 78 The values of % oil removed in the contaminated soils.	322

## List of Abbreviations

A - Area  
D or d - Diameter  
k - Permeability  
krw - Relative permeability of water.  
kro - Relative permeability of oil,  
L - Length  
p - Pressure  
pc - Capillary pressure  
pnw - Pressure in non-wetting phase  
pw - Pressure in wetting phase  
q - Flow rate  
r - Radius  
ro - Displacement-by-water ratio  
rw - Displacement-by-oil ratio  
S<sub>o</sub> - Saturation of oil, water or gas  
Sor - Residual oil saturation  
Swc - Connate water saturation  
Swr - Irreducible water saturation  
SG - Specific gravity  
T - Temperature  
t - Time  
u - Flow velocity  
V - Volume  
V<sub>o</sub> - Volume of oil, water or gas  
V<sub>b</sub> - Bulk volume  
V<sub>g</sub> - Grain volume  
V<sub>p</sub> - Pore volume  
w - Weight  
Bd - bulk density  
ρ - Density  
∅ - porosity  
∞ - Refers to oil (o), water (w) or gas (g) phase  
Δp - Pressure difference  
γ - Specific gravity or shear rate  
λ - Mobility  
μ - Dynamic or absolute viscosity  
Θ - Contact angle  
∂ - Surface or interfacial tension  
API - American Petroleum Institute  
EOR - Enhanced oil recovery  
WI - Wettability index  
wt% - Weight percentage  
ρ<sub>np</sub> - Density of nanoparticles, (*kg/m<sup>3</sup>*)  
ρ<sub>nf</sub> - Density of nanofluids, (*kg/m<sup>3</sup>*)  
C<sub>pnf</sub> - Constant pressure specific heat of, (*kJ/kg.K*)  
C<sub>pnf</sub> - Constant pressure specific heat for nanoparticles, (*kJ/kg.K*)

## ABSTRACT

The research focused on the investigation into the cleaning behavior of nanofluids on crude oil contaminated soil at optimum conditions. This was done by contaminating 10g of soil with 5g stimulant – HV1 60 mineral oil and white mineral oil, in each case, 10 grams sandy soils was uniformly spilled with 5g each mineral oil. Subsequently, the simulated soil samples were cleaned using 15g of nanofluids prepared from 0.3 – 1wt% powdered ZnO, TiO<sub>2</sub>, and Al<sub>2</sub>O<sub>3</sub> nanoparticles each dispersed in deionised water and their cleaning behaviors were observed with and without surfactants. Differential Scanning Calorimetric Analysis was used to determine the total weight loss, heat transfer rate and mass flow after the clean-up process of the soil samples. The particle size distribution of the Al<sub>2</sub>O<sub>3</sub>, TiO<sub>2</sub> and ZnO -water nanofluids was done using dynamic light scattering technique. The pH stability study was carried out by adding 0.5g sodium hexametaphosphate and 0.1g sodium dodecylbenzenesulfonate, respectively, as surfactants, to ZnO Al<sub>2</sub>O<sub>3</sub> and TiO<sub>2</sub> water nanofluids as well as ultrasonicated for 24hours. Oil cleaning efficiency of pure Al<sub>2</sub>O<sub>3</sub> nanofluid was 74%. TiO<sub>2</sub> nanofluid was 84% and ZnO nanofluid was 78% at optimum level of 1g. The cleaning efficiency of the nanofluids increased to 84%, 99.4% and 98%, respectively, when they were surfacted. The results obtained showed that the flow characteristics properties of the different nanofluids increased with decrease in particle size concentration. The contaminated soil samples and cleanup experiments were used to determine wettability, contact angle and relative permeabilities. The imaging method was executed to investigate how the surfacted nanofluids and mass fraction of surfactants influenced the contact angle and surface tension. In the contact angle and surface tension measurements a decline was observed for the measurements with surfacted nanofluids. However, the values of both measurements increased from 0.3 wt% to 1.0 wt% of nanofluids. The reason for this is attributed to the stability of the various nanofluids, and it contradicts the assumption of more water-wet conditions for higher nanoparticle concentrations. Besides this singular contradiction, the experimental results are in conformity with the expectations of my earlier proposal. These findings are comparable to the findings of other Researchers.

Keywords: Soil, Petroleum, soil contamination, remediation, Nano-fluids, stability, mass fraction, wettability and optimum conditions.

# 1 Chapter 1.0 Introduction

## 1.1 Background

Soil contamination is the presence of natural or man-made chemicals or other alterations in the soil natural environment. This type of contamination is typically caused by the rupture of underground petroleum pipes and storage tanks, application of pesticides, percolation of contaminated surface water to subsurface strata, leaching of wastes from landfills or direct discharge of industrial wastes to the soil.

Soil contamination results when hazardous substances are either spilled or buried directly in the soil or migrate to the soil from a spill that has occurred elsewhere Figure 1-1. Contaminated lands contain substances which when present in sufficient concentrations may cause harm, directly or indirectly to man, to the environment or other targets [119]. The main hazards associated with chemical contaminated land are uptake of contaminants by food crops grown in the contaminated soil, skin contact, photo toxicity, fire and explosions as well as chemical attack on building materials and building services [43].



Figure 1-1 Soil contaminated sites [100]

Polluted rivers render the water unsafe for drinking, fishing and recreation. Polluted land results in the killing of plants and fauna, adversely affecting their natural habitat, and putting an end

to local economic practices and livelihoods such as hunting, farming as well as a multiplicity of nutritional, health related and socio cultural practices.

There is a very large set of health consequences from exposure to soil contamination depending on pollutant type, pathway of attack and vulnerability of the exposed population. Lead originating from coal burning, gasoline burning, and ore smelting causes a high risk of developmental damage to the brain and nervous system in young children [79]. Mercury is an element known as quicksilver, or hydragyrum. It is a chemical element represented in the Periodic Table with the symbols: Hg. and atomic number of 80. Mercury is a heavy, silvery d-block metal and is one of the five metals that are liquid at or near room temperature and pressure. Mercury is used in barometers, thermometers, manometers, sphygmomanometers, float valves, and other scientific tools. Exposure to Mercury can lead to poisoning, kidney damage, liver toxicity and depression of the central nervous system. There are many other health effects such as headache, nausea, fatigue, eye irritation and skin rash [21a, 21b].

In Nigeria, statistics of some possible causes of oil spillage shows that one per cent (1%) of the spillage is due to engineering drills, twenty one per cent (21%) to oil production operation, twenty eight per cent (28%) to sabotage and fifty per cent (50%) to corrosion [95]. Inability to effectively control oil wells, failure of machines and inadequate care in loading and off-loading oil vessels are also some causes of the oil spillage [95]. The materials contained in oil spills are usually in the form of biodegradable (mainly hydrocarbons and sulphur compounds), non-biodegrade (mainly inorganic elements like Iron, Zinc, lead) and hazardous compounds).

There have been recently some reports by soil scientists on a new technique for mapping and testing of oil-contaminated soils which uses visible near infrared light with diffuse reflectance spectroscopy, shining a light on a sample and reading the reflecting wavelengths [115]. This allows researchers to rapidly evaluate soils for the presence and amount of oil contamination quickly while in the field, without taking a sample to a laboratory for analysis and waiting for the results of the test. The fact that this spectroscopic technology does not need prior sample preparation has made it applicable.

The over increasing demand for enough energy supply to meet up with the extensive global industrialization demand has grossly expanded the frontiers of petroleum hydrocarbon (PHC)

exploration. In the petroleum industry it is considered that most of the easy accessible oil reservoirs has been found and set on production and currently there is a decline in conventional petroleum production. To meet the future demand of petroleum the industry will either have to find new fields, increase the recovery factor of existing fields or start to produce more unconventional resources such as shale gas, shale oil, crude oil /heavy oil and bitumen. About 80% of the easy accessible conventional petroleum is located in the Middle East, most of it in Saudi Arabia [122]. Though, taking heavy oil and bitumen reserves into account, America may be the future giant of petroleum assets as most of the reserves are located in Venezuela and Canada.

The exploration and production of crude oil is highly dependent on the oil price as the recovery methods used for extraction of heavy oil are expensive. Consequently, the exploration activities amongst others often result in pollution of environment, thus creating serious imbalance in the biotic and abiotic regimes of the ecosystem hence there is an urgent need for investigating the methods of cleaning such polluted environment of which if not taken care of will definitely contaminate the air, water and soil. It has been observed that accidental and deliberate crude oil spills have been and still continue to be a significant source of environmental pollution [128b]). Apparently, the only available solution to such environmental problem is cleaning of such ecosystem.

Cleaning, otherwise known as remediation, is the means of returning the polluted environment to its natural form by cleaning-up and / or treatment using some materials which may be biologically, physically or chemically sourced [90]. Several cleaning techniques have been in use (or the restoration of petroleum polluted site). These include the naturally occurring bioremediation and phyto remediation which have been used for centuries. Take for example; desalination of agricultural land by phyto extraction has a long tradition. Fungal biodegradation, which refers to the degradation of a wide variety of organo pollutants utilizing fungi lignin – degrading wood rotting enzyme system. Petroleum cleaning products (PCP) consist of long spheres of treated wax and nutrients which when they come in contact with the spilled oil ‘bind’ with the hydrocarbons. Others include soil vapour extraction; recirculating well technology, air sparing and in-situ chemical oxidation (ISCO) methods [124].

Biological cleaning or remediation refers to any cleaning technique that uses biological means such as micro-organisms, green plant or their enzymes to return the polluted sites to its original

form or condition, that is utilizing micro-organisms to reduce to the barest minimum or completely remove the concentration and toxicity of various petroleum hydrocarbon pollutants (PHP). These PHP include polycyclic aromatic hydrocarbons, polychlorinated biphenyls, phthalate esters, nitro-aromatic compounds, petrochemical solvents and metals.

Chemical cleaning or remediation refers to the use of various minerals or chemicals to absorb, adsorb, bind, precipitate or co-precipitate trace elements and heavy metals in contaminated soils and water thereby reducing their bioavailability, toxicity and mobility. The application of the two processes simultaneously is referred to as biochemical remediation. The goal of biochemical remediation, therefore, is to degrade organic and inorganic pollutants to concentrations that are not detectable or if detectable, to concentrations that are permissible by regulatory agencies [96].

On the other hand, physical cleaning refers to the means of returning the contaminated environment to its original form by use of equipment and materials that do not involve either biological or chemical reactions. A typical example of such cleaning technique is the application of pulverized used water sachet polyethylene whose characteristic length is less than 100 nanometer (100 nm) in cleaning petroleum hydrocarbon polluted river or sea. Other examples include the application of particle production technologies in the production of large quantities of colloids typical of solid metal oxide particles suspended in liquids [96].

Colloids are systems that consist of small particles of one substance suspended in another whose characteristic lengths are less than 100 nm. In other words, nano fluids are colloids containing nanoparticles, particularly in the field of surface cleaning of polluted soils research. The significance of nanofluids is in the cleaning of polluted soils or in the area of heat transfer research which may be beneficial in future cooling including their thermal property, optical property and rheological properties as well as their high particle stability. The above stated properties make any investigation in the areas of surface cleaning cum heat transfer technology quite promising and interesting especially when consideration is given to their uses in removing solid and liquid contaminants from surfaces which could be beneficial to many industries. In that respect, a fundamental knowledge and understanding of how nano fluids behave with respect to a specified geometry becomes absolutely necessary. The increasing demand for hydrocarbons has led to a hope of developing more efficient recovery techniques



for unconventional resources such as heavy oil. Heavy oil is movable in the reservoir, but recovery is time-consuming and expensive.

Nanofluid is investigated as a possible enhanced oil recovery method. Nanofluid promises an alternation of wettability and a reduction of the interfacial tension as nanoparticles added to one of the fluid phases disturbs the initial equilibrium state. By bringing nanotechnology into the petroleum industry the hope is to develop recovery methods that are cheaper, more effective and have a better environmental sound. Nanofluids can be developed as a recovery method for both conventional and unconventional resources. The injection of nanoparticles as nanofluids are introduced as a possible future enhanced oil recovery method. Hydrophilic silica nanoparticles promise a decrease in the interfacial tension and a possibility of wettability alternation to strongly water-wet conditions. The motivation for investigating nanofluid for enhanced oil recovery application is development of nanofluid as a new enhanced oil recovery method. The hope is to develop an effective and less expensive recovery method for the future.

## 1.2 Causes of soil contamination

Soil contamination is the occurrence of pollutants in soil above a certain level causing a deterioration or loss of one or more soil functions. Also, Soil contamination can be considered as the presence of man-made chemicals or other alteration in the natural soil environment. This type of contamination typically arises from the rupture of underground storage tanks, application of pesticides, and percolation of contaminated surface water to subsurface strata, leaching of wastes from landfills or direct discharge of industrial wastes to the soil. The most common chemicals involved are petroleum hydrocarbons, solvents, pesticides, lead and other heavy metals. The occurrence of this phenomenon is correlated with the degree of industrialization and intensity of chemical usage in the region. Petroleum hydrocarbon pollution is one of the main environmental problems, not only by the important amounts released but also because of their toxicity.

The soluble compounds of diesel (benzene, toluene, ethyl benzene and xylenes which are known as BTEX) are toxic to aquatic life as well as animals and humans. According to [108b] hydrocarbons in the soil are considered toxic when they reach concentrations greater than 100 (MU)g/g. Where, (MU) g, Micro =  $1\mu\text{g}$  – one millionth of a gram.

The concern over soil contamination stems primarily from health risks, from direct contact with the contaminated soil, vapours from the contaminants, and from secondary contamination

of water supplies within and underlying soil. Mapping of contaminated soil sites and the resulting clean-up are time consuming and expensive tasks, requiring extensive amounts of geology, hydrology, chemistry, computer modelling skills and GIS as well as an appreciation of the history of industrial chemistry.

It is in North America and Western Europe that the extent of contaminated land is most well-known, with many of the countries in these areas having a legal framework to identify and deal with this environmental problem, this however may well be just the tip of the iceberg with developing countries very likely to be the next generation of new soil contamination cases [82].

The immense and sustained growth of the Peoples' Republic of China since the 1970s has exacted a price from the land in increased soil pollution. The State Environmental Protection Administration believes it to be a threat to the environment, to food safety and to sustainable agriculture. According to a scientific sampling, 150 million mi (100,000 square km) of China's cultivated land has been polluted with contaminated water being used to irrigate a further 32.3 million (21,670 square km) land and another 2 million (1,300 square km) land covered or destroyed by solid waste. In total, the area account for one-tenth of China's cultivatable land, and is mostly in economically developed areas. An estimated 12 million tonnes of grains are contaminated by heavy metals every year, causing direct losses of US\$2.57 billion.

#### Statement of problem

The cleaning behavior of nanofluids on crude oil contaminated soils and modelling is still in the early stages of development and therefore has not been investigated. Research is needed to advance nanotechnology and to determine the possibility of nanofluids applications for cleaning refineries and reclaiming agricultural farmlands after oil spillage. Research will help to understand the relationship of nanofluids and cleaning efficiency at various operational conditions. The research being conducted in this study uses three types of nanofluids (monotypes) and their combinations (hybrids) at different concentrations under three levels (low - 0.3g, medium - 0.7g and high - 1.0g) and at different optimum process variable conditions (temperature, pressure and time).

#### Significance of the problem

The mechanisms responsible for the cleaning behaviour of nanofluids are not yet fully understood. However, they may possess the mechanisms or ability which helps in the cleanup

process such as heat transfer, stability, flow/transport properties of nanofluids, wet and spreading, mass transfer and diffusion of nanofluids.

Definition

Nano –  $10^{-9}$

Nanoparticle – particle with a size between 1-100 nm

Nanofluid – nanoparticle mixed in a conventional fluid

Conventional Fluid – water, oil, High viscosity mineral oil

Heating Element – converts electricity into heat

Convection – heat transfer between a solid and conventional fluid

Steady State – temperatures remain constant with time

Laminar – dominated by diffusion and velocity profile is nearly linear

Turbulent – dominated by turbulent mixing

Reynolds Number – is a dimensionless number for definition of flow regime (laminar and turbulent flow).

Assumptions

It is important to assume that there was no heat loss during the cleaning from the heat exchanger through the helical coil tubing. Experiments were conducted using the same procedures and equipment and have the same factors monitored. Temperature and flow rates were measured at steady state which was indicated by the steady temperatures for a ten minute period [58].

#### 1.2.1.1 Limitations

The study will be limited to laboratory conditions. First of all, financial limitations were my prime concern. Budgetary constraint limits the items being used to conduct the experiment. The burettes that were used for the soil contamination and clean-up process affected oil removal due to the size of the burettes as well as a financial constraint. Due to cost consideration the nanofluids used was restricted to  $\text{Al}_2\text{O}_3$ ,  $\text{TiO}_2$  and  $\text{ZnO}$  with their combinations (hybrids). Testing was restricted to only three concentrations (3 levels – low, medium and high/optimum of nanofluid) to accommodate the time schedule. Use of water as conventional fluid to mix with the nanoparticles for cleanup experiments, however, to lessen our environmental impact and requirements for disposal, this research was conducted using deionised and distilled water. The Study is limited to evaluating heat transfer rates at predetermined flow rates and temperatures, specific heat capacity, thermal conductivity and to

measure viscosity, density, surface tension of the different water nanofluids as well as thermaloptical of the nanofluids. The study focused on the evaluation of stability of different water nanofluids using zetapotential, pH, thermaloptical – absorbancy, wavelength and particle size distribution as well as cleanup process using pure and surfacted nanofluids on 10g soil contaminated with 5g of HV1 60 mineral oil. The wettability, relative permeabilities of oil and water were determined using the endpoint/products from the cleanup process of the different nanofluids on crude oil contaminated soils.

### 1.3 Aims and Objective of the study

The main objective of this study was to investigate the cleaning behaviour of nanofluids namely ZnO, TiO<sub>2</sub> and Al<sub>2</sub>O<sub>3</sub> on crude oil contaminated soils at optimum conditions with and without surfactants.

The aim of the present study was to apply different water based nanofluids in cleaning simulated crude oil contaminated soil samples so as to determine their cleaning efficiency. The scope of the study included the following:

To investigate the cleaning behavior of nanofluids using (powdered ZnO, Al<sub>2</sub>O<sub>3</sub> and TiO<sub>2</sub> dispersed in deionised water) on the simulated crude oil contaminated samples using 3 x 3 simplex Lattice design (3<sup>2</sup>). Specifically, it aimed at studying the effect of:

i Behaviour of ZnO – water nanofluid on the cleaning of crude oil contaminated soils using Sodium hexametaphosphate to enhance ZnO – water nanofluid stability, based on 2,2 Simplex Lattice Design.

ii Absorbancy behaviour of Al<sub>2</sub>O<sub>3</sub> – water nanofluid on cleaning crude oil contaminated soils using SDBS surfactant to enhance Al<sub>2</sub>O<sub>3</sub> – water nanofluid stability, based on 2,2 Simplex Lattice Design

iii Behaviour of TiO<sub>2</sub> – water nanofluid on the cleaning crude oil contaminated soils using SDBS surfactant and nitric acid to enhance TiO<sub>2</sub> – water nanofluid stability/optical properties.

iv Concentration on the stability of the nanofluids. This is formulated using 3, 3 simplex Lattice Design.

The different concentrations of nanoparticle size dispersed in deionised water will be used to clean mineral oil contamination soil samples with and without stabilised/surfacted nanofluids. Evaluating remediation efficiency of each nanofluid so as to choose the best nanofluid based on economy, and cleaning efficiency as well as most recent applications to laboratory scale and commercial scale soil remediation, with a focus on crude oil (mineral oils) pollutants.

via It is very important to optimize the various conditions such as mass fraction/concentration of nanoparticles, surfactants to obtain the nanofluids with desired properties. Three process variables (temperature ,at 0 °C – 400°C at interval of 10°C/min pressure - 150mbars and time – 60min) on the cleaning behaviour of the different nanofluids on two mineral oil grades contaminated soils using 3,3 simplex Lattice Design at optimum conditions.

vib Different surfactants (ionic and non ionic surfactants) on the wettability and contact angle of the various nanofluids.

vii Thermophysical/transport properties (flow characteristics) study which is density, viscosity, specific heat capacity and surface tension. Thermal optical properties such as absorbancy and wavelength through the evaluation of stability of the various surfacted – stabilized nanofluids.

viiia. Application of statistical analysis to determine the contributions of the remediation factors on the cleaning of crude oil contaminated soils.

viiib. Application of statistical analysis to the experimental data and comparison of cleaning efficiency/oil recovery with wettability using mixture experiments based on 3, 3 simplex Lattice Design at optimum conditions.

ix. Wetting analysis study consisting of Wettability (water wettability index and oil wettability index), contact angle and relative permeabilities of water nanofluids and oil using oil contaminated cores oilflood samples and cleanup process of nanofluid flooding based on using Amott Harvey tests.

x. Comparison of the wettability index using contact angle, Amott Harvey and USBM Index.

### 1.3 Report Outline

The thesis is divided into eight chapters and the outline is as follows:

Chapter 1 is the introduction. This chapter defines the main objectives of the thesis.

Chapter 2 of this thesis is dedicated to the general description of theory relevant to the background of this study including some concepts in nanofluids, description of soil pollution, remediation techniques. Interaction between fluids and soil, wetting properties of soil (soil reservoir parameters) with a special focus on wettability in soil as a reservoir.

Chapter 3.0 describes the experimental work performed in the laboratory including formulation, preparation of different nanofluids based on experimental design, characterization, measurement of themophysical and thermal optical properties of various nanofluids. The methodology of soil contamination and cleanup process using nanofluids and

differential scanning calorimetry (DSC) in chapters 3& 4. Chapter 4 is the mineral oil soil contamination and clean-up process. The key results are presented in chapter 4. Chapters 5 and 6 are discussions of the results presented in Chapter 4 with wettability study. Chapter 7 is general discussion and summary. The conclusions & recommendation/future work are given chapter 8.

## 2 Chapter 2.0 Literature Review

This chapter provides the literature review on the different aspects of the present study. It comprises of a summary of the theory relevant to the study of the most important physical properties of soil, fluid and fluid-soil interaction formulation, preparation, characterization and measurement of properties of water nanofluids, wettability and contact angle through oil contamination soil and cleanup process. The various sections explain/emphasize the geological origin, classification, properties and chemical composition of crude oil. Different methods of soil remediation were reviewed. Nanotechnology is introduced. Nanoparticles, nanofluid and surfactants as a possible enhanced oil cleaning / recovery method are introduced. Propagation of nanofluids through porous media and their wettability is covered. Also, a short review of current literature on mineral oil and nanotechnology is given.

### 2.1 Soil properties

Soil properties are the physical characteristics of reservoir soils that make them able to store fluids and allow for fluid flow [113]. The most important soil properties are bulk density, porosity and permeability.

### 2.2 Porosity

Porosity,  $\phi$ , is a measure of the storing capacity of the soil as a reservoir. Porosity is defined as the ratio of the pore volume to bulk volume as:

$$\phi = \frac{V_b - V_g}{V_b} = \frac{V_p}{V_b} \dots \dots \dots (2.1)$$

Where, the bulk volume,  $V_b$ , is the sum of the pore volume,  $V_p$ , and the grain volume,  $V_g$ . Porosity is given in fraction or in percentage of the bulk volume. Fluid flow is not possible in the total pore space. Residual porosity is the ratio of the volume of the pores that are closed off by the reservoir matrix to the bulk volume. Effective porosity is the ratio of the volume of the pores that are interconnected to the bulk volume. Effective porosity is of most importance as it reflects the volume available for fluid flow, and it is usually measured in the laboratory. Helium porosimeter is a common method used to measure porosity of core soil samples in the laboratory. The experimental set-up and procedure for another method is given in Chapter 3.

### 2.2.1 Permeability (Hydraulic conductivity)

Permeability,  $k$ , is a property of porous medium, and it is a measure of the capacity of the medium to transmit fluid. Permeability measures the ease at which a fluid flows through porous media. The easiness at which fluid flows through the soil decreases with the depth.

The coefficient or permeability is also known as hydraulic conductivity. Hydraulic conductivity,  $k$ , is a measure of soil permeability;  $k$  is determined in the lab using two methods: Constant-Head Test and Falling-Head Test. Darcy's law relates the flow rate,  $q$ , to the permeability,  $k$  and according to Darcy they are proportional. Darcy's law is given as follows:

$$K = QL/Aht \dots\dots\dots (2.2)$$

Where,  $Q$ = flow rate ( $\text{cm}^3/\text{s}$ )

$k$ = coefficient of permeability ( $\text{cm}/\text{s}$ )

$A$  = area of the specimen ( $\text{cm}^2$ )

$L$  = length or distance ( $\text{cm}$ )

$H$  = height of water ( $\text{cm}$ )

$t$  = time (second)

The rate,  $q$ , is proportional to permeability and inversely proportional to the viscosity. In other words, if the viscosity of the oil or water is decreased or if the permeability is increased, the oil rate will increase. This test applies a constant head of water to each end of a soil in a “permeameter”.

In the present thesis a constant head permeater is used for measurement of permeability. The experimental set-up and procedure for this method is given in Chapter 3.

### 2.2.2 Saturation

For a given porous soil, fluid saturation is defined as the ratio of the volume of the fluid to the pore volume of the rock [126]. In a water, oil and gas (air) system, the respective saturations are defined as:

$$S_w = \frac{V_w}{V_p}, S_o = \frac{V_o}{V_p}, S_g = \frac{V_g}{V_p} \dots\dots\dots (2.3)$$

Where  $V_w, V_o, V_g$  and  $V_p$  are water, oil, gas and pore volumes respectively.

$$S_w + S_o + S_g = 1$$

The pore volume is referred to as the interconnected pore volume only, then the saturation is referred to as the effective saturation. A normalized value of the saturation is used where the



irreducible saturations are subtracted from the bulk saturations. Saturation is given as a fraction or as a percent. The irreducible water saturation ( $S_{wirr}$ ) is the lowest water saturation obtainable when a water displacement process is occurring (ie water retained in the soil after cleaning process). Increasing the capillary pressure will not reduce the water saturation below  $S_{wirr}$ . The residual oil,  $S_{or}$  or gas saturation,  $S_{gr}$  is the ultimate trapped value of oil or gas after the capillary pressure is decreased from a high positive value to a high negative value, and finally, the critical water saturation is defined as the highest water saturation for which the water is immobile.

### 2.3 Fluid Properties

Fluid properties are the physical characteristics of fluids that affect their flow. The most important fluid properties are density, viscosity and surface tension.

#### 2.3.1 Density

Density ( $\rho$ ) is defined as mass per unit volume. It is a function of temperature and pressure. Density has the SI-unit of  $\text{kg/m}^3$ .

Specific gravity (SG) and API gravity are two terms used to describe the density of a fluid. For liquid, SG is defined as the ratio of density of the liquid to density of water at the same temperature. For gases, it is the ratio of density of the gas to density of air at the same temperature. The density of water at standard conditions is  $1000 \text{ kg/m}^3$  while for air at standard conditions it is  $1.23 \text{ kg/m}^3$ . The standard conditions in the petroleum industry for international trade of petroleum are  $15^\circ\text{C}$  ( $60^\circ\text{F}$ ) and  $1 \text{ atm}$ . This is different from the standards in chemistry where standard conditions are  $25^\circ\text{C}$  and  $1 \text{ atm}$ .

API gravity was developed by the American petroleum institute (API). It is referred to on an API scale where most values falls within the range of  $10^\circ$  until  $70^\circ$  [113]. The formula for API gravity is:

$$\text{API} = \frac{141.5}{\text{SG}_{60^\circ\text{F}}} - 131.5 \dots \dots \dots (2.4)$$

Where, SG is the specific gravity of the fluid at standard conditions. Density does not have a direct impact on the physical flow properties such as permeability, but it usually increase with viscosity which has a high impact on the fluid flow. The density will be measured using a pycnometer as described in Chapter 3.

### 2.3.2 Surface and interfacial tension (IFT)

Surface tension is the tendency of a liquid to expose a minimum free surface, and it may be defined as the contractile tendency of a liquid surface exposed to gases. The interfacial tension (IFT) is a similar tendency which exists when two immiscible liquids are in contact. Surface and interfacial tension of fluids result from molecular properties occurring at the surface or interface [126].

Molecules in a given fluid are attracted to each other by an electrostatic force called cohesion. If several fluids are present in a system, cohesive forces also exist between the different fluids. In a water/oil/gas system, the intramolecular forces (within a fluid) are often greater than the intermolecular forces (between two or more fluids), causing the different fluids to be immiscible. In such systems, the area of the contact surfaces is minimized. If a solid is introduced to the system, the molecules are attracted to the solid by an electrostatic force called adhesion [129].

This intermolecular force to contract the surface is called the surface tension, and it is responsible for the shape of liquid droplets. In practice, external forces such as gravity deform the droplet; consequently, the contact angle is determined by a combination of surface tension and external forces (usually gravity). Theoretically, the contact angle is expected to be characteristic for a given solid-liquid system in a specific environment [120a]. Surface and interfacial tension (IFT)  $\sigma$ , is a property of the interface of two immiscible phases. When both of the phases are liquids, like oil and water, the term interfacial tension is used. When the phases are different, like gas and liquid, surface tension is used. Interfacial tension is the tendency of a liquid to expose a minimum free surface when it is in contact with an immiscible fluid, and interfacial tension acts perpendicular to the interface as shown in Figure 2-1.

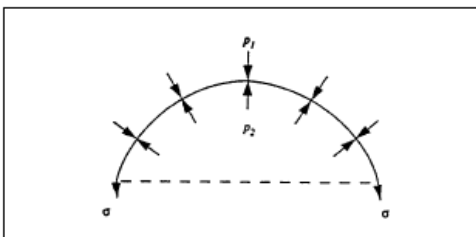


Figure 2-1 Interfacial tension acts perpendicular to the interface between the two immiscible fluids [126]

The Young-Laplace equation describes the discontinuity in pressure,  $p_2 - p_1$ , across the interface between two immiscible fluids as follows:

$$P_2 - P_1 = \sigma \left( \frac{1}{r_1} + \frac{1}{r_2} \right) \dots \dots \dots (2.5)$$

Where,  $r_1$  and  $r_2$  are the curvature of the surfaces and  $\delta$  is the interfacial tension between the two immiscible fluids. In this thesis, surface tension is measured in place of interfacial tension. This is because, the Attestation Theta for measuring surface tension comprises of liquid which is water-nanofluid and gas is the air.

### 2.3.3 Viscosity

Absolute or dynamic viscosity,  $\mu$ , of a fluid is a measure of the internal resistance to flow. The absolute viscosity is defined as the relation between the shear stress,

T, and shear rate,  $y$ , as follows:

$$\mu = \frac{T}{y} \quad (2.6)$$

This equation holds only for Newtonian fluids where the shear stress is proportional to the shear rate. The unit used for viscosity is Pascal second (Pas) in SI units and centipoise (cp) in field units. One centipoise is equal to 1/100 poise and 0.001 Pas. Kinetic viscosity,  $\nu$ , is also used by the oil industry. It is defined as the dynamic viscosity divided by the density of the fluid, and the unit is centistokes (cSt).

## 2.4 Properties of Fluid-Soil Interaction

The most important properties of fluid-rock interaction are wettability, saturation, capillary pressure and relative permeability. These parameters describe the interaction of the fluid-soil interaction on a micro scale.

### 2.4.1 Wettability

Wettability is the tendency of one fluid to spread on or adhere to a solid surface in the presence of other immiscible fluids [10b]. Wettability is an important determining factor in a multiphase flow in reservoir rock, fluid distribution and trapping [122b]. Fluid distributions in porous media are affected both by forces at fluid-fluid interfaces and fluid-solid interfaces. Usually, one phase is more strongly attracted to the solid than the other phase, when two immiscible fluids are placed in contact with a solid surface. The more strongly attracted phase is called the wetting phase. Also, soil wettability affects the nature of fluid saturations and the general relative permeability characteristics of fluid-rock system. The location of a fluid within the pore structure depends on the wettability of that phase [50b].

The reservoir wettability is a critical parameter in many types of oil recovery processes. Recovery of oil by spontaneous imbibition of water into the matrix of fractured reservoirs is a frequently cited example. [81b] also noted that capillary pressure is the driving

force in spontaneous imbibitions. Wettability remains the key factor in determining capillary driving force and the related imbibition rate.

#### 2.4.2 Classification of wettability

Wettability can be classified as homogeneous when the rock surface has uniform molecular affinity to either water or oil. This is again split into strongly water-wet, strongly oil-wet, and intermediate-wet categories. For a strongly oil-wet soil, the oil will contact most of the rock surface and occupy the smallest pores and the water is in the middle of the larger pores. When this soil is waterflooded, the oil will remain as a film on the soil surface and in the smallest pores where water does not penetrate. The water will mainly flow through the soil in the larger pore channels as illustrated by Figure 2-3.

On the other hand, if water contacts most of the rock surfaces and fills the smallest pores of the soil, we have strongly water-wet soil. The oil is located in the center of the larger pores. If the soil is waterflooded, a snapping phenomenon may occur, leaving oil globules trapped in the center of the large pores, as shown in Figure 2.2 [122b]. Intermediate wettability occurs when both fluid phases tend to wet the solid, but one is only slightly more attracted than the other [50b].

Moreover, the concept of intermediate wettability assumes that all portions of the soil have a slight but equal preference to being wetted by oil or water.

In contrast, the internal surface of the reservoir soil is composed of many minerals with different surface chemistry and adsorption properties, leading to variations in wettability. This heterogeneous wettability may be divided into fractional or mixed wet. In fractional wettability, (also called heterogeneous, spotted, or dalmatian) crude oil components are strongly adsorbed in certain areas of the soil. Thus, some portion of the soil is strongly oil-wet, while the rest is strongly water-wet. The mixed wet is a special type of fractional wettability when the soil has continuous water-wet and oil-wet regions [111b, 122b]. Mixed wettability results from a variation or heterogeneity in chemical composition of the exposed rock surfaces or cementing-material surfaces in the pores [50b]. In addition, both water and oil can spontaneously imbibe, in some mixed-wet or fractional wet system [10b, 27c]. Furthermore, [50b] gave a quantitative classification of wettability based on contact angles. Contact angle by convention, is measured through the water phase and it is a measure of wettability. From Figure 2.1, the solid is water-wet if  $\theta < 90^\circ$  and oil-wet if  $\theta > 90^\circ$ . A contact angle approaching  $0^\circ$  indicates a strongly water-wet system and an angle approaching  $180^\circ$  indicates a strongly oil-wet system. Intermediate

wettability occurs when  $\theta$  is close to  $90^\circ$ . Small contact angles ( $<90^\circ$ ) correspond to high wettability, while large contact angles ( $>90^\circ$ ) correspond to low wettability.

Wettability is a surface phenomenon where two immiscible fluids are in contact with a solid surface. Wettability describes the interactions between fluid(s) and soil, i.e. how the fluid(s) tends to spread on the soil surface. The wettability and wetting condition can be expressed through the wettability index, WI, or the contact angle which is measured through the densest fluid phase relative to the soil surface. In an oil-water system as shown in Figure 2.2, the soil surface can be described as water-wet, intermediate-wet or oil-wet. In such a system the contact angle is determined through the densest phase which in most cases is water.

#### 2.4.3 Methods of wettability measurement

Many different methods have been proposed for measuring the wettability of a system [10b]. They include quantitative methods- contact angles, Amott (imbibition and forced displacement), and USBM wettability method. The qualitative methods include: imbibition rates, microscope examination, flotation, glass slide method, relative permeability curves, capillarimetric method, displacement capillary pressure, reservoir logs, nuclear magnetic resonance, and dye adsorption.

Finally, there is a new quantitative wettability test method for carbonates [122b] based on chromatographic separation between sulfate ions,  $\text{SO}_4^{2-}$  and thiocyanate, SCN, as a tracer. However, there is no single accepted method and many of the wettability measurements are also imprecise, particularly close to neutral wettability. One method may show that a core is mildly oil-wet, while another shows that a core is mildly water-wet [10b].

#### 2.4.4 Amott method for the calculation of Wettability Index (WI)

There are many quantitative and qualitative methods for calculation of wettability index, as follows:

Amott test is one of the commonly used methods of characterizing wettability of a porous medium [81b]. It combines imbibition and forced displacement (of water and oil) to measure the average wettability of a core [10b]. The method is based on the fact that the wetting fluid generally imbibes spontaneously into the core, displacing the nonwetting one. Forced displacement is either by centrifuging, as originally proposed by Amott, or by waterflooding [27d]. No stepwise capillary pressure values are measured during the test. The Amott wettability measurement consists of 5 steps which include: (1) immerse the core in oil, and measure the volume of water displaced by the spontaneous (free) imbibition of oil after 20 hours; (2)

centrifuge the core in oil until irreducible water saturation (IWS) is reached, and measure the total amount of water displaced, including the volume displaced by spontaneous imbibitions; (3) immerse the core in brine, and measure the volume of oil spontaneously displaced by imbibitions of water after 20 hours; and (4) centrifuge the core in oil until residual oil saturation (ROS) is reached, and measure the total amount of oil displaced [10b].

The modified Amott wettability test, called Amott-Harvey relative displacement index ( $I_{AH}$ ) is used by some researchers [10b]. This method offers a single value that can be used for mathematical modeling.

The Amott wettability indices to water  $I_w$  and oil  $I_o$  are defined respectively as:

$$I_w = \frac{\Delta S_{w\text{ imb}}}{\Delta S_{w\text{ imb}} + \Delta S_{w\text{ f}}} \dots \dots \dots (12b)$$

$$I_o = \frac{\Delta S_{o\text{ imb}}}{\Delta S_{o\text{ imb}} + \Delta S_{o\text{ f}}} \dots \dots \dots (12c)$$

Where:

$\Delta S_{w\text{ imb}}$  = the saturation change during a spontaneous imbibitions of water (water recovered after cleanup process)

$\Delta S_{w\text{ f}}$  = the saturation change during a forced imbibition of water (water retained in the soil after cleaning with nanofluids)

$\Delta S_{o\text{ imb}}$  = the saturation change during a spontaneous drainage of oil (oil recovered after cleanup process)

$\Delta S_{o\text{ f}}$  = the saturation change during a forced drainage of oil (oil retained after cleanup process).

The Amott-Harvey relative displacement index is the displacement-by-water ratio minus the displacement-by-oil ratio. This is expressed as  $WI = WWI - OWI$ . (Ie  $I_{AH} = I_w - I_o$ )

Thus, this combines the two ratios into a single wettability index that varies from +1 for complete water wetness to -1 for complete oil wetness. [27d] further gave the index ranges as:  $+0.3 \leq I_{AH} \leq 1.0$

for water-wet system,  $-0.3 < I_{AH} < 0.3$  for intermediate wet system, and  $-1 \leq I_{AH} \leq -0.3$  for oil-wet system. The Amott test gives a defined scale for the wettability. The test is widely used and measurement is easy to perform. However, Amott method is insensitive close to neutral wettability [10b]. It does not discriminate adequately between systems that give high wettability index to water [81b].

Amott Test combines spontaneous and forced imbibition to measure the average wettability of a specimen (soil). The method is based on the fact that the wetting fluid will generally imbibe spontaneously into the specimen (soil) and displace the nonwetting one. The ratio of spontaneous to forced imbibition is used to reduce the influence of other factors such as relative

permeability, viscosity and initial saturation of the specimen (soil).Based on the test, the Amott-Harvey wettability index WI can be calculated. The index compares the imbibition potential of water and oil, which varies from +1 for strongly water-wet specimens (soils) to -1 for strong oil-wet specimens (soils) [11].

#### 2.4.4.1 USBM Test

The USBM test [34] measures the average wettability of the core.

It has advantage over Amott wettability test because of its sensitivity close to neutral wettability.A minor disadvantage is that USBM wettability index can only be measured on plug-size samples because the sample must be spun in a centrifuge. Also, the USBM test also cannot determine whether a system has fractional or mixed wettability.

This method compares the work necessary for one fluid to displace the other.Because of the favourable free-energy change, the work required for the wetting fluid to displace the nonwetting fluid from the specimen (soil) is less than the work required for the opposite displacement.Based on the USBM test, the USBM wettability index can be calculated.Experimentally though the index usually falls within -1 to +1. According to [79a], the specimen (soil) is preferentially water-wet if the index is greater than zero (+ve).If the index is less than zero (-ve), the specimen (soil) is preferentially oil-wet. The specimen (soil) is neutral-wet if the index is approximately zero.

#### 2.4.4.2 Contact angle

The contact angle method is the best measure of the wettability when pure fluids and artificial cores are used [10b].A typical oil/water/solid system is shown in Figure 2.1b and 2.2, where the surface energies in the system are related by Young’s equation.By convention, the contact angle,  $\theta$ , is measured through the water and the interfacial energy  $\partial_{ow}$  is equal to  $\partial$ .

$$\partial_{ow} \text{Cos}\Theta = \partial_{os} - \partial_{ws} ; \dots\dots\dots (12c) ..$$

Contact angles can be either static or dynamic.Static contact angles are formed with a surface under no applied force other than gravity.Dynamic contact angles are distorted from the static case by an applied force and can advancing or receding.Advancing contact angles are formed at the front of the encroaching wetting phase, whereas receding contact angles are formed at the front of the encroaching non-wetting phase [122b].Such motion of a phase boundary, involving advancing and receding contact angles, is known as dynamic wetting.

The commonly used methods in the petroleum industry are the sessile drop method and the modified sessile drop method [10b]. The sessile drop method uses a single flat, polished mineral crystal.

#### 2.4.4.3 The static and dynamic sessile drop method

The most frequently used is the goniometer-telescope measurement of sessile-drop contact angles. Commercial contact angle goniometers employ a microscope objective to view the angle directly. In the static method a drop is deposited on a surface and the contact angle can be measured by looking at the drop through a goniometer (an instrument that measures contact angles). The dynamic method is similar to the static one but the drop of liquid which is deposited on a surface is modified. The droplet is being deposited via a syringe and the droplet's volume is changed dynamically without increasing its solid-liquid interface area and this maximum angle is the advancing angle. Volume is then removed to produce the smallest possible angle, which is called the receding angle. The difference between those two measured angles is called contact angle hysteresis.

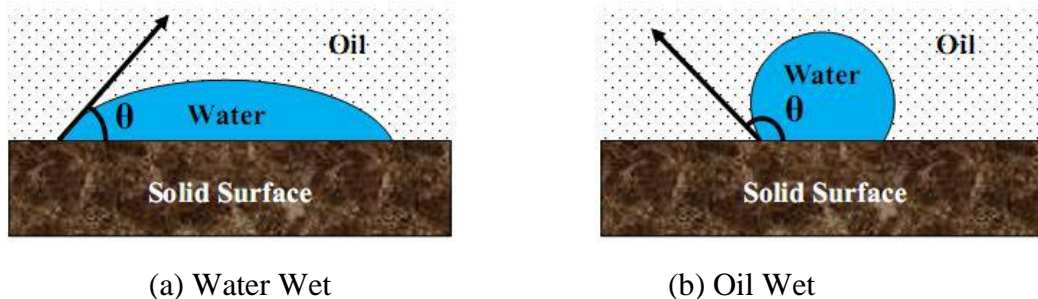


Figure 2-2 Contact angle measurements through the water phase [107]

The modified sessile drop method uses two flat, polished mineral crystals that are mounted parallel to each other on adjustable posts. Drop method will be used in this thesis.

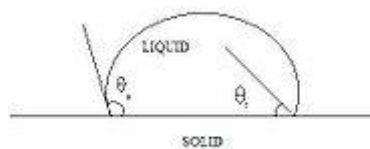


Figure 2-3 Schematic of advancing and receding contact angles

Unlike ideal surfaces, real surfaces do not have perfect smoothness, rigidity, or chemical homogeneity. Such deviations from ideality result in phenomena called contact-angle



hysteresis. Contact-angle hysteresis is defined as the difference between the advancing ( $\theta_a$ ) and receding ( $\theta_r$ ) contact angles [122b].

$$H = \theta_a - \theta_r$$

In simpler terms, contact angle hysteresis is essentially the displacement of a contact line by either expansion or retraction of the droplet. Figure 6 depicts the advancing and receding contact angles. The advancing contact angle is the maximum stable angle, whereas the receding contact angle is the minimum stable angle. Contact-angle hysteresis occurs because there are many different thermodynamically stable contact angles on a non-ideal solid [122b].

#### 2.4.4.4 Applications of contact angle

The interest in contact angles is because it plays a significant role in a number of technological, environmental and biological phenomena. Water imbibition into porous media theory has been shown to have a multidisciplinary validity in food, soil physics, geology, printings and more. Imbibition of a liquid by a porous solid is a phenomenon highly dependent on wetting. Capillary imbibition is a mechanism that plays a significant role during rehydration of dry food particles that are considered as porous media. Imbibition is highly dependent on the wettability of the porous media, which is usually determined by measuring contact angles which liquids form with the solid.

#### 2.4.5 Contact angle and wettability

When a liquid comes in contact with a solid surface, the liquid either spreads out on the surface or forms drops on the surface [126]. If the liquid spreads out, the liquid is said to be wetting the surface, while in the other case a contact angle  $\Theta = 0$  will develop between the surface and the drop. If there are more than one fluid present in the system, one of the fluids (the most adhesive one) has a higher tendency of wetting the surface than the other fluids. This fluid is called the wetting phase and a measure of how much the fluid is wetting can be determined by the contact angle. This angle reflects the equilibrium between the fluids' interfacial tension and the fluids' individual adhesive attraction to the solid [129]. In some cases the different fluids can have equal affinity to the solid surface. This is called a neutral system. The process of decreasing the wetting phase saturation is defined as drainage. The opposite, increasing the wetting phase saturation is defined as imbibition. In other words, hysteresis in contact angle in a water-wet porous medium (a) increase in the wetting fluid (imbibition) and (b) decrease in the wetting fluid (drainage).

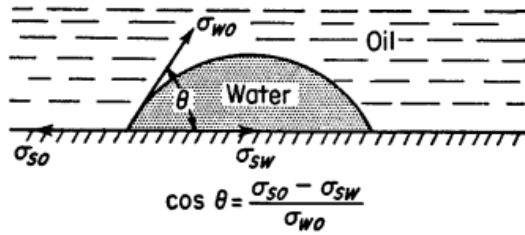


Figure 2-4 Illustration of the nomenclature used for defining the contact angle [126]

In figure 2-4,  $\delta_{so}$ ,  $\delta_{sw}$  and  $\delta_{wo}$  are the interfacial tensions between the solid and oil, solid and water and water and oil, respectively.[126] give the following Table 2-1 that relates the contact angle to the wettability.

The values of the wettability index and contact angle and their corresponding wetting conditions are shown in Table 2-1.

Table 2-1 Wettability index (WI) and contact angle for different wetting conditions

Wetting Index $\cos \Theta$	Contact angle $\Theta$	Wetting condition
1	$0^\circ$	Completely water-wet
0	$90^\circ$	Neutral system
-1	$180^\circ$	Completely oil-wet

When more than 50 % of the soil surface is wet by water in a water/oil/soil system, the soil is considered water-wet [35].The smallest pores and crevices are fully saturated with water, and the water also coats the grains in bigger pores as surface films, surrounding the oil that exists as droplets in the center of the pore bodies.The oil can exist as globules, which means that oil can be connected between two or more pores, but the oil is not a continuous phase unless the water saturation is very low.In a water-wet system the water will exist as a continuous phase and wets the surfaces even if we reduce the saturation to the irreducible water saturation.Another core of the same reservoir soil that is 100 % water-filled will not spontaneously imbibe oil [35].For an oil-wet soil the roles of water and oil is the opposite compared to the water-wet case.Oil fills the smallest pores and crevices and coats the surfaces of the grains, while the water exists in the center of the pore bodies.The behavior of oil for an oil-wet core is the same as for water in a water-wet core soil sample described above.

Table 2-2 Relationship between wettability, contact angle USBM and Amott – Harvey wettability indices [10b]

Wetting conditions	Water-wet	Neutral – wet	Oil – wet
Contact angle $\theta^\circ$			

Minimum	0°	60° to 75°	105° to 120°
Maximum	60° to 75°	105° to 120°	180°
USBM Wettability Index	W near 1	W near zero	W near -1
Amott test			
Displacement by H <sub>2</sub> O ratio	+ve	Zero	-ve
Displacement by oil ratio	Zero	Zero	+ve
Amott – Harvey Wettability Index	0.3 ≤ WI ≤ 1.0 WI < 1.0	-0.3 < WI < 0.3	-1.0 ≤ WI ≤ -0.3 WI ≤ -0.3

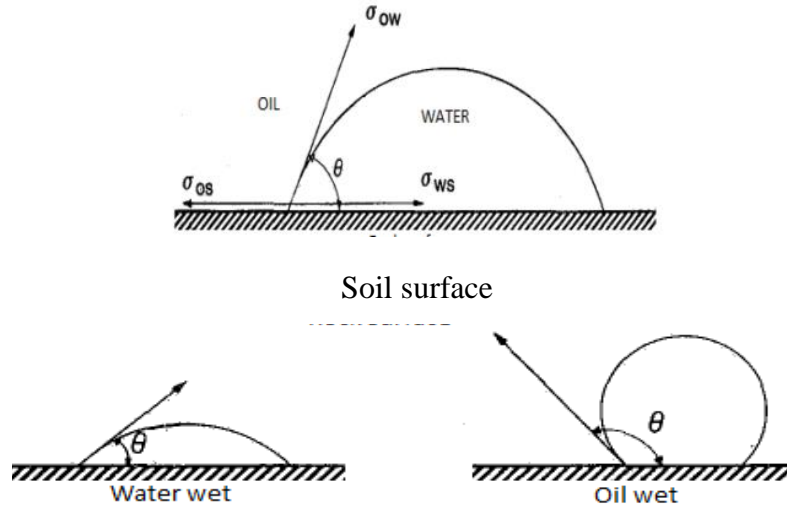


Figure 2-5 Illustration of interfacial tension for a two-phase system with water and oil on a soil surface [10b]

Where,  $\sigma_{wo}$  is the interfacial tension between water and oil,  $\sigma_{wo}$  is the surface tension between solid and oil and  $\sigma_{sw}$  is the surface tension between solid and water.

#### 2.4.5.1 Spreading, wetting, and contactangle

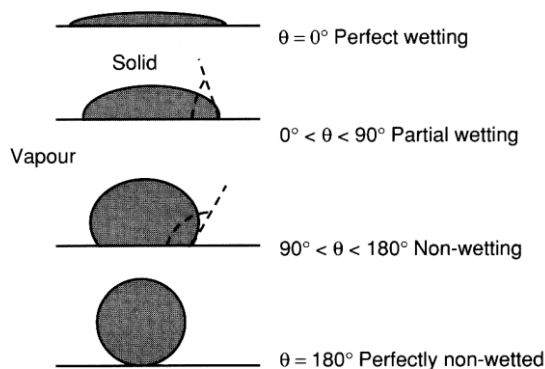


Figure 2-6 Illustration of a porous system of mixed wettability

Some grains are oil-wet where the oil is coating the grain while others are water-wet [51].

Figure 2-6 is an illustration of a porous media where different grains have unlike wetting preference. It is referred to as a system of mixed wettability. In a water-wet system, water is coating the soil surface completely and tends to be occupying the smaller pores while oil is situated in the center of the larger pores. After water flooding residual oil is trapped as big droplets in the center of the larger pores due to the discontinuous phase. In an oil-wet system it will be the other way around. Oil is then coating the soil surface and occupying the smaller pore space while water is in the center of the larger pores. The residual oil is then the oil that is coating the soil.

Residual oil saturation is defined as the fraction of volume of oil that cannot be displaced over pore volume. The same applies for irreducible water saturation. Both irreducible water saturation and Residual oil saturation are affected by permeability.

In a neutral system (intermediate wet) the situation in the porous media is a mix of the two described above. Wettability is the main characteristic evaluated in the present thesis. The contact angle is measured by the Imaging method as described in Chapter 3: 3.4.3 and the relative wettability change is evaluated with the spontaneous imbibition test as described in Chapter 3: 3.4.2.

## 2.5 Saturation

Saturation,  $S$ , is the relative amount of a fluid in the pore space and is expressed as follows:

$$S_{\alpha} = \frac{V_{\alpha}}{V_p} \dots \dots \dots (2.7a)$$

Where,  $V_p$  is the volume of the pore space,  $V_{\alpha}$  is the volume of a fluid in the pore space and  $\alpha$  refers to the oil, water or gas phase. As porosity, saturation is given as fraction or in percentage of the pore volume.

The sum of the saturation of the phases (oil, water and/or gas) present in the pore space is equal to one:

$$S_o + S_w + S_g = 1 \dots \dots \dots (2.7b)$$

Saturation is a function of the soils wettability and is important when it comes to how easy the fluid flows through porous media. If the fluid phase is continuously connected through the pore space then it flows more easily than fluid that is surrounded by another phase. Droplets or 'blobs' of a phase may be trapped in the pore space when completely surrounded by another phase. When oil is displaced by water and the remaining oil no longer flows, the amount of oil left behind in the porous media is referred to as the residual oil saturation,  $S_{or}$ . When water is displaced by oil and the water no longer flows, it is called the irreducible water saturation,

Swr.Connate water/oil saturation, Swc, is the water/oil saturation in the reservoir before starting production. In other words, initial moisture content of the soil sample. The movable fraction of oil is:  $1 - Swr - Sor$ . The use of enhanced oil recovery (i.e surfacted nanofluids) techniques may reduce the residual oil saturation. This will lead to a higher recovery.

Note: Saturation is not directly measured in present thesis, but residual oil saturation (oil retained in the soil after cleaning) and the irreducible water saturation (water retained in the soil after cleaning) are calculated for the experiments performed on soil contamination and cleanup process.

### 2.5.1 Capillary Pressure

Capillary pressure is the difference in pressure between two immiscible phases in the pores space, and it is given by Equation 2.9 which is the pressure in the nonwetting phase minus the pressure in the wetting phase. The pressure difference is caused by a discontinuity in pressure on the interface between the two fluids. For an oil-water system, the capillary pressure is defined as:  $p_c = p_o - p_w$  where o stands for oil and w for water. Recall that the Young Laplace (Equation 2.5) gives the relation between the capillary pressure and the curvature of the interfaces.

The same equation may be modified to give the capillary pressure as follows:

$$p_c = p_{nw} - p_w = \sigma \left( \frac{1}{r_1} + \frac{1}{r_2} \right) \dots\dots\dots (2.8)$$

Where  $p_{nw}$  is the pressure of the non-wetting phase,  $p_w$  is the pressure of the wetting phase,  $\sigma$  is the interfacial tension, and  $r_1$  and  $r_2$  is the curvature of the interfaces.

Drainage is defined as the process where the non-wetting phase is displacing the wetting phase. Imbibition is defined as the process where the wetting phase is displacing the non-wetting phase. For simplicity, imbibition in an oil-water system refers to the process where oil is displacing water even though oil is the wetting phase and drainage refers to the opposite, e.g. the process where water is displacing.

This is due to the underlying assumption that all soil reservoirs are considered to be water-wet. Porous media has a distribution of different pore throat sizes where the wetting fluid is occupying the smaller space and the non-wetting fluid is occupying the center in the larger space. During drainage more pressure is applied to the nonwetting phase. Gradually smaller pore throats are invaded of the non-wetting phase which leads to a decrease in the saturation of the wetting phase. Typical imbibition and drainage curves are shown in Figure 2-7. The upper-most curve is the primary drainage curve. Primary drainage is when the core is initially fully saturated

with water,  $S_w = 1$ , and water is displaced by oil. The imbibition curve is the lower-most curve going from  $S_{cw}$  to  $S_{or}$ . The imbibition curve is found by first letting water spontaneously imbibe the core soil sample until the spontaneous water saturation,  $S_{spw}$ , is reached. After forced imbibitions are performed, i.e. until no more oil is released, then  $S_{or}$  is reached. The secondary drainage curve is the curve in the middle going from  $S_{or}$  to  $S_{cw}$ . The secondary drainage curve is found by first drain the oil spontaneously until the spontaneous oil saturation,  $S_{spo}$ . Second, forced drainage is performed until no more water is released at  $S_{cw}$ . The capillary pressure is not measured in the present thesis. The methods used in laboratory experiments to measure the capillary pressure can be found in the literature.

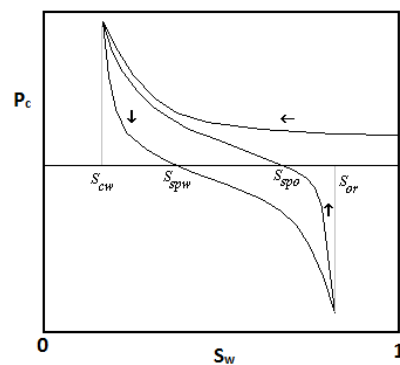


Figure 2-7 Illustration of the capillary pressure as a function of saturation showing the drainage and imbibition curve

### 2.5.2 The Effects of Wettability on Capillary Pressure

Wettability affects the capillary pressure together with the saturation and the pore throat Distribution [11]. USBM, also called the centrifuge method, is an experimental method used for determination of wettability based on the correlation between the areas under the capillary pressure curves and the wetting condition. The imbibition and drainage curves are obtained only by forced imbibition and forced drainage. For a water-wet system the area under the forced drainage curve,  $A_1$ , is expected to be larger than the area under the forced imbibition curve,  $A_2$ . For an oil-wet system,  $A_2$  is expected to be larger than  $A_1$ . While for a system of neutral wettability  $A_1$  and  $A_1$  are expected to be equal.

### 2.5.3 Effective and Relative Permeability

Effective permeability,  $k_e$ , is a measure of how easy a fluid is transmitted through porous media when another phase is present. The dimension of effective permeability is the same as for absolute permeability: Darcy, D, or  $m^2$ . Relative permeability,  $k_r$ , describes the interaction of the phases while flowing through a porous medium as a function of the saturation. It is the ratio of effective permeability to absolute permeability as follows:

$$K_{r\alpha} = \frac{k_e \alpha}{K} \dots \dots \dots (2.9)$$

Where  $\alpha$  refers to the oil, water or gas phase. With the use of effective and relative permeability, Darcy's law (Equation 2.2) can be modified so that the equation holds for two- or three-phase flow in porous media:

$$u_{\alpha} = \frac{k \cdot k_{r\alpha}}{\mu_{\alpha}} \cdot \frac{\Delta p}{L} \dots \dots \dots (2.10)$$

### 2.5.4 Effects of Wettability on Relative Permeability

Wettability effects relative permeability as the wetting condition of the porous media determines the distribution of the fluids in the pores and hence the flow [12a]. As a consequence the shape of the relative permeability curve is dependent on wettability as shown in Figure 2.5. The fluid path for the wetting fluid is often through the smaller and low permeable pores. At low saturations of the non-wetting fluid, this phase will be discontinuous through the pore space and left as droplets in the larger pores. This blocks the pore throats, and lowers the available flow area for the continuous wetting phase.

Hence, it also lowers the relative permeability of the wetting phase. As the non-wetting fluid has its fluid path in the center of the larger pores the non-wetting phase has a higher permeability at any saturation.

Figure 2-8: shows that the oil relative permeability is always higher in the water-wet case, and the water relative permeability is higher in the oil-wet case. Also, at low saturation of the wetting fluid the relative Permeability of the non-wetting fluid often approaches the absolute permeability.

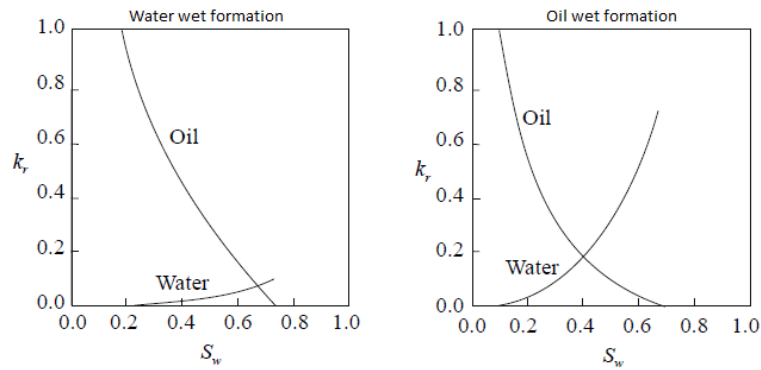


Figure 2-8 Visualizaion of the effect of wettability on the relative permeability curves [129].

Crude oil also known as petroleum (from Greek: Petra (rock) & Latin oleum (oil) is a composition of hydrocarbons (chemicals composed solely of hydrogen and carbon in various molecular arrangements) and other compounds which is usually brown or black in colour. It is extracted from the earth, formed naturally from the fossil of animals and plants. The viscosity and relative weight of crude oil varies and it can exist in either liquid or solid state.

### 2.5.5 Crude oil

Crude oil can also be defined as a highly complex mixture, containing hundreds of thousands of Hydrocarbons [15]. Compounds in crude oil can be divided into three general classes consisting of saturated hydrocarbons, aromatic hydrocarbons and polar organic compounds. Crude oil is physically, chemically and biologically harmful to soil because it contains many toxic compounds in relatively high concentrations (e.g. polycyclic aromatic hydrocarbons, benzene and cycloalkane rings). The presence of high molecular weight compounds with very low solubility in water prevents natural biodegradation process from working efficiently in hydrocarbon contaminated soils. These compounds also prevent macro- and micro-pores in soil and thus limit water and air transport that would be necessary for organic matter conversion. Generally, petroleum hydrocarbons compounds bind to soil components and are difficult to remove or degrade. Biosurfactants (BS) can emulsify hydrocarbons, thus enhancing their water solubility, decreasing surface tension and increasing the displacement of oily substance from soil particles. Sites contaminated by petroleum compounds ranged from leaking household oil tanks to areas polluted by oil tanker spills, e.g. old and new petrol stations as well as areas surrounding oil storage facilities, pipelines, terminals and refineries.



Crude oil is a naturally occurring flammable liquid consisting of a complex mixture of hydrocarbons of various molecular weights and other liquid organic compounds that are found in geologic formations beneath the Earth's surface. A fossil fuel is formed when large quantities of dead organisms, such as zooplankton and algae, are buried underneath sedimentary rock and undergo intense heat and pressure.

Crude oil varies greatly in appearance depending on its composition. It is usually black or dark brown (it can be yellowish, reddish or greenish), It is found in the reservoir as natural gas, which being lighter forms a gas cap over the petroleum, and saline water, which, being heavier than most forms of crude oil, generally sinks beneath it [141]. Crude oil may also be found in semi-solid form mixed with sand and water as well as other components (Table 2-3), where it is usually referred to as crude bitumen (bitumen is considered as a sticky, black, tar-like form of crude oil which is so thick and heavy that it must be heated or diluted before it flows). Crude oils are classified as: paraffin base, naphthene base, asphalt base or mixed base. There are some crude oils which have up to 80% aromatic content, and these are known (as aromatic-base oil). Attempts have been made to define or classify petroleum based on various distillation properties when combined with another property such as density. It has been suggested that crude oil should be called asphaltic if the distillation residue contained less than 2% wax and paraffinic if it contained more than 5%.

### 2.5.6 Classification of Hydrocarbon Reservoir Fluids

Petroleum and crude oil are equal terms and their definition is "a natural occurring mixture of hydrocarbons which may also include compounds of sulfur, nitrogen, oxygen, metals and other elements" (Table 2-2 and [122]). The term conventional petroleum covers the petroleum fluids that are produced and recovered through utilizing the easily free flow of the liquid. Unconventional petroleum is used for resources such as shale gas, shale oil, heavy oil, extra heavy oil and bitumen.

Table 2-3 2005 Composition and Percentage of the Trecate crude oil (AGIP, 1995)

Enrollment in local colleges,

<b>Component</b>	<b>Percentage (%)</b>
Water	0.1
H <sub>2</sub> S	0.01
Hydrocarbons	

Gaseous (fraction compounds)	11 (Methane 4%, C <sub>2</sub> – C <sub>4</sub> 7%)
Polycyclic Aromatic Hydrocarbons	8
Sulphur Organic compounds	0.16
Light fuel	6.5
Kerosene	20
Diesel fuel	11
Lubricating oils	25.23
<b>Residue</b>	<b>18</b>
100	

The different types of crude oil are classified based on the America Petroleum Institute (API), (an oil industry measure of density and its sulphur content) and viscosity. The properties may vary in terms of proportion of hydrocarbon elements, sulphur content etc. as it is extracted from different geographical locations all over the world.

Light crude oil is defined as having an API gravity higher than 31.1° API: i.e. Crude oil is considered light if it has low density or heavy if it has high density. Medium oil is defined as having an API gravity between 22.3° API and 31.1° API. Heavy oil is defined as having an API gravity below 22.3° API.

Crude oil classifications: Classifications are made based on the sulphur content. Crude oil with low content of sulphur means ‘sweet’ and the presence of high sulphur content is known as ‘sour’. One of the largest and major classifications of crude oil is Brent, which is found in the North Sea. With an API gravity of 38.3 degrees and 0.37% of sulphur, this blend of crude oil comes from 15 various oil fields in the North Sea. Some of the common reference crudes are: West Texas Intermediate (WT) known as Texas Light sweet, OPEC Reference Basket, a weighted average of oil blends from various OPEC (The Organization of the Petroleum Exporting Countries) countries and Dubai-Oman Crude (Middle East sour crude oil flowing to the Asia-Pacific region) are other major benchmarks or references. The deposits for West Texas Intermediate (a very-quality, sweet, light oil delivered at Cushing, for North American) are found in Texas and Mexico. Tapis (from Malaysia, used as a reference for light Far East oil) Minas (from Indonesia), is used as a reference for heavy Far East oil.

Whereas for OPEC Reference Basket oil is sourced from Bonny light (Nigeria), Arab light (Saudi Arabia), Basra light (Iraq), Saharan blend (Algeria) and Minas (Indonesia). Although, Brent blend is graded as a light crude oil, it is not as light as (WT). Russian Export Blend, the Russian benchmark crude, is a mixture of several crude grades used domestically or sent for

export. Russian Export blend is a medium, sour crude oil with an APL gravity of approximately 32 and a sulphur content of 1.2%. It is used in countries like Augusta, Italy and Rotterdam, Netherlands, which act as the two primary points. Light, sweet crude is more expensive than heavier, sourer crude because it requires less processing and produces a slate of products with a greater percentage of value-added products such as gasoline, diesel, and aviation fuel. Heavier, sourer crude typically sells at a discount to lighter, sweeter grades since it produces a greater percentage of lower value-added products with simple distillation and require additional processing to produce lighter products [47].

Crude oil pollution causes among other things low permeability and low infiltration of water into the soil [13]. These conditions can lead to accumulation of water on the soil surface and artificial drought in the subsurface layer of soil. The growth of plant root into soil help to create pores in the soil and thereby enhance water penetration and infiltration in soil polluted with crude oil. Water: It is a fundamental requirement that liquefied petroleum gas should not contain free water (ASTM D-2713). Dissolved water may give trouble by forming hydrates and giving moisture vapor in the gas phase. Both of these will lead to blockages. Test methods are available to determine the presence of water using electronic moisture analyzers (ASTM D-5454), dew-point temperature (ASTM D-1142).

Sulfur Content: weight percentage of Sulfur content and API gravity are two properties which have had the greatest influence on the value of crude oil, although nitrogen and metals contents are increasing in Importance. The sulfur content is expressed as percent sulfur by weight and varies from less than 0.1% to greater than 5%. Crudes with greater than 0.5% sulfur generally require more extensive processing than those with lower sulfur content. Although the term "sour" crude initially had reference to those crudes containing dissolved hydrogen sulfide independent of total sulphur content, it has come to mean any crude oil with a sulfur content high enough to require special processing. There is no sharp dividing line between sour and sweet crudes, but 0.5% sulfur content is frequently used as the criterion.

Metallic Compounds: Metallic compounds exist in all crude oil types in very small amounts. Their concentration must be reduced to avoid operational problems and to prevent them from contaminating the products. Metals affect many upgrading processes. They cause poisoning to the catalysts used for hydro processing and cracking. Even minute amounts of metals (iron, nickel and vanadium) in the feedstock to the catalytic cracker affect the activity

of the catalyst and result in increased gas and coke formation and reduced gasoline yields. For high-temperature power generators, the presence of vanadium in the fuel may lead to ash deposits on turbine blades and cause severe corrosion, and the deterioration of refractory furnace linings.

Parts of the metallic constituents of crude oils exist as inorganic water-soluble salts, mainly as chlorides and sulphates of sodium, potassium, magnesium and calcium. These are removed in desalting operations. More important are metals which are present in form of oil-soluble organometallic compounds. Zinc, titanium, calcium and magnesium appear in the form of organometallic soaps. However, vanadium, nickel, copper and iron are present as oil-soluble compounds, capable of complexing with pyrrole compounds.

**Nitrogen Compounds:** Crude oils contain very low amounts of nitrogen compounds. Generally, the more asphaltic the oil, the higher its nitrogen content. Nitrogen compounds are more stable than sulphur compounds and therefore are harder to remove. Even though they are present at very low concentrations, nitrogen compounds have great significance in refinery operations. They can be responsible for the poisoning of a cracking catalyst, and they also contribute to gum formation in finished products.

#### 2.5.7 Chemical components

The most common elements in natural hydrocarbons are Carbon, Hydrogen, Nitrogen, Sulfur and Oxygen. These elements make up the main chemical components in hydrocarbons which can be divided into three groups: Paraffins, Naphthenes and Aromatics and examples of their structure are shown in Figure 2-6.

Crude oils are often characterized based on the amount of the different hydrocarbon compounds.  $n$  alkanes with the general formula  $C_nH_{2n+2}$  where  $n$  from 1 to 4 are gases,  $n$  from 5 to 15 are liquids and  $n$  above 15 are wax-like solids such as paraffin waxes. Paraffins are saturated, where the carbon atoms are arranged in chains by single bonds, both branched and straight. Naphthenes form a ring of carbonates saturated with hydrogen and has the general formula  $C_nH_n$  where  $n$  is 5, 6 or 7.

Aromatics contain at least one carbon ring, e.g. benzene  $C_6H_6$ , where every other bond is a double and single bond. Aromatics are undersaturated and may bond with hydrogen or other elements to the unsaturated ring. Paraffins are mineral oils known as lubricating oils.

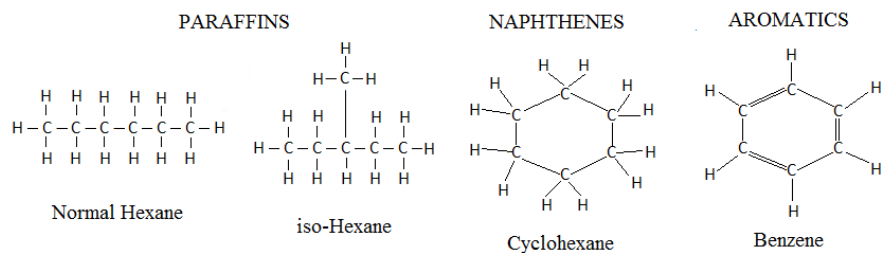


Figure 2-9 Examples of typical hydrocarbon components. Normal hexane and iso-hexane are paraffins. Cyclohexane belongs to the naphthenes, and aromatic benzene [51].

Non-hydrocarbon compounds can include any of the three hydrocarbon components mentioned above, but are considered to be non-hydrocarbons as they contain nitrogen, sulfur or oxygen in their molecular structure. Non-hydrocarbon compounds are often found in heavier crude oils. Resins and asphaltenes are large molecules with similar basic structure of rings, mostly aromatics. Resins dissolve in petroleum while asphaltenes are dispersed colloidal. Resins become asphaltenes by oxidation. The black color of heavy oils and bitumen compared to light oils are mainly due to presence of resins and asphaltenes.

## 2.5.8 Petroleum and petroleum products

### 2.5.8.1 Petroleum definition

Petroleum (also called crude oil) is a naturally mixture of hydrocarbons, generally in the liquid state, that may also include compounds of sulfur, nitrogen, oxygen, and metals and other elements (ASTM D-4175). Inorganic sediment and water may also be present.

The elementary composition of crude oil usually falls within the following ranges as shown on Table 2-4.

Petroleum is recovered mostly through oil drilling. Oil drilling comes after the studies of structural geology, sedimentary basin analysis, reservoir characterization (in terms of porosity and permeable structures). It is refined and separated, most easily by boiling point, into a large number of consumer products, from petrol (or gasoline) and kerosene to asphalt and chemical reagent used to make plastics and pharmaceutical [141].

**Petroleum Composition:** Petroleum is commonly known as crude oil which includes all liquids, gaseous and solid (such as paraffin) hydrocarbons. Lighter hydrocarbons methane, ethane, propane and butane, under surface pressure and temperature conditions; occur as gases, while

pentane and heavier ones are in the form of liquids or solids. The proportion of gas, liquid and solid in an underground oil reservoir, however, depends on the subsurface conditions and on the phase diagram of the petroleum mixture.

The proportion of light hydrocarbons in the petroleum in the petroleum mixtures varies greatly among different oil fields, ranging from 97 per cent by weight in the lighter oils to 50 per cent in the heavier oils and bitumen. The hydrocarbons in crude oil are mostly alkanes, cycloalkanes and various aromatic hydrocarbons while the other organic compounds contain nitrogen, oxygen and sulphur and trace amounts of metals such as iron, nickel, copper and vanadium. The exact molecular composition varies widely from formation to formation but the chemical elements proportions vary uniformly (Table 2-1).

Table 2-4. Composition of hydrocarbon elements by weight

<b>Element</b>	<b>Percentage range %</b>
Carbon	83 to 87
Hydrogen	10 to 14
Nitrogen	0.1 to 2
Oxygen	0.05 to 1.5
Sulphur	0.05 to 6
<b>Metal</b>	<b>&lt;0.1</b>

Petroleum is used mostly, by volume, for producing fuel oil and petrol, very important primary energy sources. 84 per cent by volume of the hydrocarbons contain in petroleum is converted into energy-rich fuels (petroleum-based fuels), which includes petrol, diesel, jet, heating and other fuel oils as well as liquefied petroleum gas. Lighter grades of crude oil produce the best yields of petroleum-based fuels. Oil refineries are increasingly processing heavy oil and bitumen using more complex and expensive methods to produce the products required as the world's reserves of light and medium oil are depleted. Heavier crude oils have too carbon and less hydrogen, these processes generally involve removing carbon from or adding hydrogen to the molecules, using fluid catalytic cracking to convert the longer, more complex molecules in the oil to shorter, simpler ones in the fuels.

Oil has become the world's most important source of energy since the mid-1950s due to its high energy density, easy transportability and relative abundance. Petroleum is also the raw material for many chemical products such as pharmaceuticals, solvents, fertilizers, pesticides and plastics. Petroleum is found in porous rock formations in upper strata of some areas of the

Earth's crust. There is also petroleum in oil sands (tar sand) with estimates of  $190\text{km}^3$  (1.2 trillion) barrels without sand and  $595\text{ km}^3$  (3.74 trillion barrels) with oil sand.

#### 2.5.8.2 Chemistry of Petroleum

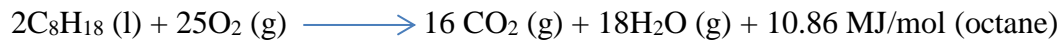
Petroleum is a mixture of a very large number of different hydrocarbons; the most commonly found molecules are alkanes (linear or branched), cycloalkanes, aromatic hydrocarbons and complicated chemicals like asphaltenes. Each petroleum variety has a unique mixture of molecules, which define its physical and chemical properties (e.g. colour and viscosity). The alkanes, known as paraffin, are saturated hydrocarbons with straight or branched chains which contain only carbon and hydrogen with general formula  $\text{C}_n\text{H}_{2n+2}$ . They generally have from 5 to 40 carbon atoms per molecule with trace amounts of shorter or longer molecules present in the mixture.

The alkanes (or straight and branched-chain alkanes) from propane ( $\text{C}_3\text{H}_8$ ), pentane ( $\text{C}_5\text{H}_{12}$ ) to octane ( $\text{C}_8\text{H}_{18}$ ) are refined into petrol, the ones from nonane ( $\text{C}_9\text{H}_{20}$ ) to hexadecane ( $\text{C}_{16}\text{H}_{34}$ ) into diesel fuel, kerosene and jet fuel. Alkanes with more than 16 carbon atoms can be refined into fuel oil and lubricating oil. Paraffin wax is an alkane with close to 25 carbon atoms, while asphalt has 35 and above, they are usually cracked by modern refineries into more valuable products. The shortest molecules, those with four or fewer carbon atoms, are in a gaseous state at room temperature. They are the petroleum gases. Depending on the cost of recovery and demand, these gases are either flared off, or sold as liquefied petroleum gas under pressure or used to power the refinery's own burners. Butane ( $\text{C}_4\text{H}_{10}$ ), during the winter, is blended into the petrol pool at high rates, since butane's high vapor pressure assist with cold starts. Butane, when liquefied under pressure slightly above atmospheric, is used for powering cigarette lighters. It is also a main fuel source for many developing countries. Propane can be liquefied under modest pressure and is consumed as petroleum for energy as well as in other applications like cooking, heating and transportation.

The cycloalkanes, known as naphthenes, are saturated hydrocarbons which have one or more carbon rings in which hydrogen atoms are attached according to formula  $\text{C}_n\text{H}_{2n+2}$ . Cycloalkanes have similar properties to alkanes except that Cycloalkanes have higher boiling points.

The aromatic hydrocarbons are highly unsaturated hydrocarbons which have one or more planar six-carbon rings called benzene rings, to which hydrogen atoms are attached with the formula,  $\text{C}_n\text{H}_n$ . Aromatic hydrocarbons include also toluene, ethyl benzene, and xylene

(collectively known as BTEX). When carbon atoms are shared between rings, compounds are called polycyclic aromatic hydrocarbons (PAHs). They tend to burn with a sooty flame and many have a sweet aroma while some are carcinogenic. These different molecules are separated by fractional distillation at an oil refinery to produce, petrol, jet fuel, kerosene and other hydrocarbons. Example, 2, 2, 4-Trimethylpentane (isooctane), widely used in petrol, has a chemical formula of  $C_8H_{18}$ , it reacts with oxygen exothermically [141].



The amount of various molecules in an oil sample can be determined in laboratory. The molecules are extracted in a solvent, then separated in a gas chromatograph and finally determined with a suitable detector, such as a flame ionization detector or a mass spectrometer. As a result of the large number of co-eluted hydrocarbons within oil, many cannot be resolved by traditional gas chromatography which appears as a hump in the chromatogram. This unresolved complex mixture of hydrocarbons is especially apparent when analysing weathered oils and extracts from tissues of organisms exposed to oil. Incomplete combustion of petroleum results in production of toxic by-products. Too little oxygen results in carbon monoxide. Exhaust gases from petrol combustion in car engines which includes nitrogen oxides that are responsible for creation of photochemical smog due to the high temperatures and pressures involved. Octane known as paraffin wax or paraffin oil. Octane is found in UK, Ireland and South African as paraffin oil which is called Kerosine in US, Canada, Australia etc. The property of this organic compound can be found on Table A-3 in Appendix A-3.

### 2.5.8.3 Chemical Compounds and Wettability

Chang et.al investigated the effects of crude oil components on soil wettability. The heavier components in crude oil can change the wettability of a reservoir when in contact with the reservoir soil for a longer period of time. Polar compounds containing nitrogen, sulfur and oxygen were found to alter wettability. As the fraction of higher boiling point compounds increased the wettability of the sand stone increases also. The wettability was altered to less water-wet.

Brief origin of crude oil: There are five geological features that have to be in place in the correct sequence for hydrocarbon to be trapped in a soil reservoir. These are a good source, a migration pathway, a reservoir, a trap and a seal, the source of hydrocarbon is sediment with a high content of biogenic decay deposited in a low-energy environment. If the biological material is buried and exposed for a certain range of temperature and pressure through geological time then hydrocarbons can be generated (biogradation). After migration from the source due to



buoyancy the hydrocarbons hopefully enters a storage unit, i.e. a reservoir which is a porous and permeable rock. A trap is needed to accumulate the hydrocarbons in the reservoir. The seal prevent further upward fluid migration. The seal is often a zone with low permeability. The reservoir is typically sandstone with good permeability and with a reservoir temperature of 40 - 60 °C.

#### 2.5.9 Recovery of crude Oil

How easily a fluid flows in the reservoir can be expressed by its mobility which is a function of both fluid and soil properties. Mobility of a phase is the ratio of the effective permeability to the viscosity of that phase, i.e. mobility is inversely proportional to the viscosity. The lower the mobility value the less mobile the in-situ fluid is in the soil reservoir for most crude oil reservoirs the low mobility is often the main challenge in production.

#### 2.5.10 Use of Nanotechnology as Enhanced Oil Recovery

Nanotechnology may have the solution to several challenges faced by the oil industry today, and it ranges from finding the oil, drilling wells for production, the extraction process through field life and the process facilities and transport. Above all, cleaning oil spillages and refineries with nanotechnology.

Nanotechnology is engineering of functional systems at the molecular scale. Nanotechnology can refer to measurement or visualization at the scale of 1-100 nanometers.

#### 2.5.11 Nanoparticles and Nano fluids

##### 2.5.11.1 Backgrounds

Nanoparticles are very small nanometer sized particles with dimensions 1-100 nm (nanometers) in size. Some of the common oxide nanoparticles being used in heat transfer research are: Zinc Oxide (ZnO), Zirconia (ZrO<sub>2</sub>), Copper Oxide (CuO), Silica (SiO<sub>2</sub>), Aluminum Oxide (Al<sub>2</sub>O<sub>3</sub>), and Titanium Oxide (TiO<sub>2</sub>) while some of the metal nanoparticles are Gold (Au), Silver (Ag), and Copper (Cu). Conventional fluids being mixed with nanoparticles are: water, ethylene glycol, and oil.

Water is a convenient and safe medium; however, it has poor heat transfer characteristics which are a major disadvantage. For example, water is roughly three orders of magnitude poorer in heat conduction than copper; as is the case with coolants such as engine coolants, lubricants, and organic coolants. The use of nanofluids (nanoparticles + conventional fluids), like water,

may possess the ability to increase the convection heat transfer characteristics of that particular fluid.

Nanofluids are dilute liquid suspensions of nanoparticles with at least one critical dimension smaller than 100nm. A nanofluid is a mixture of liquid and nanoparticles. Nano-particles suspended in base fluids is a new Innovative called 'nanofluids'. These nano-particles were make changes in the thermal and transference properties of the base fluid. Much attention has been paid in the past decade to this new type of composite material which has enhanced properties and behaviour associated with heat transfer [80, 25], mass transfer [70], wetting and spreading [136], antimicrobial activities [148], and the number of publication related to nanofluids increases in an exponential manner.

Nanofluids are also important for the production of nanostructure materials [65], for the engineering of complex fluids [127a] as well as for cleaning oil from surface due to their excellent wetting and spreading behaviour [136]. Despite considerable research effort and significant progress in the past decade, the fundamental understanding of Nanofluids is limited. This is indeed reflected in the scattering/disagreement of published works and less convincing arguments in experimental data. It is fair to say that there is a long way to go before we can actually tailor-make nanofluids for targeted applications. Advanced material engineering techniques can structure surfaces that allow dynamic turning of their wettability all the way from super hydrophobic/ water hating (i.e repelling) behaviour to almost complete wetting equipment (i.e. super hydrophilic/ water loving or strongly absorbing) , but these surfaces only work with high surface-tension liquids. Almost all organic liquids that are ubiquitous (seeming to be in all places) in human environment such as oils, solvents, detergent etc. have fairly low surface tensions and thus readily wet even super hydrophobic surfaces [82].

Nanofluids are emerging as one of the most promising cooling reagent in the present world; Alumina has been used by many researchers as nanoparticles because of its stability and can dispersed easily in water, thus forming colloidal solution. Silver and gold though have higher thermal conductivities; they are much more expensive than alumina. Copper oxide, though not very unstable, requires a dispersant to form a colloidal solution with the base fluid. Carbon Nano Tubes have high thermal conductivity but it is difficult to disperse them in base fluid as they entangle and agglomerate to settle [4].

A new type of fluids, which can be labelled as “smart fluids” is becoming increasingly available to the oil and gas industry. These nanofluids are designed by adding nano-fabricated particles to a fluid in order to enhance or improve some of its properties. Essential nano scale particles are suspended in the liquid phase in low volumetric fractions. The liquid phase can be any liquid such as oil, water or conventional fluid mixtures. The nanoparticles used in the design of such fluids are preferably inorganic with properties of no dissolution or aggregation in the liquid environment. They can be designed to be compatible with reservoir fluids and are environmentally friendly.

Recent experiments have shown some promising nano fluids with amazing properties such as fluids with advanced drag reduction, binders for sand consolidation, gels, products for wettability alteration and anticorrosive coating [136].

Gardea-Torresdey et.al [62] carried out research in order to better understand that why the thermal conductivity of nano fluids increases with the decrease in the particle size of the nanoparticles. They explored four possible causes, i.e., Brownian motion of the particles, molecular level layering of the liquid at the liquid particle interface, the nature of heat transport in nanoparticles and the clustering of nanoparticles.

Palma et.al [130] investigated theoretical reasons for heat transfer enhancement in nanofluids by applying hyperbolic heat conduction constitutive relationship and comparing the same with the corresponding Fourier conduction results. They proposed that the hyperbolic thermal conduction was the reason behind high heat transfer in nanofluids.

Gupte, et al [72] in their investigation on copper oxide-ethylene glycol nano fluids observed that the thermal conductivity with respect to particle concentration is attainable only when concentration is below the dilute limit of  $3\phi$ , with  $\phi$  denoting the nanoparticle volume fraction. Volume fraction at dilute limit is 0.002. Therefore dilute limit is 0.006. Well-dispersed and stable nanofluids are formed after properly dispersing nanoparticles into base fluids and the resulting nanofluids are expected to exhibit several beneficial features: a) High stability of nanofluids. Because the nanoparticles are small, the particles are stably staying in the liquid phases for months or even years without sedimentation. Brownian motion (the random thermally driven movement of particles suspended in a fluid) can increase the stability of the suspension.

b) Greatly improved heat conduction. Nanofluids demonstrate higher thermal conductivities than the base fluid due to several factors. The large surface area of nanoparticles per unit volume allows for more heat transfer between solids particles and base fluids. Another advantage is that the high mobility of the nanoparticles due to the tininess, which may introduce micro-convection of fluids to further stimulate heat transfer.

c) Elimination of clogging. Nanoparticles are only composed of hundreds or thousands of atoms, about 1 ~ 100 nm in diameter and are well-dispersed in nanofluids, so that they will not causing any clogging problem. Nanofluids can therefore be used in microchannels, which can further promote the heat transfer rate by combining enhanced thermal conductivity of fluids and increased ved heat conduction.

Choi, [36b] stated fluids such as water, oil, and ethylene glycol are poor heat transfer properties and they are widely used in many industries nowadays. Nanofluids are modern heat transfer fluids organized by dispersing metallic or non-metallic nanoparticles into fluid. Many researchers demonstrated that nanofluids have created a variety of advantages, such as better long-term stability, greater thermal conductivity compared with millimeter or even micrometer sized particle.

Nanofluid is a pioneering heat transfer fluid with better potential for enhancing the heat transfer performance and cleaning properties. Many pioneers have been made to study its thermophysical properties which is important before determine the heat transfer performance.

Basically, the main idea is to disperse small solid particles in common base liquids in order to enhance their heat transfer properties. However, before starting to determine the heat transfer performance of nanofluids, it is necessary to know about their thermophysical properties.

Know that, viscosity, density and specific heat are the most important transport properties of nanofluids. From the researcher, [94] stated that publications about the viscosity and specific heat of nanofluids are still bare compared with thermal conductivity properties. From the theoretical, [94] also stated that a nanofluid represents a fascinating new challenge to researchers in fluid dynamics and heat transfer because of the fact that it appears very difficult, if not practically impossible, to formulate any theory that can reasonably predict behaviors of a nanofluid by considering it as a multi-component fluid.

Chandrasekar et al [31] found that, in general, dynamic viscosity of nanofluid increases considerably with particle volume concentration but clearly decreases with a temperature

increase. Then, they also state that the hysteresis phenomenon has raised serious doubts regarding the reliability of using nanofluids for heat transfer enhancement purposes.

### Properties of Nanofluids

A fluid is any substance which flows because its particles are not rigidly attached to one another. The properties outlined below are general properties of fluids which are of interest in engineering. These properties can readily be found at many reference books.

### Viscosity

Viscosity is one of the properties that is needed to know to determine the heat transfer rate of a fluid. Viscosity is a scientific term describing the internal friction of a fluid or gas. Both have adjacent layers, and when pressure is applied, the friction between layers affects how much the substance will respond to external force. [195] said in his book, viscosity, in its simplest form, can be evaluated by the thickness of a substance. A general rule is that gases are less viscous than liquids, and thicker liquids exhibit higher viscosity than thin liquids.

### Density

Yunus A. Cengel [195] also explicitly discusses a material's density and it is defined as its mass per unit volume. It is, essentially, a measurement of how tightly matter is crammed together or can also refer to how closely "packed" or "crowded" the material appears to be. For example: A rock/soil is obviously denser than a crumpled piece of paper of the same size. This can be simplified to the equation below. The unit of density is  $\text{kg/m}^3$ .

$$\rho = \frac{m}{V} \quad (2.1)$$

$m$  = mass of the object

$\rho$  = density of the object

$V$  = volume of the object

### Specific heat capacity

The other property that is important to determine before conducting the experiment to predict the heat transfer of fluid as a cooling agent. Specific heat is defined as the ratio of the amount of heat required to raise the temperature of a unit mass of a substance by one unit of temperature

to the amount of heat required to raise the temperature of a similar mass of a reference material, usually water, by the same amount.[151] said it is also can be define as the amount of heat, measured in calories, required to raise the temperature of one gram of a substance by one Celsius degree.

There are two types of specific heat which are specific heat at constant pressure,  $c_p$  and specific heat at constant volume,  $c_v$ . [195] define the specific heat at constant volume,  $c_v$  can be viewed as the energy required to raise the temperature of a unit mass of as substance by one degree as the volume is constant. The energy required to do the same as the pressure is held constant is the specific heat at constant pressure  $c_p$ . Common unit is  $\text{kJ/kg}\cdot^\circ\text{C}$  or  $\text{kJ/kg}\cdot\text{K}$ . Notice that  $\Delta T(^{\circ}\text{C}) = \Delta T(\text{K})$  and  $1^{\circ}\text{C}$  change in temperate is equivalent to a change of 1K.

There are many types of nanoparticles examples, carbon nanotubes, aluminium, alumina, zinc, zinc oxide, gold nanoparticles, silver nanoparticles, diamond, tin oxide, metal oxides etc. Studies has shown that a mixture of Nano scale  $\text{SiO}_4$  and  $\text{TiO}_4$  can increase nitrate reductase activity in Soybean, enhance its ability to absorb and utilize water and fertilizer, stimulate its antioxidant system and hasten its germination and growth [152] Nano- $\text{TiO}_2$  has further been reported to promote photosynthesis and nitrogen metabolism, and thus greatly improve growth of spinach at certain concentration.

So far no general mechanisms have been formulated to explain the strange behaviour of the nanofluids [143] including the highly improved effective thermal conductivity, although many possible factors have been considered, including Brownian motion, liquid-solid interface layer and surface charge state. Currently there is no reliable theory to predict the anomalous thermal conductivity of nanofluids satisfactorily. From the experimental results of many researchers, it is known that thermal conductivity of nanofluids depends on parameters including the thermal conductivities of the base fluid and the nanoparticles, the volume fraction of the nanoparticles, the surface area, and the shape of the nanoparticle and the temperature [133]. Recent research of nanofluids has offered particle clustering as a possible mechanism for the abnormal enhancement of thermal conductivity when nanoparticles are dispersed in the liquids [102].

## 2.6 Preparation of nanofluids

There are two primary methods to prepare nanofluids: Single or one-step methods and two-step methods.

### 2.6.1 Production of Nano fluids

Nano fluids preparation using Dispersion method, also called two-step method, is generally favoured for preparing nano fluids containing high volume fraction metals, oxides and carbon nanotubes. Here the dry nano powder is dispersed in the liquid by application of one or many dispersion techniques [88]. This method is more economical in comparison to one-step method, due to the low cost of nano powders in the market. Decline of the price of nano powders is a result of the rapid development of high throughput nanoparticle production technologies over the years. Nano fluids prepared by dispersion method, however commonly have shown a stability problem [88]. These Nano fluids gradually start to settle after a period of time depending on the properties of base liquid, surfactant or dispersant used type of nanoparticles and the likelihood of nanoparticles to aggregate. The validity of a nano fluid is as only long as it is stable.

An agglomerated nano fluid is different in properties, and may cause operational problems similar to those encountered with micron-sized particulate suspensions; sedimentation and clogging of the system. Unstable nano fluids moreover are most likely a root cause for the wide discrepancies in literature data on their heat transfer behaviour.

#### 2.6.1.1 One-Step Methods

The nanoparticles may agglomerate during the drying, storage, and transportation process, leading to difficulties in the following dispersion stage of two-step method. Consequently, the stability and thermal conductivity of nanofluid are not ideal. In addition, the production cost is high. To reduce the agglomeration of the nanoparticles, one-step methods have been developed. There are some ways for preparing nanofluids using this method including direct evaporation condensation [69, 38, 39] chemical vapour condensation [121] and single-step chemical synthesis. The nanofluids are homogenized with or without surfactants depending on the interface properties of between nanoparticles and base fluids. This method is mainly limited by the availability of nanoparticles

### 2.6.1.2 Two-Step Methods

Several studies, including the earliest investigations [76] of nanofluids, used a two-step process in which nanoparticles are first produced as a dry powder. This method is more extensively used to produce nanofluids because nanopowders are commercially available nowadays. Some authors suggested that two-step process is very suitable to prepare nanofluids containing oxide nanoparticles than those containing metallic nanoparticles [56b].

Stability is a big issue that inherently related to this operation as the powders easily aggregate due to strong van der Waals force among nanoparticles. In spite of such disadvantages this process is still popular as the most economic process for nanofluids production.

There are also three methods of preparing nanofluids, namely ballmilling. This method is used in the one-step method of preparing nanofluids. It is the poorest method of preparing nanofluids because there is some extent you can not reduce particle size into powder. The nanofluid tends to aggregate very easily. The second is ultrasonification method which is good but the best method is pressure homogenization method.

Kelvin [85] prepared Copper oxide and Aluminium oxide nanofluids by the introduction of each of the nanofluid to the tank of water caused an immediate discoloration of the water. For example, when the CuO nanofluid was introduced to the water, the water turned a dark dirty brown and when the Al<sub>2</sub>O<sub>3</sub> nanofluid was introduced to the water it turned a silvery color even though the concentrations were extremely low (2g of nanoparticles in 6 liters of water & 4 grams of nanoparticles in 6 liters of water).

A variety of physical, chemical, and laser-based methods are available for the production of the nanoparticles to be used for nanofluids [1, 2] [28a].

### 2.6.2 Stability of nanofluids

The production of a nanofluid faces some major challenges such as agglomeration of particles in solution due to very strong van der Waals interactions and the rapid settling of particles in fluids. The special requirements for preparation of a nanofluid are durability and stability of suspension with low agglomeration of particles, and no chemical change of the fluid [128a]. Stability of a nanofluid is strongly affected by the characteristics of the suspended particles and base fluids such as the particle morphology and the chemical structure of the particles and base fluid [57]. In order to make a stable suspension, one should reduce the density difference between the particles and the fluid, increase the viscosity of the fluid, and make the



particles very small to prevent agglomerating [22]. Stability of any liquid is a homogenized mixed solution. I.e, it is in equilibrium between liquid phase and solid phase.

### 2.6.3 Methods of Improving the Stability of a Nanofluid

To obtain stable nanofluids, several methods such as electrical, physical, or chemical [30] are used. General common methods are:

(1) Controlling the surface charge of the nanoparticles by controlling the pH. The stability of a nanofluid directly links to its electrokinetic properties. Through a high surface charge, density, strong repulsive forces can stabilize a well-dispersed suspension [46]. As the pH of the solution departs from the isoelectric point (IEP) of particles, the colloidal particles get more stable [145] and [75]. The IEP is the concentration of potential controlling ions at which the zeta potential is zero. Thus, at the IEP, the surface charge is zero.

(2) Modifying the surface by addition of some surfactants: This is one of the general methods to avoid sedimentation of nanoparticles. Surfactants can modify the particles-suspending medium interface and prevent aggregation over long time periods. The reason is that the hydrophobic surfaces of nanoparticles/nanotubes are modified to become hydrophilic and *vice versa*. Selection of suitable surfactants and dispersants depends mainly upon the properties of the solutions and particles.

Surfactant molecules adsorbed on the nanoparticle's surface can decrease the surface energy and thus prevent the agglomeration of particles. Popular surfactants that have been used in literature can be listed as sodium dodecylsulfate [61], sodium dodecylbenzenesulfonate [135b], cetyltrimethylammoniumbromide [14], dodecyltrimethylammonium bromide, sodium octanoate [78] and polyvinylpyrrolidone [150]. Adding surfactants restricts the application of nanofluids at high temperatures [149] when the bonding between surfactant and nanoparticles is damaged and hence, the nanofluid loses its stability and sedimentation of nanoparticles occurs [133].

The use of additives (surfactants) is a technique applied to enhance the heat transfer performance of base fluids.

(3) Using ultrasonic vibration. Ultrasonic bath, processor, and homogenizer are powerful tools for breaking down the agglomerations in comparison with other methods like magnetic and high shear stirrer as experienced by researchers [46]. Each of the above techniques or

combination of them such as simultaneous use of ultrasonic agitation and addition of surfactants are sometimes used to minimize particle aggregation and to improve dispersion behaviour. The best way to produce a stable suspension may be a single-step method where instead of nanoparticles; nanofluids are produced directly, thus reducing the chance of agglomeration [30].

#### 2.6.4 Stability Evaluation

The Derjaguin-Landau-Verwey-Overbeek (DLVO) theory [32b] and [130b] for colloidal interactions dictates that a colloidal system will remain stable if and only if the columbic repulsion, arising from the net charge on the surfaces of the particles in a colloid, is greater than the van der Waals forces.

When the reverse is true, the colloidal particles will cluster together and form flocculates and aggregates. Although the stability of nanofluids is very important for their applications, there are limited studies on estimating the stability of a suspension. There are some ways for evaluating the stability of a nanofluid:

[25] Measuring the zeta potential which is the overall charge that a particle acquires in a specific medium and is a good [52] indicator for the colloidal stability of a nanofluid [96b]. The higher the absolute zeta potential, the stronger the columbic repulsion between the particles, and therefore, the lower impact of the van der Waals forces on the colloid. Zetapotential measurement is one of the most critical tests to validate the quality of the nanofluids stability via a study of its electrophoretic behaviour [130a].

(2) Measuring particle size distribution by transmission electron microscopy (TEM) or light scattering methods. The nanofluid becomes more stable when nanoparticles have narrow particle size distribution.

(3) UV-Vis spectrophotometric measurements. UV-Vis analysis is an efficient way to evaluate the stability of nanofluids. If nanomaterials dispersed in fluids have characteristic absorption bands in the wavelength range of 190-1100 nm, it is an easy and reliable method to evaluate the stability of nanofluids using UV-Vis spectral analysis. The variation of supernatant particle concentration of nanofluids with sedimentation time can be obtained by the measurement of absorption of nanofluids because there is a linear relation between the supernatant nanoparticle concentration and the absorbance of suspended particles. The outstanding advantage of UV-Vis spectral analysis compared to other methods is that it can present the quantitative concentration

of nanofluids [147a]. The first work to quantitatively characterize colloidal stability of the dispersions of CNT by UV-Vis scanning spectrophotometric measurements was reported by [61]. However, this method is unsuitable for high concentration of nanofluids because these dispersions are too dark to differentiate the sediment visibly [46].

Absorbance is a material's ability to soak up a liquid. Example, nanoparticle and water. Absorbance indicates the stability of a solution in terms of wavelength. Typically, absorbance of a dissolved substance is measured using absorption spectroscopy/UV-Vis spectrophotometer. This involves shining a light through a solution and recording how much light and what wavelengths were transmitted onto a detector. Solutions are placed in a small cuvette cell and inserted into the holder. The UV-Vis spectrophotometer is controlled through a computer and, once you "blank" it, will automatically display the absorbance plotted against wavelength.

(4) Cryogenic electron microscopy (Cryo-TEM, Cryoscanning electron microscopy) is another efficient method to distinguish the shape, size, distribution, and aggregation of nanoparticles in a fluid if the microstructure of nanofluids is not changed during cryoation [142].

#### 2.6.5 Surfactants

A surfactant is surface active agent, or wetting agent, capable of reducing the surface tension of a liquid. Surfactant is force acting on a liquid surface, minimizing the surface area. Surfactants are compounds that lower the surface tension of a liquid, the interfacial tension between two liquids, or that between a liquid and a solid. Surfactants may act as detergents, wetting agents, emulsifiers, foaming agents, and dispersants.

There are essentially three types of surfactants - anionic, cationic and non-ionic.

**Anionic surfactants** have a negatively charged ion. Common types include soaps and alkyl benzene sulfonates.

**Cationic surfactants** have a positively charged ion. Common types include alkyl ammonium chlorides.

**Non-ionic surfactants** have a polar, but uncharged, ion. Common types include polyethylene ethoxylates. When a single surfactant molecule exhibit both anionic and cationic dissociations, it is called amphoteric or Zwitterionic.

Polymeric surfactants or surface active (surface) polymers which result from the association of one or several macromolecular structure exhibiting hydrophilic and lipophilic characters. They

are commonly used in formulating products such as cosmetics, paints, foodstuffs and petroleum production additives.

Sodium hexametaphosphate is a hexamer of composition  $(\text{NaPO}_3)_6$ . Sodium hexametaphosphate of commerce is typically a mixture of polymeric metaphosphates, of which the hexamer is one, and is usually the compound referred to by this name. Sodium hexametaphosphate is used to disperse the different nanofluids used in the experiments.

#### Thermophysical properties of nanofluids

Thermal conductivity, viscosity, density, specific heat, and surface tension of the nanofluids have been investigated up to now as the physical properties of nanofluid.

#### 2.6.6 Thermal Conductivity:

Among all the physical properties of nanofluids, the thermal conductivity is the most complex and for many applications the most important one [69b]. By suspending some of the nanoparticles in heating or cooling fluids, the heat transfer performance of the fluid can be improved significantly. The main reasons of such enhancement may be listed as follows [145b]:

1. The suspended nanoparticles increase the surface area and the heat capacity of the fluid.
2. The suspended nanoparticles increase the effective (or apparent) thermal conductivity of the fluid.
3. The interaction and collision between particles and fluid are intensified.
4. The mixing fluctuation and turbulence of the fluid are intensified.
5. The dispersion of nanoparticles flattens the transverse temperature gradient of the fluid.

From the experimental results of many researchers, it is known that the thermal conductivity of nanofluids depends on many parameters including:

Thermal conductivity of base fluid: [85b] measured some physicochemical properties including thermal conductivity, viscosity, and surface tension of ZnO nanoparticles in ethylene glycol and glycerol as base fluids. They found that the enhanced thermal conductivity ratio decreases with increasing thermal conductivity of the base fluid.

2. Thermal conductivity of nanoparticles: The thermal conductivity of a nanofluid containing a metal is greater than that of oxide of that metal at the same conditions [87b].
3. Volume fraction: The thermal conductivity of a nanofluid is strongly dependent on the nanoparticle volume fraction [145b]. [146a] measured thermal conductivity enhancements of

nanodiamond particles suspended in deionized water with different volume fractions in the range from 0.8% to 3%. They observed the highest enhancement in the thermal conductivity (7.2%) for a volume fraction of 3% (ie enhanced thermal conductivity increased with increase in concentration of nanoparticles suspended in deionized water).

2.6.7 Heat Transfer: An investigation in heat transfer characteristics with nanofluids has revealed that when nanoparticles are introduced to a conventional fluid in certain concentrations they enhance the ability to transfer heat. Water is a very common fluid used in heat transfer applications; therefore the data collected from many experiments proved that nanofluids are a viable option in heat transfer applications. A research conducted using a heated aqueous mixture of aluminum and copper oxide nanoparticles was passed through helical coiled copper tubing (heat exchanger) while being cooled by a fan [64]. Measured data from this research were temperature and flow to determine Reynolds Number and heat transfer rate.

Nanoparticles are very small nanometer sized particles with dimensions 0.1-1000 nm (nanometers) in size. Some of the common oxide nanoparticles being used in heat transfer research are: Zinc Oxide (ZnO), Zirconia (ZrO<sub>2</sub>), Copper Oxide (CuO), Aluminum Oxide (Al<sub>2</sub>O<sub>3</sub>), and Titanium Oxide (TiO<sub>2</sub>) while some of the metal nanoparticles are Gold (Au), Silver (Ag), and Copper (Cu). Conventional fluids being mixed with nanoparticles are: water, ethylene glycol, and oil.

Water is a convenient and safe medium; however, it has poor heat transfer characteristics which are a major disadvantage. For example, water is roughly three orders of magnitude poorer in heat conduction than copper; as is the case with coolants such as engine coolants, lubricants, and organic coolants. The use of nanofluids (nanoparticles + conventional fluids), like water, may possess the ability to increase the convection heat transfer characteristics of that particular fluid.

As fluids stream through a heat exchanger, the flow can be two distinct types: laminar or turbulent. Laminar flow is smooth and the fluid moves in layers or paths parallel to each other and leads to low heat transfer rates. In turbulent flow, the layers of fluid mix until they are no longer distinguishable and leads to higher heat transfer rate. Deficiencies in efficient heat transfer rates should be a result of design flaws in the exchanger, not an effect of nanofluids. This section will review recent research of flow characteristics within heat exchangers, the understanding of Reynolds number, and the influence of nanoparticles on

modern heat exchange research with respect to thermal conductivity and viscosity. Although research has been conducted on heat exchange designs for a long time, the field of nanofluids with respect to heat exchange transfer is relatively new. Current research indicates, however, that nanoparticles do not pose a problem to heat transfer designs.

Currently, researchers [61b] are conducting experiments to examine the effects of the nanoparticles dispersed into the fluid. Experiments are being conducted routinely with helical coiled tubing. These experiments are being conducted because most heat exchangers, condensers, and steam generators are constructed with helical coiled tubing. The helical coiled tubing presents an interesting challenge because of the effects of centrifugal force through the radial sections, especially in small radial bends. The centrifugal force causes the fluid to become unstable resulting in a Reynolds number that is no longer a constant value when transitioning from laminar to turbulent flow.

The hydraulic performance is influenced by centrifugal force and that has a pronounced effect on the Reynolds number by causing it to increase significantly.

All et.al [9] conducted hydrodynamic experiments on spiral coiled tubing referred to as ascending equiangular spiral tube coils. Equiangular spiral tube coils are spirals with no constant pitch but varies along the length of the spiral whereas an Archimedian spiral has a constant pitch. They wrote how the helical coil and spiral coil differ in flow characteristics because the coil curvature remains constant which produces fully developed downstream flow. The spiral coil, with its nonconstant spiral pitch and varying curvature, does not produce a fully developed flow but instead creates a secondary flow that varies intensity. Therefore; they determined there was a need for a calculation for critical Reynolds number that incorporated the Reynolds numbers calculation for both straight and helical coiled tubing. The following equation was also a basis for this experiment:

$$\text{Critical Re} = 2100 [1 + 12\{d/2(R_{\max})\}^{0.5}] \dots\dots\dots (2.11)$$

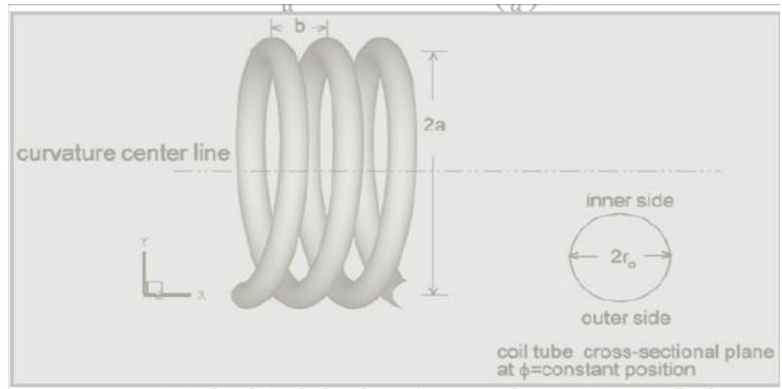


Figure 2-10 Helical Coiled Tubing (Heat Exchanger) Layout [69c]

Thermal Conductivity of nanofluids has been debated for years with many different experiments being conducted to determine the many different factors, like Reynolds number, or heat transfer coefficient, or heat transfer rate at laminar and turbulent flow rates. In theoretical models A.K.Singh [120b] remarks that thermal conductivity depends on nanoparticle size, material, and concentration.

### 2.6.8 Contact Angle

One of the fundamental methods of characterizing the properties of pure/Surfacted nanofluid is to determine the contact angle. The contact angle is a measure of the wetting behavior of a particular liquid (ie nanofluid or water) on the surface (a glass slide) under investigation and directly relates to the interfacial energies of the systems. The contact angle on the solid surface gets changed merely by changing the chemistry of the outermost monolayer [77], [99].

It can be defined geometrically as the angle formed by a liquid at the three phase boundary where a liquid, gas and solid intersect as shown below:

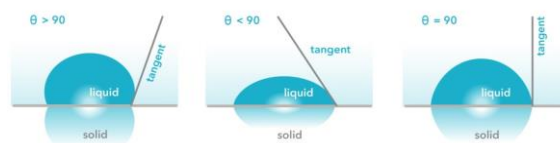


Figure 2-11 A water droplet in equilibrium over a horizontal solid surface

It can be seen from the Figure 2.8 that a low values of contact angle ( $\theta$ ) indicates that the liquid spreads, or wets well i.e. hydrophilic nature of surface of solid under test, while a high contact angle indicates poor wetting. If the angle  $\theta$  is less than  $90^\circ$  the liquid is said to wet the solid. If it is greater than  $90^\circ$  it is said to be non-wetting i.e. hydrophobic nature. A zero contact angles represents complete wetting.

### 2.6.9 Porosity and contact angle

Contact angle on a smooth surface ( $\Theta$ ) for which a porous substrate with pore fraction  $f_i$  will be wetted ( $\Theta'=90^\circ$ ) is shown on Table 2-5

Table 2-5 Porosity and contact angle values

Porosity ( $f_1$ )	Contact angle $\Theta^\circ$	Porosity ( $f_2$ )	Contact angle $\Theta^\circ$
0	90	0.45	35
0.2	75	0.48	23
0.4	48	0.5	0

This can be understood by the following relation, derived by Cassie and Batter (121):

$$\cos\Theta' = f_1 \cos\Theta - f_2, \dots\dots\dots (2.12)$$

$f_1$  and  $f_2$  are the fractions of the composite surface which are liquid-solid and liquid-air, respectively. This equation can only be used if  $f_2 < f_1$ . In the other case ( $f_2 > f_1$ )  $\cos\Theta$  would be smaller than zero, which means that  $\Theta$  is always larger than  $90^\circ$ . This should mean that such a surface could never be wetted. However, it can be easily understood that, if  $\Theta$  becomes zero or approaches zero, the surface of the material (even inside the pores) becomes completely wetted.

### 2.7 Application of Nano fluids

These are fluids with a colloidal dispersion of nanometer-sized particles of Metals, oxides, carbides, nitrides, or nanotubes. Typically, a Nanofluid may contain Carbon nanotube (CNT),  $\text{TiO}_2$ ,  $\text{Al}_2\text{O}_3$ ,  $\text{MoS}_2$ , and diamond. Size of the nanoparticles is between 1 and 100 nm. Nano fluids show enhanced thermal conductivity and heat transfer coefficient. With the addition of nanoparticles, the thermal conductivity of the fluids can enhance by several hundred per cents. This is mainly due to more surface-to-volume ratio of nanoparticles [25].

The enhanced thermal behaviour of Nano fluids could provide a basis for an enormous innovation for heat transfer intensification, which is of major importance to a number of industrial sectors including transportation, power generation, micro-manufacturing, thermal therapy for cancer treatment, chemical and metallurgical sectors, as well as heating, cooling, ventilation and air-conditioning. Nano fluids are also important for the production of nano



structured materials, for the engineering of complex fluids as well as for cleaning oil from surfaces due to their excellent wetting and spreading behaviour.

There have been increasing research activities in heat intensification using nano fluids. An exhaustive review of this is found in [134]. Previous studies under nano fluids include effective thermal conductivity studies under the static conditions [138], convective heat transfer studies [88] and phase change heat transfer studies [25]. [134] and [138] gave a detailed report on Nanofluids behaviour under these static conditions. [134] have reported the investigations on nano fluids behaviour under forced convective and enhancement in heat transfer characteristics.

Few studies concluded that the particle shape or aspect ratio of the particle is a significant parameter to affect the thermal performance of Nano fluids. The conflicting results observed from limited data for the effect of nanoparticles on the boiling heat transfer performance indicated that the understanding of the thermal behaviour of nano fluids related to the boiling heat transfer is still poor. In the reviewed studies, however, only the surface roughness is the most often considered parameter. Systematic studies should be carried out to include the interaction between the surface and nano fluids (wettability), also as suggested by [138]. Compared with the research effort in forced convective and phase change heat transfer, relatively few studies have been carried on natural convective heat transfer. Golubovic et.al [66] numerically investigated the heat transfer behaviour of nanofluids in a two-dimensional horizontal enclosure. The random motion of nanoparticles was considered through a dispersion model similar to thermal dispersion models for flows through porous media.

It has been shown by the available results that the heat transfer behaviour of nano fluids is very complex and the application of nano fluids for heat transfer enhancement should not depend on their effective thermal conductivity. Many other factors such as particle–fluid interactions particle size, shape and distribution, micro-convection and pH value have important influence on the heat transfer performance of the nanofluids in natural convective heat transfer, which should be identified further in future work. This apparently paradoxical behaviour of heat transfer has motivated the authors to carry out a critical analysis of all the possible factors that affect the heat transfer process using nanofluids with a special focus on the particle–fluid interactions which is greatly influenced by the sonication time. CuO nano fluids of different

concentrations were prepared at various sonication times and their effects on the heat transfer characteristics were investigated [66].

Recently, nanofluids have been used with Minimum Quantity Lubrication (MQL) systems. The nanofluid is supplied to the machining area in the form of mist mixed with highly pressurised compressed air. Nanofluids have been containing MoS<sub>2</sub>, diamond, and Al<sub>2</sub>O<sub>3</sub> in grinding and milling. Khovakh [88] applied nanofluid containing 30-nm size diamond particles with the basefluids of paraffin and vegetable oils in drilling aluminium work piece. The performance of nanofluid MQL was compared with compressed air lubrication and pure MQL. The nano diamond concentration of 1% and 2% by volume was considered for the study. The addition of nano diamond particles improved lubrication and cooling effects with their enhanced penetration and entrapments at the drilling interface. It is reported that nanoparticles have ball/rolling bearing effect and enhance tribological and wear characteristics significantly. Meanwhile, the magnitude of torques and thrust forces were significantly reduced.

Khovakh [88] observed that paraffin oil based nanofluid MQL was more effective than the vegetable oil based one. In the case of the paraffin oil, the 1 vol% of nano diamond particles was more effective than 2 vol% of particles. On the other hand, in the case of the vegetable oils, the nanofluid with 2 vol% was found better.

### 2.7.1 Nanofluid Detergent

Nanofluids do not behave in the same manner as simple liquids with classical concepts of spreading and adhesion on solid surface [88]. This fact opens up the possibility of nanofluids being excellent candidates in the processes of soil remediation, lubrication, oil recovery and detergency. Future engineering applications could abound in such processes.

### 2.7.2 Application of Nanotechnology in Oil and Gas Industries

Nanotechnology is exciting because the science and engineering behind it are largely unknown. In fact, most scientists are aware that the laws that govern materials at nano scale are very different from those that have been widely accepted in larger scales [59], but nanotechnology is poised to impact dramatically on all sectors of industry. In oil and gas

application, nanotechnology could be used to increase opportunities to develop geothermal resources by enhancing thermal conductivity, improving whole separation, and aiding in the development of non-corrosive materials that could be used for geothermal – energy production. Nano scale metals already have been used to delineate ore deposits for geothermal exploration [132].

Nanotechnology could be used to enhance the possibilities of developing unconventional and stranded gas resource. Nanotechnology can address the problems associated with accessing stranded natural gas resources by developing nano– catalysts and nano-membrane for gas-to liquid (GTL) production and creating nanostructured materials for compressed natural gas transport or long-distance electricity transmission [112]. Nanotechnology could help improve oil and gas production by making it easier to separate oil and gas in the reservoir for instance, through improved understanding of processes at the molecular level.

There are many other potential clean energy sources that could be enhanced through the use of nanotechnology. The practical application of nanotechnology in the soil opens interesting prospects for improved oil recovery, not least through better understanding of processes at the interface between liquids and solids. The oil industry needs strong, stable materials in virtually all of its processes. By building up such substances on a nano scale, could produce equipment that is lighter, more resistant, and stronger [111a].

The productions of petroleum and petroleum processing have resulted in the spillage of oil and gas flaring in the Niger Delta of Nigeria. Oil spills and waste water has significant polluting properties due to its high levels of chemical oxygen demand (COD), biochemical oxygen demand (BOD) and phenols.

New research by Capasso's team at the University of Naples and Dr. Baoshan Xing's group [21a] at the University of Massachusetts has investigated the interaction of complexing dissolved organic matter with aluminium oxide nanoparticles. The researchers demonstrated that it is possible to use polymerin to adsorb phenanthrene – one of the most hazardous compounds in the ecosystem, derived mostly from the combustion of carbon fuels such as coal, oil, gas, wood, etc. – from polluted waters and spilled oil and that by mixing aluminium oxide nanoparticles with polymerin and drying the complex they can notably increase the effectiveness of this process.

Different experimental results showed that alumina oxide nanoparticles adsorbed an amount of polymerin nearly 100 times higher than micro particles” says Xing “In addition, we found that a dry complex using nanoparticles and polymerin adsorbed twice the amount of phenanthrene than polymerin alone and 70 times the amount compared to a polymerin micro particles complex” (Baoshan Xing’s group [21a].Polymerin is a negatively charged water-soluble matrix and therefore it is difficult to separate it from the once the binding process is done.Xing and Capasso had the idea to immobilize polymerin on an insoluble support [21a].Since aluminium oxides are positively charged at neutral and acidic pH, they seemed suitable for this purpose.

By coating the oxides with a negatively charged organic matter, it is possible to change their hydrophilic surface into relatively hydrophobic after drying the complex, which have a great affinity for soil and oil polluting compounds such as hydrophobic organic chemicals.Manganese Oxide Nano powder (MnO), nanoparticles are high surface area particles. Nano scale Manganese Oxide Nanoparticles are typically 5 - 100 nanometers (nm) with specific surface area (SSA) in the 25 - 50 m<sup>2</sup> /g range.

### 2.7.3 Remediation methods

Oil spill is subject to physical, chemical and biological changes. Non-biological weathering processes include evaporation, dissolution, dispersion, photochemical oxidation, water – in – oil emulsification, adsorption onto suspended particulate material, sinking and sedimentation [18].Biological processes include ingestion by organisms and microbial degradation – (bioremediation).Methods of remediation are vaporization, which takes care of one or two thirds of the oil spilt; physical removal and chemical treatments.Remediation processes are used to restore the contaminated area to a status as close as possible to the original.

Successful clean up may require a combination of remediation processes [126].The potential impact will depend on the remediation process used and the type of habitat being cleaned. The need to remediate the crude oil contaminated soils( to recover oil) has led to development of a wide variety of innovative processes such as chemical, physical, thermal and biological, that eliminate hazardous organics from the environment without causing further ecological

damages. As a result of public concern towards the conservation of the environment, demands have made for new and more environmentally efficient low cost strategies for clean-up contaminated sites.

In respect of oil pollution, soil remediation methods aim at preventing the further spread of the pollutants and also its removal from the soil. Comparative Analyses of Remediation methods: Five criteria are used to evaluate the different remediation methods based on their efficiency, applicability, cost, time and cleanliness. Soil remediation can take place either in-situ or ex-situ using different remediation technologies. A number of physical (natural attenuation, leaching), thermal, chemical amendments and biological methods have been developed to remediate the oil contaminated soils [3]. Each of the remediation methods has its advantages and disadvantages.

#### **2.7.4** Natural processes

For some contaminated sites, the best remediation process may be to do nothing and let natural processes degrade and remove any contaminants. Natural processes that can remove hydrocarbons include evaporation, photo – oxidation and bacterial action, coupled with dispersion from wind and wave action. Natural processes can be enhanced by manually removing free oil with absorbents. Natural attenuation describes the processes that act on a contaminant in the natural environment to reduce contaminant concentrations. These processes may include dilution, volatilization, biodegradation, adsorption, and chemical reactions.

Although not a technology per se, natural attenuation has been employed at sites where the potential for contaminant migration is low, or where other remedial measures are impractical. Advantages: it involves no handling of contaminated materials which could put workers at risk, No site disturbance, no capital costs. It can be a permanent solution.

*Disadvantages:* Modelling and long term monitoring are generally required. Degradation of products may be more mobile and toxic than the original contaminant. Regulatory and public acceptance is low because it may be perceived as a "do-nothing" option. Less regulatory and public acceptance is low because it may be perceived as effective for some halogenated volatiles and semi-volatiles, pesticides. The use of cheap and sustainable agricultural wastes or by products which are natural polymers as raw materials for the adsorption of heavy metals

from waste water have been severally reviewed [51, 56-60]. Rice husk, sugarcane bagasse, soya bean hulls, rice bran and straw sawdust are among the numerous agricultural wastes mentioned as materials used for such application [51].

Saw dust, egg shell and chitosan were found to be suitable for the chromium (VI), iron (III), nickel (II) and mercury (II) from waste water. It was reported that the materials significantly adsorbed 90% of the initial metal concentration present in 1g-2g/l of solution containing the metals [57]. Sorbents made of rice husk had efficiency of almost 100% when used to remove metals in complex matrix containing iron, Manganese, zinc, copper, cadmium and lead. Agricultural and sewage wastewater are reported to contain these metals [61].

### 2.9.2 Soil washing

Soil washing is when a wash solution (water, surfactant or both) is added to soil to remove contaminants. The contaminant is transferred from the soil to the wash solution, which then must be treated. Residual sludge is often associated with this method. Water alone is not effective in removing PAHs. [53] reported that the amount of total PAHs in the soil decreased by about 50% after soil washing as the PAHs were transferred into the washing water. The higher the soil particle size, the lower the washing rate. The combined effect of particle size and total petroleum hydrocarbons concentration, determines the total petroleum hydrocarbons removal efficiencies. These facts are very important for designing an appropriate soil washing remediation process. Leaching is washing away of soil nutrients and contaminants through erosion is an intrinsic natural process.

### 2.9.3 Pump and treat

Traditionally, the most common way to remediate hydrocarbon contaminated groundwater is to pump the ground water from on-site wells or trenches and then treat the water. Due to capillary trapping of hydrocarbons in the pore spaces, pump and treat does not completely recover all of the hydrocarbons at a spill site, additional remediation may be required.

The conventional technique used for remediation have been to dig up contaminated soil and remove it to a land fill, or to cap and contain the contaminated areas of a site. The method has some drawbacks. The method simply moves the contamination elsewhere and may create significant risks in the excavation, handling and transport of hazardous material. It is also very difficult and increasingly expensive to find new landfill sites for the final disposal of the material. The cap and contain method is only temporal measure since the contamination

remains on site, requiring monitoring and maintenance of the isolation barrier for long period of time, with high costs.

Some technologies that have been used are high temperature incineration and various types of chemical decomposition such as base-catalysed dechlorination, UV Oxidation. They can be very effective at reducing levels of a range of contaminants, but have several drawbacks due principally to their technological complexity, the cost for small-scale application, and lack of public acceptance.

#### 2.9.4 Thermal gravimetric analysis (TGA)

TGA is a useful technique or method of thermal analysis in which changes in physical and chemical properties of materials are measured as a function of increasing temperature (with constant heating rate), or as a function of time, with constant temperature and/or constant mass loss [28].<sup>1</sup> TGA is commonly used to determine selected characteristics of materials that exhibit either mass loss or gain due to decomposition, oxidation, or loss of volatiles (such as moisture). Common applications of TGA are (1) materials characterization through analysis of characteristic decomposition patterns, (2) studies of degradation mechanisms and reaction kinetics, (3) determination of organic content in a sample, and (4) determination of inorganic (e.g. ash) content in a sample, which may be useful for corroborating predicted material structures or simply used as a chemical analysis.

Thermo gravimetric analysis relies on a high degree of precision in three measurements: mass change, temperature, and temperature change. Therefore, the basic instrumental requirements for TGA are a precision balance with a pan loaded with the sample, and a programmable furnace. The furnace can be programmed either for a constant heating rate, or for heating to acquire a constant mass loss with time.

Though a constant heating rate is more common, a constant mass loss rate can illuminate specific reaction kinetics. For example, the kinetic parameters of the carbonization of polyvinyl butyric were found using a constant mass loss rate of 0.2 wt. %/min. [27a]. Regardless of the furnace programming, the sample is placed in a small, electrically heated furnace equipped with a thermocouple to monitor accurate measurements of the temperature by comparing its voltage output with that of the voltage-versus-temperature table stored in the computer's memory. A reference sample may be placed on another balance in a separate chamber. The

atmosphere in the sample chamber may be purged with an inert gas to prevent oxidation or other undesired reactions. A different process using a quartz crystal microbalance has been devised for measuring smaller samples on the order of a microgram (versus milligram with conventional TGA). Figure 1 provides schematic diagrams of a typical TGA instrument.

#### 2.9.5 Bioremediation

The biological processes also known as bioremediation has become a valuable alternative to chemical and physical (traditional) methods. Bioremediation can be defined as any process that uses microorganisms, green plants or their enzymes to return the environment altered by contaminants to its original condition. Petroleum hydrocarbons will degrade over time, given the right conditions, as a result of metabolism by bacteria normally present in soil. Under normal conditions, it will take many years before the contamination is reduced to acceptable levels. The process can be vastly accelerated under controlled conditions by bio-remediation to reduce the time frame to months rather than years.

Bio-remediation of contaminated soil uses living organisms to remove pollutants including hydrocarbons, from soil. It can be carried out either in-situ or ex-situ. In situ remediation efforts focus on treating the contaminant at the polluted site. Ex situ remediation refers to the treatment of contaminated water or soil at an off-site location. In such cases, soil and groundwater from the contaminated site are transported to a place (like a bioreactor), where conditions favourable for biological degradation can be controlled and enhanced. Ex-situ treatment can deal with higher levels of contamination and more difficult soil types. It allows for immediate removal of contaminated soil so that development of the site can continue. Bioremediation is the oldest method of soil remediation.

It is cumbersome and complex. It has low operation cost, and can remove small amount of contaminations that usually will be remained after applying a traditional method. These biological processes are simpler than traditional methods and can be employed without huge transport of chemicals to contaminated sites/soils. Recent awareness of the dangers of many chemicals has led to products that are more easily degraded in the environment. Three important disadvantages of the traditional methods are harsh side effects, high costs and are inconvenient application [46].



Bioremediation can be used to destroy or render harmless various contaminants using natural biological activity. It uses relatively low-cost, low technology techniques, which generally have a high public acceptance and can often be carried out on site. Fertile soil naturally contains up to one million hydrocarbon degrading bacteria per gram of dry soil [124]. By adding nutrients and ensuring the availability of oxygen, in-situ bioremediation can effectively degrade many hydrocarbon contaminants. This process can take several months to several years to complete; however, it is difficult to control (U.S. Environmental Protection Agency, 1990).

The microorganisms transform contaminants to less harmful compounds through aerobic and anaerobic respiration, fermentation, co-metabolism and reductive de-halogenation. The rate at which natural biodegradation occurs is slow and this is due to the following reasons: low counts of hydrocarbon – degrading microbes, toxicity of some components, limited oil / soil interface, insufficiency of oxygen, sub optimal temperatures, pH and lack of mineral nutrients and electron acceptors and biotic factors such as predation by protozoa [ 16, 28].

Immobilized microorganisms have been used and studied for the treatment of waste waters [45a], [23d] and the bioremediation of contamination from numerous toxic chemicals. [33] reported that immobilization of bacterial cells significantly enhanced the biodegradation rate of crude oil compared to free living cells over a wide range of culture medium salinity. Although immobilized cells have been successfully employed as biocatalysts in environmental protection, especially in pharmaceutical, chemical and food industry processes, as well as in aquatic environments, there are very few reports of their direct application in the bioremediation of contaminated soils. Many synthetic and natural polymeric materials have been proposed as carrier material but the uses of locally available cellulosic materials (such as straw, wood fibre, rice husk, peat moss, coconut shell etc.) have not been reported.

Taguchi Method for optimization of crude oil bioremediation in soil was used by Syed Ford, [7] to optimize bioremediation of crude oil in contaminated soils putting into consideration all the factors influencing bioremediation (such factors like aeration, bacteria, urea, glucose (used as additional carbon source), humidity, compost, salt and temperature) in the first experiment. In the second experiment he replaced aeration and temperature with time and activated sludge while molasses was used as additional carbon source. The contribution percentage of each factor was determined by analysis of variance. The oil removal was 64.4% and 68% at 35 – 40°C temperature within 20 days for optimum conditions of the first and second set of

experiments, respectively. Addition of molasses and urea reduced the effect of oil removal, while aeration showed 98% of oil removal from the contaminated soil. Enhanced natural attenuation/process:

Remediation by enhanced natural attenuation (RENA) is a land farming treatment technology for intervention in petroleum hydrocarbon contaminated soils in the Niger Delta regions of Nigeria [18]. RENA is a full-scale bioremediation technology in which contaminated soils, sediments and sludge's, are periodically turned over or tilled into the soil to aerate the waste. Soil conditions are often controlled to increase the rate of contaminant degradation [49]. Bioremediation process enhances the indigenous bacteria via the addition of oxygen and nutrients to degrade petroleum hydrocarbon to carbon dioxide and water. The actual mechanism involved, which is mediated by microbes, is known as biodegradation [17]. RENA process was used while spanning for 10 weeks, to ascertain the total petroleum hydrocarbon, nitrogen and phosphorus levels, total hydrocarbon utilizing bacteria and total heterotrophic bacteria in a contaminated farm settlement in Rivers State, Nigeria.

#### 2.9.6 .Biodegradation

Biodegradation of petroleum hydrocarbons in soil could be limited by physico-chemical factors (e.g. nutrient, pH, temperature, oxygen) as well as biological factors (e.g. number and species of indigenous microbes, bio surfactant and seeding). Besides, the above factors could affect the rate of uptake and mineralization of organic compounds in contaminated soils [83]. Temperature plays a significant role in controlling the nature and extent of microbial hydrocarbon metabolism [83]. Hence, temperature affects the rate of biodegradation, as well as the physical and chemical composition of hydrocarbon [117]. Complete degradation might be obtained by longer incubation time and higher temperature above 50°C.

In-situ biodegradation: Biodegradation involves stimulating naturally occurring microbes to convert contaminants into less toxic compounds such as carbon dioxide and water. Nutrients and oxygen are added to enhance the biodegradation. Advantages: •Minimal site disturbance, low capital costs. It can be a permanent solution. Public acceptance is high. Disadvantages: contaminant mobility may increase due to microbe enhancement,. Not effective in highly layered, clay, or bedrock sub-surfaces. Not effective at sites with high concentrations of heavy metals, inorganic salts, or chlorinated organics, Regulatory acceptance is low due to potential

of increased contaminant mobility. Remediation may take several months to years. Not cost effective for small volumes.

### 2.9.7 Bioventing

This is a form of biodegradation in which oxygen in the form of air is delivered to contaminated unsaturated soils through a system of extraction and injection wells. Unlike soil vapour extraction, lower air flow rates are used to provide just enough oxygen to enhance biodegradation while minimizing volatilization of contaminants to the atmosphere.

*Advantages:* Better oxygen delivery to less permeable formations. Minimal site disturbance, low capital and organic matter costs. It can be a permanent solution. Regulatory and public acceptance is moderate to high. No off-gas treatment if there is a closed system operation.

*Disadvantages:* Not recommended where water table is near surface. Monitoring of off-gases at the soil surface may be required. Remediation may take several months to years [60].

### 2.9.8 Air sparging/Soil Vapour Extraction (SVE) Enhancement Technology

2.9. 8.1 Air sparging: Air sparging, also known as in situ air stripping (in-situ aeration), is an in situ remediation technology that involves the injection of air into the subsurface saturated zone and venting through the unsaturated zone to remove subsurface contaminants. During air sparging, air bubbles traverse horizontally and vertically through the saturated and unsaturated zones, creating an underground stripper that removes contaminants by enabling a phase transfer of hydrocarbons stripper that removes contaminants by enabling a phase transfer of hydrocarbons from dissolved or adsorbed state to a vapour phase. When used in combination with soil vapour extraction (SVE), air bubbles carry vapour phase contaminants to a SVE system controls vapour plume migration by creating a negative pressure in the unsaturated zone through a series of extraction wells. Using air sparging as an SVE (soil venting) enhancement technology increases contaminants movement and enhances oxygenation in the subsurface which increase the rate of contaminant extraction.

In-situ air sparging (IAS) is becoming a widely used technology for remediating soils contaminated by volatile organic materials such petroleum hydrocarbons. When it is used in combination with SVE can increase removal rates in comparison to SVE alone for cases where hydrocarbons are distributed within the water saturated zone. Air sparging systems are almost always coupled with soil vapour extraction to control the subsurface air flow. Proper hydraulic

control is key to preventing migration of contaminants to uncontaminated areas. It is a relatively new treatment technology. The target contaminant groups for air sparging are volatile organic compounds (VOCs) and fuels. Air sparging is generally more applicable to the lighter gasoline constituents such as benzene, ethyl benzene, toluene, and xylene. It is less applicable to heavier constituents such as diesel fuel and kerosene. The use of in-situ air sparging poses risks, in terms of health implications not generally associated with most practiced remediation technologies. Vapour extraction (soil venting) has been demonstrated to be a successful and cost effective remediation technology for removing volatile organic compounds from unsaturated zone soils.

2.9.8.2 Soil vapour extraction: Soil vapour extraction is a process of inducing air flow through unsaturated soils to remove volatilized contaminants. The air flow is induced by applying a vacuum to the soil through a network of extraction wells. The technology is applicable to volatile compounds with a high vapour pressure. The process requires a system for handling off-gases. Volatilisation may be enhanced by heating the subsurface with injected steam or applied electrical currents. *Advantages:* Control vapour migration to structures, therefore inhalation/explosive risk reduced, Minimal site disturbance, low capital costs. It is found to be a permanent solution. Regulatory and public acceptance is high when off-gas is treated. *Disadvantages:* Volatilization inhibited by high humic content of soil, best suited for relatively permeable, homogeneous soils. Residual liquid from treated air requires disposal thermal enhancement of volatilization may sterilize the subsurface, killing microbes required for biodegradation. High organic matter costs. Remediation may take many years.

#### 2.9.9 Solidification/stabilization

Solidification or stabilization, contaminants are physically or chemically bound to the medium to produce a non-leachate material. Commonly used binding agents include cement, lime, organic polymers, and silicates. This can be accomplished either in-situ or ex-situ. Commercially available off-site facilities are also available. *Advantages:* Most soils can be treated. Time to complete cleanup is relatively short. Low organic matter costs. *Disadvantages:* Permanent immobilization of organic contaminants cannot be assured. Organic compounds may interfere with binding agents. Volume of contaminated material can increase 50 to 100% due to addition of Solidifying agents. High capital costs

#### 2.9.10 Surface capping (Encapsulation)

Surface capping utilizes an impermeable ground cover to isolate the contaminants from the surface and redirect surface water percolation away from the contaminated soil. Surface caps are typically made of synthetic membranes, soil-bentonite mixtures, asphalt, steel or concrete. An extension of surface capping is encapsulation where impermeable barriers are extended vertically around and sometimes underneath the contaminated soils to redirect groundwater around the contaminated soils. *Advantages:* Easily installed, reduces exposure/contact of public with contaminants, low organic matter costs. *Disadvantages:* Long term liability. Periodic maintenance and monitoring may be required, groundwater controls may be needed.

#### 2.9.11 Phyto-extraction

Phyto-extraction is a relatively new technique that exploits the property of some plants to absorb large amounts of heavy metals for storage in their roots and shoots. Phyto-extraction involves selecting and cultivating plants that are amenable to the local soil and climate in the contaminated zone. These plants may accumulate metals up to 1000 times greater than would the normal species. Their shoots may be harvested and subsequently treated as waste. *Advantages:* Low capital and organic matter costs, can treat large areas of contaminated soil. *Disadvantages:* Long time period required. Not yet a recognised full scale treatment technology. Treatment only extends to the depth of the roots. Not effective for highly contaminated soils. Plants must be removed and properly disposed of. Biodegradation of pollutants using plants (i.e., phytoremediation) and their associated microorganisms has been shown to be effective for remediation of oil contaminated soils [84].

#### 2.9.12 Bio-stimulation

This is the stimulation of a group of organisms in order to shift the microbial ecology toward the desired process. Bio-stimulation can be achieved through changes in pH, moisture, aeration or nutrient additions. Bio-stimulation with inorganic fertilizer and bio-augmentation with hydrocarbon utilizing indigenous bacteria were employed as remedial methods for 12 weeks in a crude oil – contaminated soil. To promote oil removal, bio carrier for immobilization of indigenous hydrocarbon – degrading bacteria was developed using peanut hull powder. Biodegradation was enhanced with free-living bacterial culture and bio carrier with a total petroleum hydrocarbon removal ranging from 26% to 61% after 12 weeks treatment. Oil removal was also enhanced when peanut hull powder was only used as a bulking agent, which accelerated the mass transfer rate of water, oxygen, nutrients and hydrocarbons, and provided nutrition for micro flora. Dehydrogenase activity in soil was remarkably enhanced by the application of carrier material. Bio-augmentation is a widely approach where organisms

selected for high degradation abilities are used to inoculate the contaminated site. Bio-stimulation and bio-augmentation can be used simultaneously.

According to [5] a combination of treatments consisting of the application of poultry manure, piggery manure, goat manure, and chemical fertilizer was evaluated in the in situ during a period of 4 weeks of remediation. Each treatment contained petroleum hydrocarbon mixture (kerosene, diesel oil, and gasoline mixtures) (10% w/w) in soil as a sole source of carbon and energy. After 4 weeks of remediation, the results showed that poultry manure, piggery manure, goat manure and NPK (nitrogen, phosphorous, and potassium/potash) fertilizer exhibited 73%, 63%, 50% and 39% total petroleum hydrocarbon degradation, respectively. However, a first-order kinetic equation was fitted to the biodegradation data and the specific degradation rate constant (k) values obtained showed that the ordered of effectiveness of these bio-stimulating strategies in the clean-up of soil contaminated with petroleum hydrocarbon mixtures (mixtures of kerosene, diesel oil and gasoline) was improved in this order, poultry manure, piggery manure and goat manure treatments showing greater petroleum hydrocarbon reductions than NPK fertilizer treatment. Therefore, application of animal manure and chemical fertilizer could enhance oil removal with poultry manure showing a greater effectiveness and thus could be one of the severally environmentally friendly ways of remediating natural ecosystem contaminated with crude oil.

#### 2.9.13 Thermal process

This process uses heat to increase the volatility, to burn, decompose, destroy or melt the contaminants. The principle is based on the increase in the soil temperature to a level where pollutants become volatile and change into gas phase (best suited for non-biodegradable organic pollutants and mercury).

Physico – chemical process /treatment (shallow and mixing oxidation-reduction, hydrolysis-neutralization, stabilization-solidification, mobilisation-immobilisation, soil flushing-washing). Physical methods, such as stripping or sorption, are not as effective as biological methods for treating hazardous organic compounds. The principle is based on the pollutants extraction, as a result of a physico – chemical or washing treatment (or washing process) suitable for many types of mixed pollution, organic/metals. Chemical methods are used to remove heavy metals. Biological processes (bioventing, bio purging, hydraulic-pneumatic fracturing, soil bio injection, air and water flushing, biopolymer shields and

phytoremediation). The question of which method should be used in oil polluted lands depends on the chemical, physical and biological properties of both contaminants and soil source

#### 2.9.14 Eco-friendly treatments.

This is a new biological degreaser's approach which unlike traditional cleaning technique, they clean and as well as digest unwanted oil emulsions. There are a number of oil degrading natural microbes and enzyme treatments for all manner of oil incidents. The enzymes in ideal Microbial oil Remover rapidly biodegrade mineral oils into harmless constituent parts and the enzymatic action breaks down oil pollution on soil, grass and concrete as well as converts hydrocarbons to basic water soluble elements and nutrients.

2.9.14.1 Ideal Group has developed a range of specialist chemical and biology solutions for cleaning oil spills ranging from a small spill on a forecourt, driveway, fuel pumping, mechanical workshop and garage to a major spillage in a plant room or other location.

Ideal Group Chemical Solutions are:

2.9.14.2 Ideal biological removal of oil and stains: Oil stain removal rapidly digests and removes oil stains from porous block work and hard surface, including road surfaces, floors, equipment, tarmac and Asphalt oil remover removes oil from contaminated surfaces.

2.9.14.3 Ideal Marine Safe: A very fast solution which is an emulsion free degreaser, excellent for use in environmentally sensitive marine areas. Degreasing, cleaning oil, contaminated birds and general oil spill pollution can be combated using this chemical solution.

2.9.14.4 Ideal Power Wash: A powerful, biodegradable oil degreaser that efficiently removes oil and grease contamination.

2.9.14.5 Ideal BIO GEL: Ideal BIO GEL: is a biological solution which is poured over the area to digest the remaining oil. It can handle contaminations of any type, from diesel to heavy fuel oil. Biological oil removers are very effective on hard surfaces.

2.9.14.6 Ideal Soil treatment: Ideal Soil treatment removes fuel, hydraulic and lubricating oils from soil or sports turf. A bioremediation composting system, dry powder bacteria is applied to contaminated soil which will achieve a 99% reduction in Total Hydrocarbon and Polycyclic Aromatics.

Chemical cleaning or remediation refers to the use of various minerals or chemicals to absorb, adsorb, bind, precipitate or co-precipitate trace elements and heavy metals in contaminated soils and water thereby reducing their bioavailability, toxicity and mobility. The application of the two processes simultaneously is referred to as biochemical remediation. The goal of biochemical remediation, therefore, is to degrade organic and inorganic pollutants to concentrations that are not detectable or if detectable, to concentrations that are permissible by regulatory agencies [132].

Hydrogen peroxide was used to oxidize absorbed petroleum hydrocarbons contaminant in a clay soil with 5000 gKg<sup>-1</sup> of crude oil by using nano zero-valent iron as catalyst [4]. 5 grams crude oil was spilled in 1kg soil and left 3 weeks before tests were carried out for crude oil sorption by soil. From the results, it was found that optimum molar ratio of H<sub>2</sub>O<sub>2</sub>:Fe<sup>0</sup> was 33.7:1 with maximum TPH removal, 91%. It was found that hydrogen peroxide was heterogeneously decomposed by the soil (due to its organic and/or inorganic components) and its decomposition rate decreases when the iron was previously precipitated–impregnated into the soil [5].

2.9.14.7 Fenton's Reagent: This is a solution of hydrogen peroxide and ferrous iron catalyst, used for an in-situ chemical oxidation of organic contaminants (Seol and Javandel, 2008). Fenton reagent is a mixture of hydrogen peroxide (H<sub>2</sub>O<sub>2</sub>) and ferrous iron salts that reacts to form hydroxyl radicals (HO), ferric iron (Fe<sup>+</sup>), hydroperoxyl radicals (HO<sub>2</sub>) and/or superoxide radicals (O<sub>2</sub><sup>-</sup>).

Fenton's Reagent – Remediation of soil and groundwater contaminated with organic contaminants is accomplished by injecting a strong chemical oxidizer, like a mixture of hydrogen peroxide, together with a catalyst, ferrous sulphate and an optimum pH (3-5) adjusted, using sulphuric acid. Concentrated pumping of Fenton Reagent (FR) into an area is done in order to oxidize / destroys those contaminants to the maximum extent possible. It is a chemical oxidation method which uses strong oxidants to destroy organic contaminants. The process works best on compounds, such as olefins and substituted aromatics, which contain unsaturated carbon-carbon bonds. Several chemical combinations can be used: peroxide, peroxide and iron (Fenton's reagent), ozone, hydrogen peroxide and ozone (peroxide), and potassium permanganate [ 89].



Weak organic acids such as citrate, tartrate (ammonium salts), citrate-oxalate are very effective in removing heavy metal at optimum pH of contaminated soils at different textures. Ammonium salts are very effective in removing heavy metals in sandy clay loam soil at large scale level in a plastic container (tub), using citrate as flushing liquid. EDTA and DTPA (chelating agent) are effective in removing heavy metals except Hg.

#### 2.9.15 Soil Reclamation

This is process of liming soil using Calcium sulphate ( $\text{CaSO}_4$ ). Ammonium salts are very effective in removing heavy metals in sandy clay loam soil at large scale level in a plastic container (tub).

#### 2.9.16 Frelu Technology

This consists of the following –

2.9.16.1 Frelu Hydrocarbon Converter is a technique used for soil remediation as an alternative to dig and haul method that is used for oil spill clean-up. Frelu Hydrocarbon Converter is a non-toxic planet-friendly solution that reduces costs and saves time.

2.9.16.2 Frelu Maxclean is unique in its matrix as it actually breaks down harmless organic silicate material as a product. It can be used on all types of petroleum products and related materials.

2.9.16.3 Frelu Catalyst is a non-toxic liquid solution that makes lead contaminated materials safe for handling and disposal. It uses the silicates in the product to tie up the heavy metals. This is inexpensive way to enhance the performance of many processes. Soluble silica reacts with all multivalent cationic metal ions to form insoluble metal silicate.

#### 2.9.17 Quantification of oil content methods using Mass balance method.

2.9.17.1 Gravimetric method: This is the method of drying crude oil polluted soils in the oven. The weight of oil loss is obtained using bulk density method which is given as below:

Bulk density =  $(\text{Total weight of wet soil (soil containing crude oil)} - \text{Weight of oven dried soil}) / \text{Total volume of the wet soil}$ , which is equal to the weight of the oil loss.

2.9.18 Biodiesel is a cleaning agent comprising of vegetable oil blended with an alcohol. Literature revealed that research into biodiesel started more than a decade ago. Review indicates that biodiesel is a promising agent for cleanup of oil spills; its efficacy is far from

conclusive. Biodiesel is produced from a wide range of oil seed crops, such as corn, soybean, rapeseed/canola, sunflower, palm kernel [135c]. The oil from these seeds is pressed and extracted, then subjected to transesterification [108a]. Through transesterification, the vegetable oil is reacted with alcohol, often methanol, ethanol and a basic catalyser, usually sodium hydroxide (NaOH) or potassium hydroxide, KOH [43]. Temperature and time of reaction, as well as the experimental reagents, influence the yield and the optimal reaction conditions which are specific to each type of oil.

Pereira and Mudge [135a] evaluated the efficiency of extraction of light crude oil by rapeseed, soybean and waste cooking oil biodiesels in three sets of experiments. Rapeseed biodiesel was the most effective of the three biodiesels tested, removing 90% - 96.5% of the crude oil depending upon the volume of biodiesel applied. The removal rate of 96.5% resulting from the application of 75ml of biodiesel was significantly greater than the 90% of crude oil removed by the 30ml application. Soyabean biodiesel approached the removal efficiency of rapeseed biodiesel whereas waste cooking oil was much less effective than the other two at all volumes (varying volumes – 30, 40, 50 & 75ml).

## 2.10 Pollutants

Examples of pollutants: Pollutants found in soils present a variety of different human health risks. These are listed below:

### 2.7.1 Petroleum by-products

BTEX – benzene, toluene, ethyl benzene and xylene are by-products of petroleum product. The biodegradability of these compounds is relatively well known and remediation can be achieved by creating favourable conditions for BTEX degrader's growth.

### 2.7.2 Methyl tert-butyl ether

MTBE is a gasoline additive introduced to replace lead. MTBE raises the oxygen content of fuel, allowing for more complex combustion and less emissions. MBTE, however, is highly soluble, does not adsorb well in soil and can move quickly through soil and into groundwater.

### 2.7.3 Polychlorinated biphenols

PCHs are used in industrial applications are very recalcitrant and many are known carcinogens.

### 2.7.4 Chlorinated solvents

Chlorinated solvents are used extensively as cleaning agents. Many chlorinated solvents are carcinogenic. Trichloroethylene (TCE) can be degraded to vinyl chloride under anaerobic

conditions. Vinyl chloride, in turn, needs different conditions to transform and this should be seriously considered due to its high toxicity.

### 2.7.5 Polycyclic aromatic compounds

PAHs are found in high concentrations at industrial sites especially sites that use or process petroleum products. They are considered carcinogens and mutagens, and are very recalcitrant, prevailing for many years in the natural environment.

**General Discussion and Conclusions:** There are many remediation methods which include: chemical, physical, thermal and biological. Thermal process: This process uses heat to increase the volatility, to burn, decompose, destroy or melt the contaminants (best suited for non-biodegradable organic pollutants and mercury).

Physico – chemical process /treatment (shallow and mixing oxidation-reduction, hydrolysis-neutralization, stabilization-solidification, mobilisation-immobilisation, soil flushing-washing). Physical methods, such as stripping or sorption, are not as effective as biological methods for treating hazardous organic compounds. Chemical methods are used to remove heavy metals. Biological processes (bioventing, bio purging, hydraulic-pneumatic fracturing, soil bio injection, air and water flushing, biopolymer shields and phytoremediation). The question of which method should be used in oil polluted lands depends on the chemical, physical and biological properties of both contaminants and soil source. Bio-augmentation is a widely approach where organisms selected for high degradation abilities are used to inoculate the contaminated site. Bio-stimulation and bio-augmentation can be used simultaneously. Table 2.7.6 – shows the summary of the comparative analysis of the remediation techniques based on advantages and disadvantages of each major remediation technique. The analysis showed that nanotechnology is the best due to its simplicity, low cost, timeliness and high cleaning efficiency /effectiveness. Therefore, nanofluid was considered for this thesis.

Table 2-6 Summary of the major remediation methods

Remediation techniques	Advantages	Disadvantages
Physical	Efficient and effective as final cleanup	Expensive, complex, labour intensive, required maintenance and longer period for cleanup.

<p>Bioremediation</p>	<p>Less manpower needed, simpler than traditional technique, low operation cost and environmentally friendly, Bioremediation can be used to destroy or render harmless various contaminants using natural biological activity. It has a high public acceptance and can often be carried out on site.</p>	<p>Long period of treatment. Oldest method of remediation. It is cumbersome and complex. It has low operation cost, and can remove small amount of contaminations that usually will be remained after applying a traditional method.</p>
<p>Phytoremediation</p>	<p>Permanent removal of the metal. More than one contaminant can be remediated at the same time. Reduces the amount of hazardous waste to be disposed. Relatively low cost Easily implemented and maintained Several mechanisms for removal. Environmentally friendly Aesthetically pleasing Reduces landfilled wastes Harvestable plant material.</p>	<p>It can only be used for surface soil contamination. Remediation takes longer than with conventional treatments, 18-60 months. Longer remediation times. Climate dependent. Effects to food web might be unknown. Ultimate contaminant fates might be unknown Results are variable.</p>
<p>Chemical</p>	<p>Less manpower needed, less expensive than mechanical methods, quick, effective on wide range of oil, accelerates the degradation of the oil by natural processes.</p>	<p>Efficiency of the remediation is reduced by the presence of large concentrations of other ions. Promotes the separation of HgS, which is a very stable form of mercury, generating higher volumes of metallic mercury to remediate. Harmful. Dangerous to the surrounding underground area.</p>

Thermal	Effective, quick, less manpower needed, cost effective and requires minimal but specialized equipments	Fear of flashback and secondary fires. Emit many petroleum related compound to air environment, threats to ecosystem. High cost
Nanotechnology	Nanotechnology is very simple, applicable to remediation of surface and ground water, surface and subsurface soils as well. It has low cost, timeliness and high cleaning efficiency. The solution for the treatment can be prepared on site. The stabilizer is a low cost, water soluble, environmentally friendly compound. Compounds used are commercially available. Does not generate additional waste. It has low energy demand. High oil recovery.	The effects of the soil pH in the kinetics of the treatment are yet to be determined. Deployment strategy needs to be designed, in terms of separation and depth of injection points. Requires further evaluation of the geochemistry of the nanoparticle, nanofluid and the effects on the soil, Microorganisms. Nanofluid must be stabilized before any application.
Biodiesel	Biodiesel degrades faster and to a greater degree than heavy oil. Environmental friendly, timeliness.	High importation cost of the source materials due to due to deforestation, erosion. The use of biodiesel as a cleansing agent for oil spill is still in its infancy. Limited range of biodiesels. Unavailability and dispersant toxicity.

### 3 Chapter 3.0 | MATERIALS AND METHODS |

This section comprises of materials, equipment and experimental procedure to be used in this research [57].

#### 3.1 Materials and Equipment

These are given in Tables 3.1 and 3.2

Table 3-1 List of Materials

<b>Materials</b>	<b>Source (UK)</b>	<b>Comment</b>
ZnO, Al <sub>2</sub> O <sub>3</sub> and TiO <sub>2</sub> (ZnO: 40 -100nm)	Available in the lab,	Clean-up materials
Mineral oil (White liquid mineral oil, CAS No. 8020 – 83 - 5) HV1 60 mineral oil, Polyol Caradol SN 9765	Available in the lab,	Pollution material
Soils storage bottle jar	Obtained from Leeds	Pollution medium  Dried soil sample
Sodium hexametaphosphate (Na <sub>2</sub> HPO <sub>4</sub> ), and Sodium dodecylbenzene sulfonate (SDBS)	Available in the lab ,	Surfactants
<b>Deionised water</b>	<b>Available in the lab</b>	<b>Dissolving liquid</b>

Table 3-2List of Equipment

<b>Equipment</b>	<b>Model/Manufactur er</b>	<b>Comment</b>
Hand auger	Auger Edelman clay (Eijkelkamp)	Soil drilling and sampling.

Standard A.P.I sand Sieve	NL Baroid	Sieving dried soil samples
Bohlin Rotational Rheometer	Bohlin Gemini	Measurement of Rheological properties such as viscosity.
Dynamic Light Scattering	HP 6890 Series	Measurement of particle size distribution of nanofluids.
Thermo gravimetric Analyser	Mettler Toledo,	Identification, characterization & measurement of mass change with time at high temp./heating rate, total weight loss, amount & composition of materials /crude oil to be used.
pH Meter	Mettler Toledo and Zetasizer	Measurements of electrochemical parameters such as pH, electrical conductivity, ion concentration as well as Oxidation, Reduction Potential (ORP).

Weighing balance		Mettler Toledo	For measuring mass of materials for the experiments.
Digital Camera			For direct visual analysis.
Clock			For measuring time.
Density meter			Measurement of density and specific gravity of nanofluids as well as mineral oils.
Zetasizer		Malvern	Measurement of particle size distribution and zeta potential. To prevent aggregation of particles.
Separating funnel Lab	Available in the		Separating/Removing of water from oil.
Picnometer	Available in the lab		Measurement of density of nanofluids
UV vis-Spectrophotometer.		Available in the Lab	Measurement of absorbancy & wavelength of ZnO, TiO <sub>2</sub> & Al <sub>2</sub> O <sub>3</sub> , optical properties of TiO <sub>2</sub>
Attension Theta.			



### 3.2 Experimental Work /procedures

The aim of this chapter is to give an overview of the experimental work executed.

All experiments were performed at the student lab at IPSE and ERRI. The experimental theory, setup and procedure in the present chapter is based on experience from the laboratory work and [57, 165]. Figures 3.1a& b is an overview of the laboratory work. It is given to help the reader understand the sequence of the laboratory work and the preparation needed for each experiment. The main goal of the soil contamination and cleanup experiments is to have a look at how nanofluids affect the wettability and interfacial tension of a two-phase system of crude oil and an aqueous phase, deionised water/pure/hydrophobic nanofluids and hydrophilic/surfacted nanofluids. Two experiments are prepared for wettability; the imaging method for measurement of the contact angle,  $\Theta$ , and the spontaneous imbibition test for investigation of relative permeabilities. One experiment is prepared for the interfacial tension; the drop method. Initially the Amott method was intended for wettability determination, but the method was later reduced to spontaneous imbibition testing. This is discussed in Chapter 4.

#### 3.2.1 ZnO, TiO<sub>2</sub> & Al<sub>2</sub>O<sub>3</sub> Nanofluid (s) formulation and Preparation

The required/appropriate amount of dry powder was weighed using a Mettler Toledo laboratory balance with accuracy of  $10^{-4}$ g. ZnO – water nanofluid, TiO<sub>2</sub>– water nanofluid and Al<sub>2</sub>O<sub>3</sub> were formulated by using ZnO, TiO<sub>2</sub> and Al<sub>2</sub>O<sub>3</sub> nanopowder (FigA1-3) 0.3-1wt % (0.3 g), monodispersed in 99.70 - 99.0% deionised water (pH of 7), as basefluid (See Table 2) The nanofluid formulated in this Table was made based on to make 100g nanofluid). This composition was prepared taking the original nanofluid after 24 hours ultrasonification with magnetic stirrer for uniformity of nanofluid/solution. Each nanofluid obtained was further ultrasonicated by means of low power, high frequency (12W, 55 KHz) water bath for 15 mins, in order to improve the dispersion of nanoparticles in water as well as to **prevent aggregation of particles**. No dispersant was added to each nanofluid Figs 1 - 9.



Figure 3-1.  $\text{Al}_2\text{O}_3$  nanoparticles

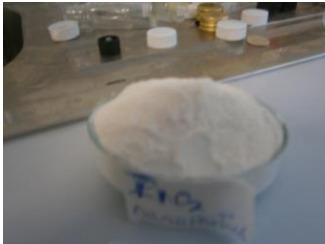


Figure 3-2  $\text{TiO}_2$  nanoparticles

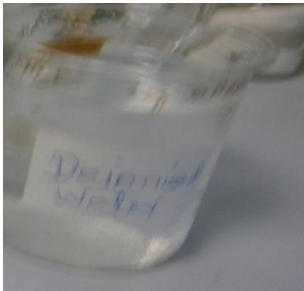


Figure 3-3. Deionised water

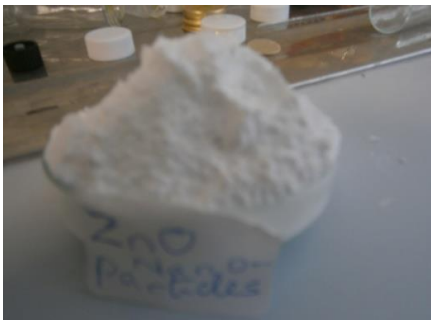


Figure 3-4  $\text{ZnO}$  powder

The volume fraction of the powder is calculated from the weight of dry powder using the density provided by the supplier and the total volume of the suspension.

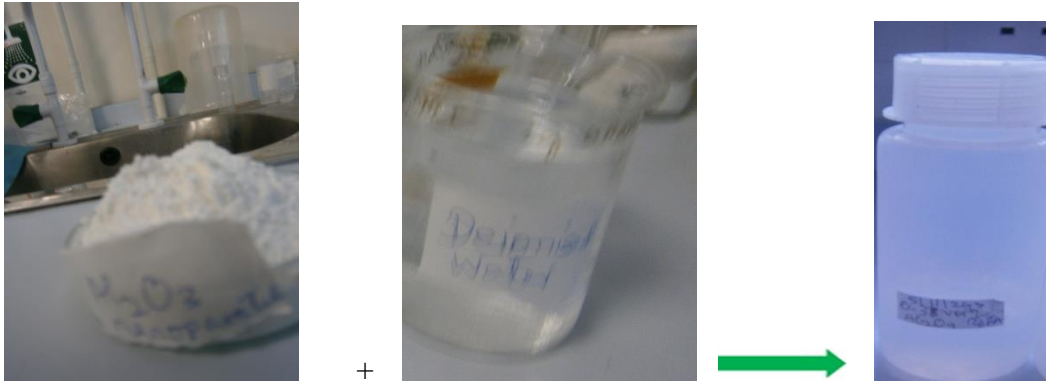


Figure 3-5 Al<sub>2</sub>O<sub>3</sub> nanoparticles Figure 3-6 Deionised water Figure 3-7 Al<sub>2</sub>O<sub>3</sub> nanofluid

$$\text{Vol\%} = \frac{m}{\rho} \times 100 \text{ml water} + \frac{m}{\rho} \dots\dots\dots (3.1)$$

Where *m* and *ρ* are the mass and density of the Al<sub>2</sub>O<sub>3</sub> nanoparticles, respectively

The surfactant, SDBS with the density, 1.3115 g/cm<sup>3</sup> at volume percentage of around 0.01-0.02 can stabilize the nanofluids [145]. The amount of 0.01 vol % SDBS was added into the Al<sub>2</sub>O<sub>3</sub> water-based nanofluids to keep the nanoparticles well dispersed in the base fluid, water. The nanofluid was then stirred by a magnetic stirrer for 19 hours before undergoing Ultrasonification process (Fisher scientific Model 500) for one and a half hours. This is to ensure uniform dispersion of nanoparticles and also to prevent the nanoparticles from the aggregation in the nanofluids. Stabilization of nanofluid

3.2.2 Nanofluid Stability Characterization/Sedimentation study and stability optimization [57, 161]. For stability optimization experiments, samples of ZnO, nanofluids with different concentrations of ZnO nanoparticles (ranging from 0.3g to 1g increments of 0.3% (0.3 - 1wt %)) was dispersed in 99.70g (99.70ml) of deionised water (pH of 7) as basefluid, first and later 0.5% Sodium hexametaphosphate (Na<sub>2</sub>HPO<sub>4</sub>) as dispersant was added to it in the ratio of 1/2th concentration of nanoparticles, to enhance the stability of nanoparticles in the fluids, leaving it for settling time of 16 - 24hrs. Each with sonification time of 19 hrs. The stable suspension has Sodium hexametaphosphate ZnO as 0.3:0.15 in deionised water following an optimization study [161]. The formulation was made based on making 100g of each nanofluid (ZnO/TiO<sub>2</sub>/Al<sub>2</sub>O<sub>3</sub>). The Sodium dodecylbenzene sulfonate, anionic surfactant was added to Al<sub>2</sub>O<sub>3</sub> and TiO<sub>2</sub> in the ratio of 1/10<sup>th</sup> for nanofluid Stability Characterization. (See. Table 3-3)

### 3.3 Experimental Design

Table 3-3 Samples ZnO/TiO<sub>2</sub>/Al<sub>2</sub>O<sub>3</sub> formulation & preparation using factorial designs 23

(8 samples from each nanoparticles) using different concentration of nanoparticles in the range of 0.3 – 1%

No	Name/Sample Nanofluid	%nano Particles	ZnO(g)	TiO <sub>2</sub> (g)	Al <sub>2</sub> O <sub>3</sub> (g)	Na <sub>2</sub> HPO <sub>4</sub> Mg	Sodium dodecyl benzen e sulfonate Mg	Deionised H <sub>2</sub> O (g)
1	S <sub>1</sub> (ZnO)	0.3	0.3	0.3	0.3	0	0	0 99.70
2	S <sub>2</sub> (ZnO)	0.70 & 1	0.70 & 1	0.70 & 1	0.70 & 1	1	1	1 9 9.30& 99
3	S <sub>3</sub> (TiO <sub>2</sub> )	0.3	0.3	0.3	0.3	0	0	0 99.70
4	S <sub>4</sub> (TiO <sub>2</sub> )	0.70&1	0.70 & 1	0.70 & 1	0.70 & 1	10	10	10 99.30 & 99
5	S <sub>5</sub> (Al <sub>2</sub> O <sub>3</sub> )	0.3	0.3	0.3	0.3	15	15	15 99.70
6	S <sub>5</sub> (Al <sub>2</sub> O <sub>3</sub> )	0.3&1	0.70 & 1	0.70 & 1	0.70 & 1	20	20	20 99
7	S <sub>7</sub> (ZnO+ TiO <sub>2</sub> + Al <sub>2</sub> O <sub>3</sub> )	0.3 +0.3+ 0.3=1.0	90	50	50	0	0	0 99
8	S <sub>8</sub> (ZnO+ TiO <sub>2</sub> + Al <sub>2</sub> O <sub>3</sub> )	0.3 +0.3 + 0.3=1	90	50	50	Na <sub>2</sub> HPO <sub>4</sub> + Sodium dodecylbenzene sulfonate		99

To prepare/make: 100g nanofluid (ZnO, Al<sub>2</sub>O<sub>3</sub> & TiO<sub>2</sub>) for 0.3% - 1% representing 3 – levels design: low (0.3g), medim (0.7g) and high (1.0g)

$$\frac{0.3 \times 100}{100} = 0.3\text{g of ZnO, Water to be used } 100 - 0.3 = 99.70\text{g}$$

$$1\%, = \frac{1 \times 100}{100} = 0.1\text{gZnO, Water to be used } 100 - 0.1 = 99.9\text{g}$$

$$0.70\% = \frac{0.7 \times 100}{100} = 0.7\text{gZnO, Water to be used: } 100 - 0.70 = 99.30\text{g}$$

The graphs of the different concentrations against the different nanoparticles/nanofluids are plotted.

Table 3-4 Formulation 2. Using 3, 3 Simplex Lattice Design

This can be used to formulate crude oil contaminated soils and nanofluid for optimum formulations. Here values are approximated to one decimal place.

Nanofluid formulation	Simplex Lattice Design			
	X1(ZnO)g	X2(TiO <sub>2</sub> )g	X3(Al <sub>2</sub> O <sub>3</sub> )g	Deionised H <sub>2</sub> O(g)
Al <sub>2</sub> O <sub>3</sub> nanofluid	0	0	1(1%)	99.00
TiO <sub>2</sub> +Al <sub>2</sub> O <sub>3</sub> nanofluid	0	0.7(0.7%)	0.3(0.3%)	99.00
TiO <sub>2</sub> nanofluid	0	1 (1%)	0	99.00
ZnO + Al <sub>2</sub> O <sub>3</sub> 0.3(0.3%) nanofluid	0.3(0.3%)	0	0.7 (0.7%)	99.00
ZnO + TiO <sub>2</sub> +Al <sub>2</sub> O <sub>3</sub> 0.3 (0.3%) nanofluid	0.3 (0.3%)	0.3(0.3%)	0.3(0.3%)	99.10
ZnO + TiO <sub>2</sub> nanofluid 0.3 (0.3%)	0.3 (0.3%)	0.7 (0.7%)	0	99.00
TiO <sub>2</sub> +Al <sub>2</sub> O <sub>3</sub> nanofluid 0.7( 0.7%)	0.7( 0.7%)	0	0.3(0.3%)	99.00
ZnO + TiO <sub>2</sub> nanofluid 0.7 (0.7%)	0.7 (0.7%)	0.3(0.3%)	0	99.00
ZnO nanofluid 1 (1)	1 (1)	0	0	99.00

Table 3-5 (2.2) Simplex Lattice Design for formulation of mixture of two surfactants

X <sub>1</sub> (Na <sub>2</sub> HPO <sub>4</sub> )	X <sub>2</sub> (Sodium dodecylbenzene sulfonate)
0	0
0.5g	0
0	0.1g for 1wt%
0.5g for 1wt%	0
0	0.03 – 0.07g for 0.3wt% - 0.7 wt%
0.15 – 0.35g for 0.3wt% - 0.7 wt%	0.15 – 0.35g for 0.3wt% - 0.7 wt%

Each surfactant was dispersed together with nanoparticles (i.e. 0.3% nanoparticles + 0.15% Na<sub>2</sub>HPO<sub>4</sub> surfactant = 0.45% surfacated nanoparticles, 100 – 0.45 = 99.55%) in 99.55% deionised water for ZnO nanoparticles. 0.1% SDBS is for Al<sub>2</sub>O<sub>3</sub> and TiO<sub>2</sub>, 0.01% Nitric acid was added to surfacted TiO<sub>2</sub> – water nanofluid to enhance the stability.

Table 3-6 Process Variables design using 3, 3 Simplex Lattice Design for optimum cleanin of crude oil contaminated soils

Process variables: Temperature T, Time t, and Pressure, p

Process variable formulation		Simplex Lattice Design		
		Temperature (400°C)	Time (60 mins)	Pressure (150 bars) Interactions
Pressure	0		0	1(150) P
Temperature x time	0		0.667(40 mins)	0.333(49.95 = Pt 50bars)
Time	0		1 (60 mins)	0 T
Temperature pressure	x 0.333X400 = 133.2 °C		0	0.667 (100.05) TP

Temperature x time 400 °C x Pressure	40mins	150bar	TtP
Temperature x time 0.333 (133.2°C)	0.667 (40 mins)	0	Tt
Temperature x 0.667(266.8 °C) pressure	0	0.333 (49.95 = TP 50bars)	
Temperature x time 0.667 (266.8 °C)	0.333 (19.98mins = 0 20mins)		Tt
Temperature 1 (400 °C)	0	0	T

Table 3-7 (3,3) Simplex Lattice Design for formulation of time,( max 60 mins) for optimum time of cleaning crude oil contaminated soils using nanofluids.

t <sub>1</sub>	t <sub>2</sub>	t <sub>3</sub>
0	0	1.0
1	0	0
0	1	0
0.5	0	0.5
0	0.5	0.5
0.5	0.5	0

Table 3-8 (3,2) Simplex Lattice Design for formulation of mixture of soil with two oil grades.

X <sub>1</sub> (Soil)g (ratio of 1)	X <sub>2</sub> (mineral oil)g	X <sub>3</sub> (HV1 60 mineral oil)g
1	1	0
1	0	0
1	0	1
1	½	0
1	½	½
1	0	½

### 3.3.1 Stability Analysis [41a]

The stability of nanofluid is carried out using dynamic light scattering.

Zetasizer: Particle size distribution and the zeta potential are measured using Dynamic light scattering (DLS). Stabilized nanofluid should have particle size <100 nanometer, with zeta potential of  $\pm 40$  to 60mV, which indicates a good stable nanofluid and  $\geq 60$  mV, which indicates excellent stable nanofluid. ZnO –water nanofluid is very difficult to stabilise so must be surfactated using 0.15 to 0.5wt%  $\text{Na}_2\text{HPO}_4$  & SDBS- Sodium dodecylbenzene sulfonate, 0.03 – 0.1wt% for 0.3 – 1wt%  $\text{Al}_2\text{O}_3$  and  $\text{TiO}_2$  (ie for 1wt% ZnO = 1gZnO).

### 3.3.1.1 Dynamic Light Scattering

Dynamic light scattering (DLS) is particularly suited to determine small changes in mean diameter such as those due to adsorbed layers on the particle surface or slight variations in manufacturing processes. In the present case, DLS is used to elucidate the effect of surfactants on overall size of the prepared nanofluids as well as to determine the hydrodynamic size of the coated nanoparticles when dispersed in the water.

DLS measurements were carried out using a Malvern 4800 Autosizer (Fig 3-8) employing 7132 digital correlator. The light source was He-Ne laser operated at 632.8 nm. All measurements were carried out at  $25.0 \pm 0.1^\circ\text{C}$  using a circulating water bath. Cylindrical cells of 10 mm diameter were used in all of the light scattering experiments. The intensity of scattered light was measured five times for each sample at  $130^\circ$ . The autocorrelation function was obtained using a 192-channel photon correlator. According to the semi-classical light scattering theory when light impinges on matter, the electric field of the light induces an oscillating polarization of electrons in the molecules. The molecules then serve as secondary source of light and subsequently radiate (scatter) light. The frequency shifts, the angular distribution, the polarization, and the intensity of the scatter light are determined by the size, shape and molecular interactions in the scattering material. Dynamic light scattering method is one of the light scattering methods. Figure 3-9 shows the sketch block diagram of instrument of Dynamic light scattering. The working DLS is on the basis of three assumptions as mentioned below [15, 16]:





Figure 3-8 Photographic view of a Malvern 4800 zetasizer

The disperse particles or macromolecules suspended in a liquid medium undergo **Brownian motion**, in this situation we know the probability density function, given by the formula:  $P(r,t|0,0)=(4\pi Dt)^{-3/2}\exp(-r^2/4Dt)$  where  $D$  is the diffusion constant, which causes fluctuations of local concentration of the particles, resulting in local in homogeneities of the refractive index. This in turn results in fluctuations of intensity of the scattered light.

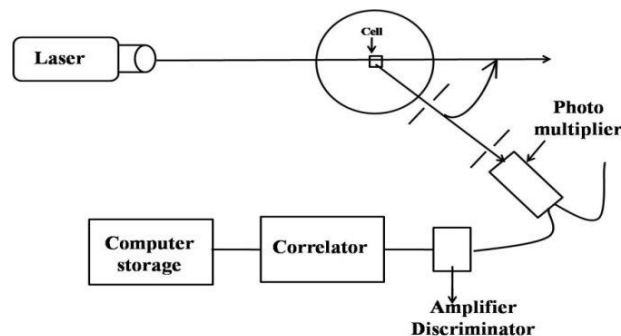


Figure 3-9A sketch block diagram of Dynamic Light Scattering instrument.

pH Meter Calibration: pH meter was calibrated with pH 7 buffer solution and pH 4 buffer solution at room temperature, rinsed with distilled water and wiped with Kim wipe before submersing the pH meter electrode into each nanofluid for the measurement of pH and zetapotential.

### 3.3.1.2 Zeta potential Analyzer

For nanotechnology application it is necessary to dispersed nanoparticles in deionised water. Zetapotential analyzer was used to study the dispersion stability, aggregability and sedimentation property. Zeta potential and corresponding pH values of the prepared suspension were measured by using Zetasizer (Malvern Instruments Ltd.) and pH meter (waterproof pH

scan-2, Eutech Instrument), respectively. Zeta potential of each nanofluid was measured using pH meter (Figure 3-10). The results are shown on Table A-K-1.



Figure 3-10 Photographic view of pH meter

Zeta potential is the potential difference between the dispersion medium and the stationary layer of fluid attached to the dispersed particle. Zeta potential can be calculated using theoretical models and an experimentally determined electrophoretic mobility or dynamic electrophoretic mobility. The potential at the surface of shear for a particle is defined as the zeta potential. Derivations show that the zeta potential is the double-layer potential close to the particle surface and one of its applications is the measurement of surface charges of particle surfaces, such as nanoparticles.

The liquid layer of a particle in suspension migrating in an electric field moves at the same velocity as the surface (shear surface). This shear surface occurs well within the double layer, likely at a location roughly equivalent to the Stern surface. Although the precise location of the surface of shear is unknown, it is assumed to be within a couple of molecular diameters of the actual particle surface for smooth particles. This thickness is associated with the zeta potential and defines the ion atmosphere near a surface.

The magnitude of the zeta potential gives an indication of the potential stability of the colloidal system. If all the particles in suspension have a large negative or positive zeta potential then they will tend to repel each other and there is no tendency to flocculate. However, if the particles have low zeta potential values then there is no force to prevent the particles aggregation. The general dividing line between stable and unstable suspensions is generally taken at either +30mV or -30mV. Particles with zeta potentials more positive than +30mV or more negative than -30mV are normally considered stable.

### 3.3.1.3 Optical transmittance method/ UV – Vis Spectrophotometer.

Along with zeta potential measurements, optical transmittance/ UV – Vis Spectrophotometer. Experiment was carried out for suspension stability of prepared nanofluid by studying sedimentation behaviour [16].The sedimentation behaviour of  $\text{Al}_2\text{O}_3$ ,  $\text{TiO}_2$  and  $\text{ZnO}$  nanoparticles in water was studied by optical method using red He-Ne laser of wavelength  $6328 \text{ \AA}$  and glass beaker of volume (40 ml) with suspension solution was placed between the laser source and the photo detector.The transmittance/absorbancy was recorded by interface in terms of voltage as function of time.The experimental set up is as shown in the Figures 3-11 to 3-13.When an incident beam falls on suspension then part of it gets reflected and some part transmitted through the particles and the suspension solution.

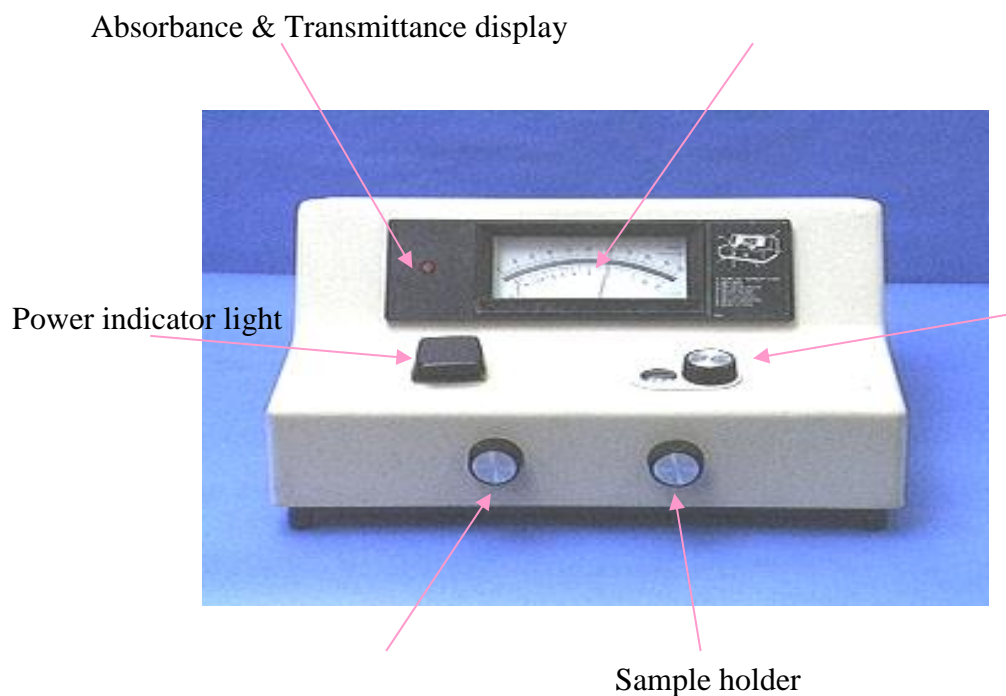


Figure 3-11 Photographic View of UV-Vis Spectrophotometer



Figure 3-12 Absorption Cell/Cuvettes

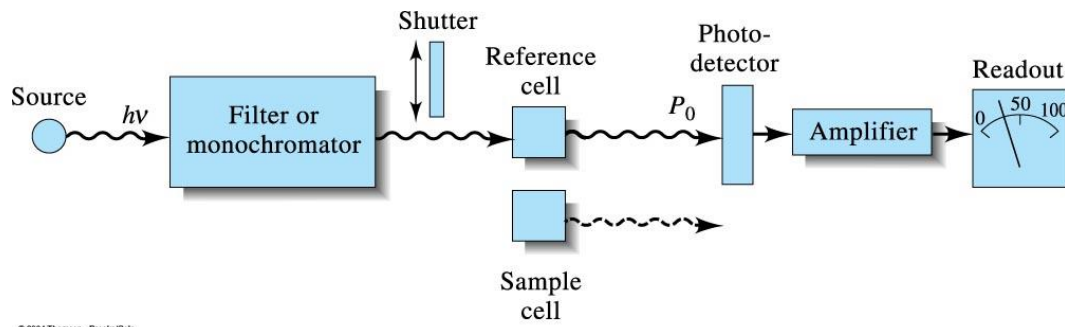


Figure3-4c: Block diagram of uv-visible spectrophotometer

### 3.3.1.4 Contact angle measurements

One of the fundamental methods of characterizing the hydrophobic/hydrophilic properties of a solid surface is to determine the contact angle. The contact angle is a measure of the wetting behavior of a particular liquid on the surface under investigation and directly relates to the Interfacial energies of the systems. The contact angle on the solid surface gets changed merely by changing the chemistry of the outermost monolayer [18, 19]. It can be defined geometrically as the angle formed by a liquid at the three phase boundary where a liquid, gas and solid intersect as shown below.

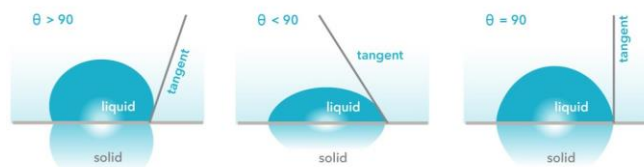


Figure 3-13 More reviewed on water droplet in equilibrium over a horizontal solid surface. It can be seen from the Figure 3-13 that a low value of contact angle ( $\theta$ ) indicates that the liquid spreads, or wets well i.e. hydrophilic nature of surface of solid under test, while a high contact angle indicates poor wetting. If the angle  $\theta$  is less than  $90^\circ$  the liquid is said to wet the solid. If it is greater than  $90^\circ$  it is said to be non-wetting i.e. hydrophobic nature. A zero contact angle represents complete wetting.

## 3.4 Measurement of thermo physical and thermal optical properties of different monotype nanofluids and their hybrids.

3.4.1. Density: The densities of the monotype nanofluids were measured using density meter, while those of the hybrids were measured using Picnometer (Figure3-5) due to unavailability of density meter. The results are discussed in Figures 5-14 & 5-15.



Figure 3-14 Photographic view of a Picnometer for measuring the density of mineral oil and nanofluids

#### 3.4.2: Measurement of viscosity of the different nanofluids.

3.4.2 Viscosity: The Viscosity of nanofluids was measured using a Bohlin Rotational Rheometer (model: 50 Bohlin Gemini) using an Ultra-low (UL), adaptor with geometry of 14mm, gap size of 150 $\mu$ m (Figure3-14).The results obtained are shown on Figures 5-26 to 5-31.



Figure 3-15. Photographic view of Bohlin Rheometer

Using Bohlin Rheometer (Figure3-15) the controlled shear rate rheometer (Contraves LS 40) was applied to measure the viscosity of the monotype and hybrid nanofluids. The rheometer has a cup and bob geometry. The bob is connected to the spindle drive while the cup is mounted onto the rheometer. As the cup is rotated, the viscous drag of the fluid against the spindle is measured by the deflection of the torsion wire. The cup and bob geometry requires a sample volume of around 5 ml; hence, the temperature equilibrium can be achieved quickly within 5 minutes.

The spindle type and speed combination would produce satisfactory results when the applied torque is up to 100% of the maximum permissible torque. In the measurement, the cup was placed onto the rheometer while the bob was inserted into the top shaft. The nanofluids were then transferred to the cup in preventing any bubbles forming. Afterwards, the bob was lowered down until it was completely inserted into the cup and immersed in the nanofluids. The lever knob was then adjusted until the bob and cup were concentric. After the measuring settings such as the minimum and maximum shear rates were set, the experiment was run.

The viscosity as a function of the shear rate was plotted.

For the temperature effect, the rheological property of the nanofluids was measured by viscometer/ Bohlin Rheometer with the thermostat, which controls temperature. The viscosity measurement was started at 20 °C, and temperature was gradually increased to 70 °C at an interval of 10 °C. The nanofluid temperature was also measured by using a thermocouple. All the viscosity measurements were recorded at steady state conditions. Chandrasekar et.al.[31] found that, in general, dynamic viscosity of nanofluid increases considerably with particle volume concentration but clearly decreases with a temperature increase.

### 3.1.1 Surface tension

Table 3-9 Measured surface tension data for the different nanofluids

Nanofluid system	Volume (μL) microlitre)	Area (mm <sup>2</sup> )	Surface tension(mN/m)
1 vol%TiO <sub>2</sub>	7.2528	18.08	52.46
1 vol%ZnO	8.6725	20.27	46.74
1 vol% Al <sub>2</sub> O <sub>3</sub>	4.5330	12.87	39.76
0.3 vol% Al <sub>2</sub> O <sub>3</sub>	32.2535	47.84	46.98
0.7 vol% Al <sub>2</sub> O <sub>3</sub>	30.8395	46.68	25.73
0.3 vol% ZnO	30.8955	45.66	88.03
0.7 vol% ZnO	37.5676	57.18	22.61
0.3 vol%TiO <sub>2</sub>	48.7350	64.55	36.1
0.7 vol%TiO <sub>2</sub>	54.8070	69.91	40.3
0.7ZnO + 0.3Al <sub>2</sub> O <sub>3</sub>	8.8925	21.4257	42.05
0.3ZnO + 0.7TiO <sub>2</sub>	4.8706	11.7353	50.21

0.7Al <sub>2</sub> O <sub>3</sub> + 0.3TiO <sub>2</sub>		5.8940	14.2011	65.5253
0.7TiO <sub>2</sub> + 0.3Al <sub>2</sub> O <sub>3</sub>		6.2149	14.9742	69.0923
0.3Al <sub>2</sub> O <sub>3</sub> +0.3TiO <sub>2</sub> + 0.3ZnO		8.9049	21.4556	45.3651
0.3ZnO + 0.7Al <sub>2</sub> O <sub>3</sub>		6.8889	16.5982	47.6593
0.7ZnO + 0.3TiO <sub>2</sub>		4.9067	11.8223	31.4966
0.3TiO <sub>2</sub> + SDBS		29.1135	46.47	114.11
0.7TiO <sub>2</sub> + SDBS		25.3286	41.46	129.97
1.0 TiO <sub>2</sub> + SDBS		31.4628	45.62	94.34
0.7 ZnO + Na <sub>2</sub> HPO <sub>4</sub>		25.1265	41.43	104.91
1.0 ZnO + Na <sub>2</sub> HPO <sub>4</sub>		27.9566	44.04	180.81
0.3 ZnO + Na <sub>2</sub> HPO <sub>4</sub>		32.4725	49.09	181.61
0.3Al <sub>2</sub> O <sub>3</sub> + SDBS		25.6804	41.58	147.21
0.7Al <sub>2</sub> O <sub>3</sub> + SDBS		40.8309	57.37	191.41
1.0Al <sub>2</sub> O <sub>3</sub> + SDBS		39.1810	52.97	91.76
0.7ZnO + 0.3Al <sub>2</sub> O <sub>3</sub> + surfactants		18.5969	33.95	152.44
0.3ZnO + 0.7TiO <sub>2</sub> + surfactants		12.9062	25.16	646.1

0.7Al <sub>2</sub> O <sub>3</sub> + 0.3TiO <sub>2</sub> + SDBS		30.6779	47.61	214.84
0.7TiO <sub>2</sub> + 0.3Al <sub>2</sub> O <sub>3</sub> + SDBS		22.2020	38.18	214.15
0.3Al <sub>2</sub> O <sub>3</sub> +0.3TiO <sub>2</sub> + 0.3ZnO surfactants		29.2999	45.20	878.64
0.3ZnO + 0.7Al <sub>2</sub> O <sub>3</sub> + surfactants		20.3948	36.11	195.92
0.7ZnO + 0.3TiO <sub>2</sub> + surfactants		19.1950	34.26	878.64



Figure 3-16 Photographic view of Attension Theta (Potential meter)

### 3.1.1 Contact angle measurements

The contact angle is a measure of the wetting behavior of nanofluids. In the present thesis, contact angle measurements used to deduce the successful attachment of hydrophilic ligands of secondary surfactant on the surface of prepared nanofluids. Water Contact Angles of the surfacted and pure nanofluids were measured using Pendant drop method by deposition of 4-6  $\mu$ L droplets of nanofluid water on a horizontal surface (glass slide) and their observation in cross-section. Each drop was observed directly with an Olympus BX-41 microscope objective lens, whereas its image was digitally captured using a 1.4 megapixel computer-controlled



digital CCD camera. The instrument used for measuring the contact angle is shown in Figure 2-11. The results obtained for contact angles are shown on Table 6-6 and fig.6-8.



Figure 3-17 The picture view of Contact Angle Instrument.

Attestion Theta / Optical Tensiometer is a mobile contact angle meter enabling characterization of solid surfaces and liquid - solid interactions. It is primarily used for quality control measurements and characterization of large objects. The contact angle is the angle at which the liquid/solid/air interface meets the solid surface. When a liquid droplet is set onto a smooth homogeneous horizontal surface, it may spread out over substrate and the contact angle will approach zero if complete wetting takes place. Conversely, if wetting is partial, the resulting contact angle reaches equilibrium in the range of the material's surface energy. The smaller the contact angle the greater the wettability or surface energy of the substrate is said to be. Contact angle is a good measure of surface wettability. Attestion Theta is used in measuring Wettability, Surface tension, Interfacial tension, Contact angles, Absorption, Surface free energy, Adsorption, Spreading, Cleanliness, Surface heterogeneity and Interfacial rheology (Figures 2-16 & 2-17).

Contact angle,  $\theta$ , is a quantitative measure of the wetting of a solid by a liquid. It is defined geometrically as the angle formed by a liquid at the three phase boundary where a liquid, gas and solid intersect as shown on Fig 3-13.

When attracted by the solid, the liquid spreads, forming a drop with low contact angles ( $\theta < 90^\circ$ ). If repelled, the contact angles are high ( $\theta > 90^\circ$ ). The contact angle is determined by the interactions between the gas, liquid and solid phases. A change in one of the phase properties will lead to a change in contact angle measurable with Theta QC. Using a known liquid (typically water) and gas (typically air) enables checking the solid properties. It is also possible to test liquid properties on a known surface.

3.5: Evaluation of dispersion of the different nanofluids by using the UV–visible spectrophotometer/absorption spectrum.

Evaluation of dispersion characteristics of the  $\text{Al}_2\text{O}_3$ ,  $\text{TiO}_2$  and  $\text{ZnO}$  nano-suspensions was accomplished using the UV–Visible spectrophotometer (Fig.3-11).The experiments were conducted using 100 ml of 0.3% - 1%  $\text{Al}_2\text{O}_3$ ,  $\text{TiO}_2$  and  $\text{ZnO}$  nano-suspensions.Different concentrations of the surfactants (SDBS and  $\text{Na}_2\text{HPO}_4$ ) were added to the nanosuspensions, which were thoroughly stirred with magnetic stirrer for at least 1 hour with 1100 rpm and sonicated with the ultrasonic disruptor for 24hrs at  $25^\circ\text{C}$ . In addition, a blank of deionised water sample in the test tube was measured first using spectrophotometer then 2 ml of each nanosuspension was added to the blank water sample and diluted 99 times with deionised water then pass through a light The absorbency of the nano-suspensions was measured on a UV–Visible **spectrophotometer**.When the original suspension concentration was greater than 0.1mg/ml, the dispersions were rapidly diluted to 0.1mg/ml (99times) and then spread over a blank of water for the UV – Vis spectrophotometer measurements.During the experiment, if the absorbency value is greater than, (eg 1 – 3 and above).It means that the testing sample is highly concentration and have to be diluted until the absorbency is less than +1 (0.0 to 0.9 ie stable /stability).When the absorbency is negative (ie unstable), the test sample has to be diluted by adding more nanofluid until the absorbency is +ve.Stability increases as absorbency approaches 1 and beyond that is unstability.

### 4 4.0: Soil preparation and characterization

#### 4.1 Study site

The study was conducted from 2012 to 2014 on a garden at Chapeltown, 16 km east of the Leedcity, Leeds (27°32'50"S; 70°15'50"W). Soil evaluations were done at the former Institute of Particle Science Engineering, University of Leeds, during last year of preliminary experimental set -up (2012). The study site is characterized by high winter precipitation of around 65.5 mm per year, with daily average temperatures fluctuating between 25° C in summer and 5° C in winter.

##### 4.1.1 Soil Sampling

On August 2012, 24 hours after rainfall, soil sampling was done using a hand auger at the depth of 0 - 50cm. This type of soil was chosen because of low cost, its physical and chemical properties as arable soils favourable to plant growth. Samples were taken at 0-10 and 10-30 cm in order to measure the soil physical properties.

4.1.2 Soil Analysis: Soil samples collected were transferred to the Laboratory, oven dried at 25°C for 24hrs. Samples were sieved to sieve cut of 1.18 mm and coarse materials were hand picked and the samples were stored for the analysis. Particle density (DP) was measured using picnometer [61]. Soil texture was determined by the Bouyoucos method [63] using samples from each depth.

In parallel, a portion of undisturbed soil sample was oven dry for 48 h at 105 °C until a constant weight is reached to 16% moisture content, for bulk density (Db) [57]. The measured values of bulk density are showed on Table 4.1.2. All the methodologies are detailed in [142]. With the values of DP and Db, the total porosity (TP, %) was calculated by  $TP = [1 - (Db / Dp)] \times 100$ . The total porosity result is showed on Table 4.1.1. Hydraulic conductivity (permeability) was measured using constant head permeameter; the experimental set up is illustrated as shown in Fig.4-1.

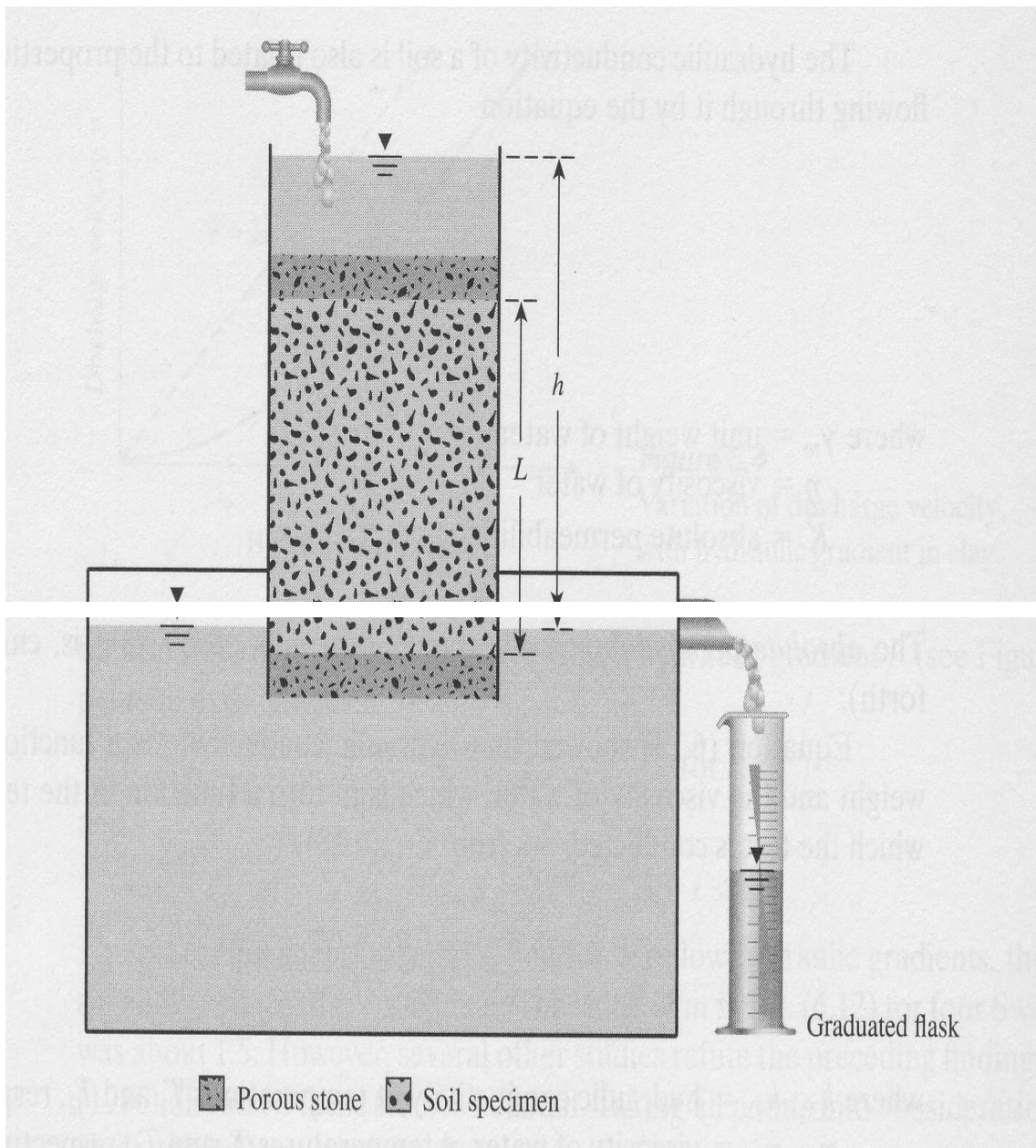


Figure4-1.Illustration of the Constant Head permeability test apparatus experimental setup

The core/soil sample is placed in the beaker which is a core holder. The tap supplies water  $Q$ , to the soil sample in the beaker at a constant rate, which is recorded. The water flowing out of the system (or water that permeates through the soil) is collected in a graduated cylinder and recorded. The constant – head permeability test arrangement is shown in Fig 4-1. The test gives these values showed on Table 6.1.3.

The results of the physical properties of experimental soils are shown on Table 6-1.

#### 4.2 Soil Characterization

The soil was classified according to soil taxonomy series. The soils were classified into fine (<2mm) and coarse (>2mm). Following [136], textures are clay loam to Sandy clay loam (22 to 33% of clay content and 36 to 54% of sand content).

#### 4.3 Soil contamination



Figure 4-2 Burette/Imbibition Flask with Core soil sample

Burette/Imbibition Flask with Core soil sample under Spontaneous Imbibition and also Figure 4-2 were used for the core nanofluid flood system used for the wettability alteration investigation at soil reservoir conditions [57]. The core flood apparatus was used to determine oil recovery, saturations of oil and end-point effective permeabilities. A core soil flood data from the experiments were used to calculate wetting properties of the soil and oil/water relative permeabilities.



Figure 4-3 Laboratory clean-up experimental Set-up of oil contaminated soil using nano fluid

The experiment was set-up by artificial pollution of the soil samples with different quantities of mineral oil (crude oil/petroleum) Fig4-2, based on the following formulation procedure [57]: The soil samples were contaminated in the ratio of 1:1 (10g of soil: 10g (10ml) of mineral oil) and later in the ratio of 1:1/2. Each of the mineral oil Figures 4.2 & 4-3 contaminated soil was left for 24 hrs for uniform absorption of oil by the soil.

**Thermal analysis:** The contaminated soil samples were later transferred to thermal gravimetric analyzer to determine rate of mass change and weight loss of the mineral oil contaminated soils. Oil contaminated samples of 10 – 50mg was taken from each of the bulk oil contaminated soil (10g of soil: 10g (10ml) of mineral oil) for Tga test. This was done using Mettler, TG 50 under controlled temperature rise from room temperature to 400°C at the rate of 30°C / min, interval of 30 °C , period of 60mins, pressure of 50ml/min. TGA test was carried out on the oil contaminated samples before and after cleaning with nanofluids. Taking small soil sample from the top, middle and bottom to ensure uniform/even contamination (fully saturation) of the soil sample from which average values were determined. The experimental results are shown in figures A-34 to A-123.



Figure 4-4 White mineral oil.



Figure 4-5 HV160

These oils Figs 4-4 & 4-5 were used to simulate crude oil contamination soil.

#### 4.4 Cleaning Process using different nanofluids & their combinations with and without surfactants.

Each of the powdered nanoparticles, ZnO, TiO<sub>2</sub> and Al<sub>2</sub>O<sub>3</sub> (dispersed in water, base fluid) was added to the contaminated soils, and left for 24hrs for cleaning. Cleaning efficiency was quantified using Mass balance method. TGA test was used to determine the amount and weight loss of crude oil before and after the cleaning process under three process variables (Onset temperature, T<sub>1</sub> = 30 °C /min & T<sub>2</sub> = 400°C, pressure, 50 & 150 bars and time, 30, 40 & 60mins) of 3,2 simplex lattice design after which optimum process variables for cleaning crude oil contaminated soil samples were determined statistically with ANOVA and modelled using Regression and correlation analysis. From the Mettler Toledo Tga test already carried out, the optimum process variables were found to be 400°C, 150 bars and 40mins with onset temperature of 30°C/mins. Tga test starts heating from 30°C/mins to 400°C and cooling down to 30°C/mins for max of 40mins. Cleanup ratio: (soil: oil: nanofluid) ie (1:1/2, 1/2) for primary cleaning, or (1:1/2: 3/2) for secondary cleaning. Oil recovered after the cleaning is shown on Fig 4-6.

Reason for using mineral oil instead of crude oil to simulate crude oil contaminated soil sample. The use of mineral (laboratory) oil is common because crude oil often precipitate polar compounds at ambient temp, hence, the experiments must be performed at elevated temps when using crude oil. In other cases crude oil is simply not available and mineral oil must be used instead. Sometimes, mineral oil is used for establishing initial water saturation because it has a more favourable viscosity than crude oil which makes it easier to displace the water. When the correct initial water saturation is obtained, the mineral oil is displaced with crude oil at elevated temperature [151].

**Procedure I.** Sandy soil of 10g increment up to 50g was taken and simulated with mineral oil by adding 5% 10%, 15% .in the increments of 5% up to 40% weight/volume % of various mineral/lubricant oil grades. Subsequently, they are mixed thoroughly (Table 4-1). Then 1g of powdered nanoparticles (ZnO Al<sub>2</sub>O<sub>3</sub> and TiO<sub>2</sub>,) is dispersed in water (in the ratio of Xg of nanoparticles: (100-Xg) of water, ml) to form nanofluids. Concentrations of, 0.3% - 1% of ZnO, nanofluids were added to the contaminated soils in the burette and observations were made based on the extent to which each nanofluid cleaned the contaminated soils. Al<sub>2</sub>O<sub>3</sub> and TiO<sub>2</sub> nanofluids cleaning behaviour was investigated in the same way as explained above. Take for

example, 10g of dry soil was measured into a burette; 5ml of mineral oil was added into the burette to contaminate the soil (15g). This was left for 24hrs after which the amount of oil that drained from the contaminated soil is recorded, Figure 4-3. By the second day, 10 – 50mg of soil sample is taken from the top, centre and bottom of the contaminated soil sample in the burette for analysis using TGA. Soil sample was taken from the top, centre and bottom of the contaminated soil sample to ensure fully saturation of the soil sample in the burette. Nanofluid was added to the contaminated soil sample in the burette. The amount of oil that drained per day and secondary cleaning (rinsing) was recorded. After this, the soil sample was taken to TGA for analysis [41a]. Cleaned soils from TGA were stored in a bottle jar.



Figure 4-6 Refined golden Oil recovered from the contaminated soil using nanofluids

Table 4-1 **Summary of Experimental set-up** using 2 x 3 factorial designs ( $2^3$ ) for simulation and cleaning of crude oil contaminated soils.

Soil contamination & Clean-up process

Samples		TGA	DLS	Density meter	Viscometer
No.	Name	Soil (g)	Oil (g)	Nanofluid (g)	Surfactant (g)
1	V <sub>1</sub>	100	0	0	0
2	V <sub>2</sub>	10	5	0	0
3	V <sub>3</sub>	10	5	5	0.5
					depending on the type of nanofluid
4	V <sub>4</sub>	20	10	0	0



5	V <sub>5</sub>	20	10	10	0.15
6	V <sub>6</sub>	30	15	0	0
7	V <sub>7</sub>	30	15	15	0.35
8	V <sub>8</sub>	40	20	0	0
9	V <sub>9</sub>	40	20	20	0.5
10	V <sub>10</sub>	50	25	0	0
<b>11</b>	<b>V<sub>11</sub></b>	<b>50</b>	<b>25</b>	<b>25</b>	<b>0.5</b>

---

Mass balance: Mineral oil (in) = Mineral oil (out)

#### 4.3.3 Saturation of soil samples

The experimental setup was represented on Fig.4-1. First, the empty burette was weighed and setup as in Fig 4-1. Second, the dry soil was weighed and placed in the burette. Third, mineral oil (which is less viscous) was added to the soil in the burette and left for 24hrs for full saturation of oil by the soil. Fourth, each nanofluid was poured into the burette with soil through flooding. The burette was filled with measured substantial amount of nanofluid covering the soil. It was left for 24 hours to let the soil fully saturate. The results obtained are showed on Table 6-3.

#### 4.4.0 Wetting Analysis

##### 4.4.1 Wettability Determination

Amott and USBM are two quantitative methods that were used for wettability determination. The Amott method is an empirical method based on spontaneous imbibition and drainage with the use of burette as shown on Fig 4-1 for oil contamination soil and cleanup process. Figure4-2 is a burette with a core soil sample saturated by flooding it with oil. Figure4-2 is a saturated oil core soil sample flooded with nanofluids. The spontaneous oil and water are separated and recorded. Both oil and water spontaneous as well as free production volume were noted during the measurements.

These were the measurement of contact angle and Amott imbibition test based on contaminated soil sample. The imbibition test consists of spontaneous and frees (gravitational force) imbibition to measure the average wettability of the soil. The method is based on the fact that during the artificial oil contamination of soil sample, the wetting fluid (oil) imbibe spontaneously into the soil and displace the non wetting air. After contamination, during the clean-up process, the nanofluid imbibe spontaneously into the contaminated soil sample displacing the oil until the irreducible water saturation ( $S_{wir}$ ) and the residual oil saturation ( $S_{orw}$ ) were reached. The water saturation was further increased by forced displacement of oil

by water. The wettability index to water is given as the ratio of the volume of the spontaneously imbibed water, to the total increase in water saturation after spontaneous and forced imbibition. The ratio of spontaneous to forced imbibition is used to reduce the influence of other factors such as relative permeability, and the initial saturation of the soil; the results obtained are showed on Table 6-3. The amount of oil and water displaced were measured using separating funnel. The wettability index to water is given as the ratio of the volume of the spontaneously imbibed water -nanofluid, to the total increase in water saturation after spontaneous and forced imbibition.

$$I_w = \text{Spontaneous Water nanofluid Imbibition} = \frac{V_{o1}}{V_{o1} + V_{o2}} \dots\dots\dots \text{eqn4.2a}$$

$V_{o1} + V_{o2} = \text{Total Water nanofluid Imbibition}$

$$I_o = \text{Spontaneous Oil Imbibition} = \frac{V_{w1}}{V_{w1} + V_{w2}} \dots\dots\dots \text{eqn4.2b}$$

$V_{w1} + V_{w2} = \text{Total Oil Imbibition}$

Where  $V_{O1}$  is the volume of oil produced/displaced during spontaneous imbibitions/during cleaning,  $V_{O2}$  is the volume of oil retained after water nanofluids flooding/after cleaning,  $V_{W1}$  is the water produced/displaced during nanofluid flooding/ spontaneous "imbibition" and  $V_{W2}$  is the volume of water retained after nanofluids flooding. The wettability of the soil was determined quantitative with the wettability index,

Based on the test, the wettability index WI was calculated as:  $WI (I_{wo}) = I_w - I_o$ . The index compares the imbibition potential of water and oil, and varies from +1 for strongly water-wet soil to -1 for strongly oil-wet soil [11, 12].

Discussion based on mineral oil contamination and cleanup process (Figures 4-2 & 4-3).

Soil contamination (Figure 4-2). During a cleanup process (Figure 4-3), water nanofluid flooding of water – wet system, water moves through the porous soil in a fairly uniform front. The ponded water tends to imbibe into any small or medium –size pores, moving oil into the larger pores where it is easily displaced, only oil is moving ahead of the front. Figure 4-3 (of my Master’s thesis) shows water displacing oil from water – wet pore. The soil surface is preferentially wetted by the water, so water will advance along the walls of the pore, displacing oil in front of it. At some point, the neck connecting the oil in the pore with the remaining oil becomes unstable and snap off, leaving a spherical oil globule trapped in the centre of the pore. After the water front passes, almost all the remaining oil and water is immobile (residual

oil & irreducible water). Because of such immobility in this water – wet case, there is little or no production of oil after water breakthrough [38, 113].

In this study, nanofluid flooding, water –wet soil is an imbibitions process, while nanofluid flooding oil- wet soil (soil contamination) is a drainage process. Ie primary cleaning of a contaminated soil with nanofluid is a drainage process, while the secondary cleaning process is the imbibition process.

Imbibition is often used to refer to flow that results in increasing wetting –phase saturations, while drainage refers to flow with decreasing wetting phase saturations. Wetting refers to water – wet, nonwetting is for oil –wet state.

#### 4.4.3 Measurement of the Contact Angle

The contact angle,  $\theta$ , of mineral oil and nanofluid, a water phase ) was measured using Cam 100 (KSV instrument) through the imaging method. The imaging method is based on Young's law (Equation 2.6). The contact angle is measured through the denser phase which in this case was the aqueous phase. Figure 4-7 include three examples of how a droplet of oil on a solid can behave when in contact with a water phase.

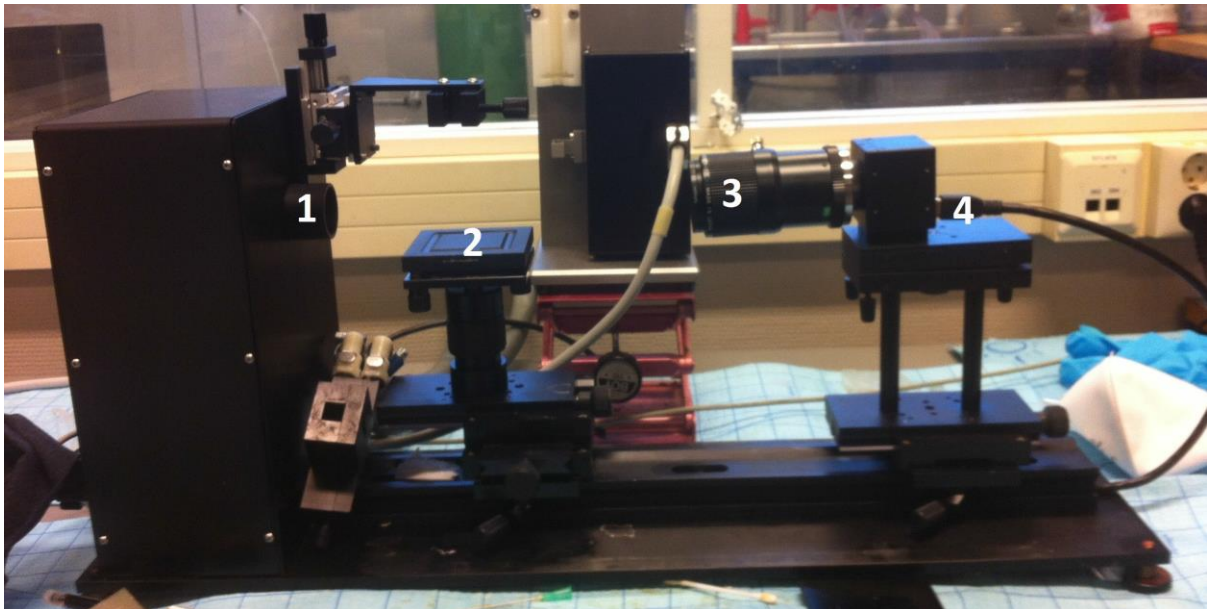


Figure 4-7 Set-up of the Cam 100 (KSV instrument) camera

Cam 100 (KSV instrument) camera used for measurement of the contact angle between nanofluid, oil and a slide glass plate. Index 1 shows the back light, index 2 the placement of the glass box, index 3 is the camera and lens to sharpen the picture while index 4 is the cable connected to the computer.

The setup of the Imaging Method is shown in Figure 4-14. The glass box with a smooth and clean glass plate was filled with deionised water first and later with different nanofluids. A syringe with a hooked needle was filled with the mineral oil and was used to place a droplet under the slide glass plate as shown in Figure 4-13 (b). The glass box was then put in front of the camera. To allow for the system to reach equilibrium the oil droplet, water-nanofluid phase and glass plate was left to rest for at least 30 mins before recordings were made. Lastly, the camera, computer and software "Adhesion theta" were used to take pictures of the droplet and to calculate the average of the contact angle measurements. 60 frames of 60 seconds were chosen. The results are shown in Chapter 5.

#### 4.4.4 Wetting properties of soil

**4.4.4 .1** Wetting Analysis comprising of Determination of Wettability indices, contact angle and relative permeabilities. The series experiments conducted for these analyses/calculations were from my Master's thesis. The calculations were computed based on Brook-Corey equations and modified Brook and Corey model as shown on Figs and Tables. Brook-Corey equations used do not always result in a good curve fit of the laboratory results (as can be seen on Figs of plotted pure & surfactant nanofluids on relative permeabilities Figs 6-10 & 6-11). In addition, due to the difficulty of determining all parameters, therefore, the most useful model in petroleum industry, the modified Brook and Corey model was used for the final calculations. The results obtained were plotted on graphs and presented on Tables as shown in Chapter 6.0.

##### **4.4.4 .1 .1** Determination of Oil-Water Relative Permeabilities.

The following functions (Modified Brook and Corey relationship) are used to generate the relative permeabilities from coreflood data:

A detailed summary of results for experiments conducted in this study is shown in Tables 4-2 & 4-3. End-point relative permeabilities were measured for the system at various surfactant concentrations. The characteristics of relative permeability curves, initial water saturation, end-point relative permeabilities to water and oil and cross-over points were used to interpret surfactant induced wettability alterations. This investigation is focused on wettability alteration

using mineral oil simulated soil samples and cleanup process at soil reservoir conditions. The mechanism behind this process is reduction in surface tension as well as wettability alteration. Modified Brook and Corey relationship [26]:

For oil –wet, & gas –oil formation /systems

$$K_{ro} = \frac{K_{ro} (1 - S_w - S_{or})^{n_o} K_{ro} (1 - S_w - S_{or})}{S_{wir} - S_{or}} \dots \dots \dots (4.3a)$$

For water – wet formation (system)

$$K_{rw} = \frac{K_{rw} (S_w - S_{wir})^{n_w}}{S_w - S_{wir}} \dots \dots \dots (4.3b)$$

Where,  $K_{ro}$  = End point relative permeability normalized to oil absolute plug air permeability  
 $K_{rw}$  = End point relative permeability normalized to water absolute plug air permeability  
 $S_{or}$  = Residual oil saturation,  $S_w$  = Water saturation,  $n_o$  = Corey exponent to oil and  $n_w$  = Corey exponent to water. Parameters used for the recalculation of replotted graphs were based on values contained on Table 4-2&4-3.

Table 4-2 Critical phase saturation & relative permeability data based on [26, 27]

Initial parameters	Initial values
Connact water saturation, $S_{wc}$	0.16
Relative oil permeability at $1 - S_{wc}$ , $K_{ro}$	1
Oil residual saturation, $S_{ro}$	0.2
Relative water saturation at $S_{ro}$ , $K_{rw}$	0.3
Initial water saturation, $S_w$	0.2
Initial oil saturation, $S_{or}$	0.8
Initial permeability, $K$	$3.36 \times 10^{-5} \text{m/s}$
Initial porosity, $\phi$	42 - 44%

Note:  $S_{wir}$  = lowest value of the saturation,  $S_w$ . It ranges from 0.16 to 0.168 at porosity = 0.31 to 0.305. Porosity,  $\phi$  from 40 – 50%,  $S_{wir} = 0.2$ . Generally,  $S_{wir} = 0.1 - 0.2$ .

$$K = \frac{0.136\phi^{4.4}}{S_{wir}^2} \dots \dots \dots (4.4), S_{wir} = \frac{BVWi}{\phi_t} \dots \dots \dots (4.5)$$

Where,  $BVWi$  is the irreducible bulk volume water and  $\phi_t$  is the total porosity

Table 4-3 Summary of the different parameters used for the calculations.

Name	Min	Mean	Max	Std
$n_w$	2.09	2.61	3.32	0.21
$n_o$	2.14	2.7	3.37	0.18
$\phi$	0.05	0.20	0.35	
$S_w$	0.00	0.50	1.00	
$S_{or}$	0.10	0.25	0.4	
$S_{wi} = S_{wir}$ (sometimes)	0.10	0.35	0.60	

Most of my calculations were done using  $n_w = 7$ ,  $n_o = 2$  for water – wet condition. Then  $n_o = 6$ ,  $n_w = 1$  for oil-wet condition and  $S_{wir} = 0.2$

4.5 Experimental Errors: These include – i. Measurement errors.

ii. Environmental/surrounding Errors. iii. Human Errors

Several problems were encountered during the soil contamination (imbibition testing) and experience concerning the experiment was gained. The main challenges (disadvantages) are summarized below, and the main learning points (advantages) are given.

Lack of experience in the laboratory and with the experimental method led to several mistakes in the first experiments especially during the formulations, preparation and characterisation of nanofluids as well as mineral oil soil contamination & cleanup process. The main error performed was in the cleanup the experiments. The core soil samples were fully saturated with mineral oil for one day, the use of a burette with a too small size, filter and control valve made oil to trap in the burette after clean up leading to improper oil drainage and improper cleaning of separating funnel. Improper cleaning of separating funnel lead to blockage of the measuring tube of the separating funnel as it is shaped as a bottleneck. In some cases the mineral oil lost its grip by shaking the apparatus.

Last, based on the results of the cleaning efficiency, most of the cores obtained a very high or low cleaning/recovery rate. There might be a problem that the optimization and cleanup process explained in Chapter 4 was too short. However, it had to be kept short due to the time limitation of the thesis.

The main learning points for the measurement of properties and spontaneous imbibition test are important and can be used in the next wettability investigation of mineral oil. The size of needles for measuring surface tension and contact angle of the nanofluids must be big and clean to avoid the blockage of the needles. Further advantages are as follow:

The preparatory conditions must be kept stable. Experience with the method performed is important. Proper cleaning is important as the nanofluid is sticky and easily attaches to glass. Proper cleaning is done by first cleaning with ethanol, then with distilled water and last properly cleaning with soap and water. The cleaning is important for the burettes, separating funnel and needles.

4.6: Remediation Factors/ Contribution Factors to the clean-up of experimental simulated crude oil contaminated soils. These are nanofluid, time and temperature. They contributed directly to the cleaning of the contaminated soils and restoring it to its original status. TGA has indirect effect on the cleaning behaviour of nanofluids on crude oil contaminated soils. Contribution factors were statistically analysed using Path analysis and Time series analysis.

The results were presented in Tables and Figures (graphs). The data were analysed using IBM Statistical Analysis of Regression, Correlation (path analysis) and Time series from which model(s) were developed. Comparisons were made based on the two techniques used in the experiments (i.e. cleaning of the crude oil contaminated soils with pure and surfacted nano fluids (ZnO, Al<sub>2</sub>O<sub>3</sub>, and TiO<sub>2</sub>) [57].

4.7. Comparison of cleaning efficiency and wettability using mixture experiment technique (3,3 Simplex Lattice Design). The statistical data analysis was done using IBM SPSS statistics, version 20 & SAS Software. The statistical analysis is contained in the Appendice.

## 5 Chapter 5.0

### 5.1 Experimental Results and Discussions.

This chapter is a summary of the results and main findings from the experimental work. An evaluation of the results from the measurements and of the experimental methods are given.

#### 5.1.1 Characterization of the mineral oil used in the experiment.

This was done using Physical and chemical properties of the experimental mineral oil.

Table 5-1 Physical and chemical properties of the experimental mineral oil

Temp(°C )	Density (g/cm <sup>3</sup> ) without surfactant	Density (g/cm <sup>3</sup> ) with surfactant	Specific gravity	Specific gravity with surfactant	pH at 17.1°C
10	0.9196	0.9346	0.9199	0.9349	7.01
15	0.9197	0.9324	0.9205	0.9333	
20	0.9166	0.9317	0.9183	0.9334	
25	0.9122	0.9289	0.9149	0.9317	
30	0.8453	0.9765	0.8472	0.9805	

Emf = -10.47 mV

Table 5-2 Physical and Chemical properties of the experimental mineral oil (IARC 1984)

Property	Value range
Specific gravity	Heavy: 0.845 - 0.905, Light: 0.818 - 0.880
Boiling point	260 – 330 °C
Vapor pressure	<0.5
Appearance	Clearly oily liquid, odorless or of a pale yellow color (when not highly distilled),
pH	7 – 7.6
Density	About 0.8g/cm <sup>3</sup> , 0.976 g/cm <sup>3</sup> at 25°C



Table 5-3 Property table for organic compounds used in the experiments [22]

Name	Mineral oil/paraffin oil (Octane)	Ethanol
Chemical formula	C <sub>8</sub> H <sub>18</sub>	CH <sub>3</sub> CH <sub>2</sub> OH
Molecular weight	C <sub>n</sub> H <sub>2n+2</sub> , n = 16 – 24	46.1
Density at 25°C (g/cm <sup>3</sup> )	0.85	0.785
Boiling temp at 1atm (°C)	300	78.3
Melting temp(°C)	-24	-114.1
CAS No.	8012 – 95 -1	
Refractive index	N20/D1.467	

Table 5-4 Property table for water (which is an inorganic compound) [22]

Name	Water (oxide)
Chemical Formular	H <sub>2</sub> O
Molecular weight	18.0
Density at 25°C (g/cm <sup>3</sup> )	1.0
Boiling temp at 1atm (°C)	100
Melting temp(°C)	0
Contact angle	28.05° – deionised water

Comparing the measured mineral oil values in Table 5.1 with those of literature values in Table 5.2, the measured mineral oil density ranged from 0.845 to 0.9197 g/cm<sup>3</sup>. The mineral oil used in the experiment can be identified as cyclic paraffin (petroleum jelly, otherwise known as "white petrolatum"), in the family of Alkane hydrocarbon oils. There are many types of mineral oils; the Chemical Abstracts Service (CAS) has assigned unique registry numbers to mineral oil types. CAS number 8020-83-5 is used to indicate white mineral oil is being referred to liquid paraffin or deodorized kerosene (8020-83-5). Liquid paraffin (White mineral oil) is mildly toxic by ingestion and is a skin and eye irritant. It has a flash point of 195 degrees C (195 degrees C), an auto ignition temperature of 338 degrees C (338 degrees C) and a density of 0.845 below is the plot of viscosity of the mineral oil against temperature as measured using Rheometer.

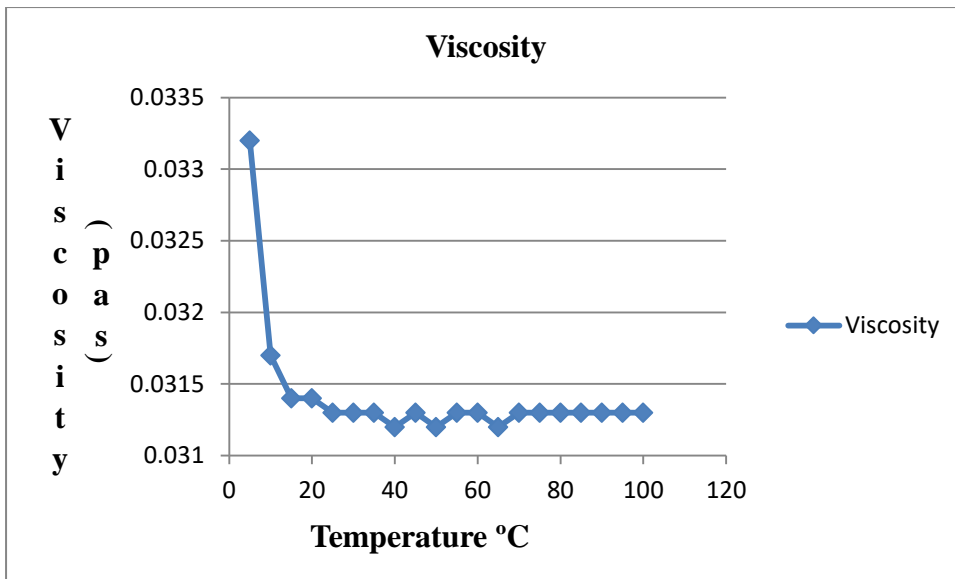


Figure5-1 Viscosity of the experimental mineral oil [57]

Figure5-1 shows the graph of the viscosity of the mineral oil used in the experiment. Viscosity decreased with increased in temperature and remained constant with further increased in temperature.

#### 5.1.2 Characterization of nanofluids

The results of average particle size determined by Dynamic Light Scattering studies using zetasizer (Nano-ZS, Malvern Instruments, and USA) are shown in Figures 5-2 to 5-7. The zeta potential and pH of the nanofluids were measured using pH meter; results are shown in Table

#### 4. 6.0 Results and Discussion

Graphs for nanofluids characterization (Figures5-2 to 5-7)

A Zetasizer Nano ZS (Malvern) was used for measuring the average dimension of the nanoparticles in solution. The particles in a liquid move about randomly and their speeds of movement are used for determining the size of the particles. The particles move by Brownian motion in which the small / light particles move quickly and form particle size distribution (stable solution) while large/heavy particles move slowly, to form large aggregate (cluster-unstable solution) [57, 16]

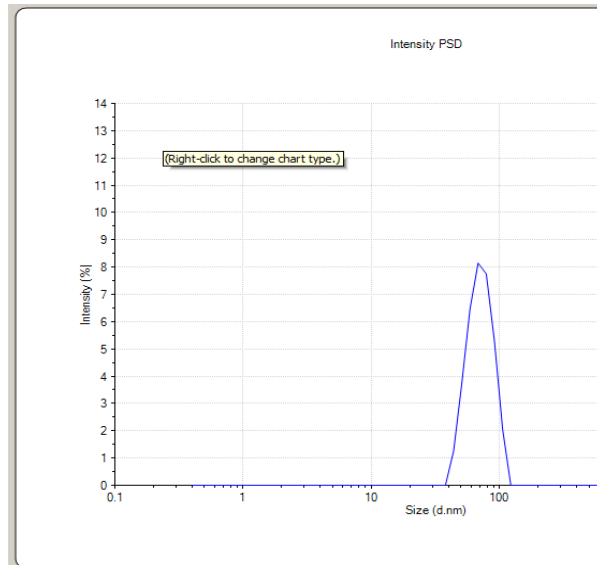


Figure 5-2 Particle size distribution of pure 0.3 vol% Al<sub>2</sub>O<sub>3</sub> water nanofluid

Particle size distribution: Figure 5-2 shows the hydrodynamic particle size distribution of 0.3 vol% Al<sub>2</sub>O<sub>3</sub> –water nanofluid at 25°C, room temperature. The nanofluid formulated with 0.3g Al<sub>2</sub>O<sub>3</sub> nanopowder +99.70ml deionized water calcined at 25°C had the average aggregate size, 71.77 d.nm, peak diameter aggregate size, total surface area of 0.0214 nm<sup>2</sup>, with percentage intensity of 100%. The Particle size distribution is less than 100nm which revealed the powdered nature of the nanoparticles. The zeta potential of pure 0.3vol% Al<sub>2</sub>O<sub>3</sub> water nanofluid was determined to be 190mV which showed excellent stability with pH of 3.15 and remained stable for more than 6months. The viscosity of nanofluids increased linearly with nanoparticle concentration. The 0.3vol% Al<sub>2</sub>O<sub>3</sub> – water nanofluid has cleaning efficiency of 82% with mean viscosity of  $5.264 \times 10^7$  Pas.

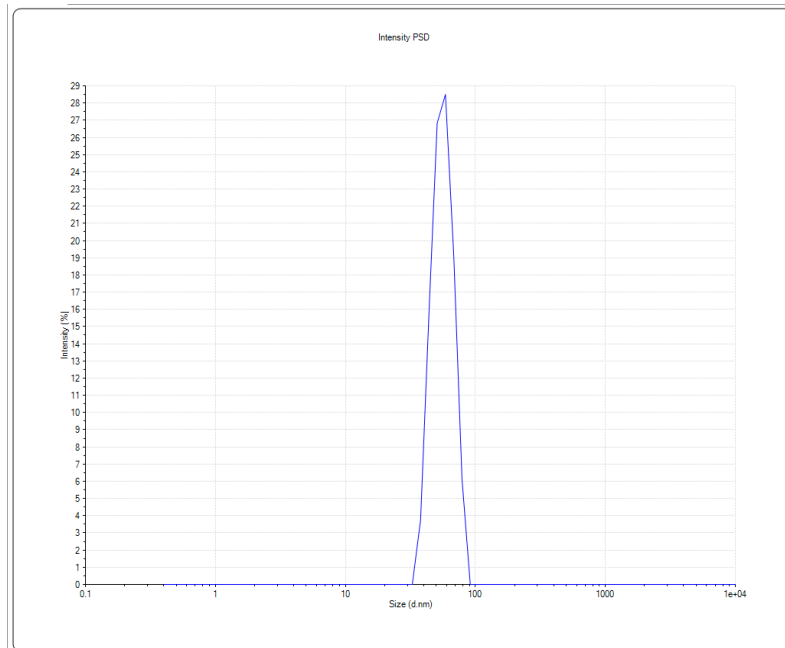


Figure 5-3 Particle Size Distribution of 0.3wt%  $\text{Al}_2\text{O}_3$  + 0.03wt% SDBS- deionised water nanofluid

Particle size distribution: Figure 5-3 Shows the hydrodynamic particle size distribution of 0.3 vol%  $\text{Al}_2\text{O}_3$  + 0.03%SBDS –water nanofluid at 25°C, room temperature. The nanofluid formulated with 0.3g  $\text{Al}_2\text{O}_3$  nanopowder +0.03%SBDS +99.67ml deionized water calcined at 25°C had the average aggregate size, 56.52 d. nm, total surface area of 0.0272nm<sup>2</sup> with percentage intensity of 100%. The Particle size distribution is less than 100nm. The average diameter is less than 100% which formed smaller particle size due to sufficient agitation of the nanofluid before particle size distribution analysis. The zeta potential of 0.3vol%  $\text{Al}_2\text{O}_3$  + 0.03%SDBS water nanofluid was determined to be 168mV which showed excellent stability with pH of 3.16 and remained stable for more than 6months. The viscosity of nanofluids increased linearly with nanoparticle concentration. The 0.3vol%  $\text{Al}_2\text{O}_3$  + 0.03%SBDS – water nanofluid has cleaning efficiency of 84% with mean viscosity of  $3.4177 \times 10^4$  Pas.

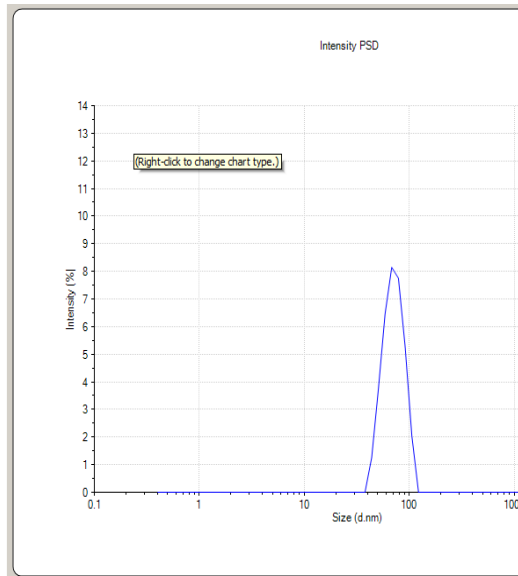


Figure 5-4 Particle size distribution of pure 0.7 vol%  $\text{Al}_2\text{O}_3$  water nanofluid

Figure 5-4 shows the hydrodynamic particle size distribution of 0.7 vol%  $\text{Al}_2\text{O}_3$  –water nanofluid at 25°C, room temperature. The nanofluid formulated with 0.7g  $\text{Al}_2\text{O}_3$  nanopowder +99.30ml deionized water calcined at 25°C had the average aggregate size, 41.77 d. nm, total surface area of 0.03667  $\text{nm}^2$ , with percentage intensity of 100%. The peak Particle size distribution is less than 100nm which revealed the powdered nature of the nanoparticles. The zeta potential of 0.7vol%  $\text{Al}_2\text{O}_3$  water nanofluid was determined to be 178mV which showed excellent stability with pH of 3.37 with stability lifespan of more than 6months. The viscosity of nanofluids increased linearly with nanoparticle concentration. The with cleaning efficiency of 70%

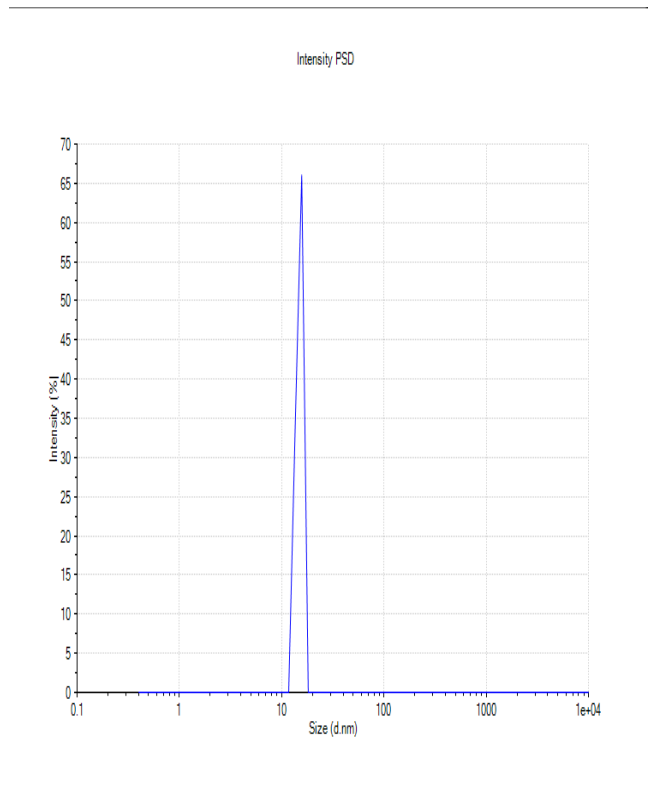


Figure5-5 Particle Size Distribution of 0.7wt% Al<sub>2</sub>O<sub>3</sub> + 0.07wt% SDBS –deionised water nanofluid

Particle size distribution: Figure5-5 shows the hydrodynamic particle size distribution of 0.7 vol% Al<sub>2</sub>O<sub>3</sub> + 0.03% SDBS –water nanofluid at 25°C, room temperature. The nanofluid formulated with 0.7g Al<sub>2</sub>O<sub>3</sub> nanopowder + 0.07% SDBS + 99.23ml deionized water calcined at 25°C had the average aggregate size, 14.96 d. nm, total surface area of 0.1024nm<sup>2</sup>, . The peak Particle size distribution is less than 100nm which revealed the powdered nature of the nanoparticles. The zeta potential of 0.7vol% Al<sub>2</sub>O<sub>3</sub> + 0.07% SDBS - water nanofluid was determined to be 136mV which showed excellent stability with pH of 3.72 and remained stable for more than 6months. The viscosity of nanofluids increased linearly with nanoparticle concentration. The 0.7vol% Al<sub>2</sub>O<sub>3</sub> + 0.07% SDBS – water nanofluid has oil cleaning efficiency of 76% with mean viscosity of 7057.16 Pas.

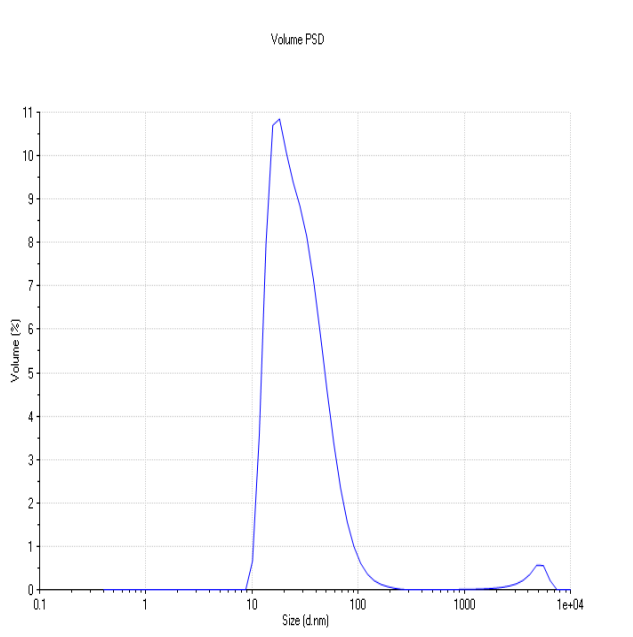


Figure 5-6 Particle size distribution of 1vol% pure $\text{Al}_2\text{O}_3$  water nanofluid

Particle size distribution: Figure 5-6 shows the hydrodynamic particle size distribution of 1 vol%  $\text{Al}_2\text{O}_3$  –water nanofluid at  $25^\circ\text{C}$ , room temperature. The nanofluid formulated with 1g  $\text{Al}_2\text{O}_3$  nanopowder +99ml deionized water calcined at  $25^\circ\text{C}$  had the average aggregate size, 30.71nm d. nm, total surface area of  $0.04972\text{nm}^2$ . Particle size distribution is less than 100nm, zetapotential of 202mV which showed excellent stability with pH of 2.94 and remained stable for more than 6months. The 1vol%  $\text{Al}_2\text{O}_3$  – water nanofluid has oil cleaning efficiency of 74% with mean viscosity of 0.05923 Pas.

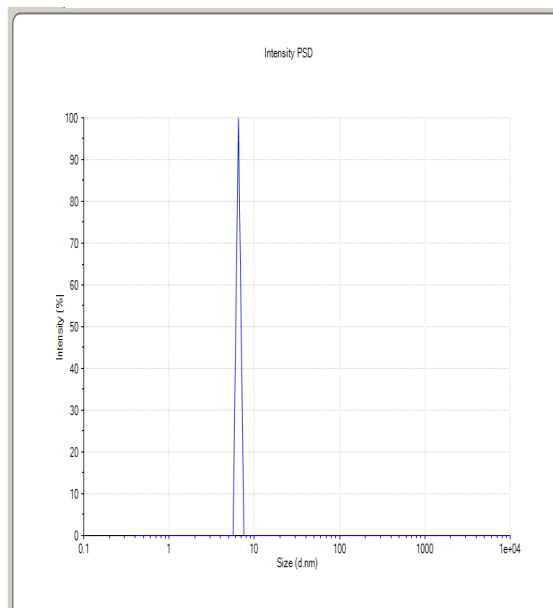


Figure 5-7 Particle Size Distribution of 1wt%Al<sub>2</sub>O<sub>3</sub> + 0.1wt%SDBS –deionised water nanofluid

Figure 5-7 shows the hydrodynamic particle size distribution of 1 vol% Al<sub>2</sub>O<sub>3</sub> + 0.1% SDBS –water nanofluid at 25°C, room temperature. The nanofluid formulated with 1g Al<sub>2</sub>O<sub>3</sub> nanopowder + 0.1% SDBS +98.90ml deionized water calcined at 25°C had the average aggregate size, 6.503 d.nm, total surface area of 0.255nm<sup>2</sup> Particle size distribution is less than 100nm, zetapotential of 170mV which showed excellent stability with pH of 3.28 and remained stable for more than 6months. The 1vol% Al<sub>2</sub>O<sub>3</sub> – water nanofluid has oil cleaning efficiency of 88% with mean viscosity of 2832.76 Pas.

TiO<sub>2</sub> and ZnO - nanofluids were characterised in the same trend as Al<sub>2</sub>O<sub>3</sub> nanofluids. The experimental data obtained are shown on Tables 5-5 and 5-6 with the particle size distribution graphs on Appendix A-1.

### 5.2.1 Cleaning efficiency

Cleaning efficiency is the ability to clean/remediate oil from the contaminated soil with a minimum amount of effort or no human interference. Cleaning efficiency describes the effectiveness of the nanofluid used for the cleaning. The cleaning efficiency of each nanofluid may be defined as the difference between the percentage of mineral oil fed to the soil before cleanup (A) and the percentage of mineral oil recovered/removed from the soil after cleanup (B) expressed as percentage of oil cleaning/removal. It is calculated as follows: With the



values of A and B, from the cleanup results, the cleaning efficiency (CE, %) was calculated by

$$CE\% = [ (A - B)/A ] \times 100.$$

Table 5-5 Characterization of different pure nanofluids and their combinations/hybrids at 25°C [57]

Types of nanofluid	Average size (d.nm)	Total surface area(nm <sup>2</sup> )	Mean viscosity (pas)	pH	Zetapotential (mV)	Cleaning efficiency (%)
0.3vol% Al <sub>2</sub> O <sub>3</sub>	71.77	0.0214	5.264 x 10 <sup>7</sup>	3.15	190	82
0.7 vol% Al <sub>2</sub> O <sub>3</sub>	41.77	0.03667	0.32236	3.37	178	70
1.0 vol% Al <sub>2</sub> O <sub>3</sub>	30.71	0.04972	0.05923	2.94	202	74
0.3vol% TiO <sub>2</sub>	45.09	0.03114	8.98 x 10 <sup>7</sup>	4.26	120	72
0.7 vol% TiO <sub>2</sub>	40	0.03497	0.0083568	3.35	178	76
1.0 vol% TiO <sub>2</sub>	71.66	0.01946	0.4075	4.08	138	84
0.3vol% ZnO	50	0.02133	33.68 x 10 <sup>4</sup>	7.89	63.4	62
0.7 vol% ZnO	82.02	0.01295	12.14 x 10 <sup>-3</sup>	8.85	-60	63
1.0 vol% ZnO	86.4	0.01226	13594	8.92	-86.7	78
0.7 TiO <sub>2</sub> + 0.3 Al <sub>2</sub> O <sub>3</sub>	45	0.0564	62592.48	3.04	196	70
0.3 TiO <sub>2</sub> + 0.7 Al <sub>2</sub> O <sub>3</sub>	44.68	0.0539	1.4026 x 10 <sup>-2</sup>	3.62	167	68
0.7ZnO + 0.3 Al <sub>2</sub> O <sub>3</sub>	50.58	0.03438	11.54682 x 10 <sup>3</sup>	8.89	-80	71
0.3ZnO + 0.7Al <sub>2</sub> O <sub>3</sub>	86.01	0.0580	1.499	7.45	48	62
0.7 ZnO + 0.3 TiO <sub>2</sub>	16.37	0.03022	6.88 x 10 <sup>4</sup>	7.35	-44	68
0.3 ZnO + 0.7 TiO <sub>2</sub>	62.23	0.05629	69715.3	5.24	78	70

0.3ZnO + 0.3TiO <sub>2</sub> +0.3Al <sub>2</sub> O <sub>3</sub>	50	0.06003	7.77 x 10 <sup>-4</sup>	5.19	73	74
---	----	---------	-------------------------	------	----	----

Table 5-6 Characterization of different surfacted nanofluids and their combinations/hybrids at 25°C [41a, 123]

Nanofluid System	Average size (nm)	Total surface area (nm <sup>2</sup> )	pH	Zeta potential (mV)	Mean viscosity (pas)	Cleaning efficiency (%)
0.3wt% Al <sub>2</sub> O <sub>3</sub> + 0.03%SDBS	56.52	0.0272	3.16	168	3.4177 x 10 <sup>4</sup>	84
0.7wt% Al <sub>2</sub> O <sub>3</sub> + 0.07%SDBS	14.96	0.1024	3.72	136	7057.16	76
1wt% Al <sub>2</sub> O <sub>3</sub> + 0.1%SDBS	6.503	0.255	3.28	170	2832.76	88
0.3wt% TiO <sub>2</sub> + 0.03%SDBS	33.32	0.04214	1.23	277	10038.27	78
0.7wt% TiO <sub>2</sub> + 0.07%SDBS	2.696	0.5188	1.31	294	3530.9	88
1wt% TiO <sub>2</sub> + 0.1%SDBS	50.9	0.02739	1.30	273	3467.01	99.4
0.3wt% ZnO + 0.15%Na <sub>2</sub> HPO <sub>4</sub>	24.81	0.04298	10.73	-196	350.812	74
0.7wt% ZnO + 0.35%Na <sub>2</sub> HPO <sub>4</sub>	20	0.0531	10.93	-205	5101.99	90
1wt% ZnO + 0.1%Na <sub>2</sub> HPO <sub>4</sub>	65.31	0.1621	8.98	140	3491.29	98
0.7 TiO <sub>2</sub> + 0.3 Al <sub>2</sub> O <sub>3</sub> +0.07%SDBS+0.03 %SDBS	60	0.5460	2.91	108	2.973 x 10 <sup>-3</sup>	87.4
0.3 TiO <sub>2</sub> + 0.7 Al <sub>2</sub> O <sub>3</sub> +0.03%SDBS+0.07 %SDBS	25	0.1335	3.93	146	2.7 x 10 <sup>-3</sup>	80
0.7ZnO + 0.3Al <sub>2</sub> O <sub>3</sub> +0.35%Na <sub>2</sub> HPO <sub>4</sub> +0.03%SDBS	34.73	0.08031	9.66	-167	2.808 x 10 <sup>-3</sup>	80

0.3ZnO +0.7Al <sub>2</sub> O <sub>3</sub> + 0.15%Na <sub>2</sub> HPO <sub>4</sub> + 0.07%SDBS	40.58	0.1454	9.31	-156	13298.16	76
0.7 ZnO + 0.3 TiO <sub>2</sub> + 0.35%Na <sub>2</sub> HPO <sub>4</sub> +0.03%SDBS	26.36	0.08424	3.85	121	8.84 x 10 <sup>4</sup>	72
0.3 ZnO + 0.7 TiO <sub>2</sub> + 0.15%Na <sub>2</sub> HPO <sub>4</sub> + 0.07%SDBS	23.16	0.5617	5.24	86	19101	78
0.3ZnO + 0.3TiO <sub>2</sub> +0.3Al <sub>2</sub> O <sub>3</sub> +0.15% Na <sub>2</sub> HPO <sub>4</sub> + 0.03%SDBS+ 0.03%SDBS	9.963	0.10133	3.74	118	9.195 x 10 <sup>-4</sup>	92

The above monotype nanofluids have been stabilised with excellent stability and stability life span of more than 6 months.

5.3. Total surface area: The values are shown on figures.5-8 and 5-9.

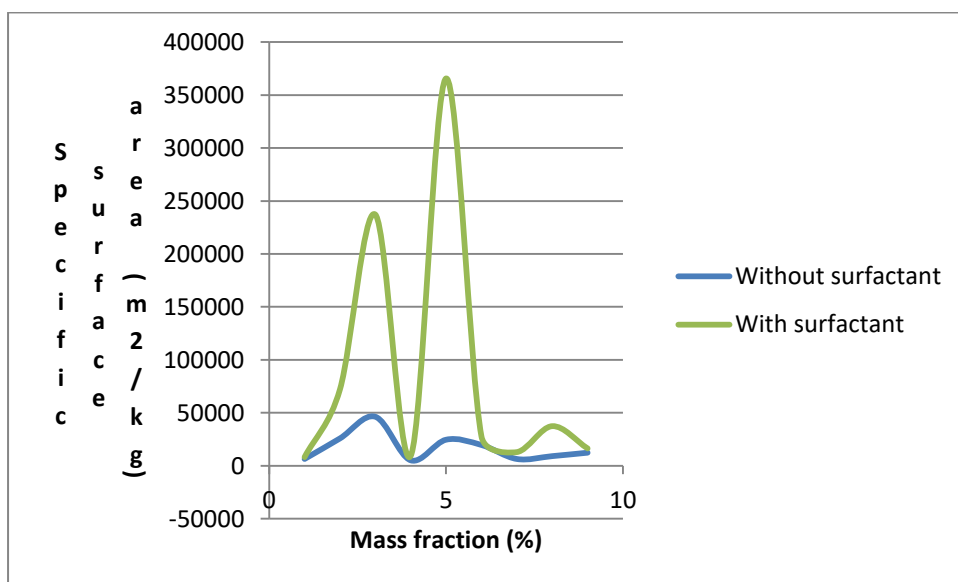


Figure 5-8 Total surface area of the different monotype nanofluids.

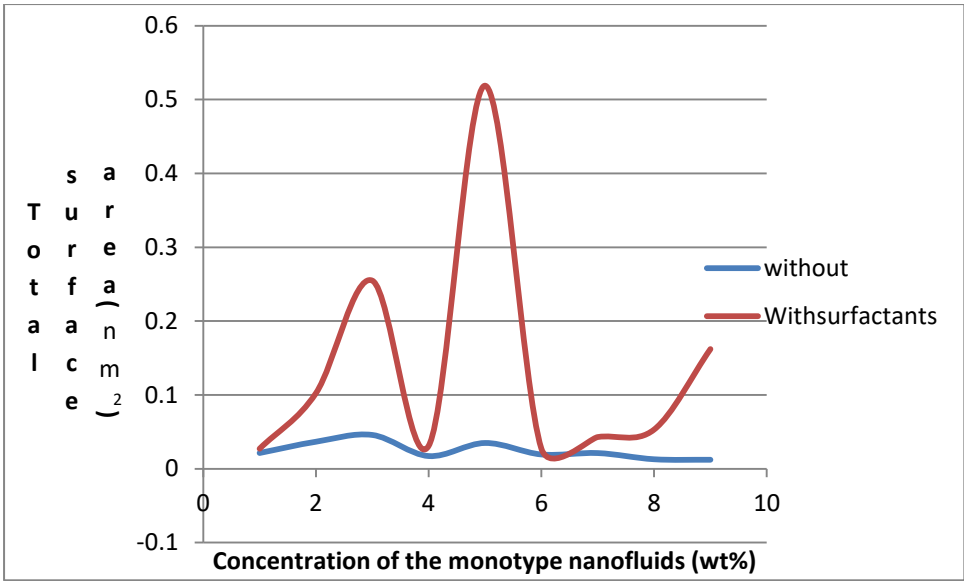
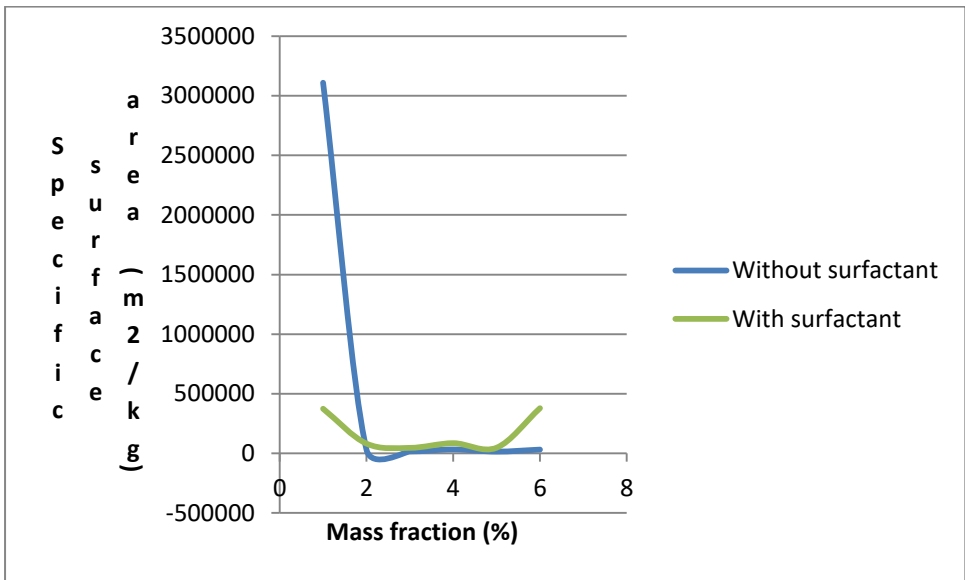


Figure 5-9 Total surface area of the different monotype nanofluids [137].

From Figure 5-9, the total surface area of surfacted monotype nanofluids is far higher than that of pure monotype nanofluids.



OR

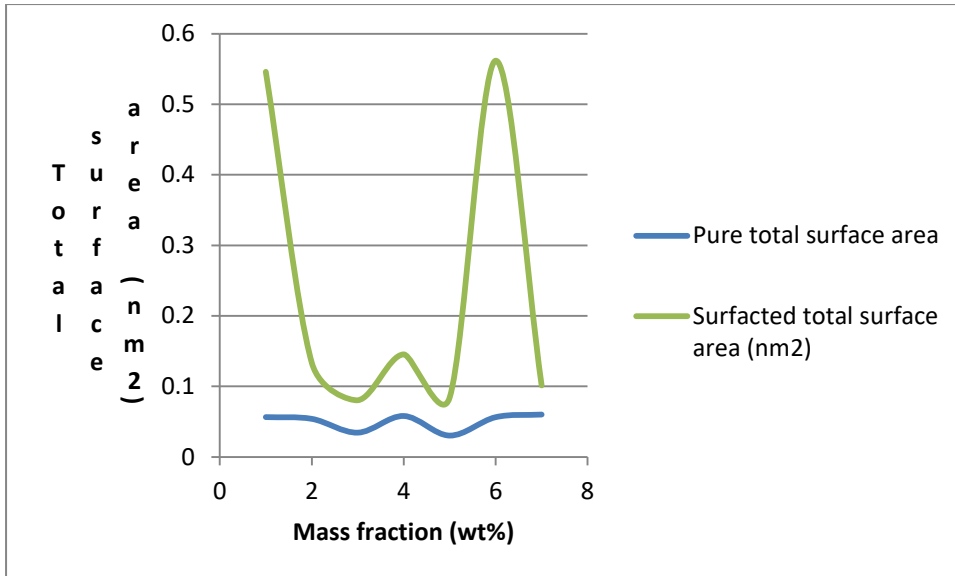


Figure 5-10 Total surface area of the different hybrid nanofluids [137].

Fig.5-10 indicates that the total surface area with surfactants is far higher than that without surfactants. Addition of surfactants to the nanofluids reduces the particle size and greater surface area thereby increasing the cleaning efficiency. I.e the smaller the particle sizes, the larger the total surface area of the nanofluids and the better the nanofluids activity. The graph indicates that the total surface area of the surfacted hybrid nanofluids increases linearly as mass fraction decreases. Also as mass fraction increases, the total surface area is reduced dramatically at constant rate. The total surface area of surfacted hybrid nanofluids equals to the total surface area of pure hybrid nanofluids at  $0.3\text{Al}_2\text{O}_3 + 0.7\text{ZnO}$  ( $0.080308 \text{ nm}^2$ ) and  $0.7\text{Al}_2\text{O}_3 + 0.3\text{ZnO}$  ( $0.057994 \text{ nm}^2$ ) [137]. Other measured flow properties of the various nanofluids are contained in the Appendice.

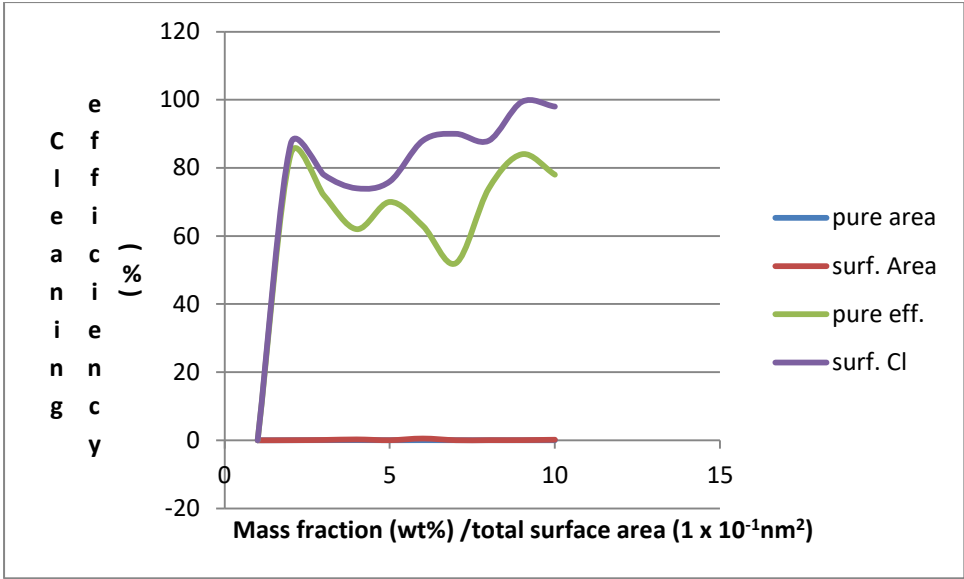


Figure 5-11 Comparison of cleaning efficiency with total surface area of Monotype nanofluids

Figure 5-11 indicates that there is a linear relationship between the total surface areas and cleaning efficiency. As the total surface area increases, the cleaning efficiency increases also and vice versa.

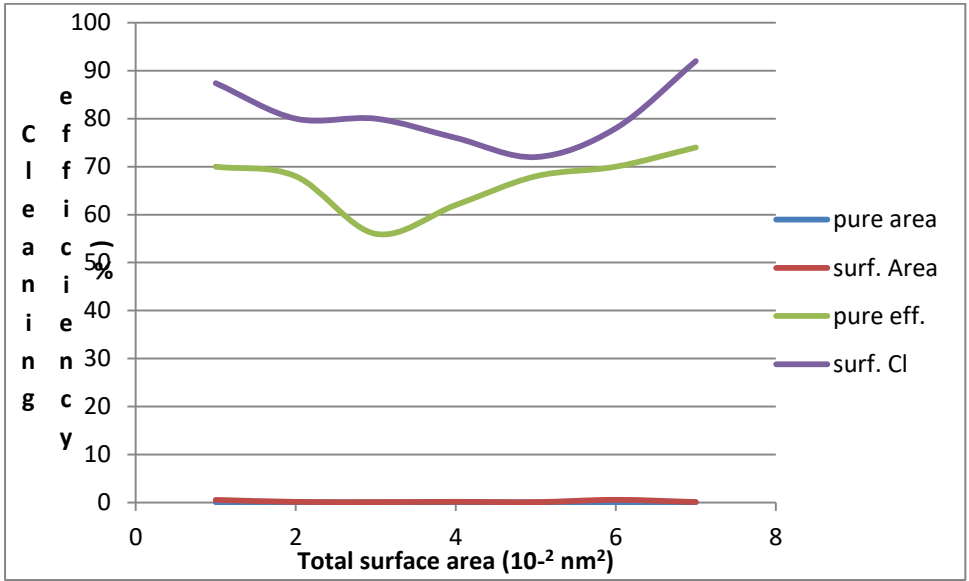


Figure 5-12 Comparison of cleaning efficiency with total surface area of hybrid nanofluids

It is observed from Figure 5-12 that addition of surfactants to the nanofluids led to increase in total surface area, thereby increasing the cleaning efficiency of the various hybrid nanofluids. The cleaning efficiency of pure hybrid nanofluids is lower than the surfacted hybrid nanofluids. There is nonlinear relationship between total surface area and cleaning efficiency of pure hybrid nanofluids. The

surfactants breakdown the particle into smaller sizes, thereby increasing the total surface of the nanofluids and cleaning efficiency.

### 5.3.2 Density

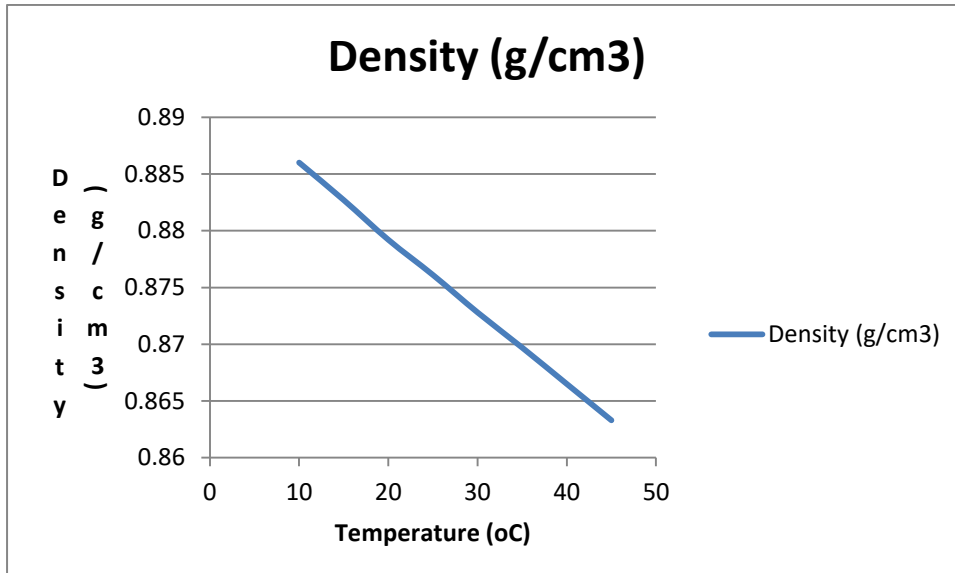
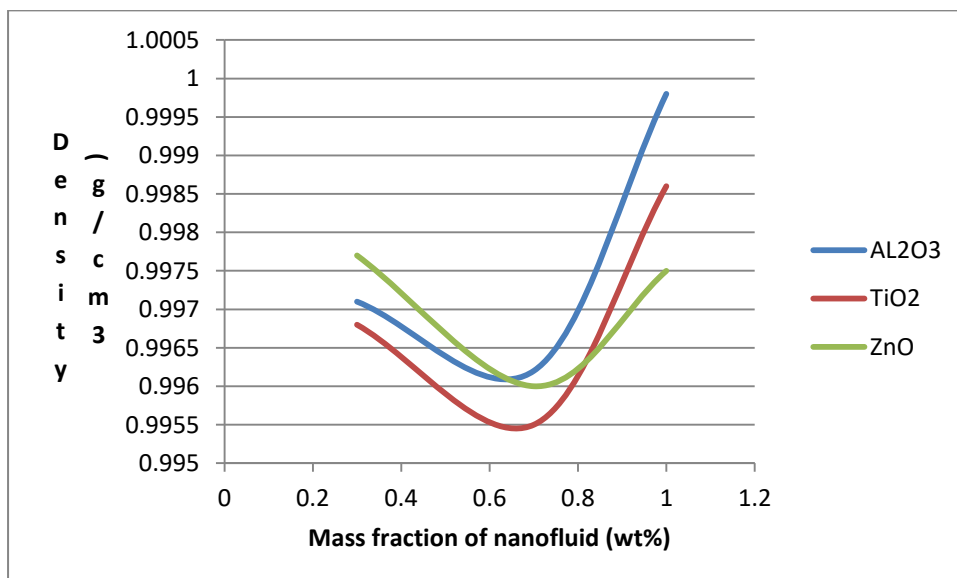


Figure 5-13 Measured density of experimental mineral oil Hv1 60

The measured density of the experimental mineral oil is showed on Figure5-13.The figure indicates that density increases with decrease in temperature, the same as viscosity.



OR

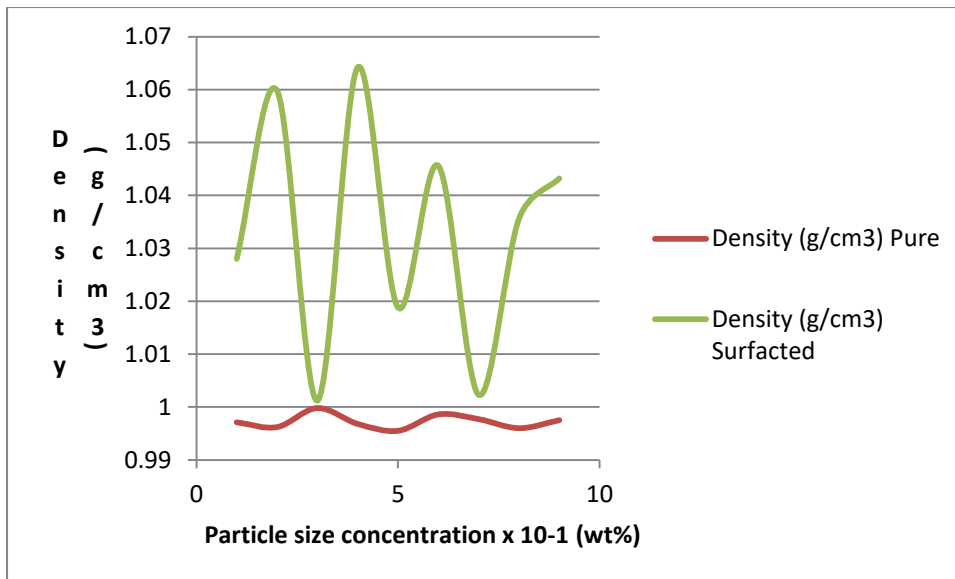


Figure 5-14 Experimental results of monotype nanofluids density measurements

Density: From Figure 5-14, it is can be seen that the density of the monotype nanofluids increases linearly with Increase in particle size concentration from 0.7 to 1.0wt%.The density decreases from mass fraction of 0.3wt% to 0.7wt%.The density of TiO<sub>2</sub>/water equals the density of ZnO/water at mass fraction of 0.7wt%.This is followed by the density of ZnO/water and Al<sub>2</sub>O<sub>3</sub>/water at the same mass fraction.Figure5-14 shows the measured results of the weight fractions of the different nanofluids with the change of density under different temperature.The increase in added concentration of nanoparticles enhances the density of the nanofluids, whereas temperature rise reduces the density of nanofluids.The influence of weight fractions on density change appears to be approximately linear.Density usually increases with viscosity which has a high impact on the fluid flow.



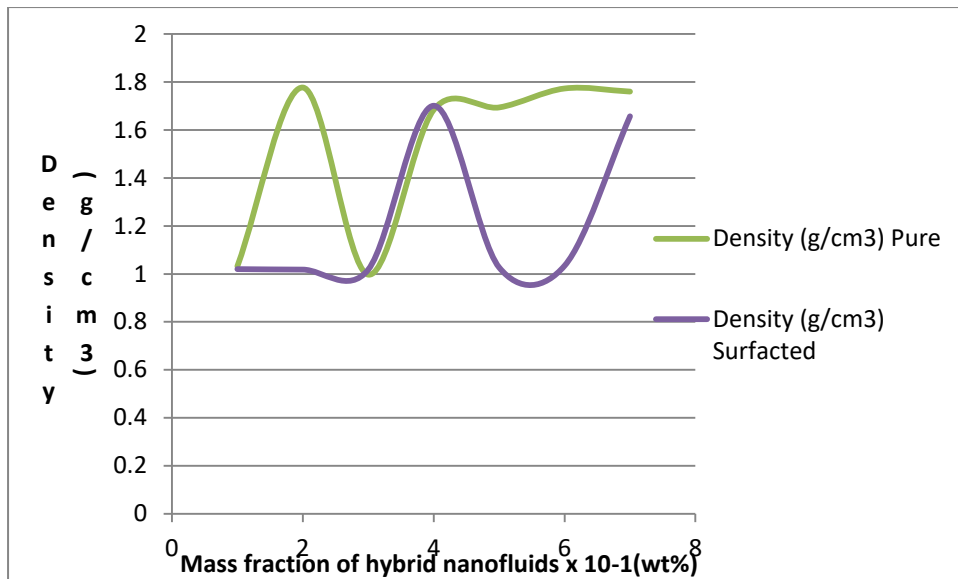


Figure 5-15 Comparison of the density of the various hybrid nanofluids

Figure 5-15 indicates that addition of surfactants to the pure hybrid nanofluids decreases the density of the various surfacted hybrid nanofluids. Both are equal at 0.3Al<sub>2</sub>O<sub>3</sub> + 0.7ZnO/water and 0.7Al<sub>2</sub>O<sub>3</sub> + 0.3ZnO /water, 0.3% and 0.4% particle size concentration, density of 1.018g/cm<sup>3</sup> and 1.684g/cm<sup>3</sup>, respectively. They are symmetrical to each other as the particle size concentration increases.

5.3.3 Surface tension: The surface tension data obtained using Attention Theta is plotted on Figs 5-17 to 5-18. The curves of pure and surfacted hybrid nanofluids are symmetrical to each other as the particle size concentration increases.

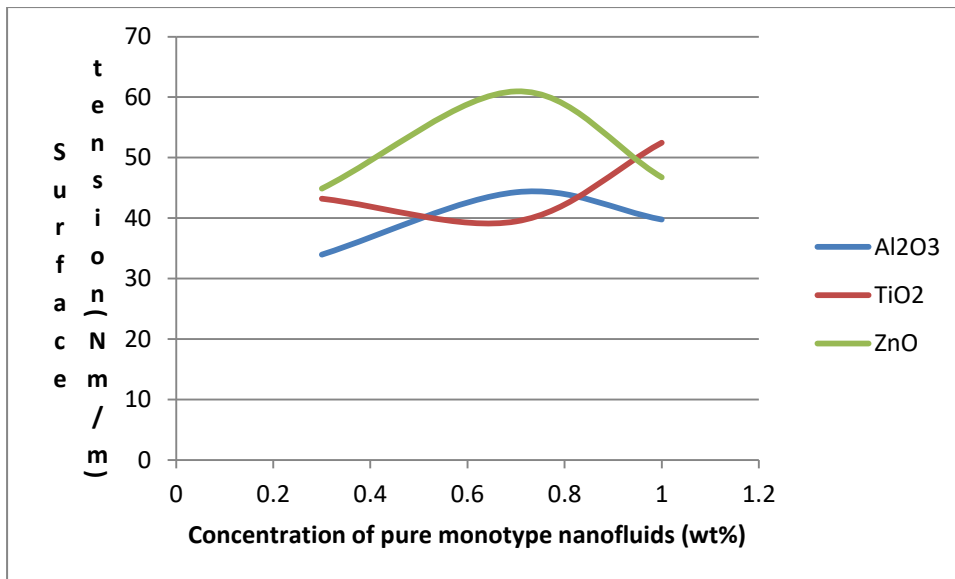


Figure 5-16 Measured surface tension of the various weight fractions of the pure monotype nanofluids.

Surface tension (interfacial properties of nanofluids) is used to study wet and spreading mechanism of nanofluids on solid surfaces eg soil or glass slide through droplet formation. It is found that the existence of nanoparticles near the liquid/solid contact line can improve its spreading.

It can be seen from Fig 5-17 that surface tension of the nanofluids decreases with increase in weight fractions of the different nanofluids. The results showed that the surface tension of Al<sub>2</sub>O<sub>3</sub>/water, TiO<sub>2</sub>/water and ZnO/water are significantly lower than those of the pure water. It can be concluded that particle volume concentration does not have a major effect on the surface tension of the nanofluids. As the volume concentration increases, the surface tension of the nanofluids remain almost unchanged or decreases at constant rate [66] & [90] [24],[47]. For deionied water containing Al<sub>2</sub>O<sub>3</sub>, the surface tension remains almost unchanged at low particle concentrations. This is likely because for such dilute suspensions, the distance between particles are much larger than the particle size, thus the forces and the interactions between particles at/near the liquid/gas interface has little impact on the surface energy. However, when the particle concentration increases, particles are getting closer to each other, thus the van der Waals force increases. This will increase the free energy at surface and results in higher surface tension. When the nanofluids are surfacted, the surface tension tends to decrease at small particle concentration, while the surface tension does not change much with pure nanofluids [28, 30]. Nanofluids are used for cleaning oil from surfaces due to their excellent wetting and spreading behaviour [180].

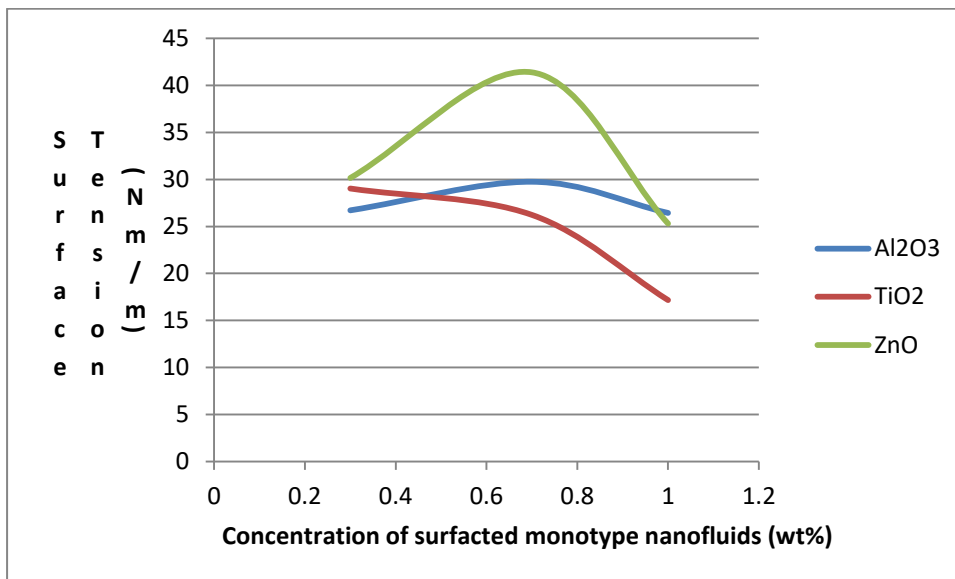


Figure 5-17 Measured surface tension of the various weight fractions of the surf acted monotype nanofluids.

From Figure 5-18, the addition of surfactants into the nanofluids reduced the surface tension [21] in Al<sub>2</sub>O<sub>3</sub> and TiO<sub>2</sub> nanofluids but it increases with weight fractions in ZnO/water. We believe that the reduction in surface tension is attributed to the adsorption of ionic surfactant on the nanoparticle surface imparting an electrostatic repulsive force between the particles in the nanofluid. This electrostatic repulsion between nanoparticles surrounded by the surfactant at the liquid-gas interface results in the reduction of the surface tension of the nanofluid. This is consistent with the conclusions of [57] and [49], both of which show that for low surfactant concentrations, the surface tension remains unchanged and starts to decrease beyond a certain concentration level.

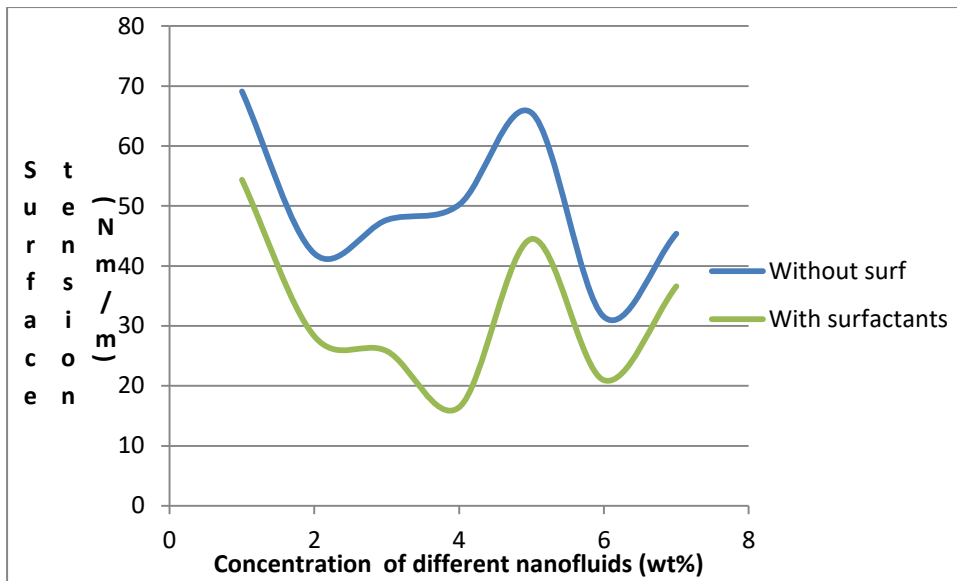


Figure 5-18 Surface tension of hybrid nanofluids

It can be seen from the Figure 5-19 above that surfactant reduces surface tension of nanofluids. It is observed from Figure 5-19 that pure  $0.7\text{TiO}_2 + 0.3\text{Al}_2\text{O}_3$  /water and  $0.7\text{ZnO} + 0.3\text{TiO}_2$  /water have the highest (69.09Nm/m) and lowest (31.50 Nm/m) surface tension respectively. Whereas surfacted  $0.7\text{TiO}_2 + 0.3\text{Al}_2\text{O}_3$  /water and  $0.3\text{ZnO} + 0.7\text{TiO}_2$  /water has the highest (54.36 Nm/m and lowest (16.43Nm/m) surface tension, respectively. However, the surface tension of both pure and surfacted hybrids nanofluids are below the pure water surface tension of 72.80Nm/m.

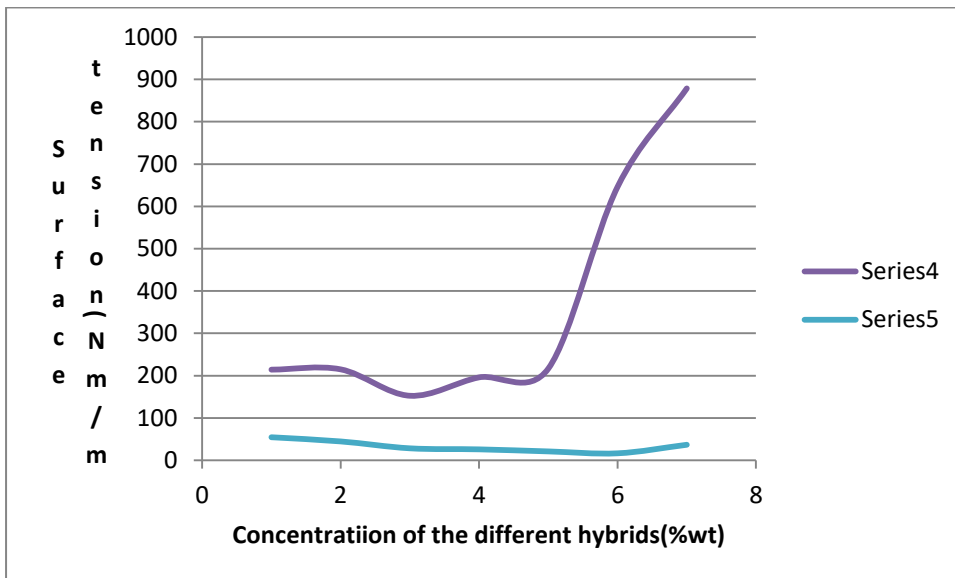


Figure 5-19 Surface tension of different hybrid nanofluids

Series 4 - pure nanofluids & series 5 – surfacted nanofluids

It can be seen from Figure 5-20 that the addition of surfactants reduces dramatically the surface tension of the different nanofluids.

### 5.3.4 Contact Angle

The measured contact angles of the different nanofluids are shown on Tables 6-6 to 6-7 and Figure 5-21

#### 5.3.4.1 Measured contact angle Results

The results from the measurements are shown in Figure 5-21: where the contact angle is plotted against wettability. The contact angle is given through the denser water phase. A decrease in contact angle is an indication of a more water-wet condition which is taking to be  $\theta \leq 45^\circ$ . A contact angle average of  $28.05^\circ$  was found for the deionised water.

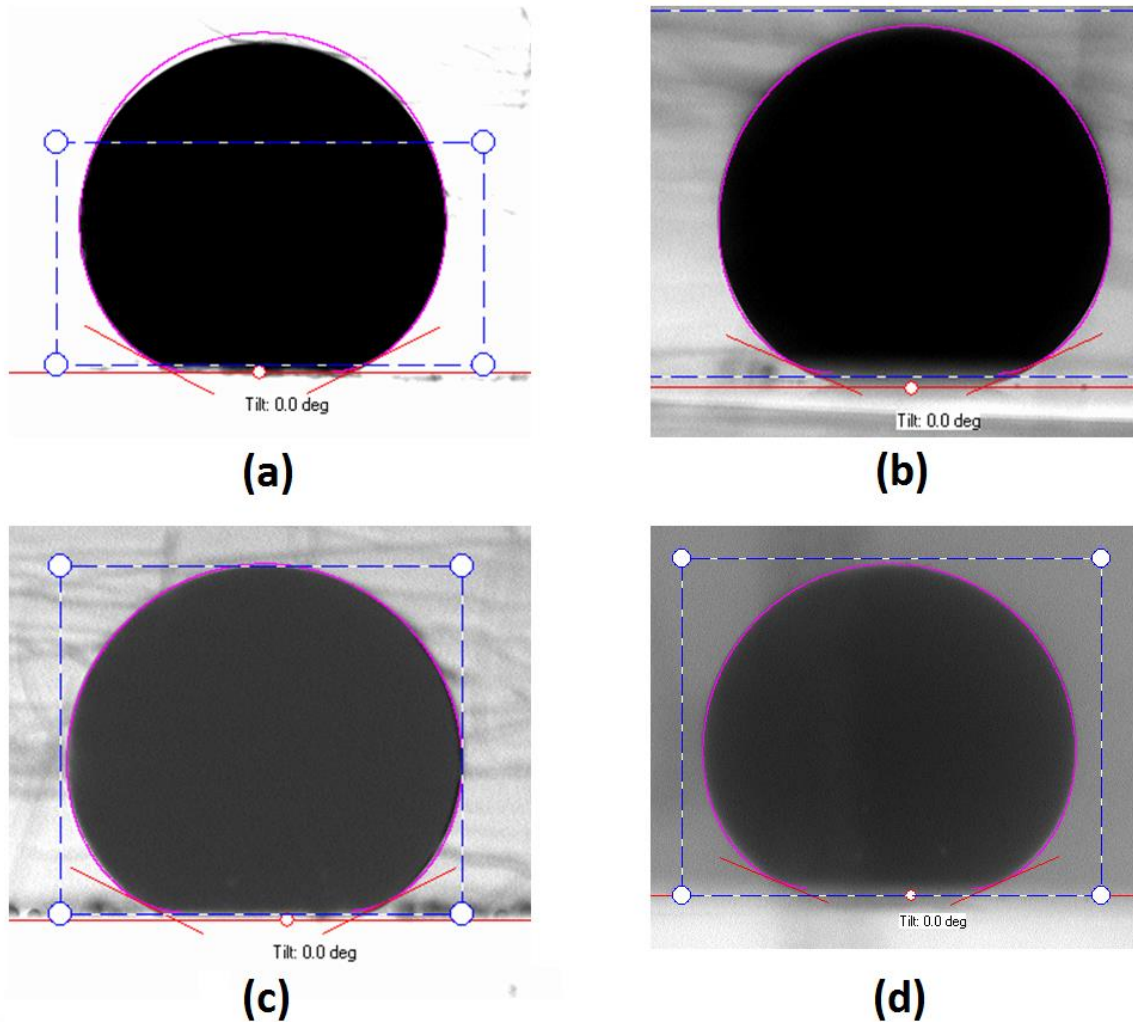


Figure 5-20 .Vertically flipped frames recorded during the measurements

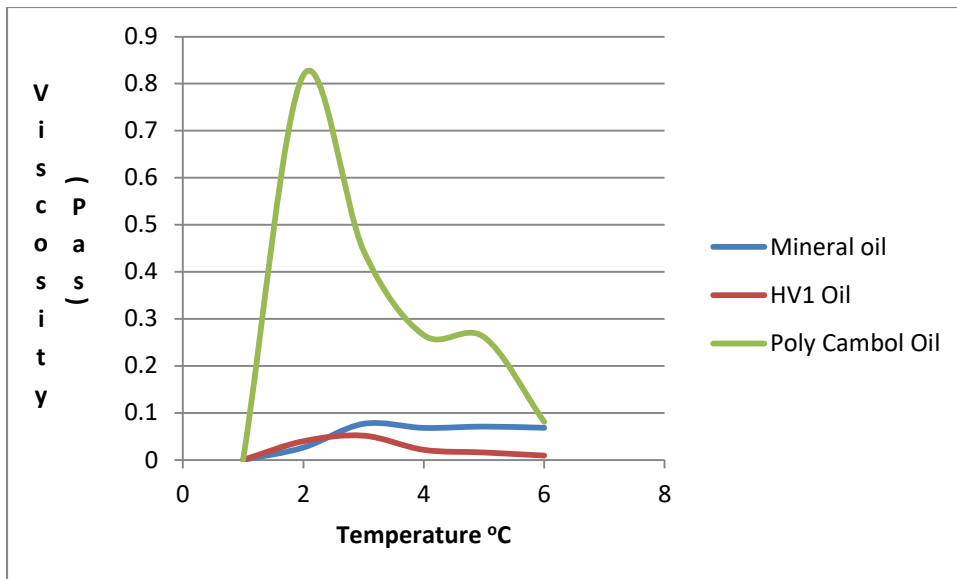


Figure 5-21 Viscosities of the experimental oils

From the Figure 5-22 and Table 5-7 below, PolyCambol oil has the highest viscosity followed by High Viscosity Index oil, highly refined mineral oil (HV1 60) and white liquid mineral oil has the least. Hence, the oil with the lower Viscosity Index (VI) uses less Viscosity Index improvers. Therefore, the oil with the lower VI is the "better" oil. Hence, HV1 oil is the best oil to use in the contamination of soil before cleaning. This is followed by white liquid mineral oil. In other words, Higher VI base oils can cover a larger spread than lower VI base oils and therefore require less VI improver (modifier).

Table 5-7 Viscosities of Poly Cambol oil, HV1 60 oil & white liquid mineral oil

	Poly Cambol oil	HV1 oil	White liquid mineral oil
Temp°C	Viscosity(pas)	Viscosity(pas)	Viscosity(pas)
20	0.818	0.03974	0.0263
30	0.4449	0.05152	0.0768
40	0.2653	0.0214	0.06805
50	0.2612	0.01578	0.0708
70	0.08096	0.009129	0.06821

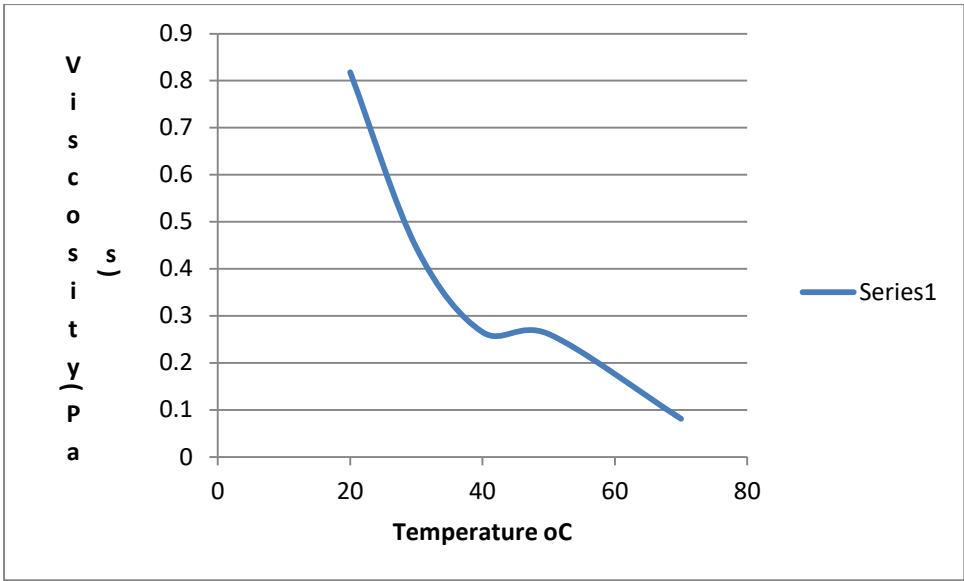


Figure 5-22 Viscosity of Poly Cambol oil

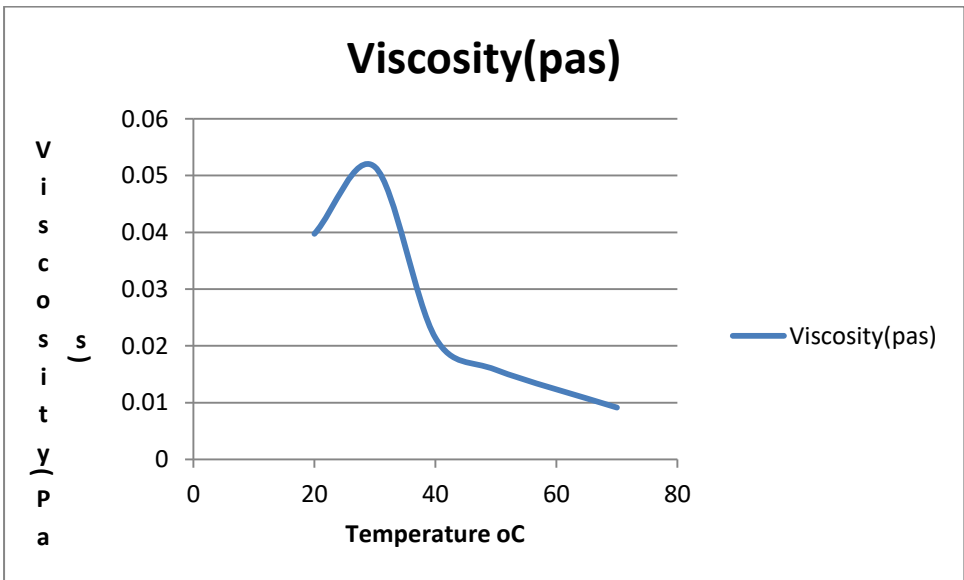


Figure 5-23 Viscosity of High Viscosity Index Oil

Viscosity of High Viscosity Index Oil (HVI 60) decreases with increase in temperature having the peak viscosity of 0.0512 pas at 30°C (Figure5-23).

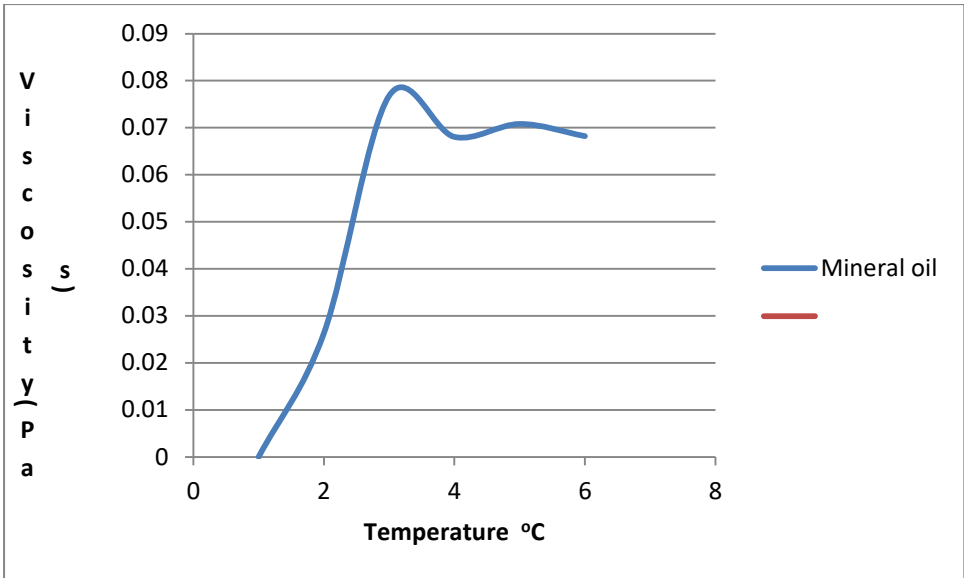


Figure 5-24 Viscosity of Mineral oil

Viscosity of mineral oil increases linearly with increase in temperature having maximum viscosity at 0.0768Pas (30°C) and the lowest at 0.06805Pas (40°C).

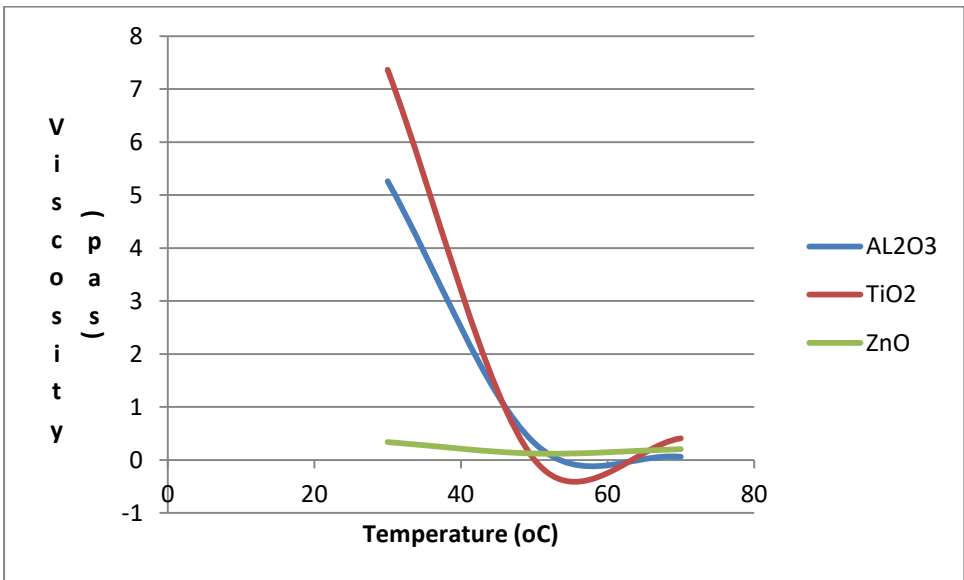


Figure 5-25 Viscosity of 0.3wt% concentration of the various nanofluids against temperature

From the plot above, the viscosity of the 0.3 wt% concentration of the different nanofluids gently decreases with increase in temperature but the viscosity of all of them are the same at 50°C. The viscosity of ZnO/water is very low. From 50°C, there is a sharp increase in viscosity as temperature increases onwards to 100°C, the boiling point of water. Above 50°C, the water



in the nanofluids start to dry up leading to increase in viscosity. This is in accordance with works of [124] and [104]. The nanofluids exhibit Newtonian behaviour

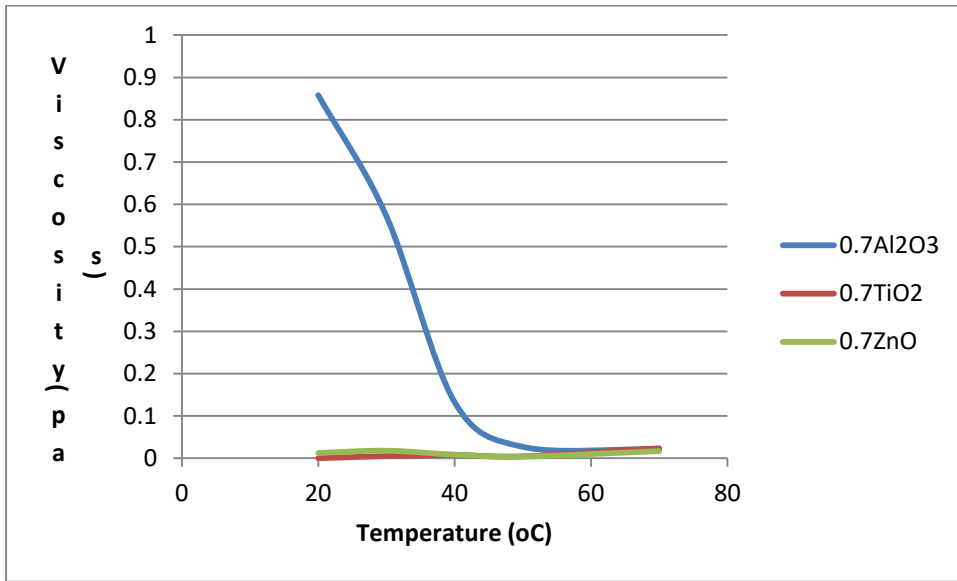


Figure 5-26 Viscosity of 0.7wt% concentration of the various nanofluids against temperature

It can be seen from Figure 5-27 above that the viscosity of 0.7wt% TiO<sub>2</sub>/water and 0.7wt% ZnO/water are constantly very low as the temperature increases with the viscosity of Al<sub>2</sub>O<sub>3</sub>/water above 50°C. For all the nanofluids measured the temperature, the gradient of viscosity is generally steeper at the temperature from 20 to 40°C. This is more pronounced as the particle size concentration increases [124].

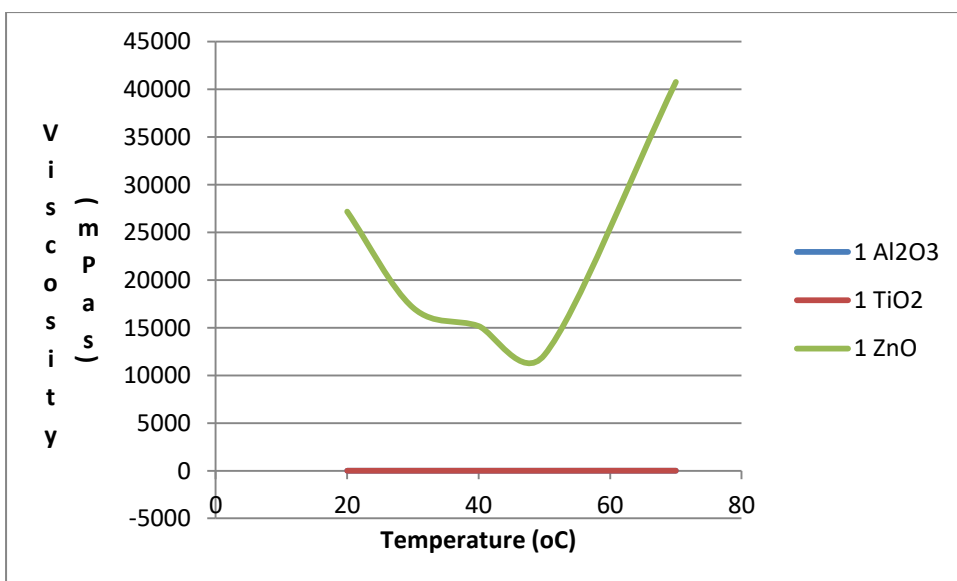


Figure 5-27 Viscosity of 1.0wt% concentration of different nanofluids against temperature [57]

From the experimental results (Figure 5-28) as the particle size increase, the effect of viscosity decreases significantly and reaches in almost constant value at the end [164]. The viscosities of  $\text{Al}_2\text{O}_3/\text{water}$  and  $\text{TiO}_2/\text{water}$  nanofluids are very low as the temperature increases for high level concentration (1.0wt%) of nanoparticles, but there is an increase in viscosity of  $\text{ZnO}/\text{water}$  nanofluid which is far higher than that of the other two nanofluids at this level (Figure 5.28). In my experiments, attempts were made to measure viscosity at the temperature higher than  $50^\circ\text{C}$ , an erratic increase of nanofluid viscosity was observed. This occurrence may have resulted from the fast evaporation of nanofluid at a relative high temperature. It can also be that beyond the temperature of  $50^\circ\text{C}$ , the surfactant might be broken down and accordingly the performance was considerably reduced or even destroyed affecting the suspension capability [124] and [104].

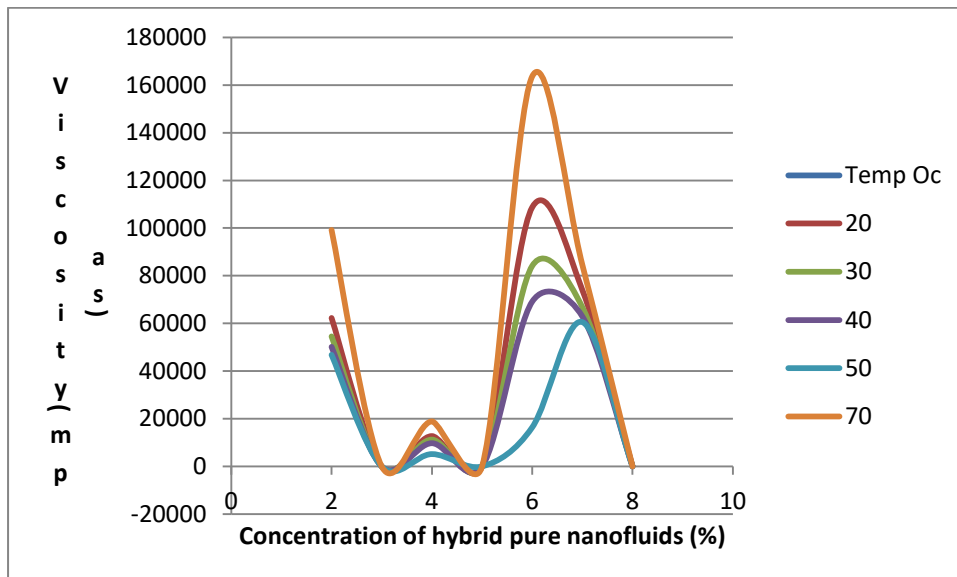


Figure 5-28 Viscosity of the various pure hybrid nanofluids

From Figure 5-29, it is observed that the viscosity of the various pure hybrids decreases with temperature but it increases sharply at  $70^\circ\text{C}$ .

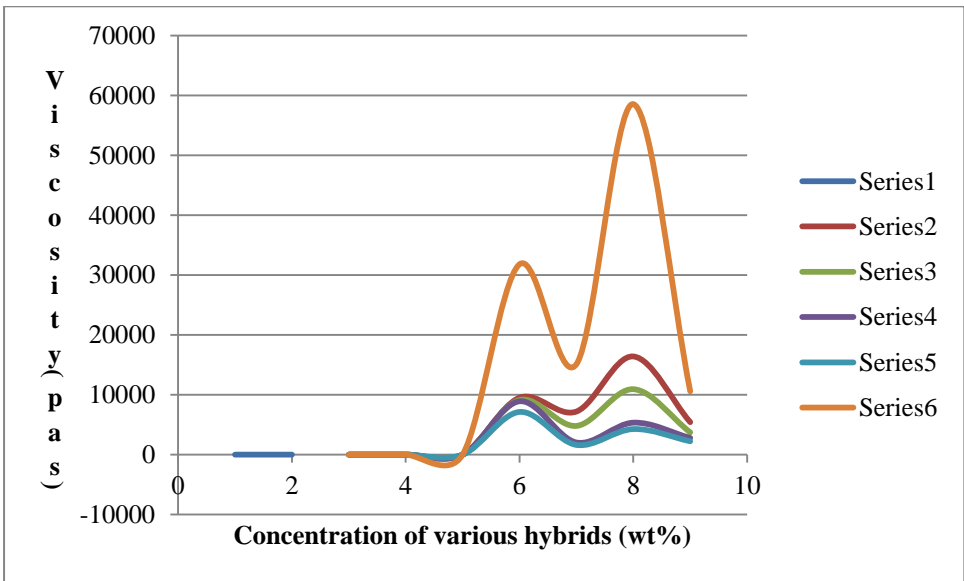


Figure 5-29 Viscosity of surfacted hybrid nanofluids

Series1 - 20 deg C, Series2 - 30 degC, Series 3 - 40 degC, Series 4 - 50degC,

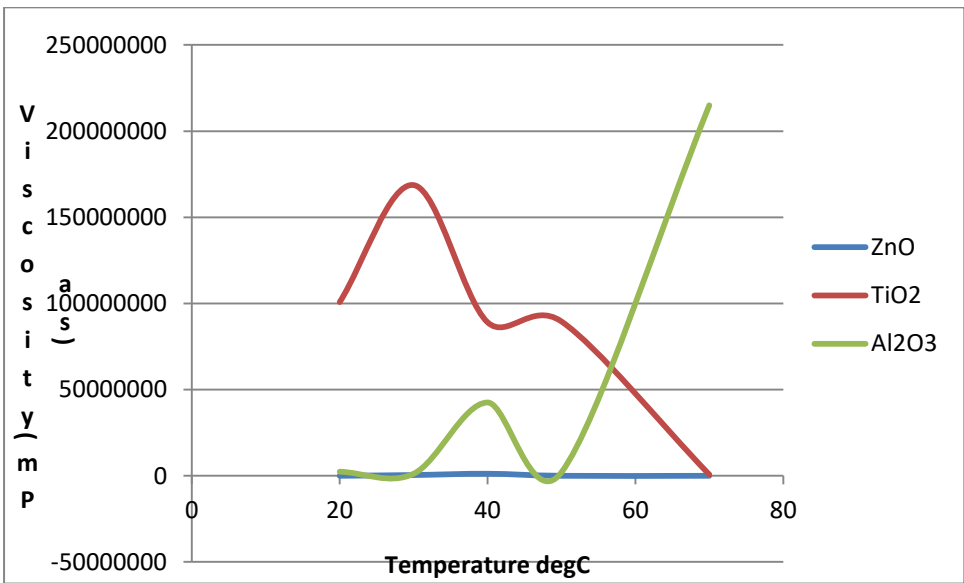


Figure 5-30 Viscosities of the different 0.3 vol% nanofluids against temperature

The viscosity of the different monotype nanofluids at 0.3wt% particle size concentration decreases with temperature for  $TiO_2$ /water and it is equal to  $ZnO$ /water at  $70^\circ C$ .  $ZnO$ /water is persistently lower than  $TiO_2$ /water and  $Al_2O_3$ /water. The viscosity of  $Al_2O_3$ /water increases with temperature from  $50^\circ c$

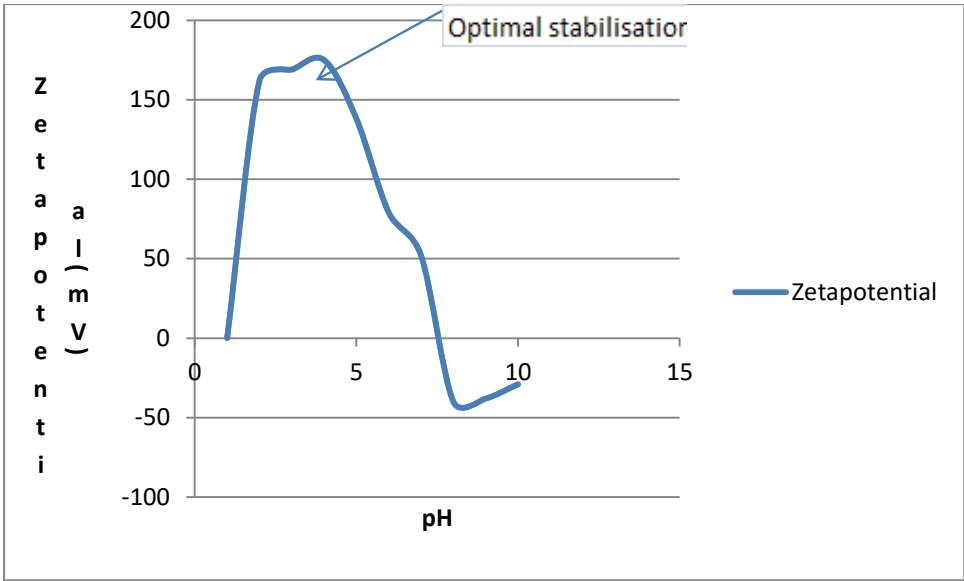


Figure 5-31 Zetapotential of the different monotype nanofluids vs pH for optimum stabilization

From the Figure5-32, the point of optimum stabilization is at 169mV and pH of 3 for monotype **nanofluids**.

Optimal stabilization

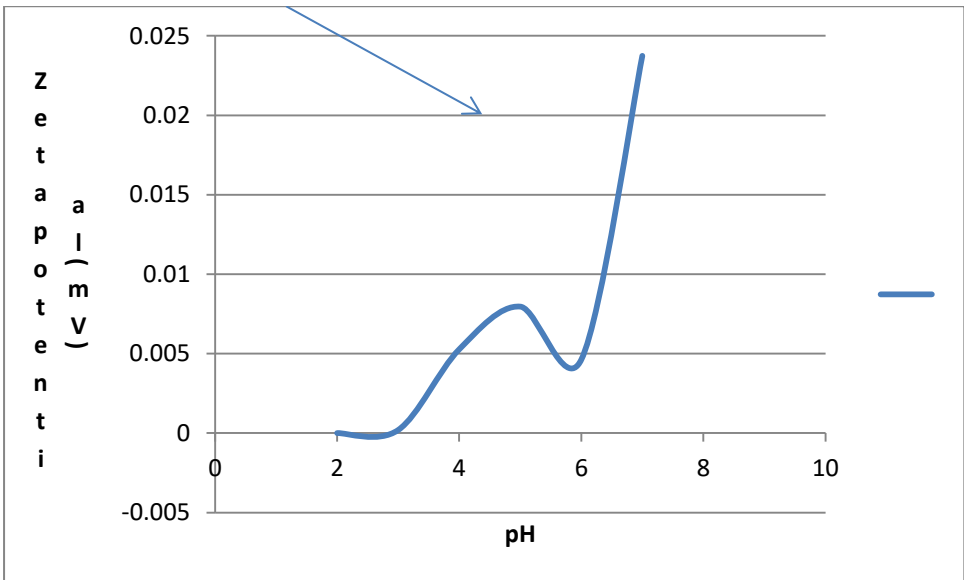


Figure 5-32 Zeta potential of the different hybrid nanofluids vs.pH for optimum stabilization

From the Figure5-33, the point of optimum stabilization is at 175mV and pH of 5 for hybrid nanofluids.

## 5.14 Comparison of cleaning efficiency of the different nanofluids

### 5.14.1 Cleaning efficiency

Cleaning efficiency is the ability to clean/remediate oil from the contaminated soil with a minimum amount of effort or no human interference. Cleaning efficiency describes the effectiveness of the nanofluid used for the cleaning. The cleaning efficiency of each nanofluid may be defined as the difference between the percentage of mineral oil fed to the soil before cleanup (A) and the percentage of mineral oil recovered/removed from the soil after cleanup (B) expressed as percentage of oil cleaning/removal. It is calculated as follows: With the values of A and B, from the cleanup results, the cleaning efficiency (CE, %) was calculated by  $CE\% = [(A - B)/A] \times 100$ .

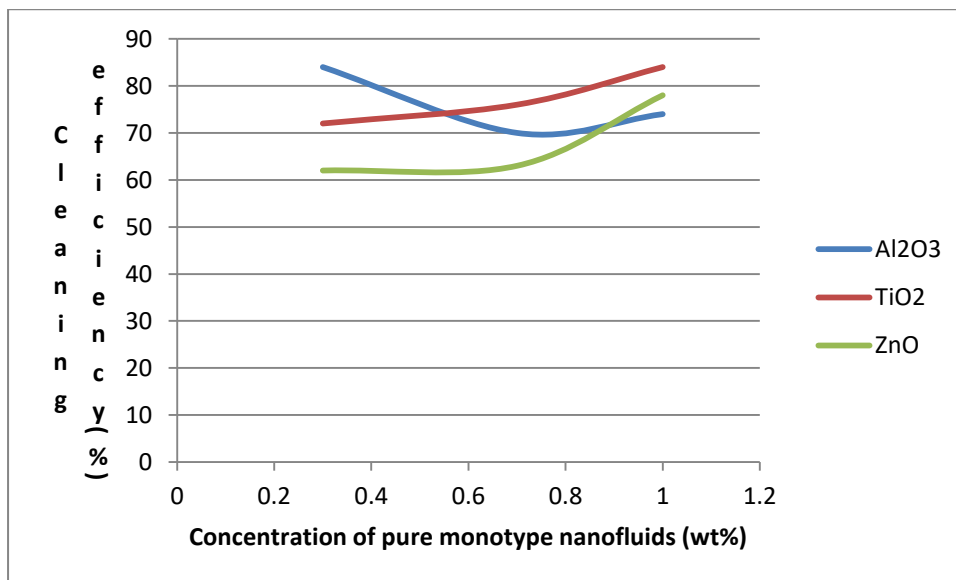


Figure 5-33 Experimental results of the cleaning efficiency of the different pure monotype nanofluids

It can be observed from the Figure5-34, the cleaning efficiency of the different pure monotype nanofluids increases along the three levels of concentration. It increases from 0.3 – 1.0 wt%. The cleaning efficiencies of Al<sub>2</sub>O<sub>3</sub> and TiO<sub>2</sub> are the same at 0.7% volume fraction. While the cleaning efficiencies of Al<sub>2</sub>O<sub>3</sub> and ZnO/water is the same at 0.7% volume fraction. Each of the nanofluid trying to outsmart one another through their strange behaviours.

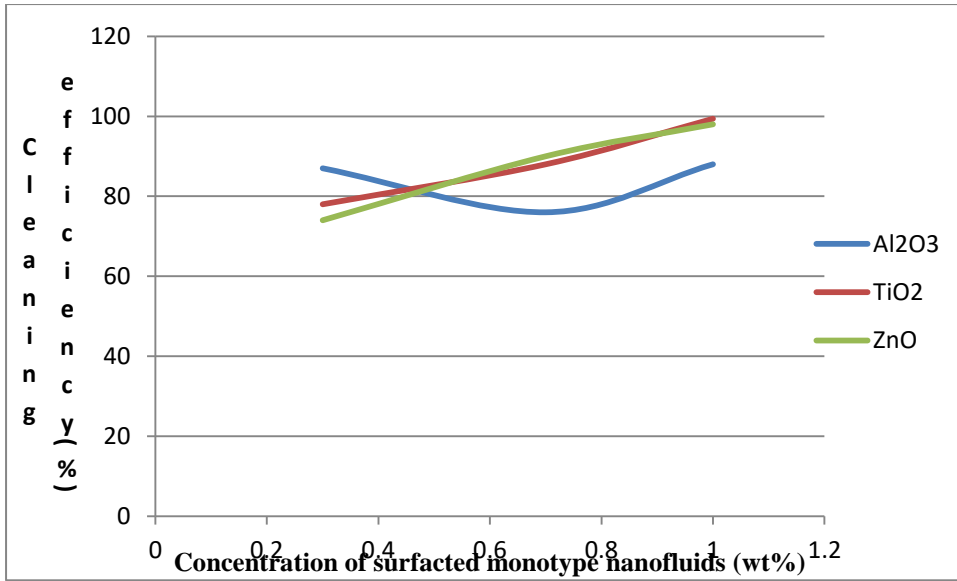


Figure 5-34 Comparison of the cleaning efficiency of different surfacted monotype nanofluids

It can be seen on Figure 5-35 that the cleaning efficiency of the different surfacted monotype water nanofluids increases with increase in volume fractions of nanofluids. Al<sub>2</sub>O<sub>3</sub> /water behaving strangely with TiO<sub>2</sub>/water and ZnO/water at medium concentration (0.7wt %). This is because Al<sub>2</sub>O<sub>3</sub>/water is a bacterial and ceramic nanofluid while TiO<sub>2</sub>/water and ZnO /water are antibacterial nanofluids. This is the reason why TiO<sub>2</sub>/water and ZnO /water behave the same at medium level concentration (0.7wt %). The strange behaviours of cleaning efficiency of TiO<sub>2</sub> and ZnO was observed when their cleaning efficiency values were plotted, each of them trying to outsmart each other. This strange behavior of nanofluids was also observed by [187]. TiO<sub>2</sub> is selected as the best monotype nanofluid since it has the highest cleaning efficiency both for pure and surfacted monotype nanofluids.

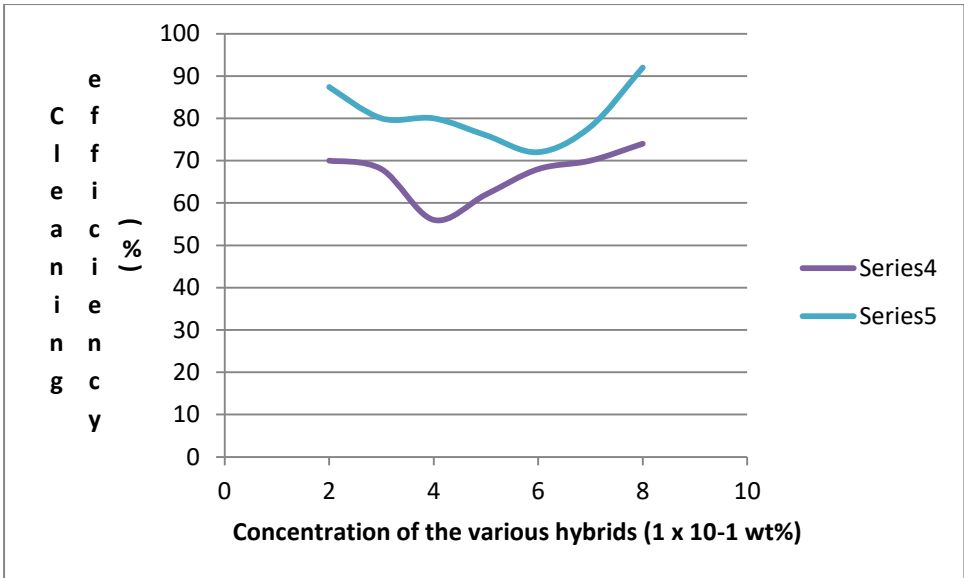


Figure 5-35 Comparison of the cleaning efficiency different pure (series 4) and surfacted (series 5) hybrid nanofluids

From the Figure 5-36 pure  $0.3\text{Al}_2\text{O}_3 + 0.3\text{TiO}_2 + 0.3\text{ZnO}/\text{water}$  and  $0.3\text{Al}_2\text{O}_3 + 0.7\text{ZnO}/\text{water}$  gave the highest and lowest cleaning efficiency, respectively. Whereas, surfacted  $0.3\text{Al}_2\text{O}_3 + 0.3\text{TiO}_2 + 0.3\text{ZnO}/\text{water}$  gave the highest cleaning efficiency. Therefore,  $0.3\text{Al}_2\text{O}_3 + 0.3\text{TiO}_2 + 0.3\text{ZnO}/\text{water}$  is selected as the best among the hybrid nanofluids. One will not be surprised why  $0.3\text{Al}_2\text{O}_3 + 0.3\text{TiO}_2 + 0.3\text{ZnO}/\text{water}$  is the best among the hybrids because the three characteristics of the three nanoparticles are combined together.

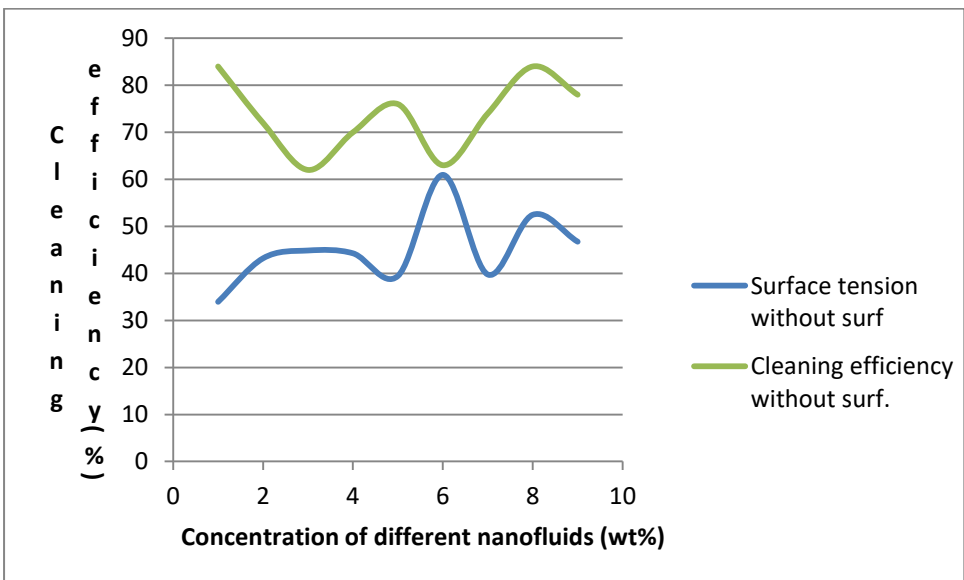


Figure 5-36 Comparison of cleaning efficiency with surface tension of pure monotype nanofluids

From Fig 5-37, comparing surface tension of pure monotype nanofluids with cleaning efficiency, it can be seen that the cleaning efficiency is higher than surface tension but they are close to each at 0.7wt% Particle size concentration.

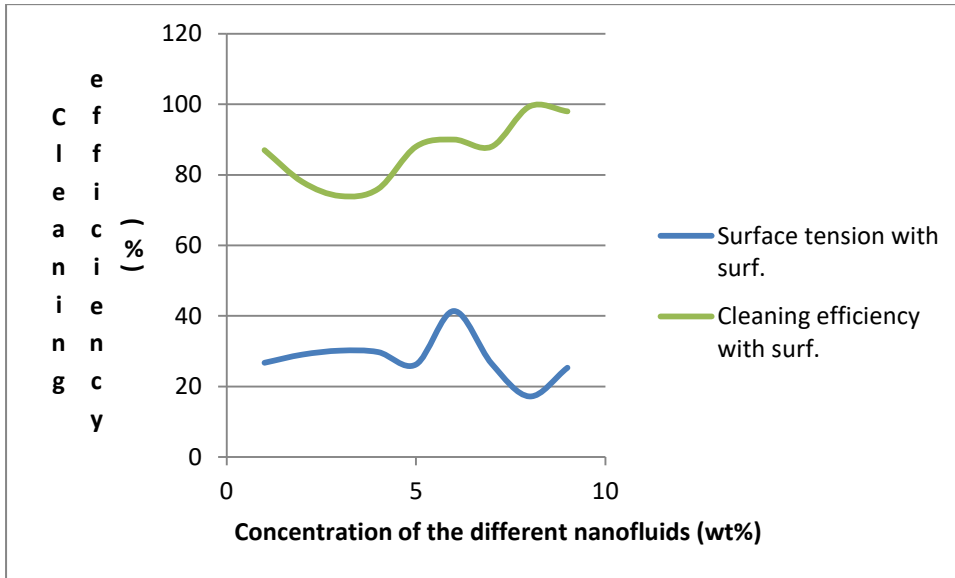


Figure 5-37 Comparison of cleaning efficiency and surface tension of surfacted monotype nanofluids.

The figure shows the effect of surfactants on surface tension. It reduces the surface tension and increases the cleaning efficiency as seen above. There is a wide gap between the cleaning efficiency and surface tension. In other words, the smaller the surface tension, the higher the cleaning efficiency.



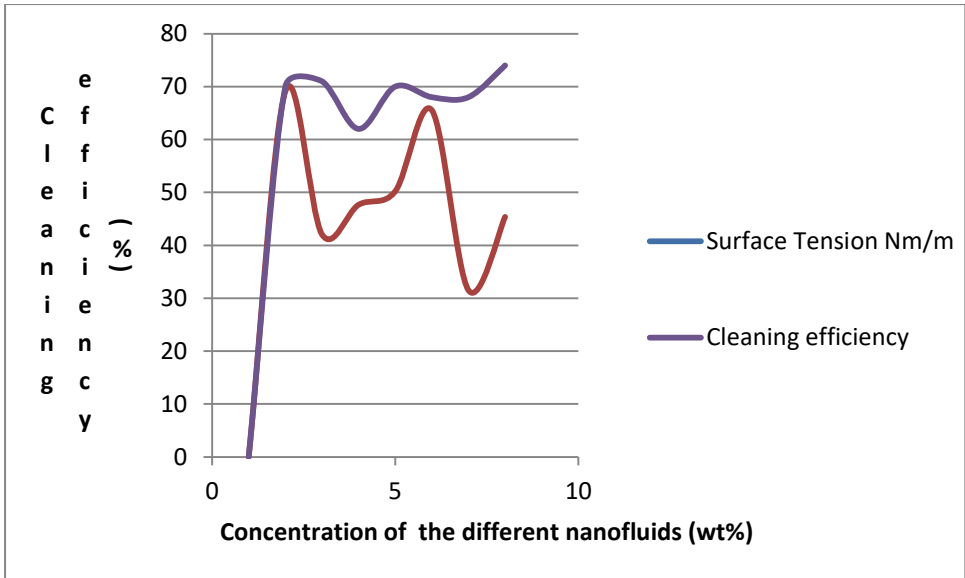


Figure 5-38 Comparison of cleaning efficiency and surface area of pure hybrid nanofluids

Figure 5-39 indicates that the cleaning efficiency increases linearly with decrease in surface tension.

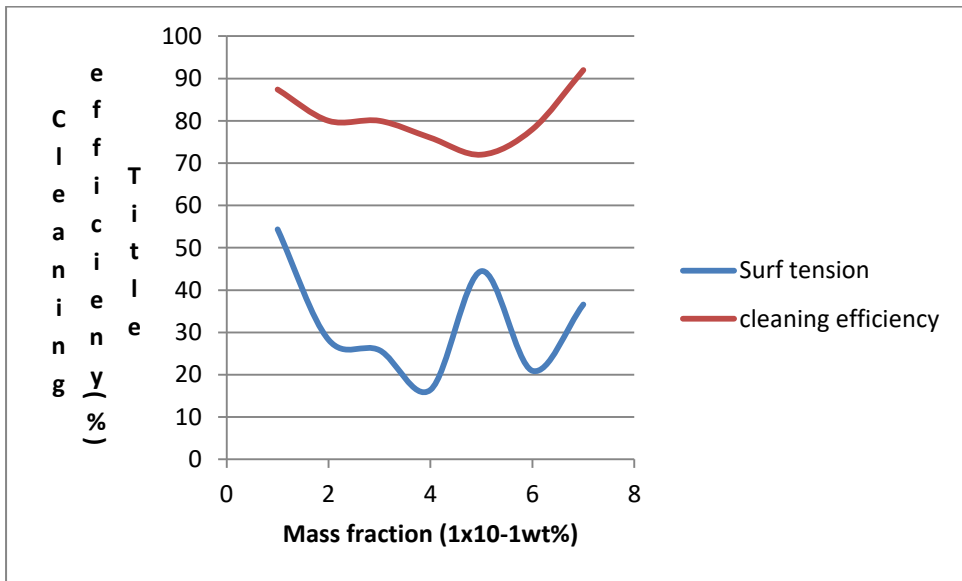


Figure 5-39 Comparison of cleaning efficiency and surface tension of surfacted hybrid nanofluids.

This is the same as discussed above for surfacted monotype nanofluids, both increase linearly, after which there is a dramatic decrease in surface tension and a large increase in cleaning efficiency due to addition of surfactants.

### 5.18 Cleaning Efficiency of different nanofluids

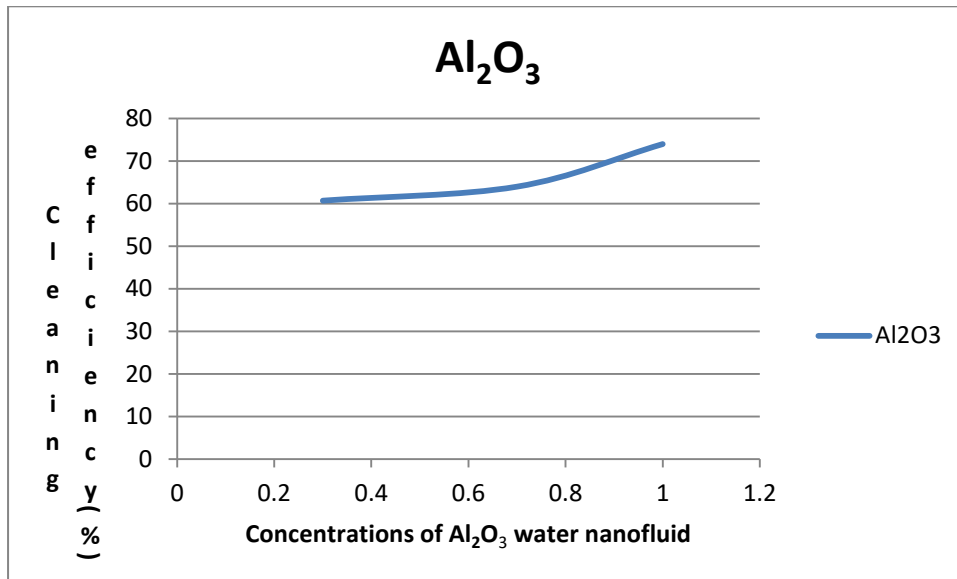


Figure 5-40 Cleaning efficiency (%) of different concentrations of Al<sub>2</sub>O<sub>3</sub> monotype deionised water nanofluid (%), Table 5-4

Cleaning efficiency of Al<sub>2</sub>O<sub>3</sub> nanofluid increases with increase in the concentration of Al<sub>2</sub>O<sub>3</sub> nanoparticles dispersed in deionised water. Concentration of 1g is the highest, followed by 0.7g and 0.3g is the least as shown on the Figure5-41.

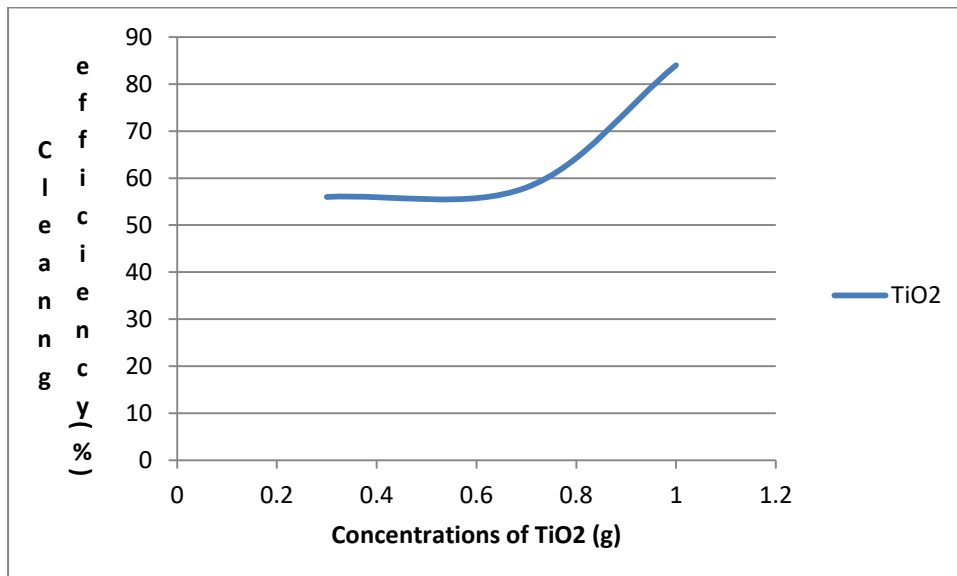


Figure 5-41 Cleaning efficiency of different concentrations of TiO<sub>2</sub> water nanofluid (%)

Cleaning efficiency of TiO<sub>2</sub> nanofluid increases with increase in the concentration of TiO<sub>2</sub> nanoparticles dispersed in deionised water. Concentration of 1g is the best, followed by 0.7g and 0.3g is the least as shown on the Figure5-42.

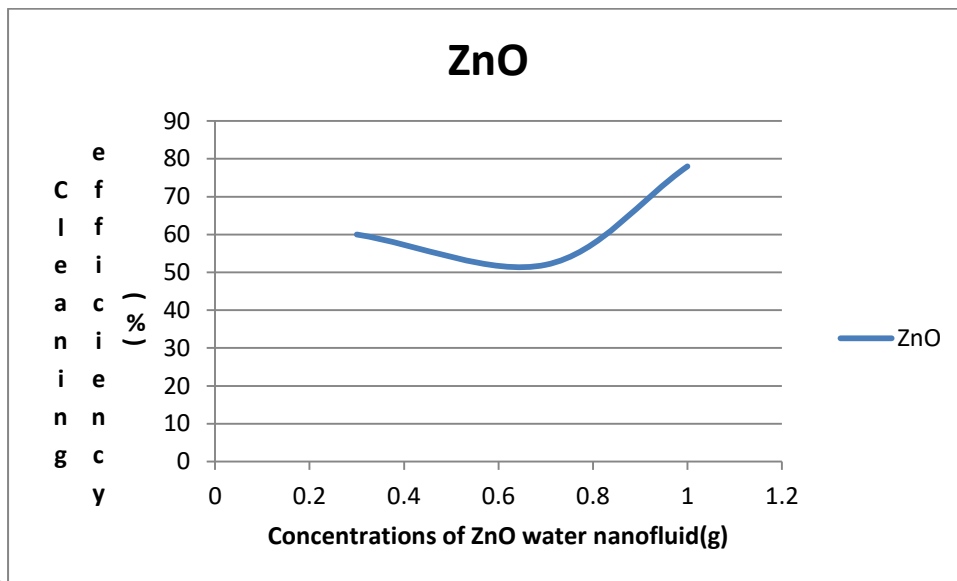


Figure 5-42 Cleaning efficiency of different concentrations of ZnO water nanofluid (%),  
Table 5-4

Cleaning efficiency of ZnO nanofluid increases with increase in the concentration of ZnO nanoparticles dispersed in deionised water. Concentration of 1g is the best, followed by 0.3g and 0.7g is the least as shown on the Figure5-43.

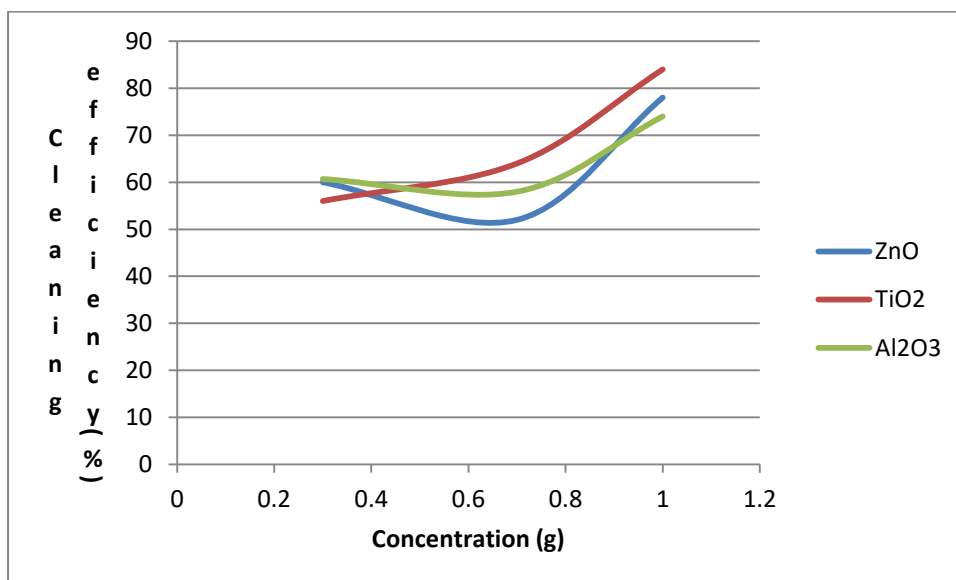


Figure 5-43 Comparison of cleaning efficiency values for different monotype -water nanofluids

Table 5-8 Comparison of the cleaning efficiency of the different pure and surfacted nanofluids

Nanofluids	Cleaning efficiency (%)						
	without			With surfactant			
	0.3	0.7	1.0	0.3	0.7	1.0	
Al <sub>2</sub> O <sub>3</sub>	84	70	74	82	76	84	
TiO <sub>2</sub>	72	76	84	62	88	99.4	
ZnO	62	63	78	74	90	98	
0.3Al <sub>2</sub> O <sub>3</sub> + 0.7TiO <sub>2</sub>	70			87.4			
0.7Al <sub>2</sub> O <sub>3</sub> + 0.3TiO <sub>2</sub>	68			80			
0.3Al <sub>2</sub> O <sub>3</sub> + 0.7ZnO	71			80			
0.7Al <sub>2</sub> O <sub>3</sub> + 0.3ZnO	62			76			
0.3TiO <sub>2</sub> + 0.7ZnO	68			72			
0.7TiO <sub>2</sub> + 0.3ZnO	70			78			
Al <sub>2</sub> O <sub>3</sub> +0.3TiO <sub>2</sub> + 0.3ZnO	74			92			

Influence of physical properties of nanofluids (Al<sub>2</sub>O<sub>3</sub>, TiO<sub>2</sub> and ZnO) on the cleaning behaviour of nanofluids on the crude oil contaminated at optimum conditions. This is determined by calculating the total surface area using different equations:

Surface area of nanofluids: The values of the surface area of each nanofluid and their hybrids are shown on Table 5-9.

Table 5-9 Total surface area (nm<sup>2</sup>) of the different nanofluids calculated with equation (C1.1) in Appendix C.

Concentration (%)	0.3	0.7	1.0
Al <sub>2</sub> O <sub>3</sub>	323.64nm <sup>2</sup>	73.53nm <sup>2</sup>	55.81nm <sup>2</sup>
TiO <sub>2</sub>	456.17nm <sup>2</sup>	1974.99nm <sup>2</sup>	8507.95nm <sup>2</sup>

ZnO	39,699.76 nm <sup>2</sup>	22,740.7 5 nm <sup>2</sup>	4400.62 nm <sup>2</sup>
-----	------------------------------	-------------------------------	----------------------------

From the Table 5-9 above, The total surface area of ZnO – water nanofluid decreases with increase in concentration of ZnO nanoparticles dispersed in deionised water (ie the surface area of each concentration decreases from 39,699.76nm<sup>2</sup> to 4,400.62nm<sup>2</sup> but the cleaning efficiency increases with increase in concentration from 60 – 78%, the same as that of surface area of Al<sub>2</sub>O<sub>3</sub> nanofluid which decreased from 323.64 nm<sup>2</sup> to 55.81nm<sup>2</sup> with increase in cleaning efficiency from 58 – 74%. The surface area of TiO<sub>2</sub> – water nanofluid increases with increase in concentration of TiO<sub>2</sub> nanoparticles dispersed in deionised water, the same as the cleaning efficiency, from 56 – 84% without surfactant.

Comparison of total surface area wth the cleaning efficiency (%)

Table 5-10 Total surface area (nm<sup>2</sup>) with the cleaning efficiency (%).

Hybrid type (vol %)	Surface area (nm <sup>2</sup> )	Cleaning efficiency (%)
0.3ZnO + 0.7Al <sub>2</sub> O <sub>3</sub>	390.10	62
0.7ZnO + 0.3Al <sub>2</sub> O <sub>3</sub>	41629.12	50
0.3ZnO + 0.7TiO <sub>2</sub>	210	78
0.7ZnO + 0.3TiO <sub>2</sub>	30.51	66
0.3 TiO <sub>2</sub> + 0.7Al <sub>2</sub> O <sub>3</sub>	619.57	68
0.7 TiO <sub>2</sub> + 0.3Al <sub>2</sub> O <sub>3</sub>	566.07	70
0.3Al <sub>2</sub> O <sub>3</sub> +0.3 TiO <sub>2</sub> +0.3ZnO	133.52	74

#### 5.4Thermal optical (Absorbency) Results

Absorbency is a material's ability to soak up a liquid.(Eg nanoparticle and water).Typically, absorbance of a dissolved substance is measured using Uv-Vis spectrophotometer.This involves shining a light through a solution and recording how much light and what wavelengths were transmitted onto a detector.The wavelengths that were absorbed can be determined. First,

measurements on a "blank" are taken using just the solvent (water) for reference purposes. The solutions are placed in a small cuvette (Figure 3-12) and inserted into the holder (Figure 3-11). The machine is controlled through a computer and, once it is "blank", it automatically displays the absorbance plotted against wavelength. The absorbance at a given wavelength is

$$A_{\lambda} = \log_{10} \frac{I_0}{I}$$

Where,  $I_0$  = intensity of light source,  $I$  = intensity of the solution sample and  $A_{\lambda}$  = absorbency of the solution. The absorbance spectrum is plotted on a graph of absorbance vs. wavelength. The significance of absorbency is for the evaluation of stability of a solution (nanofluid) and determination of the concentration of that solution.

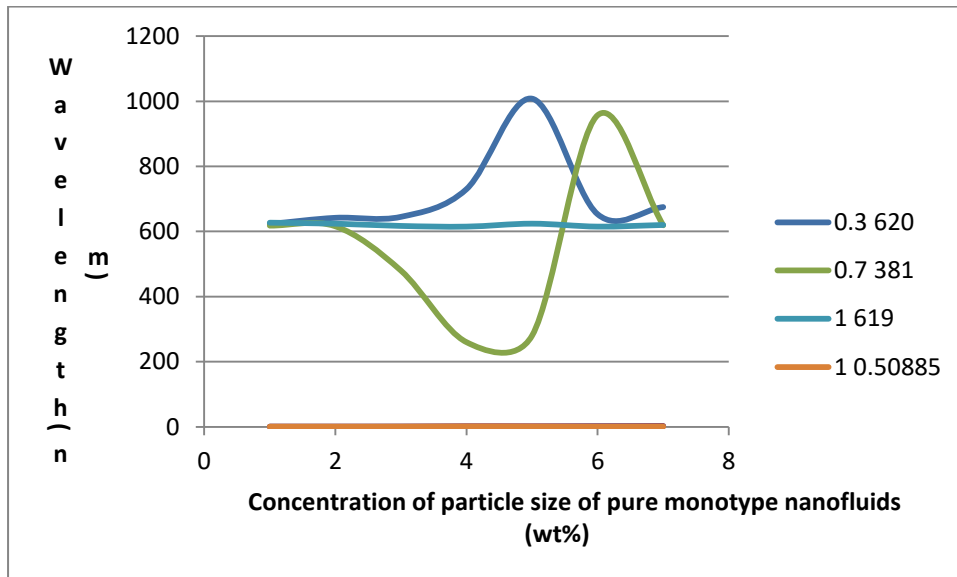


Figure 5-44 Wavelength of the different pure monotype nanofluids

The results of the pure monotype nanofluids thermal optical are plotted in the Figure 5-45. The graph shows that the particle size concentration of 0.3 wt %  $\text{TiO}_2$  has the highest wavelength (1008nm) with absorbance of 0.9897au. This is followed by 0.7 wt %  $\text{TiO}_2$  with 957nm wavelength and absorbance of 0.9897au, showing the stability of the  $\text{TiO}_2$  nanofluids. 0.7wt%  $\text{TiO}_2$  /water has the lowest wavelength (260nm) with absorbance of 0.74327au. However, the wavelength and absorbance of the different monotype nanofluids decreases as the particle size increases as can be seen from the figure. The wavelength of the pure monotype nanofluids ranges from 260 – 1008nm which is comparable with the literature values of 190 – 1100nm.

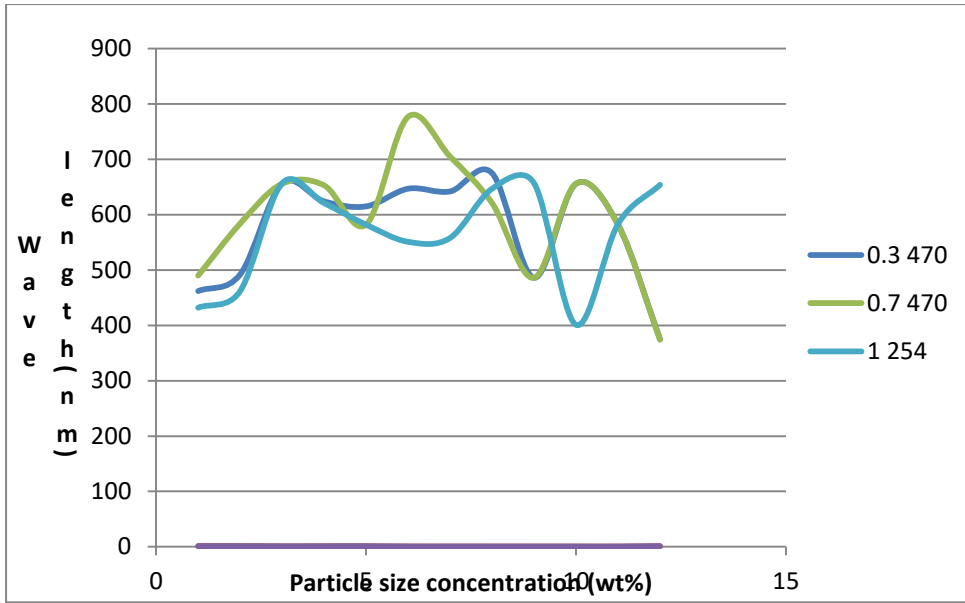


Figure 5-45 Wavelength of different surfacted monotype nanofluids

From the Figure 5-46, the wavelength ranges from 375 – 777nm for 0.7% ZnO and 0.7% TiO<sub>2</sub>  
OR

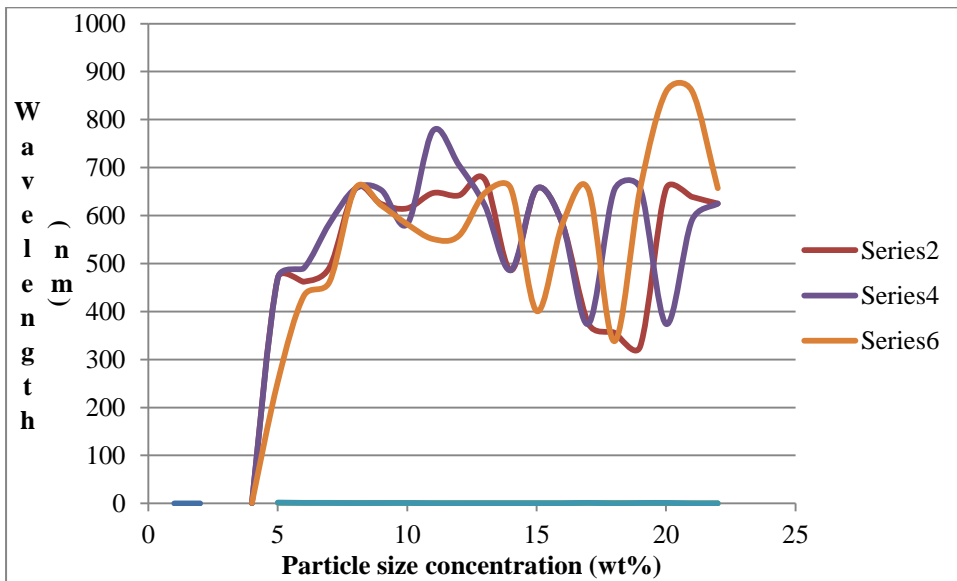


Figure 5-46 Wavelength of the various surfacted monotype nanofluids Series6 - 1.0% ZnO = 860nm

It is observed from Fig 5-47 that 1.0% ZnO/water gave the highest wavelength of 860nm, followed by 0.7% TiO<sub>2</sub> with wavelength of 777nm and 0.3% ZnO gave the least wavelength of 327nm. In summary, when the pure monotype nanofluids were surfacted, their wavelengths range from 327 – 860nm. The peak wavelength was reduced from 1008 – 860nm.

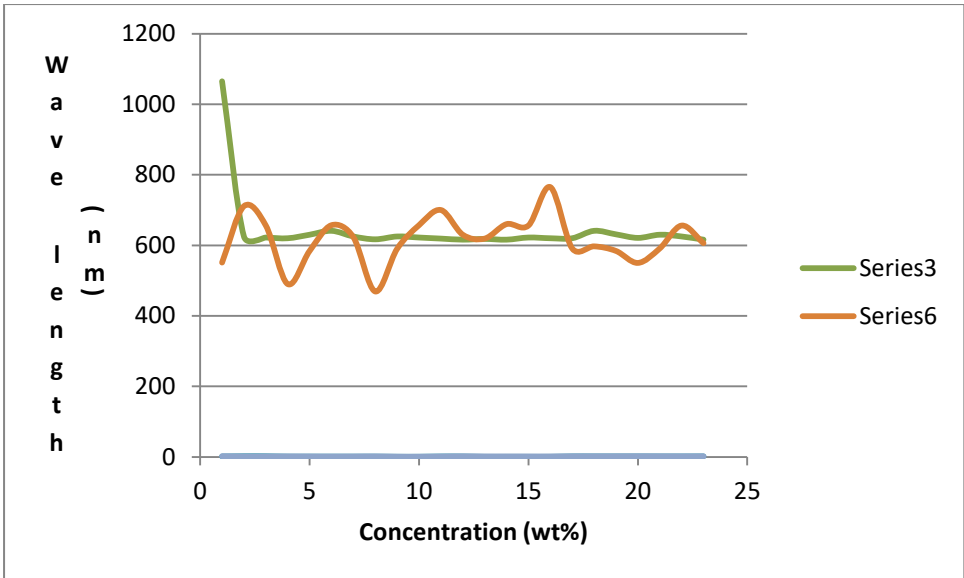


Figure 5-47 Comparison of wave length of pure (series 3) and surfacted (series 6) hybrid nanofluids

It can be seen from the Figure 5-48 that the wavelength of pure hybrid nanofluids range from 616 – 1065nm and that of surfacted hybrid nanofluids range from 606 – 765nm. This indicates that surfactant reduces the wavelength of water nanofluids in general. Surfactant as a wetting agent enhances thermophysical and thermal optical strength.

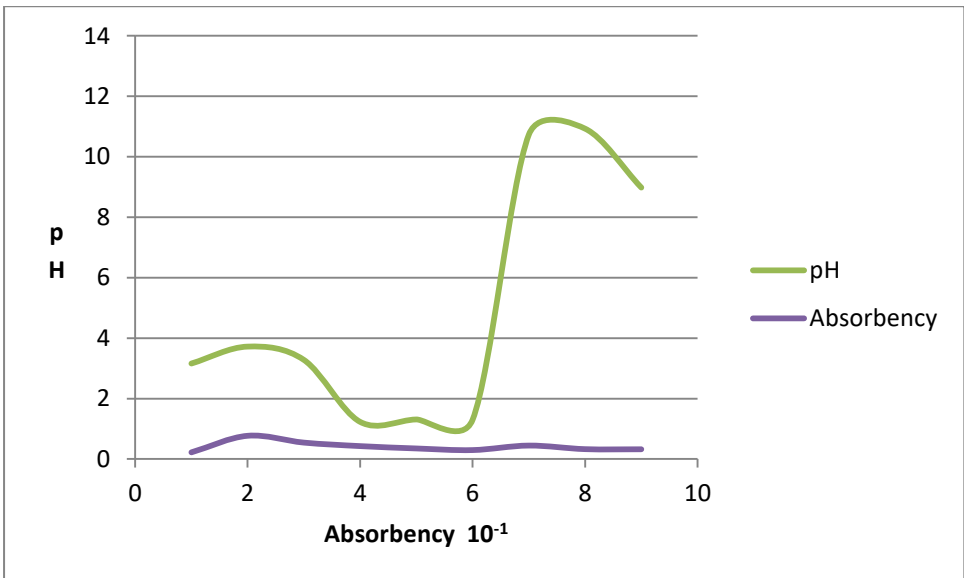


Figure 5-48 Effect of pH on the absorbency of different surfacted monotype nanofluids.

Figure 5-49 can be compared with the Fig of pure and surfacted surface tension of the various nanofluids.



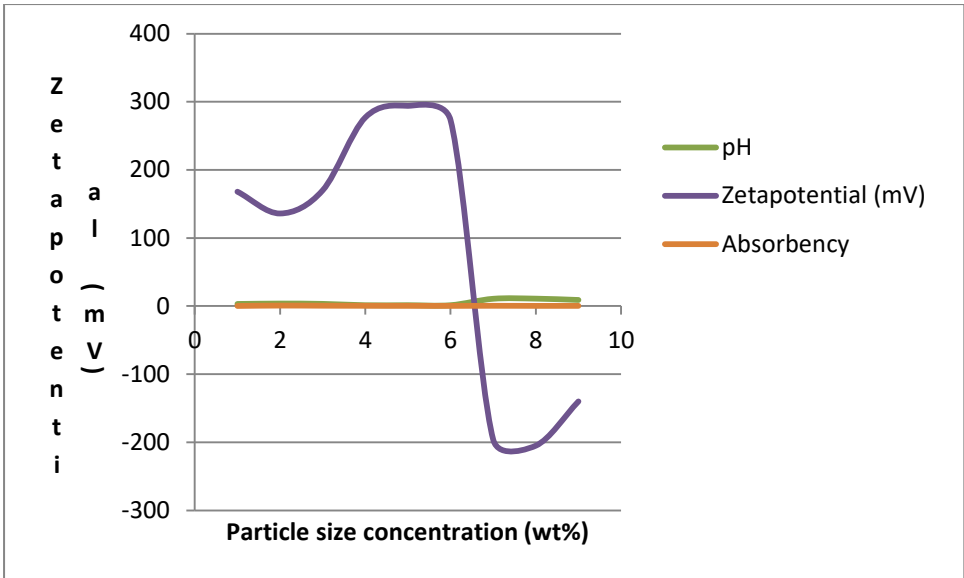


Figure 5-49 Effect of pH on the zetapotential and absorbency for surfacted monotype nanofluids

Zetapotential measurement is used to study the absorption mechanisms of the surfactants on water nanofluids. From the Figure 5-50, as pH increases the zetapotential of the surfacted monotype increases also, so the electrostatic repulsion force between nanofluids/nanoparticles becomes adequate to prevent attraction and collision between nanoparticles caused by brown motion. pH, absorbency and zetapotential are equal to each other at 1.0 wt%  $\text{TiO}_2$ /water which makes  $\text{TiO}_2$ /water the best among all the monotype nanofluids.

The significance of zetapotential is that its value can be related to the stability of nanofluids, so nanofluids with high negative zetapotential as on Figure 5-51 are electrically stabilized.

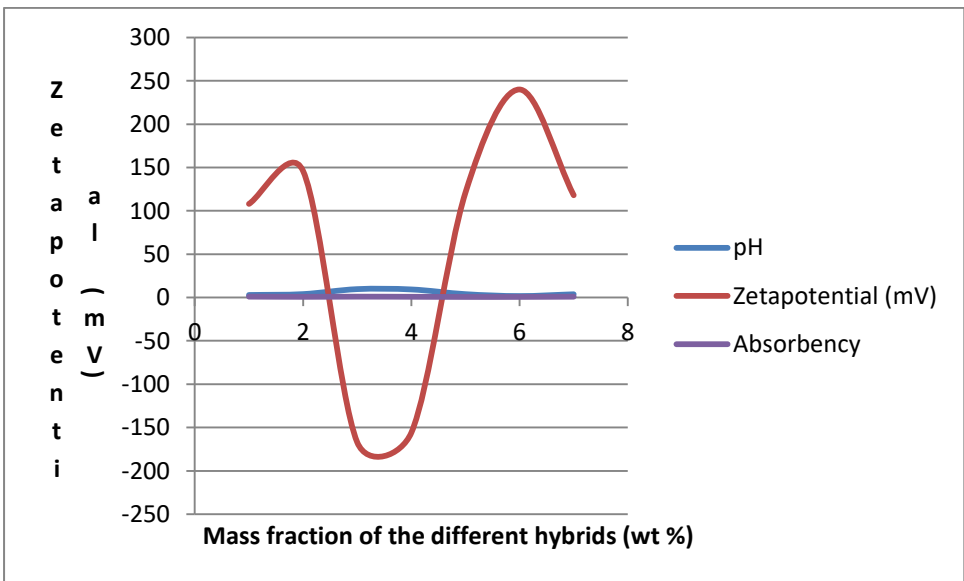


Figure 5-50 Effect of pH on the zetapotential and absorbency of the surfacted hybrid nanofluids.

The Figure 5-51 shows the optimum /peak pH of 9.66 with absorbency of 0.99356 and peak zetapotential of 240, lowest zetapotential of -167mV.

The absorbency becomes higher with rise in pH leading to an improvement of the scattering stability of the different nanofluids. Having pH 9.66 for surfactant the zetapotential and absorbency become even higher. The electrostatic repulsion force between particles becomes stronger and the coagulated nanoparticles can be re-dispersed through mechanical force, so the scattering stability of the nanofluids is at their best. As the pH value continues to increase, the concentration of the pH regulation reagents ( $\text{Na}_2\text{HPO}_4$  and SDBS) in the system increases, which causes the compressions of electrical double – layer, so lowering the zetapotential of the nanofluids surface and electrostatic repulsion force and the nano- suspension illustrates a poorer scattering.

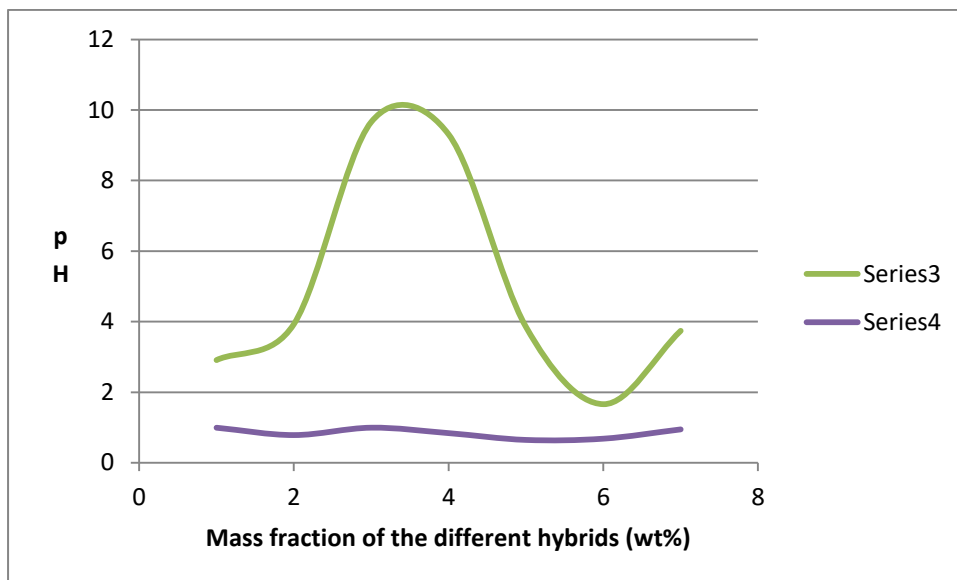


Figure 5-51 Effect of pH on absorbency of surfacted hybrid nanofluids. Series3 - pH and Series4 - Absorbency.

Optimum pH = 9.66 with absorbency of 0.99356.

Figure 5-52 can be compared with the Figure of pure and surfacted surface tension of the various nanofluids.

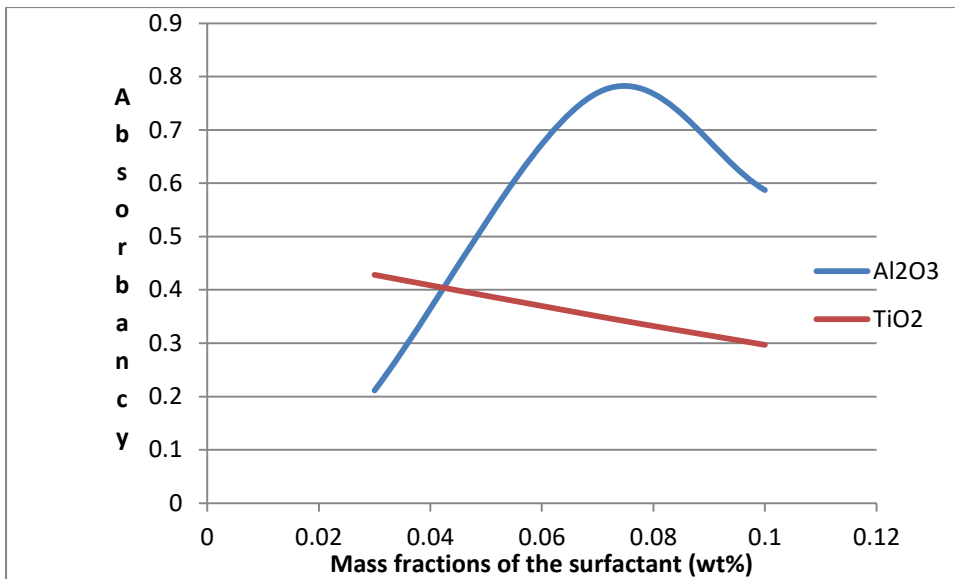


Figure 5-52 Effect of mass fraction of SDBS surfactant on absorbance of the surfacted monotype nanofluids.

From the Figure 5-53, the absorbance of Al<sub>2</sub>O<sub>3</sub>/water increases as the mass fraction increases until it reaches the optimum value of 0.76982, at 0.07% mass fraction, after which it decreases with increase in mass fraction. The absorbance of TiO<sub>2</sub>/water decreases with increase in mass fraction of SDBS but the two surfacted monotype nanofluids are best at the medium mass fraction of 0.07% SDBS. A simple scheme to solubilize high weight fraction nanoparticles in water has been demonstrated. Suspension concentrations were improved by a factor of 10 – 100 with respect to the used experimentally surfactants, and the ultrasonication technique also dramatically reduced particle fragmentation. The optimum concentration of SDBS is found equal to 0.1wt% and Na<sub>2</sub>HPO<sub>4</sub> is 0.5wt%, at this concentration, the absolute value of zeta potential and the absorbance is maximal and the system is more stable.

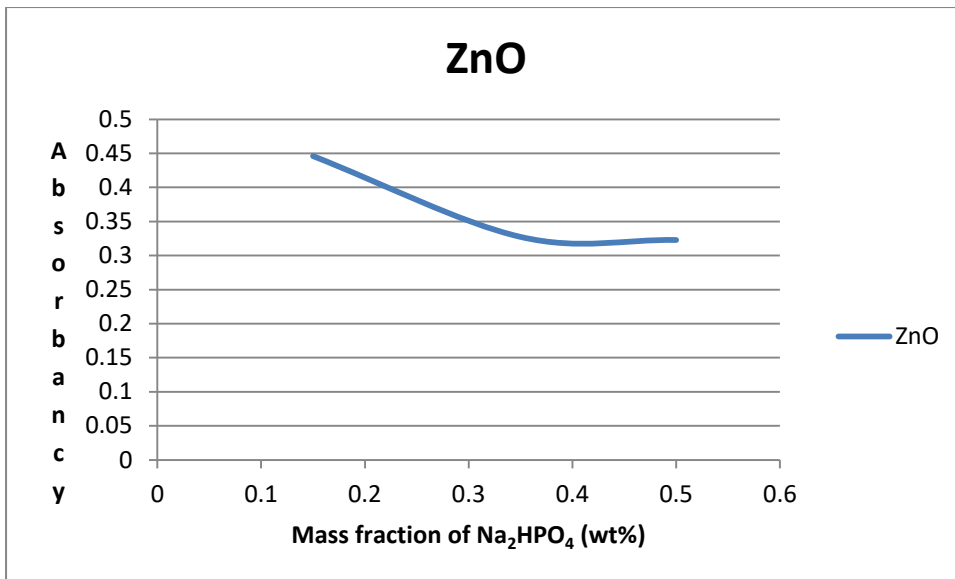


Figure 5-53 Absorbance of surfacted ZnO with different mass fraction of Na<sub>2</sub>HPO<sub>4</sub>

It can be observed from the Figure 5-54 that the absorbance of ZnO/water decreases sharply with increase in mass fraction and optimum at 0.1 wt%, absorbance of 0.44. Addition of surfactants enhanced significantly the absorption performance. Comparing the solubilising capacities of the various surfactants, any successful method must reckon with the substantial van der Waals attractions of bare particles. Figure 5-53 & 5-54, indicate that SDBS did better than Na<sub>2</sub>HPO<sub>4</sub>. It is believed that SDBS disperse the nanofluids better than Na<sub>2</sub>HPO<sub>4</sub> because of its benzene rings which improve the surfactant energetic. The spacing between the benzene rings on the surfactants and the particle surface is large enough to accommodate the SO<sub>3</sub><sup>-</sup> charged groups [121]. This is comparable with the cleaning efficiency of ZnO/water in which cleaning efficiency increases with increase in particle size concentration while absorbance increases with decrease in surfactant concentration.

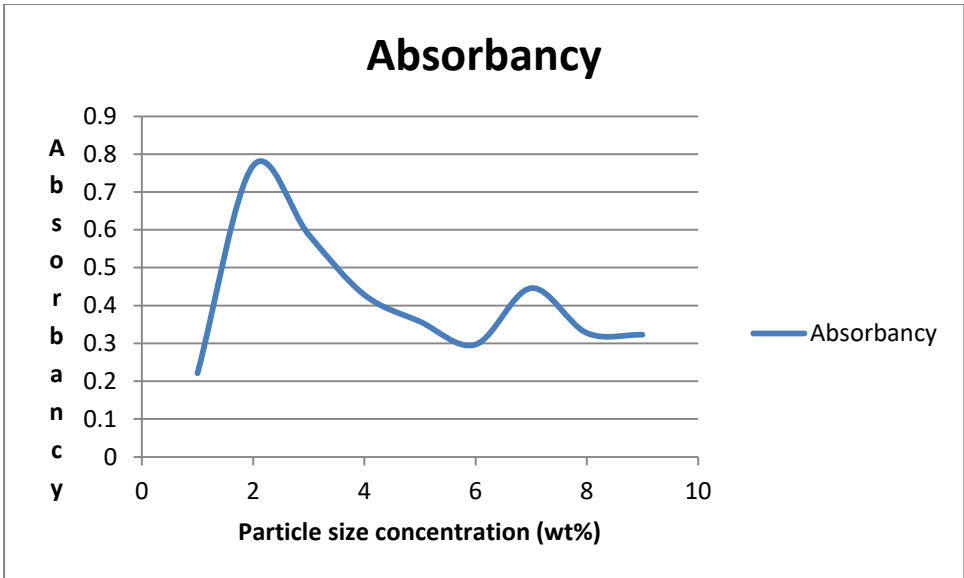


Figure 5-54 Absorbancy of the different surfacted monotype nanofluids

From the Figure5-55, it can be observed that surfacted 0.7% Al<sub>2</sub>O<sub>3</sub>/water has absorbancy peaks at 260nm (0.76952) and 0.3%ZnO has absorbancy peak at 480nm (0.44597)..Stability increases as absorbancy approaches 1 and beyond that is unstability.Absorbancy increases with decrease in particle size concentration.

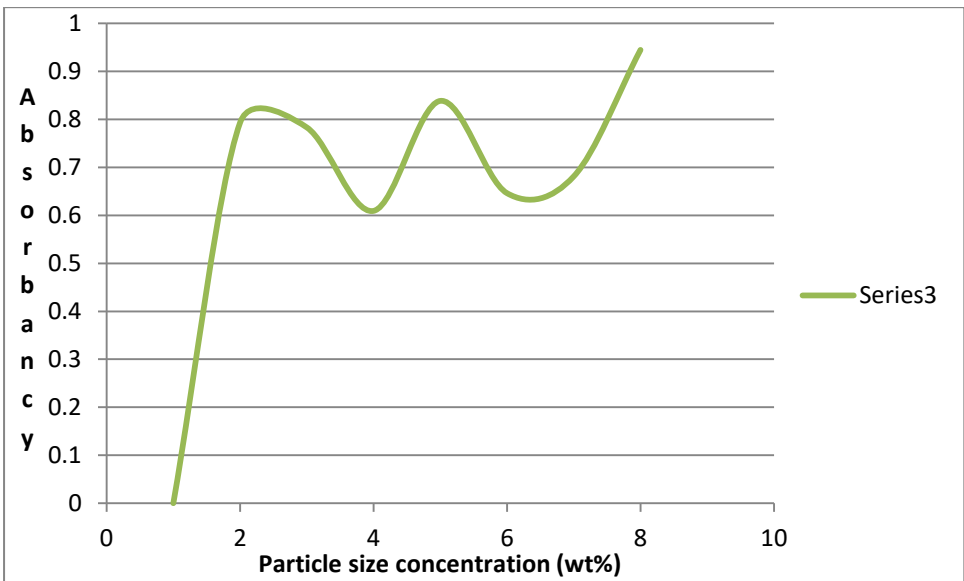


Figure 5-55 Absorbancy of the surfacted hybrid nanofluids

In general, there is a linear relationship between the absorbancy intensity and the concentration of nanoparticles in fluid.Stability increases as absorbancy approaches 1 and beyond that is unstability.The greater the absorbancy as tends or goes close to 1.0, the more stable is the nanofluids.

Table 5-11 Comparison of the cleaning efficiency of the different nanofluids

Nanofluids (monotypes)	Cleaning Efficiency (%)					
	Without surfactants			With surfactants		
Wt (g)	0.3	0.7	1.0	0.3	0.7	1.0
Al <sub>2</sub> O <sub>3</sub>	84	70	74	87	76	88
TiO <sub>2</sub>	72	76	84	78	88	99.4
ZnO	62	63	78	74	90	98
0.3 Al <sub>2</sub> O <sub>3</sub> + 0.7 TiO <sub>2</sub>			70	87.4		
0.7 Al <sub>2</sub> O <sub>3</sub> + 0.3 TiO <sub>2</sub>			68	80		
0.7ZnO + 0.3 Al <sub>2</sub> O <sub>3</sub>			71	80		
0.3ZnO + 0.7Al <sub>2</sub> O <sub>3</sub>			62	76		
0.7 ZnO + 0.3 TiO <sub>2</sub>			68	72		
0.3 ZnO + 0.7 TiO <sub>2</sub>			70	78		
0.3ZnO + 0.3TiO <sub>2</sub> +0.3Al <sub>2</sub> O <sub>3</sub>			74	92		

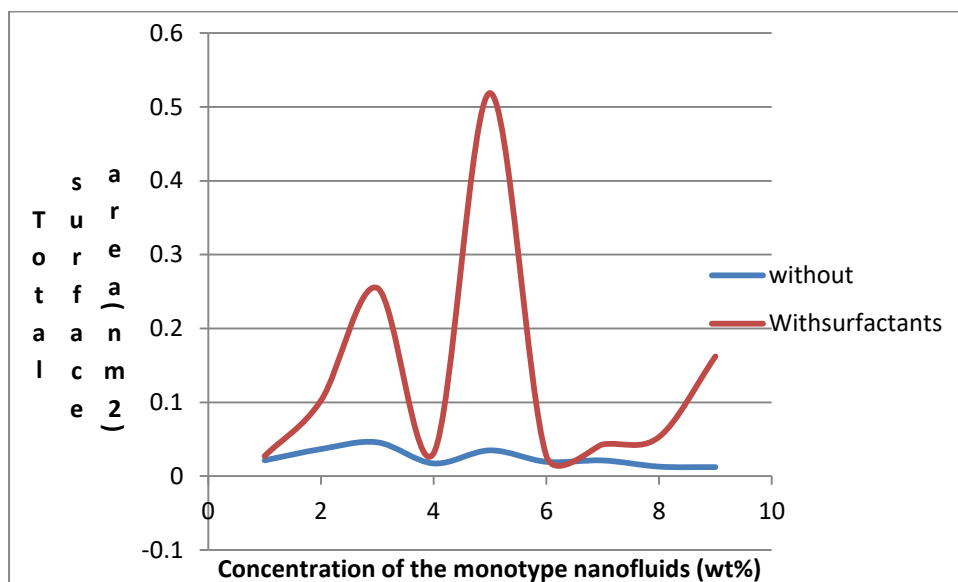


Figure 5-56 Comparison of the total surface area of the different monotype nanofluids

The total surface area of the surfacted nanofluids is larger than that of pure nanofluids. The total surface area of different nanofluids is equal at the concentration of 1wt%, 4wt% and 6wt%,

total surface area of  $0.021427 \text{ nm}^2$ ,  $0.0172764 \text{ nm}^2$  and  $0.027394 \text{ nm}^2$  for  $0.3\text{Al}_2\text{O}_3/\text{water}$ ,  $0.3\text{TiO}_2/\text{water}$  and  $1.0\text{TiO}_2/\text{water}$ , respectively.

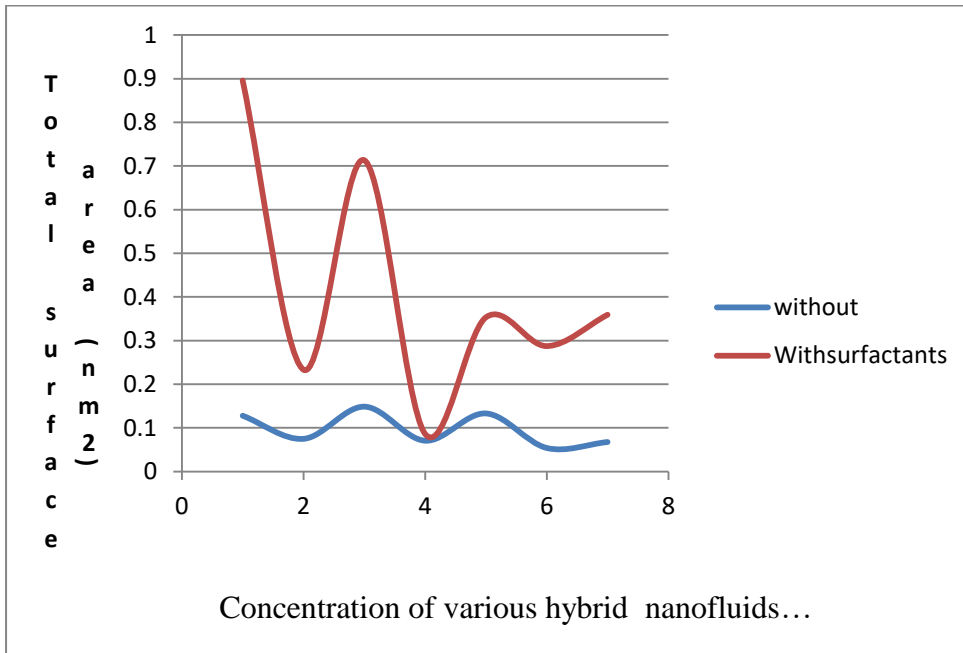


Figure 5-57 Comparison of the total surface area of the different hybrid nanofluids

Figure5-58 shows the effect of surfactants on the total surface area of the hybrid nanofluids. Surfacted nanofluids have higher total area than the pure nanofluids but both have equal total surface of  $0.7133 \text{ nm}^2$  and  $0.07057 \text{ nm}^2$  at the concentrations of 0.3wt% and 0.4wt% for  $0.3\text{Al}_2\text{O}_3 + 0.7\text{ZnO}/\text{water}$  and  $0.7\text{Al}_2\text{O}_3 + 0.3\text{ZnO}/\text{water}$ , respectively.

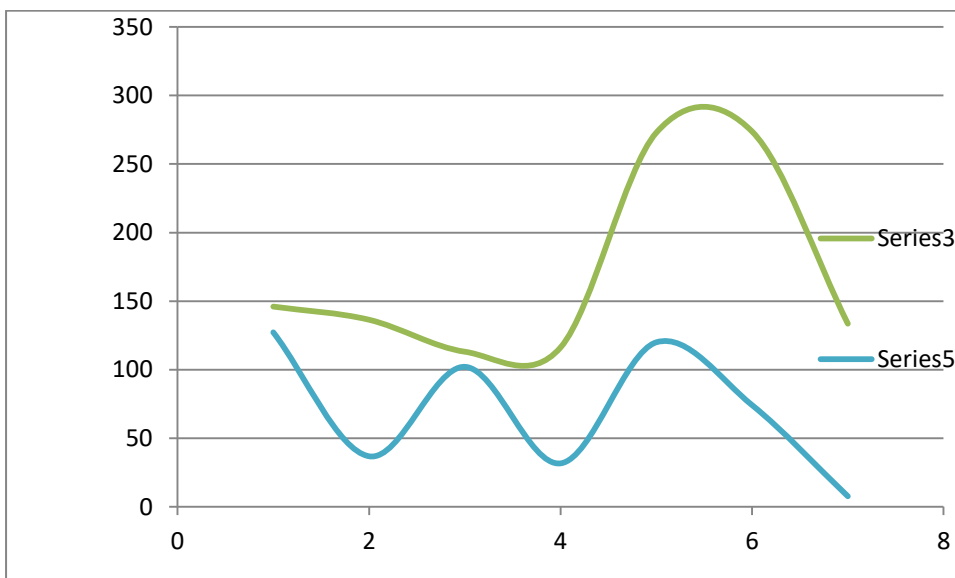


Figure 5-58 Total surface area of the hybrid nanofluids. (Series3 – surfacted hybrids & series5 – Pure hybrids)

Total surface area of the nanofluids of surfacted hybrid nanofluids is higher than those of the pure nanofluids.

## Chapter Six

### 6.0 Soil preparation And Characterization

#### 6 6.1 General soil physical and chemical properties

Soils showed high texture homogeneity, at the surface and at subsurface. The sand, silt and clay content varied, respectively, between 41-47%, 23-29% and 22-31% in the surface horizon (0-10 cm) and 36-46%, 24-34% and 29-34% at different depths (10-50 cm). The textural classes varied from clay loam to sandy clay loam. Particle density ( $D_p$ ) ranged between 2.58 and 2.71  $Mg\ m^{-3}$  within the range expected for mineral soils [179]

The capacity of soil to transport and store water depends on the proportion and functionality of its pores, thus an adequate proportion of all sizes is important for water flow across the profile. For example, a minimum of 12 % of coarse pores ( $>50\ \mu m$ ). This high porosity was generated by the development of roots, which are able to displace particles, generating coarse porosity as they grow in length and diameter [62]. At high tensions water retention is due mainly to adsorption to solid surfaces, which depends on properties such as soil texture and the surface area of the particles, and is less influenced by the structure [192].

#### 6.2 Soil Characterization

The soil belongs to soil taxonomy series, corresponding to Fine loamy, mixed, calcareous, thermic, Typic Haplocambid Family, according to [26]. It is located in an alluvial remnant terrace with a slight slope (1%) and is well drained. Following [105], textures are clay loam to sandy clay loam (22 to 33% of clay content and 36 to 54% of sand content), but below 80 cm there is a sandy substrate.

The results of the physical properties of experimental soils are shown on Table 6.1.

Table 6-1 Mean physical properties of the soils



Properties	Bulk density(g/cm <sup>3</sup> )	Ks(m/s) at depth of 25cm	Gs	Porosity (%)	Particle density (g/cm <sup>3</sup> )
Values	1.6	3.36 x 10 <sup>-5</sup>	2.70	44	2.65

The top/surface soil (0 – 10cm) of the experiment (Table 6-1) showed porosity >12%, which as classified by [98] is in the range of very porous soils. However, the percentage of coarse pores declined sharply in the depth of 10 – 30cm. Porosity decreases as you go down the soil depth/profile.

Table 6-2 Distribution of pore sizes, porosity (%) for the treatments as a function of soil depth. Means  $\pm$  standard error of the mean). Pore size ( $\mu$ m) (>50  $\mu$ m)

Porosity (%) measurement.

0 – 10cm	10 – 30cm
14.1 $\pm$ 0.97	9.3 $\pm$ 0.90
16.1 $\pm$ 0.79	11.7 $\pm$ 0.36
14.5 $\pm$ 0.8	11.0 $\pm$ 0.38
14.2 $\pm$ 0.64	14.0 $\pm$ 0.67

Table 6-2 shows that porosity decreases with increase in soil depth.

Table 6-3 Result of bulk density (g/m<sup>3</sup>) measurements

0 – 10cm	10 – 30cm
$\pm$ 0.03	1.62 $\pm$ 0.04
$\pm$ 0.01	1.57 $\pm$ 0.02

Table 6-3 indicates that bulk density increases with soil depth.

Table 6-3 Hydraulic conductivity (permeability) results

Q (cm <sup>3</sup> )	L (cm)	A (cm <sup>2</sup> )	h (cm)	Time (mins)	K (cm/sec)
33.8	18	3.5	28	3	0.0345cm/sec = 3.45 x 10 <sup>-5</sup> m/s
33.6	18	3.5	28	3	0.032cm/sec = 3.2 x 10 <sup>-5</sup> m/s
34.0	18	3.5	28	3	0.0347cm/sec = 3.47 x 10 <sup>-5</sup> m/s

				Mean K	$3.36 \times 10^{-5} \text{ m/s}$
--	--	--	--	--------	-----------------------------------

### 6.3 Wetting Analysis

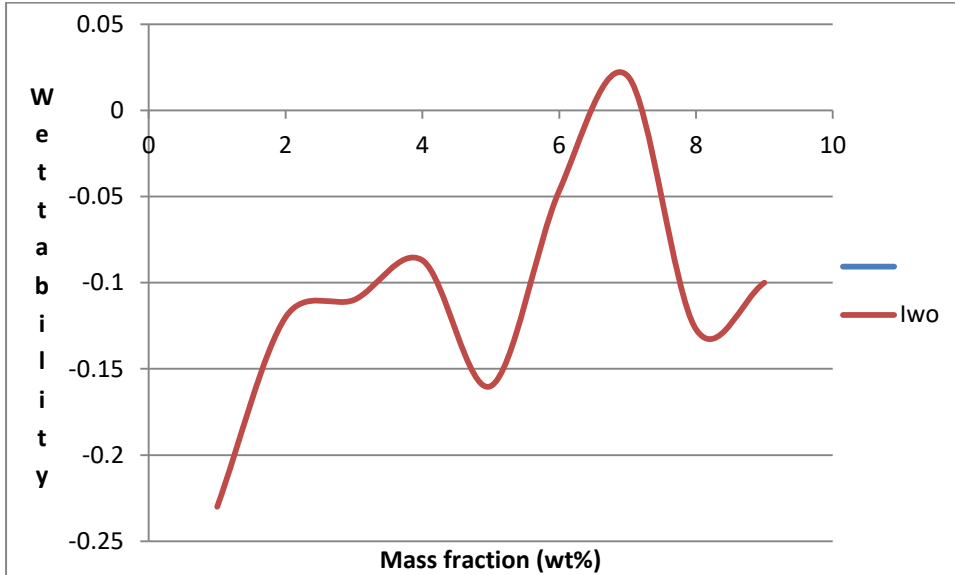


Figure 6-1 Measured oil-wet of the various pure monotype nanofluids during the cleanup process

It can be seen from Figure 6-1, that the mineral oil contaminated soil sample (strong oil wet) after the cleanup with pure monotype nanofluids was changed to more oil - wet and slightly water-wet state since all wettability index as shown in Fig 6-1 are all negative, indicating the oil wetness state. But as more nanofluids are imbibed into the contaminated soil and water saturation increases about 60%, wetting becomes water wet and finally oil - wet condition after cleaning. Then the sample was further analysed using TGA. It shows the moderate cleaning and wetting of the soil sample. In other words, the soil sample was not perfectly restored its original water wet condition. Therefore, the necessity of TGA.

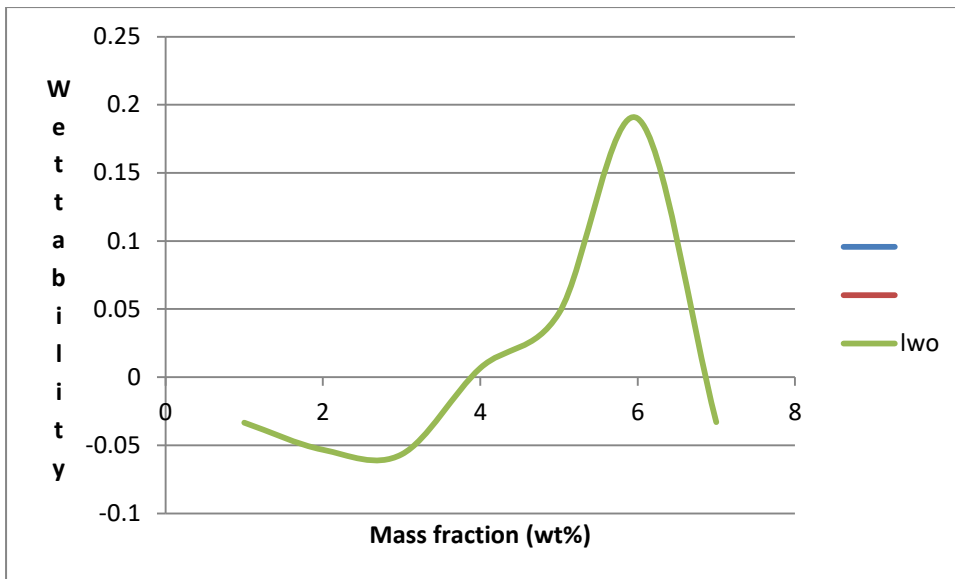


Figure 6-2 Measured water-wet of the various pure hybrid nanofluids during the cleanup process.

It can be seen from Figure6-2 , that the mineral oil contaminated soil sample (strong oil wet) after the cleanup with pure hybrid nanofluids was changed to more water- wet and slightly oil-wet state since all wettability index as shown in Figure6-2 are all positive , indicating the water wetness state of the soil sample after cleaning.It shows the perfect cleaning and wetting of the soil sample.In otherwords, the soil sample was restored its original water wet condition.Pure hybrid nanofluids are better than the pure monotype nanofluids in restoring the soil sample back to its original water wetness.

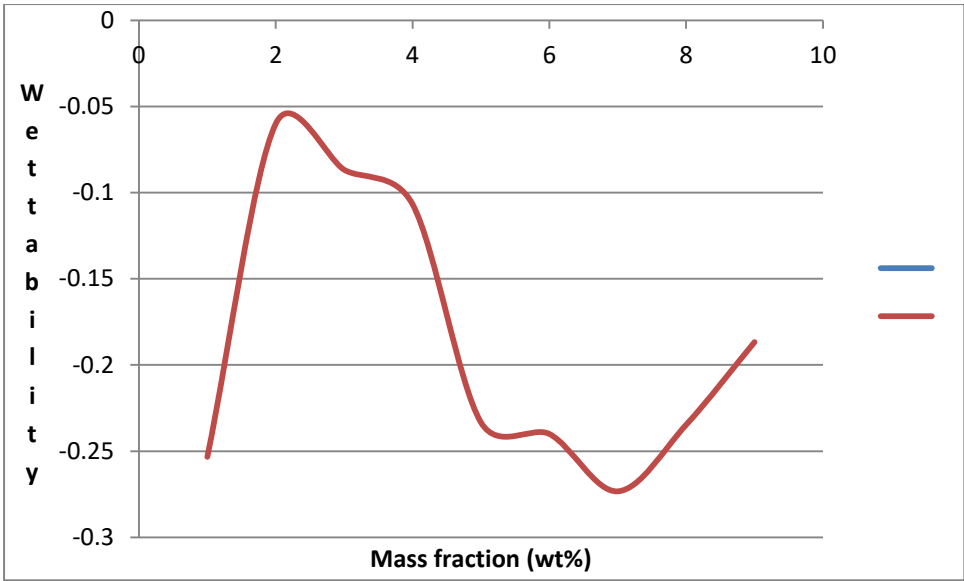


Figure 6-3 Measured oil-wet of the various surfacted monotype nanofluids during the cleanup process.

It can be observed in Figure 6-3 that the surfacted monotype nanofluids used to clean the mineral oil contaminated soil sample altered the strongly water wet state to strongly oil-wet state since all the wettability index are all negative describing the oil wet characteristics of the soil sample which is now, non-wettable.

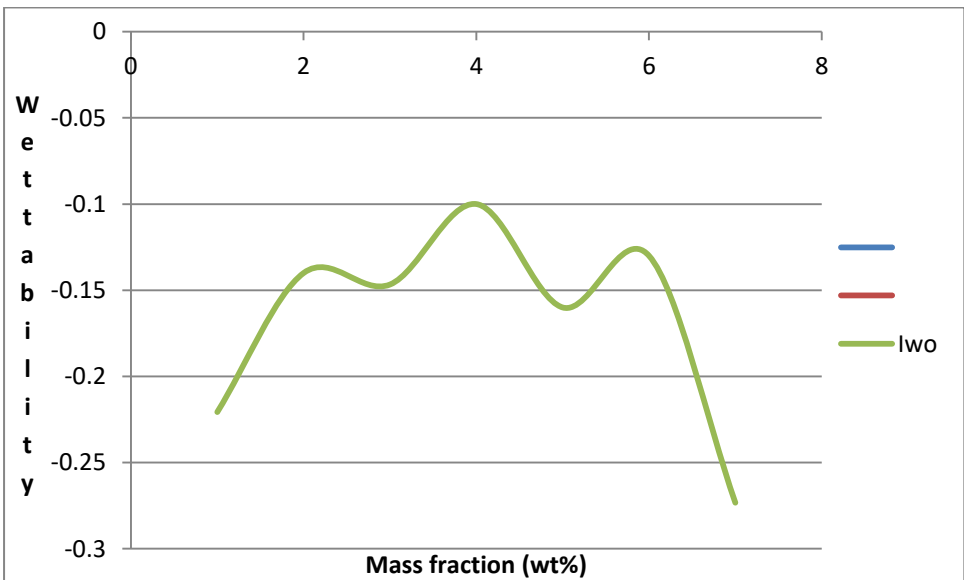


Figure 6-4 Measured oil-wet of the various surfacted hybrid nanofluids during the cleanup process.

It can be observed in Figure 6-4 that the surfacted nanofluids used to clean the mineral oil contaminated soil sample altered the strongly water wet state to strongly oil –wet state since all the wettability index are all negative describing the oil wet characteristics of the soil sample which is now , non wettable.

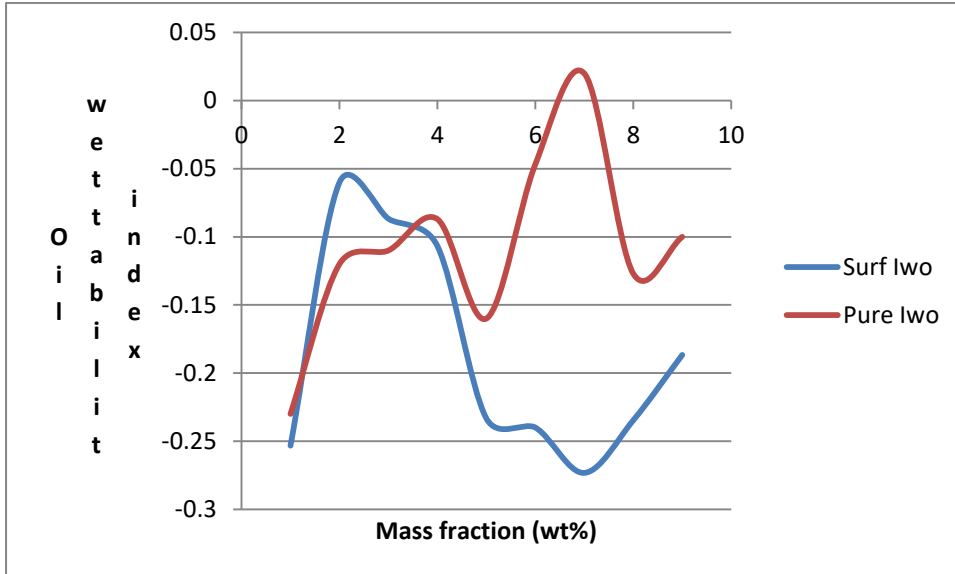


Figure 6-5 Comparison of lwo from pure and surfacted monotype nanofluids

Figure 6-5 indicates that pure nanofluids alter wettability to more oil – wet and slightly water wetness condition while surfacted nanofluids alter wettability to strongly oil-wet condition because of the presence of surfactants which improve/enhance higher oil recovery.

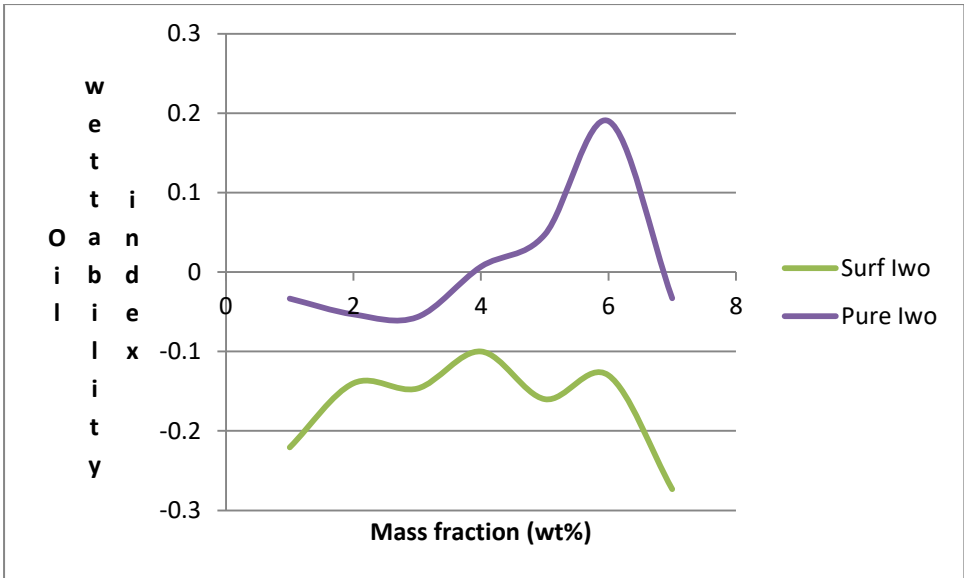


Figure 6-6 Comparison of lwo from pure and surfacted hybrid nanofluids

Figure 6-6 indicates that the wetting condition of soil sample cleaning with pure nanofluids is moderately water – wet and slightly oil – wet state while that cleaned with surfacted nanofluids showed strongly oil – wet condition. It means that soil sample cleaned with surfacted nanofluids is perfectly cleaned than that cleaned with pure nanofluids. More oil was recovered with surfacted nanofluids. More oil is retained in the soil sample cleaned with pure nanofluids than that cleaned with surfacted nanofluids. This can be comparable with the tga results analysis.

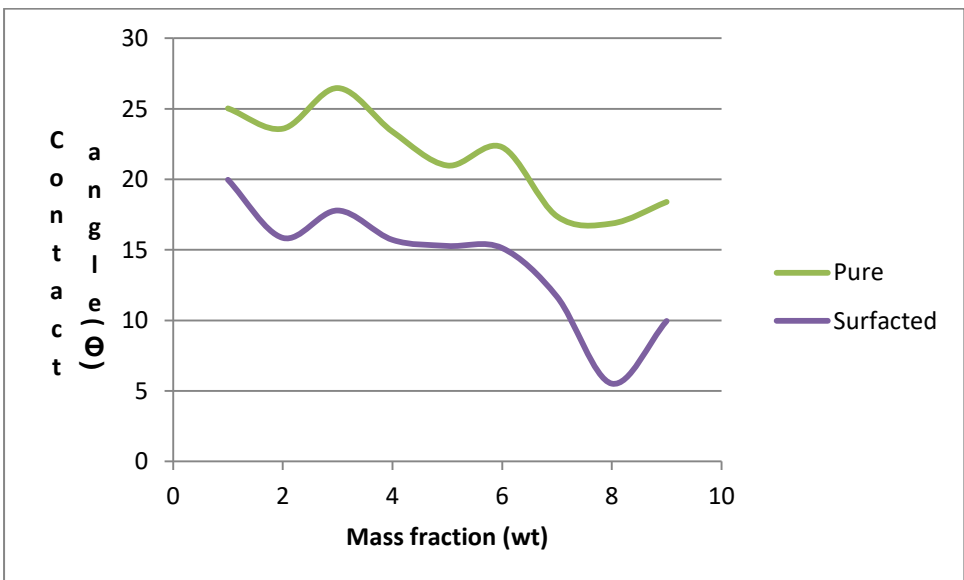


Figure 6-7 Measured contact angles of the different monotype nanofluids

Figure 6-7 shows the effect of surfactants on contact angle, just as surfactant decreases the surface tension of the different nanofluids; it does the same on the contact angle of the nanofluids as can be seen on Figures 6-7 & 6-8. The contact angle and surface tension (interfacial tension) was altered by the presence of surfactants in the nanofluids (hydrophilic nanoparticles in the deionised water). With the imaging method, it is difficult to get accurate measurements of the contact angle on strongly water-wet surfaces. Also, nanofluids with a high concentration of nanoparticles are less transparent than deionised water. This makes it difficult to focus on the droplet and the glass slide edge at the same time. Based on the experimental work performed it is concluded that mass fraction of both nanofluids (pure & hybrids) and surfactants have an effect on the surface tension and the wettability. It is also observed that the concentration of nanoparticles has an impact.

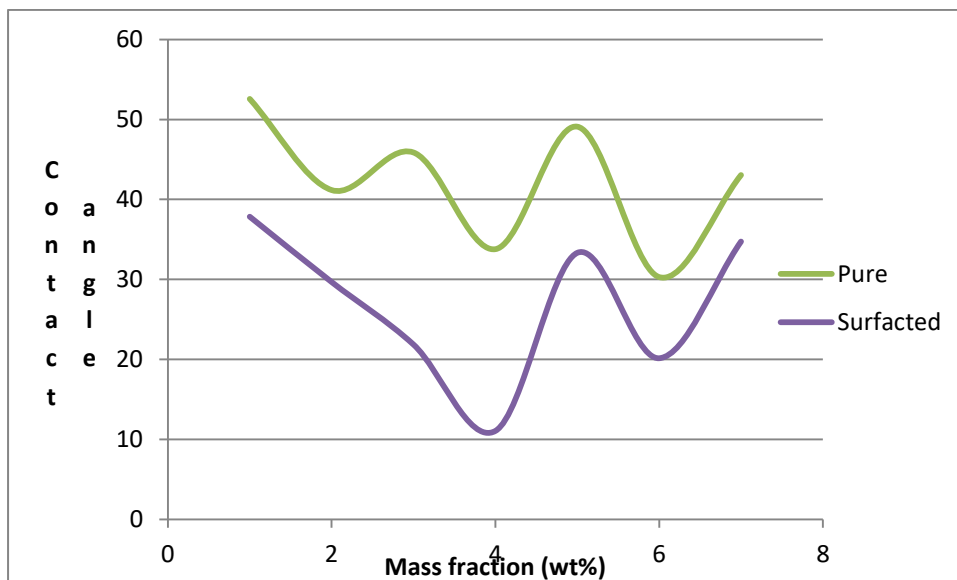


Figure 6-8 Measured contact angles of the different hybrid nanofluids

The contact angle gives information on the wettability of a surface. It indicates the relative wetting tendencies of the fluids in contact with the solid (soil) medium. From Fig 6-8, comparing the contact angle of pure and surfacted nanofluids, it can be seen that surfacted nanofluids have smaller contact angles than pure nanofluids. It shows that surfacted nanofluids wetted the soil more than the pure nanofluids. But all their contact angles are water-wetness. It also shows that the porosity is within 50% which is perfect wetting. When the porosity is above 50%, the wettability decreases, it becomes nonwettability state which indicates oil-wet condition. The soil becomes more of clay, so water breakthrough is restricted.

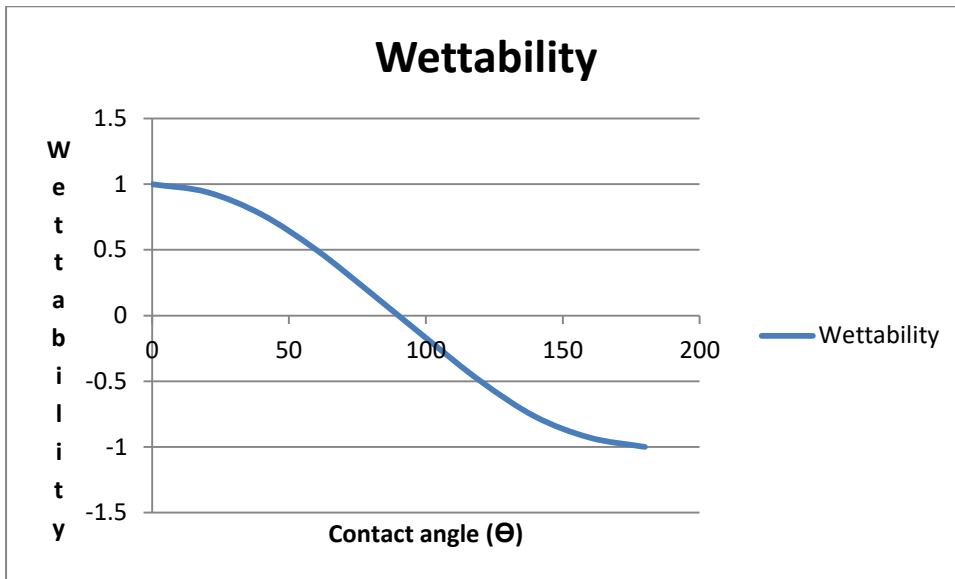


Figure 6-9 Measured wettability with contact angles of the best surfacted hybrid nanofluid

Fig. 6-9 shows that as contact angle increases the wettability decreases. Almost all the contact angle is less than  $90^\circ$  ( $0^\circ = 1$ , strongly water – wet, one intermediate ( $90^\circ = 0$ ), perfectly wetted condition and few strongly oil-wet ( $>90^\circ = -1$ ) conditions. A decrease in contact angle is an indication of a more water – wet condition. A contact angle average of  $28.05^\circ$  was measured for the deionised water.

#### 6.4 Effect of surfactants on contact angle

This is similar to that of effect of surfactants on stability of nanofluids. Surfactants help to breakdown large aggregates to smaller size therefore improving stability. Likewise, surfactants breakdown contact angle into smaller/lesser angles making it more water – wet and wetting state. Larger contact angles indicate strong oil – wet and nonwetting state. In Fig 6-9, wettability index of 0 to 1.0 has contact angle of 0 to  $80^\circ$  which is less than  $90^\circ$  indicating strongly water – wetness condition. Wettability index of below zero ie from -0.5 to -1. Indicates larger contact angle showing slightly to strongly oil – wet of nonwetting condition and clayey nature of the soil at this depth

Table 6-4 Calculation of wettability index & contact angle  $\theta$  for pure nanofluids & summary of wettability index compared with Amott –Harvey and USBM test.



Nanofluid system	I <sub>w</sub>	I <sub>o</sub>	I <sub>w</sub> - I <sub>o</sub>	Θ <sub>water</sub> (degree) Water – Wet	Θ <sub>oil</sub> (degree) Water – Wet	Θ <sub>wo</sub> (degree) Oil- Water
0.3Al <sub>2</sub> O <sub>3</sub>	0.6	0.84	-0.24	53.13	32.86	103.89
0.3TiO <sub>2</sub>	0.6	0.72	-0.12	53.13	43.95	96.89
0.3ZnO	0.66	0.78	-0.11	48.70	38.74	96.32
0.7Al <sub>2</sub> O <sub>3</sub>	0.61	0.70	-0.09	52.41	45.57	95.16
0.7TiO <sub>2</sub>	0.6	0.76	-0.16	53.13	40.54	99.21
0.7ZnO	0.59	0.64	-0.05	53.84	50.21	92.87
1.0Al <sub>2</sub> O <sub>3</sub>	0.76	0.74	0.02 = 0	40.54	42.27	90
1.0TiO <sub>2</sub>	0.71	0.84	-0.13	44.77	32.86	97.47
1.0ZnO	0.68	0.78	-0.1	47.16	38.74	95.74
0.3Al <sub>2</sub> O <sub>3</sub> +0.7TiO <sub>2</sub>	0.67	0.70	-0.033	47.93	45.57	91.89
0.7Al <sub>2</sub> O <sub>3</sub> +0.3TiO <sub>2</sub>	0.63	0.68	-0.053	50.95	47.16	93.04
0.3Al <sub>2</sub> O <sub>3</sub> +0.7ZnO	0.65	0.71	-0.057	49.46	44.77	93.27
0.7Al <sub>2</sub> O <sub>3</sub> +0.3ZnO	0.63	0.62	0.007 = 0	50.95	51.68	90
0.3TiO <sub>2</sub> +0.7ZnO	0.71	0.66	0.047	44.77	48.70	87.31
0.7TiO <sub>2</sub> +0.3ZnO	0.97	0.78	0.19	14.07	38.74	79.05
0.3Al <sub>2</sub> O <sub>3</sub> +0.3TiO <sub>2</sub> +0.3ZnO	0.71	0.74	-0.033	44.77	42.27	91.89

Note: The closer I<sub>ow</sub> is to -1, the more oil-wet the soil and the I<sub>w</sub> & I<sub>o</sub> values are closer to +1, the more water-wet the soil. The closer I<sub>w</sub> is to 1, the more water-wet the soil is. Similarly, the closer I<sub>o</sub> is to 1, the more oil-wet the soil is. The behaviour of oil for an oil-wet soil is the same as for water in a water-wet core soil sample described above. It can be observed from Table 6-5 that the wettability of pure nanofluids are intermediate and slightly oil-wet. The soil pore surfaces are all well /perfectly wetted with oil, more water is drained. Almost all the contaminated soil samples cleaned with the different pure nanofluids are altered neutral to slightly oil-wet and water wet. As can be observed from Table 6-5 that pure 1.0% Al<sub>2</sub>O<sub>3</sub>/water (I<sub>wo</sub> = 0.02 = 0) and its hybrid, 0.7Al<sub>2</sub>O<sub>3</sub>+0.3ZnO/water (I<sub>wo</sub> = 0.007 = 0) indicating perfectly wetted condition. The pure nanofluids indicate slightly oil-wet to strongly oil –

wet state. The receding and advancing contact angles for pure nanofluids are 14.07 & 103.89, respectively. The contact angle hysteresis for pure nanofluids is  $(103.89 - 14.07) = 89.82^\circ$ . The receding and advancing contact angles for surfacted nanofluids are 6.28 & 105.66, respectively. The contact angle hysteresis for surfacted nanofluids is  $(6.28 - 105.66) = 99.38^\circ$ .

Table 6-5 Calculation of wettability index & contact angle  $\theta$  for surfacted nanofluids & summary of wettability index compared with Amott –Harvey and USBM test.

Nanofluid system	I <sub>w</sub>	I <sub>o</sub>	I <sub>w</sub> o = I <sub>w</sub> - I <sub>o</sub>	$\Theta$ water (degree) Water – Wet	$\Theta$ oil (degree) Water – Wet	$\Theta$ wo (degree) Oil -Wet
0.3Al <sub>2</sub> O <sub>3</sub>	0.57	0.82	-0.25	55.25	34.92	104.45
0.3TiO <sub>2</sub>	0.56	0.62	-0.06	55.94	51.68	93.44
0.3ZnO	0.65	0.74	-0.087	49.46	42.27	94.56
0.7Al <sub>2</sub> O <sub>3</sub>	0.65	0.76	-0.107	49.46	40.54	96.14
0.7TiO <sub>2</sub>	0.65	0.88	-0.23	49.46	28.36	103.30
0.7ZnO	0.74	0.98	-0.24	42.27	11.48	103.89
1.0Al <sub>2</sub> O <sub>3</sub>	0.57	0.84	-0.27	55.25	32.86	105.66
1.0TiO <sub>2</sub>	0.76	0.994	-0.23	40.54	6.28	103.30
1.0ZnO	0.71	0.90	-0.19	44.77	25.84	100.95
0.3Al <sub>2</sub> O <sub>3</sub> +0.7TiO <sub>2</sub>	0.65	0.874	-0.22	49.46	29.07	102.71
0.7Al <sub>2</sub> O <sub>3</sub> +0.3TiO <sub>2</sub>	0.66	0.80	-0.14	48.70	36.87	98.05
0.3Al <sub>2</sub> O <sub>3</sub> +0.7ZnO	0.65	0.80	-0.15	49.46	36.87	98.63
0.7Al <sub>2</sub> O <sub>3</sub> +0.3ZnO	0.66	0.76	-0.1	48.70	40.54	95.74
0.3TiO <sub>2</sub> +0.7ZnO	0.56	0.72	-0.16	55.94	43.95	99.21
0.7TiO <sub>2</sub> +0.3ZnO	0.65	0.78	-0.13	49.46	38.74	97.47
0.3Al <sub>2</sub> O <sub>3</sub> +0.3TiO <sub>2</sub> +0.3ZnO	0.65	0.92	-0.27	49.46	23.07	105.66

Note: Since I<sub>w</sub> & I<sub>o</sub> values are less than 1.0, then the values are all water –wet and all the contact angles are less than 90°C. Where, *w* and *o* is for water and a perfectly wetting liquid, mineral oil, respectively. In other words, the wetting angle of

water in the investigated soil is determined from two experiments where water sorptivity and mineral sorptivity are measured. It is assumed here that mineral oil, as a polar low-surface-tension liquid, perfectly wets the soil, e.g.  $\theta_{oil} = 0^\circ$ . Surface tension of mineral oil is 28.21N/m. The experimental wet soil sample is described as strongly water-wet. Spontaneous imbibition of water into the strongly oil-wet soil samples cleaned with pure and surfacted nanofluids was in the range of 82 - 84%. The water imbibed rapidly, and approximately 84% of the spontaneous imbibition was completed within an hour. No water could be forced into samples after spontaneous imbibition. It is concluded that soil can be altered towards a homogeneous neutral to slightly oil-wet state using crude oil added with 0.3, 0.7 and 1.0 weight% nanoparticles dispersed in deionised water as well as addition of surfactants.

Tables 6-5 & 6-6 illustrate how nanofluid(s) is situated on the interface dependent on their wettability. As discussed in Literature Review, Section 2.3.1, a contact angle of 90 degree is considered intermediate wet and the nano fluid(s) will then ideally have 50 % surface area covered with oil and 50 % with water. A contact angle of less than 90 degrees is water-wet and a larger fraction of the surface area of the nanofluid(s) is then covered with water than oil. A contact angle of more than 90 degrees is oil-wet, and a smaller fraction of the surface area of the nanofluid(s) is then covered with water than oil. Recall that the contact angle is determined by the densest liquid phase. It is observed that the contact angle is the function of porosity. Since all the soil pore spaces were filled up during the oil –soil contamination and cleanup process, the porosity is from 40 – 50% which is wettable condition, the wettability index is 1 (strongly water -wet), therefore the contact angles are less than  $90^\circ$  ( $\Theta < 90^\circ$ ), this is why all the core soil samples were fully saturated with water and oil. Porosity, above 50%, the wettability index is -1 (strongly oil-wet) and non wettable condition with all the contact angles greater than  $90^\circ$  ( $\Theta > 90^\circ$ ).

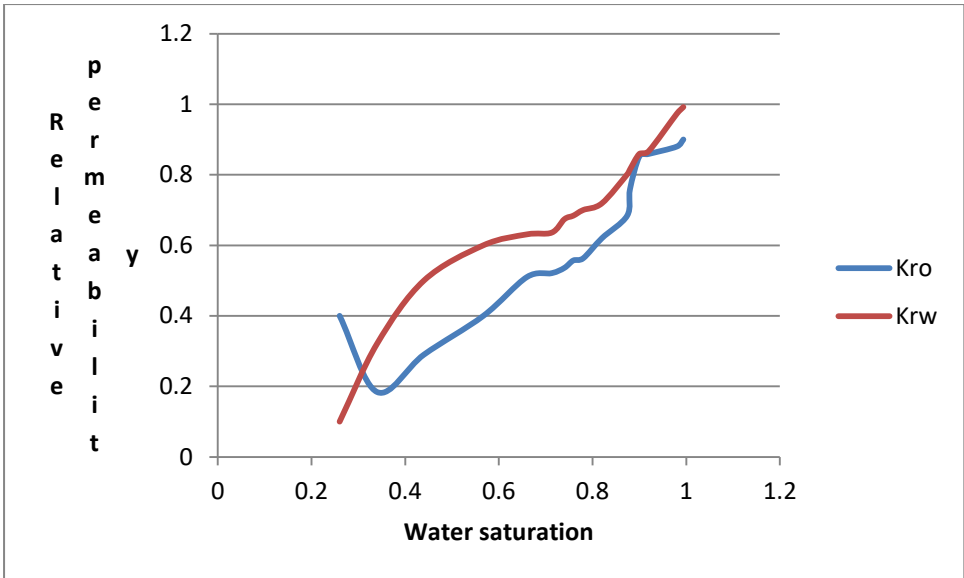


Figure 6-10 Effect of wettability on relative permeability of surfacted nanofluids based on Brook – Corey

Figure 6-10 indicates that the relative permeability of water and oil are equal at water saturation of 0.42 (42% water, 54% oil) which is water-wet as the saturation increases, they cross each other again at 84% water, 74% oil. Further interpretations are as follows based on the rule of Thumb shown on Table 6.2b. The resulting relative permeability shows that the initial water saturation ( $S_{wi} = 34\% > 25\%$ ,  $K_{rw} = 26\% < 30\%$  and  $S_{w_{c-o}} = 88\% > 50\%$  indicate water – wet nature. However,  $K_{ro}$  of 32.1% < 70% indicates oil – wet characteristics.

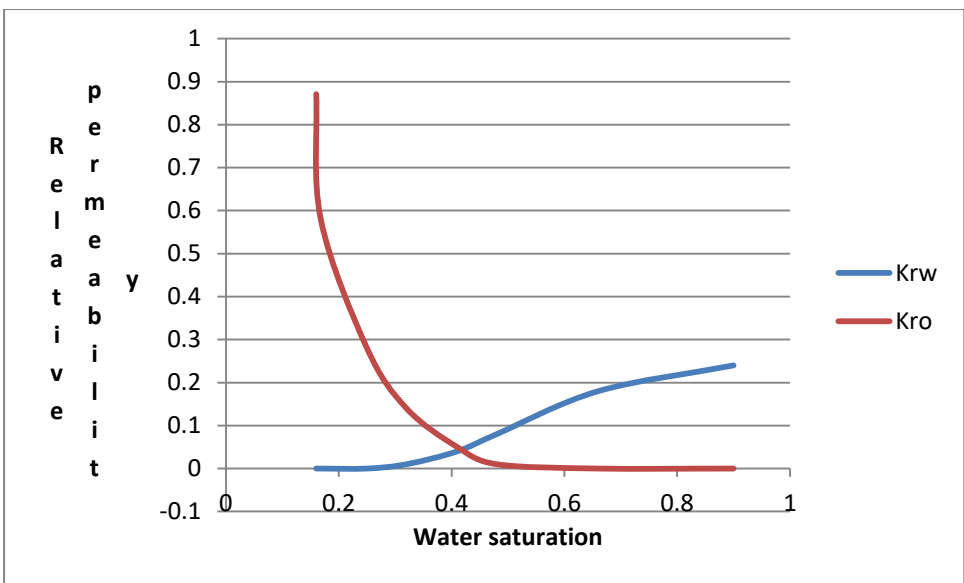


Figure 6-11 Effect of wettability on relative permeability curves for surfacted nanofluids (oil – wet formation) based on modified Brook-Corey method [170].

Figure6-11 shows a clear cross over of oil – wet ness based on modified Brook –Corey equation.The interpretations are as follows based on the rule of Thumb shown on Table 6.2b. The resulting relative permeability shows that the initial water saturation ( $S_{wi} = 16.8\% > 25\%$ ,  $K_{rw} = 24\% < 30\%$  and  $S_{w_{c-o}} =$  at 40%. However,  $K_{ro}$  of 41% < 70% indicates oil – wet characteristics.

These curves are believed to be accurate because of good agreement between results obtained from the earlier Figure6-10.and the new method (recalculated graphs) Figure6-11/Table 6-8.

Table 6-6 Relative permeability of the best surfacted nanofluid (Recalculated values from the former graph (Fig6-11) for surfacted nanofluids)

Sw	Krw	Kro
0.16	0	0.871
0.168	0	0.58
0.25	0	0.28
0.32	0.01	0.14
0.41	0.04	0.05
0.48	0.08	0.01
0.66	0.18	0
0.9	0.24	0
0.99	0	0

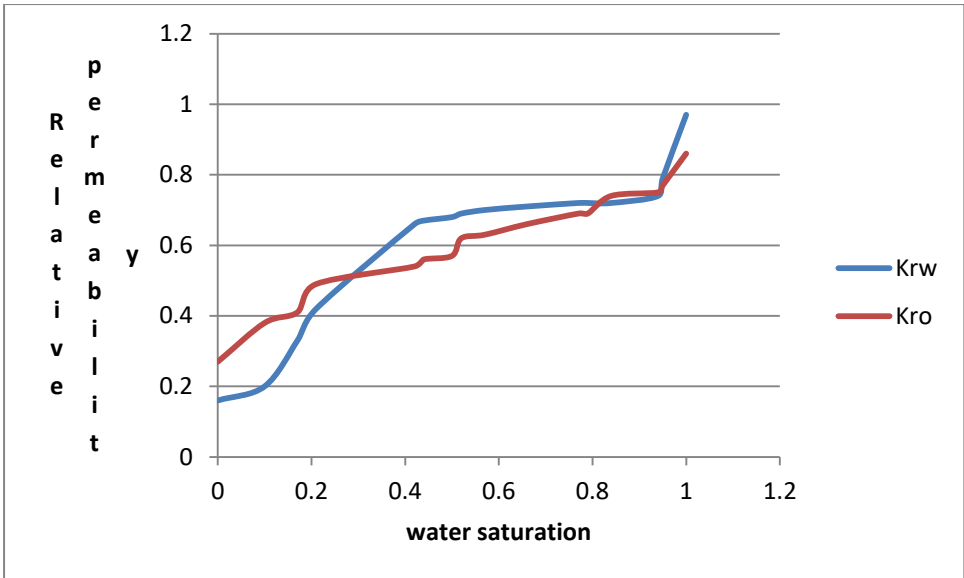


Figure 6-12 Effect of wettability on relative permeability of pure nanofluids based on Brook – Corey equation

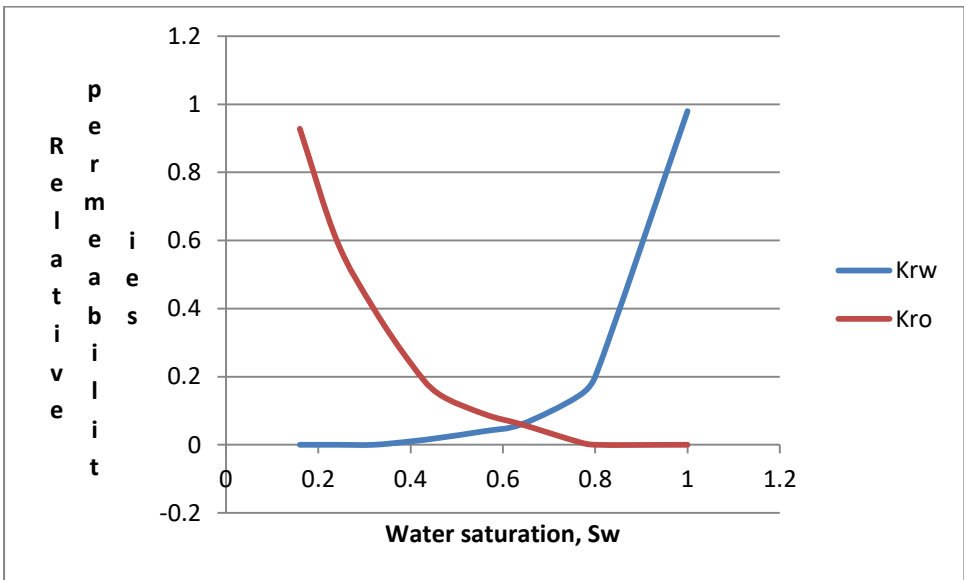


Figure 6-13 Effect of wettability on relative permeability of pure nanofluids (Strongly water – wet soil) based on modified Brook – Corey (Caig’s rules of thumb, Table 6.2b, [170]).

These curves are believed to be accurate because of good agreement between results obtained from the Figure 6-12 and the new method (recalculated graphs).

In Fig 6.13, water and oil relative permeability are equal at  $K_{rw} = 64\%$  and  $K_{ro}$  at  $60\%$  ( $S_{w_c} = 0.6$ ).

## 6.5 General discussion on relative permeability:

Soil saturation is governed by fluid densities, wettability, surface tension, pore size (porosity) and geometry. Generally, irreducible water saturation increases as the pore size decreases, which is not a simple linear function. Water becomes movable or is displaced in the soil when water saturation is higher than water retain in the soil known as irreducible water saturation. The movable water is the difference between water saturation and irreducible water saturation timing pore volume. However, the increase in water saturation is higher than the irreducible water saturation, which causes the water to be movable/displaced.

### 6.5.1 Effect of surfactants on wettability

Surfactants are used primarily to lower oil-water interfacial tension (IFT) and thus improve production. However, surfactants possess the ability to alter soil wettability and hence increase oil cleaning /recovery/production.

The use of Sdbs surfactant at different concentrations with crude oil in corefloods experiments showed significantly higher oil recoveries indicating that the surfactant has altered wettability. The optimum surfactant concentration has been established at 0.1% and 0.5% for SDBS and  $\text{Na}_2\text{HPO}_4$ , respectively. Other experiments conducted using  $\text{Na}_2\text{HPO}_4$  surfactant has also shown a favorable wettability alteration as soil sample core cleaned with  $\text{Na}_2\text{HPO}_4$  surfacted nanofluid s was altered from strongly water-wet to strongly oil wet consequently higher oil recoveries. Surfactants can be used to alter soil wettability from oil-wet to water-wet hence increase Spontaneous water imbibition and improve recovery [86b].

Increase in surface tension is measures of surfactant instability. They concluded that oil recovery can be improved with low concentration of surfactant for both spontaneous and forced imbibition of water and that reduction in soil surface adsorption is achievable by reducing surfactant concentration. It is observed that the core's wettability was moderately altered to water-wet at ambient/room temperatures. [108b] demonstrated that an increase in temperature in soil always resulted in increased water wetness, which improves spontaneous imbibition of water and hence increased oil recovery. The wettability of the soil is altered from oil-wet to water-wet to improve the displacement of oil by nanofluids (spontaneous imbibitions) and hence higher oil recovery [138].

## 6.6 Effect of Wettability on relative permeability.

In an oil contaminated soil sample (strongly oil - wet) as shown by relative permeability and USBM wettability measurements. Craig's rules of thumb (Table 6-4) show that the contaminated soil shown in Fig 4-1 is strongly oil – wet. The cross over point for the oil and water relative permeabilities occurs at a water saturation of 44.0%, while the water relative permeability at floodout is about 88%. In general, the cleaned soil samples were strongly water – wet.

Some soil samples were cleaned only to neutral (contact angles =  $90^\circ$  or approximately =  $90^\circ$ ) wettability, possibly because of the presence of surfactants or because both the pure and surfactant nanofluids were stabilized before the cleanup process as can be seen on Tables 6-5 and 6.6, which is naturally neutrally wet. Finally, the restored – state soil samples were neutrally wet, with relative permeability characteristics intermediate between measurements in the contaminated, strongly oil – wet state and the cleaned, strongly water – wet state.

At any saturation, the relative oil permeabilities were lower and the relative water permeabilities were higher for restored – state soil sample when compared with the more water – wet cleaned soil sample. Relative permeabilities were determined on the cleaned soil sample using surfactant nanofluids and mineral oil. Based on Craig's rules of thumb for wettability (Table 6-4), the cleaned soil sample is significantly more water – wet than the native –state one. This is confirmed by contact – angle measurements. The water contact angles  $\Theta$  were less than  $90^\circ$  and  $>90^\circ$  for oil – wet (Tables 6-5 & 6-6 as contained in Appendix I. 2) [114], [148] and [173]. By evaluating the contact angle and surface tension, it was found that wettability alteration plays a more dominant role in the oil displacement mechanism through nano-EOR. These results reveal a potential way to use  $\text{Al}_2\text{O}_3$ ,  $\text{ZnO}$  and  $\text{TiO}_2$ -based nanofluids for enhanced oil recovery purposes for a wide range of soil reservoir wettabilities at a given soil temperature.

In summary, soil sample was oilflooded followed by water nanofluid flooding, the water /oil relative permeability ratio increased for given water determined. Imbibition tests showed that the cleaned soil sample was more water – wet than the native- state sample because it imbibed water more rapidly. When oil is the wetting fluid, that soil sample is treated as oil-wet. In both cases, the non wetting fluid (eg nanofluid) displaces the wetting fluid (drainage) during the experiment.



Unsteady – state relative permeability will appear more oil –wet when measurements are made on strongly water – wet systems initially 100% saturated with oil [98, 96).

According to [123], which is similar to my own findings, water-nanofluid flooded water – wet sandpacks initially saturated with refined mineral oil and obtained significant amounts of simultaneous oil and water production after breakthrough. Generally, there is little or no production after water breakthrough in a strongly water – wet soil sample with a low oil/water viscosity ratio, so this soil sample behaved as if it were somewhat oil- wet [39], [139],[128],[49] and [96].

## CHAPTER 7.0

### 7.0: GENERAL DISCUSSION &SUMMARY

The thermal conductivity, viscosity, and surface tension of the various water-based nanofluids were measured. It is found the thermal conductivity increases significantly with the decrease in nanoparticle volume fraction. This is contrary to existing classical models which reported that thermal conductivity increases with increase in mass fraction. Models are for large aggregates (cluster) or large diameter greater than 100nm. With an increase of temperature, the thermal conductivity increases for a certain volume concentration of nanofluids, but the viscosity decreases. The size of nanoparticle also influences the thermal conductivity of nanofluids. It is indicated that existing classical models cannot explain the observed enhanced thermal conductivity

in the nanofluids. Similarly, the viscosity increases as the concentration increases at room temperature. At the volume concentrations of 5%, the viscosity has an increment of 60%. The effect of particle sizes on the viscosity is limited. The addition of surfactant is believed to be the reason behind the decrease in surface tension in comparison with the base fluid.

Surface tension measurements of nanofluids

Figure 5-18 shows the surface tension as a function of the volume concentration. The results demonstrate that the surface tensions of the different water-based nanofluids are significantly

lower than those of the base fluid, pure water. However, as the volume concentration increases, the surface tension remains almost unchanged in the  $Al_2O_3$  nanofluids. Hence we can deduce that particle volume concentration does not have a major effect on the surface tension of the nanofluids. The experimental results of [66] and [90] have shown that the surface tension of all the nanofluids without surfactant is independent on concentration and has the close values as that of pure water. The addition of a small amount of surfactant into the liquid reduced the surface tension [28], [30].

### 7.1 Effect of particle size on viscosity

From Fig.5-27, our experimental results show that as the particle sizes increase, the effective viscosity decreases significantly and reaches an almost constant value at the end. This trend is similar to the results of other researchers shown in Fig.5-29 except for particle size greater than 100 nm. [165] suggested the big particle size can form larger aggregates.

7.2 Effect of volume concentrations on viscosity. The nanofluids exhibit a Newtonian behavior. Figure 5-26 shows that the effective viscosity ratio increases as the volume concentrations increase [106] and [124].

### 7.3 Effect of temperature on viscosity

The viscosities were measured for the nanofluids as a function of temperature. The viscosity under the particle volume fraction ranging at 0.3%, 0.7%, and 1.0% from 20 to 70 °C is shown in Fig.5-28, the nanofluid viscosity decreases with an increase in temperature. The increasing temperature would weaken the inter-particle and inter-molecular adhesion forces. For all the nanofluids measured, the temperature gradient of viscosity is generally steeper at the temperature from 20 to 40 °C. Such the viscosity gradient is particularly more pronounced as the particle volume concentration increases. With an increase of temperature, the measured viscosity data have shown a gentle decrease with an increase of temperature. n

our experiments, we have attempted to measure viscosity at the temperature higher than 55 °C, but a critical temperature has been observed, above the temperature of 50°C (specifically at 70°C), an ‘erratic’ increase of nanofluid viscosity was observed. The phenomenon may be resulted from the fast evaporation of nanofluids in the related small volume at a relative high temperature. Another possibility is that beyond the critical temperature, the surfactant might be broken down and accordingly the performance was considerably reduced or even destroyed, affecting the suspension capabilities. Thus, the particles have a tendency to form aggregation, resulting in the observed unpredictable increase of the nanofluid viscosity. As known, the water

viscosity decreases with an increase of temperature. The viscosity values of the different concentration nanofluids measured from 20 to 70 °C are compared with a reference of the viscosity of water at these temperatures. This observations can be substantiated by [124] and [106].

#### 7.4 General discussion on wettability.

A review of the literature shows that the wettability is a very complex parameter which is dependent on many variables in the reservoir (soil). These include properties of the soil and properties of the oil, nanofluids, surfactants and the soil conditions, suggesting that the wettability is a result of the equilibrium between the forces acting on the solid and the fluids ( adhesive and cohesive) present in the system. Wettability affects the fluid saturation distribution in the soil. Different wettability characteristics of a reservoir soil leads to different oil displacement mechanisms on a pore-scale level. The wettability also affects the residual oil (ie oil retained in the soil after cleaning) saturations. The experimental results/ current view is that wettabilities close to neutral gives the lowest residual oil and therefore the highest recovery. Hence, the knowledge of the wettability state of a given reservoir (soil) and how it can be altered to lower the residual oil is crucial in enhanced oil recovery projects. Because of its complexity, the wettability is still a variable that is not fully understood, and research is continuously ongoing.

## CHAPTER 8.0

### 8.0 CONCLUSIONS AND RECOMMENDATION/Future work

#### 8.1 conclusions

The strange behaviour of nanofluids as reported in the literature (Xiang et. al., 2008) which was observed between the three monotypes - nanofluids used in the experiments during the plotting of cleaning efficiency. Al<sub>2</sub>O<sub>3</sub> and ZnO nanofluids showed their strange behaviour at the concentration of 0.7vol%. At this concentration the cleaning efficiency of these two nanofluids are lower than that of 0.3vol% nanofluid. At 0.7wt% nanoparticles dispersed in deionised water, the cleaning efficiency decreased but increased at both 0.3 and 1.0 vol%. This is because the surface area of the Al<sub>2</sub>O<sub>3</sub> and ZnO nanofluids decreased with increased in concentration of nanoparticles dispersed in deionised water (ie increased in volume fraction of Al<sub>2</sub>O<sub>3</sub> and ZnO nanofluids). ZnO and TiO<sub>2</sub> nanofluid behaved strangely at concentration of 0.3 volume fraction. This is because the two monotype water nanofluids are antibacterial

nanofluids. ZnO nanofluid is also anticorrosive agent. In case of TiO<sub>2</sub>, the cleaning efficiency increased with increased surface area of TiO<sub>2</sub> as well as concentration of nanoparticles dispersed in deionised water. The three monotypes - nanofluids behaviour strangely at the concentration of 0.7vol% as shown on the Fig. above. From the cleaning efficiency without surfactants, TiO<sub>2</sub> nanofluid is the best.

The three monotype nanofluids behaviour strangely at the 0.7vol% concentration with each other, but their hybrids of 0.3Al<sub>2</sub>O<sub>3</sub> + 0.3TiO<sub>2</sub> + 0.3ZnO vol% agreed together at this 0.7vol% concentration with cleaning efficiency of 74% the same as that of Al<sub>2</sub>O<sub>3</sub> nanofluid. Nanofluid being a smart fluid, the three experimental nanofluids behaved strangely to each other. Al<sub>2</sub>O<sub>3</sub> nanofluid is a ceramic and bacterial nanofluid. Al<sub>2</sub>O<sub>3</sub> nanofluid is recommended for cleaning oil refineries and oil spillage (in the literature) but TiO<sub>2</sub> and ZnO nanofluids are better than Al<sub>2</sub>O<sub>3</sub> nanofluid in cleaning crude oil polluted soils. They outsmarted Al<sub>2</sub>O<sub>3</sub> nanofluid even the same with their hybrids. TiO<sub>2</sub> and ZnO nanofluids are both antibacterial nanofluids, ZnO nanofluid is also anticorrosive nanofluid. TiO<sub>2</sub> is used as coolant in engines. Investigation on the stability is a key issue that influences the properties of nanofluids for applications. Zetapotential, pH, and absorbancy are used to evaluate the stability of the different nanofluids. Although, addition of surfactants leads to enhancement of thermophysical properties of the nanofluids but the improvement is still well comparable to the expected value. These observations suggest that the efficiency of property improvement depends on the particle size, concentration of nanoparticles, type of surfactants as wetting agent, preparation technique/sonication procedure. The excellent thermal conductivity of the surfacted nanofluids significantly improve the thermal transport and optical properties/strength of the different nanofluids which lead to their usage as cleaning agent for crude oil.

The biggest challenge in realizing the full potential of nanofluids is to achieve homogeneous dispersion (stability) of nanofluids so that maximum total surface area will be available for efficient recovery of oil. This can be seen in the plot of total surface area and cleaning efficiency with surfacted nanofluids Fig 5-39. Although, hybrid nanofluids (new technique/improved method of preparing nanofluid) produce high cleaning efficiency but monotype nanofluids are much simpler and provide option for large scale production. Further comparison of monotype and hybrid nanofluids was based on their wettability study which showed that the pure hybrids nanofluids cleaned the contaminated soil better than the pure monotype nanofluids on comparing their relative permeabilities. Improvement in both monotype and hybrid nanofluids

enhances their properties and processing conditions. So finally we can conclude that nanofluid is an ideal agent /solution for cleaning crude oil polluted soils/sites.

Based on the work performed in this study, the following overall conclusions can be presented: When the  $\text{Al}_2\text{O}_3$  /water,  $\text{TiO}_2$  /water and  $\text{ZnO}$  /water as well as their hybrid –water nanofluids were synthesized by two-steps method, the observed particle size analysis showed better scattering. It can be concluded that since the particle size distribution of  $\text{Al}_2\text{O}_3$  /water are less than 100nm. It shows that the  $\text{Al}_2\text{O}_3$  nanoparticles /powder used for the study is gamma alumina (<100nm) not Alpha alumina which is greater than 100nm (>100nm). To select appropriate conditions for scattering nanoparticles, absorbency and zeta potential are essential basis. In addition, there is an excellent relationship between absorbency and zeta potential. The efficacy of pH on the stability of the  $\text{Al}_2\text{O}_3$ ,  $\text{TiO}_2$  and  $\text{ZnO}$  nano-suspension was investigated. At pH values of <4, are excellent dispersion of  $\text{Al}_2\text{O}_3$  and  $\text{TiO}_2$  /nanoparticles, while pH values >8 are excellent dispersion of  $\text{ZnO}$  nanoparticles were obtained. The smaller the particle size concentration, the higher the catalytic activities of the nanofluids. Most of the activities occurred at compatible medium. In other words, stable suspension of water nanofluids is achieved in physiological compatible medium.

The stability comportment of the 0.3 – 1.0%wt  $\text{Al}_2\text{O}_3$ ,  $\text{TiO}_2$  and  $\text{ZnO}$  as well as their hybrids nano-suspensions with SDBS and  $\text{Na}_2\text{HPO}_4$  surfactants and particle size concentrations was investigated at different pH values by making use of zeta potential, absorbency techniques. The optimum process variables for tga soil analysis after cleaning with the different nanofluids are: During the tga analysis, water evaporates by 15mins or less depending on the amount of water retained in the soil after cleaning the contaminated soil with nanofluid at 100°C. The oil burnt off at the solubility temperature (338°C) of the mineral oil. In summary, the optimum process variables to restore the contaminated soil after cleaning with nanofluids during tga analysis are 40mins, 400°C and 150 bars.

In this work also, we present results of  $\text{Al}_2\text{O}_3$ ,  $\text{TiO}_2$  and  $\text{ZnO}$  - Nanofluids' impact on enhanced oil recovery during soil sample /core flood experiments on oil-wet soil contaminated samples.

Based on the results obtained the following conclusions can be drawn:

1.  $\text{Al}_2\text{O}_3$ ,  $\text{TiO}_2$ , and  $\text{ZnO}$  nanofluids are wettability modifiers for soil porous medium systems, and they can change the wettability of soils from strongly oil-wet to strongly water-wet condition.

2. Wettability change by adsorption of Nanoparticles on the soil surface is a fast process, requiring a period of at least 1 hr.
3. Use of these Nanofluids in flooding tests revealed the strong capability of these new agents for oil recovery from crude oil soil reservoirs. The mechanism of oil recovery by the selected Nanofluids during Nanofluid flooding and after aging of Nanofluid/crude oil attributed to wettability alteration.
4. The originally strongly water-wet cores are altered to be intermediate-wet or oil-wet by the surfactants, depending on the type and their concentrations.
5. The wettability indices (either water index, oil index, or combined index) correlate well with the traditional Amott–Harvey indices, suggesting that quantitative information about soil wettability can be gained from surface tension measurements.(4) After surfacted nanofluids imbibition, residual oil saturation decreases from water-wet to intermediate-wet region, while it increases from the intermediate wet to oil-wet region.

Based on the experimental work performed it is concluded that surfactants have an effect on the surface tension, contact angle and the wettability. It is also observed that the concentration has an impact. Though, a deviation in the expected behavior when comparing the results was observed.

Relative permeabilities are a function of wettability, pore geometry, fluid distribution, saturation and saturation history. Wettability affects relative permeability by controlling the flow and spatial distribution of fluids in a soil medium. In a uniformly wetted soil sample, the effective oil permeability at a given initial water saturation decreases as the wettability is varied from water – wet to oil – wet. In addition, the water relative permeability decreases as the soil sample becomes more oil – wet.

In fractionally wetted soil samples, where the size of the individual water and oil – wet surfaces are on the order of a single pore, relative permeabilities appear to be similar to those in uniformly wetted systems. The water relative permeability increases and the oil relative permeability decreases as the fraction oil – wetted surfaces increases. Increasing the sulphate concentration which has a catalytic effect on the wettability alteration, improved both the imbibition rate and ultimate recovery.

Finally, In a nutshell, nanofluid is all about nanoparticle diameter of less 100 nm dispersed in water, the fewer diameters are from 100nm, the more stability it is. So also is the contact angle

of wettability,  $<90^\circ$ . The smaller the contact angle, the more/strongly water -wet condition (ie wetting state) and porosity from 40 - 50% for efficient oil recovery/cleaning. Larger contact angle indicates non-wet table condition and strongly oil - wet state, porosity of above 50% describing the clayey nature of the soil in that soil depth. Therefore, nanofluid can be propagated through a porous soil medium (wettability). Pure nanofluid enhances oil recovery but surf acted nanofluid super enhances oil recovery.

The experiments were an extensive test of nanofluid as an oil spill cleaner. Thus it is confirmed that nanofluid is an effective solvent for spilled oil and that greater volumes of nanofluid relative to the amount of oil spilled lead to a greater cleaning effectiveness. Based on the performance in laboratory settings, nanofluid should be considered a potential oil spill remediation agent but the results obtained in the laboratory settings do not always translate to the field, hence, nanofluid needs to be trialled on a full-scale in a marine and land settings.

## 8.2: Future Work / Recommendations

One of the strongest recommendations that can be made regarding subsequent research into the efficacy of nanofluid as an oil spill cleaning agent is that studies need to move out of laboratory into the field. Laboratory studies in controlled conditions limit confounding factors but also fail to indicate how real world performance might be affected by which confounding conditions. Of key concern to developing a practical field work trial are the following:

Determine realistic application rates,

Develop, optimise and evaluate field work protocol,

Develop field work protocol into oil spill response protocol,

Effects of nanofluid application on a large and over the long term.

Enhancement of oil cleaning efficiency of  $\text{Al}_2\text{O}_3$ /water nanofluids using *Staphylococcus Aureus* /*E. Coli* bacteria surfactants, since Aluminum Oxide is a bacterial nanoparticle. The *Staphylococcus Aureus* bacterial will help to eat up the crude oil thereby improving the cleaning efficiency. Investigation on the Inhibitory effect of *E. coli* on cleaning crude oil contaminated soils using  $\text{ZnO}$  /water and  $\text{TiO}_2$  /water as well, knowing that both are antibacterial nanoparticles  $\text{ZnO}$  /water is anticorrosive nanofluid also. More experimental work is needed on crude oil contamination and cleanup process.

## References

- [1]Abareshi, M.Goharshadi, E.K.Zebarjad, S.M.Khandan Fadafan, H. Youssefi, A (2010): Journal of Magnetism and Magnetic Materials 322 (2010) 3895.
- [2]Abareshi, M.Sajjadi, S.H.Zebarjad, S.M.Goharshadi, E.K.(2011): Journal.Molecular.Liquids.163 (2011) 27.
- [3]Adekunle, I.M, Arowolo, T.A, Ndahi, N.P, Bello, B and Owolabi (2007): Chemical characteristics of humic acids in relation to lead, copper and cadmium levels in contaminated soils of South West, Nigeria.Annals Environmental Science 1: 23 – 34.
- [4]Aditya, S.(2008): Benzopyrene degradation by *Sphingomonas yanoikuyae* JAR02.Environmental Pollution.151, pp. 669677.
- [5]Agarry, S.E, Owabor C.N.and Yusuf, R.O.(2011): Bioremediation of Soil Artificially Contaminated with Petroleum Hydrocarbon Oil Mixtures; Evaluation of the use of Animal Manure and Chemical Fertilizer.Bioremediation Journal, Volume 14.Page 189 – 195.
- [6]Agbalaka, C., Dandekar, A.Y., Patil, S.L.et al.2008.The Effect of Wettability on Oil Recovery: A Review.Paper 114496 presented at the SPE Asia Pacific Oil and Gas Conference and Exhibition, Perth, Australia, 20-22 October. <http://dx.doi.org/10.2118/114496-MS>.
- [7]Aghamiri, Seyed Foad, Kasra Kabiri and Giti Emtiazi (2011): A Novel Approach for optimization of Crude Oil Bioremediation in Soil by the Taguchi Method. Journal of Petroleum Environment Biotechnology 2: 108.
- [8]Ali, S.(2001).Pressure drop correlations for flow through regular helical coils. Fluid Dynamics Research, 295-310.
- [9]All, S., & Zaidl, A.H.(1979). Head Loss and Critical Reynolds Number for Flow in Ascending Equiangular Spiral Tube Coils.*Ind. Eng.Process Des.Dev*, 349-353
- [10]Anderson, W.(1986).Wettability literature survey - part 2: Wettability measurement.Journal of Petroleum Technology.
- [11]Anderson, W.G., 1986a, Wettability literature survey—Part 1, Rock/oil/brine interactions and the effects of core handling on wettability: Journal of Petroleum Technology, v.38, p.1125–1144., 10, 2118/13932-PA
- [12]Anderson, W. G., 1986f, Wettability literature survey—Part 6, Effects of wettability on waterflooding: Journal of Petroleum Technology, v.38, p.1605–1622
- [13]Anderson, W.(1987a).Wettability literature survey - part 4: Effects of wettability on capillary pressure.Journal of Petroleum Technology.



- [14] Anderson, W. (1987b): Wettability literature survey - part 5: The effects of wettability on relative permeability. *Journal of Petroleum Technology*.
- [15] Andersen, M.A., 1995. "Petroleum Research in North Sea Chalk." Amoco Norway Oil Company and RF –Rogaland Research. ISBN 82-7220-725-7.
- [16] Andrade, M.L, Covelo, E.F, Vega, F.A. and Marcet, P.(2004): Effect of the Prestige Oil spill on salt marsh soils on the coast of Galicia (North western Spain). *Journal of Environmental Quarterly* 33, 2103 – 2110.
- [17] Assael, M.J, Metaxa, I.N, Kakosimos, K. Constantinou, D. (2006): *Int. J. Thermophys.* 27 (2006) 999
- [18] *Asian Journal of Biotechnology* 3 (3): 206 – 213, 2011. ISSN 1996 – 0700 / Doi: 10.3923/ajbkr.2011.206 – 213. 2011 Knowledge Review, Malaysia.
- [19] Atlas, R.M and Bertha, R. (1972): Degradation and mineralization of petroleum in seawater. Limitation by nitrogen and phosphorus. *Biotechnology and Bioengineering* 14, 309 – 318.
- [20] Atlas, R.M (1981): Microbial degradation of Petroleum hydrocarbons. An environmental perspective microbiology *Reviews* 45, 180-209.
- [21] Awobajo, S.A (1981): An analysis of spill incidents in Nigeria (1976-1980): In Seminar on petroleum Industry and the Nigerian Environment, NNPC/FMOW and Housing PT, Warri.
- [22] Aylward, G. and Findlay, T.(2002): *SI Chemical Data*, 5th edition. John Wiley & Sons Australia, Ltd, second edition edition. Monograph Volume 20
- [23] Baker Institute Study (2005): *Energy and Nanotechnology: Strategy for the Future*. Houston: Rice U: 30, 1-20.
- [24] Baoshan Xing (2011): Bacterial Toxicity of Oxide Nanoparticles and Their Effects on Bacterial Surface Biomolecules. PhD Dissertations presented by Jiang, Wein. Open Access Paper 386, submitted to the Graduate School of the University of Massachusetts. Bentor, Yinon. *Chemical Element.com-Mercury*. Retrieved on Mar. 17, 2013 <<http://www.chemicalelements.com/elements/hg.html>>.
- [25] Bentor, Yinon. *Chemical\_\_Element\_com\_\_Mercury*. Retrieved on Mar. 17, 2013 <<http://www.chemicalelements.com/elements/hg.html>>.
- [26] Behrenbruch, P. and H.M. Goda (2006): Two-phase relative permeability prediction: a comparison of the modified Brook-Corey methodology with a new Carman-Kozeny based flow formulation. SPE 101150, SPE Asia Pacific Oil and Gas Conference and Exhibition, Adelaide, Australia.

- [27]Behrenbruch Peter and Ta Quoc Dung (2011): **Estimation** of new relative permeability curves due to compaction case study at bachaquero field – Venezuela.Science & Technology Development, Vol 14, No.M2- 2011.
- [28]Blinks, B.(2002).Particles as surfactants - similarities and differences. *Curr.Opin.Colloid Interface Sci.*, 7, 21-41.
- [29]Boennemann, H, Botha, S.S., Bladergoen, B.Linkov, V.M.(2005; Applied.Organometry.Chemistry.19 (2005) 768.
- [30]Bresme, F&Faraudo, J.(2007):Particles as surfactants - similarities and differences.*J.Phys.Condens.Matter*, 19, 375110.
- [31]Chandrasekar, M.; Suresh, S. & Chandra Bose, A.(2010):Experimental investigations and theoretical determination of thermal conductivity and viscosity of Al<sub>2</sub>O<sub>3</sub>/water nanofluid.*Exp.Therm.Fluid Sci.*, 34, 210-216.
- [32]Chang, H.Tsung, T.T.Chen, L.C, Jwo.C.S, Tsung, J.W., Lu, Y.C. (2005): Journal Material Engineering.Perform.14 (2005) 158.
- [33] Chaudhurry, M.K.(2003).Complex Fluids: Spread the World about Nano fluids.Nature 423, 10, 131-132.
- [34]Chen, K.C, Chen, J.J. and Hounq, J.Y (2000): Improvement of nitrogen removal efficiency using immobilized microorganisms with oxidation-reduction potential monitoring. Journal Industrial Microbiology.Biotechmol 25, 229-234.
- [35]Chieruzzi Manila, Gian Cerritelli, Adio Miliozzi and José Kenny.(2013): Effect of nanoparticles on heat capacity of nanofluids based on molten salts as PCM for thermal energy storage. Nanoscale Research Letters 2013, 8:448 Page 2 – 8,<http://www.nanoscalereslett.com/content/8/1/448>
- [36a]Choi, S.U.S. (1995): in D.A. Singer, H.P. Wang (1995): (Eds.), Enhancing Thermal Conductivity of Fluids with Nanoparticles, Developments and Applications of Nonnewtonian Flows, American Society of Mechanical Engineers, New York, 1995.
- [36b]Choi, S. U. S."Nanofluid technology: current status and future research."*Korea-U.S.Technical Conference on Strategic Technologies*, Vienna, VA, 1998.
- [37] CIREN.2007.Estudio Agrológico Del Valle Del Copiapó y Valle Del Huasco.Descripciones de suelos, materiales y símbolos.Publicación N° 135.126 p.
- [38]Coats, A.W., and Redfern, J. P. (1963): Thermo gravimetric Analysis: A Review.Analyst **88**: 906-924.doi:

10.1039/AN9638800906.[Http://en.wikipedia.org/wiki/thermogravimetric\\_analysis](http://en.wikipedia.org/wiki/thermogravimetric_analysis) 10 Thermo gravimetric Analysis.pdf.Retrieved on 14/1/2013.

[39]Craig, F.F.1971.The Reservoir Engineering Aspects of Waterflooding, Vol.2.Millet the Printer, Texas: Monograph Series, SPE.

[40]Cuiec, L.E., 1999. “*Evaluation of Reservoir Wettability and its Effect on Oil Recovery.*” In: Surfactant Science Series, Vol. 36.Interfacial Phenomena in Petroleum Recovery.Ed.orrow, N.R., Marcel Dekker, Inc., New York and Basel.

[41]Cuiec, L. 1984. “*Rock/Crude-oil interactions and Wettability: An Attempt to Understand the Interaction.*” Paper SPE 13211 presented at the SPE 59<sup>th</sup> Annual Technical Conference and Exhibition in Houston, TX, USA, September 16-19.

[42]Cunningham, C.J.,Ivshina, I.B., Lozinaky, V.I, Kuyukina, M.S.and Philip, J.C. (2000): Bioremediation of diesel contaminated soil by microorganisms immobilized in polyvinylalchol.International bio deterioration and biodegradation.Vol. 54, issues 2-3, 167-174.

[43]Damoko, D., Cheryan, M. (2000): Kinetics of palm oil transesterification in a batch reactor.Journal of the American oil Chemists’ society, 2000, 77 (12), 1263 – 1267.

[44a]Das, S.K, Putra, N., Roetzel, W.(2003): International Journal.Heat Mass Tran.46 (2003) 851.

[44b]Das, S., Choi, S.U.S. Patel, H.E (2006): Heat Transfer.Engineering.27 (2006) 3.

[45]Deqian Huang\*, Quan Xu, Jiongjia Cheng, Xiaocheng Lu, and Hong Zhang (2012): Electrokinetic Remediation and Its Combined Technologies for Removal of Organic Pollutants from Contaminated Soils.International Journal of Electrochemical Science 7 (2012) 4528 – 4544

[46]Denekas, M., Mattax, C., and Davis, G. (1959): Effects of crude oil components on rock wettability.Presented at the AIChE-SPE Joint Symposium in Kansas City, Mo.(SPE 1276-G).

[47]Derjaguin B.V.and Landau, L.D (1941): Acta Physicochim. URSS, 14, 633 (1941)

[48]Diaz, M.P.Boyd, K.G., Grigson, S.J.W.and Burgess, J.G. (2002): Biodegradation of crude oil across a wide range salinities by an extremely halo tolerant bacteria consortium MPD-M, immobilized onto polypropylene fibres.Biotechnology and Bioengineering.79, 145-153.

[49]Donaldson, E.C., Thomas, R.D., and Lorenz, P.B.1969.Wettability Determination and Its Effect on Recovery Efficiency. *SPE Journal* **9** (1): 13-20. SPE-2338-PA.<http://dx.doi.org/10.2118/2338-PA>.

- [50]Donaldson, E.C. and Alam, W. 2008.*Wettability*. Houston: Gulf Publishing Company.
- [51]Donaldson, E.C, Thomas, R.D and Lorenz, B (1969): Wettability Determination and its effect on Recovery Efficiency, SEJ (March 1969) 13 – 20.
- [52]Duangthongsuk, W.Wongwises S (2009): Exp. Therm. Fluid Sci. 33 (2009) 706.
- [53]Eastman J.A., Choi S.U.S, Li S., Thompson, L.J. Lee S. (1996): Materials Research Society Symposium Proceedings, 1996.
- [54]Eastman, J.A. Choi, U.S. Li, S. Thompson, L.J. and Lee, S. (1997): Proceedings of the Materials Research Symposium (Nanophase and Nanocomposite Materials II), 1997.
- [55]Eastman, J.A. Choi, S.U.S. Li, S. Soyez, G. Thompson, L.J. DiMelfi, R.J. (1998): Journal of Metastable and Nanocrystalline Materials. 2 (1998) 629.
- [56a]Eastman J.A. Lee, S. Choi, S.U.S. Li, S. (1999): Journal of Heat Transfer 121 (1999) 280.
- [56b] Eastman, J.A, Choi, S., Li, U.S.Yu, S.W. and Thompson, L. J(2001): Anomalously increased effective thermal conductivities f ethylene glycol-based nanofluids containing copper nanoparticles, Applied Physics Letters, vol. 78, no. 6, pp.718–720, 2001.
- [57]Edoga, Rita N, Hassanpour, Ali, Dixon Hardy, Darron and Ding, Yulong (2014): Investigation into the cleaning behaviour of ZnO nanofluid on crude oil contaminated soil under controlled environmental conditions.Applied Petroleum Chemical Research (2014) 4 :1-2.D01.10.1007/S 13203 – 014 – 0061 -2.
- [58]Ershadi L, Ebadi T, Ershadi V and Rabbani A: Chemical Oxidation of crude in oil contaminated soil by Fenton process using nano Zero Valent Iron.2011 2<sup>nd</sup> International Conference on Environmental Science and Technology IPCBEE volume 6 (2011) IACSIT Press, Singapore.
- [59]European Commission (2005): Joint Research Centre, Institute for Environment and sustainability
- [60]Flemming, G (1991): Recycling Derelict Land Institution of Civil Engineers, Thomas Telford Ltd., London. 218pp.
- [61]Flint, A.L., Flint L.E. 2002.The solid phase. Particle density.In: J.Dane, G.C.Topp.(eds.) Methods of soil analysis.Part 4.Physical methods.SSSA.Madison, Wisconsin, USA, pp: 229-240.

- [62] Gardea-Torresdey J L, Gonzalez JH, Tiemann JL, Rodingnuez O, Gamez G (1998): Phytosorption of cadmium, chromium, lead and zinc ions by biomass of *Medicago sativa* (Alfalfa). *J Hazard.Mater.*57: 29 - 39.
- [63]Gee, G.W., Or, D.2002. Particle size analysis.In: J.Dane, G.C.Topp. (Eds.) *Methods of soil analysis.Part 4.Physical methods.SSSA.Madison, Wisconsin, USA*, pp: 255-293.
- [64]Ghadimi, A Saidur, R.Metselaar, H.S.C (2011): *International Journal of Heat Mass Transfer* 54 (2011) 4051.
- [65] Global Crude Supply (2011): [http://global\\_crude\\_supply.blogspot.co.uk/2011-02-01\\_archive.html](http://global_crude_supply.blogspot.co.uk/2011-02-01_archive.html).Retrieved on 06/08/12.
- [66] Golubovic MN, Madhawa Hettiarachchi HD, Worek WM, Minkowycz WJ: **Nanofluids and critical heat flux, experimental and analytical study.** *Applied Thermal Engineering* 2009, **29**:1281-1288.
- [67] Guillet, D.W., (1992): Crop choice and soil management. In: D.W. Guillet, *Covering Ground*, Chapter 5, p.67 -84, University of Michigan Press, 250 p.
- [68] Gradi, P.C (1985): *Bioremediation. Its Management and Microbiology Basis Biotechnology and Bio-Engineering* 27: 660-674.
- [69]Greeves, N. and Clayden, J. (2001): *Organic Chemistry Oxford* ISBN 0 -19-850346-6 p.21.
- [70] Green, D. W. and Willhite, G. P., 1998. “*Enhanced Oil Recovery.*” Society of Petroleum Engineer, *Vol. 6*, Richardson, Texas
- [71]Guo, H. (2011). Aes 1300 properties of hydrocarbons and oilfield fluids. TU Delft Lecture notes.
- [72] Gupte, S.K. Advani, S.G. and Huq, P. (1995): *International Journal. Heat Mass Transfer* 38 (1995) 2945.
- [73] Haapea, P and Tuhkanen, T. (2006): Integrated treatment of PAHs contaminated soil by soil washing, ozonation, and biological treatment. *J. Hazardous materials*, 136: 244~827
- [74] Heris, S. Z., Etemad, S. G., & Esfahany, M. N. (2006). Experimental investigation of oxide nanofluids laminar flow convective heat transfer. *International Communications in Heat and Mass Transfer*, 529-535.
- [75] Hiemenz, P.C and Rjagopalan, R.( 1997): *Principles of Colloid and surface chemistry*, 3<sup>rd</sup> ed. Marcel Dekker, New York, 1997.
- [76]Hunter, R.J. (2001): *Foundations of Colloid Science*, Second edition, Oxford University Press, 2001.

- [77] Hwang, Y, Lee, J.K, Lee, C.H, Jung, Y.M. Cheong, S. I . Lee, C.G. Ku, B.C and Jang, S.P. (2007) *Thermochimica Acta* 455 (2007) 70
- [78] Incropera, F.P. & DeWitt, D. P. (1996): *Introduction to Heat Transfer*. New York: John Wiley & Sons, Inc.
- [79] Islam, M.R. (2004), Unravelling the Mysteries of Chaos. *EEC Innovation*, 2 (2): 54 – 87.
- [80] Jacob Eapen, Ju Li and Sidney Yip. (2007): Thermal Conduction in Nanofluids with Percolating Fluid Structures. *Theoretical Division, Los Alamos National Laboratory, Los Alamos, NM 875445 (eapen@lanl.gov)*. *Physics Review Letter*. (2007).
- [81] Jiang, L, GAO, L and Sun, J. (2003): *Journal of Colloid Interface Science*. 260 (2003) 89.
- [82] Ju, H., Huang, Z., Xu, Y., Duan, B., & Yu, Y. (2001): Hydraulic Performance of Small Bending Radius Helical Coil-Pipe. *Journal of Nuclear Science and Technology*, 38, 826-831.
- [83] Kay, B. 1990. Rates of change of soil structure under different cropping systems. *Advance Soil Science* 12, 1- 4.
- [84] Koblinski, P., Phillpot, S.R., Choi, S.U. and Eastman, J.A.(2002): Mechanisms of Heat Flow in Suspensions of Nano-sized Particles (Nano fluids). *International Journal of Heat and Mass Transfer*, 45 (2002). 855 – 863.
- [85] Kevin G Wallace (2010): Research in Heat Transfer with Nanofluids. A M.Sc thesis submitted to Purdue University Calumet School of Technology.
- [86] Kinloch, I.A., Roberts, S.A., and Windle, A.H. (2002): A Rheological Study of Concentrated Aqueous Nanotube Dispersions, *Polymer*, 43, 7483-7419.
- [87] Khanafer, K. Vafai, K. and Lightsome, M. (2003): Buoyancy-driven heat transfer enhancement in a two-dimensional enclosure utilizing nanofluids”, *International Journal of Heat and Mass Transfer* 46, 3639–3653
- [88] Khovakh, M (1979): Motor vehicle engines. Mir publishers Moscow, p.548
- [89] Kim, J.K. Jung, J.Y. Kang, Y.T. (2006): *Int. J. Refrigeration*. 30 (2006)50.
- [90] Kim S, Bang I, Buongiorno J, Hu L (2007): **Surface wettability change during pool boiling of nanofluids and its effect on critical heat flux.** *International Journal of Heat and Mass Transfer* 2007, **50**:4105-4116.
- [91] Kim, K.S. Won, M.H, Kim, J.W. Back, B.J. (2003): *Applied Therm. Eng.* 23 (2003) 1137.
- [92] Kleinstreuer Clement\*, Yu Feng (. 2011): Experimental and theoretical studies of nanofluid thermal conductivity enhancement: a review. *Nanoscale Research Letters* 2011, 6:229 <http://www.nanoscalereslett.com/content/6/1/229>

- [93] Ko, T., & Ting, K. (2006). Optimal Reynolds number for the fully developed laminar forced convection in a helical coiled tube. *Energy*, 2142-2152.
- [94] Krishnamurthy .S, L. hattarcharya, P., Phelan, P.E. and Prasher, R.S (2006): Enhanced Mass Transfer in Nanofluids, *Nano Letter*, 6 (3), 419-426.
- [95]Kwak, K., Kim, C. (2005): Viscosity and Thermal Conductivity of Copper Oxide Nanofluid Dispersed in Ethylene Glycol, *Korea – Australia Rheology Journal* 17 (2005) 35 – 40.
- [96] Kyte, J.R. Naumann, V.O .and Mattax, C.C: Effect of Reservoir Environment on water – oil Displacements, *JPT* (June 1961) 579 -82; *AIME*, 222.
- [97] Laurence M. Harwood, Christopher J. Moody (2001) *Experimental organic chemistry: Principles and Practice* (Illustrated edition.). pp.145–147.ISBN 978-0-632-02017-1.
- [98] Leach, R.O., Geffen, T.M and Berry, V.J (1956): Discussion of wettability versus Displacement in water flooding in unsolidated sand columns (*JPT* march 1956) 61 – 63.
- [99] Lee, D, Kim, J. Kim, B.G (2006): *Journal of Physical Chemistry B* 110 (2006): 4323.
- [100] Lee, S, Choi, S.U, Li, S. and Eastman, J.A (1999): *J. Heat Transf.*121 (1999) 280.
- [101] Li, M., Xu, J.Lu, Q. (2007): *Journal of Material Chemistry.*17 (2007) 4772-4776.
- [102] Madni, I., Hwang, C.Y, Park, S.D., Choa, Y.H. and Kim, H.T.(2010): *Colloids and Surfaces A: Physicochemical and Engineering Aspects* (Elsevier) Volume 358 Issue 1-3, (pp. 1-178) April 5, 2010. Volume 357: Issue 1-3.
- [103] Man and Jing (2000): Wettability of reservoir rock and fluid systems from complex resistivity measurements.2000.19 pp.Paper presented at 6th International Symposium on Evaluation of Reservoir Wettability and its Effect on Oil Recovery, Socorro, New Mexico, United States
- [104] Martin Novák, Simon Emmanuel, and Melanie A.Vile, Yigal Erel (2003): Origin of Lead in Eight Central European Peat Bogs Determined from Isotope Ratios, Strengths, and Operation Times of Regional Pollution Sources.*Environment Science.Technology.* 2003, 37 (3), pp 437–445.DOI: 10.1021/es0200387
- [105] Masuda, H., Ebata, A. Teramae, K and Hishinuma, N (1993): Alteration of thermal conductivity and viscosity of liquid by dispersing ultra-fine particles (Dispersion of G-Al<sub>2</sub>O<sub>3</sub>, SiO<sub>2</sub> and TiO<sub>2</sub> ultra-fine particles), *NetsuBussei* (Japan) 4, 227–233.
- [106] Masoumi, N.; Sohrabi, N.& Behzadmehr, A. (2009).A new model for calculating the effectiveviscosity of nanofluids.*J. Phys. D: Appl. Phys.*, 42, 055501.

- [107] Maxwell, J.C. (1904): A Treatise on Electricity and Magnetism, Oxford University Press, Cambridge, 1904
- [108a] Ma, F., Hanna, M.A. (1999): Biodiesel production: a review *Bioresource Technology* 1999, 70 (1), 1-15.
- [108b] Ma, S. M., Morrow, N. R., Zhang, X., and Zhou, X., (1999.): “*Characterization of Wettability from Spontaneous Imbibition Measurements.*” *Journal of Canadian Petroleum Technology*, Vol.38, pp 94-47.
- [109] Michael, B (2008): Novel Nanotechnology Materials. Addresses Water Pollution and Old Spills.
- [110] Molina Rodriguez-Vazquez R, Hernandez – Velasco M, Vega – Jarquin C, Zapata – Perez O, et al.(2004) Diesel removal from contaminated soils by biostimulation and supplementation with crop residues, *Applied Soil Ecology* 27: 165 - 175
- [111] Minai – Tehrani, D and Herfatmanesh, A (2007): Biodegradation of aliphatic and aromatic fractions of heavy crude oil-contaminated soil: A Point Study, *Bioremediation Journal*, 11: 71 – 76.
- [112] Moore, T.F and Slobod, R.L (1956): The Effect of viscosity and capillarity on the Displacement of oil by water. *Production monthly* (Aug 1956) 20, No.10, 20- 30.
- [113] Moosavi, M, Goharshadi, E.K and Youssefi, A (2010): "Fabrication, characterization, and measurement of some physicochemical properties of ZnO nanofluids," *International Journal Heat Fluid FL*, 31[4] 599-605 (2010).
- [114] Morgan, J.T and Gordon, D.T (1970): Influence of pore geometry on water – oil. *Relative Permeabilities JPT* (Oct 1970) 1199 -1208.
- [115] Morrow, R. N. & Mason G., “Recovery of oil by spontaneous imbibition” *Current opinion in Colloid and Interface Science*, 6, 231-337 (2001).
- [116] Murshed, S.M.S, Leong, K.C. Yang, C(2005); *International Journal Thermophysical Science*. 44 (2005) 367.
- [117] Murshed SMS, Leong KC, Yang C, Nguyen NT (2008) Convective heat transfer characteristics of aqueous TiO<sub>2</sub> nanofluid under laminar flow conditions. *International Journal of Nanoscience* 7:325–331.
- [118] Nam J.J, Song B.H, Eom K.C, Lee S.H and Smith A (2011): Distribution of polycyclic aromatic hydrocarbons in agricultural soils in South Korea, *Chemosphere*, 50: 1281 – 1289.
- [119] National Research Council (1997): Innovations in groundwater and soil clean-up from concept to commercialization: Washington, D.C., National Academies Press, 310 p.




- [120] Nationwide spill and emergency response service, oil cleaning bioremediation (2012): Bio-remediation and oil spill Containment.<http://www.idealgroupuk.co.uk/services/cleaning/oil-cleaning-bioremediation>.
- [121] Nanofluids Letter, Volume 3, No .2(2003).
- [122] Nanofluids for Heat Transfer Enhancement-A Review/**Phys. Chem. Res.**, Vol. 1, No. 1, 1-33, June 2013.
- [123] New combe, J.McGhee, J andRzasa, M.J: Wettability versus Displacement in waterflooding in Unconsolidated sand columns, Trans.AIME (1955) 204,227 – 32.
- [124] Nguyen, C.T. Roy, G. Gauthier, C. Galanis, N (2007): Applied Thermophysical.Engineering 27 (2007) 1501.
- [125] Nwilo, P.C. & O.T. Badejo, (2005): Oil Spill Problems and Management in the Niger Delta. International Oil Spill Conference, Miami, Florida, USA
- [126] Okoh, A.I. and M.R. Trejo-Hernandez,( 2006): Remediation of petroleum hydrocarbon [http://www.fspublishers.org/ijab/past-issues/IJABVOL\\_13\\_NO\\_2/16.pdf](http://www.fspublishers.org/ijab/past-issues/IJABVOL_13_NO_2/16.pdf).
- [127] Olle B, Bromberg L, Hatton TA, Wang DIC (2006) Enhancement of oxygen transfer in fermentation by use of functionalized magnetic nanoparticles.In: 2006 NSTI nanotechnology conference and trade show—NSTI Nanotech 2006 technical proceedings, pp 411–414.
- [128] Owens, W.W and Archer, D.L (1971): The effect of Rock wettability on oil –wet Relative permeabilities relationships.Journal of Petroleum Technology (July1971) 873 -78; Trans, AIME, 25.
- [129] Pagliai, M., Vignozzi, N. 2002.The soil pore system as an indicator of soil quality.In: M. Pagliai, R. Jones (Eds).Sustainable land management-environmental protection.A soil physical approach.Advances in Geocology.35.IUSS. Catena Verlag.Reiskirchen.Germany, pp: 71-82.
- [130] Palma, R.D. Peters, S. Van Bael, M.J. Rul, H.V. Bonroy, K. Laureyn, W. Mullens, J. Borghs, G. (2007): Chem. Mater. 19 (2007) 1821- 1831.
- [131] Panagos, P., Van Liedekerke, M., Yigini, Y., Montanarella, L. (2013) Contaminated Sites in Europe: Review of the Current Situation Based on Data Collected through a European Network. Journal of Environmental and Public Health In Press. doi:10.1155/2013/158764
- [132] Patel, H.E, Das, S.K., Sundararajan, T. Sreekumaran, N.A. George, B. (2003): Pradeep, Applied Physical Letter 83 (2003) 2931.
- [133] Pawel, K., Jeffrey, A., and David, G. C.(2005): Nanofluids for thermal transport Materials today, **8**, pp. 36-44.

- [134] Petroleum – Wikipedia, the free encyclopedia 2012 (<http://en.wikipedia.org/wiki/petroleum>) Retrieved on 06/08/2012.
- [135a] Pereira, M.G., Mudge, S.M (2004): Cleaning oiled shores: Laboratory experiments testing the potential use of vegetable oil biodiesels. *Chemosphere* 2004, 54, (3), 297 – 304.
- [135b] Perry, R. H., & Green, D. W. (1997): Perry's Chemical Engineering *Handbook* New York: McGraw-Hill.
- [135c] Pinto, A.C., Guarieiro, L.L.N., Rezende, M.J.C, Ribeiro, N.M., Torres, E.A., Lopes, W.A., Pereira, P.A.P., Andrade, J.B.(2005): Biodiesel: an overview. *Journal of the Brazilian chemical society*, 2005, 16, 1313 – 1330.
- [136] Poblete (2011): *The Soils of Chile*. Manuel Casanova, Osvaldo Salazar, Oscar Seguel, Walter Luzio.
- [137] Preparation and Dispersion stability study of CoFe<sub>2</sub>O<sub>4</sub> nanofluid. D.Y Patil University, Kolhapur.
- [138] Rao, D.N and Ayirala, S. C (2004): Beneficial effects of wettability Altering Surfactant in Oil-wet fractured reservoirs” 8<sup>th</sup> International symposium on Reservoir wettability and its effect on oil recovery. Houston, TX, USA May 2004.
- [139] Raza, S.H., Treiber, L.E and Archer, D.L (1968): Wettability of Reservoir Rocs and its Evaluation *Production monthly* 32, No. 4, 2 – 7.
- [140] Riser-Roberts, E.(1998): *Bioremediation of petroleum contaminated soils*. Lewis Publishers. Boca Raton Florida.
- [141] Roosta, A., Escrochi, M., Varzandeh, F. et al (2011): Investigating the Mechanism of Thermally Induced Wettability Alteration. Paper SPE 120354 presented at the SPE Middle East Oil and Gas Show and Conference, Bahrain, Bahrain, 15-18 March. <http://dx.doi.org/10.2118/120354-MS>. OR cross check for Rosen (2011)
- [142] Sadzawka, A., Carrasco, M.A., Grez, R., Mora, M. L.(2004): Métodos de análisis recomendados para los suelos chilenos. Comisión de Normalización y Acreditación. Sociedad Chilena de la Ciencia Del Suelo. Santiago, Chile, 113 p.
- [143] Saeid, M., Mariela, A. And Islam, M.R (2006): *Application of Nanotechnology in oil and Gas E & P*, Imperial College, London.
- [144] Salathiel, R.A.(1973): “*Oil Recovery by Surface Film Drainage in Mixed-Wettability Rocks.*” *Journal of Petroleum Technology*, October, pp.1216-1224.
- [145] Sakamoto, M.; Kanda, Y.; Miyahara, M. & Higashitani, K.(2002). Origin of long-range attractive force between surfaces hydrophobized by surfactant adsorption. *Langmuir*, 18, 5713-5719.

- [146] Sayanrayana, L.; Madhusudan, R.K. and Manorama, S.V (2003): Synthesis of Nanocrystalline A Material for Liquified Petroleum Gas Sensing Sensors and Actuator B, 89 (1) 62-67.
- [147] Schlumberger: ECLIPSE reservoir simulation software, ECLIPSE Technical Description. Version 2013.2.2013. Schlumberger (2013) Oil field glossary [www.glossary.oilfield.slb.com](http://www.glossary.oilfield.slb.com).
- [148] Schmid, C: The wettability of Petroleum Rocks and results of Experiments to study the effects of variations in wettability of core samples. *Erdol und Kohle – Erdgas – Petrochemi* (1964) 17, No.8, 605 – 09.
- [149] Science Daily (2010): Predicting amount of oil in contaminated soils: Scientists develop faster method for testing soils around oil spills.
- [150] Seethepalli, A., Adibhatla, B., and Mohanty, K.K., 2004. “Physiochemical Interactions during Surfactant Flooding.
- [151] Selboe K. G., Hadia, N., Heldal Lehne, H., Kumar, , K., Stensen, J. Å. and Torsæter, O.(2011): “Laboratory Investigation of Low Salinity Waterflooding on Reservoir Rock Samples from the Frøy Field”, Paper SPE 141114 accepted for presentation at the SPE Middle East Oil and Gas Show and Conference to be held in Manama, Bahrain, 25-28 Sept.2011.
- [152] Seol, Y., and Javandel, I.(2008): Citric acid- modified Fento’s reaction for the oxidation of chlorinated ethylenes in soil solution systems: Lawrence Berkeley National Laboratory, 21 p.
- [153] Semple KT, Reid BJ, Fermor TS (2001): Impact of composting strategies on the treatment of soils contaminated with organic pollutants. *Environmental Pollution* 112:269 – 283.
- [154] Silberberg, Martin (2004): *The Molecular Nature of Matter and Change*. New York: McGraw- Hill Companies, 2004. ISBN 0-07-310169-9.
- [155] Smith, S.R., 1991. Effects of sewage sludge application on soil microbial processes and soil fertility. *Advances in Soil Science*, 16, 191-212.
- [156] Snoeijer, J.H, Andreotti B, Antonin Marchand1, Siddhartha Das (2008): Contact angles on a soft solid: from Young’s law to Neumann’s law, *Phys. Fluids* **20**, 057101 (2008). Institute for Nanotechnology, University of Twente,
- [157] Singh, A.K.(2008). Thermal Conductivity of Nanofluids. *Defense Science Journal* , 58, 600-607.
- [158] Srdic, V.V., Winterer, M. Iler, A.M Mieke, G. Hahn, H. (2001): *Journal American Ceramic Society* 84 (2001) 2771.

- [159] Speight, J.G.(2009).Enhanced recovery methods for heavy oil and tar sands. Gulf Publishing Company.
- [160]Strand, S.( 2005): “*Wettability Alteration in Chalk: A Study of Surface Chemistry*,” PhD Thesis, University of Stavanger, Norway.
- [161] Suganthi, K.S and Rajan, K.S (2012): Investigations on the role of surfactants on stability and rheology of ZnO – water nanofluids using surface response methodology, in proceedings of international Conference on nanoscience and technology (ICOSAT -2012).Hyderabad India, 2012.RA -42, Page 185 – 185.
- [162] Testa, S.M. and Winegardner, D.L (1991): Restoration of Petroleum-Contaminated Aquifers. Lewis Publishers, Chelsea, Michigan, PP.1-180, 211-229.
- [163] Tikhonov, N.A., Arkhangelsky, I.V., Belyaev, S. S. and Matveev, A.T.(2009): Carbonization of polymeric nonwoven materials. *Thermochimica Acta* 486: 66-70.Doi:10.1018/j.tca.2008.12.020.
- [164] Timofeeva, E.V.; Gavrilov, A.N.; McCloskey, J.M. & Tolmachev, Y.V.(2007).Thermal conductivity and particle agglomeration in alumina nanofluids: Experiment and theory. *Phys. Rev. E*, 76, 061203.
- [165]Torsæter, O.and Abtahi, M.2003.Experimental Reservoir Engineering Laboratory Workbook.Department of Petroleum Engineering and Applied Geophysics, Norwegian University of Science and Petroleum (NTNU), Norway.
- [166]Tohver V, Chan A, Sakurada O, Lewis JA (2001).Nanoparticle engineering of complex fluid behavior.*Langmuir*.17: 8414-8421.
- [167] Treatment of petroleum-contaminated soils, 0271-2801P-MTDC, Petroleum. Retrieved on <http://www.fs.fed.us/t-d/pubs/htmlpubs/html02801/section02.htm> 5/12/2012.
- [168] Trisaksria, V. Wongwises, S. (2007): *Renewal Sustainable Energy Review*.11 (2007) 512.
- [169] Torres, I.E. (1999): The Mineral Industry of Trinidad and Tobago. In Country Report: U.S. Geological Service.
- [170]Ursin, J. R. and Zolotukhin, A.(2000).Introduction to petroleum reservoir engineering.Høyskoleforlaget, Norwegian Academic Press.
- [171]Vadasz, J.J., Govender, S., Vadasz, P. (2006): Heat Transfer Enhancement in Nano-fluid Suspensions: Possible Mechanisms and Explanations, *International Journal of Heat and Mass Transfer* 48 (2006) 2673-2685.

- [172] Verwey E.F. and Overbeek, G (1948): Theory of the Stability of Lyophobic Colloids, Elsevier, Amsterdam (1948).
- [173] Wang, F.H.L (1986): Effect of wettability Alteration on water oil relative permeability, Dispersion and Flowable saturation in porous media. Paper SPE 15019 presented at the 1986 SPE Permian Basin oil and Gas Recovery Conference, Midland, TX March 13 – 14.
- [174] Wang, X., Chang, Z., Lu, Y., Xu, L., and Xie, X. (1997): Nano Scaled Metals in Earth gas and Mobile Forms of Metal in Overburden in Wide-Spaced Regional Exploration for Giant Deposits in Overburden Terrains. *Journal of Geochemical Exploration*, 58, 63-72
- [175] Wang, X. Q., Mujumdar, A. S.(2007) : Heat transfer characteristics of nanofluids: a review. *International Journal of Thermal Sciences*, **46**, pp. 1-19.
- [176] Wang X. Q and. Mujumdar, A.S (2008): A review on nanofluids - part II: experiments and applications," *Brazilian Journal of Chemical Engineering*, 25 631-648 (2008).
- [177] Wang, X.J. Zhu, D.S. and Yang, S.Y (2009): *Chemical Physics Letter* 470 (2009) 107.
- [178] Wassan, D.T., and Nikolov, A.D. (2003): Spreading of Nanofluids on Solids. *Nature*, 423 (156-159).
- [179] Warrick, A.W. (Ed.).2002. *Soil Physics Companion*. CRC Press. Boca Raton, USA, 389 p.
- [180] Wasan, D., Nikolov, A., and Kondiparty, K. (2011): The wetting and spreading of nanofluids on solids: Role of the structural disjoining pressure. *Current Opinion in Colloid & Interface Science*, Elsevier
- [181] Weindorf David, Cristine Morgan and John Galbraith (2010): Predicting Amount of Oil in Contaminated Soils: Scientists Develop Faster Method for Testing Soils Around Oil Spills.
- [182] Wen, D.S., Ding, Y.L (2004): Effective thermal conductivity of aqueous suspensions of carbon nano tubes (Nanofluids), *Journal of Thermophysics and Heat Transfer* 18 (4), 481–485.
- [183] Wen, D. S. and Ding, Y.L (2005): "Formulation of nanofluids for natural convective heat transfer applications," *International Journal of Heat and Fluid Flow*, vol. 26, pp. 855-864.
- [183] Williams, B.J and C.A. Ortiz-Solorio, (1981): Middle American folk soil taxonomy. *Annals of the Association of American Geographers* 71(3): 335 – 358.
- [184] World Crude Oil Production.Pdf Retrieved Sept. 27 2012.
- [185] Wu, D., Zhu, H., Wang, L and Liua, L.(2009): Critical issues in nanofluids preparation, characterization and thermal conductivity, *Curriculum Nanoscience*, volume 5, 2009, p.103-112.

- [186] Wu Weidong\*, Sheng Wei, Zhang Hua, Kang Yong Tae (2012): Mass Transfer Enhancement by Binary Nanofluids (NH<sub>3</sub>/H<sub>2</sub>O + Ag Nanoparticles) for Bubble Absorption Process, *International Journal of Refrigeration*, Vol.35, pp.2240-2247, 2012.
- [187] Xiang-Qi Wang; and Arun S. Mujumdar (2008): A review on nanofluids - part II: experiments and applications, *Braz. J.Chem. Eng.*, 25, 631-648.
- [188] Xiang-Qi Wang and Arun S.Mujumdar (2007): Heat transfer characteristics of nanofluids.A review, *International Journal of Thermal Sciences*, 46, 1-19.
- [189] Xie, H.Wang, J.Xi, T. Liu, Y Ai, F. Wu, Q.(2002):*Journal Applied Physics* 91 (2002) 4568.
- [190] Xuan Y. &Li, Q.(2000):Heat transfer enhancement of nanofluids. *Int. J. Heat Fluid Flow*, 21.58-64.
- [191]Yeganeh, M (2010): Volume fraction and temperature variations of the effective thermal conductivity of nanodiamond fluids in deionized water.*International.Journal.Heat and Mass Transfer*.53, 3186–3192 (2010).
- [192] Yoon, Y., Kim, J., Hyun, S. (2007): Estimating soil water retention  in a selected range of soil pores using tension disc infiltrometer data. *Soil Tillage Res.* 97, 107-116
- [193]Yu, W andXie, H. (2011): A review on nanofluids: Preparation, stability mechanisms, and applications. Article ID 435873, *Journal of Nanomaterials*.
- [194]Yu L, Evje S, Kleppe H, Karstad T, Fjelde I, Skjæveland SM, (2008): Analysis of the wettability alteration process during seawater imbibition into preferentially oil-wet chalk cores, Presented at SPE/DOE Improved Oil Recovery Symposium. Tulsa, USA, SPE Paper No. 113304.
- [195]Yunus A. Cengel, (2006): *VISCOUS FLUID FLOW, THIRD EDITION* International Edition 2006
- [196] Zhang, L., Jiang, Y., Ding, Y.L., Povey, M., and York, D.W (2007): Investigation into the Antibacterial Behaviour of Suspension of ZnO Nanoparticles (ZnO nanofluids) *Journal of Nanoparticle Research*, 9, 479-489.
- [197] Zhang, T., Davidson, A., Bryant, S and Huh, C.(2010): Nanoparticle-stabilized emulsion for applications in enhanced oil recovery.SPE paper 129885 prepared for presentation at the SPE Improved Oil Recovery Symposium, Tulsa, Okla- homa, USA.
- [198]Zhu, H Zhang, C. Tang, Y.Wang, J.Ren, B. and Yin, Y (2007): Preparation and thermal conductivity of suspensions of graphite nanoparticles. **Carbon** 2007; 45(1):226–8.

[199] Zhou J Li, Y.Tung, S Schneider, E. & Xi, S. (2009): A review on development of nanofluid preparation and characterization. *Powder Technol.*, 196, 89-101.

[200] Zheng, Z.G Wu, G.(2005): *Journal Nanoscience Nanotechno.*5 (2005) 571.

[201] Zhou S.Q. and Ni, R (2008): Measurement of the specific heat capacity in Water-based Al<sub>2</sub>O<sub>3</sub> nanofluid,” *Applied Physics Letter* 92, 093123 (2008).

List of publications from this thesis

[57] Edoga, Rita N, Hassanpour, Ali, Dixon Hardy, Darron and Ding, Yulong (2014): Investigation into the cleaning behaviour of ZnO nanofluid on crude oil contaminated soil under controlled environmental conditions. *Applied Petroleum Chemical Research* (2014) 4: 1-2. doi:10.1007/S 13203 – 014 – 0061 -2.

In Press: 1. Edoga, Rita N, Hassanpour, Ali, and Edoga, M.O (2015): Possibility of using TiO<sub>2</sub> nanofluids on cleaning crude oil contaminated soil under optimum conditions.

2. Edoga, Rita N, Hassanpour, Ali, and cayre, O (2015): Cleaning efficiency of Al<sub>2</sub>O<sub>3</sub> nanofluids on crude oil contaminated soil under optimum conditions.

3. Edoga, Rita N (2015): A book on cleaning crude oil contaminated soil/oillspill with nanofluids.

## CURRICULUM VITAE

**NAME: Rita Ngozi, EDOGA (Mrs)**

PRESENT RANK READER (2013) IN SOIL SCIENCE.

Educational QUALIFICATIONS with dates:

Ph. D. (Soil Science) Dec, 1999

M. Sc. (Agric. Engineering) June, 1993

B. Eng. (Agric. Engineering) August, 1989

Employment: Teaching & Research at Federal University of Technology, Minna – Nigeria.

Teaching Responsibilities: I teach both undergraduate and postgraduate courses.

Research Responsibilities: I supervise Undergraduate and Postgraduate students.

Professional Societies: i. Member of Soil Science Society of Nigeria (SSSN). ii Member of Women Engineering Society, UK branch (2012 – date)

iii. Member of STEM Ambassador, West Yorkshire branch., Leeds – United Kingdom (2012 – date).





## Appendices

### A Properties of experimental materials

#### A-1 Nanoparticles

Table A- 1 Properties of Alumina Nanopowder.

	Alpha Al <sub>2</sub> O <sub>3</sub>	Gamma Al <sub>2</sub> O <sub>3</sub>
Appearance	White powder	White powder
Purity	99.9+	99.9+
Grain size	>100nm	5nm, <100nm
Specific surface area (m <sup>2</sup> /g)	≤ 25m <sup>2</sup> /g	500 – 600m <sup>2</sup> /g

Table A- 2 Properties of Titanium Oxide Nanopowder

	Anatase – TiO <sub>2</sub>	Rutile – TiO <sub>2</sub>
Appearance	White powder	White powder
Purity	99.5+%	99+%
Grain size (nm)	20nm	80nm
Specific surface area (m <sup>2</sup> /g)	>120	>30
Apparent density (g/cm <sup>3</sup> )	0.3	0.85
pH value of aqueous	7 – 8	

Table A- 3 Properties of Zinc Oxide Nanopowder, ZnO

	ZnO -20nm
Appearance	White or pale yellow powder.
Purity	99%
Grain size (nm)	20nm
Specific surface area (m <sup>2</sup> /g)	>90

Table A- 4 Properties of Disodium Phosphate Na<sub>2</sub>HPO<sub>4</sub> (inorganic compound)

Name	Sodium hydrogen phosphate
Appearance	Hygroscopic, anhydrous salt, white crystalline odorless solid.
Molecular formular	Na <sub>2</sub> HPO <sub>4</sub>
Molar mass	141.96 g/mol

Melting point	250°C
Density	1.7g/cm <sup>3</sup>
pH	Between 8 and 11, moderately basic.
CAS No.	7558 – 79 – 4

Table A- 5 Properties of Sodium dodecyl Sulphate (Organic compound)

Molecular formular	C <sub>12</sub> H <sub>25</sub> C <sub>6</sub> H <sub>4</sub> SO <sub>3</sub> Na
Molar mass	348.48g/mol
CAS No.	25155 – 30 – 0

## A.2 Organic and Inorganic Compounds

Table A- 6 Property table for water (which is an inorganic compound) [19].

Name	Water (oxide)
Chemical Formular	H <sub>2</sub> O
Molecular weight	18.0
Density at 25°C (g/cm <sup>3</sup> )	1.0
Boiling temp at 1 atm (°C)	100
Melting temp (°C)	0

Table A- 7 Property table for organic compounds used in the experiments [19]

Chemical formular	Mineral oil/paraffin (wax) oil/Octane	Ethanol
Chemical formular	C <sub>8</sub> H <sub>18</sub>	CH <sub>3</sub> CH <sub>2</sub> OH
Molecular weight	C <sub>n</sub> H <sub>2n+2</sub> , n = 16 – 24	46.1
Density at 25°C (g/cm <sup>3</sup> )	0.85	0.785
Boiling temp at 1 atm (°C)	300	78.3
Melting temp (°C)	-24	-114.1
CAS Number	8012 – 95 – 1	
Refractive index	N20/D1.467	

## A.3 Characterization of experimental nanofluids [57]

### A.3.1 Particle size distribution

Particle size distribution: The particle size of the various nanofluids are shown on Appendix A.3

A Zetasizer Nano ZS (Malvern) was used for measuring the average dimension of the nanoparticles in solution. The particles in a liquid move about randomly and their speeds of movement are used for determining the size of the particles. The particles move by Brownian motion in which the small / light particles move quickly and form particle size distribution (stable solution) while large/heavy particles move slowly, to form large aggregate (cluster-unstable solution)[57, 161].

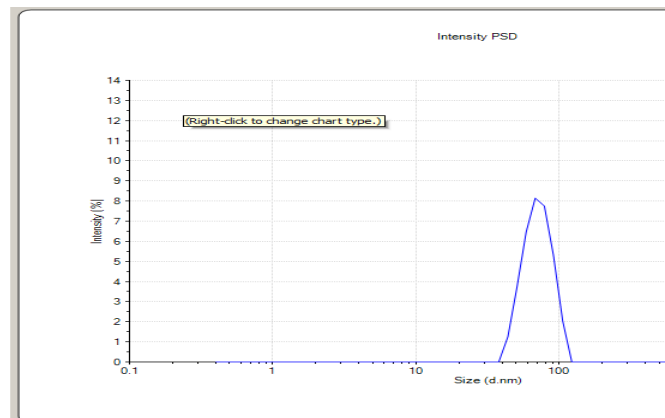


Figure A- 1 Particle size distribution of pure (without surfactant) 0.3 vol%  $\text{Al}_2\text{O}_3$  water nanofluid

Particle size distribution: Figure A-1 shows the hydrodynamic particle size distribution of 0.3 vol%  $\text{Al}_2\text{O}_3$  –water nanofluid at 25°C, room temperature. The nanofluid formulated with 0.3g  $\text{Al}_2\text{O}_3$  nanopowder +99.70ml deionized water calcined at 25°C had the average aggregate size, 71.77 d.nm, peak diameter aggregate size, total surface area of 0.0214  $\text{nm}^2$ , with percentage intensity of 100%. The Particle size distribution is less than 100nm which revealed the powdered nature of the nanoparticles. The zeta potential of pure 0.3vol%  $\text{Al}_2\text{O}_3$  water nanofluid was determined to be 190mV which showed excellent stability with pH of 3.15 and remained stable for more than 6months. The viscosity of nanofluids increased linearly with nanoparticle concentration. The 0.3vol%  $\text{Al}_2\text{O}_3$  – water nanofluid has

cleaning efficiency of 82% with mean viscosity of  $5.264 \times 10^7$  Pas.

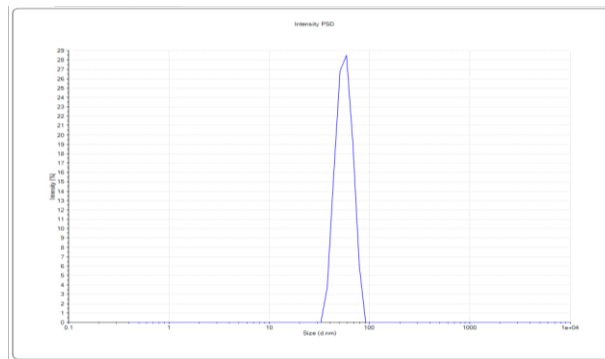


Figure A- 2 Particle Size Distribution of 0.3wt%Al<sub>2</sub>O<sub>3</sub> + 0.03wt% SDBS- deionised water nanofluid

Particle size distribution: Figure A-2 Shows the hydrodynamic particle size distribution of 0.3 vol% Al<sub>2</sub>O<sub>3</sub> + 0.03%SBDS –water nanofluid at 25°C, room temperature. The nanofluid formulated with 0.3g Al<sub>2</sub>O<sub>3</sub> nanopowder +0.03%SBDS +99.67ml deionized water calcined at 25°C had the average aggregate size, 56.52 d. nm, total surface area of 0.0272nm<sup>2</sup> with percentage intensity of 100%. The Particle size distribution is less than 100nm. The average diameter is less than 100% which formed smaller particle size due to sufficient agitation of the nanofluid before particle size distribution analysis. The zeta potential of 0.3vol% Al<sub>2</sub>O<sub>3</sub> + 0.03%SDBS water nanofluid was determined to be 168mV which showed excellent stability with pH of 3.16 and remained stable for more than 6months. The viscosity of nanofluids increased linearly with nanoparticle concentration. The 0.3vol% Al<sub>2</sub>O<sub>3</sub> + 0.03%SBDS – water nanofluid has cleaning efficiency of 84% with mean viscosity of  $3.4177 \times 10^4$  Pas.

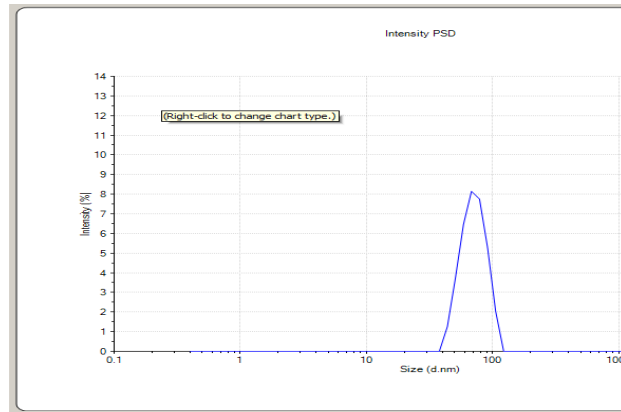


Figure A- 3 Particle size distribution of pure 0.7 vol% Al<sub>2</sub>O<sub>3</sub> water nanofluid

Figure A-3 shows the hydrodynamic particle size distribution of 0.7 vol% Al<sub>2</sub>O<sub>3</sub> –water nanofluid at 25°C, room temperature. The nanofluid formulated with 0.7g Al<sub>2</sub>O<sub>3</sub> nanopowder +99.30ml deionized water calcined at 25°C had the average aggregate size, 41.77 d.nm, total surface area of 0.03667 nm<sup>2</sup>, with percentage intensity of 100%.The peak Particle size distribution is less than 100nm which revealed the powdered nature of the nanoparticles.The zeta potential of 0.7vol% Al<sub>2</sub>O<sub>3</sub> water nanofluid was determined to be 178mV which showed excellent stability with pH of 3.37 with stability lifespan of more than 6months.The viscosity of nanofluids increased linearly with nanoparticle concentration.The 0.7vol% Al<sub>2</sub>O<sub>3</sub> – water nanofluid has oil cleaning efficiency of 70% with mean viscosity 0.32236 Pas

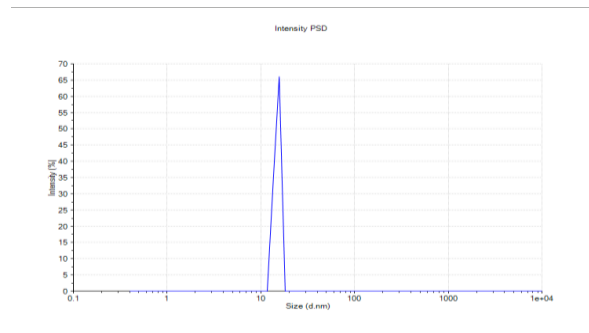


Figure A- 4 Particle Size Distribution of 0.7wt% Al<sub>2</sub>O<sub>3</sub> + 0.07wt%SDBS –deionised water nanofluid

Figure A-4 shows the hydrodynamic particle size distribution of 0.7 vol% Al<sub>2</sub>O<sub>3</sub> + 0.03%SDBS –water nanofluid at 25°C, room temperature. The nanofluid formulated with 0.7g Al<sub>2</sub>O<sub>3</sub> nanopowder + 0.07%SDBS + 99.23ml deionized water calcined at 25°C had the average aggregate size, 14.96 d. nm,

total surface area of  $0.1024\text{nm}^2$ . The peak Particle size distribution is less than 100nm which revealed the powdered nature of the nanoparticles. The zeta potential of 0.7vol%  $\text{Al}_2\text{O}_3 + 0.07\%\text{SDBS}$  - water nanofluid was determined to be 136mV which showed excellent stability with pH of 3.72 and remained stable for more than 6months. The viscosity of nanofluids increased linearly with nanoparticle concentration. The 0.7vol%  $\text{Al}_2\text{O}_3 + 0.07\%\text{SDBS}$  - water nanofluid has oil cleaning efficiency of 76% with mean viscosity of 7057.16 Pas.

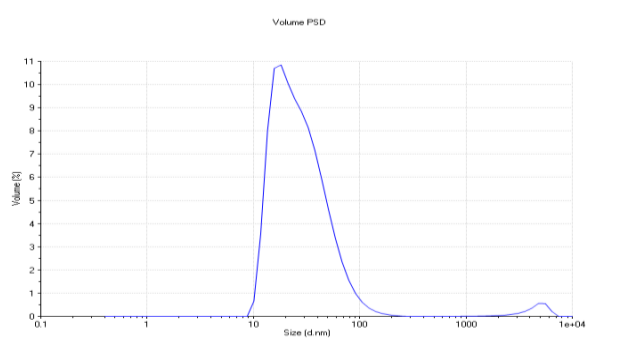


Figure A- 5 Particle size distribution of 1vol%  $\text{Al}_2\text{O}_3$  water nanofluid without surfactant

Figure A-5 shows the hydrodynamic particle size distribution of 1 vol%  $\text{Al}_2\text{O}_3$  –water nanofluid at 25°C, room temperature. The nanofluid formulated with 1g  $\text{Al}_2\text{O}_3$  nanopowder +99ml deionized water calcined at 25°C had the average aggregate size, 30.71nm d.nm, total surface area of  $0.04972\text{nm}^2$ . Particle size distribution is less than 100nm, zetapotential of 202mV which showed excellent stability with pH of 2.94 and remained stable for more than 6months. The 1vol%  $\text{Al}_2\text{O}_3$  – water nanofluid has oil cleaning efficiency of 74% with mean viscosity of 0.05923 Pas.

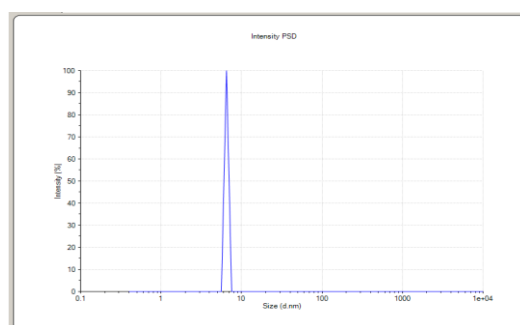


Figure A- 6 Particle Size Distribution of 1wt%  $\text{Al}_2\text{O}_3 + 0.1\text{wt}\%\text{SDBS}$  –deionised water nanofluid.

Figure A-6 shows the hydrodynamic particle size distribution of 1 vol% Al<sub>2</sub>O<sub>3</sub> + 0.1% SDBS –water nanofluid at 25°C, room temperature. The nanofluid formulated with 1g Al<sub>2</sub>O<sub>3</sub> nanopowder + 0.1% SDBS +98.90ml deionized water calcined at 25°C had the average aggregate size, 6.503 d. nm, total surface area of 0.255nm<sup>2</sup> Particle size distribution is less than 100nm, zetapotential of 170mV which showed excellent stability with pH of 3.28 and remained stable for more than 6months. The 1vol% Al<sub>2</sub>O<sub>3</sub> – water nanofluid has oil cleaning efficiency of 88% with mean viscosity of 2832.76 Pas.

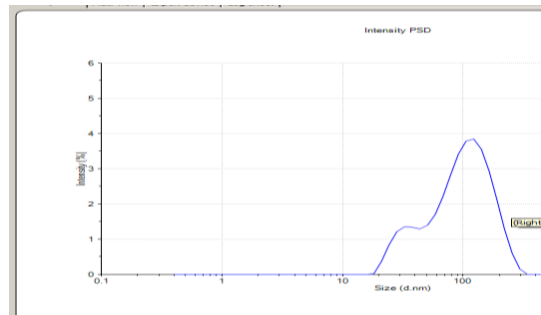


Figure A- 7 Particle size distribution of 0.3vol% TiO<sub>2</sub> water nanofluid without surfactant

Figure A-7 shows the hydrodynamic particle size distribution of 0.3 vol% TiO<sub>2</sub> –water nanofluid at 25°C, room temperature. The nanofluid formulated with 0.3g TiO<sub>2</sub> nanopowder +99.70ml deionised water calcined at 25°C had the average aggregate size, 45.09 d. nm, total surface area of 0.03114nm<sup>2</sup> Particle size distribution is less than 100nm, zetapotential of 120mV which showed excellent stability with pH of 4.26 and remained stable for more than 6months. The 0.3 vol% TiO<sub>2</sub> – water nanofluid has oil cleaning efficiency of 72% with mean viscosity of 8.98 x 10<sup>7</sup> Pas.

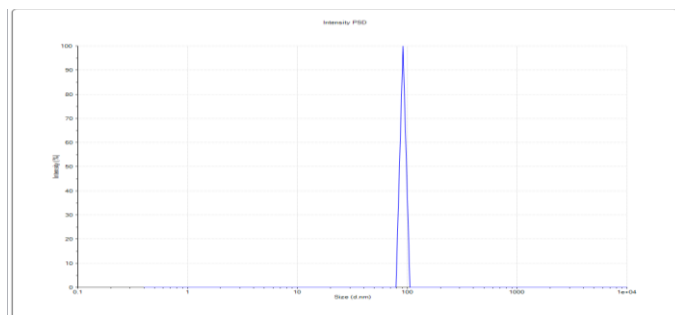


Figure A- 8 Particle Size Distribution of 0.3wt% TiO<sub>2</sub> + 0.03wt% SDBS – deionised water nanofluid.

Figure A-8 shows the hydrodynamic particle size distribution of 0.3 vol%

TiO<sub>2</sub> + 0.03% SDBS –water nanofluid at 25°C, room temperature. The nanofluid formulated with 0.3g TiO<sub>2</sub> nanopowder + 0.03%SDBS + 99 .67ml deionized water calcined at 25°C had the average aggregate size, 33.32 d. nm, total surface area of 0.04214nm<sup>2</sup>. Particle size distribution is less than 100nm, zetapotential of 277mV which showed excellent stability with pH of 1.23 and remained stable for more than 6months. The 0.3vol% 0.3wt%TiO<sub>2</sub> + 0.03wt%SDBS – water nanofluid has oil cleaning efficiency of 78% with mean viscosity of 10038.27 Pas.

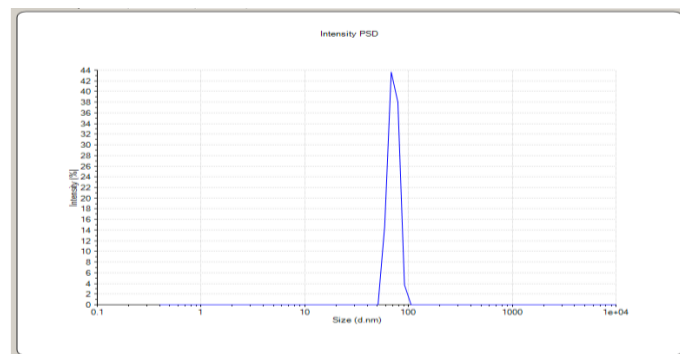


Figure A- 9 Particle size distribution of pure 0.7vol% TiO<sub>2</sub> water nanofluid

Figure A-9 shows the hydrodynamic particle size distribution of 0.7 vol%TiO<sub>2</sub> –water nanofluid at 25°C, room temperature. The nanofluid formulated with 0.7g TiO<sub>2</sub> nanopowder +99.30ml deionized water calcined at room temperature had the average aggregate size, 40 d. nm, total surface area of 0.03497nm<sup>2</sup>.With excellent stability of 178mV zetapotential and pH of 3.35, remained stable for more than 6months. The 0.7 vol% TiO<sub>2</sub> – water nanofluid has oil cleaning efficiency of 76% with mean viscosity of 0.0083568 Pas.

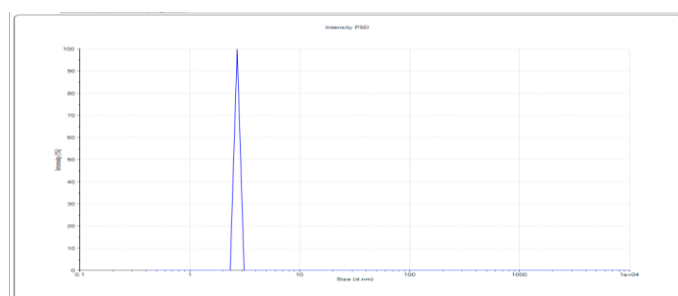


Figure A- 10 Particle Size Distribution of 0.7wt%TiO<sub>2</sub> + 0.07wt%SDBS – deionised water nanofluid.

Figure A-10 shows the hydrodynamic particle size distribution of 0.7 vol% TiO<sub>2</sub> +0.07%SDBS –water nanofluid at 25°C, room temperature.The nanofluid



formulated with 0.7g TiO<sub>2</sub> nanopowder +0.07%SDBS + 99.23ml deionized water calcined at 25°C had the average aggregate size, 2.696 d.nm, total surface area of 0.5188nm<sup>2</sup>. Particle size distribution is less than 100nm, zeta potential of 294mV which showed excellent stability with pH of 1.31 and remained stable for more than 6months. The 0.7vol% 0.7wt%TiO<sub>2</sub> + 0.07%SDBS – water nanofluid has oil cleaning efficiency of 88% with mean viscosity of 3530.9 Pas.

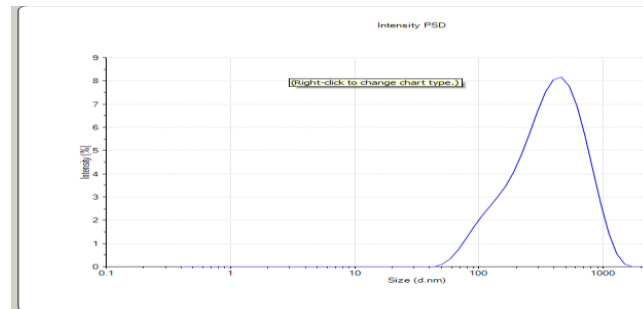


Figure A- 11 Particle size distribution of pure 1.0 vol% TiO<sub>2</sub> water nanofluid

Figure A-11 shows the hydrodynamic particle size distribution of 1 vol%TiO<sub>2</sub> –water nanofluid at 25°C, room temperature. The nanofluid formulated with 1g TiO<sub>2</sub> nanopowder +99ml deionized water calcined at room temperature had the average aggregate size, 71.66 d. nm, total surface area of 0.01946.nm<sup>2</sup>. Particle size distribution is less than 100nm, with excellent stability of 138mV zeta potential and pH of 4.08, remained stable for more than 6months. The 1 vol% TiO<sub>2</sub> – water nanofluid has oil cleaning efficiency of 84% with mean viscosity of 0.4075 Pas.

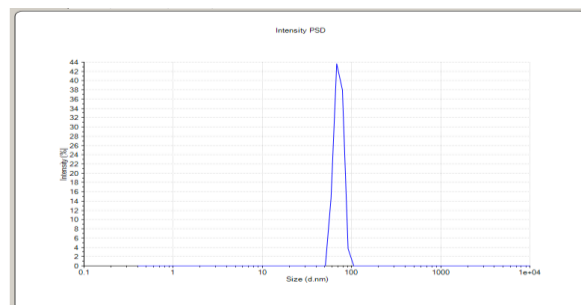


Figure A- 12 Particle Size Distribution of 1wt%TiO<sub>2</sub> + 0.1wt%SDBS – deionised water nanofluid.

Figure A-12 shows the hydrodynamic particle size distribution of 1 vol%TiO<sub>2</sub> + 0.1%SDBS –water nanofluid at 25°C, room temperature. The

nanofluid formulated with 1g TiO<sub>2</sub> nanopowder + 0.1%SDBS +98.90ml deionized water calcined at 25°C had the average aggregate size, 50.9 d. nm, total surface area of 0.02739nm<sup>2</sup>. Particle size distribution is less than 100nm, zetapotential of 273mV which showed excellent stability with pH of 1.30 and remained stable for more than 6months. The 1vol% TiO<sub>2</sub> + 0.1%SDBS – water nanofluid has oil cleaning efficiency of 99.4% with mean viscosity of 3467.01 Pas.

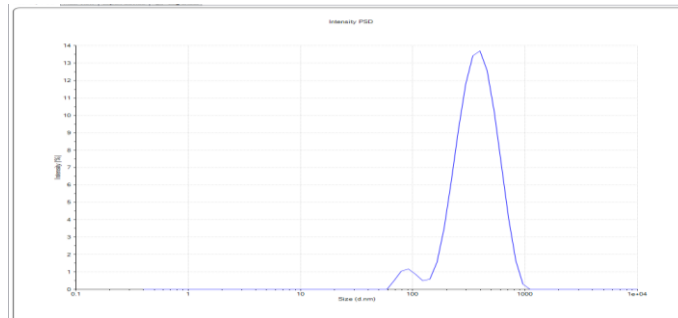


Figure A- 13 Particle Size Distribution of pure 0.3wt% ZnO -water nanofluid.

Figure A-13 shows the hydrodynamic particle size distribution of 0.3 vol%ZnO –water nanofluid at 25°C, room temperature. The nanofluid formulated with 0.3g ZnO nanopowder +99ml deionized water calcined at 25°C had the average aggregate size, 50 d. nm, total surface area of 0.02133nm<sup>2</sup>. Particle size distribution is less than 100nm, zetapotential of 63.4mV which showed excellent stability with pH of 7.89 and remained stable for more than 6months. The 0.3vol% ZnO – water nanofluid has oil cleaning efficiency of 62% with mean viscosity of 33.68 x 10<sup>4</sup>Pas.

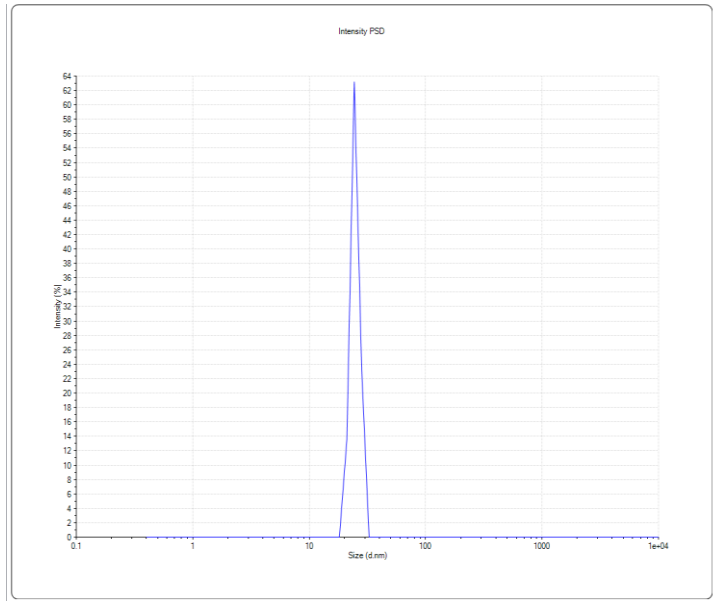


Figure A- 14 Particle Size Distribution of 0.3wt%ZnO + 0.15wt%Na<sub>2</sub>HPO<sub>4</sub> – deionised water nanofluid.

Figure A-14 shows the hydrodynamic particle size distribution of 0.3 vol%ZnO+ 0.15%Na<sub>2</sub>HPO<sub>4</sub> –water nanofluid at 25°C, room temperature. The nanofluid formulated with 0.3g ZnO nanopowder + 0.15%Na<sub>2</sub>HPO<sub>4</sub> + 99.55ml deionized water calcined at 25°C had the average aggregate size, 24.81, total surface area of 0.04298nm<sup>2</sup>. Particle size distribution is less than 100nm, zetapotential of -196mV which showed excellent stability with pH of 10.73 and remained stable for more than 6months. The 0.3vol% ZnO+ 0.15%Na<sub>2</sub>HPO<sub>4</sub> – water nanofluid has oil cleaning efficiency of 74% with mean viscosity of 350.812 Pas.

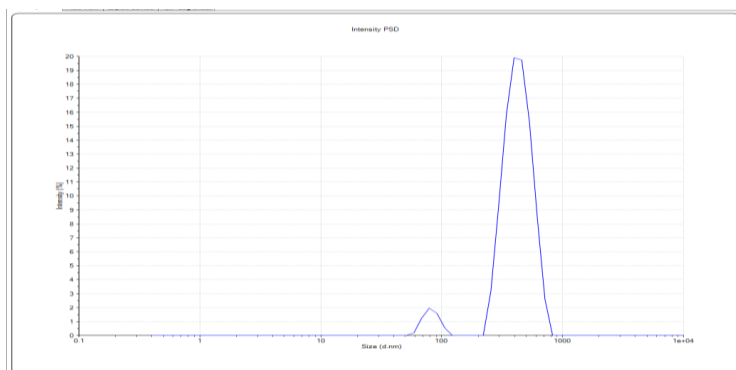


Figure A- 15 Particle Size Distribution of 0.7wt% pure ZnO water nanofluid.

Figure A-15 shows the hydrodynamic particle size distribution of 0.7 vol% ZnO –water nanofluid at 25°C, room temperature. The nanofluid formulated with 0.7g ZnO nanopowder +99ml deionised water calcined at 25°C had the average aggregate size, 82.02 d. nm, total surface area of 0.01295nm<sup>2</sup> Particle size distribution is less than 100nm, zetapotential of -60mV which showed excellent stability with pH of 8.85 and remained stable for more than 6months. The 0.7vol% ZnO – water nanofluid has oil cleaning efficiency of 63% with mean viscosity of 12.14 x 10<sup>-3</sup>Pas.

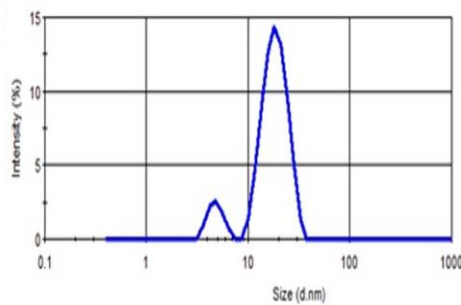


Figure A- 16 Particle Size Distribution of 0.7wt% surfactedZnO + 0.35wt% Na<sub>2</sub>HPO<sub>4</sub> – deionised water nanofluid.

Figure A-16 shows the hydrodynamic particle size distribution of 0.7 vol% ZnO + 0.35% Na<sub>2</sub>HPO<sub>4</sub> –water nanofluid at 25°C, room temperature. The nanofluid formulated with 0.7g ZnO nanopowder + 0.35% Na<sub>2</sub>HPO<sub>4</sub> +98.95ml deionised water calcined at 25°C had the average aggregate size, 20d.nm, total surface area of 0.0531nm<sup>2</sup>. Particle size distribution is less than 100nm, zetapotential of -205mV which showed excellent stability with pH of 10.93 and remained stable for more than 6months. The 0.7vol% ZnO+ 0.35% Na<sub>2</sub>HPO<sub>4</sub> – water nanofluid has oil cleaning efficiency of 90% with mean viscosity of 5101.99 Pas.

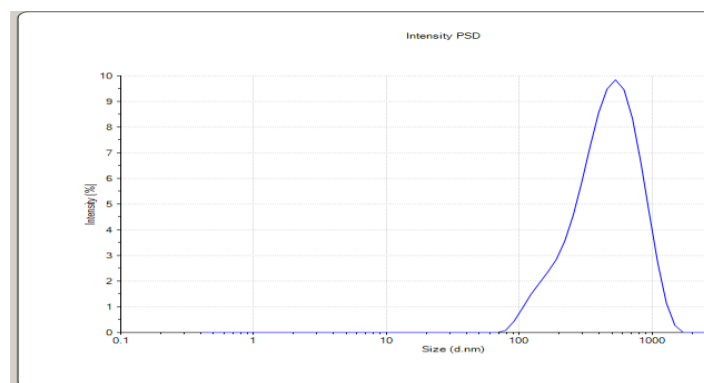


Figure A- 17 Particle Size Distribution of 1wt% pure ZnO -water nanofluid

Figure A-17 shows the hydrodynamic particle size distribution of 1.0 vol% ZnO –water nanofluid at 25°C, room temperature. The nanofluid formulated with 1.0g ZnO nanopowder +99ml deionized water calcined at 25°C had the average aggregate size, 86.4 d. nm, total surface area of 0.01226nm<sup>2</sup>. Particle size distribution is less than 100nm, zetapotential of -86.7mV which showed excellent stability with pH of 8.92 with stability lifespan of more than 6months. The 1.0vol% ZnO – water nanofluid has oil cleaning efficiency of 78% with mean viscosity of 13594 Pas.

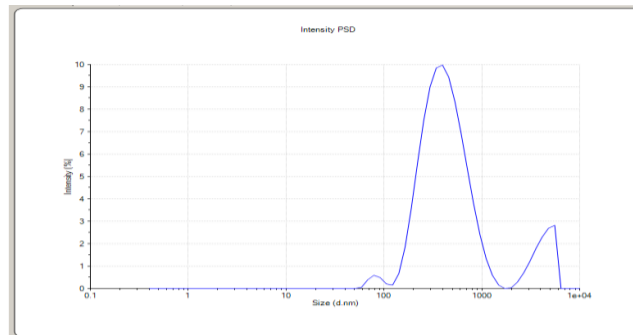


Figure A- 18 Particle Size Distribution of 1wt%ZnO + 0.5wt%Na<sub>2</sub>HPO<sub>4</sub> –deionised water nanofluid.

Figure A-18 shows the hydrodynamic particle size distribution of 1.0 vol%ZnO + 0.5% Na<sub>2</sub>HPO<sub>4</sub> –water nanofluid at 25°C, room temperature. The nanofluid formulated with 1.0g ZnO nanopowder + 0.5% Na<sub>2</sub>HPO<sub>4</sub> +98.50ml deionized water calcined at 25°C had the average aggregate size, 65.31 d.nm, total surface area of 0.1621 nm<sup>2</sup> Particle size distribution is less than 100nm, zetapotential of -140mV which showed excellent stability with pH of 8.98 and remained stable for more than 6months. The 1.0vol% ZnO+ 0.5wt%Na<sub>2</sub>HPO<sub>4</sub> – water nanofluid has oil cleaning efficiency of 98% with mean viscosity of 3491.29 Pas.

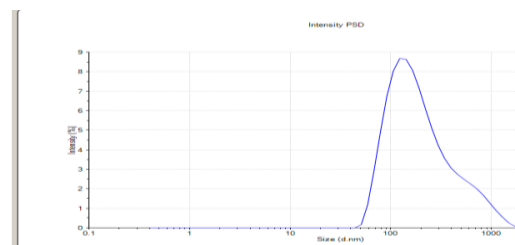


Figure A- 19 Particle size distribution of pure 0.3wt% Al<sub>2</sub>O<sub>3</sub> + 0.7wt% TiO<sub>2</sub> - deionised water nanofluid

Figure A-19 shows the hydrodynamic particle size distribution of 0.7TiO<sub>2</sub> + 0.3Al<sub>2</sub>O<sub>3</sub> vol% deionised water nanofluid at 25°C, room temperature. The nanofluid formulated with 0.7TiO<sub>2</sub> + 0.3Al<sub>2</sub>O<sub>3</sub> nanopowder +99ml deionized water calcined at 25°C had the average aggregate size, 45 d. nm, and total surface area of 0.0564nm<sup>2</sup>. Particle size distribution is less than 100nm, zetapotential of 196mV which showed good stability with pH of 3.04 and remained stable for more than 6months. The 0.7 TiO<sub>2</sub> + 0.3Al<sub>2</sub>O<sub>3</sub> vol% deionised water nanofluid has oil cleaning efficiency of 70% with mean viscosity of 62592.48 Pas.

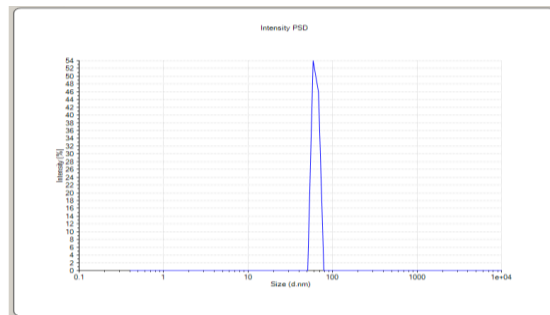


Figure A- 20 Particle size distribution of 0.3wt% Al<sub>2</sub>O<sub>3</sub> + 0.7wt% TiO<sub>2</sub> + 0.1wt% SDBS - deionised water nanofluid

Figure A-20 shows the hydrodynamic particle size distribution of 0.3wt%Al<sub>2</sub>O<sub>3</sub> + 0.7wt%TiO<sub>2</sub> + 0.1wt% SDBS vol% deionised water nanofluid at 25°C, room temperature. The nanofluid formulated with 0.3wt%Al<sub>2</sub>O<sub>3</sub> + 0.7wt%TiO<sub>2</sub> nanopowder +99ml deionized water calcined at 25°C had the average size diameter of 60 d. nm and total surface area of 0.5460nm<sup>2</sup>. Particle size distribution is less than 100nm, zetapotential of 108mV which showed good stability with pH of 2.91 and stability lifespan of more than 6months. The 0.3wt% Al<sub>2</sub>O<sub>3</sub> + 0.7wt%TiO<sub>2</sub> + 0.1wt% SDBS vol% deionised water nanofluid has oil cleaning efficiency of 87.4% with mean viscosity of 2.973 x 10<sup>-3</sup> Pas.

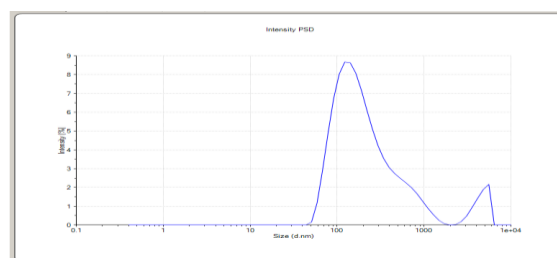


Figure A- 21 Particle size distribution of 0.7 pureAl<sub>2</sub>O<sub>3</sub> + 0.3 TiO<sub>2</sub>deionised water nanofluid

Figure A-21 shows the hydrodynamic particle size distribution of 0.7Al<sub>2</sub>O<sub>3</sub> + 0.3TiO<sub>2</sub> vol% deionised water nanofluid at 25°C, room temperature. The nanofluid formulated with 0.7 Al<sub>2</sub>O<sub>3</sub> + 0.3 TiO<sub>2</sub> nanopowder +99ml deionized water calcined at 25°C had the average aggregate size, 44.68 d. nm and total surface area of 0.0539nm<sup>2</sup>. Particle size distribution is less than 100nm, zetapotential of 167mV which showed good stability with pH of 3.62 and remained stable for more than 6months. The 0.7 Al<sub>2</sub>O<sub>3</sub> + 0.3 TiO<sub>2</sub> vol% deionised water nanofluid has oil cleaning efficiency of 68% with mean viscosity of 1.4026 x 10<sup>-2</sup> Pas.

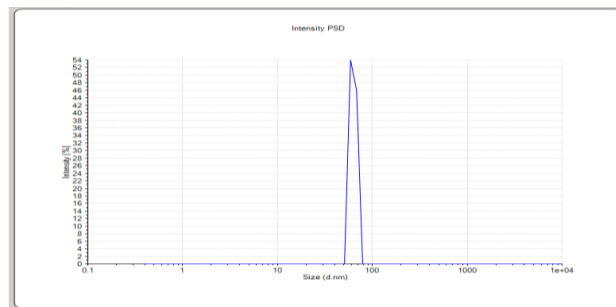


Figure A- 22 Particle size distribution of 0.3wt% TiO<sub>2</sub> + 0.7wt%Al<sub>2</sub>O<sub>3</sub> + 0.03wt%SDBS + 0.07wt%SDBS – deionised water nanofluid.

Figure A-22 shows the hydrodynamic particle size distribution of 0.7 Al<sub>2</sub>O<sub>3</sub> + 0.3 TiO<sub>2</sub> + 0.03wt%SDBS + 0.07wt%SDBS vol% deionised water nanofluid at 25°C, room temperature.The nanofluid formulated with 0.3wt%TiO<sub>2</sub> + 0.7wt%Al<sub>2</sub>O<sub>3</sub> + 0.03wt%SDBS + 0.07wt%SDBS – deionised water nanofluid +98.99ml deionized water calcined at 25°C had the average aggregate size, 25 d. nm and total surface area of 0.1335nm<sup>2</sup>.Particle size distribution is less than 100nm, zetapotential of 146mV which showed excellent stability with pH of 3.93 and stability lifespan of more than 6months.The 0.3wt% TiO<sub>2</sub> + 0.7wt%Al<sub>2</sub>O<sub>3</sub> + 0.03wt%SDBS + 0.07wt%SDBS – deionised water nanofluid has oil cleaning efficiency of 80% with mean viscosity of 2.7 x 10<sup>-3</sup> Pas.

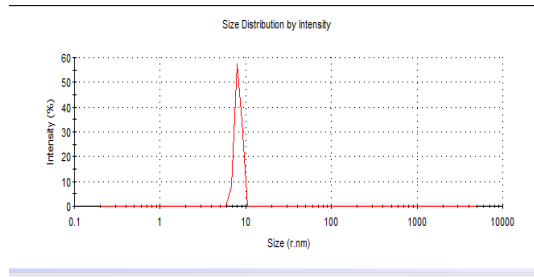


Figure A- 23 Particle size distribution of pure 0.3Al<sub>2</sub>O<sub>3</sub> + 0.7ZnO vol% deionised water nanofluid

FigureA-23 shows the hydrodynamic particle size distribution of 0.3 Al<sub>2</sub>O<sub>3</sub>+ 0.7ZnO vol% –water nanofluid at 25°C, room temperature.The nanofluid formulated with 0.7gZnO + 0.3gAl<sub>2</sub>O<sub>3</sub> nanopowder +99ml deionized water calcined at room temperature had the average aggregate size, 8.184 d.nm, and total surface area of 0.03438nm<sup>2</sup>.With excellent stability of 88mV zetapotential and pH of 8.89, remained stable for more than 6months.The 0.3Al<sub>2</sub>O<sub>3</sub> + 0.7 ZnO vol% – water nanofluid has oil cleaning efficiency of 71% with mean viscosity of 11.54682 x 10<sup>3</sup> pas.

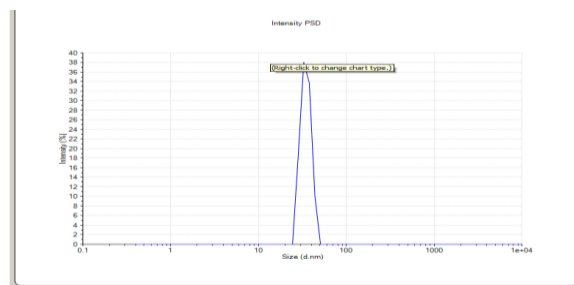


Figure A- 24 Particle size distribution of 0.7wt%ZnO + 0.3wt% Al<sub>2</sub>O<sub>3</sub> + 0.35wt%Na<sub>2</sub>HPO<sub>4</sub> + 0.03wt%SDBS

Figure A-24 shows the hydrodynamic particle size distribution of 0.7ZnO + 0.3Al<sub>2</sub>O<sub>3</sub> vol% deionised water nanofluid at 25°C, room temperature.The nanofluid formulated with 0.7ZnO + 0.3Al<sub>2</sub>O<sub>3</sub> nanopowder + 0.35wt%Na<sub>2</sub>HPO<sub>4</sub> + 0.03wt%SDBS - +98.62ml deionized water calcined at 25°C had the average aggregate size, 34.73 d. nm and total surface area of 0.08031nm<sup>2</sup>.Particle size distribution is less than 100nm, zetapotential of -167mV which showed excellent stability with pH of 9.66 and remained stable for more than 6months.



The 0.7ZnO + 0.3Al<sub>2</sub>O<sub>3</sub> + 0.35wt%Na<sub>2</sub>HPO<sub>4</sub> + 0.03wt%SDBS vol% deionised water nanofluid has oil cleaning efficiency of 80%, mean viscosity of 2.808 x 10<sup>-3</sup> Pas.

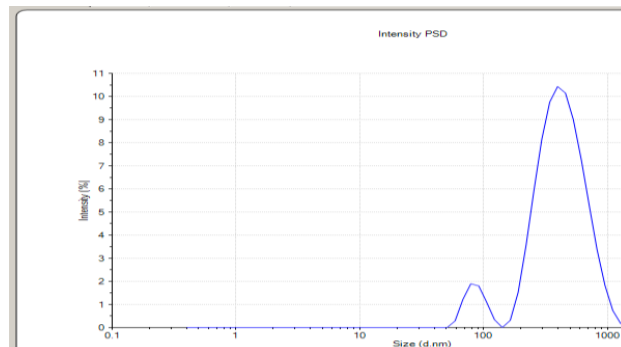


Figure A- 25 Particle size distribution of pure 0.3ZnO + 0.7Al<sub>2</sub>O<sub>3</sub> vol% deionised water nanofluid

Figure A-25 shows the hydrodynamic particle size distribution of 0.3ZnO + 0.7Al<sub>2</sub>O<sub>3</sub> vol% deionised The nanofluid formulated with 0.3ZnO + 0.7Al<sub>2</sub>O<sub>3</sub> nanopowder +99ml deionized water calcined at 25°C had the average aggregate size, 86.01 d. nm, total surface area of 0.0580nm<sup>2</sup>.Particle size distribution is less than 100nm, zetapotential of 48mV which showed good stability with pH of 7.45 and remained stable for more than 6months.The 0.3ZnO + 0.7Al<sub>2</sub>O<sub>3</sub> vol% deionised water nanofluid has oil cleaning efficiency 62%, mean viscosity of 1.499 Pas.

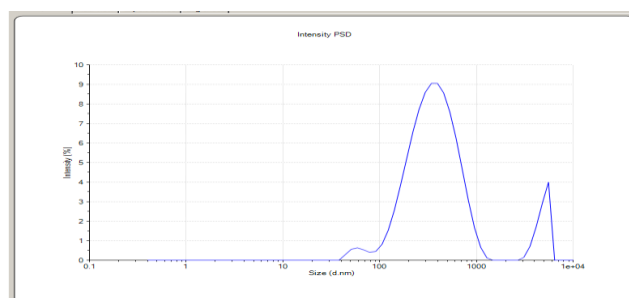


Figure A- 26 Particle size distribution of 0.3wt% ZnO + 0.7wt% Al<sub>2</sub>O<sub>3</sub> + 0.15wt% Na<sub>2</sub>HPO<sub>4</sub> + 0.07wt% SDBS – deionised water.

Figure A-26 shows the hydrodynamic particle size distribution of 0.3wt% ZnO + 0.7wt% Al<sub>2</sub>O<sub>3</sub> + 0.15wt% Na<sub>2</sub>HPO<sub>4</sub> + 0.07wt% SDBS – deionised water nanofluid at 25°C, room temperature.The nanofluid formulated with 0.3wt% ZnO + 0.7wt% Al<sub>2</sub>O<sub>3</sub> + 0.15wt% Na<sub>2</sub>HPO<sub>4</sub> + 0.07wt% SDBS nanopowder and surfactants +99ml deionized water calcined at room temperature had the average aggregate size, 40.58d.nm, total surface area of 0.1454.nm<sup>2</sup>.With stability of -156mV

zeta potential and pH of 9.31, stability lifespan of more than 6 months. The 0.3wt% ZnO + 0.7wt% Al<sub>2</sub>O<sub>3</sub> + 0.15wt% Na<sub>2</sub>HPO<sub>4</sub> + 0.07wt% SDBS vol% – water nanofluid has oil cleaning efficiency of 76% with mean viscosity of 13298.16

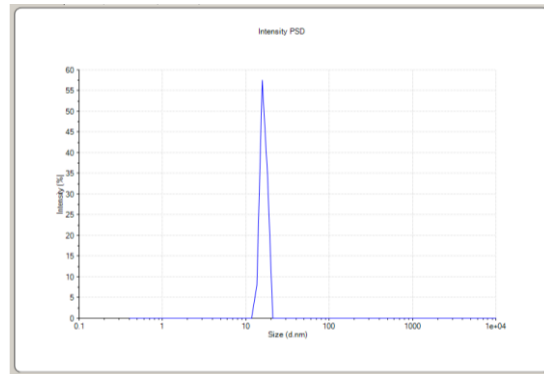


Figure A- 27 Particle size distribution of pure 0.3TiO<sub>2</sub> + 0.7 ZnO vol% deionised water nanofluid.

Figure A-27 shows the hydrodynamic particle size distribution of 0.7ZnO + 0.3TiO<sub>2</sub> vol% –water nanofluid at 25°C, room temperature. The nanofluid formulated with 0.7gZnO + 0.3gTiO<sub>2</sub> nanopowder +99ml deionized water calcined at room temperature had the average aggregate size, 16.37 d. nm, and total surface area of 0.03022nm<sup>2</sup>. With stability of -44mV zeta potential and pH of 7.35, stability lifespan of more than 3 months. The 0.3TiO<sub>2</sub> + 0.7 ZnO vol% – water nanofluid has oil cleaning efficiency of 68% with mean viscosity of 6.88 x 10<sup>4</sup> pas.

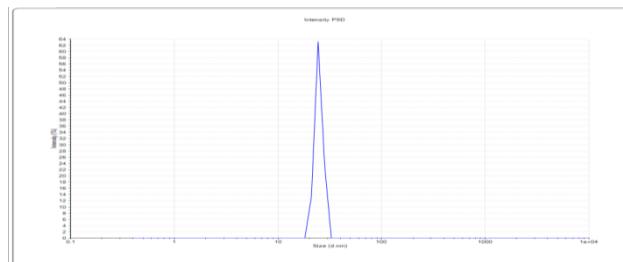


Figure A- 28 Particle size distribution of 0.7ZnO + 0.3TiO<sub>2</sub> + 0.35wt%Na<sub>2</sub>HPO<sub>4</sub> + 0.03wt%SDBS – deionised water

Figure A-28 shows the hydrodynamic particle size distribution of 0.7ZnO + 0.3TiO<sub>2</sub> + 0.35wt% Na<sub>2</sub>HPO<sub>4</sub> + 0.03wt% SDBS vol% deionised water nanofluid at 25°C, room temperature. The nanofluid formulated with 0.7ZnO + 0.3TiO<sub>2</sub> + 0.35wt% Na<sub>2</sub>HPO<sub>4</sub> + 0.03wt% SDBS nanopowder +98.62ml deionized water calcined at 25°C had the average aggregate size, 26.36d.nm and total surface area of 0.08424nm<sup>2</sup>. The particle size distribution is less than 100nm,

zeta potential of 121mV which showed excellent stability with pH of 3.85 and remained stable for more than 6 months. The 0.7ZnO + 0.3TiO<sub>2</sub> + 0.35wt% Na<sub>2</sub>HPO<sub>4</sub> + 0.03wt% SDBS – deionised water nanofluid has oil cleaning efficiency of 72% with mean viscosity of 8.84 x 10<sup>4</sup> Pas.

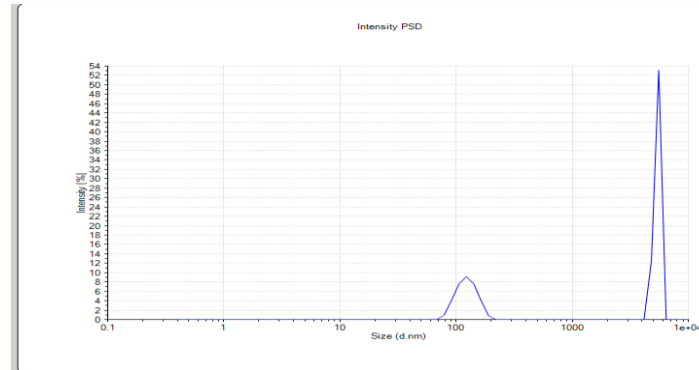


Figure A- 29 Particle size distribution of 0.3ZnO + 0.7TiO<sub>2</sub> vol% –water nanofluid

Figure A-29 shows the hydrodynamic particle size distribution of 0.3ZnO + 0.7TiO<sub>2</sub> vol% –water nanofluid at 25°C, room temperature. The nanofluid formulated with 0.3gZnO + 0.7gTiO<sub>2</sub> nanopowder + 99ml deionized water calcined at room temperature had the average aggregate size, 62.23 d. m, and total surface area of 0.05629nm<sup>2</sup>, with excellent stability of 78mV zeta potential and pH of 5.24, remained stable for more than 3 months. The 0.3ZnO + 0.7TiO<sub>2</sub> vol% – water nanofluid has oil cleaning efficiency of 70% with mean viscosity of 69715.3 pas.

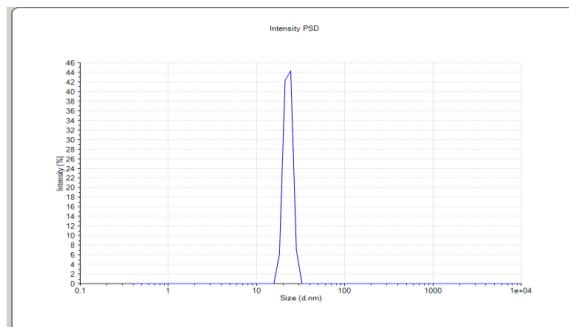


Figure A- 30 Particle size distribution of 0.3wt%ZnO + 0.7wt%TiO<sub>2</sub> + 0.15wt%Na<sub>2</sub>HPO<sub>4</sub> + 0.07wt%SDBS -deionised water nanofluid

Figure.A-30 shows the hydrodynamic particle size distribution of 0.3ZnO + 0.7TiO<sub>2</sub> + 0.15wt%Na<sub>2</sub>HPO<sub>4</sub> + 0.07wt%SDBS vol% –water nanofluid at 25°C, room temperature. The nanofluid formulated with 0.3gZnO + 0.7g TiO<sub>2</sub> + 0.15wt%Na<sub>2</sub>HPO<sub>4</sub> + 0.07wt%SDBS nanopowder + 99ml deionized water calcined at

room temperature had the average aggregate size, 23.16d.nm, total surface area of 0.5617 nm<sup>2</sup>. With excellent stability of 86mV zetapotential and pH of 5.24, remained stable for more than 3months. The 0.3ZnO + 0.7TiO<sub>2</sub> + 0.15Na<sub>2</sub>HPO<sub>4</sub> + 0.07SDBS vol% – water nanofluid has oil cleaning efficiency of 78% with mean viscosity of 19101 pas.

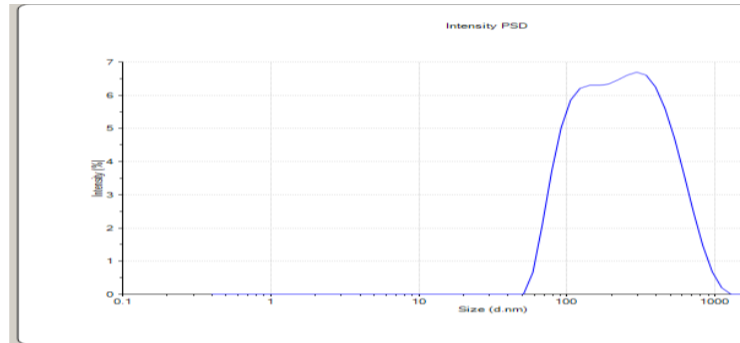


Figure A- 31 Particle size distribution of pure 0.3Al<sub>2</sub>O<sub>3</sub> + 0.3TiO<sub>2</sub> + 0.3ZnO vol% deionised water nanofluid.

Figure A-31 shows the hydrodynamic particle size distribution of 0.3Al<sub>2</sub>O<sub>3</sub> + 0.3TiO<sub>2</sub> + 0.3ZnO vol% –water nanofluid at 25°C, room temperature. The nanofluid formulated with 0.3gAl<sub>2</sub>O<sub>3</sub> + 0.3gTiO<sub>2</sub> + 0.3gZnO nanopowder +99ml deionized water calcined at room temperature had the average aggregate size, 50 d. nm,.total surface area of 0.06003nm<sup>2</sup> with excellent stability of 73mV zetapotential and pH of 5.19, remained stable for more than 6months. The 0.3Al<sub>2</sub>O<sub>3</sub> + 0.3TiO<sub>2</sub> + 0.3ZnO vol% – water nanofluid has oil cleaning efficiency of 74% with mean viscosity of 7.77 x 10<sup>-4</sup> pas.

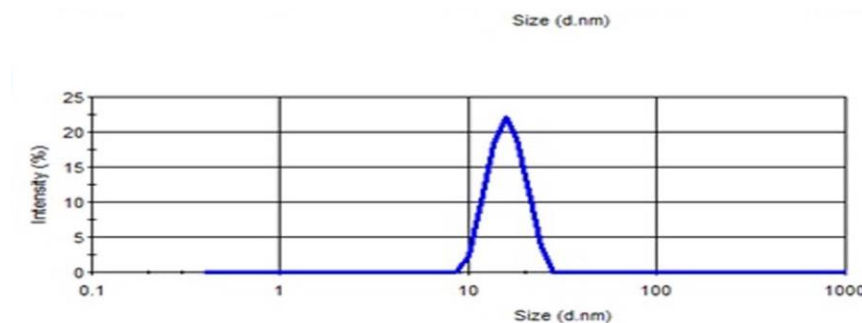


Figure A- 32 Particle size distribution of surfacted 0.3Al<sub>2</sub>O<sub>3</sub> + 0.3TiO<sub>2</sub> + 0.3ZnO vol% deionised water nanofluid

Figure A-32 shows the hydrodynamic particle size distribution of 0.3Al<sub>2</sub>O<sub>3</sub> + 0.3TiO<sub>2</sub> + 0.3ZnO vol% –water nanofluid at 25°C, room temperature. The nanofluid formulated with 0.3gAl<sub>2</sub>O<sub>3</sub> + 0.3gTiO<sub>2</sub> + 0.3gZnO nanopowder

+0.03gSDBS +0.03gSDBS + 0.15gNa<sub>2</sub>HPO<sub>4</sub>+99ml deionized water calcined at room temperature had the average aggregate size, 9.963.0 d.nm, total surface area of 0.10133nm<sup>2</sup> with excellent stability of 118mV zetapotential and pH of 3.74, remained stable for more than 6months.The 0.3Al<sub>2</sub>O<sub>3</sub> + 0.3TiO<sub>2</sub> + 0.3ZnO vol% – water nanofluidhas oil cleaning efficiency of 92% with mean viscosity of 9.195 x 10<sup>-4</sup> pas

B.Results from the measurements of soil sample and fluid properties

B.1 Permeability measurements

B.1 is the measurement of porosity results.

Table A- 8 Porosity (%) measurement

0 – 10cm	10 – 30cm
14.1± 0.97	9.3 ± 0.90
16.1± 0.79	11.7 ± 0.36
14.5 ± 0.8	11.0 ± 0.38
14.2 ± 0.64	14.0 ± 0.67

Table A-8 shows that porosity decreases with increase in soil depth.

Table A- 9 Result of bulk density (g/m<sup>3</sup>) measurements

0 – 10cm	10 – 30cm
± 0.03	1.62 ± 0.04
± 0.01	1.57 ± 0.02

TableA-9 indicates that bulk density increases with soil depth.

B.2 Results from the mean permeability.

Table A- 10 Hydraulic conductivity (permeability) results

Q (cm <sup>3</sup> )	L (cm)	A (cm <sup>2</sup> )	h (cm)	Time (mins)	K (cm/sec)
33.8	18	3.5	28	3	0.0345cm/sec= 3.45 x 10 <sup>-5</sup> m/s
33.6	18	3.5	28	3	0.032cm/sec = 3.2 x10 <sup>-5</sup> m/s
34.0	18	3.5	28	3	0.0347cm/sec = 3.47 x 10 <sup>-5</sup> m/s
				Mean K	3.36 x 10 <sup>-5</sup> m/s

Table A- 11 The density of mineral oil, nanofluids and distilled water was measured with a picnometer of 25ml at room temperature of 25°C.

Fluid	Wt (g)	Picnometer (cm <sup>3</sup> )	Density (g/cm <sup>3</sup> )
Mineral oil	22.38	25	0.895
Distilled water	24.979	25	0.99956
Pure nanofluid 0.3%	19.741	25	0.78964
0.7%	19.751	25	0.79004
1.0%	19.79	25	0.7916
Surfacted nanofluid 0.3%	24.979	25	0.99916
0.7%	25.003	25	1.00012
1.0%	23.47	25	1.0188

Table A- 12 Viscosity of different nanofluids without surfactants

Nanofl.syst.	0.3Al <sub>2</sub> O <sub>3</sub>	0.7Al <sub>2</sub> O <sub>3</sub>	1.0Al <sub>2</sub> O <sub>3</sub>	0.3TiO <sub>2</sub>	0.7TiO <sub>2</sub>	1.0TiO <sub>2</sub>	0.3ZnO	0.7ZnO	1.0ZnO
Temp(°C)	Viscosity(mPas)	Viscosity	Viscosity	Viscosity	Viscosity	Viscosity	Viscosity	Viscosity	Viscosity
20	2.15E8	0.8581	0.1627	1.687E8	0.0001929	2.035	8800	0.01275	4.07
30	4.255E7	0.5721	0.06084	1.008E8	0.005271	0.000784	7054	0.01805	2.71
40	2.372E6	0.1327	0.04056	8.91E7	0.00796	0.0006636	4438	0.0087	1.71
50	2.021E6	0.02717	0.01780	8.956E7	0.00462	0.000608	3151	0.004121	1.51
70	1.178E6	0.02174	0.01424	7.274E5	0.02374	0.00040533	1193	0.01707	1.21
Mean $\mu$	5.264E7	0.32236	0.05923	8.98E7	0.0083568	0.4075	33.68E4	0.012138	135

Table A- 13 Viscosity of different hybrid - water nanofluids without surfactants

Nanofl. Syst.	0.3Al <sub>2</sub> O <sub>3</sub> + 0.7TiO <sub>2</sub>	0.7Al <sub>2</sub> O <sub>3</sub> + 0.3TiO <sub>2</sub>	0.3 ZnO + 0.7TiO <sub>2</sub>	0.7 ZnO + 0.3TiO <sub>2</sub>	0.3 ZnO + 0.7Al <sub>2</sub> O <sub>3</sub>	0.7 ZnO + 0.3Al <sub>2</sub> O <sub>3</sub>	0.3Al <sub>2</sub> O <sub>3</sub> + 0.3TiO <sub>2</sub>

							+ 0.3 ZnO
Temp (°C)	Viscosity( mPas)	Viscosit y(Pas)	Viscosity( mPas)	Viscosity( mPas)	Viscosit y(Pas)	Viscosity( mPas)	Viscosit y(Pas)
20	62267.5	0.00142 3	73939.6	108702	1.58863	12721.7	0.00121 6
30	54539.8	0.00139 15	66757.9	84128.7	1.47598	11239.2	0.00095 01
40	50162	0.00135 92	62857.6	69140.6	1.38687	9729.99	0.00071 26
50	46812.1	0.00124 0	60532.8	16378.7	1.26754	5164.69	0.00068 77
70	99181	0.00159 95	84488.6	163628	1.77456	18878.5	0.00103 1
Mean $\mu$	62592.48	0.01402 6	69715.3	88395.6	1.49872	11546.82	0.00077 7

Table A- 14 Viscosity of different monotype nanofluids with surfactants

Nanofl.syst.	0.3Al <sub>2</sub> O <sub>3</sub>	0.7Al <sub>2</sub> O <sub>3</sub>	1.0Al <sub>2</sub> O <sub>3</sub>	0.3ZnO	0.7ZnO	1.0ZnO	0.3TiO <sub>2</sub>	0.7TiO <sub>2</sub>	1.0TiO <sub>2</sub>
Temp(°C)	Viscosity(Pas)	Viscosity	Viscosity	Viscosity	Viscosity	Viscosity	Viscosity	Viscosity	Viscosity
20	75510	18500	4530	561	6164	4229	13820	2734.37	1876
30	30340	12333.33	3020	374	4109.33	2819.33	9213.33	1822.91	1250.67
40	16470	2070	2265	280.5	3082	2114.5	6910	2430.55	938
50	13176	992.7	1812	224.4	2465.6	1691.6	5528	1944.44	750.4
70	35390	1389.78	2536.8	314.16	9689	6602	14720	5177.67	12520
Mean $\mu$	34177.2	7057.162	2832.76	350.812	5101.99	3491.29	10038.27	3530.9	3467.01

Table A- 15 Viscosity of different hybrid nanofluids with surfactants

Nanofl. Syst.	0.3Al <sub>2</sub> O <sub>3</sub> + 0.7TiO <sub>2</sub>	0.7Al <sub>2</sub> O <sub>3</sub> + 0.3TiO <sub>2</sub>	0.3 ZnO + 0.7TiO <sub>2</sub>	0.7 ZnO + 0.3TiO <sub>2</sub>	0.3 ZnO + 0.7Al <sub>2</sub> O <sub>3</sub>	0.7 ZnO 0.3Al <sub>2</sub> O <sub>3</sub>
Temp(°C)	Viscosity(Pas)	Viscosity(Pas)	Viscosity(Pas)	Viscosity(Pas)	Viscosity(Pas)	Viscosity(P

20	0.003349	0.002926	16400	108702	9507	0.002655
30	0.003035	0.002743	10933	84128.7	9138	0.002616
40	0.002811	0.002341	5340	69140.6	8916	0.002428
50	0.001874	0.002743	4272	16378.7	7132.8	0.002358
70	0.003794	0.002743	58560	163628	31800	0.003983
Mean $\mu$	0.0029726	0.002700	19101	88395.6	13298.76	0.002808

Table A- 16 Viscosity of pure hybrid nanofluids

$0.3Al_2O_3 + 0.7TiO_2$	62267.5	54539.8	50162
$0.7Al_2O_3 + 0.3TiO_2$	0.001423	0.001392	0.001
$0.3Al_2O_3 + 0.7ZnO$	12721.7	11239.2	9729
$0.7Al_2O_3 + 0.3ZnO$	1.58863	1.47598	1.386
$0.3TiO_2 + 0.7ZnO$	108702	84128.7	69140
$0.7TiO_2 + 0.3ZnO$	73939.6	66757.9	62857
$0.3Al_2O_3 + 0.3TiO_2 + 0.3ZnO$	0.001216	0.00095	0.000

Table A- 17 Measured density of experimental mineral oil Hv160

Temp (oC)	Density (g/cm3)
10	0.886
15	0.8827
20	0.8792
25	0.8761
30	0.8728
35	0.8697
40	0.8665
	0.8633

Table A- 18 Measured density of different monotype nanofluids

Nanofluids	Density (g/cm3)	
	Pure	Surfacted
0.3Al2O3	0.9971	1.028
0.7Al2O3	0.9962	1.0598
1.0Al2O3	0.9998	1.0012
0.3TiO2	0.9968	1.0642
0.7TiO2	0.9955	1.0188
1.0TiO2	0.9986	1.0456



0.3ZnO	0.9977	1.0023
0.7ZnO	0.996	1.0356
1.0ZnO	0.9975	1.0432

Table A- 19 Measured density of different hybrid nanofluids

Nanofluids	Density (g/cm <sup>3</sup> )	
	Pure	Surfacted
0.3Al <sub>2</sub> O <sub>3</sub> +0.7TiO <sub>2</sub>	1.032	1.02
0.7Al <sub>2</sub> O <sub>3</sub> +		
0.3TiO <sub>2</sub>	1.777	1.018
0.3Al <sub>2</sub> O <sub>3</sub> +0.7ZnO	0.997	1.018
0.7Al <sub>2</sub> O <sub>3</sub> +0.3ZnO	1.684	1.701
0.3TiO <sub>2</sub> + 0.7ZnO	1.694	1.027
0.7TiO <sub>2</sub> + 0.3ZnO	1.773	1.034
0.3Al <sub>2</sub> O <sub>3</sub> +0.3TiO <sub>2</sub> + 0.3ZnO	1.76	1.657

C. Results from the total surface area of the different nanofluids is calculated using three equations:

1.  $A_T = npA_p \dots \dots \dots (Ci)$ , Where,  $np$  = total no. of nanoparticles which can be obtained from the peak of the particle size distribution graph of mass fraction of each of the experimental nanofluid.

$A_p$  is the area of each nanofluid =  $\pi d^2/4$ ,  $d$  = average diameter of the particle size distribution graph of mass fraction of each of the experimental nanofluid. The results are shown on Table C-1

2.  $A_s = \frac{6m \times 106}{PD} (\text{unit} - \text{m}^2/\text{g}) \dots \dots \dots (Cii)$

Where,  $m$  = mass fraction /concentration of nanoparticles (%).

$P$  = density of nanoparticle (g/cm<sup>3</sup>).

$D$  = diameter of nanofluid from the graph of particle size distribution (nm).

The results obtained from equation are shown on Table C.1.2

3.  $A_T = \frac{6(100 - W)}{PD} (\text{unit} - \text{nm}^2) \dots \dots \dots (Ciii)$

Where,  $100 - W = m$ .  $W$  = weight or mass fraction of nanoparticles (%)

$PD$  as defined in equation (Cii). The results obtained from equation are shown on Table A-20

Table A- 20 Total surface area of the different nanofluids calculated using equation (C1.1)

Nanofluid system	Total surface area (nm <sup>2</sup> ).	Surfacted nanofluids (nm <sup>2</sup> ).	Cleaning efficiency (%) PureNanofluids	Cleaning efficiency (%)

	pure nanofluids			Surfacted Nanofluids
0.3Al <sub>2</sub> O <sub>3</sub>	323.64	75.269	84	87
0.3TiO <sub>2</sub>	518.87	150.099	72	78
0.3ZnO	30.94	19.63	62	74
0.7Al <sub>2</sub> O <sub>3</sub>	112.37	11.425	70	76
0.7TiO <sub>2</sub>	105.56	0.57	76	88
0.7ZnO	105.67	46.50	63	90
1.0Al <sub>2</sub> O <sub>3</sub>	33.13	33.21	74	84
1.0TiO <sub>2</sub>	177.46	162.79	84	99.4
1.0ZnO	586.30	335.0	78	98
0.3Al <sub>2</sub> O <sub>3</sub> +0.7TiO <sub>2</sub>	146.00	127.23	70	87.4
0.7Al <sub>2</sub> O <sub>3</sub> +0.3TiO <sub>2</sub>	136.41	36.82	68	80
0.3Al <sub>2</sub> O <sub>3</sub> +0.7ZnO	113.10	30.51	71	80
0.7Al <sub>2</sub> O <sub>3</sub> +0.3ZnO	116.20	31.04	62	76
0.3TiO <sub>2</sub> +0.7ZnO	272.87	74.14	68	72
0.7TiO <sub>2</sub> +0.3ZnO	273.74	49.28	70	78
0.3Al <sub>2</sub> O <sub>3</sub> +0.3TiO <sub>2</sub> +0.3ZnO	133.52	7.64	74	92

Table A- 21 Total surface area of the different nanofluids calculated using equation (C1.2)

Nanofluid system	Total surface area (m <sup>2</sup> /g).pure nanofluids	Surfacted nanofluids	Cleaning efficiency (%) Pure Nanofluids	Cleaning efficiency (%) Surfacted Nanofluids
0.3Al <sub>2</sub> O <sub>3</sub>	6447.33	8186.92	84	87
0.3TiO <sub>2</sub>	25848.49	72171.89	72	78
0.3ZnO	46291.01	237185.37	62	74
0.7Al <sub>2</sub> O <sub>3</sub>	5198.51	9370.93	70	76
0.7TiO <sub>2</sub>	24647.89	365695.66	76	88
0.7ZnO	19654.63	27670.94	63	90
1.0Al <sub>2</sub> O <sub>3</sub>	6417.11	12932.51	74	84

1.0TiO <sub>2</sub>	9127.81	37433.16	84	99.4
1.0ZnO	12378.69	16376.03	78	98
0.3Al <sub>2</sub> O <sub>3</sub> +0.7TiO <sub>2</sub>	31095.22	373882.58	70	87.4
0.7Al <sub>2</sub> O <sub>3</sub> +0.3TiO <sub>2</sub>	31047	81542.82	68	80
0.3Al <sub>2</sub> O <sub>3</sub> +0.7ZnO	15575.14	45620.08	71	80
0.7Al <sub>2</sub> O <sub>3</sub> +0.3ZnO	32265.6	85104.4	62	76
0.3TiO <sub>2</sub> +0.7ZnO	14326.32	46804.09	68	72
0.7TiO <sub>2</sub> +0.3ZnO	31065	378628.17	70	78
0.3Al <sub>2</sub> O <sub>3</sub> +0.3TiO <sub>2</sub> +0.3ZnO	18062.95	30490.36	74	92

Table A- 22 Total surface area of the different nanofluids calculated using equation (C.1.3)[106]

Nanofluid system	Total surface area (nm <sup>2</sup> ). Pure nanofluids	Surfacted nanofluids(nm <sup>2</sup> )	Cleaning efficiency (%) Pure Nanofluids	Cleaning efficiency (%) Surfacted Nanofluids
0.3Al <sub>2</sub> O <sub>3</sub>	0.021427	0.027208	84	87
0.3TiO <sub>2</sub>	0.0172764	0.031143	72	78
0.3ZnO	0.021326	0.042979	62	74
0.7Al <sub>2</sub> O <sub>3</sub>	0.036668	0.102381	70	76
0.7TiO <sub>2</sub>	0.034965	0.51877	76	88
0.7ZnO	0.012948	0.05310	63	90
1.0Al <sub>2</sub> O <sub>3</sub>	0.0458281	0.254814	74	84
1.0TiO <sub>2</sub>	0.019458	0.027394	84	99.4
1.0ZnO	0.012255	0.162122	78	98
0.3Al <sub>2</sub> O <sub>3</sub> +0.7TiO <sub>2</sub>	0.056392	0.545978	70	87.4
0.7Al <sub>2</sub> O <sub>3</sub> +0.3TiO <sub>2</sub>	0.0539444	0.133524	68	80
0.3Al <sub>2</sub> O <sub>3</sub> +0.7ZnO	0.034375	0.080308	71	80
0.7Al <sub>2</sub> O <sub>3</sub> +0.3ZnO	0.057994	0.145336	62	76
0.3TiO <sub>2</sub> +0.7ZnO	0.0302244	0.084243	68	72
0.7TiO <sub>2</sub> +0.3ZnO	0.056291	0.561749	70	78

0.3Al <sub>2</sub> O <sub>3</sub> +0.3TiO <sub>2</sub> +0.3ZnO	0.0600294	0.10133	74	92
--	-----------	---------	----	----

D. Results from the surface tension of both pure and surfacted nanofluids.

Table A- 23 Surface tension results

Nanofluid system	Volume (μL)	Area (mm <sup>2</sup> )	Surface tension (Nm/m)	Density (g/cm <sup>3</sup> )	Density, pw
1 vol% Al <sub>2</sub> O <sub>3</sub>	4.5330	12.87	39.76		0.9986 g/cm <sup>3</sup>
1 vol% TiO <sub>2</sub>	7.2528	18.08	52.46		Density of air = 0.0013g/cm <sup>3</sup>
1 vol% ZnO	8.6725	20.27	46.74		Surface tension for water = 72.80Nm/m

Table A- 24 Surface tension of the different nanofluids

Nanofluid system	Surface tension	
	Pure nanofluids	Surfacted nanofluids
0.3Al <sub>2</sub> O <sub>3</sub>	33.95	26.711
0.3TiO <sub>2</sub>	43.2036	29.0322
0.3ZnO	44.87	30.152
0.7Al <sub>2</sub> O <sub>3</sub>	44.27	29.7488
0.7TiO <sub>2</sub>	39.4482	26.2265
0.7ZnO	60.953	41.3855
1.0Al <sub>2</sub> O <sub>3</sub>	39.76	26.4338
1.0TiO <sub>2</sub>	52.46	17.1678
1.0ZnO	46.74	25.3023

0.7TiO <sub>2</sub>	+		
0.3Al <sub>2</sub> O <sub>3</sub>		69.0923	54.36
0.7ZnO	+		
0.3Al <sub>2</sub> O <sub>3</sub>		42.0545	28.26
0.3ZnO			
+0.7Al <sub>2</sub> O <sub>3</sub>		47.6593	25.8
0.3ZnO			
+0.7TiO <sub>2</sub>		50.2056	16.43
0.3TiO <sub>2</sub>	+		
0.7Al <sub>2</sub> O <sub>3</sub>		65.5253	44.49
0.7ZnO	+		
0.3TiO <sub>2</sub>		31.4966	20.94
0.3Al <sub>2</sub> O <sub>3</sub>	+		
0.3TiO <sub>2</sub>			
+0.3ZnO		45.3651	36.6

E Thermal Conductivity enhancement (%)

Table A- 25 Thermal Conductivity enhancement (%)

Nanofluid system	K (%)
0.3 Al <sub>2</sub> O <sub>3</sub>	2.34
0.7 Al <sub>2</sub> O <sub>3</sub>	0.51
1.0 Al <sub>2</sub> O <sub>3</sub>	0.52
0.3 TiO <sub>2</sub>	0.57
0.7 TiO <sub>2</sub>	0.72
1.0 TiO <sub>2</sub>	0.32
0.3 ZnO	0.93
0.7 ZnO	1.05
1.0 ZnO	0.3
0.3Al <sub>2</sub> O <sub>3</sub> + .7TiO <sub>2</sub>	Enhancement(% )17.62
0.7Al <sub>2</sub> O <sub>3</sub> + 0.3TiO <sub>2</sub>	71.34

0.3Al <sub>2</sub> O <sub>3</sub> + 0.7ZnO	44.41
0.7Al <sub>2</sub> O <sub>3</sub> + 0.3ZnO	63.05
0.3TiO <sub>2</sub> + o.7ZnO	59.95
0.7TiO <sub>2</sub> + 0.3ZnO	90.82
0.3Al <sub>2</sub> O <sub>3</sub> + 0.3TiO <sub>2</sub> + 0.3ZnO	92.08

Table A- 26 Thermal conductivity (W/m-k) of the various hybrid nanofluids

Nanofluids	Thermal Conductivity (W/m-k)	
	Without surfactants	With surfactants
	0.3Al <sub>2</sub> O <sub>3</sub> + 0.7TiO <sub>2</sub>	3.914008
0.7Al <sub>2</sub> O <sub>3</sub> + 0.3TiO <sub>2</sub>	0.370131	1.291271
0.3Al <sub>2</sub> O <sub>3</sub> + 0.7ZnO	8.54148	15.36629
0.7Al <sub>2</sub> O <sub>3</sub> + 0.3ZnO	0.245358	0.664058
0.3TiO <sub>2</sub> + o.7ZnO	0.139846	0.349196
0.7TiO <sub>2</sub> + 0.3ZnO	0.190509	2.074659
0.3Al <sub>2</sub> O <sub>3</sub> + 0.3TiO <sub>2</sub> + 0.3ZnO	0.169155	2.137045

Table A- 27 Thermal conductivity of the various Monotype nanofluids

Nanofluids

	without surfactants	
0.3Al <sub>2</sub> O <sub>3</sub>	3.785	9.9399
0.7Al <sub>2</sub> O <sub>3</sub>	0.09714	1.4788
1.0Al <sub>2</sub> O <sub>3</sub>	0.11096	1.5764
0.3TiO <sub>2</sub>	0.1122	1.5777
0.7TiO <sub>2</sub>	0.129	2.0131
1.0TiO <sub>2</sub>	1.1765	2.0139
0.3ZnO	3.425	5.8116
0.7ZnO	0.134	2.8555
1.0ZnO	0.0896	0.8852

Table A- 28 Specific heat capacity and thermal capacity of the various nanofluids

0.3Al <sub>2</sub> O <sub>3</sub> + 0.7TiO <sub>2</sub>	10.867	12.8041
0.7Al <sub>2</sub> O <sub>3</sub> + 0.3TiO <sub>2</sub>	15.328	13.196
0.3Al <sub>2</sub> O <sub>3</sub> + 0.7ZnO	9.147	13.422
0.7Al <sub>2</sub> O <sub>3</sub> + 0.3ZnO	15.829	13.53
0.3TiO <sub>2</sub> + 0.7ZnO	5.099	17.254
0.7TiO <sub>2</sub> + 0.3ZnO	2.741	13.589
0.3Al <sub>2</sub> O <sub>3</sub> + 0.3TiO <sub>2</sub> + 0.3ZnO	12.115	12.646

Table A- 29 Specific heat capacity of the different nanofluids concentration (%)

Nanofluids	0.3	0.7	1
Al <sub>2</sub> O <sub>3</sub>	2.1158	1.1488	0.791
TiO <sub>2</sub>	1.9335	1.0271	0.7118
ZnO	2.1687	1.54	1.34

Table A- 30 Summary of thermal capacity of the different pure hybrid nanofluids

	Thermal capacity (KJ/Kg)	
	Pure	surfacted
0.3Al <sub>2</sub> O <sub>3</sub> + 0.7TiO <sub>2</sub>	10.867	12.8041
0.7Al <sub>2</sub> O <sub>3</sub> + 0.3TiO <sub>2</sub>	15.328	13.196
0.3Al <sub>2</sub> O <sub>3</sub> + 0.7ZnO	9.147	13.422
0.7Al <sub>2</sub> O <sub>3</sub> + 0.3ZnO	15.829	13.53
0.3TiO <sub>2</sub> + 0.7ZnO	5.099	17.254

0.7TiO <sub>2</sub> + 0.3ZnO	2.741	13.589
0.3Al <sub>2</sub> O <sub>3</sub> + 0.3TiO <sub>2</sub> + 0.3ZnO	12.115	12.646

Table A- 31 Thermal capacity of pure monotype nanofluids

Nanofluids	Concentration (%)		
	0.3	0.7	1
Al <sub>2</sub> O <sub>3</sub>	13.69	15.613	10.307
TiO <sub>2</sub>	14.11	13.167	6.288
ZnO	13.78	6.8113	5.453

Table A- 32 Thermal capacity of pure monotype nanofluids

Nanofluids	Concentration (%)		
	0.3	0.7	1
Al <sub>2</sub> O <sub>3</sub>	13.69	15.613	10.307
TiO <sub>2</sub>	14.11	13.167	6.288
ZnO	13.78	6.8113	5.453

G. Thermal optical/Absorbancy Results for the different nanofluids

Table A- 33 Pure nanofluids thermal optical results

	Wave length(nm)		Absorbancy (AU)		Wave length(nm)	
	0.3	0.7	0.3	0.7	0.3	0.7
Without surfactants						
Al <sub>2</sub> O <sub>3</sub>	620	0.262	381	1.506	619	0.50885
	623	0.27581	618	0.69873	627	0.49296
	642	0.25943	616	0.6963	624	0.49164
TiO <sub>2</sub>	645	0.27581	480	0.97838	617	0.50735
	730	1.7669	260	0.74327	615	0.76767
	1008	1.7577	280	0.45528	624	0.39296
ZnO	653	1.7485	957	1.7455	615	0.40437
	675	2.7729	619	1.3524	620	0.56045
	756	2.09708	641	1.3284	624	0.54711

Table A- 34 Results of thermal optical measurement for surfacted monotype nanofluids.



Wave length(nm)	Absorbancy (AU)	Wave length(nm)	Absorbancy (AU)	Wave length(nm)	Absorbancy (AU)
With surfactants					
	0.3		0.7		1
Al <sub>2</sub> O <sub>3</sub>	470	1.2555	470	1.779	254 2.5523
	462	1.2516	490	1.1415	432 1.4734
	492	1.2303	584	0.9246	462 1.43796
	656	0.86801	656	0.75129	657 0.91399
	624	0.99557	653	0.82896	621 1.0851
TiO <sub>2</sub>	615	1.0073	582	0.90468	582 1.126
	647	0.54777	777	0.43582	551 0.37082
	642	0.54727	705	0.43034	558 0.37038
	675	0.54701	621	0.41941	647 0.36842
	486	0.49721	486	0.38608	657 0.3395
ZnO	656	0.50445	656	0.40133	401 0.35882
	582	0.51814	582	0.40342	583 0.36051
	375	0.93875	374	1.1807	654 0.13644
	356	0.77595	653	0.13704	338 0.91544
	327	0.75344	657	0.88816	656 0.84841
	656	0.20323	374	1.1422	858 0.10159
	639	0.23494	590	0.19493	860 0.10192
	625	0.24025	625	0.17788	657 0.13275
ZnO		582	0.51814		582
		375	0.93875		374
		356	0.77595		653
		327	0.75344		657
		656	0.20323		374
		639	0.23494		590
		625	0.24025		625

Table A- 35 Thermal optical of the different nanofluids

Nanofluid system	Wave length(nm)	Absorbance (AU)	Wave length(nm)	Absorbance (AU)	Wave length(nm)	Absorbance (AU)
	0.3		0.7	1.506	1	0.50885
Al <sub>2</sub> O <sub>3</sub>	620	0.262	381	0.69873	619	0.49296
	623	0.27581	618	0.6963	627	0.49164
	642	0.25943	616	0.97838	624	0.50735
TiO <sub>2</sub>	645	0.27581	480	0.74327	617	0.76767
	730	1.7669	260	0.45528	615	0.39296
	1008	1.7577	280	1.7455	624	0.40437
ZnO	653	1.7485	957	1.3524	615	0.56045
	675	2.7729	619	1.3284	620	0.54711
	756	2.09708	641		624	

#### H. Summary of the wettability of the different nanofluids

Table A- 36 Wettability index of pure nanofluids

Nanofluid system	lw	lo	lwo
0.3Al <sub>2</sub> O <sub>3</sub>	0.6	0.84	-0.23
0.3TiO <sub>2</sub>	0.6	0.72	-0.12
0.3ZnO	0.66	0.78	-0.11
0.7Al <sub>2</sub> O <sub>3</sub>	0.61	0.7	-0.087
0.7TiO <sub>2</sub>	0.6	0.76	-0.16
			-
0.7ZnO	0.59	0.64	0.0467
1.0Al <sub>2</sub> O <sub>3</sub>	0.76	0.74	0.02
1.0TiO <sub>2</sub>	0.71	0.84	-0.127
1.0ZnO	0.68	0.78	-0.1
			-
0.3Al <sub>2</sub> O <sub>3</sub> +0.7TiO <sub>2</sub>	0.67	0.7	0.0334
			-
0.7Al <sub>2</sub> O <sub>3</sub> +0.3TiO <sub>2</sub>	0.63	0.68	0.0533
			-
0.3Al <sub>2</sub> O <sub>3</sub> +0.7ZnO	0.65	0.71	0.0567
0.7Al <sub>2</sub> O <sub>3</sub> +0.3ZnO	0.63	0.62	0.0067

0.3TiO <sub>2</sub> +0.7ZnO	0.71	0.66	0.047
0.7TiO <sub>2</sub> +0.3ZnO	0.97	0.78	0.19
0.3Al <sub>2</sub> O <sub>3</sub> +0.3TiO <sub>2</sub> +0.3ZnO	0.71	0.74	-0.033

Note the Iwo for 1.0Al<sub>2</sub>O<sub>3</sub> is 0.02 which is approximated as zero and cos0 = 90° which is neutral wetting condition. All Iwo values are within the values recommended by Amott –Harvey index for completely oil-wet condition.

## H.2 Surfacted nanofluids

Table A- 37 Wettability index of Surfacted nanofluids

Nanofluid system	lw	lo	lwo
			-
0.3Al <sub>2</sub> O <sub>3</sub>	0.5667	0.82	0.2533
0.3TiO <sub>2</sub>	0.56	0.62	-0.06
			-
0.3ZnO	0.6533	0.74	0.0867
			-
0.7Al <sub>2</sub> O <sub>3</sub>	0.6533	0.76	0.1067
			-
0.7TiO <sub>2</sub>	0.6467	0.88	0.2333
0.7ZnO	0.74	0.98	-0.24
			-
1.0Al <sub>2</sub> O <sub>3</sub>	0.5667	0.84	0.2733
			-
1.0TiO <sub>2</sub>	0.7593	0.994	0.2347
			-
1.0ZnO	0.7133	0.9	0.1867
			-
0.3Al <sub>2</sub> O <sub>3</sub> +0.7TiO <sub>2</sub>	0.6533	0.874	0.2207
0.7Al <sub>2</sub> O <sub>3</sub> +0.3TiO <sub>2</sub>	0.66	0.8	-0.14
			-
0.3Al <sub>2</sub> O <sub>3</sub> +0.7ZnO	0.6533	0.8	0.1467
0.7Al <sub>2</sub> O <sub>3</sub> +0.3ZnO	0.66	0.76	-0.1
0.3TiO <sub>2</sub> +0.7ZnO	0.56	0.72	-0.16
0.7TiO <sub>2</sub> +0.3ZnO	0.6533	0.78	-0.13
			-
0.3Al <sub>2</sub> O <sub>3</sub> +0.3TiO <sub>2</sub> +0.3ZnO	0.6467	0.92	0.2733

Table A- 38 Comparison of lwo from pure and surfacted nanofluids

Nanofluid system	Surf lwo	Pure lwo
0.3Al <sub>2</sub> O <sub>3</sub>	0.2533	-0.23
0.3TiO <sub>2</sub>	-0.06	-0.12
0.3ZnO	0.0867	-0.11
0.7Al <sub>2</sub> O <sub>3</sub>	0.1067	-0.087
0.7TiO <sub>2</sub>	0.2333	-0.16
0.7ZnO	-0.24	0.0467
1.0Al <sub>2</sub> O <sub>3</sub>	0.2733	0.02
1.0TiO <sub>2</sub>	0.2347	-0.127
1.0ZnO	0.1867	-0.1
0.3Al <sub>2</sub> O <sub>3</sub> +0.7TiO <sub>2</sub>	0.2207	0.0334
0.7Al <sub>2</sub> O <sub>3</sub> +0.3TiO <sub>2</sub>	-0.14	0.0533
0.3Al <sub>2</sub> O <sub>3</sub> +0.7ZnO	0.1467	0.0567
0.7Al <sub>2</sub> O <sub>3</sub> +0.3ZnO	-0.1	0.0067
0.3TiO <sub>2</sub> +0.7ZnO	-0.16	0.047
0.7TiO <sub>2</sub> +0.3ZnO	-0.13	0.19
0.3Al <sub>2</sub> O <sub>3</sub> +0.3TiO <sub>2</sub> +0.3ZnO	0.2733	-0.033

Table A- 39 Comparison of pure and surfacted nanofluids

Nanofluid system	Surf lwo	Pure lwo
0.3Al <sub>2</sub> O <sub>3</sub>	-0.2533	-0.23
0.3TiO <sub>2</sub>	-0.06	-0.12
0.3ZnO	-0.0867	-0.11
0.7Al <sub>2</sub> O <sub>3</sub>	-0.1067	-0.087
0.7TiO <sub>2</sub>	-0.2333	-0.16
0.7ZnO	-0.24	-0.0467
1.0Al <sub>2</sub> O <sub>3</sub>	-0.2733	0.02
1.0TiO <sub>2</sub>	-0.2347	-0.127
1.0ZnO	-0.1867	-0.1
0.3Al <sub>2</sub> O <sub>3</sub> +0.7TiO <sub>2</sub>	-0.2207	-0.0334
0.7Al <sub>2</sub> O <sub>3</sub> +0.3TiO <sub>2</sub>	-0.14	-0.0533
0.3Al <sub>2</sub> O <sub>3</sub> +0.7ZnO	-0.1467	-0.0567
0.7Al <sub>2</sub> O <sub>3</sub> +0.3ZnO	-0.1	0.0067
0.3TiO <sub>2</sub> +0.7ZnO	-0.16	0.047
0.7TiO <sub>2</sub> +0.3ZnO	-0.13	0.19
0.3Al <sub>2</sub> O <sub>3</sub> +0.3TiO <sub>2</sub> +0.3ZnO	-0.2733	-0.033

Table A- 40 Measured contact angles of the different nanofluids

Nanofluid system	Pure	Surfacted
0.3Al <sub>2</sub> O <sub>3</sub>	25.03	19.97
0.3TiO <sub>2</sub>	23.59	15.85
0.3ZnO	26.47	17.79
0.7Al <sub>2</sub> O <sub>3</sub>	23.38	15.71
0.7TiO <sub>2</sub>	20.98	15.28
0.7ZnO	22.28	15.13
1.0Al <sub>2</sub> O <sub>3</sub>	17.38	11.68
1.0TiO <sub>2</sub>	16.87	5.52
1.0ZnO	18.4	9.96
0.3Al <sub>2</sub> O <sub>3</sub> +0.7TiO <sub>2</sub>	52.57	37.84

0.7Al <sub>2</sub> O <sub>3</sub> +0.3TiO <sub>2</sub>	41.17	29.67
0.3Al <sub>2</sub> O <sub>3</sub> +0.7ZnO	45.87	21.85
0.7Al <sub>2</sub> O <sub>3</sub> +0.3ZnO	33.78	11.05
0.3TiO <sub>2</sub> +0.7ZnO	49.1	33.32
0.7TiO <sub>2</sub> +0.3ZnO	30.29	20.14
0.3Al <sub>2</sub> O <sub>3</sub> +0.3TiO <sub>2</sub> +0.3ZnO	43.05	34.73

Table A- 41 Comparison of wettability with contact angle.

Contact angle	Wettability
0	1
20	0.94
40	0.77
60	0.5
80	0.17
100	-0.17
120	-0.5
140	-0.77
160	-0.93
180	-1

Table A- 42 Wettability parameters for pure nanofluids

Nanofluid system	Sor	Sw	Kro	Krw	
0.3Al <sub>2</sub> O <sub>3</sub>	0.16	0.39	0.12	0.67	0.23
0.3TiO <sub>2</sub>	0.28	0.4	0.057	0.67	0.12
0.3ZnO	0.22	0.33	0.22	0.7	0.11
0.7Al <sub>2</sub> O <sub>3</sub>	0.1	0.38	0.16	0.67	0.28
0.7TiO <sub>2</sub>	0.24	0.4	0.071	0.67	0.16
0.7ZnO	0.36	0.41	0.082	0.66	0.05
1.0Al <sub>2</sub> O <sub>3</sub>	0.26	0.24	0.63	0.74	-0.02
1.0TiO <sub>2</sub>	0.16	0.29	0.403	0.72	0.13
1.0ZnO	0.22	0.32	0.25	0.71	0.1
0.3Al <sub>2</sub> O <sub>3</sub> +0.7TiO <sub>2</sub>	0.1	0.33	0.29	0.7	0.23
0.7Al <sub>2</sub> O <sub>3</sub> +0.3TiO <sub>2</sub>	0.11	0.37	0.18	0.68	0.26
0.3Al <sub>2</sub> O <sub>3</sub> +0.7ZnO	0.097	0.35	0.24	0.69	0.25

0.7Al <sub>2</sub> O <sub>3</sub> +0.3ZnO	0.13	0.37	0.17	0.68	0.24
0.3TiO <sub>2</sub> +0.7ZnO	0.07	0.29	0.45	0.72	0.22
0.7TiO <sub>2</sub> +0.3ZnO	0.22	0.027	0.21	0.79	-0.19
0.3Al <sub>2</sub> O <sub>3</sub> +0.3TiO <sub>2</sub> +0.3ZnO	0.26	0.29	0.33	0.72	0.03

Table A- 43 Wettability parameters for surfacted nanofluids

Surfacted nanofluids					
Nanofluid system	Sw	Sor	Kro	Krw	Swro(Sw - Sor)
0.3Al <sub>2</sub> O <sub>3</sub>	0.26	0.18	0.4	0.1	
0.3TiO <sub>2</sub>	0.34	0.38	0.184	0.321	
0.3ZnO	0.44	0.26	0.29	0.5	
0.7Al <sub>2</sub> O <sub>3</sub>	0.567	0.24	0.4	0.6	
0.7TiO <sub>2</sub>	0.66	0.12	0.51	0.631	
0.7ZnO	0.713	0.02	0.521	0.636	
1.0Al <sub>2</sub> O <sub>3</sub>	0.74	0.16	0.536	0.674	
1.0TiO <sub>2</sub>	0.759	0.006	0.557	0.684	
1.0ZnO	0.78	0.1	0.563	0.7	
0.3Al <sub>2</sub> O <sub>3</sub> +0.7TiO <sub>2</sub>	0.82	0.13	0.62	0.719	
0.7Al <sub>2</sub> O <sub>3</sub> +0.3TiO <sub>2</sub>	0.874	0.2	0.684	0.801	
0.3Al <sub>2</sub> O <sub>3</sub> +0.7ZnO	0.88	0.2	0.759	0.815	
0.7Al <sub>2</sub> O <sub>3</sub> +0.3ZnO	0.9	0.24	0.852	0.859	
0.3TiO <sub>2</sub> +0.7ZnO	0.92	0.28	0.859	0.867	
0.7TiO <sub>2</sub> +0.3ZnO	0.98	0.22	0.88	0.973	
0.3Al <sub>2</sub> O <sub>3</sub> +0.3TiO <sub>2</sub> +0.3ZnO	0.994	0.08	0.9	0.992	

Table A- 44 Effect of pH on the zeta potential and absorbency of the different surfacted nanofluids.

Nanofluids	pH	Zetapotential	
			(mV)
0.3Al <sub>2</sub> O <sub>3</sub>	3.16	168	0.22112
0.7Al <sub>2</sub> O <sub>3</sub>	3.72	136	0.76952
1.0Al <sub>2</sub> O <sub>3</sub>	3.28	170	0.54387
0.3TiO <sub>2</sub>	1.23	277	0.42823
0.7TiO <sub>2</sub>	1.31	294	0.35057
1.0TiO <sub>2</sub>	1.3	273	0.29688



0.3 ZnO	10.73	-196	0.44597
0.7 ZnO	10.93	-205	0.32738
1.0 ZnO	8.98	-140	0.32282
0.3Al <sub>2</sub> O <sub>3</sub> + 0.7TiO <sub>2</sub>	2.91	108	0.99267
0.7Al <sub>2</sub> O <sub>3</sub> + 0.3TiO <sub>2</sub>	3.93	146	0.78332
0.3Al <sub>2</sub> O <sub>3</sub> + 0.7ZnO	9.66	-167	0.99356
0.7Al <sub>2</sub> O <sub>3</sub> + 0.3ZnO	9.31	-156	0.8388
0.3TiO <sub>2</sub> + 0.7ZnO	3.85	121	0.64627
0.7TiO <sub>2</sub> + 0.3ZnO	1.66	240	0.68126
0.3Al <sub>2</sub> O <sub>3</sub> + 0.3TiO <sub>2</sub> + 0.3ZnO	3.74	118	0.94487

L. Soil contamination with mineral oil and cleanup process with the different nanofluids

Table A- 45 Soil contamination & cleanup process with pure and surfacted nanofluids.

Soil Contamination			Cleanup Process						
Amount of soil used for contamination(g)	Amount of oil used for contamination(g)	Amount of excess oil drained before cleaning (g)	Nanofluid type & concentration	Amount of nanofluid used in the cleaning (g)	Amount of oil removed after cleaning (g)	Cleaning efficiency (%)	Amount of H <sub>2</sub> O removed after cleaning(g)	Amount of H <sub>2</sub> O retained in the soil after cleaning(g)	Amt of oil
10	10(HV <sub>1</sub> )	4.5	0.3vol% ZnO	10	3.3	$3.3/5.5 = 60$	5.5	4.47	2.2
10	10(HV <sub>1</sub> )	4.5	0.3vol% TiO <sub>2</sub>	10	3.1	$3.1/5.5 = 56$	5.5	4.47	2.4
10	10(HV <sub>1</sub> )	4.4	0.3vol% Al <sub>2</sub> O <sub>3</sub>	10	3.4	$3.4/5.6 \times 100 = 60.71\%$	5.57	4.43	2.2
10	10(HV <sub>1</sub> )	4.61	0.7 ZnO	10	2.8	$2.8/5.39 \times 100 = 52.0\%$	5.4	4.6	2.2
10	5(HV <sub>1</sub> )	-	0.7Al <sub>2</sub> O <sub>3</sub>	10	2.9	$2.9/5 \times 100 = 58\%$	5.0	4.0	2.1

10	5(HV <sub>1</sub> )	-	0.7TiO <sub>2</sub>	10 5 was used for 2 <sup>nd</sup> cleaning	3.2 with 2 <sup>nd</sup> cleaning	3.2/5x10 0 = 64%	5.4	4.6	1.8
10	5(HV <sub>1</sub> )	-	1.0 ZnO	10 5 was used for 2 <sup>nd</sup> cleaning	3.9 with 2 <sup>nd</sup> cleaning	3.9/5x10 0 = 78%	5.2	4.8	1.1
10	5(HV <sub>1</sub> )	-	1.0 TiO <sub>2</sub>	10 5 was used for 2 <sup>nd</sup> cleaning	3.4+0.8 = 4.2 with 2 <sup>nd</sup> cleaning	4.2/5 x 100 = 84%	5.1+ 0.6 = 5.7	4.3	1.6 – 0.8 =
10	5(HV <sub>1</sub> )	-	1.0Al <sub>2</sub> O <sub>3</sub>	10 (no2 <sup>nd</sup> cleaning)	3.7	3.7/5 x 100 = 74%	6.4	3.6	1.3
10	5(HV <sub>1</sub> )	-	0.3ZnO+0.3 TiO <sub>2</sub> + 0.3Al <sub>2</sub> O <sub>3</sub>	10 5(2 <sup>nd</sup> cleaning)	2.4	2.4+0.5 = 2.9/5x10 0 = 58%	6.6	3.4	2.1
10	5(HV <sub>1</sub> )	-	0.3ZnO + 0.7Al <sub>2</sub> O <sub>3</sub>	10 5(2 <sup>nd</sup> cleaning)	2.1	2.1+1.0 =3.1/5 x100 = 62%	4.4	5.6	1.9
10	5(HV <sub>1</sub> )	-	0.7ZnO + 0.3Al <sub>2</sub> O <sub>3</sub>	10 5(2 <sup>nd</sup> cleaning)	1.7	1.7+0.8 = 2.5/5 x 100 = 50%	4.2 +3.6 = 7.8	2.2	2.5
10	5(HV <sub>1</sub> )	-	0.7 Al <sub>2</sub> O <sub>3</sub> + 0.3TiO <sub>2</sub>	10	3.1	3.1+0.3 = 3.4/5 x	No water	1.5	3.7

				5(2 <sup>nd</sup> cleaning)		100 = 68%				
10	5(HV1)	-	0.7 TiO <sub>2</sub> + 0.3 Al <sub>2</sub> O <sub>3</sub>	10 5(2 <sup>nd</sup> cleaning)	3.2	3.2 + 0.3 = 3.5/5 x 100 = 70%	4.4	1.6	5.6	
10	5(HV1)	-	0.7 TiO <sub>2</sub> + 0.3 ZnO	10 5(2 <sup>nd</sup> cleaning)	1.8	1.8 + 2.1 = 3.9/5 x 100 =78%	6.6 + 8 = 14.6	1.1	0.4	
10	5(HV1)	-	0.3 TiO <sub>2</sub> + 0.7 ZnO (repeated)	10 5(2 <sup>nd</sup> cleaning)	2.1	2.1 + 1.2 = 3.3/5 x 100 =66%	6.4 + 2.6 = 9	2.9 -1.2= 1.7	3.6-2.6 = 1	
10	5(HV1)		1.0%Al <sub>2</sub> O <sub>3</sub> + 0.1%SDBS	10 5(2 <sup>nd</sup> cleaning)	2.1	2.1+ 1.4 = 3.5/5 x100 =70%	6.6 + 2.8 = 9.4	2.9 - 1.4 = 1.5	3	
10	5(HV1)		1%TiO <sub>2</sub> + 0.1%SDBS	10 5(2 <sup>nd</sup> cleaning)	2.6	2.6 + 1.5 = 4.1/5 x100 =82%	6 + 2.4 = 8.4	2.4 - 1.5 = 0.9	6.6	
10	5(HV1)		1%ZnO + 0.5%Na <sub>2</sub> HP O <sub>4</sub>	10 5(2 <sup>nd</sup> cleaning)	3.5	3.5 + 0.9 = 4.5/5 x100 = 90%	4.5 +3.0 = 7.5	4.3	0.5	
10	5(HV1)		0.7%ZnO + 0.35%Na <sub>2</sub> H PO <sub>4</sub>	10 5(2 <sup>nd</sup> cleaning)	2.4	2.4 + 2.5= 4.9/5 x 100=98 %	6.1 +3.3 = 9.4	3.9	0.1	

10	5(HV1)		0.7%Al <sub>2</sub> O <sub>3</sub> + 0.07%SDB S	10 5(2 <sup>nd</sup> cleaning)	3.1	3.1 + 0.7 = 3.8/5 x100 = 76%	5.1 + 3.7 = 9.8	5.2	1.2
10	5(HV1)		0.7%TiO <sub>2</sub> + 0.07%SDB S	10 5(2 <sup>nd</sup> cleaning)	3.5	3.5 + 0.9 = 4.4/5 x 100 = 88%	6.6 + 3.1 = 9.7	5.3	0.6
10	5(HV1)		0.3%Al <sub>2</sub> O <sub>3</sub> + 0.03%SDB S	10 5(2 <sup>nd</sup> cleaning)	2.8	2.8 + 1.3 = 4.1/5 x 100 = 82%	5.2 + 3.3 = 8.5	6.5	0.9
10	5(HV1)		0.3%TiO <sub>2</sub> + 0.03%SDB S	10 5(2 <sup>nd</sup> cleaning)	2.5	2.5 + 0.6 = 3.1/5 x 100 = 62%	5 + 3.4 = 8.4	6.6	1.9
10	5(HV1)		0.3%ZnO + 0.15%Na <sub>2</sub> H PO <sub>4</sub>	10 5(2 <sup>nd</sup> cleaning)	2.7	2.7 + 1 = 3.7/5 x 100 = 74%	5 + 3 = 8	7	1.3
10	5(HV1)		1.0%Al <sub>2</sub> O <sub>3</sub> + 0.1%SDBS Repeated	10 5(2 <sup>nd</sup> cleaning)	3	3 + 1.2 = 4.2/5 x 100 = 84%	5.1 + 3.5 = 8.6	6.5	0.8
10	5(HV1)		1%TiO <sub>2</sub> + 0.1%SDBS Repeated	10 5(2 <sup>nd</sup> cleaning)		2.8+2.17 =4.97/5 x 100 = 99.4%	4.1+7.2 9=11.3 9	3.61	0.03
10	5(HV <sub>1</sub> )	-	0.3ZnO- +0.3TiO <sub>2</sub> +	10 5(2 <sup>nd</sup> cleaning)					

			0.3Al <sub>2</sub> O <sub>3</sub> + surfactants						
10	5(HV1)	-	0.3ZnO + 0.7Al <sub>2</sub> O <sub>3</sub> + surfactants	10 5(2 <sup>nd</sup> cleaning)		1.9+0.8+ 0.7 = 3.8/5 x 100 =76%	8.7	1.2	5.1
10	5(HV1)	-	0.7ZnO + 0.3Al <sub>2</sub> O <sub>3</sub> + surfactants	10 5(2 <sup>nd</sup> cleaning)		2.5+1.5= 4/5 x 100 =80%	0.3+1.6 = 1.9	1.0	5.2
10	5(HV1)	-	0.7 Al <sub>2</sub> O <sub>3</sub> + 0.3TiO <sub>2</sub> + surfactants	10 5(2 <sup>nd</sup> cleaning)		2.7+1.3= 4/5 x100 =80%	4.6+3.3 =7.9	1.0	5.1
10	5(HV1)	-	0.7 TiO <sub>2</sub> + 0.3 Al <sub>2</sub> O <sub>3</sub> + surfactants	10 5(2 <sup>nd</sup> cleaning)		1.6+1.3+ 1.47= 4.37/5 x100=87. 4%	2.6+2.2 +4= 8.8	0.63	5.2
10	5(HV1)	-	0.7 TiO <sub>2</sub> + 0.3 ZnO+ surfactants	10 5(2 <sup>nd</sup> cleaning)		2.3 + 1.6 = 3.9/5 x100 = 78%	6.1+ 3.5=9.6	1.1	5.2
10	5(HV1)	-	0.3 TiO <sub>2</sub> + 0.7 ZnO + surfactants (repeated)	10 5(2 <sup>nd</sup> cleaning)		1.8+1.8 = 3.6/5 x100 =72%	5.9+2.5 = 8.4	6.6	1.4

9.4(20gOil was used for contamination)	3.6	33.1
---	-----	------

-	2.1	16.1
-	2.2	16.4
-	1.1	15.9
-	0.8	15.1
-	1.3 (after 4 day of cleaning)	14.9
-	2.1	15.5
	1.9	15.3
	2.6	14.8
	1.5	15.2
	1.6	13.6
	1.1	11.6
	1.7	12.7
	1.5	14.5
	0.9	15.1
	0.5	14.8
	0.1	14.0
	0.6	15.9
	1.2	16
	1.9	15.9
	0.9	16
	1.3	16.5
	0.8	17.3

## M. Thermal Analysis of soil after cleanup process

### M.1 Soil Analysis

The results of Tga soil analysis [38, 57] are shown on Figures presented in original graphs as Fig.A...for mass loss against time (minutes) and heatflow against temperature.The combined original graphs of weight loss and heat flows are separated by plotting them against time and temperature represented in figs as FigsA-35,A-37,A-43,A-47,A-50,A-53,A-55,A-58,A-61,A-64,A-79, A-80,A-85,A-90,A-93,A-98 and A-108.to FigureA-118 for better understanding of the analysis as follows:

i. monotype pure and surfacted nanofluids, ii.Hybrid pure and surfacted nanofluids.

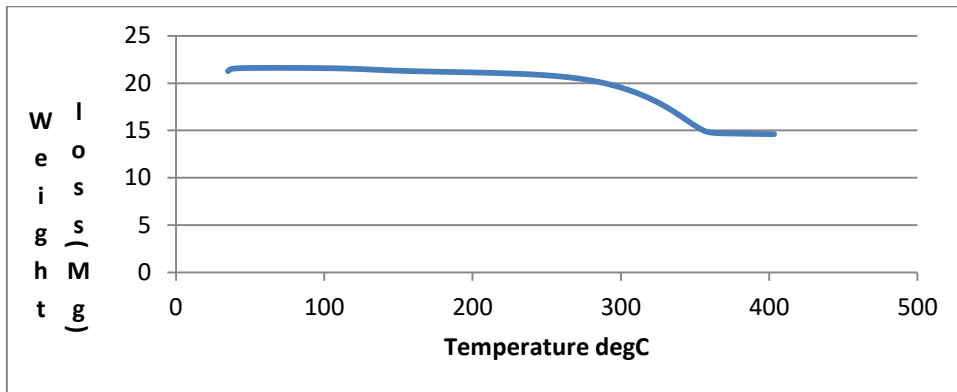


Figure A- 33 10g Soil contaminated with 5g Oil HV1 and cleaned in Tga without nanofluid [57].

The weight loss increases with increase in temp until it reaches 338°C and becomes constant at 400°C without further weight loss. At this temperature all the oil has been burnt off leaving only clean soil at controlled temperature.

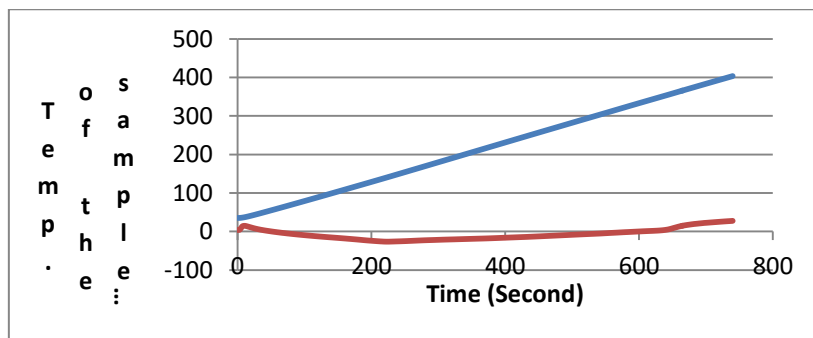


Figure A- 34 Tga heat flow of 21.33mg oil contaminated soil sample analysis cleaned without nanofluid.

Figure A-34 shows heat flow of oil contaminated soil sample weighing 21.33mg. The sample was analyzed in tga cleaned without nanofluid. After the analysis, 13.90mg (65.17%) soil sample was recovered. The quantity of oil in the contaminated soil is  $21.33 - 13.90 = 7.43\text{mg}$  (34.83%) [41a].

Below is the Tga analysis of 10g soil contaminated with 5g HV1 60 oil and cleaned with 15g of the pure and surfacted monotype as well their hybrid nanofluids.

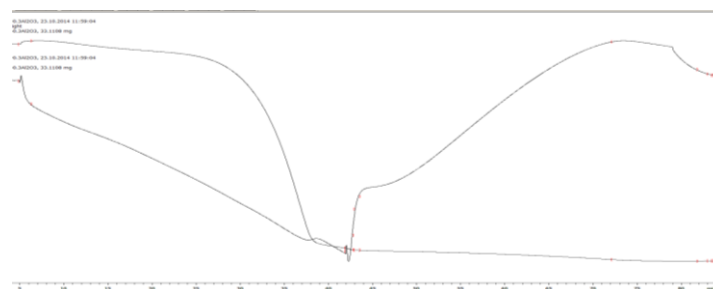


Figure A- 35 Weight loss and heatflow of 0.3 Al<sub>2</sub>O<sub>3</sub>/water –nanofluid

This graph is reported by replotting the generated tga data into weight loss and heatflow considering the temperature and time as shown on FigureA-36

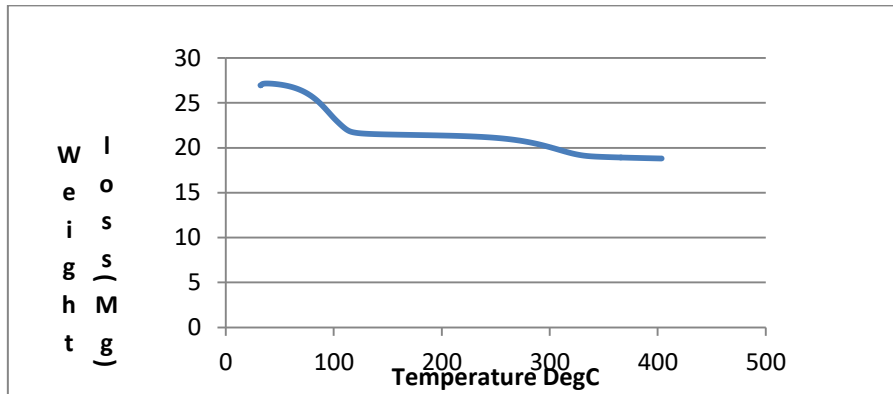


Figure A- 36 10g Soil contaminated with 5g Oil HV1 and cleaned with pure 0.3vol% Al<sub>2</sub>O<sub>3</sub>. The FigureA-36 shows the heatflow of contaminated soil after cleaning with 15g pure 0.3Al<sub>2</sub>O<sub>3</sub> /water in which 26.9585mg was taken from the bulk soil for tga analysis at controlled temperature.As heat flows through the soil sample, with onset temperature of 30.3369 °C and 12mins into the start of the analysis, water (3.6975mg) boils off with weight of sample equals to 23.261mg at 100.436°C.More weight (4.2054mg) loss occurs at 150.019 °C, burning off all the oil (0.2407mg) with weight of hot clean soil, 19.0556mg, at 338.152°C.The weight of cleaned soil(18.8149mg) remains constant even after the end temperature 400°C without further weight loss, cooling down at 397.27°C.It takes 37.3mins to restore the contaminated soil after cleaning with pure 0.3wt% Al<sub>2</sub>O<sub>3</sub>/water to its original status with total weight loss of 30.21%.

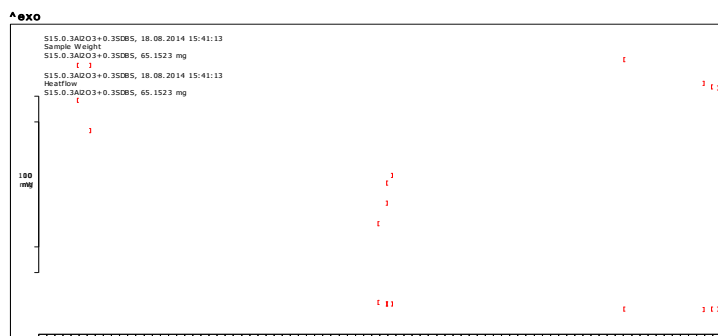


Figure A- 37 Mass loss per min and heatflow per min of surfacted 0.3wt% Al<sub>2</sub>O<sub>3</sub>/water

This graph is reported by replotting the generated tga data into weight loss and heatflow considering the temperature and time as shown on Figures A-38&A-39



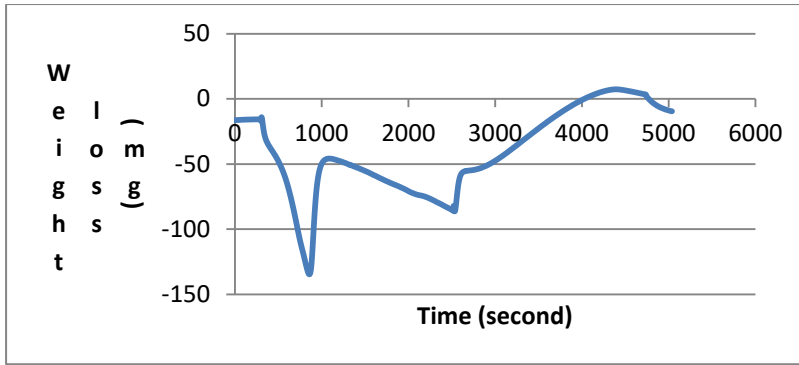


Figure A- 38 Heatflow for surfacted  $0.3\text{Al}_2\text{O}_3/\text{water}$

Tga analysis of contaminated soil after cleaning with surfacted  $0.3\text{Al}_2\text{O}_3/\text{water}$  as shown in Figures A-38 & A-39. Weight loss started at 2mins with weight of 65.1523mg and weight loss increase downwards at the interval of -20mg until it gets to weight loss of 19.4561mg/29.8625% (12mins), where most of the water retained in the soil after cleaning with surfacted  $0.3\text{Al}_2\text{O}_3/\text{water}$  is lost. As the analysis progresses, the weight loss increases upward until it gets to 16mins, here much oil is lost (0.489mg/0.75055%). Weight loss decreases again, until it reaches 42.1mins (45.2072mg/69.3870%) as all the oil is burnt off leading to constant weight of soil (45.2072mg/69.3870%), no further change in weight loss.

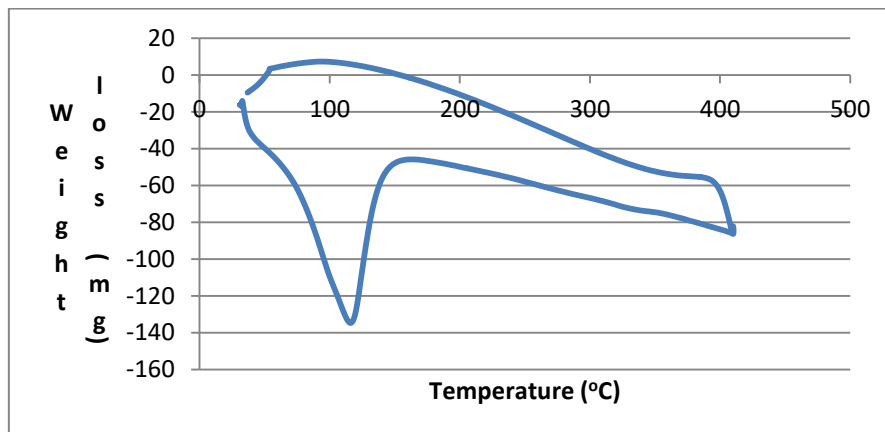


Figure A- 39 Heatflow for surfacted  $0.3\text{Al}_2\text{O}_3/\text{water}$

The Figure A-39 shows the heatflow of contaminated soil after cleaning with surfacted  $0.3\text{Al}_2\text{O}_3/\text{water}$  in which 65.1523mg was taken from the bulk soil for tga analysis. As heat flows through the soil sample by 12mins into the start of the analysis, water boils off with weight of water lost equals to 19.4561mg at  $100^\circ\text{C}$ . More weight loss occurs at  $150.019^\circ\text{C}$ , burning off all the oil (0.489mg) with weight of hot clean soil, 45.2072mg, at  $338.152^\circ\text{C}$ . The weight of cleaned soil remains constant even after the end temperature  $400^\circ\text{C}$  without further weight loss, cooling down to  $36.8561^\circ\text{C}$  with total weight loss of 30.61%, out of which water is 23.11% and oil is 7.5%.

Figure A-39 shows the change in weight of the oil contaminated soil +  $0.3\text{Al}_2\text{O}_3$  – water nanofluid + 0.03g SDBS subjected to the controlled temperature rise. The onset of a rapid decrease in weight was observed at  $30.9171^\circ\text{C}$  (the decomposition temperature of the  $0.3\text{Al}_2(\text{OH})_2$ ) which progressed up to  $320^\circ\text{C}$ . The percentage loss in weight from 0 to  $400^\circ\text{C}$  is 30.61%. At  $338^\circ\text{C}$  (boiling point of the mineral oil), the mineral oil in contaminated soil started to evaporate at constant rate to  $400^\circ\text{C}$  at the point where 100% soil cleaning was achieved and the soil was restored to its original status. Comparing the Figures A-38 and A-39, the total percentage weight loss of oil contaminated sample cleaned with nanofluid without surfactant (30.21%) was less than the total percentage weight loss of contaminated sample cleaned with  $0.3\text{Al}_2\text{O}_3$  – water nanofluid + 0.03g SDBS (30.61%).

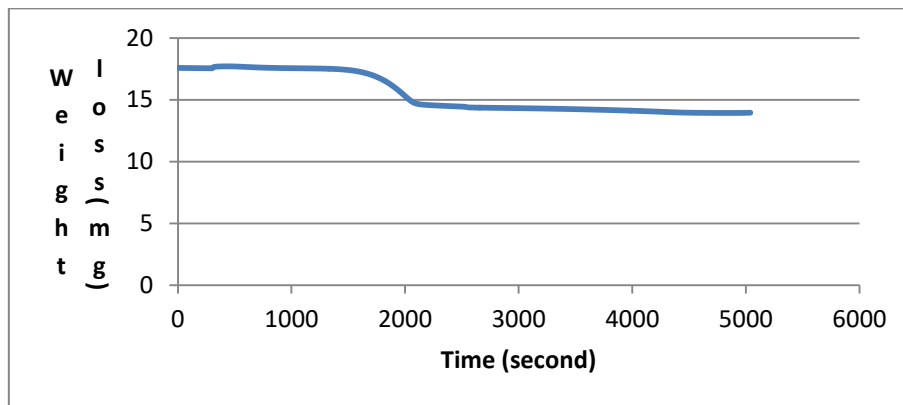


Figure A- 40 Weight loss per second of the contaminated soil cleaned with pure  $0.7\text{Al}_2\text{O}_3/\text{water}$

After the cleaning with pure  $0.7\text{Al}_2\text{O}_3$  /water, 21.2949mg soil sample (which comprises of oil and water retained in the soil after cleaning) was taken into a crucible for tga analysis at onset temperature of  $30^\circ\text{C}$ . As heatflow through the soil sample progressively, at 10.93 minutes into the start off the experiment, 6.5259mg (30.6454%) water in the sample boiled off, leaving only the oil in the soil. Further progression of the heatflow led to the removal of oil by weight, 0.1406mg (0.6603%) at 12.05mins. Finally, all the oil was removed at constant rate leaving the soil (14.6753mg /68.6944%) to its original status.

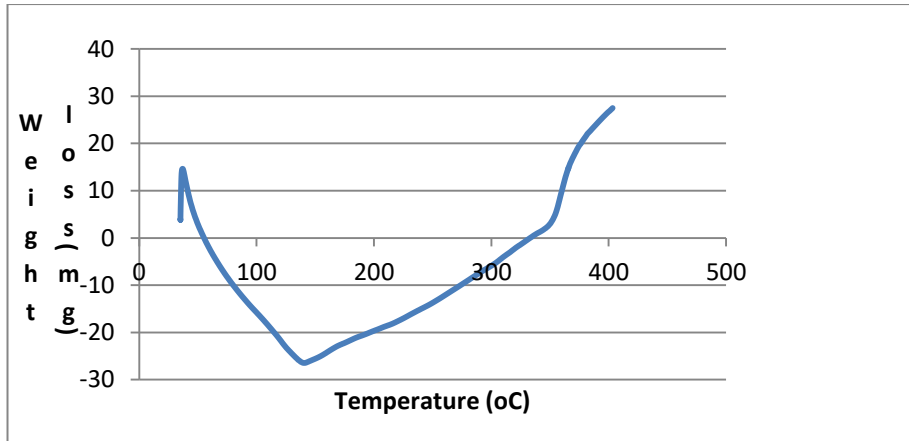


Figure A- 41 Heatflow for pure 0.7Al<sub>2</sub>O<sub>3</sub>/water

FigureA-41 shows the heatflow of 21.2949mg soil sample cleaned with pure 0.7Al<sub>2</sub>O<sub>3</sub>/water which started at onset temperature of 30°C.As the temperature increases at 100.184°C, 5.7595mg (27.0464%) water evaporated from the soil.Further advanced of heatflow at 338.598°C, 0.8952mg (4.2038%) of oil burnt off, leaving only 14.6753mg (68.9132%) cleaned soil at the end temperature of 400°C.The percentage loss in weight from 0 to400°C is 31.0854%.

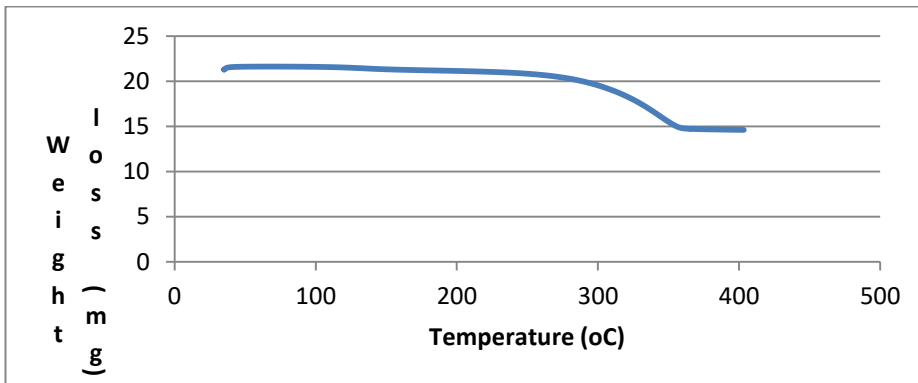


Figure A- 42 Heatflow for 0.7Al<sub>2</sub>O<sub>3</sub>/water

FigureA-42 shows the weight loss of 21.2949mg soil sample cleaned with pure 0.7Al<sub>2</sub>O<sub>3</sub>/water which started at onset temperature of 30°C.As the temperature increases at 100.184°C, 5.7595mg (27.0464%) water evaporated from the soil. Further advanced of heatflow at 338.598°C, 0.8952mg (4.2038%) of oil burnt off, leaving only 14.6753mg (68.9132%) cleaned soil at the end temperature of 400°C.

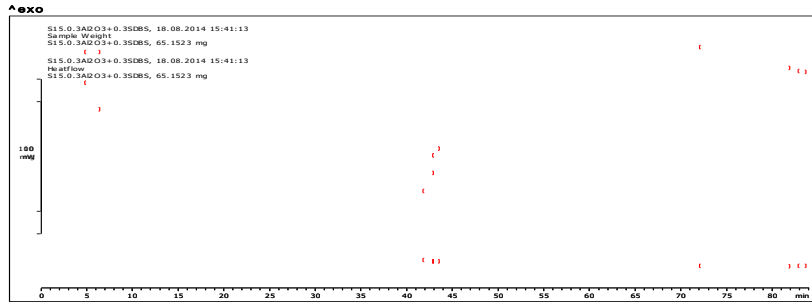


Figure A- 43 Mass loss per min and heatflow per min of surfactated  $0.7Al_2O_3/Water$   
 This graph is reported by replotting the generated tga data into weight loss and heatflow considering the temperature and time as shown on Figures A-44 &A-45.

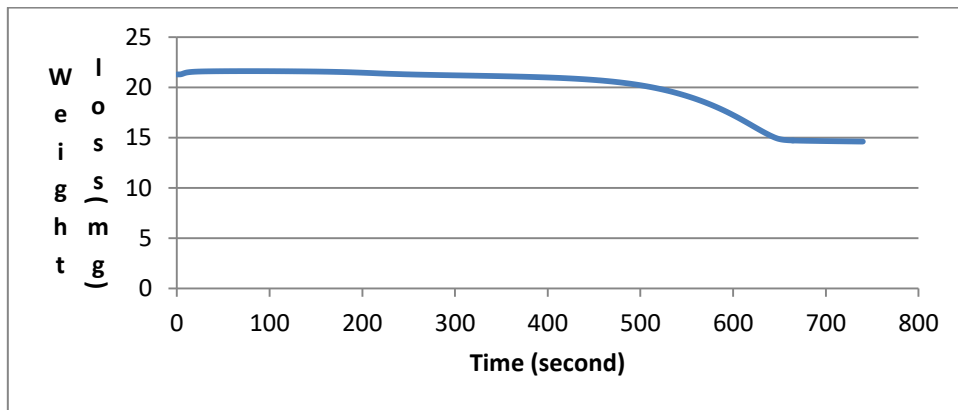


Figure A- 44 Heatflow for surfactated  $0.7Al_2O_3/water$

After the cleaning with surfactated  $0.7Al_2O_3/water$ , 41.3897mg soil sample (which comprises of oil and water retained in the soil after cleaning) was taken into a crucible for tga analysis at onset temperature of  $30^{\circ}C$ .As heatflow through the soil sample progressively, at 12.1 minutes into the start off the experiment, 6.5694mg (15.8721%) water in the sample boiled off, leaving only the oil in the soil. Further progression of the heatflow led to the removal of oil by weight, 0.0227mg (0.0548%) at 39.0mins.Finally, all the oil was removed at constant rate leaving the soil (34.7976mg/84.0731%) to its original status

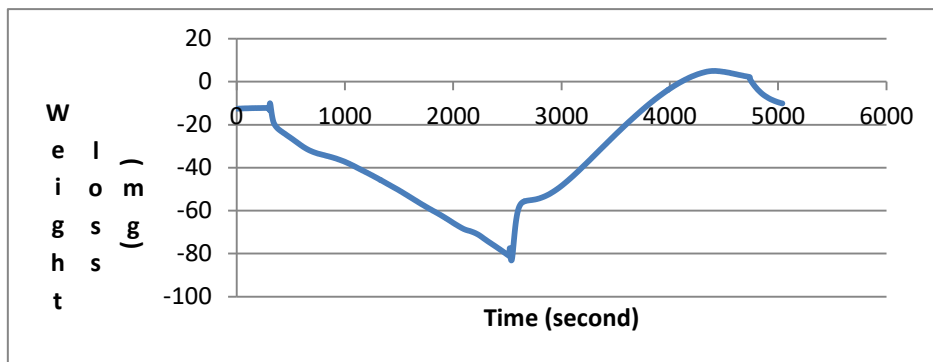


Figure A- 45 Heatflow for surfactated  $0.7Al_2O_3/water$

After the cleaning with surfacted  $0.7\text{Al}_2\text{O}_3/\text{water}$ , 41.3897mg soil sample (which comprises of oil and water retained in the soil after cleaning) was taken into a crucible for tga analysis at onset temperature of  $30^\circ\text{C}$ . As heatflow through the soil sample progressively, at 12.1 minutes into the start off the experiment, 6.5694mg (15.8721%) water in the sample boiled off, leaving only the oil in the soil. Further progression of the heatflow led to the removal of oil by weight, 0.0227mg (0.0548%) at 39.0mins. Finally, all the oil was removed at constant rate leaving the soil (34.7976mg/84.0731%) to its original status.

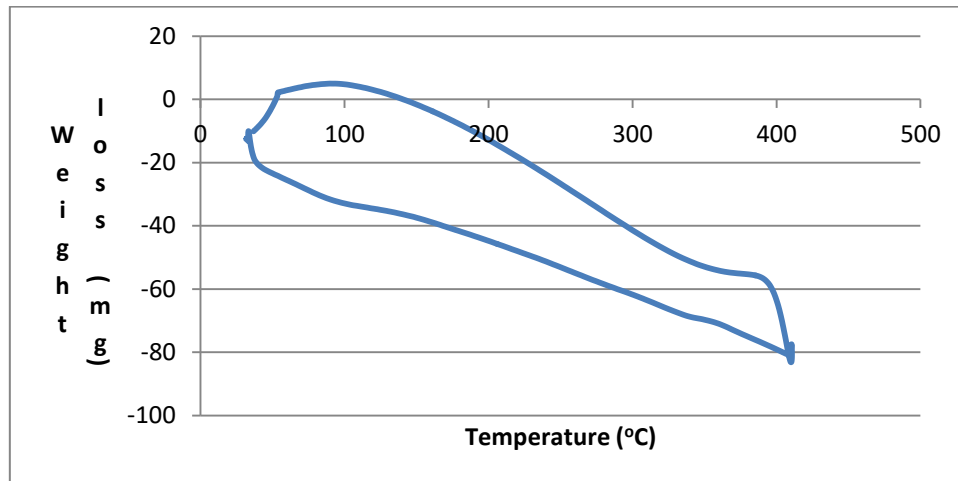


Figure A- 46 Heatflow for surfacted  $0.7\text{Al}_2\text{O}_3/\text{water}$

The Figure 46 shows the heatflow of contaminated soil after cleaning with surfacted  $0.7\text{Al}_2\text{O}_3/\text{water}$  in which 41.3897mg was taken from the bulk soil for tga analysis. As heat flows through the soil sample by 11 97mins into the start of the analysis, water boils off with weight of water lost equals to 4.7646mg at  $100.091^\circ\text{C}$ . More weight loss occurs, burning off all the oil (0.0227mg) at  $338.481^\circ\text{C}$  with weight of hot clean soil, 25.6528mg. The weight of cleaned soil remains constant after  $338.481^\circ\text{C}$  to the end temperature of  $400^\circ\text{C}$  without further weight loss, cooling down to  $30^\circ\text{C}$

Figure A-46 shows the change in weight of the oil contaminated soil +  $0.7\text{Al}_2\text{O}_3 - \text{water}$  nanofluid + 0.1g SDBS subjected to the controlled temperature rise. The onset of a rapid decrease in weight was observed at  $30.33^\circ\text{C}$  (the decomposition temperature of the  $0.7\text{Al}(\text{OH})_2$ ) which progressed up to  $320^\circ\text{C}$ . The percentage loss in weight from 0 to  $400^\circ\text{C}$  is 38.02%. At  $338^\circ\text{C}$  (boiling point of the mineral oil), the mineral oil in contaminated soil started to evaporate at constant rate to  $400^\circ\text{C}$  at the point where 100% soil cleaning was achieved and the soil was restored to its original status. Comparing the Figures A-41 and A-46, the total percentage weight loss of oil contaminated sample cleaned

with nanofluid without surfactant (4.2038%) was more than the total percentage weight loss of contaminated sample cleaned with 0.7Al<sub>2</sub>O<sub>3</sub> – water nanofluid + 0.1g surfactant ((0.0548%)

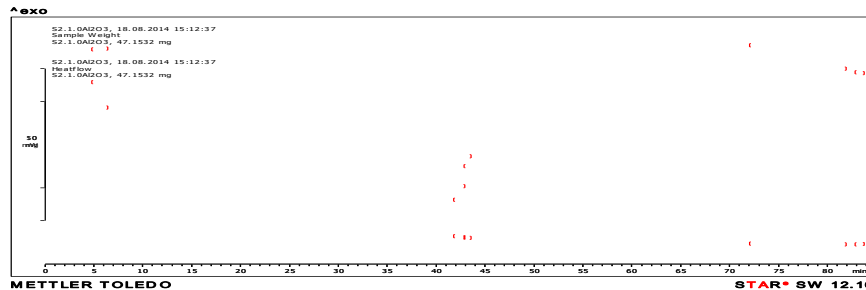


Figure A- 47 Mass loss per min and heatflow per min of pure 1.0wt%Al<sub>2</sub>O<sub>3</sub>/water

This graph is reported by replotting the generated tga data into weight loss and heatflow considering the temperature and time as shown on Figures A-48 & A-49

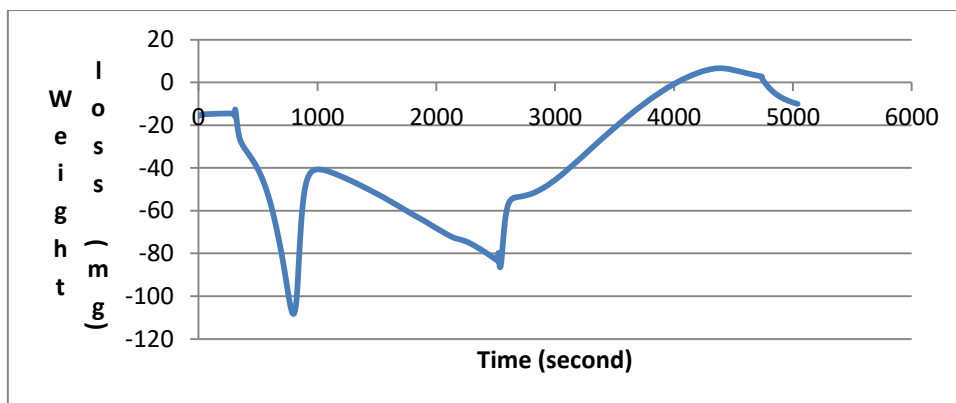


Figure A- 48 Heatflow for pure 1.0Al<sub>2</sub>O<sub>3</sub>/water.

Tga analysis of contaminated soil after cleaning with 1.0Al<sub>2</sub>O<sub>3</sub>/water as shown in FigureA-48 Weight loss started at 2mins with weight of 44.7318mg and weight loss increase downwards at the interval of -20mg until it gets to weight loss of 9.071mg (13.08mins), where most of the water retained in the soil after cleaning with 1.0Al<sub>2</sub>O<sub>3</sub> /water is lost.As the analysis progresses, the weight loss increases upward until it gets to 16mins, here much oil is lost (0.1258mg).Weight loss decreases again, until it reaches 42.1mins(35.5350mg) as all the oil is burnt off leading to constant weight of soil (35.5350mg) , no further change in weight loss.

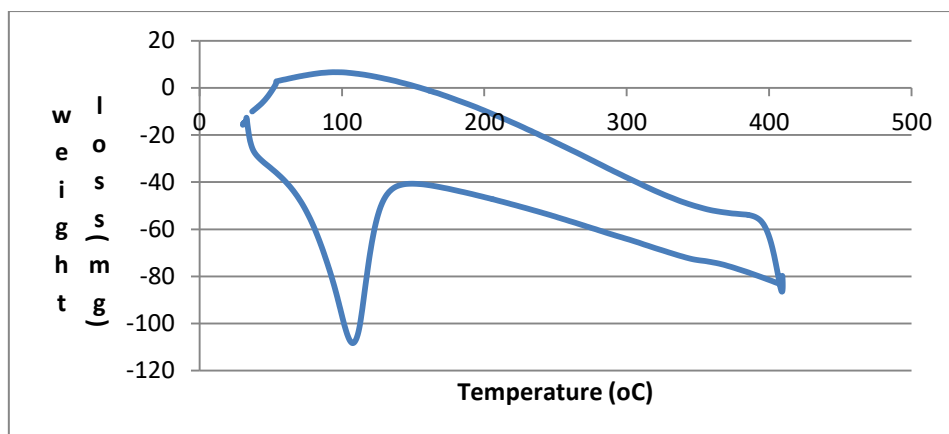


Figure A- 49 Heatflow for pure 1.0Al<sub>2</sub>O<sub>3</sub>/water.

The Figure A-49 shows the heatflow of contaminated soil after cleaning with 1.0Al<sub>2</sub>O<sub>3</sub> /water in which 47.1532mg was taken from the bulk soil for tga analysis. As heat flows through the soil sample by 11.97mins into the start of the analysis, water boils off with weight of water lost equals to 8.9089mg at 100.011°C. More weight loss occurs at 136.147°C, burning off all the oil (4.2156mg, 8.9402%) with weight of hot clean soil, 34.0287mg, at 338.218°C. The weight of cleaned soil remains constant after the 400°C without further weight loss, cooling down at 388.743°C. The percentage loss in weight from 0 to 400°C is 27.83%.

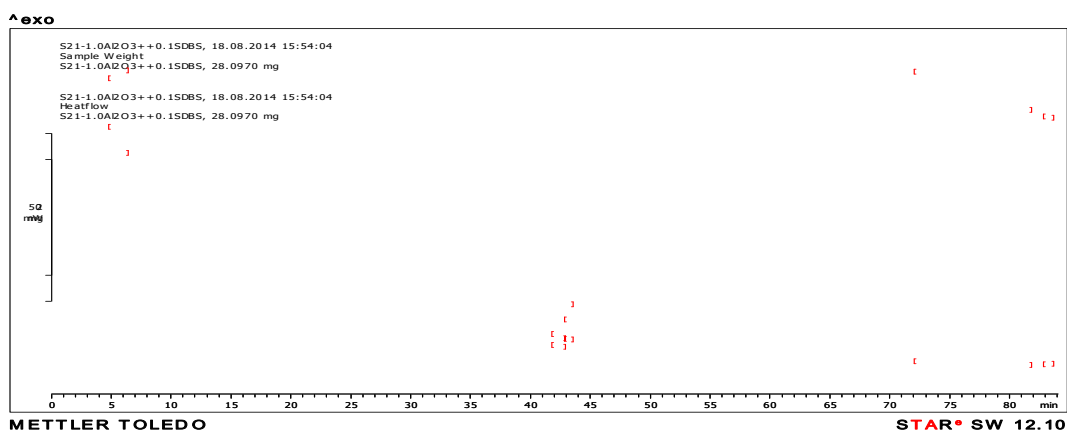


Figure A- 50 Mass loss per min and heatflow per min of surfacted 1.0Al<sub>2</sub>O<sub>3</sub>/water

This graph is reported by replotting the generated tga data into weight loss and heatflow considering the temperature and time as shown on Figures A-51& A-52

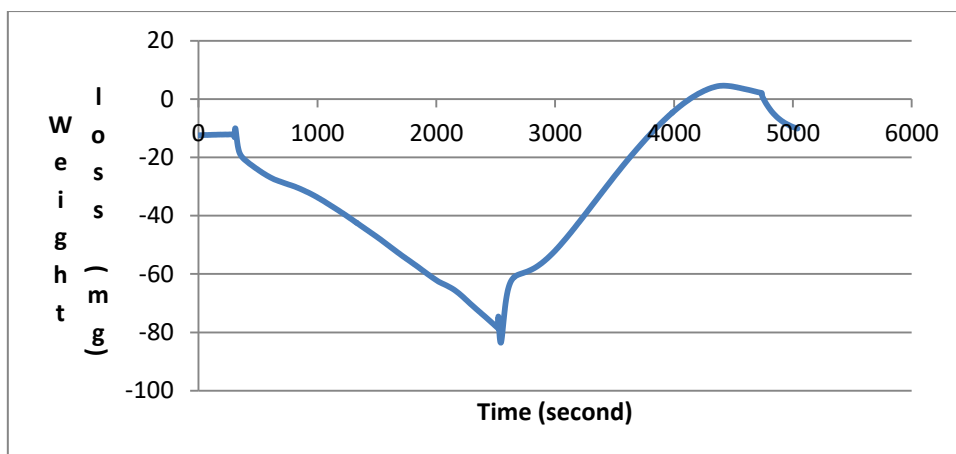


Figure A- 51 Heatflow for surfacted  $1.0\text{Al}_2\text{O}_3/\text{water}$ .

After the cleaning with pure  $1.0\text{Al}_2\text{O}_3/\text{water}$ , 47.1532mg soil sample (which comprises of oil and water retained in the soil after cleaning) was taken into a crucible for tga analysis at onset temperature of  $30^\circ\text{C}$ . As heatflow through the soil sample progressively, at 12.47 minutes into the start off the experiment, 5.1812mg (11%) water in the sample boiled off, leaving only the oil in the soil. Further progression of the heatflow led to the removal of oil by weight, 0.08716mg (0.18%) at 39.0mins. Finally, all the oil was removed at constant rate leaving the soil (41.8848mg) to its original status.

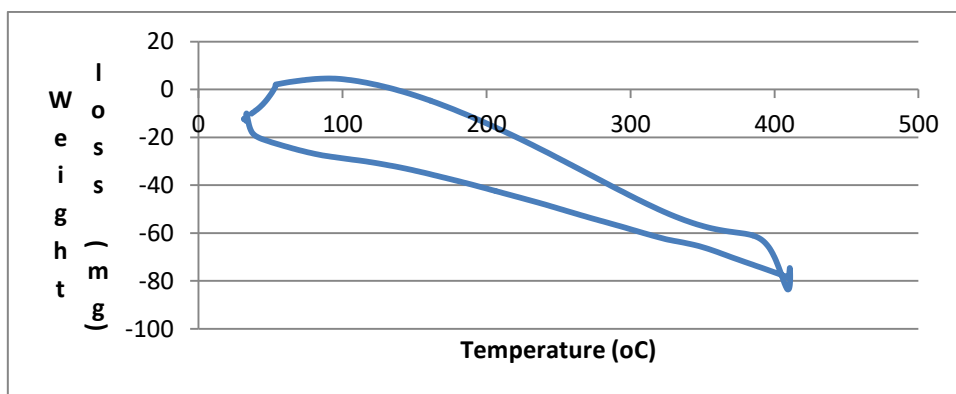


Figure A- 52 Heatflow for surfacted  $1.0\text{Al}_2\text{O}_3/\text{water}$ .

The Figure A-52 shows the heatflow of contaminated soil after cleaning with surfacted  $1.0\text{Al}_2\text{O}_3/\text{water}$  in which 53.916mg was taken from the bulk soil for tga analysis onset temperature of  $30.3369^\circ\text{C}$ . As heat flows through the soil sample  $100.038^\circ\text{C}$ , water boils off with weight of water lost equals to 14.0656mg. More weight loss occurs at  $338.819^\circ\text{C}$ , burning off all the oil (2.5277mg) with weight of hot clean soil, 37.3227mg. The weight of cleaned soil remains constant after  $388.11^\circ\text{C}$  to end temperature of  $400^\circ\text{C}$  without further



weight loss, cooling down to 30°C. The percentage loss in weight from 0 to 400°C is 30.78%.

Figure A-52 shows the change in weight of the oil contaminated soil + 1.0Al<sub>2</sub>O<sub>3</sub> – water nanofluid + 0.1g SDBS subjected to the controlled temperature rise. The onset of a rapid decrease in weight was observed at 30.33°C (the decomposition temperature of the Al (OH)<sub>2</sub>) which progressed up to 320°C. The percentage loss in weight from 0 to 400°C is 30.78%. At 338°C (boiling point of the mineral oil), the mineral oil in contaminated soil started to evaporate at constant rate to 400°C at the point where 100% soil cleaning was achieved and the soil was restored to its original status. Comparing the Figures A-49 and A-52, the total percentage weight loss of oil contaminated sample cleaned with nanofluid without surfactant (27.83%) was less than the total percentage weight loss of contaminated sample cleaned with 1.0Al<sub>2</sub>O<sub>3</sub> – water nanofluid + 0.1g SDBS (30.78%). Considering the amount of oil removed, 4.6882% was cleaned with surfacted 1.0Al<sub>2</sub>O<sub>3</sub>/water while 8.9402% was cleaned with pure 1.0Al<sub>2</sub>O<sub>3</sub>, which is more than that of surfacted 1.0Al<sub>2</sub>O<sub>3</sub>/water. In other words, more oil was removed initially with surfacted 1.0Al<sub>2</sub>O<sub>3</sub>/water than pure 1.0Al<sub>2</sub>O<sub>3</sub>/water.

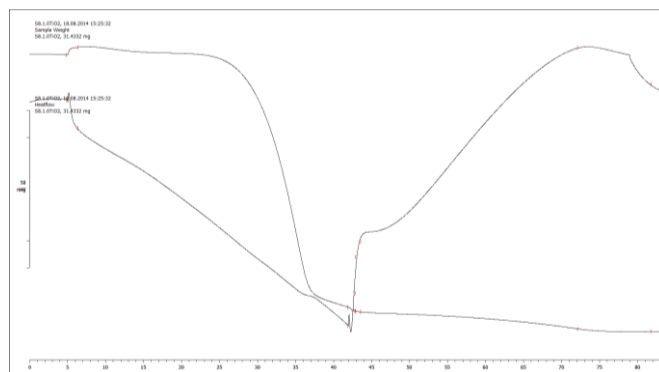


Figure A- 53 Weight loss and heatflow of pure 1.0 TiO<sub>2</sub> -Water

This graph is reported by replotting the generated tga data into weight loss and heatflow considering the temperature and time as shown on Figure A-54

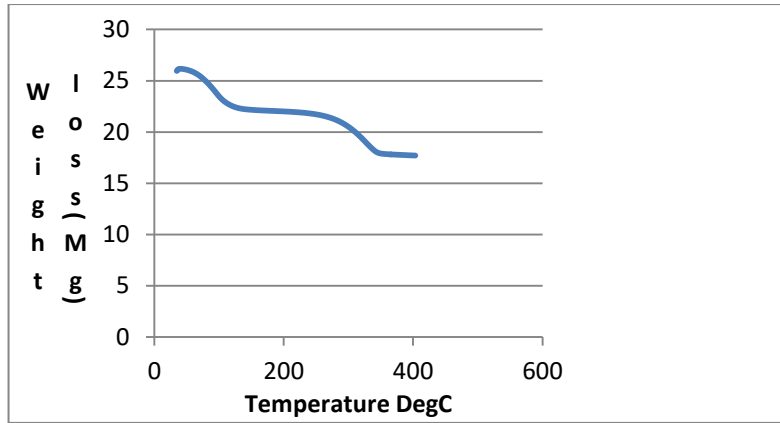


Figure A- 54 0.3vol% TiO<sub>2</sub> at controlled temperature in Thermal Analyzer.

The Figure A-54 shows the heatflow of contaminated soil after cleaning with pure 0.3vol% TiO<sub>2</sub> /water in which 25.9612mg was taken from the bulk soil for tga analysis. As heat flows through the soil sample, water boils off with weight of water lost equals to 7.9334 mg at 100.731°C. More weight loss occurs at 136.876°C, burning off all the oil (0.3084mg) with weight of hot clean soil, 25.6528mg, at 338.893°C. The weight of cleaned soil (17.7194) remains constant after the 400°C without further weight loss, cooling down at 398.907°C. The percentage loss in weight from 0 to 400°C is 31.75%.

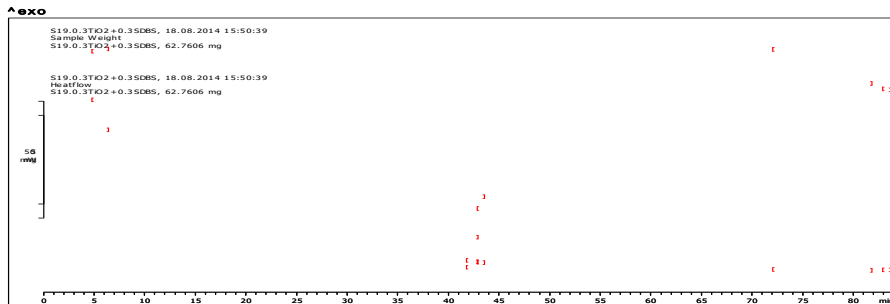


Figure A- 55 Mass loss per min and heatflow per min of Surfacted 0.3TiO<sub>2</sub>/water

This graph is reported by replotting the generated tga data into weight loss and heatflow considering the temperature and time as shown on Figures A-56 & A-57

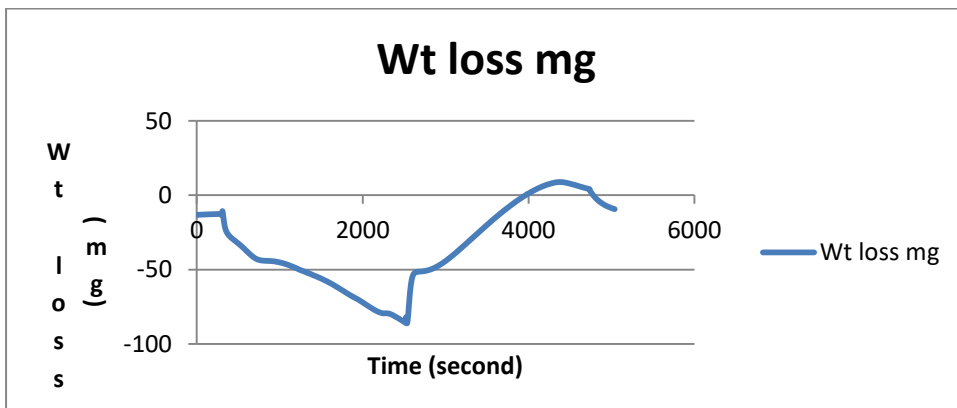


Figure A- 56 Heatflow for surfacted 0.3TiO<sub>2</sub>/water.

After the cleaning with surfacted 0.3 TiO<sub>2</sub> /water, 53.8148mg soil sample (which comprises of oil and water retained in the soil after cleaning) was taken into a crucible for tga analysis at onset temperature of 30°C. As heatflow through the soil sample progressively, at 12 minutes into the start off the experiment, 11.8392mg (22%) water in the sample boiled off, leaving only the oil in the soil. Further progression of the heatflow led to the removal of oil by weight, 0.0916mg (0.1702%) at 39.0mins. Finally, all the oil was removed at constant rate leaving the soil (41.8848mg) to its original status.

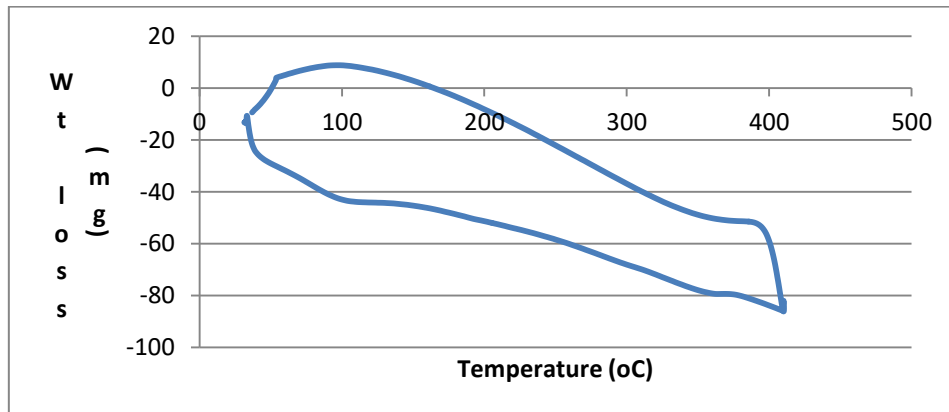


Figure A- 57 Heatflow for surfacted 0.3TiO<sub>2</sub>/water

The Figure A-57 shows the heatflow of contaminated soil after cleaning with surfacted 0.3TiO<sub>2</sub> /water in which 62.7606mg was taken from the bulk soil for tga analysis. As heat flows through the soil sample with rapid rise in temperature, water boils off with weight of water lost of 12.0812mg at 99.9282°C. Further rise in temperature led to, burning off all the oil (0.2989mg) with weight of hot clean soil, 50.3805mg, at 338.338°C. The weight of cleaned soil remains constant after 338.338°C till the end temperature of 400°C without further weight loss, cooling down to 30°C. The percentage loss in weight from 0 to 400°C is 19.73%.

Figure A-57 shows the change in weight of the oil contaminated soil + 0.3TiO<sub>2</sub> – water nanofluid + 0.1g SDBS subjected to the controlled temperature rise. The onset of a rapid decrease in weight was observed at 30°C (the decomposition temperature of the 0.3Ti (OH) <sub>2</sub>) which progressed up to 320°C. The percentage loss in weight from 0 to 400°C is 19.73%. At 338°C (boiling point of the mineral oil), the mineral oil in contaminated soil started to evaporate at constant rate to 400°C at the point where 100% soil cleaning was achieved and the soil was restored to its original status. Comparing the Figures A-54 and A-57, the total percentage weight loss of oil contaminated sample cleaned with nanofluid without surfactant (31.75%.%) was more than the total percentage weight loss of

contaminated sample cleaned with 0.3TiO<sub>2</sub> – water nanofluid + 0.1g surfactant (19.73%). More oil was cleaned with surfacted 0.3TiO<sub>2</sub> – water nanofluid than pure 0.3TiO<sub>2</sub> – water nanofluid.

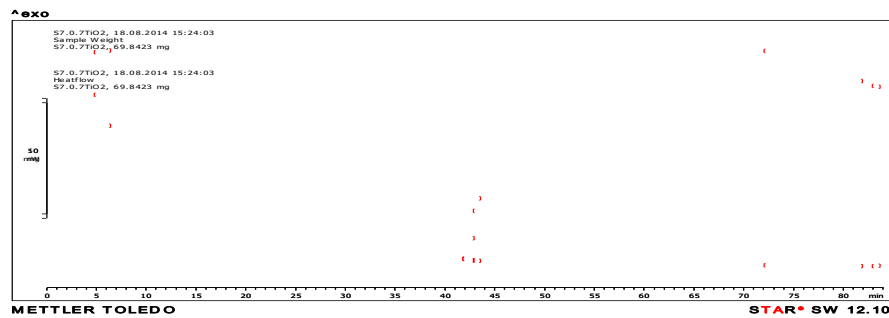


Figure A- 58 Mass loss per min and heatflow per min of pure 0.7TiO<sub>2</sub>/water

This graph is reported by replotting the generated tga data into weight loss and heatflow considering the temperature and time as shown on Figures A-59& A-60

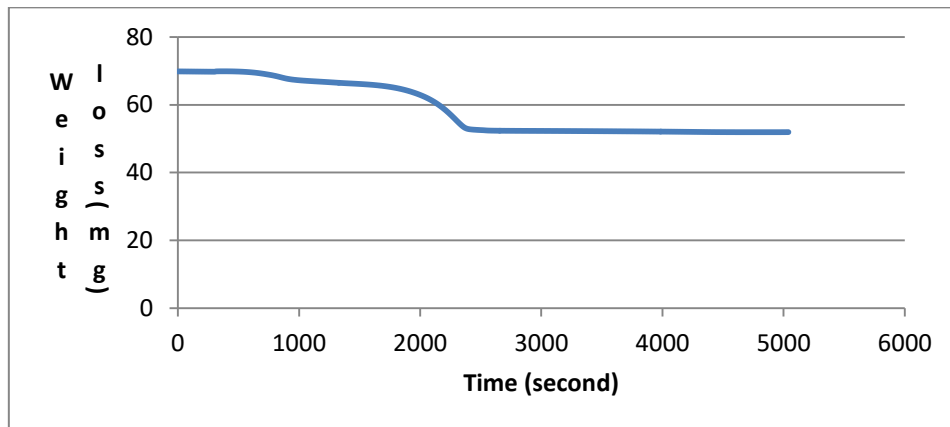


Figure A- 59 Weight loss per second of the contaminated soil cleaned with pure 0.7TiO<sub>2</sub>/water

The weight loss of this sample 69.0254mg started at 2.53 mins with weight reduced to 57.0254mg. It progressed downwards until it gets to 14.6mins (weight loss of 16.3956mg), at this point all the water hydrated and the sample continued losing oil weight at the interval of -20mg/min until it reaches the lowest point(40.33min, 51.9274mg ). Here all the oil (0.7024mg) is burnt off, leaving only the clean soil of weight 51.9274mg. After which the hot soil was cooled down at the constant rate to 84mins.

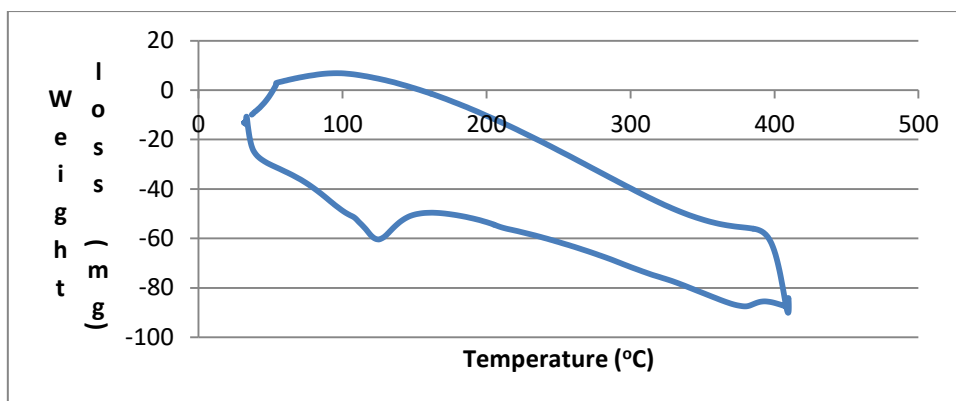


Figure A- 60 Comparison of weight loss with temperature for heatflow of 0.7TiO<sub>2</sub>/water.

The weight loss of contaminated soil cleaned with pure 0.7TiO<sub>2</sub>/water started at onset temp of 31.9145°C for water and oil retained in the soil with weight 69.0254mg and progresses downwards at interval of -20mg. Water boils off finally at 100.194°C (weight of 10.9788mg/ 15.91%) and oil burnt off at the temp of 338.945°C, weight 6.1192mg (8.8651%), leaving the hot cleaned soil cooling at constant weight to the temp of 401.046°C (and cleaned soil weight of 51.9274mg/75.2294%). The total percentage loss in weight from 0 to 400°C is 24.77%.

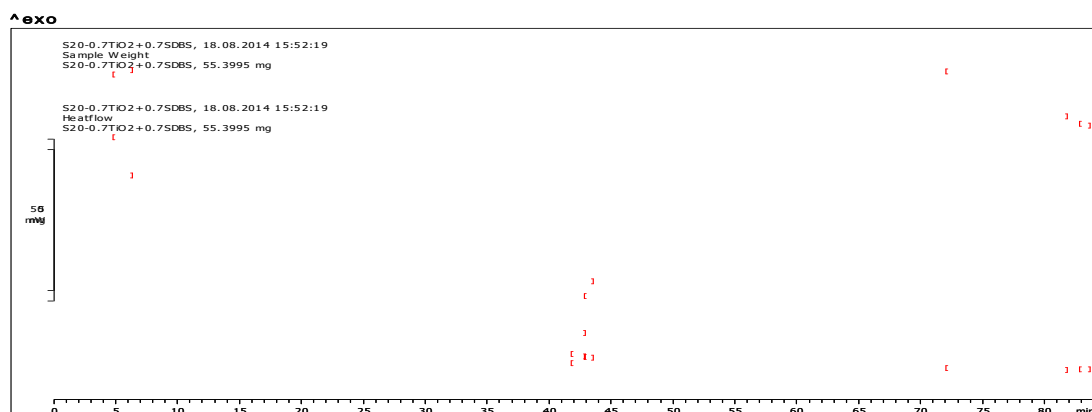


Figure A- 61 Mass loss per min and heatflow per min of surfacted 0.7TiO<sub>2</sub>

This graph is reported using tga generated data into weight loss per second and heatflow considering the temperature as shown on FiguresA-62&A-63

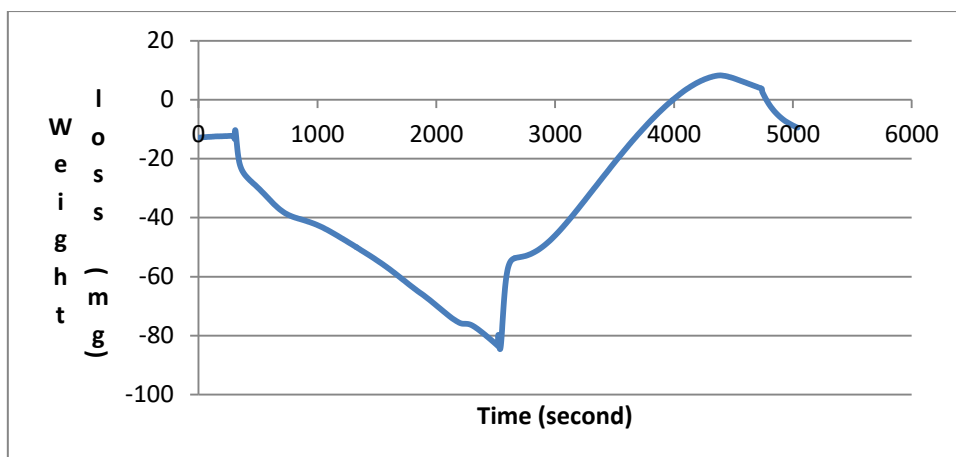


Figure A- 62 Heatflow for surfacted 0.7TiO<sub>2</sub>/water.

After the cleaning with surfacted 0.7 TiO<sub>2</sub> /water, 55.3995mg soil sample (which comprises of oil and water retained in the soil after cleaning) was taken into a crucible for tga analysis at onset temperature of 30°C. As heatflow through the soil sample progressively, at 13.2mins, 99.9697°C temperature rise, 10.2031mg (18.4173%) water in the sample boiled off, leaving only the oil in the soil. Further progression of the heatflow led to the removal of oil by weight, 0.2864mg (0.5170%) at 39.0mins. Finally, all the oil was removed at constant rate leaving the soil (44.91mg) to its original status.

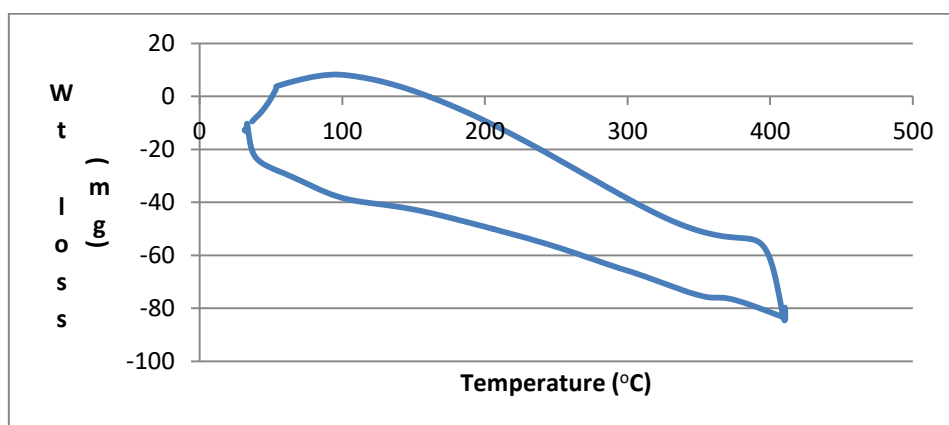


Figure A- 63 Heatflow for surfacted 0.7TiO<sub>2</sub>/water.

The Figure A-63 shows the heatflow of contaminated soil after cleaning with surfacted 0.7TiO<sub>2</sub> /water in which 55.8148mg was taken from the bulk soil for tga analysis. As heat flows through the soil sample at 100 °C, water boils off with weight of water lost equals to 10.4366mg. As the More weight loss progresses, all the oil (0.4682mg) burnt off leaving the hot clean soil (44.91mg) at 357.024°C. The weight of cleaned soil remains constant without further weight loss, cooling down to 30°C. The percentage loss in weight from 0 to 400°C is 19.54%.

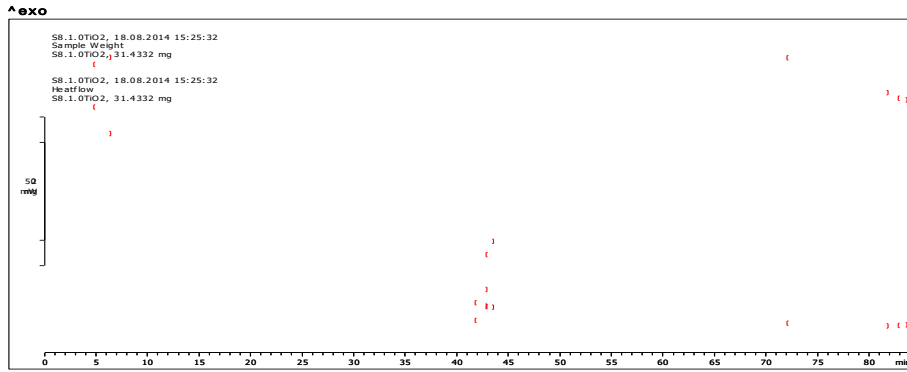


Figure A- 64 Mass loss per min and heatflow per min of pure 1.0TiO<sub>2</sub>/water

This graph is reported using tga generated data into weight loss per second and heatflow considering the temperature as shown on FiguresA-65 & A-66.

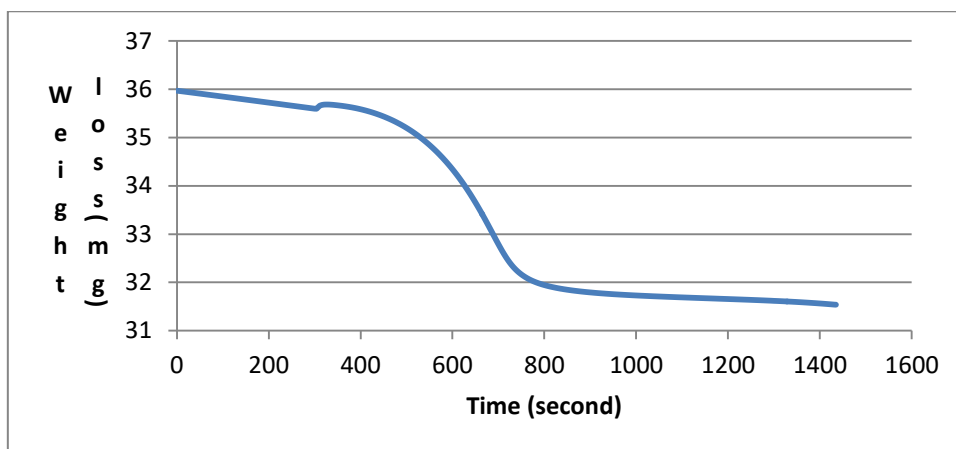


Figure A- 65 Weight loss per second of the contaminated soil cleaned with pure 1.0TiO<sub>2</sub>/water.

Soil sample (36mg) consisting of oil and water retained in the soil after cleaning with 1.0TiO<sub>2</sub>/water. Water (4.4319mg) in the soil evaporated at 3.42mins leaving only 0.2844mg oil which burnt off at 14.55mins. The contaminated soil is finally cleaned at 22.9mins with the constant soil weight of 31.5385mg without further weight loss. The percentage loss in weight from 0 to 400°C is 12.39%.

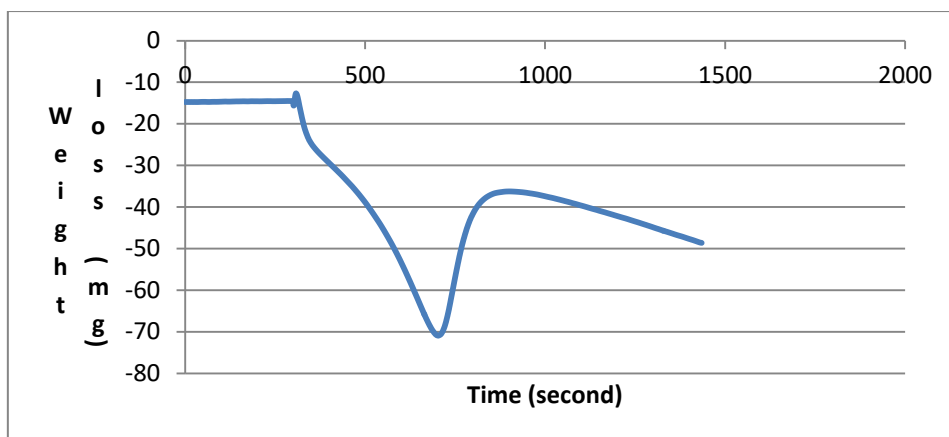


Figure A- 66 Heatflow for pure 1.0TiO<sub>2</sub> nanofluid

The heatflow of contaminated soil after cleaning with 1.0TiO<sub>2</sub>/water started at 1.48mins with weight of 35.9681mg, constantly losing water at the rate of -10mg/min until it gets to 12.28mins, all the water (4.3948mg /12.2186%) boils off. As tga analysis progresses further at 13.83mins (0.0348mg /0.09675%), the soil loses all the oil weight constantly until it gets to 23.92mins and final weight loss of 31.5385mg (87.6846%). Figure A-66 shows that the amount of oil retained in the soil after cleaning with 1.0TiO<sub>2</sub>/water was small; this is the reason why the time taken to restore the soil to its original status took shorter time (23.92mins than the designed experimental time of 40mins).

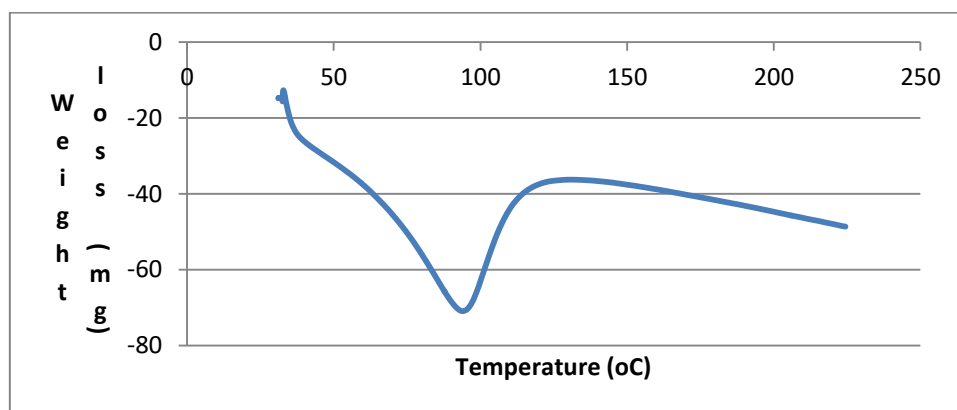


Figure A- 67 Heatflow for pure 1.0TiO<sub>2</sub>/water.

From the graph, it is observed that the soil was restored to its original status at temp of 224.43°C. Sample (35.9681mg) started losing weight after the onset temp of 30 °C. As the experiment progresses, water evaporates finally at 100.082°C (4.3948mg/12.2186%) after which all the oil (0.0348mg/0.09675%) was cleaned at end temperature of 224.428°C (leaving cleaned soil weight of 31.5385mg/87.6846%) earlier than 400°C due to little quantity of oil retained in the soil after the contaminated soil with 1.0wt% TiO<sub>2</sub>/water, this is the best pure monotype nanofluids. The total percentage loss in weight from 0 to 400°C is 12.32%.



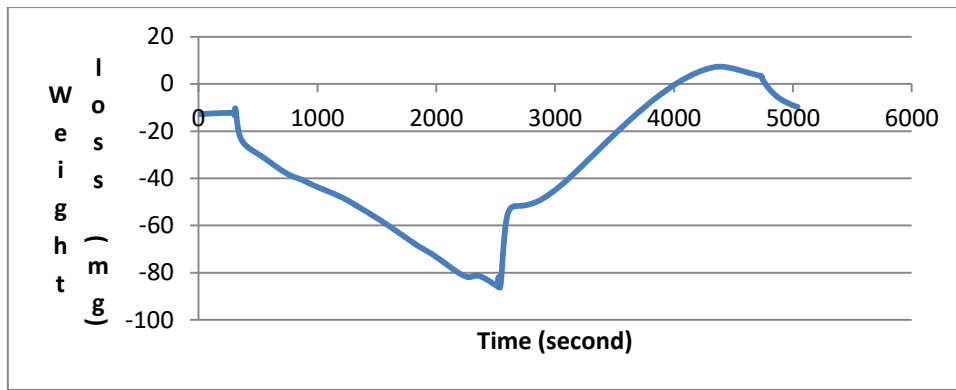


Figure A- 68 Heatflow for surfacted 1.0 TiO<sub>2</sub>/water

After the cleaning with surfacted 1.0 TiO<sub>2</sub> /water, 53.8148mg soil sample (which comprises of oil and water retained in the soil after cleaning) was taken into a crucible for tga analysis at onset temperature of 30°C. As heatflow through the soil sample progressively, at 12 minutes into the start off the experiment, 11.8392mg (22%) water in the sample boiled off, leaving only the oil in the soil. Further progression of the heatflow led to the removal of oil by weight, 0.0916mg (0.1702%) at 39.0mins. Finally, all the oil was removed at constant rate leaving the soil (41.8848mg) to its original status. The percentage loss in weight from 0 to 400°C is 22.17% of which oil is only 0.17%. This result is very good as the cleaning efficiency is 99.4%, so only 0.6% was retained in the soil before tga analysis.

Comparing Figure A-66 and Figure A-68, more oil (0.17%) was removed with surfacted TiO<sub>2</sub>/water than pure TiO<sub>2</sub>/water; oil removed was 0.097% and difference of 0.073%.

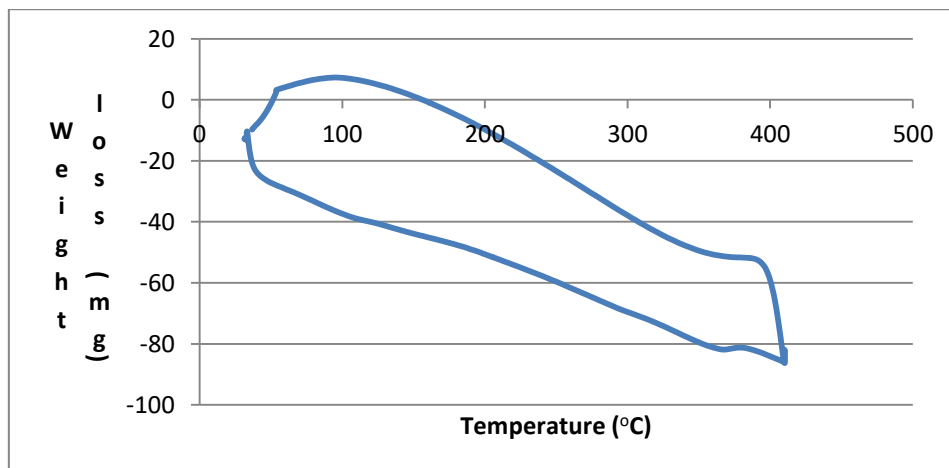


Figure A- 69 Heatflow for surfacted 1.0 TiO<sub>2</sub>/water

The Figure A-69 shows the heatflow of contaminated soil after cleaning with surfacted 1.0 TiO<sub>2</sub> /water in which 53.8148mg was taken from the bulk soil for tga analysis. As heat flows through the soil sample by 100.784°C into the start of the analysis, water boils off with weight

of water lost equals to 11.8384mg. More weight loss occurs at 338.578 °C, burning off all the oil (0.0916mg) with weight of hot clean soil, 41.8848mg, at 400°C. The weight of cleaned soil remains constant after 400°C without further weight loss, cooling down at 36.8055 °C.

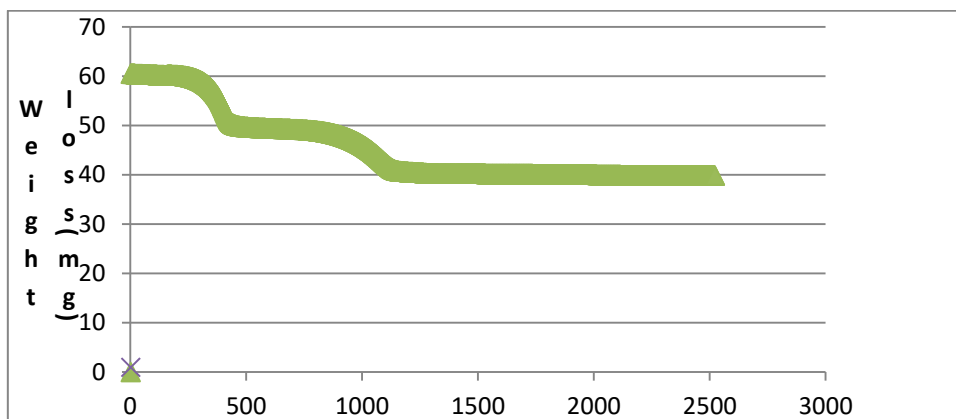


Figure A-70 shows the graph of 10g soil contaminated with 5g High viscosity oil and cleaned with 15g of pure 0.3wt% ZnO/water. After the cleaning, 60.5409mg soil sample (which comprises of oil and water retained in the soil after cleaning) was taken into a crucible for tga analysis at onset temperature of 30°C. As heatflow through the soil sample progressively, at 100°C (the boiling point of water) and 6.8 minutes, 15.5101mg (25.62%) water in the sample boiled off, leaving only the oil in the soil. Further progression of the heatflow led to the removal of oil by weight 7.7mg (12.72%) at 17.25mins, 338°C (solubility temperature of the experimental mineral oil). Finally, all the oil was removed at 40.68mins, 400°C, constantly leaving the soil to its original status. The percentage loss in weight from 0 to 400°C is 34.08 %.

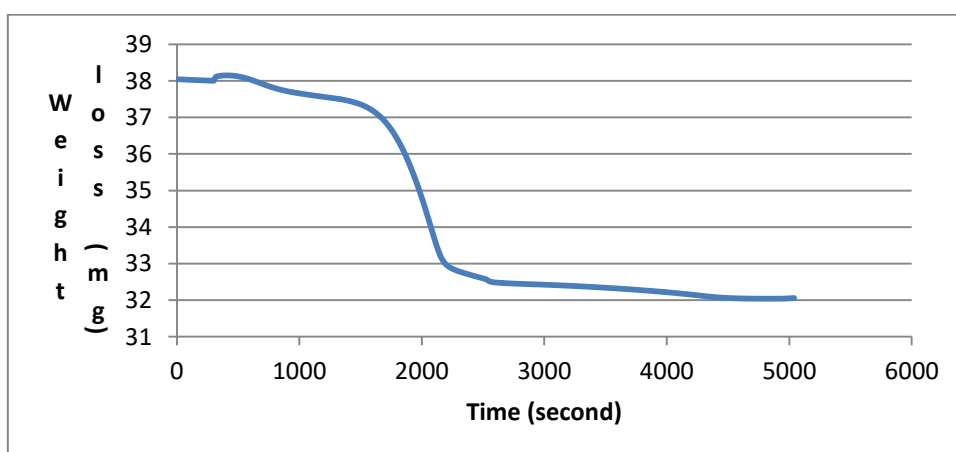


Figure A-71 Weight loss per second of the contaminated soil cleaned with surfactated 0.3ZnO/water.

Figure A-71 shows the weight loss of 45.1878mg soil sample cleaned with 0.3ZnO

deionised water nanofluid. During the tga analysis at 0.3ZnO deionised water nanofluid 100.054°C , 6.5363water boils off .As the temperature increases further 1.6055mg oil was burnt off , leaving dried 37.0486mg soil constantly at the end temperature of 400°C. The total percentage loss in weight from 0 to 400°C is 18.02%. Comparing the Figures A-69 and A-70 , the total percentage weight loss of oil contaminated sample cleaned with nanofluid without surfactant (34.08 %) was more than the total percentage weight loss of contaminated sample cleaned with 0.3ZnO – water nanofluid + 1g surfactant (18.02%).

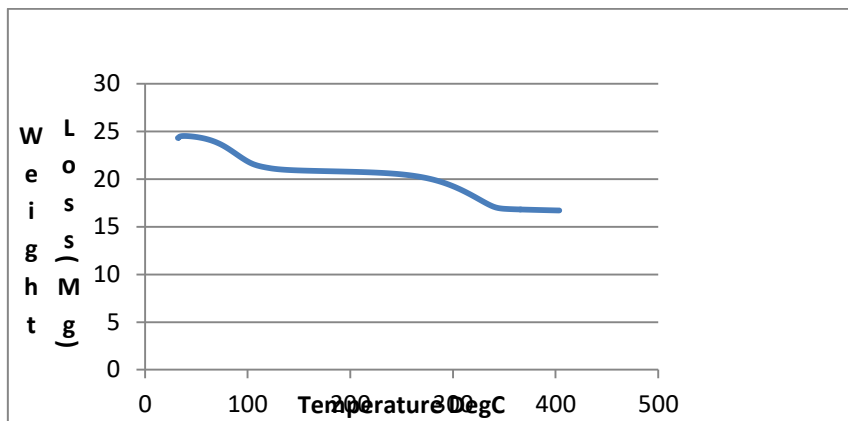


Figure A- 72 10g Soil contaminated with 5g oil HV1 and cleaned with 15g pure 0.7ZnO deionised water nanofluid

Figure A-72 shows the weight loss of 45.1878mg soil sample cleaned with pure 0.7ZnO deionised water nanofluid. During the tga analysis, 0.7ZnO deionised water nanofluid at 100.054°C, 7.5363mg water boils off As the temperature increases further 0.6055mg oil was burnt off, leaving dried 37.0486mg soil constantly at the end temperature of 400°C. The total percentage loss in weight from 0 to 400°C is 18.02% .

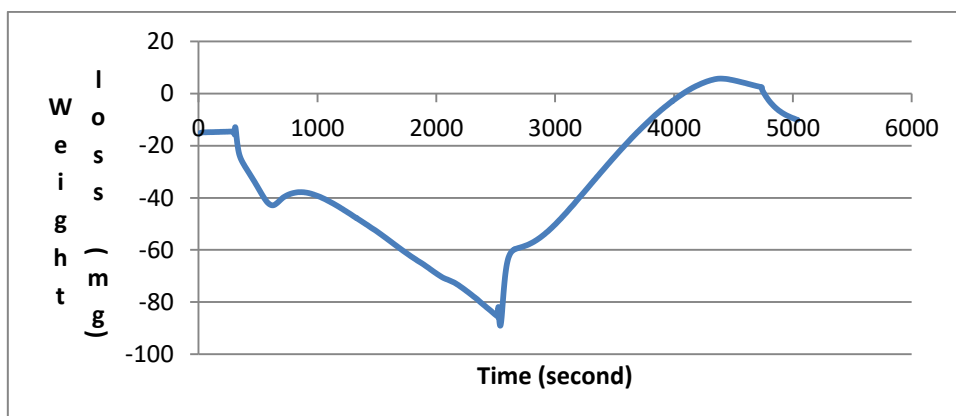


Figure A- 73 Heatflow for pure 0.7ZnO/water.

The Figure A-73 shows the heatflow of contaminated soil after cleaning with pure 0.7ZnO/water in which 45.1878mg was taken from the bulk soil for tga analysis. As heat flows through the soil sample by 12mins into the start of the analysis, water boils off with weight of water lost equals to 8.7068mg. More weight loss occurs at 21.083mins, burning off all the oil (0.69mg) with weight of hot clean soil, 35.3350mg, cooling down at 41.92mins. The weight of cleaned soil remains constant without further weight loss.

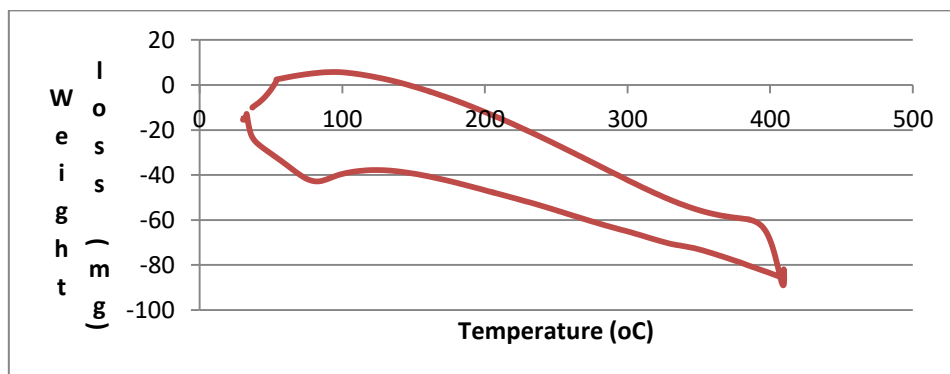


Figure A- 74 Heatflow for contaminated soil cleaned with pure 0.7ZnO/water nanofluid. The soil sample with onset temperature of 30.398°C and weight 45.1878mg lost its water (7.5337mg/16.6720%) as the analysis progresses at 100.054°C. under at controlled temperature in Thermal Analyzer The weight loss increases with increase in temp until it reaches 338°C where all the oil (0.6055mg/1.340%) burnt off and the weight becomes constant at 400°C without further weight loss. At this temperature all the oil has been burnt off leaving only clean soil by weight 37.0486mg. The percentage loss in weight from 0 to 400°C is 18.0119%.

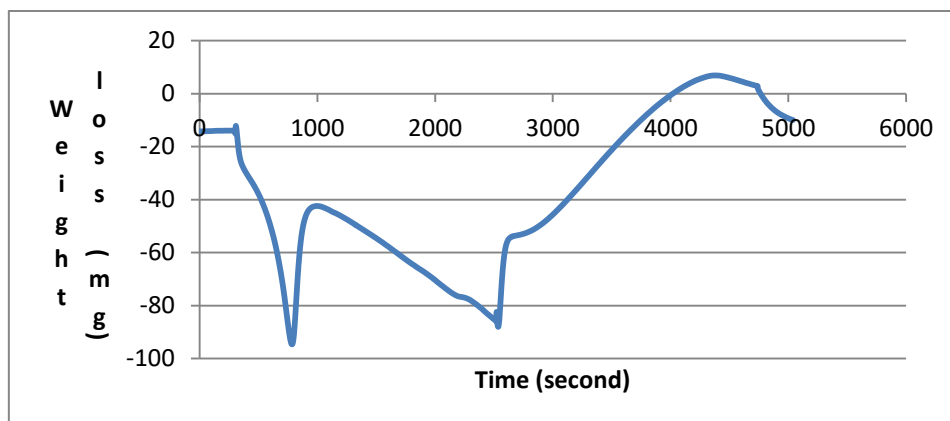


Figure A- 75 Heatflow for contaminated soil cleaned with pure 1.0ZnO/water. The Figure A-75 shows the heatflow of contaminated soil after cleaning with 1.0ZnO /water in which 47.4719mg was taken from the bulk soil for tga analysis. As heat flows through the soil sample by 12 37mins into the start of the analysis, water boils off with weight of water lost

equals to 9.3027mg. More weight loss occurs at 36.8667mins, burning off all the oil (3.0714mg/6.47%) with weight of hot clean soil, 35.0978mg, at 40.93mins. The weight of cleaned soil remains constant without further weight loss, cooling down at 83.83mins. The percentage loss in weight from 0 to 400°C is 26.07% [57].

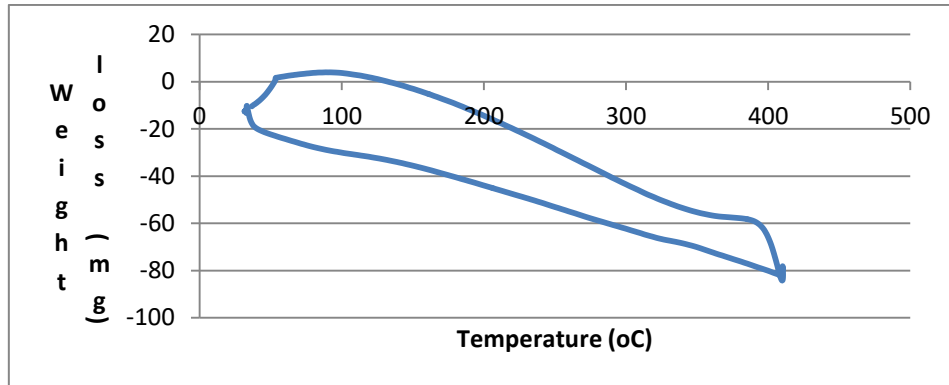


Figure A- 76 Heatflow for contaminated soil cleaned with surfacted 1g ZnO nanofluid

The Figure A-76 shows the change in weight of the oil contaminated soil + ZnO – water nanofluid + 0.5g hexametaphosphate subjected to the controlled temperature rise. The onset of a rapid decrease in weight was observed at 30.74°C (the decomposition temperature of the Zn (OH) 2) which progressed up to 319°C. The percentage loss in weight from 0 to 400°C is 15.93%. At 338°C (boiling point of the mineral oil), the mineral oil in contaminated soil started to evaporate at constant rate to 400°C at the point where 100% soil cleaning was achieved and the soil was restored to its original status. Comparing the FigureA-75 and FigureA-76 , the total percentage weight loss of oil contaminated sample cleaned with nanofluid without surfactant (26.07%.) was more than the total percentage weight loss of contaminated sample cleaned with ZnO – water nanofluid + 0.5g surfactant (22.17%).

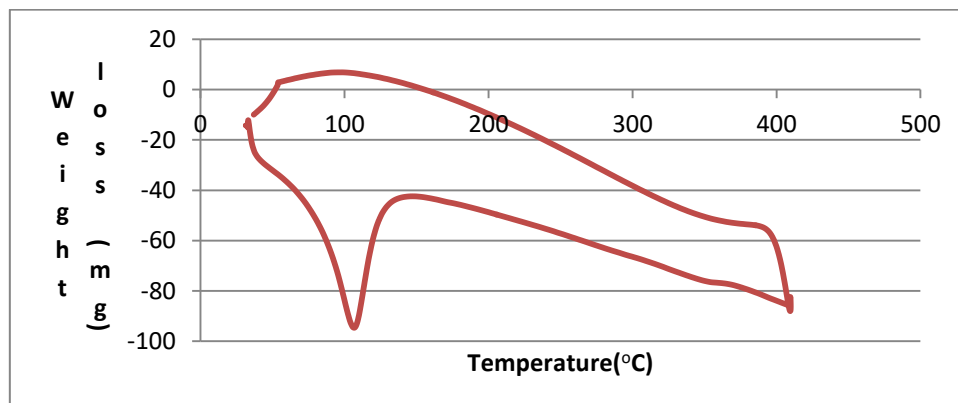


Figure A- 77 Further result on heatflow for soil cleaned with surfacted 1.0%ZnO/water.

Figure A-77 10g Soil contaminated with 5g Oil HV1 and cleaned with 15g 1.0ZnO/water deionised water nanofluid at controlled temperature in Thermal Analyzer.

Figure A-76 shows soil sample consisting of water and oil retained in the soil (wt – 47.4719mg) after clean-up process, energy/heatflow used to evaporate 12.2657mg/25.8378% of water to its boiling point (100.099°C) in the Tga as shown in Figure A-75.

While the oil retained in the soil (0.1084mg/0.2283%) burnt off at solubility point of 338°C leaving the soil to its original status. This oil vaporises completely at 364.388°C leaving the clean soil (35.0978mg) with constant weight, cooling down to 384.497°C.

Comparing Figure A-75 and FigureA-77, oil (0.2283%) removed using surfacted1.0%ZnO/water during the tga analysis is smaller than that of pure 1.0%ZnO/water (6.47%).This shows that more oil was retained in the soil after cleaning with pure 1.0%ZnO/water.Therefore, surfacted1.0ZnO%/water is more effective in removing oil from the contaminated soil.

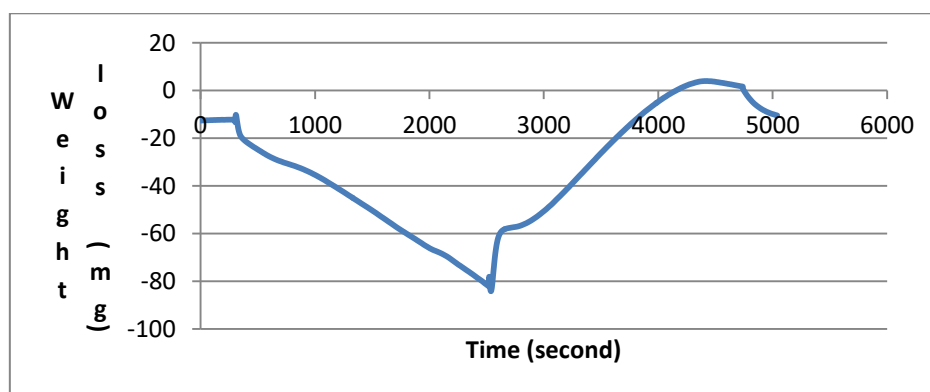


Figure A- 78 Heatflow for contained soil cleaned with surfacted 1.0ZnO/water per second.

Figure A -78 shows the change in weight of the oil contaminated soil + ZnO – water nanofluid + 0.5g hexametaphosphate subjected to the controlled temperature rise.The onset of a rapid decrease in weight was observed at 30.33°C (the decomposition temperature of the Zn (OH) 2) which progressed up to 320°C.At 338°C (boiling point of the mineral oil), the mineral oil in contaminated soil started to evaporate at constant rate to 400°C at the point where 100% soil cleaning was achieved and the soil was restored to its original status.Comparing the Figures A-78 and A-79, the total percentage weight loss of oil contaminated sample cleaned with nanofluid without surfactant (26.07%) was more than the total percentage weight loss of contaminated sample cleaned with ZnO – water nanofluid + 0.5g surfactant (22.17%) [41a].



Figure A- 79 Mass loss per min and heat flow of pure  $0.3\text{Al}_2\text{O}_3 + 0.7\text{TiO}_2/\text{water}$

This graph is reported using tga generated data into weight loss per second and heatflow considering the temperature as shown on Figures A-80 to A-81.

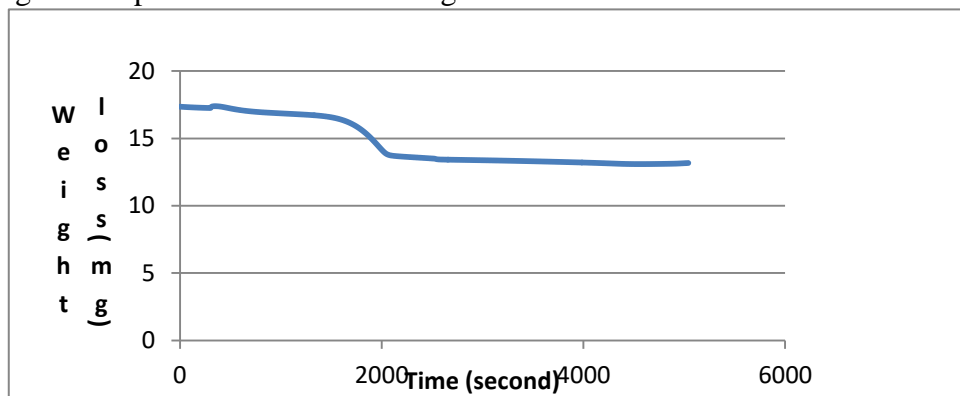


Figure A- 80 Weight loss per second of surfacted  $0.3\text{Al}_2\text{O}_3 + 0.7\text{TiO}_2/\text{water}$

The sample (17.3588mg) started losing water at 6.47mins until it gets to 13.067mins with weight loss of 3.7661mg, when all the water dried up. As the weight loss increases downwards on reaching 32.83mins, the oil burnt off with the weight loss of 0.0393mg leaving the clean soil at constant weight of 13.5534mg at 84mins. The total percentage loss from 0 to  $400^\circ\text{C}$  is 28.08%.

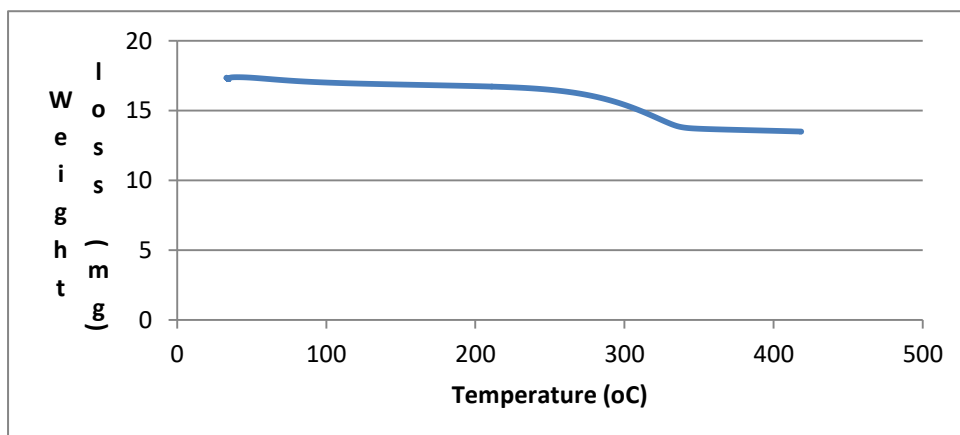


Figure A- 81 Comparison of temperature with weight loss of soil sample cleaned

with pure  $0.3\text{Al}_2\text{O}_3 + 0.7\text{TiO}_2/\text{water}$

The sample (17.3588mg) started losing water at temp of  $33.0189^\circ\text{C}$  until it gets to  $100.094^\circ\text{C}$  with weight loss of 3.7661mg, when all the water dried up. As the weight loss increases downwards on reaching the temperature of  $388.521^\circ\text{C}$ , the oil burnt off with the weight loss of 0.0393mg leaving the clean soil at constant weight of 13.5534mg at  $400.05^\circ\text{C}$ . The total percentage loss from 0 to  $400^\circ\text{C}$  is 28.08%.

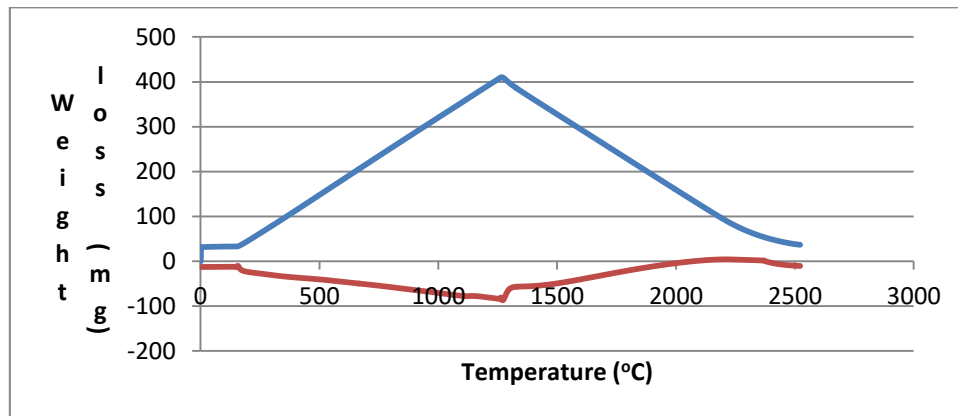


Figure A- 82 Heatflow for sample cleaned with surfacted  $0.3\text{Al}_2\text{O}_3 + 0.7\text{TiO}_2/\text{water}$ .

Figure A-82 shows the heatflow of contaminated soil after cleaning with surfacted  $0.3\text{Al}_2\text{O}_3 + 0.7\text{TiO}_2/\text{water}$  in which 57.9348mg was taken from the bulk soil for tga analysis. As heat flows through the soil sample by 11 97mins into the start of the analysis, water boils off with weight of water lost equals to 9.5352mg. More weight loss occurs at 32.4667mins, burning off all the oil (0.2271mg) with weight of hot clean soil, 48.1725mg, at 40.43mins. The weight of cleaned soil remains constant after 41.40mins without further weight loss, cooling down at 81.03mins. The total percentage weight loss of oil contaminated sample cleaned with nanofluid from 0 –  $400^\circ\text{C}$  is 16.85%.

Comparing the Figures A-81 and A-82, the total percentage weight loss of oil contaminated sample cleaned with nanofluid without surfactant (28.08%) was more than the total percentage weight loss of contaminated sample cleaned with  $0.3\text{Al}_2\text{O}_3 + 0.7\text{TiO}_2 - \text{water nanofluid} + 0.1\text{g surfactant}$  (16.85%).



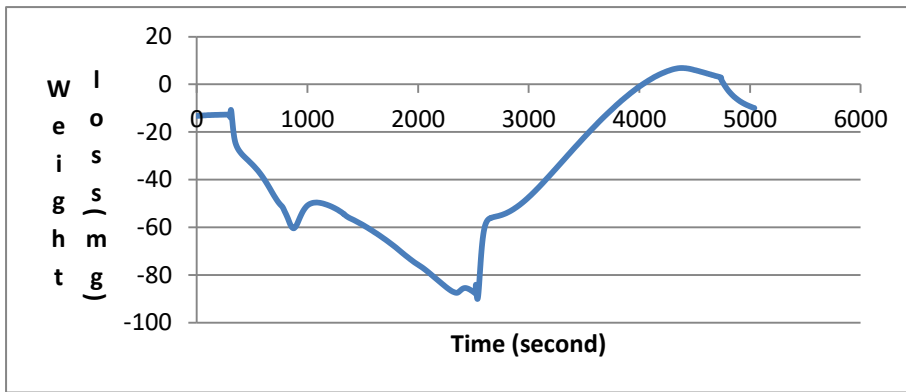


Figure A- 83 Heatflow for  $0.3\text{Al}_2\text{O}_3 + 0.7\text{TiO}_2/\text{water}$  per second.

Soil sample weighing 57.9348mg obtained from the 10g soil contaminated with 5g oil cleaned with 15g  $0.3\text{Al}_2\text{O}_3 + 0.7\text{TiO}_2/\text{water}$  was used for tga analysis. The result is shown on the Figure A-82. As heatflow through the soil sample progressively, at 14.53 minutes into the start off the experiment, 9.5352mg (16.4585%) water in the sample boiled off, leaving only the oil in the soil. Further progression of the heatflow led to the removal of oil by weight, 0.2271mg (0.3920%) at 39.1mins. Finally, all the oil was removed at constant rate leaving the soil (48.1725mg/83.1495%) to its original status.

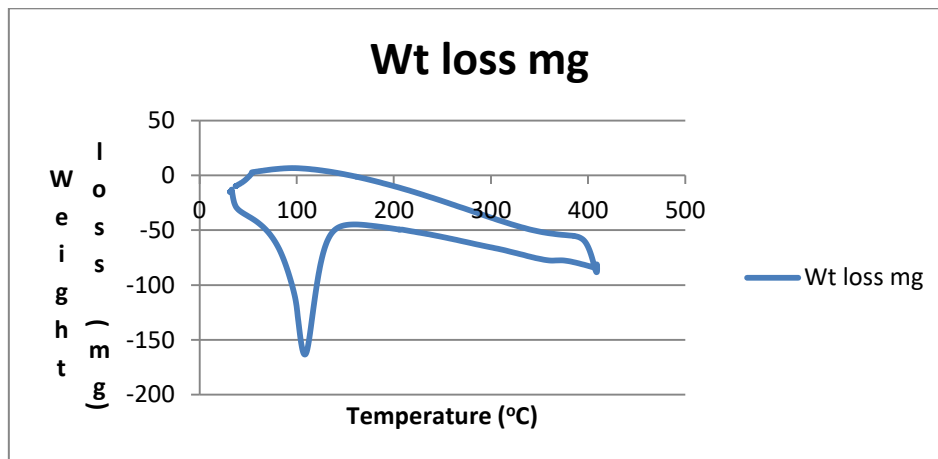


Figure A- 84 Further result on Heatflow for sample cleaned with pure  $0.3\text{Al}_2\text{O}_3 + 0.7\text{TiO}_2/\text{water}$ .

The Figure A-84 above shows the heatflow of contaminated soil after cleaning with  $0.3\text{Al}_2\text{O}_3 + 0.7\text{TiO}_2/\text{water}$  in which 57.9348mg was taken from the bulk soil for tga analysis. As heat flows through the soil sample by 11 97mins into the start of the analysis, water boils off with weight of water lost equals to 9.5352mg at 100.067°C. More weight loss occurs at 32.4667mins, burning off all the oil (0.2271mg) with weight of hot clean soil, 48.1725mg, at 338.092°C. The weight of cleaned soil remains constant after 41.40mins without further weight loss, cooling down at 36.7988°C.

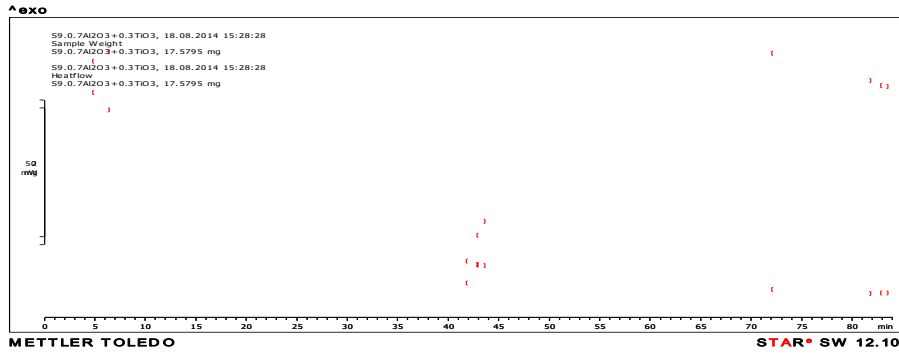


Figure A- 85 Weight loss of soil cleaned with pure  $0.7Al_2O_3 + 0.3TiO_2$ /water

This graph is reported using tga generated data into weight loss per second and heatflow considering the temperature as shown on Figures A-86 to A-89.

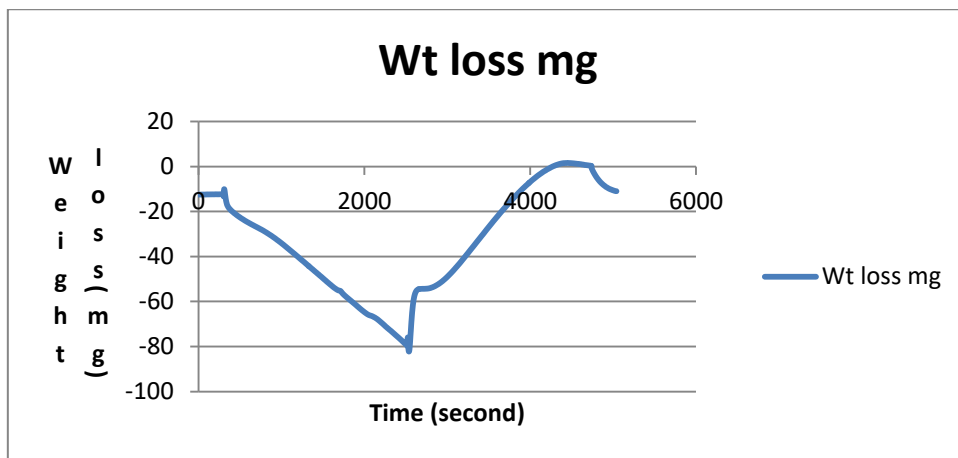


Figure A- 86 Weight loss per second of heatflow for pure  $0.7Al_2O_3 + 0.3TiO_2$

From the Figure A-86 weight loss of the 10g soil contaminated with 5g oil after cleaning with pure  $0.7Al_2O_3 + 0.3TiO_2$ /water (17.5795mg) started at 0mins until it gets to 11.93mins, weight loss of 3mg (water boils off at this time leaving only 0.6279mg oil) and progresses downwards linearly at interval of -10mg until it gets to the lowest point of 13.9516mg (42.17mins) where all the oil burns off leaving only clean soil and cooling upwards at constant rate. The hot clean soil cools down to 13.9516mg at 84mins.

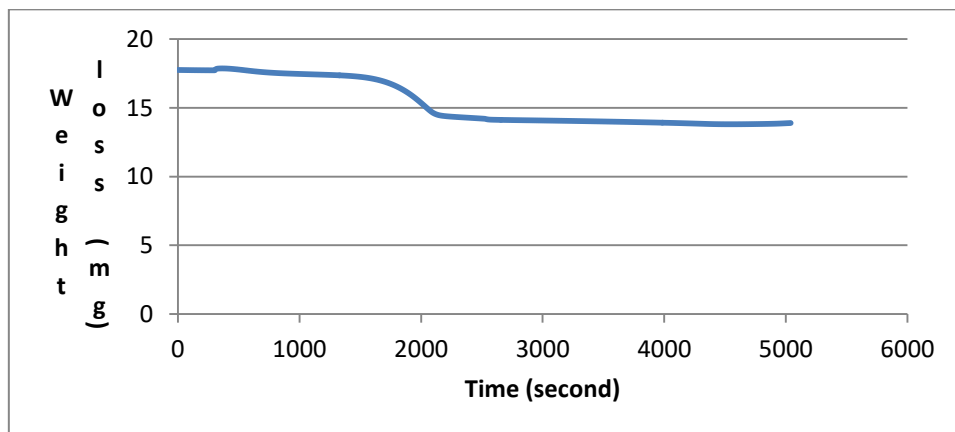


Figure A- 87 Weight loss per second for soil sample cleaned with  $0.7\text{Al}_2\text{O}_3 + 0.3\text{TiO}_2$  /water  
 From the Figure A-87 weight loss of the 10g soil contaminated with 5g oil cleaned with pure  $0.7\text{Al}_2\text{O}_3 + 0.3\text{TiO}_2$ /water (17.5795mg) started at 0mins until it gets to 11.93mins, weight loss of 3mg (water boils off at this time leaving only 0.6279mg oil) and progresses downwards linearly at interval of -10mg until it gets to the lowest point of 13.9516mg (42.17mins) where all the oil burns off leaving only clean soil and cooling upwards at constant rate. The hot clean soil cools down to 13.9516mg at 84mins.

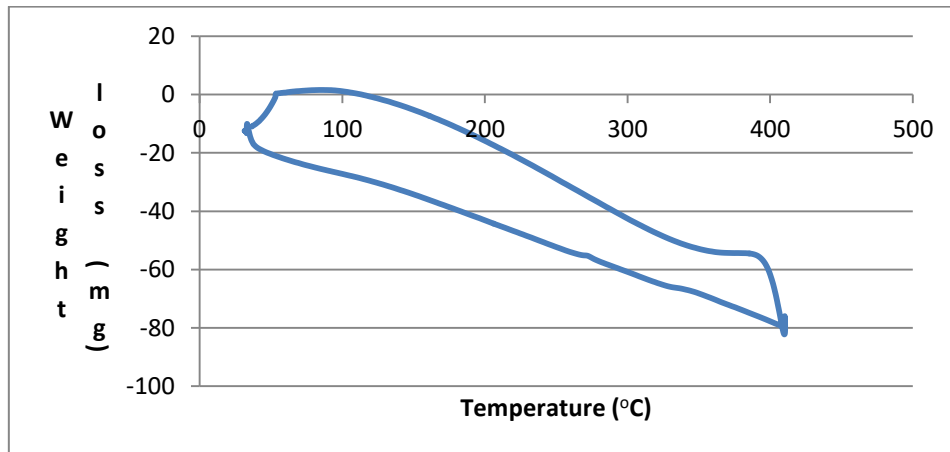


Figure A- 88 Comparison of weight loss with temperature for heatflow of  $0.7\text{Al}_2\text{O}_3 + 0.3\text{TiO}_2$ /water.

Soil sample weighing 17.7475mg obtained from the 10g soil contaminated with 5g oil cleaned with 15g  $0.7\text{Al}_2\text{O}_3 + 0.3\text{TiO}_2$ /water was used for tga analysis. The result is shown on the Figure above. As heatflow through the soil sample progressively, at 100.18°C into the start off the experiment, 3.7008mg (20.8525%) water in the sample boiled off, leaving only the oil in the soil. Further progression of the heatflow led to the removal of oil by weight, 0.1566mg (0.8824%) at 39.1mins. Finally, all the oil was removed at constant rate leaving the soil (13.8901mg/78.27%) to its original status at 37.5434°C. Total percentage loss from 0 to 400°C is 21.73%.

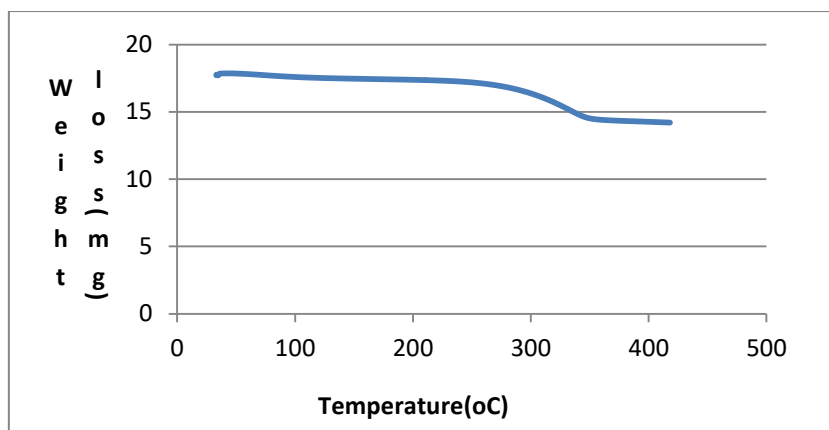


Figure A- 89 Comparison of weight loss with temperature for sample cleaned surfacted  $0.7\text{Al}_2\text{O}_3 + 0.3\text{TiO}_2/\text{water}$ .

The sample (17.5795mg) started losing water at temp of  $33.2509^\circ\text{C}$  until it gets to  $100.047^\circ\text{C}$  with weight loss of 3.6583mg, when all the water dried up. As the weight loss increases downwards on reaching the temperature of  $388.558^\circ\text{C}$ , the oil burnt off with the weight loss of 0.0693mg leaving the clean soil at constant weight of 13.9516mg at  $410.188^\circ\text{C}$ . Weight loss from 0 – 400% is 20.64%. Comparing the Figures A-87 and A-88, the total percentage weight loss of oil contaminated sample cleaned with nanofluid without surfactant (21.73%) was more than the total percentage weight loss of contaminated sample cleaned with  $0.7\text{Al}_2\text{O}_3 + 0.3\text{TiO}_2/\text{water}$  nanofluid + 0.1g surfactant (20.64%).

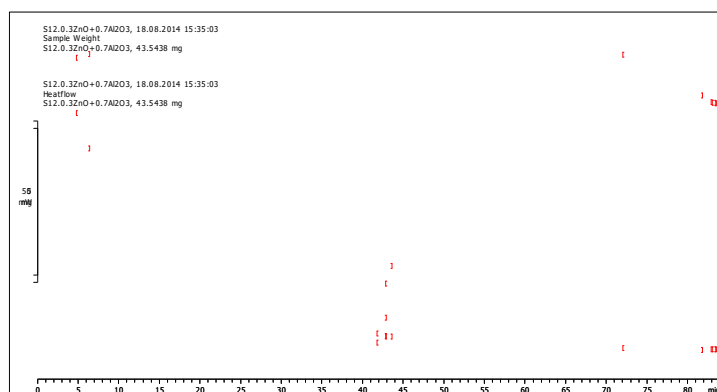


Figure A- 90 Massloss per second of contaminated soil cleaned with pure  $0.3\text{ZnO} + 0.7\text{Al}_2\text{O}_3/\text{water}$ .

This graph is reported using tga generated data into weight loss per second and heatflow considering the temperature as shown on Figure A-91.

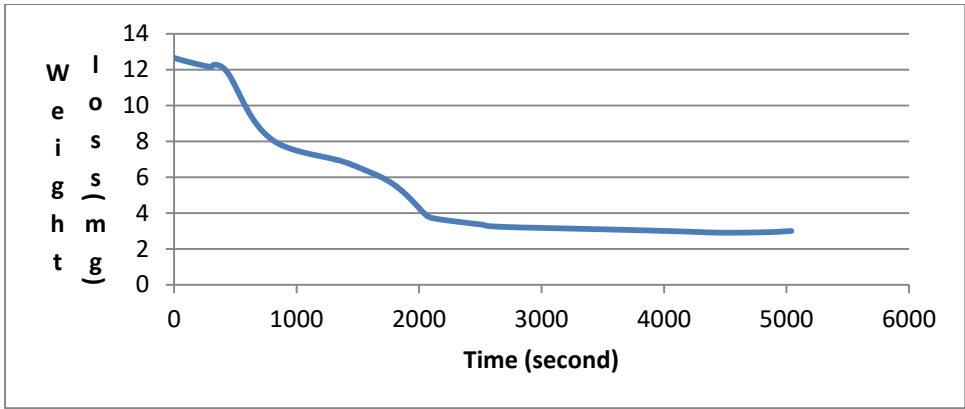


Figure A- 91 Weight loss per second of soil cleaned with pure 0.3ZnO + 0.7Al<sub>2</sub>O<sub>3</sub>/water.

The soil sample (43.5438mg) started losing water at temp of 33.2509°C until it gets to 13mins with weight loss of 9.8609mg, when all the water dried up. As the weight loss increases further, the oil burnt off with the weight loss of 0.0994mg leaving the clean soil at constant weight of 33.5835mg at 84mins. The total percentage loss from 0 – 400°C is 22.87%.

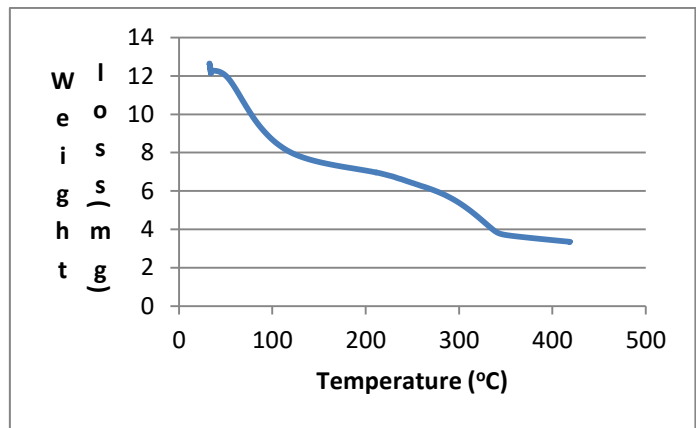


Figure A- 92 Comparison of weight loss with temperature rise for soil sample cleaned surfacted 0.3ZnO + 0.7Al<sub>2</sub>O<sub>3</sub>/water.

The Figure A-92 shows the heatflow of contaminated soil after cleaning with surfacted 0.3ZnO + 0.7Al<sub>2</sub>O<sub>3</sub>/water in which 18.6109mg was taken from the bulk soil for tga analysis. As heat flows through the soil sample at 100.24°C into the start of the analysis, water boils off with weight of water lost equals to 2.6675mg. More weight loss occurs at at 337.506°C, burning off all the oil (0.98154mg) with weight of hot clean soil, 14.9619mg. The weight of cleaned soil remains constant even after 400.208°C without further weight loss, cooling down at 37.4203°C. Total percentage loss from 0 to 400.208°C is 19.61%

Comparing Figures A-91 & A-92, the total percentage weight loss of oil contaminated sample cleaned with nanofluid without surfactant (22.87%) was more than the total

percentage weight loss of contaminated sample cleaned with  $0.7\text{Al}_2\text{O}_3 + 0.3\text{ZnO}$ /water nanofluid + 0.1g surfactant (19.61%).

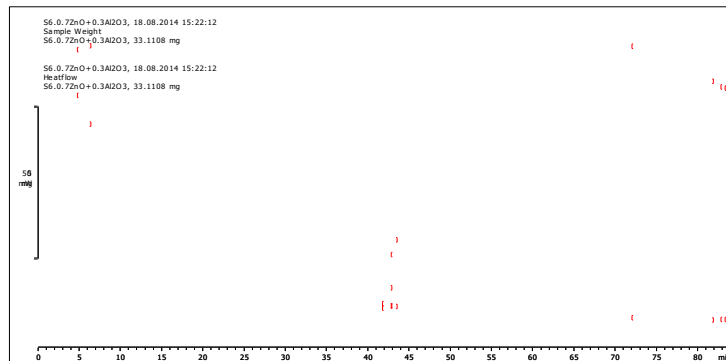


Figure A- 93 Mass loss per min and heat flow of soil cleaned with pure  $0.7\text{ZnO} + 0.3\text{Al}_2\text{O}_3$ /water. This graph is reported using tga generated data into weight loss per second and heatflow considering the temperature as shown on Figures A-94 &A-95.

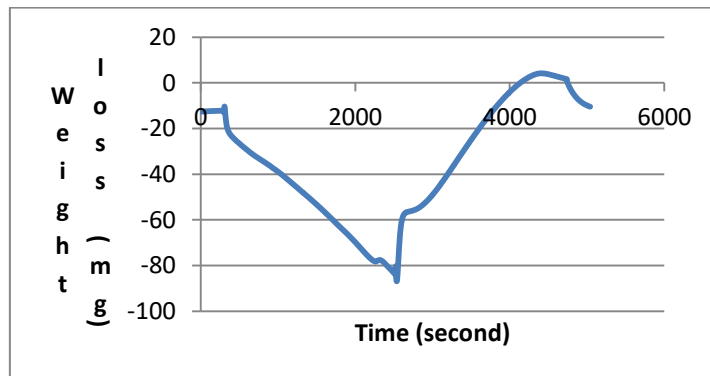


Figure A- 94 Weight loss per second for pure  $0.7\text{ZnO} + 0.3\text{Al}_2\text{O}_3$ /water. After the cleaning with pure  $0.7\text{ZnO} + 0.3\text{Al}_2\text{O}_3$ /water, 33.1108mg soil sample (which comprises of oil and water retained in the soil after cleaning) was taken into a crucible for tga analysis at onset temperature of  $30^\circ\text{C}$ . As heatflow through the soil sample progressively, at 12 minutes into the start off the experiment, 10.3957mg (31.3967%) water in the sample boiled off, leaving only the oil in the soil. Further progression of the heatflow led to the removal of oil by weight, 0.035mg (0.1057%) at 38.1mins. Finally, all the oil was removed at constant rate leaving the soil (22.6801mg) to its original status. Total percentage loss from 0 –  $400^\circ\text{C}$  is 31.47%.

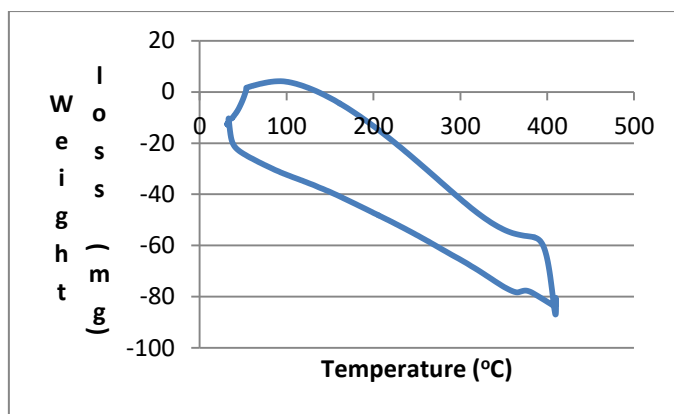


Figure A- 95 Heatflow for pure 0.7ZnO + 0.3Al<sub>2</sub>O<sub>3</sub>/water.

The soil sample with onset temperature of 30.°C and weight 33.1108mg lost its water (10.3857mg/31.37%) as the analysis progresses at 100.3°C. The weight loss increases with increase in temp until it reaches 338°C where all the oil (0.035mg) burnt off and the weight becomes constant at 400°C without further weight loss. At this temperature all the oil has been burnt off leaving only clean soil, with weight 22.6901mg. Total percentage loss from 0 – 400°C is 31.47%.

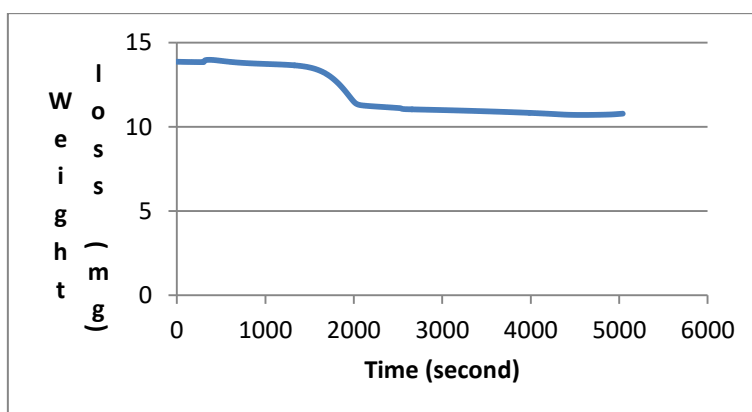


Figure A- 96 Weight loss per second of surfacted 0.3Al<sub>2</sub>O<sub>3</sub> + 0.7ZnO/water

The Figure A-96 shows the heatflow of contaminated soil after cleaning with surfacted 0.3ZnO + 0.7Al<sub>2</sub>O<sub>3</sub>/water in which 13.8721mg was taken from the bulk soil for tga analysis. As heat flows through the soil sample at 100.285°C into the start of the analysis, water boils off with weight of water lost equals to 3.0829mg. More weight loss occurs at at 337.506°C, burning off all the oil (0.0507mg) with weight of hot clean soil, (10.7385mg). The weight of cleaned soil remains constant even after 400.208°C without further weight loss, cooling down at 84mins. Total percentage loss from 0 to 400.208°C is 22.59%

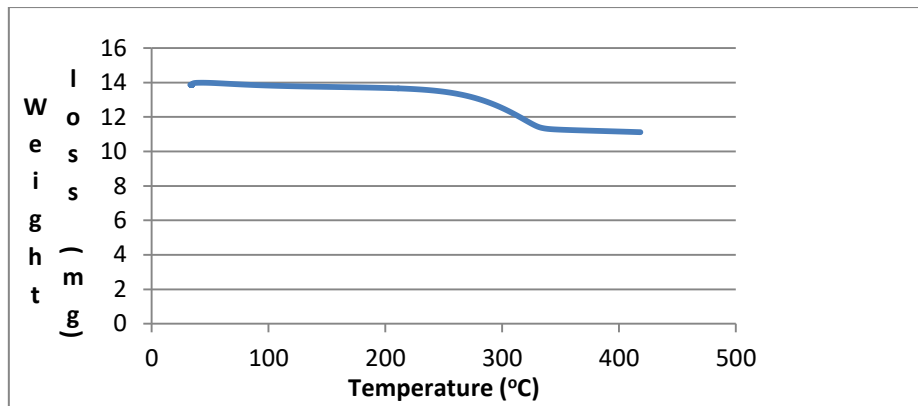


Figure A- 97 Comparison of weight loss with temperature for soil cleaned with surfacted  $0.3\text{Al}_2\text{O}_3 + 0.7\text{ZnO}/\text{water}$ .

The Figure A-97 shows the weight loss of contaminated soil after cleaning with surfacted  $0.3\text{ZnO} + 0.7\text{Al}_2\text{O}_3/\text{water}$  in which 13.8732mg was taken from the bulk soil for tga analysis. As weight loss progresses through the soil sample at 99.9931°C, water boils off with weight of water lost equals to 3.0829mg. More weight loss occurs at at 337.506°C, burning off all the oil (0.0507mg mg) with weight of hot clean soil, 10.7385mg. The weight of cleaned soil remains constant even after 400.208°C without further weight loss, cooling down at 36.7655°C. Total percentage loss from 0 to 400.208°C is 22.59%. Comparing Figures A-95 and A-96, the total percentage weight loss of oil contaminated sample cleaned with pure  $0.3\text{Al}_2\text{O}_3 + 0.7\text{ZnO}/\text{water}$  nanofluid (31.47%.) is more than the total percentage weight loss of contaminated sample cleaned with surfacted  $0.3\text{Al}_2\text{O}_3 + 0.7\text{ZnO}/\text{water}$  (22.59%).

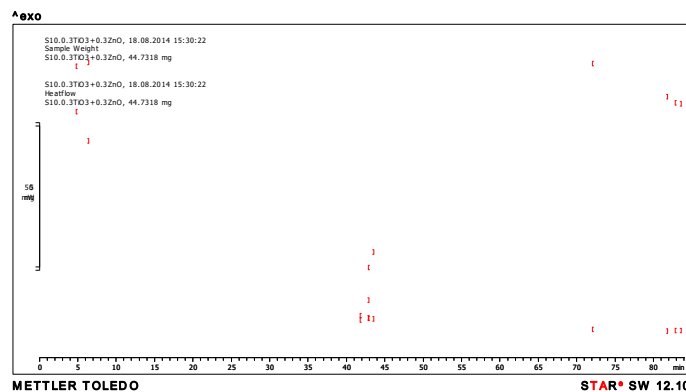


Figure A- 98 Mass loss per min and heat flow of soil cleaned with pure  $0.3\text{TiO}_2 + 7\text{ZnO}/\text{water}$   
This graph is reported using tga generated data into weight loss per second and heatflow considering the temperature as shown on Figures A-99 & A-100.



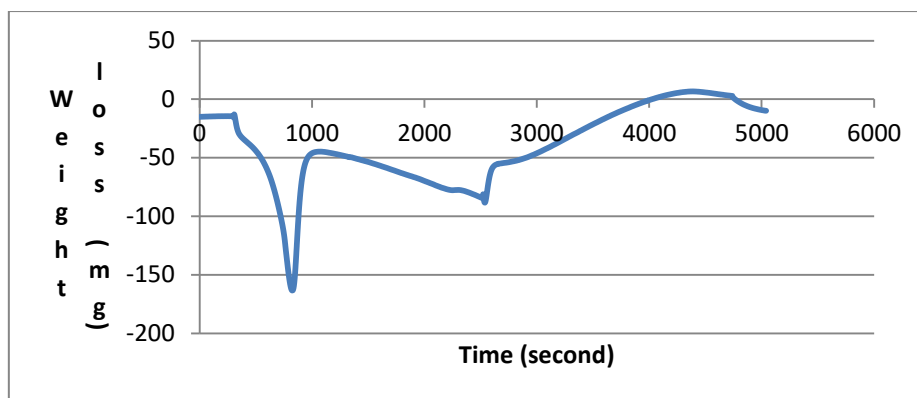


Figure A- 99 Weight loss per second for soil cleaned with pure  $0.3\text{ZnO}+0.7\text{TiO}_2/\text{water}$  Weight loss started at 2mins with weight of 60.5409mg and weight loss increase downwards at the interval of -20mg until it gets to weight loss of 9.3315mg (13.08mins), where most of the water retained in the soil after cleaning with  $0.3\text{Zn}+0.7\text{TiO}_2/\text{water}$  is lost.As the analysis progresses, the weight loss increases upward until it gets to 16mins, here much oil is lost (0.5428mg).Weight loss decreases again, until it reaches 42.1mins(50.6666mg) as all the oil is burnt off leading to constant weight of soil (50.6666mg) , no further change in weight loss.

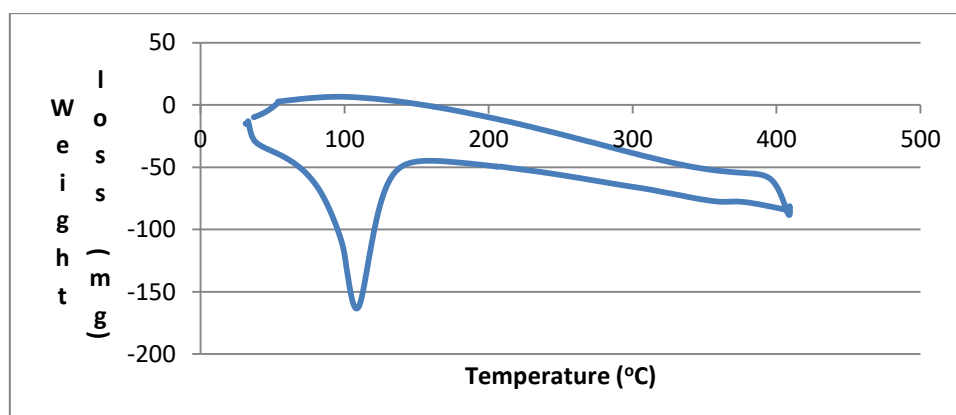


Figure A- 100 Comparison of weight loss with temperature for heatflow of  $0.3\text{ZnO} + 0.7\text{TiO}_2/\text{water}$

Weight loss of sample of contaminated soil after cleaning with 15g of  $0.3\text{ZnO} + 0.7\text{TiO}_2/\text{water}$  started with both the water at onset temp of  $30^\circ\text{C}$ , weight of 60.5409mg).The weight loss increase downwards at the interval of -20mg until it gets to  $100.084^\circ\text{C}$ , water boils off with total weight loss of 9.3315mg.0.5428mg Oil burnt off at the temp of  $338.66^\circ\text{C}$  and weight of 50.6666mg.The cleaned soil cools down at end temperature of  $36.9593^\circ\text{C}$ , constant weight of 50.6666mg.

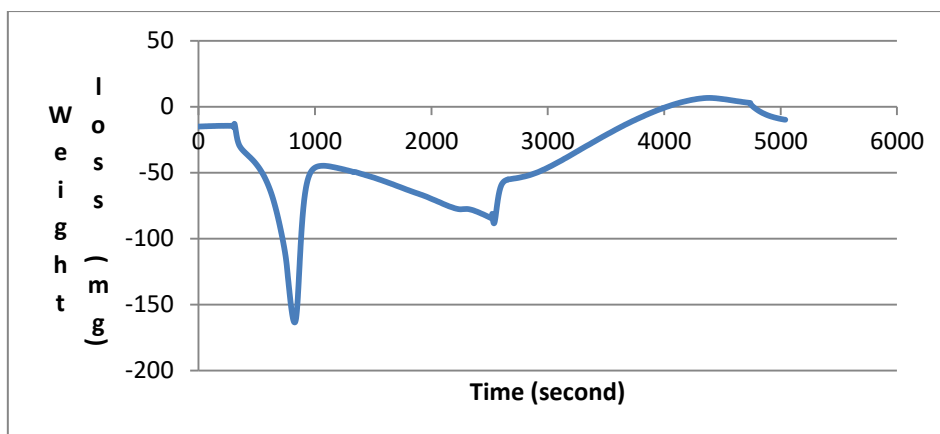


Figure A- 101 Weight loss of soil sample cleaned with pure 0.3ZnO+0.7TiO<sub>2</sub>/water

Figure A-101 heatflow of contaminated soil after cleaning with pure 0.3ZnO + 0.7TiO<sub>2</sub>/water in which 21.7385mg was taken from the bulk soil for tga analysis. As heat flows through the soil sample with rapid rise in temperature, water boils off with weight of water lost of 5.3546mg at 100.051°C. Further rise in temperature led to, burning off all the oil (0.1595mg) with weight of hot clean soil, 16.2244mg, at 338.338°C. The weight of cleaned soil remains constant after 338.338°C till the end temperature of 400°C without further weight loss, cooling down to 37.4564°C. The percentage loss in weight from 0 to 400°C is 25.37%. Weight loss started at 2mins with weight of 60.5409mg and weight loss increase downwards at the interval of -20mg until it gets to weight loss of 9.3743mg (13.08mins), where most of the water retained in the soil after cleaning with 0.3Zn0.7TiO<sub>2</sub>/water is lost. As the analysis progresses, the weight loss increases upward until it gets to 16mins, here much oil is lost (0.5mg). Weight loss decreases again, until it reaches 2.1mins(50.6666mg) as all the oil is burnt off leading to constant weight of soil (50.6666mg), no further change in weightloss. The percentage weight loss from 0 to 400°C is 16.31%

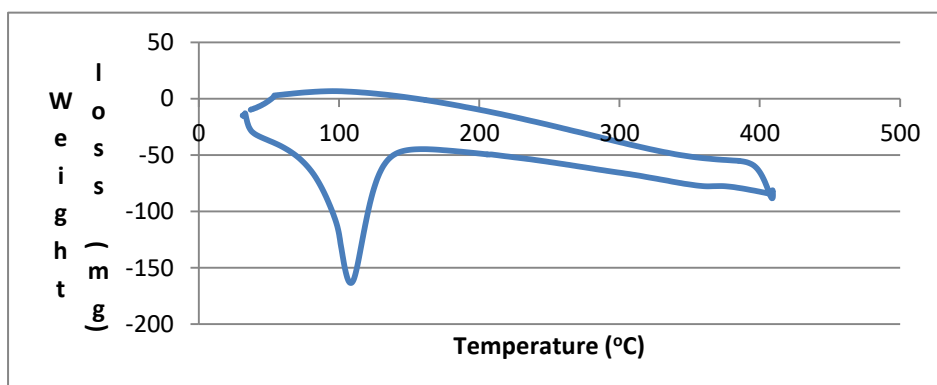


Figure A- 102 Comparison of weight loss with temperature for heatflow of pure 0.3ZnO + 0.7TiO<sub>2</sub>/water

Figure A-102 shows the heatflow of contaminated soil after cleaning with pure 0.3ZnO + 0.7TiO<sub>2</sub>/water in which 21.7385mg was taken from the bulk soil for tga analysis. As heat flows through the soil sample with rapid rise in temperature, water boils off with weight of water lost of 5.3546mg at 100.051°C. Further rise in temperature led to, burning off all the oil (0.1595mg) with weight of hot clean soil, 16.2244mg, at 338.338°C. The weight of cleaned soil remains constant after 338.338°C till the end temperature of 400°C without further weight loss, cooling down to 37.4564°C. The percentage loss in weight from 0 to 400°C is 25.37%.

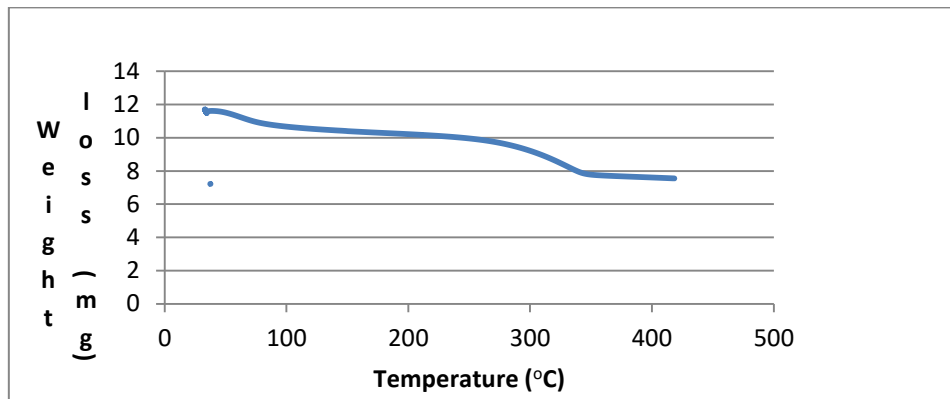


Figure A- 103 Weight loss per second for soil cleaned with pure 0.3TiO<sub>2</sub> + 0.7ZnO/water  
 In FigureA-103 Weight loss started at 2mins with weight of 44.7318mg and weight loss increase downwards at the interval of -20mg until it gets to weight loss of 9.056mg (13.08mins), where most of the water retained in the soil after cleaning with 0.3ZnO+ 0.7TiO<sub>2</sub>/water is lost. As the analysis progresses, the weight loss increases upward until it gets to 16mins, here much oil is lost (0.1258mg). Weight loss decreases again, until it reaches 42.1mins(35.54mg) as all the oil is burnt off leading to constant weight of soil (35.54mg), no further change in weight loss. The percentage total weight loss from 0 to 400°C is 20.53%.

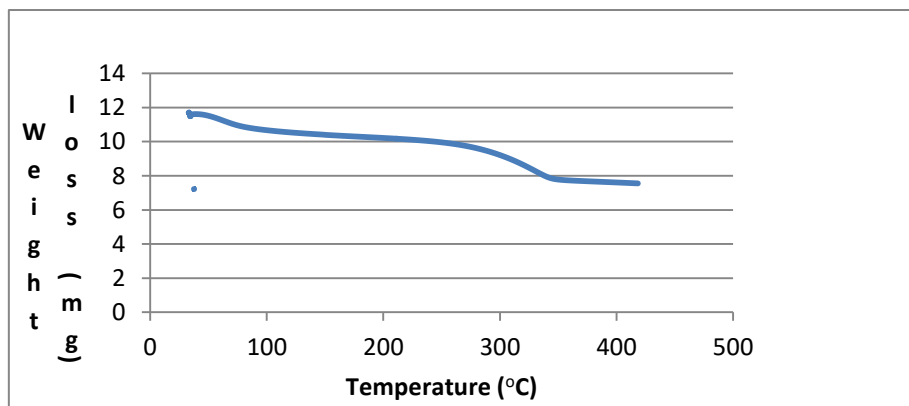


Figure A- 104 Comparison of weight loss with temperature for soil sample cleaned with surfacted 0.3TiO<sub>2</sub> + 0.7ZnO/water.

Weight loss of sample of contaminated soil after cleaning with 15g of 0.3ZnO + 0.7TiO<sub>2</sub>/water started with both the water at onset temp of 30°C, weight of 60.5409mg).The weight loss increase downwards at the interval of -20mg until it gets to 100.084°C, water boils off with total weight loss of 9.3315mg.0.5428mg Oil burnt off at the temp of 338 66°C and weight of 50.67mg.The cleaned soil cools down at end temperature of 36.9593°C, constant weight of 50.67mg.The total percentage weightloss from 0 to 400°C is 16.31%.

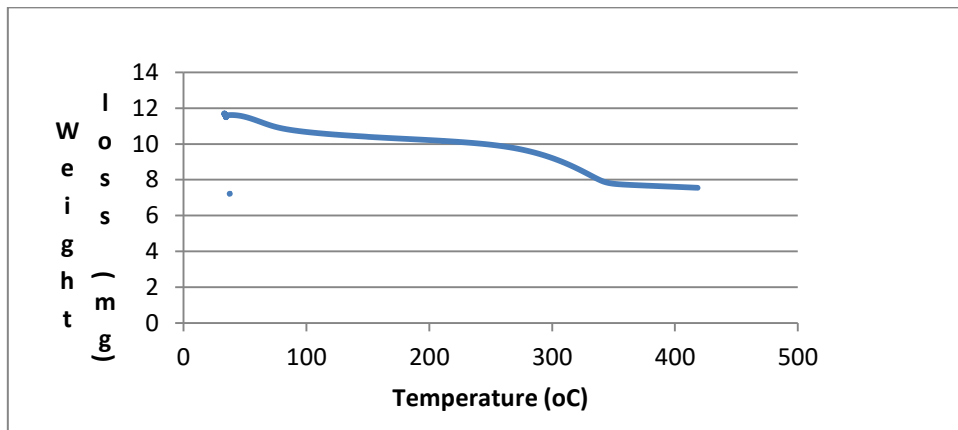


Figure A- 105 Comparison of weight loss of contaminated soil cleaned with surfactant 0.3TiO<sub>2</sub> + 0.7ZnO/water

After the cleaning, 29.6658mg pure soil sample (which comprises of oil and water retained in the soil after cleaning) was taken into a crucible for tga analysis at onset temperature of 30°C.As heatflow through the soil sample progressively, at 100.013°C (the boiling point of water) and 11.97 minutes, 6.4961mg (21.8976%) water in the sample boiled off, leaving only the oil in the soil.Further progression of the heatflow led to the removal of oil by weight, 1.4260mg (4.8067%) at 338°C (solubility temperature of the experimental mineral oil).Finally, all the oil was removed at 374.332°C, constantly leaving the soil (21.7437mg, 73.2957%) to its original status.

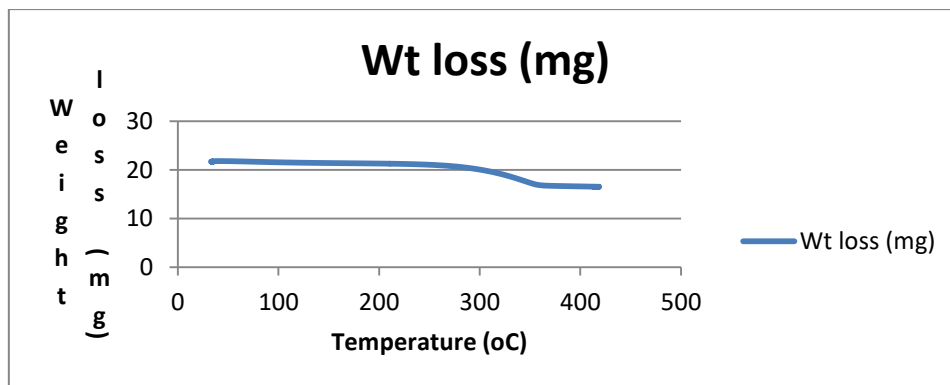


Figure A- 106 Comparison of weight loss of contaminated soil cleaned with surfactant 0.3ZnO + 0.7TiO<sub>2</sub>/water.

After the cleaning, 29.6658mg pure soil sample (which comprises of oil and water retained in the soil after cleaning) was taken into a crucible for tga analysis at onset temperature of 30°C. As heatflow through the soil sample progressively, at 100.013°C (the boiling point of water) and 11.97 minutes, 6.4961mg (21.8976%) water in the sample boiled off, leaving only the oil in the soil. Further progression of the heatflow led to the removal of oil by weight, 1.4260mg (4.8067%) at 338°C (solubility temperature of the experimental mineral oil). Finally, all the oil was removed at 374.332°C, constantly leaving the soil (21.7437mg, 73.2957%) to its original status.

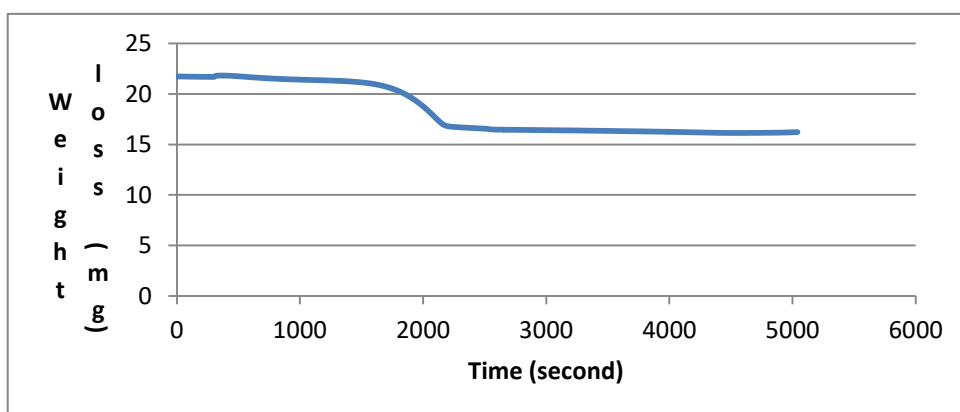


Figure A- 107 Comparison of weight loss with time for soil sample cleaned with surfacted  $0.3\text{ZnO} + 0.7\text{TiO}_2/\text{water}$

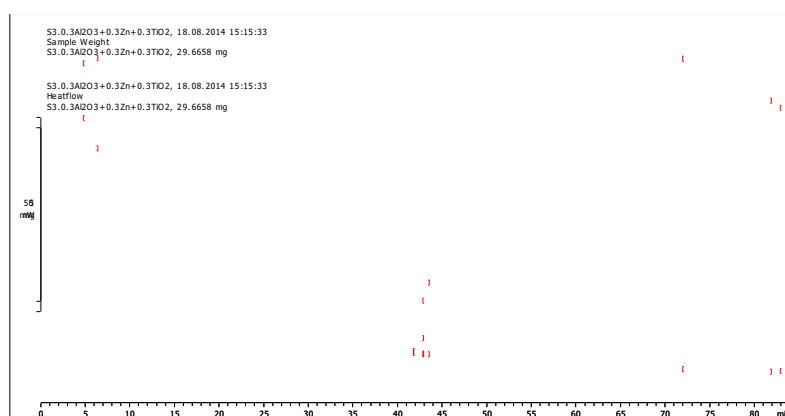


Figure A- 108 Mass loss per min of soil cleaned with pure  $0.3\text{Al}_2\text{O}_3 + 0.3\text{ZnO} + 0.3\text{TiO}_2/\text{water}$

This graph is reported using tga generated data into weight loss per second and heatflow considering the temperature as shown on Figure A-109.

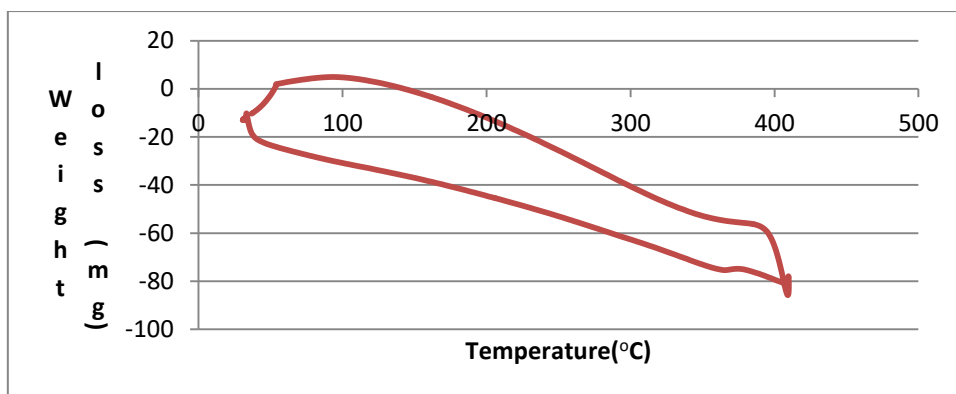


Figure A- 109 Heatflow for soil cleaned with pure  $0.3\text{Al}_2\text{O}_3 + 0.3\text{TiO}_2 + 0.3\text{ZnO}$

After the cleaning, 29.6658mg pure soil sample (which comprises of oil and water retained in the soil after cleaning) was taken into a crucible for tga analysis at onset temperature of 30°C (Figure A-108 ).As heatflow through the soil sample progressively, at 100.013°C (the boiling point of water) and 11.97 minutes, 7.9087mg (26.66%) water in the sample boiled off, leaving only the oil in the soil.Further progression of the heatflow led to the removal of oil by weight, 0.0126mg (0.0425%) at 338°C (solubility temperature of the experimental mineral oil).Finally, all the oil was removed at 374.332°C, constantly leaving the soil (21.7437mg, 73.2957%) to its original status at endtemperature of 36.883°C.Percentage weight loss from 0 to 400°C is 26.70%

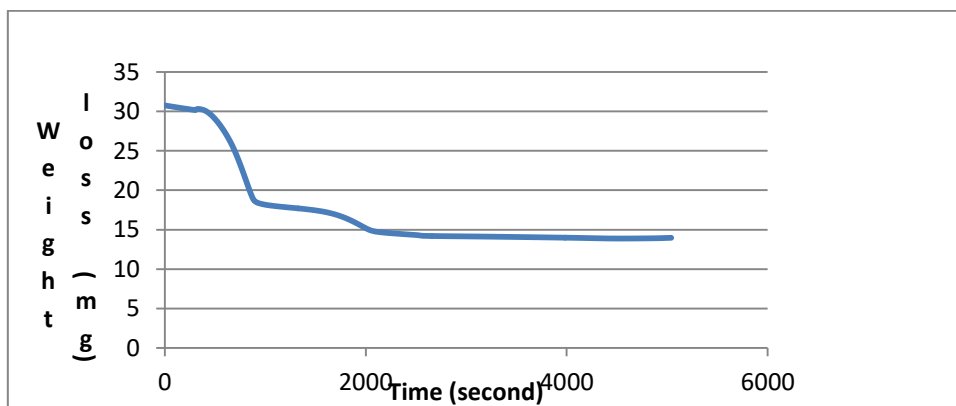


Figure A- 110 Weight loss per second of surfacted  $0.3\text{Al}_2\text{O}_3 + 0.3\text{TiO}_2 + 0.3\text{ZnO}$ /water

FigureA-110 indicated that weight loss started at 2mins with weight of 30.1150mg and weight loss increase downwards at the interval of -20mg until it gets to weight loss of 8.55631mg (13.08mins), where most of the water retained in the soil after cleaning with  $0.3\text{ZnO}+0.7\text{TiO}_2$ /water is lost.As the analysis progresses, the weight loss increases upward until it gets to 16mins, here much oil is lost, (0.0346mg).Weight loss decreases again, until it reaches 2.1mins as all the oil is burnt off leading to constant weight of soil (23.5241mg), no

further change in weight loss at endtemperature of 37.4483°C. Percentage weight loss from 0 – 400°C is 21.89%

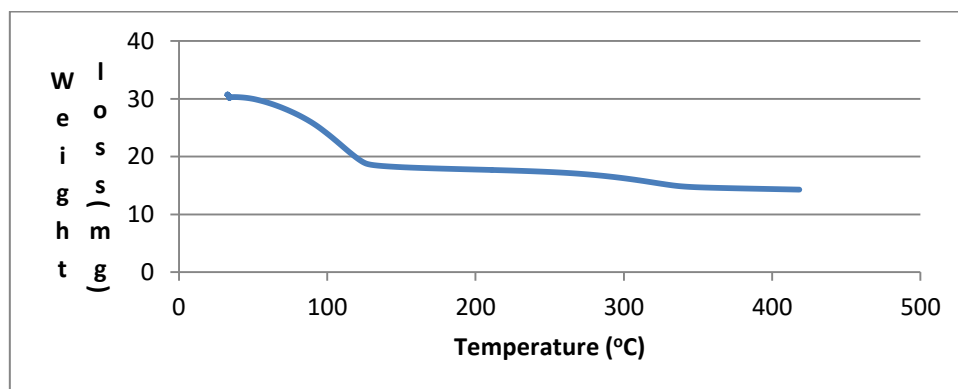


Figure A- 111 Comparison of temperature with weight loss of surfacted  $0.3\text{Al}_2\text{O}_3 + 0.3\text{TiO}_2 + 0.3\text{ZnO}$ /water.

After the cleaning, 30.1150mg pure soil sample (which comprises of oil and water retained in the soil after cleaning) was taken into a crucible for tga analysis at onset temperature of 30°C. As heatflow through the soil sample progressively, at 100.001°C (the boiling point of water) and 11.97 minutes, 8.55631mg (28.41%) water in the sample boiled off, leaving only the oil in the soil. Further progression of the heatflow led to the removal of oil by weight, 0.0346mg (0.1149%) at 338°C (solubility temperature of the experimental mineral oil). Finally, all the oil was removed at 374.332°C, constantly leaving the soil (23.5241mg, 78.11%) to its original status. The total percentage loss from 0 to 400°C is 21.89%.

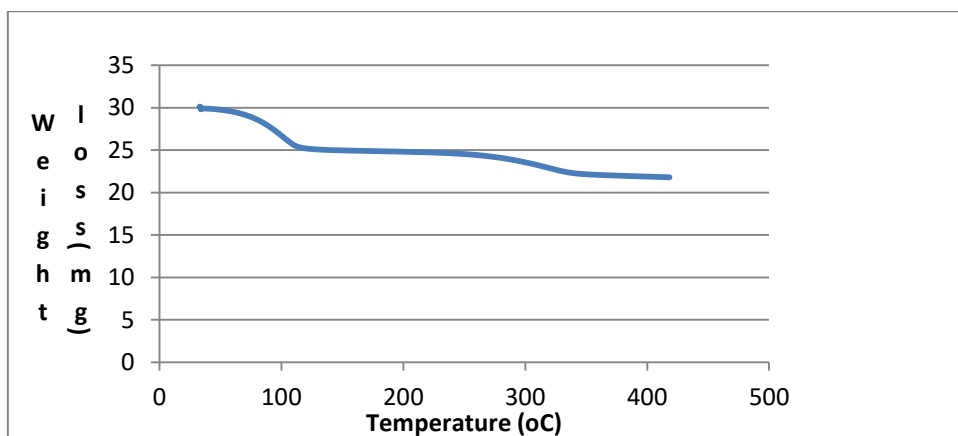


Figure A- 112 Comparison of weight loss with temperature for soil sample cleaned with surfacted  $0.3\text{Al}_2\text{O}_3 + 0.3\text{TiO}_2 + 0.3\text{ZnO}$ /water

After the cleaning, 30.1150mg pure soil sample (which comprises of oil and water retained in the soil after cleaning) was taken into a crucible for tga analysis at onset temperature of 30°C. As heatflow through the soil sample progressively, at 100.001°C (the boiling point of water)

and 11.97 minutes, 8.55631mg (28.41%) water in the sample boiled off, leaving only the oil in the soil. Further progression of the heatflow led to the removal of oil by weight, 0.0346mg (0.1149%) at 338°C (solubility temperature of the experimental mineral oil). Finally, all the oil was removed at 374.332°C, constantly leaving the soil (23.5241mg, 78.11%) to its original status. The total percentage loss from 0 to 400°C is 21.89%.

Comparing Figures A-109 and A-112, the total percentage weight loss of oil contaminated sample cleaned with pure 0.3Al<sub>2</sub>O<sub>3</sub> + 0.7ZnO/water nanofluid (26.70%) is greater than the total percentage weight loss of contaminated sample cleaned with surfacted 0.3Al<sub>2</sub>O<sub>3</sub> + 0.7ZnO/water (21.89%). This shows that more oil was recovered by surfacted 0.3Al<sub>2</sub>O<sub>3</sub> + 0.7ZnO/water during the cleaning than pure 0.3Al<sub>2</sub>O<sub>3</sub> + 0.7ZnO/water nanofluid. Tga contaminated and cleanup soil figures

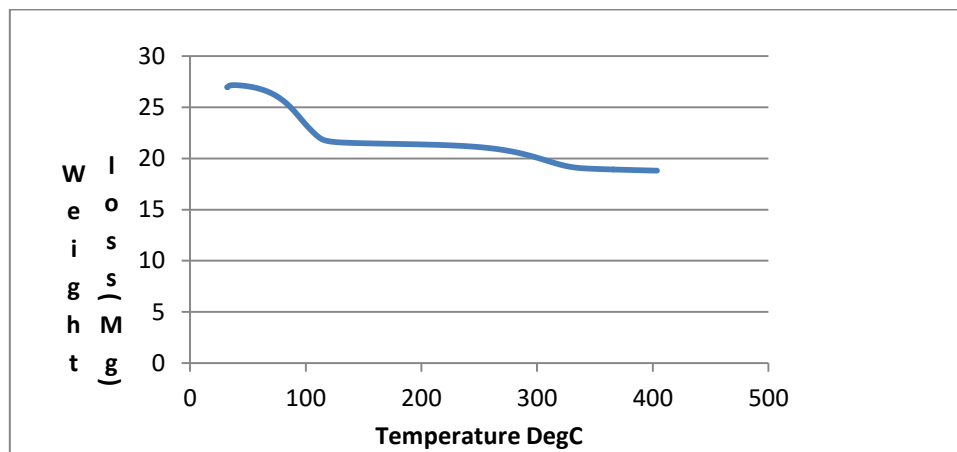


Figure A- 113 10g Soil contaminated with 4.4g Oil HV1 and cleaned with 10g 0.3vol% Al<sub>2</sub>O<sub>3</sub> Considering the water and oil retained in the soil after clean-up process, energy required to evaporate 45.5g of water to its boiling point (100°C) in the Tga as shown in FigureA-112 is calculated as below:

$Q = mH_v$  (m = mass of water retained in the soil,  $H_v$  = Heat of evaporation of water = 2260J/g)  
 $Q = 45.5g \times 2260J/g = 102830J = 102.830KJ$ . While the oil retained in the soil (3.5g) burnt off at solubility point of 338°C leaving the soil to its original status. This oil vaporises completely at 338°C at specific heat capacity of (eg amt of retained in the soil after cleaning x heat capacity of mineral oil (1670) = ....J/kg°C).

Thermal analysis: Thermal analysis of samples was done using Mettler, TG 50 under controlled temperature rise from room temperature to 400°C at the rate of 10°C min<sup>-1</sup>



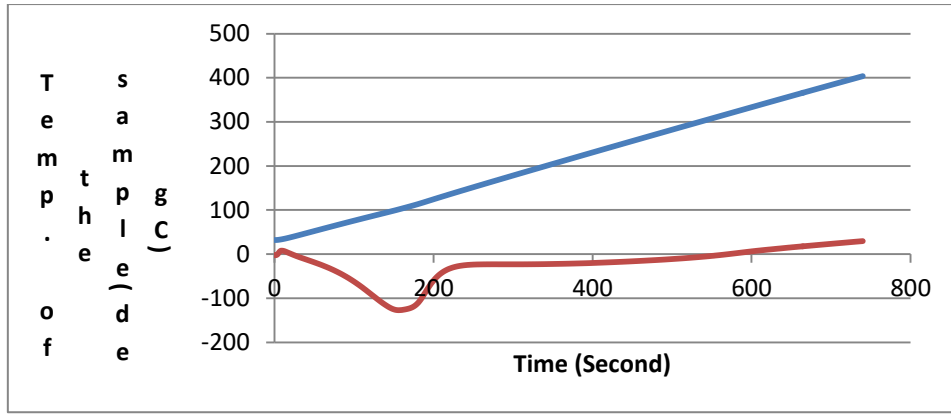


Figure A- 114 Tga heatflow curve of 27.89mg oil-0.3vol% Al<sub>2</sub>O<sub>3</sub> nanofluid soil after cleanup 27.89mg oil-0.3 vol% Al<sub>2</sub>O<sub>3</sub> water nanofluid soil sample was taken to Tga for analysis after which 15.26mg dried cleaned soil sample was restored to its original status.

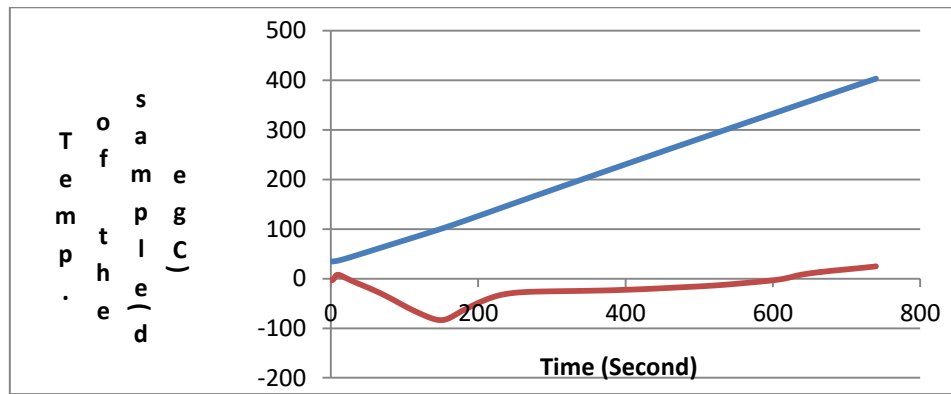


Figure A- 115 Tga heatflow curve of 27.78mg oil-0.3vol% TiO<sub>2</sub> nanofluid soil after cleanup 27.78mg mineral oil-0.3 vol% TiO<sub>2</sub> water nanofluid soil sample was taken to Tga for analysis after which 15.90mg dried cleaned soil sample was restored to its original status. Amount of oil + water loss = 11.88mg.

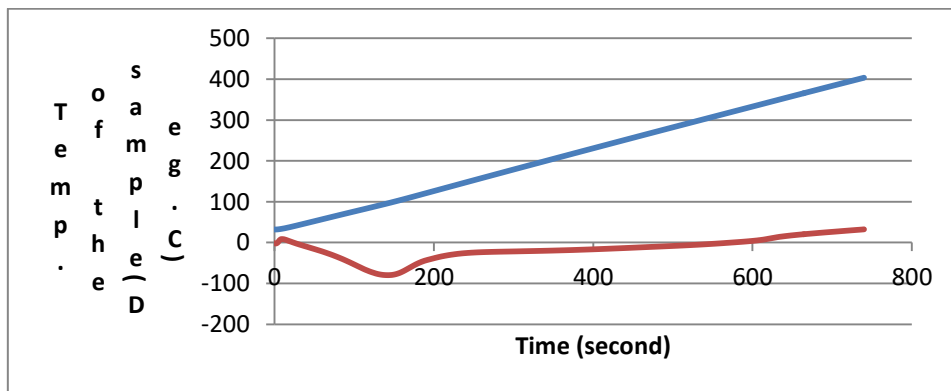


Figure A- 116 Heat flow curve of 26.01mg oil-0.7vol% ZnO nanofluid soil after cleanup [41a]. 26.01mg mineral oil-0.7 vol% ZnO water nanofluid soil sample was taken to Tga for analysis after which 17.29mg dried cleaned soil sample was restored to its original status.Amount of

oil + water loss = 8.72mg.

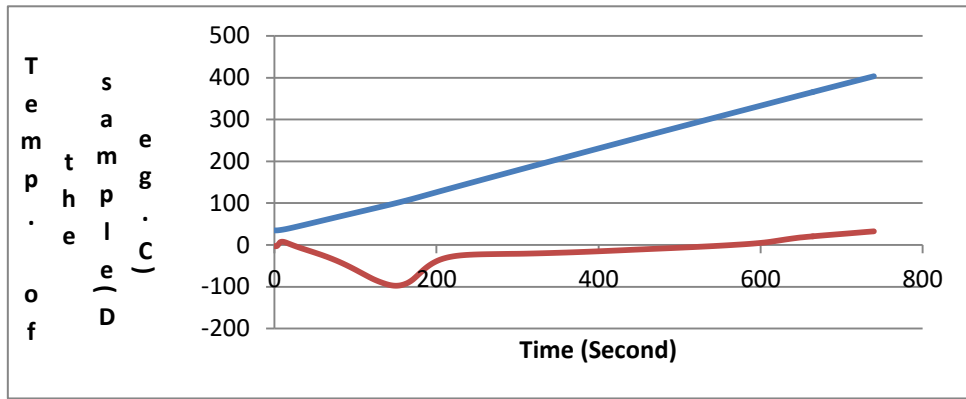


Figure A- 117 Heat flow curve of 28.24mg oil-0.3vol% ZnO nanofluid soil after cleanup. 28.24mg mineral oil-0.3 vol% ZnO water nanofluid soil sample was taken to Tga for analysis after which 17.05mg dried cleaned soil sample was restored to its original status. Amount of oil + water loss = 10.19mg

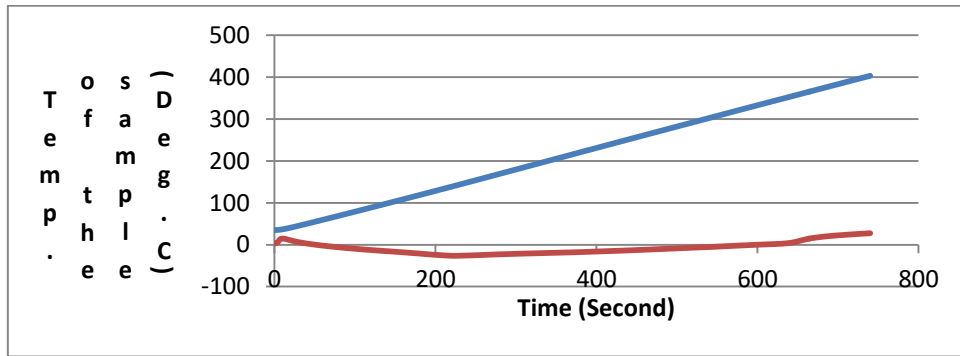


Figure A- 118 Tga heat flow of 21.33 mg oil contaminated soil sample analysis. Figure A-117 show the thermal analysis of 21.33 mg mineral oil contaminated soil sample cleaned without nanofluid. The weight of dried soil sample after Tga was 13.90mg.

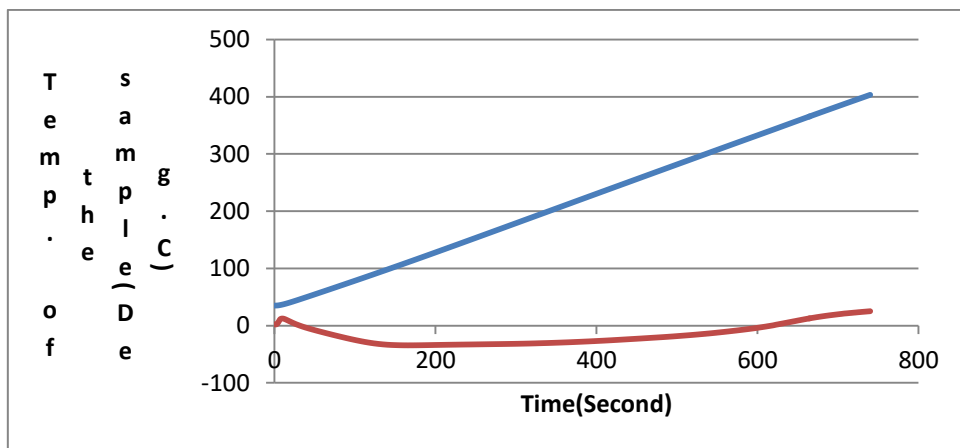


Figure A- 119 Heat flow of 37.13mg oil contaminated soil sample after cleanup

Figure A-118 shows the heat flow of 37.13mg oil contaminated soil which was taken from the bulk sample of 5g Soil contaminated with 2.5g mineral oil and cleaned using 2.5g 1vol% Al<sub>2</sub>O<sub>3</sub>- water nanofluid.

N- 1 Properties of nanofluids

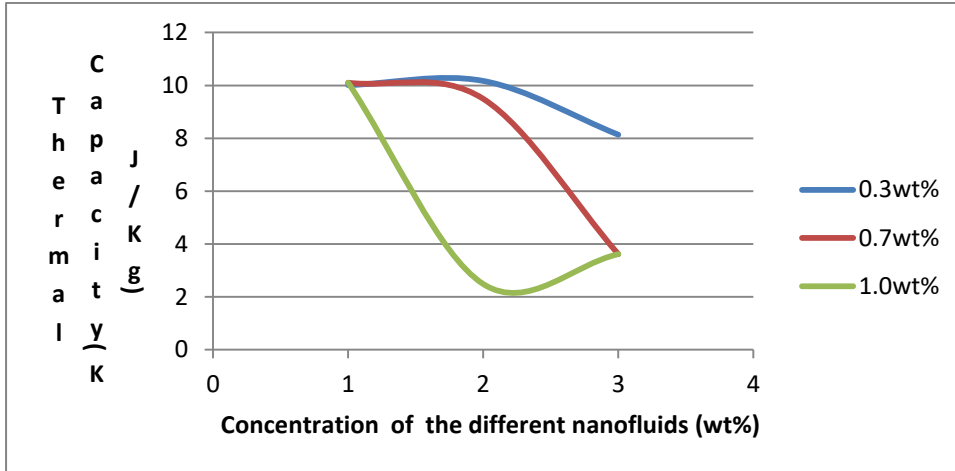


Figure A- 120 Experimental results of Thermal Capacity of the different monotype nanofluids

From the Figure A-120, the thermal capacity of the different nanofluids decreases with increase in weight fractions.

Calculations

N- 2 .Equipment Design



Figure A- 121 The DSC machine and Crucible sealing press (Mettler Toledo)

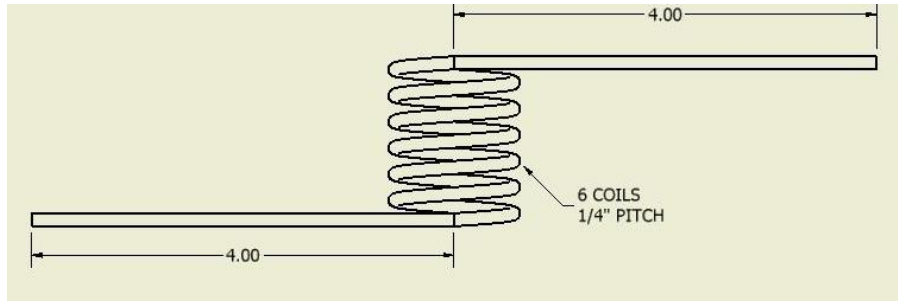


Figure A- 122 Mettler Toledo Tga helical test Coil Heat Exchanger

TestCoil	
Helical coil Diameter	3.175cm
Helical coil Radius	1.5875cm
Rmax	1.5875cm

Table 6-7 Helical Test Coil Heat Exchanger Specifications

First to observe the behaviours of nanofluids in regards to the heat transfer rate, an empty crucible was placed on top of helical coils (Figure3-19& Table2-17) inside the heat exchanger of Mettler Toledo Thermal gravical Analysis during the heat flow experiment. Thermocouples were used to monitor the onset and endset temperatures of the samples to help determine the heat transfer rate of the nanofluids during the experiment.

### Abbreviations/ **Nomenclature 2**

- Cp – Specific Heat (J / g\*K)
- d – Inside Tube Diameter (cm)
- m – Mass Flow Rate (g/s)
- R<sub>max</sub> – Maximum Radius of Coil (cm)
- Re – Renolds Number
- ΔT – Change in Temperature (K)
- v – Velocity of Fluid (m/s)
- μ- Dynamic Viscosity (kg/m\*s)
- m<sub>s</sub> – Nanoparticle Mass in Nanofluid Suspension (g)
- v – Nanoparticle Volume Fraction
- V<sub>s</sub>- Nanoparticle Volume in Nanofluid Suspension (cm<sup>3</sup>)
- V<sub>t</sub>- Total Volume of Nanofluid (cm<sup>3</sup>)
- p<sub>nf</sub>– Nanofluid Density (g/m<sup>3</sup>)
- p<sub>s</sub>– Nanoparticle Density (g/m<sup>3</sup>)
- p<sub>w</sub>– Density of Water (g/m<sup>3</sup>)
- Cp<sub>nf</sub>- Specific Heat of Nanofluid (J / g\*K)
- Cp<sub>s</sub>– Specific Heat of Nanoparticle (J / g\*K)
- Cp<sub>w</sub>- Specific Heat of Water (J / g\*K)
- Cp<sub>TiO<sub>2</sub></sub>- Specific Heat of Titania Oxide (J / g\*K)
- Cp<sub>Al<sub>2</sub>O<sub>3</sub></sub>- Specific Heat of Aluminum Oxide (J / g\*K)

Cp<sub>ZnO</sub>- Specific Heat of Zinc Oxide (J / g\*K)

DI De-Ionized

DLS Dynamic Light Scattering

DSC Differential Scanning Calorimetry

N- 3 Specific heat capacity

The following equations were utilized to determine the flow design and heat transfer

- In order to determine the Reynolds number, the following equation was used:

$$\text{Critical Re} = 2100 [1 + 12\{d/2(R_{\text{max}})\}^{0.5}] \quad [3.2]$$

The mass flow rate was calculated to determine the desired flow rate for testing and the following equation was used:

$$\text{Re} = \rho d / \mu \quad [3.3]$$

The heat transfer rate was calculated for each trial run and the following equation was used:

$$q = m \cdot C_p \cdot \Delta t \quad [3.4]$$

The nanoparticle volume in nanofluid suspension was calculated for each trial run and the following equation was used:

$$V_s = p_s / m_s \quad [3.5]$$

The nanoparticle volume fraction was calculated for each trial run and the following equation was used:

$$V = v_s / v_t \quad [3.6]$$

The nanofluid density was calculated for each trial run and the following equation was used:

$$\rho_{\text{nf}} = v \times \rho_s + (1 - v) \rho_w \quad [3.7]$$

The specific heat of Aluminum Oxide (Al<sub>2</sub>O<sub>3</sub>) was calculated for each trial run and the following equation was used:

$$C_p \text{ Al}_2\text{O}_3 = 22.18 + 0.008971T - (522500/T^2) \dots\dots\dots(3.8)$$

The specific heat of the nanofluid being tested was calculated for each trial run and the following equation was used:

$$C_{p_{\text{nf}}} = \frac{v(\rho C_{ps}) + (1 - v)\rho_w C_{pw}}{\rho_{\text{nf}}} \dots\dots\dots[3.9]$$

N- 4 Differential scanning calorimetry

Differential scanning calorimetry (DSC) tests were performed on a Mettler-Toledo DSC 822E/400 (FigureA-121).The soil samples obtained after cleaning the oil contaminated soil with different nanofluids were introduced in standard aluminum pans with lids and subjected to the following thermal cycle in nitrogen atmosphere: held at 30°C for 5 min (to remove any absorbed water in the sample), heating from 30°C to 400°C at 10°C/min, held at 400°C for 5 min, cooling from 400°C to 30°C at 10°C/min.Six consecutive cycles were run on each sample

without opening the DSC furnace to ensure good mixing of the sample and reproducibility of the results. In this way, the effect of the initial granulometry was also lost after the first cycles. The DSC thermograms were analyzed and the phase-change heat and melting temperatures were obtained using the software STARe. Moreover, the calorimetric data were used to calculate the specific heat ( $C_p$ ) of the samples. Same scanning tests were performed on the contaminated soil samples cleaned with surfacted nanofluids which were compared with those obtained with pure nanofluids [41a]. In this way, the effect of the different nanofluids could be evaluated. In particular, the DSC procedure followed to estimate specific heat values was the three-step procedure [35].

**Heat transfer rate: DSC analysis:** The thermal properties including the oil volatility temperature and latent heat capacity of both the pure water and  $TiO_2$ /Water composites were measured using a differential scanning calorimetric (DSC) instrument (Diamond DSC, Perkin Elmer, USA). Indium was used as a reference for temperature calibration. Sample with mass of 10 to 70 mg was placed and pressed into crucibles at room temperature. A lid was placed on the sample to make excellent thermal contact between the sample and the crucible. Then the crucible containing the sample was put into the DSC instrument in shielding nitrogen gas flow of 20 ml/min. After 1 min remaining at the initial temperature, the DSC measurements were performed at a linear heating rate of  $5\text{ }^\circ\text{C min}^{-1}$  in a temperature range from  $30\text{ }^\circ\text{C}$  to  $400\text{ }^\circ\text{C}$  [57]. The temperature was maintained at  $400\text{ }^\circ\text{C}$  to remove thermal history, and then cooled down to  $30\text{ }^\circ\text{C}$ .

First of all, a thermal cycle was fixed. In the first step, a measurement was taken with two empty sample pans. During this measurement, the baseline heat flux ( $Q_0$ ) was obtained. The results of this measurement indicate the bias in the DSC. In the second step, a pan containing the reference sample with a known specific heat and an empty pan were loaded into the calorimeter. The heat flux recorded was  $Q_{ref}$ . In the third step, a pan containing the sample and an empty pan were loaded into the calorimeter. The heat flux into the sample ( $Q_{sample}$ ) was recorded. The specific heat of the sample was obtained as follows:  $C_{p, sample} = [(Q_{sample} - Q_0) / (Q_{ref} - Q_0)] \times (m_{ref} - m_{sample}) \times C_{p, ref}$ , where  $m_{ref}$  and  $m_{sample}$  indicate the masses of the reference and sample, respectively.

This procedure was validated with our base fluid whose specific heat is well known. The DSC thermograms were analyzed and the phase-change heat and melting temperatures were obtained using the software STARe [35] obtained using the software STARe. Moreover, the calorimetric data were used to calculate the specific heat ( $C_p$ ) of the samples.

$$C_{p_{nf}} = \frac{\rho_{np}\phi_{np}C_{p_{np}} + \rho_f\phi_f C_{p_f}}{\rho_{np}\phi_{np} + \rho_f\phi_f} \dots \dots \dots (3.10)$$

where  $C_p$  is specific heat,  $\phi$  is the volume fraction,  $\rho$  is the density, and the subscripts np, nf, and f refer to nanoparticle, nanofluid, and base fluid, respectively, where  $C_p$  is specific heat,  $\phi$  is the volume fraction,  $\rho$  is the density, and the subscripts np, nf, and f refer to nanoparticle, nanofluid, and base fluid, respectively.

N-5 Specific heat capacity

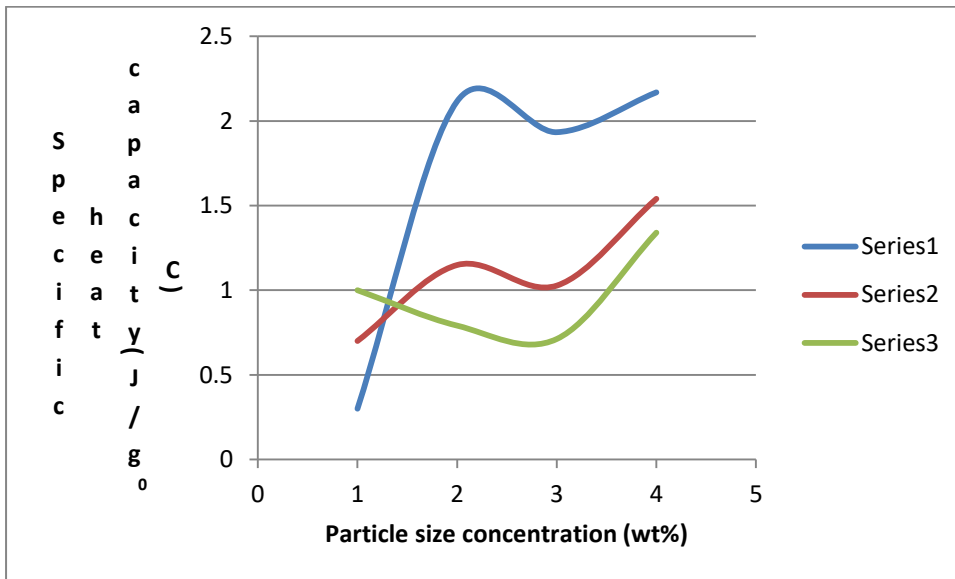


Figure A- 123 Specific heat capacity of the various monotype nanofluids

series1 - 0.3% particle size concentration,

Series2 - 0.7% particle size concentration

Series3 - 1.0% particle size concentration

The Fig A-123 indicates that the specific heat capacity decreases with increase in particle size concentration of the various monotype nanofluids, the specific heat capacity of  $Al_2O_3$  and  $TiO_2$  are nearly equal to each other at particle size concentration of 0.7wt%. It can be observed from the Figure also that the specific heat capacity of the monotype nanofluids is best at particle size concentration of 0.3wt%. The results have showed that the heat transfer performance of nanofluids is significantly enhanced at low particle size concentrations. The experimental results shown on Fig.A-123 indicates that the specific heat capacity,  $C_p$  of the nanofluids decreases gradually as the nanoparticle volume fraction  $v$  increases from 0.3 to 1.0wt% [201]. In otherwords, it increases with decrease in particle size concentration. The lesser the % weight fractions the more stable the nanofluids will be, due to

Brownian motion of particles (particle to particle movement is much easier with less particle size concentration. Particles have more freedom to move randomly in the solution). It can easily be concluded from the results of particle size distribution and zeta potential.

N- 5 Specific heat capacity J/g°C of the different nanofluids.

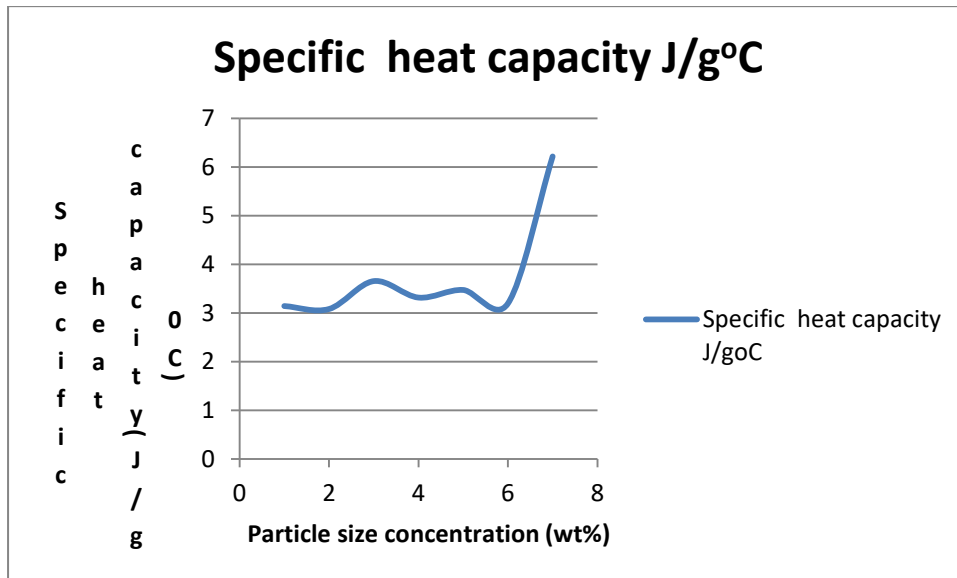


Figure A- 124 Specific heat capacity of the different hybrid nanofluids[57].

It is observed from the Fig A-124 that  $0.3\text{Al}_2\text{O}_3 + 0.3\text{TiO}_2 + 0.3\text{ZnO}$  gave the highest value of specific heat capacity. It is followed by  $0.3\text{Al}_2\text{O}_3 + 0.7\text{ZnO}$  and the least is  $0.7\text{Al}_2\text{O}_3 + 0.3\text{TiO}_2$  /water of nanofluids. Specific heat capacity increases with increase in particle size concentration.

N-6 Thermal capacity

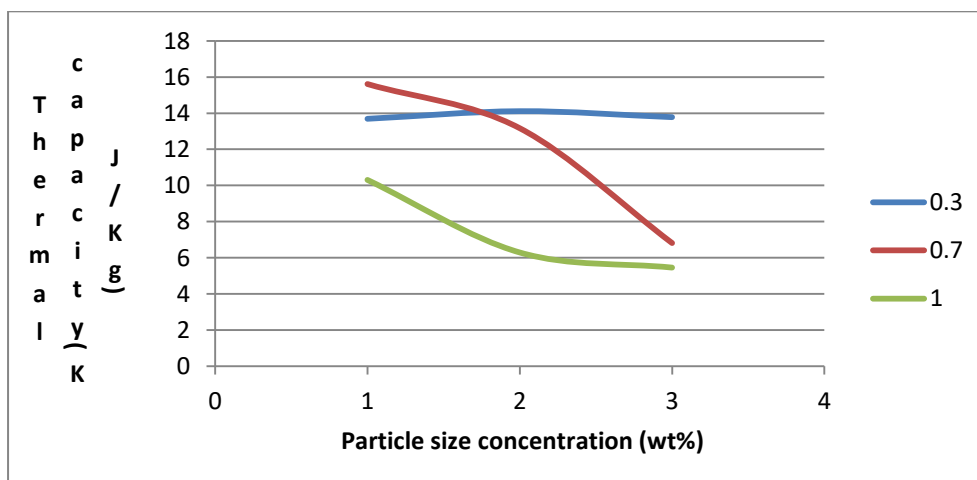




Figure A- 125 Thermal capacity of the different monotype nanofluids[57].

From the Fig.A-125 it is observed that the thermal capacity of the monotype nanofluids decreases with increase in particle size concentration but the thermal capacity of  $Al_2O_3$  and  $TiO_2$  water nanofluids are equal at the particle size concentration of 0.7 wt%.

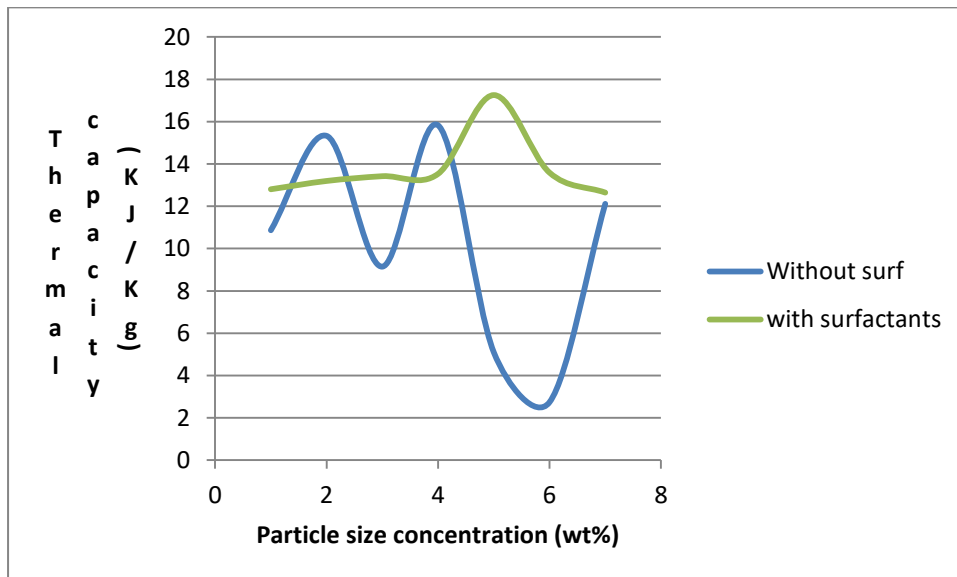


Figure A- 126 Comparison of thermal capacity of different hybrid nanofluids[57]

It is observed from the Fig.A-126 that the surfacted  $0.3TiO_2 + 0.7ZnO$  nanofluid has the highest thermal capacity of 17.254KJ/Kg while the pure  $0.3TiO_2 + 0.7ZnO$  nanofluid has the lowest thermal capacity of 2.741KJ/Kg. Generally, the addition of surfactants to the nanofluids increased/improved the heat flow (heat removed) restoring the contaminated soil to its original status.

#### N- 6 Heat transfer rate

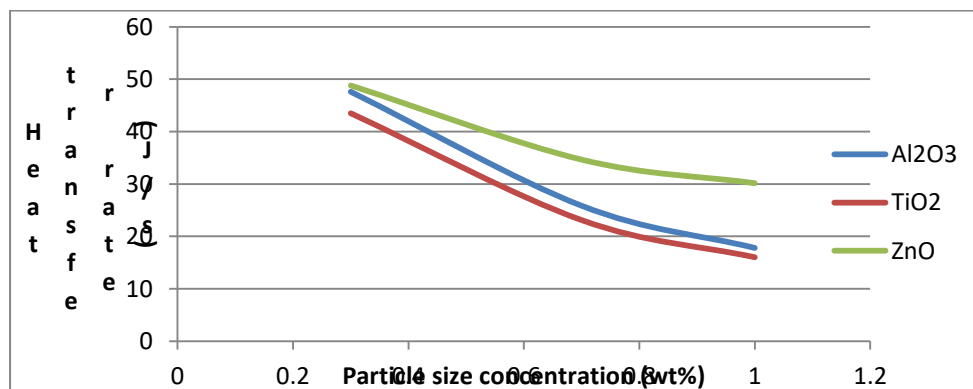


Figure A- 127 Heat transfer rate of monotype nanofluids.

The result indicates that the specific heat  $C_p$  of nanofluids decreases gradually as the particle size concentration increases from 0.3 – 1.0wt% [153]. ZnO/water has the highest specific heat capacity, follows by  $Al_2O_3$ /water and  $TiO_2$ /water has the least.

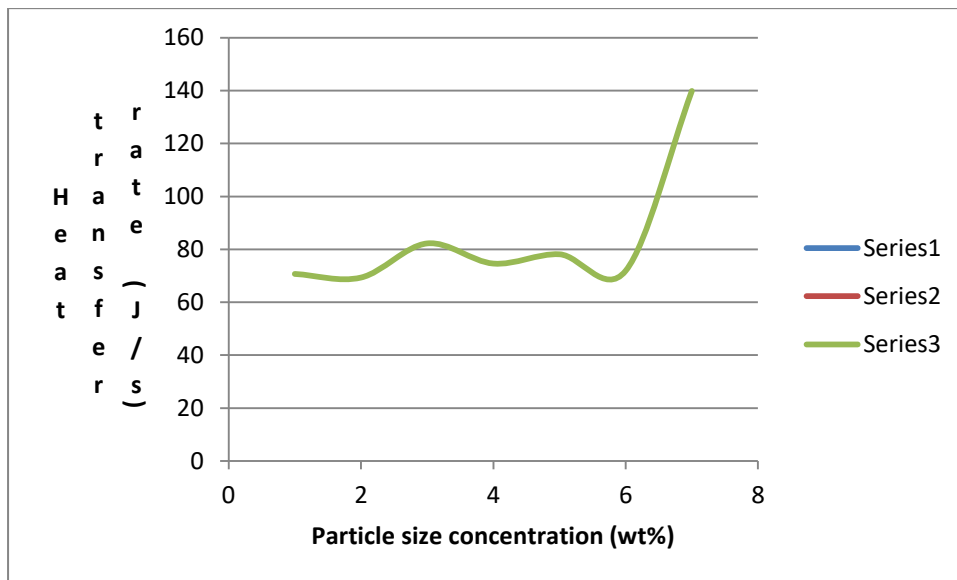


Figure A- 128 Heat transfer rate of the various hybrid nanofluids

The heat transfer rate of the various hybrid nanofluids increases with increase in particle size concentration (Fig.5.2.8b)  $0.3Al_2O_3+0.3TiO_2 + 0.3ZnO$ /water has the highest heat transfer rate of 139.8949J/S and  $0.7Al_2O_3 + 0.3TiO_2$ /water has the lowest of 69.3464J/S.

#### N- 7 Thermal conductivity measurement

The thermal conductivity of the different nanofluids was measured using KD2 Pro thermal property analyzer (Decagon Devices, InC., USA) Fig 3-20.



Figure A- 129 Photographic view of KD2 Pro thermal property analyzer

The KS -1 Sensor needle was used to measure the thermal conductivity of the various nanofluids. This was done by dipping the needle inside the nanofluids. The measurement procedure is just like that of portable pH meter. Each measurement cycle consists of 90 seconds

or at 1 second intervals. During the first 30 second, the instrument equilibrates which is then followed by heating and cooling of sensor needle for 30 second each. At the end of the reading, the controller computes the thermal conductivity internally using the change in temperature ( $\Delta T$ ) – time data from below Equation 3.11.

$$K = \frac{q(\ln t_2 - \ln t_1)}{4\pi (\Delta T_2 - \Delta T_1)} \dots \dots \dots (3.11)$$

The result was displayed; the data was plotted as shown on Figure 5-20. The result showed that the smaller needle gave better results.

N- 8 Thermal conductivity

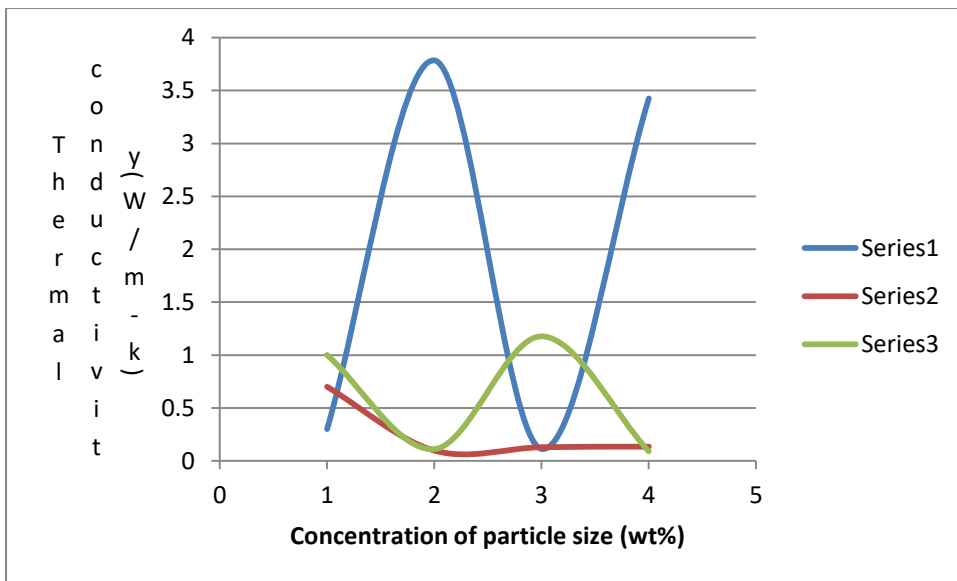
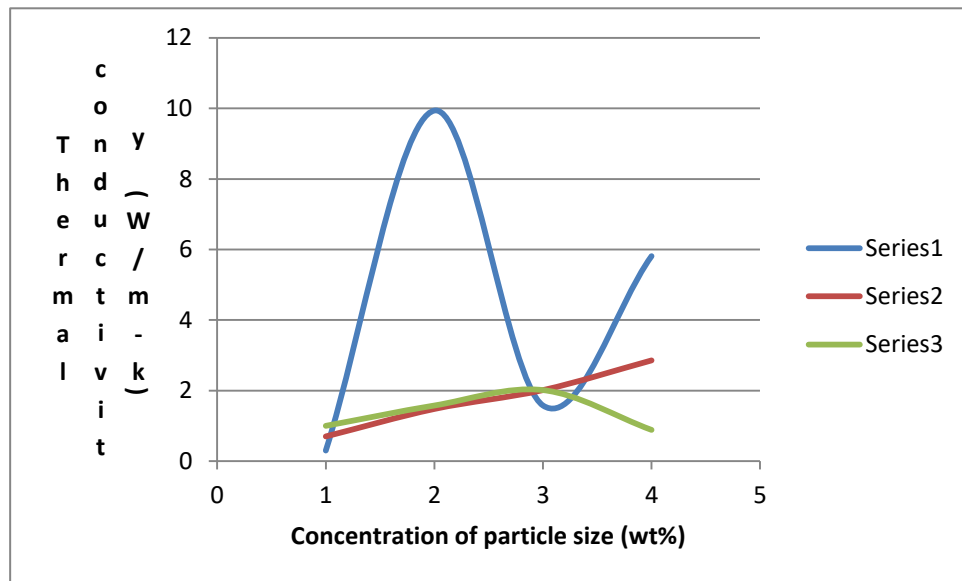


Figure A- 130 Thermal Conductivity of different pure monotype nanofluids.

Series1 - 0.3% particle size concentration (wt%), 0.7% concentration (wt%), series 2 - 0.7% particle size concentration (wt%) and series 3- 1.0% particle size concentration.

From the Fig.A-130, it is observed that thermal conductivity of the different nanofluids increases linearly with decreasing particle size. Some researchers in contrast, have shown that the thermal conductivity of nanofluids increases with increasing particle size. The study shows that the nanofluids can extraordinarily improve the thermal conductivity and enhance the heat

transfer. Moreover, nanofluid has shown its excellent performance in strengthening mass



transfer [186].

Figure A- 131 Comparison of thermal conductivity of surfacted monotype nanofluids

Series1 – 0.3% particle size concentration, Series 2 – 0.7% particle size concentration and series3 – 1.0% particle size concentration

As shown in Fig.A-131, the thermal conductivity of the monotype nanofluids decreases as the nanoparticles concentration increases. The best possible explanation for the effect is that the distance between nanoparticles decreases as the nanoparticles concentration increases. Experimental results have shown that the thermal conductivity of the nanofluids increases as the particle size decreases. This is because of the Brownian motion of the particles which is comparable with the findings of [84] . Generally it decreases with high volume concentration of nanoparticle due to low brown motion of dispersed nanoparticles [175]. The experiments showed that, on addition of surfactants to the nanofluids, an enhancement in thermal conductivity occurred [134]. This effect is shown in Fig. A-134. In this plot, the effect of nanoparticles concentration on the thermal conductivity is shown. Thermal conductivity decreases as the concentration of particle size increases [45], it is important to give attention to the particle concentration expressed in a volume fraction of nanoparticles in the base fluids.

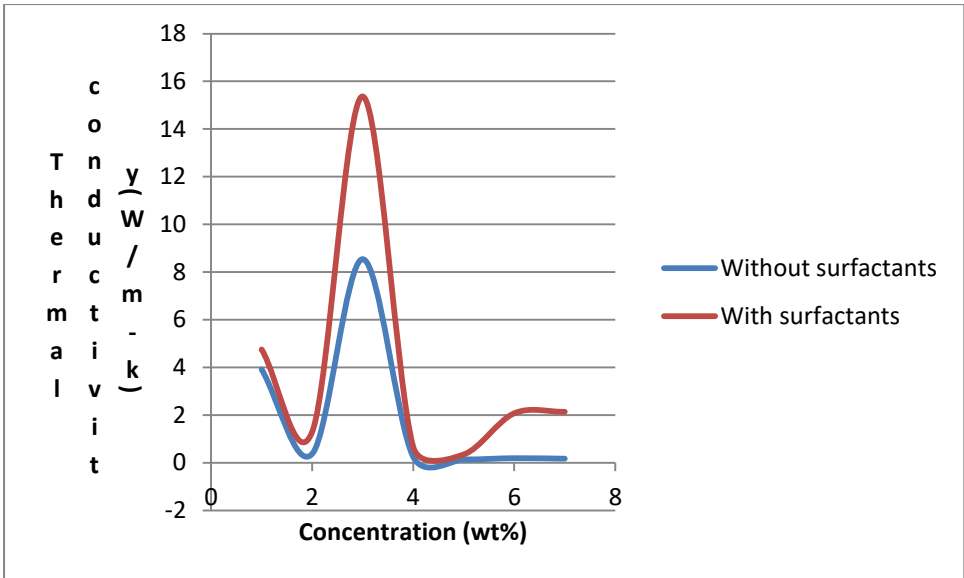


Figure A- 132 Comparison of the thermal conductivity of the different hybrid nanofluids  
 It can be observed from Fig.A-132 that surfactants enhance /improve the thermal conductivity of the different hybrid nanofluids.

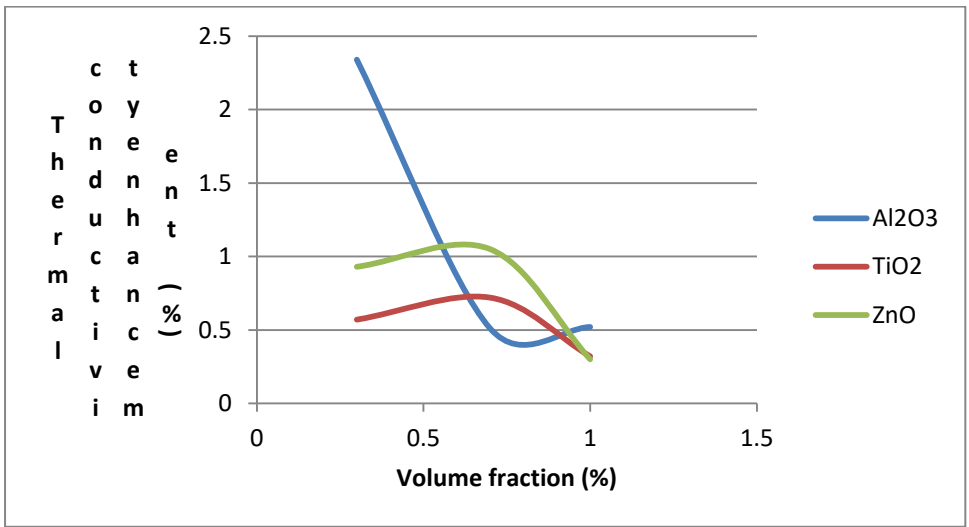


Figure A- 133 Effect of volume fraction on thermal conductivity of surfacted monotype nanofluids.

From the Fig A-133, it can be seen that surfactant decreases the thermal conductivity of the various Monotype nanofluids.

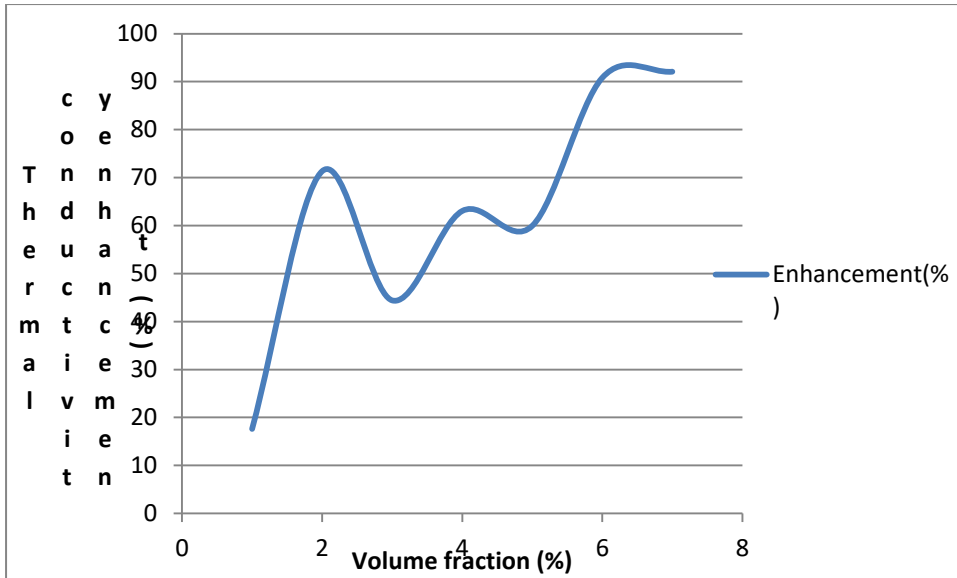


Figure A- 134 Effect of volume fraction on thermal conductivity of surfactated hybrid nanofluids  
 As shown in Fig.A-134, with addition of surfactants to the different nanofluids, the thermal conductivity enhancement increases with increase in volume fraction. That is the thermal conductivities of nanofluids improve as the concentration of particles increases (at 25°C). Notably, pH is 8 for ZnO-water with Na<sub>2</sub>HPO<sub>4</sub> surfactant. In addition, weight percent of the surfactant is 0.5. Even at a very low concentration of 1% (volume fraction), about 0.9 % increase is observed which is appropriate compared to the volume fraction of nanoparticles and also the maximum enhancement in thermal conductivity is 17% at 25°C.

O- 1 Statistical Analysis using IBM SPSS Statistics, version 20 Software

From the cleaning efficiency of the different pure and surfactated nanofluids, TiO<sub>2</sub>/water is chosen as the best among the monotype nanofluids while 0.3Al<sub>2</sub>O<sub>3</sub> + 0.3TiO<sub>2</sub> + 0.3ZnO is chosen as the best among the hybrid nanofluids, according their efficiency. Therefore, the statistical analysis was done based on these two nanofluids including the process variables.

O- 2 Comparison of means of pure and surfactated TiO<sub>2</sub>/water: This is done using compare paired sample T-Test means between pure and surfactated TiO<sub>2</sub>/water as well as their hybrids.

Table A- 46 Statistical analysis of the experimental results

Parameter	Time (second)	Temp (°C)	Weight loss of contaminated soil cleaned with pure TiO <sub>2</sub>	Weight loss of contaminated soil cleaned with surfactated TiO <sub>2</sub>
Mean	2520 (42mins)	199.2123	28.3344	46.6742

Standard Error	28.99425	2.34150	0.04823	0.10493
Standard deviation	1455.78868	117.56544	2.42136	5.26872
R Square			0.940	0.997
Std. Error of the Estimate			625.95800	

From Table A-46, it observed that addition of nanofluid to the contaminated soils increased the percentage mass loss and other properties. When comparing the means using t – test as shown on Table A-46

Comparing the two means, it is observed that the soil sample cleaned with nanofluid had higher percentage of mass loss than the other sample, but the two means were highly correlated.

Table A- 47 Comparison of pure TiO<sub>2</sub>/water with surfacted TiO<sub>2</sub>/water

		Mean	N
Pair 1	Surfacted TiO <sub>2</sub>	46.6742	N
	pure TiO <sub>2</sub>	28.3344	2521
	N	Correlation R	Sig.
Pair 1	VAR00001 & VAR00002	2521	0.997 0

The Tables A-46& A-47 indicates that there is strong relationship between pure and surfacted TiO<sub>2</sub>/water with coefficient of correlation R = 0.997. When their means were compared, the analysis shows that surfacted TiO<sub>2</sub> cleaned more oil and has higher standard error mean than pure TiO<sub>2</sub>/water. Both have strong relationship because their stability before cleaning.

	Mean	Std. Deviation	Upper	F	
			Pair 1 surfacted TiO <sub>2</sub> - pure TiO <sub>2</sub>		18.33975

When the tga result for pure & surfacted TiO<sub>2</sub>/water means are compared using paired samples Test. The paired weight loss of pure & surfacted TiO<sub>2</sub>/mean is 18.34mg with standard deviation of 2.8616mg and standard error mean of 0.0570mg.

Table A- 48 Comparison of pure TiO<sub>2</sub>/water with process variables

Correlations

		VAR00001	VAR00002	
Time(sec)	Pearson	1	.024	
	Correlation			
	Sig. (1-tailed)		.114	
	N	2521	2521	
Temp	Pearson	.024	1	
	Correlation			
	Sig. (1-tailed)	.114		
	N	2521	2521	

Comparison of process variables with weight loss using compare means that as temp increases, the weight loss increases also. It can be compared with the coefficient of correlation (R) between weight loss and temp which is highly positively correlated with R = 0.903. Comparing the temp and time for weight loss of contaminated soil cleaned with pure TiO<sub>2</sub>/water are +vely correlated at non significant level. It means then, as the temp increases, the weight loss increases at less time.

Table A- 49 Comparison of effects of temperature and time on weight loss

Using paired T- paired samples analysis for pure TiO<sub>2</sub>/water.

Paired Samples Statistics

		Mean	N	Std. Deviation	Std. Error Mean
Pair 1	VAR00002	199.2123	2521	117.56544	2.34150
	VAR00003	28.3344	2521	2.42136	.04823



Pair	VAR00001	2520.0000	2521	1455.78868	28.99425
2	VAR00003	28.3344	2521	2.42136	.04823

Var00003 = weight loss

The results on Table A-49: shows that contaminated soil cleaned with pure TiO<sub>2</sub>/water, during the Tga analysis (heating and cooling process), the temperature has the mean of 199.21°C, with standard deviation of 117.57 from the mean and standard error mean of 2.34°C on weight loss. The length of time for the process has the mean time of 2520seconds( 42minutes), standard deviation of 1455.79 seconds (24.26mins) with standard Error mean of 28.99 seconds (0.48mins) at mean weight loss of 28.33mg, standard deviation of 2.42mg from the mean, standard error mean of 0.048mg.

Table A- 50 Comparison of weight loss with temp and time for the contaminated soil cleaned with pure TiO<sub>2</sub>/water.

Paired Samples Correlations

	N	Correlation	Sig.
Pair 1 & VAR00002 & VAR00003	2521	-.285	.000
Pair 2 & VAR00001 & VAR00003	2521	-.903	0.000

The Table A-50, the –ve values of correlation between weight loss, temperature and time indicates that as the temperature increases the weight loss decreases at little amount that it is not significant. It indicates also as the time increases, the weight loss decreases significantly. In summary, as the temperature increases, the weight loss increases at dramatically reduced time period.

Table A- 51 Statistical Analysis of time and temp on weight loss using T-Test (Paired Samples Test)

Paired Samples Test

	Paired Differences			t	df
	Mean	Std. Deviation	95% Confidence Interval of the Difference		

				Std. Error Mean	Lower	Upper		
Pair 1	VAR00002 -	170.87790	118.27809	2.35569	166.25861	175.49718	72.538	2520
	VAR00003							
Pair 2	VAR00001 -	2491.66559	1457.97525	29.03780	2434.72519	2548.60598	85.808	2520
	VAR00003							

From the Table A-51, comparing the deviation of temperature from mean temperature as well as standard error means of temperature and time on weight loss, it is observed that temperature has more effect on weight loss. Ie as the temp increases, the weight loss increases also. paired Samples Test was used to compare the effect of temp on weight loss of mineral oil simulated soil sample. Comparing temp and weight loss using T – Test, it can be observed that t –value (85.81) for time and weight loss is greater than t-value (72.54) for temp and weight loss. The statistical analysis revealed that the interaction between temp and weight loss has mean temperature of 170.88°C, standard deviation from the mean of 118.28 °C and standard error mean of 2.36 °C. Comparing also the interaction of time and weight loss, the two paired parameters have mean, Standard.Deviation and Standard Error Mean values of 2491.67, 1457.97525 and 29.04, respectively. Also comparing the two process variables with weight loss using t values, t value (72.538) for temperature and weight loss is small the t value (85.808) for time and weight loss which means for weight loss of contaminated soil sample cleaned with pure TiO<sub>2</sub>, it takes longer time to restore the contaminated soil to its original status inspite the high temperature.

Surfacted TiO<sub>2</sub>/water

Table A- 52 Model Summary

Model	R	R Square	Adjusted R Square	Std. Error of the Estimate
1	.940 <sup>a</sup>	.885	.884	.82310

a. Predictors: (Constant), VAR00002, VAR00001

Table A- 53 ANOVA for Surfacted TiO<sub>2</sub> nanofluids

ANOVA

time

	Sum of Squares	df	Mean Square	F	Sig.
Between Groups	5337074512.308	2349	2272062.372	107.518	.000
Within Groups	3613567.692	171	21131.975		
Total	5340688080.000	2520			

The effect of temperature and time change on heatflow during the tga analysis of contaminated soil sample cleaned with surfacted TiO<sub>2</sub>/water is shown on Table A-53. The interaction between weight loss, time and temperature is highly significant, F =107.518, F = 92.632, respectively.

T-Test

Paired Samples Statistics

Mean	N	Std. Deviation	Std. Error Mean
time	2520.0000	2521	1455.78868
Temp	46.6742	2521	5.26872

Table A- 54 Oneway ANOVA for Time by temp(effect of temperature and time on weight loss)

	t	df	Sig. (2-tailed)			
	Mean	Std. deviation	Std. Error Mean	Upper		
Pair 1 Time – Temp	2473.32584	1460.57000	29.08946	2530.36754	85.025	2520

The effect of temperature and time on weight loss was analysis using paired samples Test. The process variables have mean value of time = 2473.33seconds, standard deviation of 1460.57seconds and standard Error mean of 29.0895seconds.

Paired Samples Correlations

	N	Correlation	Sig.
Pair 1 time & Temp	2521	-.907	0.000

As the temp increases, the time for the cleaning decreases significantly, because of the presence of surfactant. The weight loss depends so much on the temperature.

Table A- 55 Oneway ANOVA for weight loss by Temperature for surfacted TiO<sub>2</sub> time

	Sum of Squares	Df	Mean Square
Between Groups	5337074512.308	2349	2272062.372
Within Groups	3613567.692	171	21131.975
Total	5340688080.000	2520	

Oneway Correlations between time and temp on weight loss

		time	Temp
time	Pearson Correlation	1	-.907**
	Sig. (2-tailed)		0.000
Temp	N	2521	2521
	Pearson Correlation	-.907**	1
	Sig. (2-tailed)	0.000	

	N	2521	2521
--	---	------	------

Table A- 56 Paired Samples Test

		Paired Differences					t	df
		Mean	Std. Deviation	Std. Error Mean	95% Confidence Interval of the Difference			
					Lower	Upper		
Pair 1	VAR00002 - VAR00003	170.87790	118.27809	2.35569	166.25861	175.49718	72.538	2520
Pair 2	VAR00001 - VAR00003	2491.66559	1457.97525	29.03780	2434.72519	2548.60598	85.808	2520

From the Table A-56, comparing the deviation of temperature from mean temperature as well as standard error means of temperature and time on weight loss, it is observed that temperature has more effect on weight loss. Ie as the temp increases, the weight loss increases also. Paired Samples Test was used to compare the effect of temp on weight loss of mineral oil simulated soil sample. Comparing temp and weight loss using T – Test, it can be observed that t –value (85.81) for time and weight loss is greater than t-value (72.54) for temp and weight loss. The statistical analysis revealed that the interaction between temp and weight loss has mean temperature of 170.88°C, standard deviation from the mean of 118.28 °C and standard error mean of 2.36 °C. Comparing also the interaction of time and weight loss, the two paired parameters have mean, Standard.Deviation and Standard Error Mean values of 2491.67, 1457.97525 and 29.04, respectively. Also comparing the two process variables with weight loss using t values, t value (72.538) for temperature and weight loss is small the t value (85.808) for time and weight loss which means for weight loss of contaminated soil sample cleaned with pure TiO<sub>2</sub>, it takes longer time to restore the contaminated soil to its original status inspite the high temperature.

Surfacted TiO<sub>2</sub>/water

Table A- 57 Model Summary

Model	R	R Square	Adjusted R Square	Std. Error of the Estimate
1	.940 <sup>a</sup>	.885	.884	.82310

a. Predictors: (Constant), VAR00002, VAR00001

Table A- 58 ANOVA for Surfacted TiO<sub>2</sub> nanofluids

ANOVA

time

	Sum of Squares	df	Mean Square	F	Sig.
Between Groups	5337074512.308	2349	2272062.372	107.518	.000
Within Groups	3613567.692	171	21131.975		
Total	5340688080.000	2520			

The effect of temperature and time change on heatflow during the tga analysis of contaminated soil sample cleaned with surfacted TiO<sub>2</sub>/water is shown on Table A-58. The interaction between weight loss, time and temperature is highly significant, F =107.518, F = 92.632, respectively.

**.	Model	Sum of Squares	df	Mean Square	F
1	Regression	14970718.784	2	7485359.392	947.610
	Residual	19890179.817	2518	7899.198	
	Total	34860898.602	2520		

Correlation is significant at the 0.01 level (2-tailed)

When weight loss was correlated with the process variable, it is observed that the process variables have -ve effect on weight loss (R = -0.907). As the process variables increases, the weight loss reduces significantly.

Descriptive Statistics

Statistical analysis for surfacted TiO<sub>2</sub>

	N	Minimum	Maximum	Mean	Std. Deviation
time	2521	0.00	5040.00	2520.0000	1455.78868
Temp	2521	41.86	53.94	46.6742	5.26872
Weight loss	2521	31.45	410.40	199.1714	117.61671
Valid N (listwise)	2521				

T-Test

Paired Samples Statistics

Mean	N	Std. Deviation	Std. Error Mean
time	2520.0000	2521	1455.78868
Temp	46.6742	2521	5.26872

Table A- 59 Oneway ANOVA for Time by temp(effect of temperature and time on weight loss)

	t	df	Sig. (2-tailed)	Upper		
	Mean	Std. deviation	Std. Error Mean			
Pair 1 Time – Temp	2473.32584	1460.57000	29.08946	2530.36754	85.025	2520

The effect of temperature and time on weight loss was analysis using paired samples Test. The process variables have mean value of time = 2473.33seconds, standard deviation of 1460.57seconds and standard Error mean of 29.0895seconds.

### Paired Samples Correlations

	N	Correlation	Sig.
Pair 1 time & Temp	2521	-.907	0.000

As the temp increases, the time for the cleaning decreases significantly, because of the presence of surfactant. The weight loss depends so much on the temperature.

Table A- 60 Oneway ANOVA for weight loss by Temperature for surfacted TiO<sub>2</sub> time

	Sum of Squares	Df	Mean Square
Between Groups	5337074512.308	2349	2272062.372
Within Groups	3613567.692	171	21131.975
Total	5340688080.000	2520	

### Oneway Correlations between time and temp on weight loss

		time	Temp
time	Pearson Correlation	1	-.907**
	Sig. (2-tailed)		0.000
	N	2521	2521
Temp	Pearson Correlation	-.907**	1
	Sig. (2-tailed)	0.000	
	N	2521	2521

\*\* . Correlation is significant at the 0.01 level (2-tailed)

When weight loss was correlated with the process variable, it is observed that the process variables have –ve effect on weight loss (R = -0.907). As the process variables increases, the weight loss reduces significantly.

### Descriptive Statistics

Table A- 61 Statistical analysis for surfacted TiO<sub>2</sub>



	N	Minimum	Maximum	Mean	Std. Deviation
time	2521	0.00	5040.00	2520.0000	1455.78868
Temp	2521	41.86	53.94	46.6742	5.26872
Weight loss	2521	31.45	410.40	199.1714	117.61671
Valid N (listwise)	2521				

Comparing the statistical analysis of contaminated soil sample cleaned with surfacted TiO<sub>2</sub>, the result shown on Table A-61. The result shows that the time for the analysis has minimum period of 0 second, maximum of 5040 seconds(84mins), mean experimental period of 2520 second (42mins) and standard deviation of 1455.79sec(24mins). Considering the temperature, The minimum temperature is 31.45 °C which represents the onset temperature of the experiment, maximum temperature of 410oC which represent of end temperature of the experiment with mean temperature of 199.17°C and standard deviation of 117.62 oC. weight loss of 41.86mg, maximum weight loss of 53.94, mean weight loss of 46.67mg and standard deviation of 5.227g.

Model	Sum of Squares	df	Mean Square	F
Regression	14970718.7	2	7485359.3	947.610
Residual	84	251	92	
Total	19890179.8	252	7899.198	
	17	8		
	34860898.6	252		
	02	0		

When surfacted TiO<sub>2</sub>/water was statistically analysed, it was observed that temperature and time have significant effect on weight loss with F value = 107.52, F=92.63, at 0.001 level, respectively. Comparing the weight loss of surfacted TiO<sub>2</sub>/water further, reveals that weight loss significantly increase with temperature and time, both are highly significantly correlated with R= 0.655 and F = 947.6. The higher the temperature, the lesser length of time, the faster

the weightloss restoring the contaminated soil to its original status. Alternatively, if the temperature decreases dramatically, the heating time period will increase and vice versa. It can be concluded that the more temperature increases, the less time to restore the oil contaminated soil to its original conditions. Other words, the less the temperature, the more time needed for the restoration of the contaminated soil to its original status.

Table A- 62 Pure  $0.3Al_2O_3+0.3TiO_2+0.3ZnO$ /water

Descriptive Statistics

	N	Minimum	Maximum	Mean	Std. Deviation
time	2521	0.00	5040.00	2520.0000	1455.78868
Temp	2521	30.60	409.95	199.2214	117.51005
Weight loss	2521	21.73	29.79	25.0536	3.55086
Valid N (listwise)	2521				

It can be observed from Table A-62 that weight loss starts minimum time of 0 sec(min), maximum period of 5040 seconds(84mins) and mean time of 2520 (42mins) with standard deviation of 1455.789seconds(24.26mins) for contaminated soil sample cleaned with pure  $0.3Al_2O_3+0.3TiO_2+0.3ZnO$ /water. The minimum temperature (30.60°C) which is the onset temperature for the weight loss, maximum temperature of 409°C with mean temperature of 199.22 °C and standard deviation of 117.51 °C. The minimum weight loss is 21.73mg, maximum of 29.79mg, mean weight loss of 25.0536mg with standard deviation of 3.5509mg. It means then that the tga analysis for contaminated soil sample cleaned with pure  $0.3Al_2O_3+0.3TiO_2+0.3ZnO$ /water started at 0 minutes, 30.60°C with weight of 29.79mg. The cleaning finished at 42mins, 409 °C into the analysis after which the hot soil sample cooled down to 30.60°C , 84mins, leaving only the cleaned soil.

Comparison of time with weight loss

Paired Samples Statistics

	Mean	N	Std. Deviation	Std. Error Mean

Pair 1	time	2520.0000	2521	1455.78868	28.99425
	Temp	25.0536	2521	3.55086	.07072

–time, weight loss

Comparing the weight loss with time, at mean time of 2520seconds (42mins), the mean weight loss is 25.0536mg. The standard deviation and standard error mean for time and weight loss is 1455.79sec (24.26mins), 28.9943sec (0.48mins), respectively. The standard deviation and standard error mean for weight loss is 3.5509mg, 0.07072mg respectively.

Table A- 63 Paired Samples Test

	Paired Differences						t	df
	Mean	Std. Deviation	Std. Error Mean	95% Confidence Interval of the Difference				
				Lower	Upper			
Pair 1 time – Weight loss	2494.94636	1459.00406	29.05829	2437.96579	2551.92693	85.860	2520	

TableA-63 shows the effect of time on weight loss of pure  $3Al_2O_3+0.3TiO_2+0.3ZnO$ /water, the interaction is significant since t value (85.860) is greater than literature value at 95% Confidence Interval of the Difference. The mean time is 2494.9464 seconds (41.58mins), standard deviation of 1459.0041seconds (24.32 mins) and standard error mean of 29.05829seconds (0.484mins).

Table A- 64 Correlations process variables and weight loss.

		Time	Temp	Weight loss
time	Pearson	1	.025	-.905**
	Correlation			
	Sig. (2-tailed)		.209	0.000
	N	2521	2521	2521
Temp	Pearson	.025	1	-.275**
	Correlation			

	Sig. (2-tailed)	.209		.000
	N	2521	2521	2521
Weight loss	Pearson Correlation	-.905**	-.275**	1
	Sig. (2-tailed)	0.000	.000	
	N	2521	2521	2521

\*\* . Correlation is significant at the 0.01 level (2-tailed).

TableA-64 shows the correlation of process variables with weight loss of oil contaminated soil sample cleaned with pure  $0.3\text{Al}_2\text{O}_3+0.3\text{TiO}_2+0.3\text{ZnO}$ /water. The statistical analysis indicates that the temperature is positively non significantly correlated with weight loss but weight loss is negatively correlated with time. In other words, as temperature increases, the weight loss also increases in small amount. Likewise, as the length of time increases, the weight loss of the soil sample decreases significantly. The time has more effect ( $R = 0.905$  &  $F = 11442.71$ ) on the weight loss than the temperature (TablesA-65 & A-66).

Table A- 65 Model Summary And Regression of time on weight loss (ANOVAa)

Model	R	R Square	Adjusted R Square	Std. Error of the Estimate	Change Statistics			
					R Square Change	F Change	df1	df2
1	.905 <sup>a</sup>	.820	.820	618.48519	.820	11442.710	1	2519
Model	Sum of Squares		df	Mean Square	F	Sig.		
1 Regression	4377110292.591		1	4377110292.591	11442.710	.000 <sup>b</sup>		
Residual	963577787.409		2519	382523.933				
Total	5340688080.000		2520					

a. Dependent Variable: time

b. Predictors: (Constant), Weight loss

Table A- 66 Effect of process variables on Surfacted  $0.3\text{Al}_2\text{O}_3+0.3\text{TiO}_2+0.3\text{ZnO}$ /water

Correlations		Time	Temp	Weight loss
time	Pearson Correlation	1	.025	-.905**

	Sig. (2-tailed)		.209	0.000
	N	2521	2521	2521
Temp	Pearson Correlation	.025	1	-.275**
	Sig. (2-tailed)	.209		.000
	N	2521	2521	2521
Weight loss	Pearson Correlation	-.905**	-.275**	1
	Sig. (2-tailed)	0.000	.000	
	N	2521	2521	2521

\*\* . Correlation is significant at the 0.01 level (2-tailed).

From the Table A-66 of correlation between the weight loss of contaminated soil cleaned with surfacted  $0.3Al_2O_3 + 0.3TiO_2 + 0.3ZnO$ /water with process variables. Time is significantly correlated with temperature. The relationship is +ve, which indicates that as temperature increases the time, also increases on weight loss of surfacted  $0.3Al_2O_3 + 0.3TiO_2 + 0.3ZnO$ /water. The correlation of weight loss with time and temperature is -ve, which indicates that as time and temp increases, the weight loss decreases significantly with time and non significantly with temperature.

Table A- 67 Comparison of surfacted best nanofluids -  $TiO_2$  and  $0.3Al_2O_3 + 0.3TiO_2 + 0.3ZnO$

Table A- 68 Descriptive Statistics for surfacted best nanofluids -  $TiO_2$  and  $0.3Al_2O_3 + 0.3TiO_2 + 0.3ZnO$

	N	Minimum	Maximum
VAR00002	2521	26.06	31.58
Valid N (listwise)	2521		

Table A- 69 T-Test for surfacted best nanofluids -  $TiO_2$  and  $0.3Al_2O_3 + 0.3TiO_2 + 0.3ZnO$

Paired Samples Statistics

		Mean	N	Std. Deviation	Std. Error Mean
Pair 1	time	46.6742	2521	5.26872	.10493
	Temp	28.3344	2521	2.42136	.04823

From the Tables A-68 to A-69 above, comparing the surfTiO<sub>2</sub> (time) and surf0.3Al<sub>2</sub>O<sub>3</sub>+ 0.3TiO<sub>2</sub>+0.3ZnO (Temp), the contaminated soil sample cleaned with surfacted TiO<sub>2</sub>/water has the weight loss of 46.6742mg, standard deviation of 5.26872mg and standard mean error of 0.1049mg which are higher than those of surfacted 0.3Al<sub>2</sub>O<sub>3</sub>+ 0.3TiO<sub>2</sub>+0.3ZnO/water whose mean value is 28.3344mg, standard deviation of 2.4214mg and 0.04823mg, respectively. This available information shows that surfacted 0.3Al<sub>2</sub>O<sub>3</sub>+ 0.3TiO<sub>2</sub>+0.3ZnO/water is better than surfactedTiO<sub>2</sub> /water statistically.

Table A- 70 Comparing the two means using **Paired Samples Correlations**.

Paired Samples Test

	Paired Differences					T	Df	Sig. (2-tailed)
	Mean	Std. Deviation	Std. Error Mean	95% Confidence Interval of the Difference				
				Lower	Upper			
Pair 1 time - Temp	18.33975	2.86163	.05699	18.22799	18.45151	321.785	2520	0.000

Comparing the means of the two weight loss using paired samples Test, the two means paired together gives the new mean of 18.33975mg, standard deviation of 2.8616mg and standard error mean of 0.0570 with t value = 321.785 > table t value. Surfacted 0.3Al<sub>2</sub>O<sub>3</sub>+ 0.3TiO<sub>2</sub>+0.3ZnO/water and surfacted TiO<sub>2</sub>/water are highly correlated, R = 0.997 (Table A-70).

Table A- 71 Correlation of surfacted TiO<sub>2</sub> and surfacted 0.3Al<sub>2</sub>O<sub>3</sub>+ 0.3TiO<sub>2</sub>+0.3ZnO/water. Correlations

		time	Temp
time	Pearson	1	.997**
	Correlation		
	Sig. (2-tailed)		0.000
	N	2521	2521
Temp	Pearson	.997**	1
	Correlation		
	Sig. (2-tailed)	0.000	
	N	2521	2521

\*\* . Correlation is significant at the 0.01 level (2-tailed).

TableA-71 shows the correlation of surfacted  $\text{TiO}_2$  with surfacted  $0.3\text{Al}_2\text{O}_3+0.3\text{TiO}_2+0.3\text{ZnO}/\text{water}$ . The result indicates that the two nanofluids are highly correlated with the coefficient of correlation,  $R = 0.997$ . surfacted  $0.3\text{Al}_2\text{O}_3+0.3\text{TiO}_2+0.3\text{ZnO}/\text{water}$  has standard deviation of 2.169mg standard error of 0.003mg with t-value = 626.458 which is greater than that of surfacted  $\text{TiO}_2/\text{water}$  whose standard error is 0.098mg.

Table A- 72 Model Coefficients<sup>a</sup> for the best nanofluid

Model	Unstandardized Coefficients		Standardized Coefficients	t	Sig.
	B	Std. Error	Beta		
1 (Constant)	-14.783	.098		-150.140	0.000
surf0.3Al <sub>2</sub> O <sub>3</sub> +0.3TiO <sub>2</sub> +0.3ZnO	2.169	.003	.997	626.458	0.000

Dependent Variable: surfTiO<sub>2</sub>

std error of estimate = 0.42085 for surfTiO<sub>2</sub>

N- 9 Comparison of surfacted TiO<sub>2</sub> and surfacted 0.3Al<sub>2</sub>O<sub>3</sub> +0.3TiO<sub>2</sub>+0.3ZnO with process variables

Table A- 73 Paired Samples Statistics for surfacted TiO<sub>2</sub> and surfacted 0.3Al<sub>2</sub>O<sub>3</sub> +0.3TiO<sub>2</sub>+0.3ZnO with process variables

	Mean	N	Std. Deviation	Std. Error	
				Mean	
Pair 1	VAR00001	2519.0000	2520	1455.21132	28.98850
	VAR00002	203.0120	2520	119.98793	2.39022
Pair 2	VAR00003	23.4799	2520	2.75858	.05495
	VAR00004	2519.0000	2520	1455.21132	28.98850
Pair 3	VAR00005	46.6761	2520	5.26890	.10496
	VAR00006	199.2358	2520	117.59554	2.34256



Table A-73 shows the comparison of surfacted  $\text{TiO}_2/\text{water}$  and surfacted  $0.3\text{Al}_2\text{O}_3+0.3\text{TiO}_2+0.3\text{ZnO}/\text{water}$  using paired samples test. The mean lengthening time is 2519 seconds (41.98mins), standard deviation 1455.21seconds (24.25mins) and standard error mean of 28.98850seconds (0.48mins). Effect of temperature of weight loss is as follows, the mean temperature is 199.2358°C with standard deviation of 117.5955°C and standard error mean of 2.3426 °C. The weight loss of surfacted  $0.3\text{Al}_2\text{O}_3+0.3\text{TiO}_2+0.3\text{ZnO}/\text{water}$  and surfacted  $\text{TiO}_2/\text{water}$  are mean = 23.4799mg, 46.6761mg, standard deviation 2.786mg, 5.2689mg and standard error of 0.05495, 0.10496, respectively.

Table A- 74 Final Comparison of the best nanofluids with process variables

Paired Samples Statistics

		Mean	N	Std. Deviation	Std. Error Mean
Pair 1	Time	2520.0000	2521	1455.78868	28.99425
	temp	202.9461	2521	120.00974	2.39018
Pair 2	0.3aL2o3+0.3TiO2+0.3ZnO	23.4792	2521	2.75825	.05493
	surfTiO2	25.0536	2521	3.55086	.07072

Finally, in a summary, comparing the the best two nanofluids with the process variables, from Tables A-73 & A-74, it can be concluded that the surfacted  $0.3\text{Al}_2\text{O}_3+0.3\text{TiO}_2+0.3\text{ZnO}$ , statistically is the best hybrid/water as well as the overall best of 32 experimental nanofluids with the mean temperature of 202.95°C and mean time of 2520 seconds (42 mins), standard deviation of 2.758mg as well as standard error mean of 0.0549mg. Surfacted  $\text{TiO}_2$  is the best monotype nanofluid and the second among the overall 32 experimental nanofluids with the mean temperature of 199.2358°C and mean time of 2520 seconds (42 mins).

Effect of wettability on the cleaning efficiency of the different nanofluids. This is done by statistical comparison of cleaning efficiency with water saturation (water index,  $I_w$ ), oil saturation (oil index,  $I_o$ ), water and oil permeabilities. Their minimum, maximum, mean and standard deviation from the mean values is shown on Table A-75.

Table A- 75 Summary of statistical parameters of wettability and cleaning efficiency

Descriptive Statistics

	N	Minimum	Maximum	Mean	Std. Deviation	Standard Error mean
Cleaning efficiency	16	72.00	99.40	83.9875	8.41315	2.10329
Water index	16	.56	.76	.6466	.06000	0.01500
Oil index	16	.62	.99	.8243	.09829	0.02457
Water permeability	16	.00	.35	.0629	.08783	0.02196
Oil permeability	16	.10	.69	.3975	.15185	0.03796
Valid N (listwise)	16					

It can be observed from Table 6.10a that cleaning efficiency has the minimum value of 72%, maximum value of 99.4% with mean value of  $83.99 \pm 2.10329\%$ . Water saturation has the minimum water saturation of 56%, maximum value of 76% with mean value of  $64.7\% \pm 1.5\%$ . Oil saturation has the minimum of 62%, maximum value of 99% with mean Value of  $82.43 \pm 2.457\%$ . Water and oil permeabilities have minimum values of 0.0%, 10%, maximum values of 35%, 69% with mean values of 6.29% 8.8% and  $39.75 \pm 15.2\%$ , respectively. The small values of the standard error mean shows how accuracy the experimental results is.

Table A- 76 Comparison of wettability, cleaning efficiency with process variables

Correlations

		Krw	Kro	Time	Temp	Cleaning efficiency(%)		Water index	Oil index
Krw	Pearson	1		-.249	.381	.378	-.359	-	-.269
	Correlation							.220	
	Sig. (2-tailed)			.351	.146	.149	.172	.413	.313
	N	16	16	16	16	16	16	16	16
Kro	Pearson	-.249	1		.013	.029	.715*	.940	.900**
	Correlation						*	**	
	Sig. (2-tailed)	.351		.961	.915	.002	.000	.000	
	N	16	16	16	16	16	16	16	16
time	Pearson	.381	.013	1		.999*	-.130	.057	-.052
	Correlation					*			
	Sig. (2-tailed)	.146	.961	.000	.631	.833	.849		
	N	16	16	16	16	16	16	16	16
Temp	Pearson	.378	.029	.999**	1		-.115	.072	-.039
	Correlation								
	Sig. (2-tailed)	.149	.915	.000	.670	.790	.885		
	N	16	16	16	16	16	16	16	16
Cleaning efficiency	Pearson	-.359	.715**	-.130	-.115	1		.516	.857**
	Correlation						*		

	Sig. (2-tailed)	.172	.002	.631	.670		.041	.000
	N	16	16	16	16	16	16	16
Water index	Pearson Correlation	-.220	.940**	.057	.072	.516*	1	.704**
	Sig. (2-tailed)	.413	.000	.833	.790	.041		.002
	N	16	16	16	16	16	16	16
Oil index	Pearson Correlation	-.269	.900**	-.052	-.039	.857*	.704**	1
	Sig. (2-tailed)	.313	.000	.849	.885	.000	.002	
	N	16	16	16	16	16	16	16

\*\* . Correlation is significant at the 0.01 level (2-tailed).

\* . Correlation is significant at the 0.05 level (2-tailed).

Table A- 77 Summary of the Table A-76 for better understanding of the effects of wettability on the cleaning efficiency with process variables of the different nanofluids

Correlations

	Krw	Kro	time	Temp	Cleaning efficiency (%)	Water index(Iw)	Oil index (Io)
Krw	1	-0.249	0.381	0.378	-0.359	-0.220	-0.269
Sig		0.351	0.146	0.149	0.172	0.413	0.313
Kro	-0.249	1	0.013	0.029	0.715	0.940	0.900
Sig	0.351		0.961	0.915	0.002	0.000	0.000
time	0.381	0.013	1	0.999	-0.130	0.057	-0.052
Sig	0.146	0.961		0.000	0.631	0.833	0.849
Temp	0.378	0.029	0.999	1	-0.115	0.72	-0.039
Sig	0.149	0.915	0.000		0.67	0.790	0.885

Cleaning efficiency (%)	-0.359	0.715	-0.130	-0.115	1	0.516	0.857
Sig	0.172	0.002	0.631	0.072		0.041	0.000
Water index(Iw)	-0.220	0.940	0.057	0.072	0.516	1	0.704
Sig	0.413	0.000	0.833	0.790	0.41		0.002
Oil index (Io)	-0.269	0.900	-0.052	-0.039	0.857	0.704	1
Sig	0.313	0.00	0.849	0.885	0.000	0.002	

N- 10 Effect of water permeability on cleaning efficiency, wettability and process variables. It can be observed from Table7 that the water relative permeability ( $K_{rw}$ ) increases with a decrease in the oil relative permeability as it was observed in Tables 6.5 &6.6 and also in the literature. Water relative permeability increases with time and temperature (this is so because wettability depends so much on the viscosity of the fluids and porosity/permeability of the soil, hence, the reason for the use of mineral oil instead of crude oil which requires high temp in the lab.). It decreases with increase in amount of oil ( $I_o$ ) and water ( $I_w$ ) imbibed into the soil during the oilflooding (soil contamination) and nanofluid flooding (cleanup process) also. In otherwords, it decreases with strongly oil – wet condition. It decreases also with the cleaning efficiency. That is as cleaning efficiency increases, it decreases. It shows that during the cleaning, more water and oil is recovered and less water and oil is retained in the soil, the change is positively significant.

N- 11 Comparison of time, cleaning efficiency and wettability.

Table A-77 indicates that time has direct effect on water and oil relative permeabilities, temperature, water index and inversely with the cleaning efficiency and oil index (oil saturation). The oil and water relative permeabilities increase with time and temperature. Cleaning efficiency increases with oil saturation at less time. Further more, as more oil is imbibed into the soil during oilflooding (strongly oil-wet), the more oil is recovered during cleanup process (strongly water –wet.) as the soil is fully saturated.

From the Table, it can be seen that temperature has a positively significant effect on water and oil relative permeabilities, time and water saturation/index. These factors increase as the same with temperature. Cleaning efficiency and oil saturation increase with decrease in temperature significantly.

Cleaning efficiency decreases nonsignificantly with increase in water relative permeability, time and temperature but increases significantly with oil relative permeability, water and oil saturation. That is to say, as more oil and water is flooded during the soil contamination and cleanup process, the higher the cleaning efficiency with oil relative permeability at low temperature and time

Water saturation has a negative effect on the water relative permeability. In otherwords, as water saturation increases, oil relative permeability increases significantly with time, temperature, cleaning efficiency and oil saturation but decreases with water relative permeability.

There is a strong interaction between oil saturation with oil relative permeability, water saturation and cleaning efficiency. It indicates that as oil index increases these factors increase also but it decreases significantly with water relative permeability, time and temperature.

Table A- 78 The values of % oil removed in the contaminated soils.

<b>Initial mass of contaminated soils TGA(mg)</b>	<b>Mass cleaned after TGA test (mg)</b>	<b>of soils (mg)</b>	<b>Amount of oil removed (mg)</b>	<b>Oil removed (%)</b>	<b>Amount of water removed (mg)</b>	<b>Amount of nanoparticles removed (mg)</b>	<b>Amount of surfactant removed (mg)</b>	<b>+</b>
37.125	21.41		15.72	42.33				
32.88	20.87		12.01	36.53				
<b>39</b>	<b>22.50</b>		<b>16.5(oil +nanofluid+ surfactant)</b>	<b>5.2(31.5 2%)</b>	<b>10.1(61.2 1%)</b>	<b>1.2 (7.27%)</b>		

The contaminated soil samples cleaned with ZnO surfacted nanofluids in which 39 mg was analysed in TGA were restored to their original status with oil removed percentage of 30.90%, 36.53% and 31.52%, respectively.

